UNIVERSIDADE DE SÃO PAULO
ESCOLA POLITÉCNICA

ÉVERTON LINS DE OLIVEIRA

Modular Strategies Applied to the Control of Underwater Vehicle-Manipulator Systems during Cooperative Transportation

São Paulo
2023

ÉVERTON LINS DE OLIVEIRA

Modular Strategies Applied to the Control of Underwater Vehicle-Manipulator Systems during Cooperative Transportation

Corrected Version

Thesis presented to the Escola Politécnica da Universidade de São Paulo in partial fulfillment of the requirements for the degree of Doctor of Science.

São Paulo
2023

ÉVERTON LINS DE OLIVEIRA

Modular Strategies Applied to the Control of Underwater Vehicle-Manipulator Systems during Cooperative Transportation

Corrected Version

Thesis presented to the Escola Politécnica da Universidade de São Paulo in partial fulfillment of the requirements for the degree of Doctor of Science.

Research area:
Control and Mechanic Automation Engineering

Advisor:
Prof. Dr. Décio Crisol Donha

São Paulo
2023

Este exemplar foi revisado e corrigido em relação à versão original, sob responsabilidade única do autor e com a anuência de seu orientador.

São Paulo, _____ de _____ de _____

Assinatura do autor: _____

Assinatura do orientador: _____

Catalogação-na-publicação

de Oliveira, Éverton L.
Modular Strategies Applied to the Control of Underwater Vehicle Manipulator Systems during Cooperative Transportation / É. L. de Oliveira -- versão corr. -- São Paulo, 2023.
281 p.

Tese (Doutorado) - Escola Politécnica da Universidade de São Paulo. Departamento de Engenharia Mecânica.

1.Modelagem matemática 2.Controle não-linear 3.Sistemas multicorpos 4.Veículos subaquáticos 5.Sistema veículo-manipulador I.Universidade de São Paulo. Escola Politécnica. Departamento de Engenharia Mecânica II.t.

DE OLIVEIRA, É. L. **Modular Strategies Applied to the Control of Underwater Vehicle-Manipulator Systems during Cooperative Transportation.** 2023. 281 f. Thesis (Doctor of Sciences in Control and Mechanic Automation Engineering) – Escola Politécnica, Universidade de São Paulo, São Paulo, 2023.

Approved on:

Examining Committee

Prof. Dr. _____

Institution: _____

Judgment: _____

Prof. Dr. _____

Institution: _____

Judgment: _____

Prof. Dr. _____

Institution: _____

Judgment: _____

Prof. Dr. _____

Institution: _____

Judgment: _____

Prof. Dr. _____

Institution: _____

Judgment: _____

Dedicated to my parents.

ACKNOWLEDGEMENTS

First of all, I would like to thank God for allowing me to carry out this work.

To my friend and advisor, Prof. Dr. Décio Crisol Donha, for his support, guidance, patience and belief in the work.

To my friend, Prof. Dr. Renato Maia Matarazzo Orsino, for his support, encouragement, attention and suggestions on the work.

To Profs. Drs. Agenor de Toledo Fleury and Celso Pupo Pesce, for their suggestions on the work.

To Profs. Drs. António Manuel dos Santos Pascoal, Asgeir Johan Sørensen, Giovanni Indiveri and Bruno Augusto Angélico for participating in the defense committee of this thesis.

To the Polytechnic School of the University of São Paulo (USP), for the opportunity that I had to take the doctorate course.

To the Higher Education Personnel Improvement Coordination (CAPES) for the scholarship that made this research possible.

Thanks to all those who contributed to the development of this thesis.

Finally, to my parents, Adeilda and Valter, who have always donated a lot to my education. This work is dedicated to them.

“First do what is necessary. Then do what is possible.
And before you know it you are doing the impossible.”

(Saint Francis Assisi)

ABSTRACT

DE OLIVEIRA, É. L. **Modular Strategies Applied to the Control of Underwater Vehicle-Manipulator Systems during Cooperative Transportation.** 2023. 281 p. Thesis (Doctor of Sciences in Control and Mechanic Automation Engineering) – Escola Politécnica, Universidade de São Paulo, São Paulo, 2023.

The demand for natural resources (e.g., oil and gas, minerals, etc.), together with the high cost and operators fatigue associated with the classical teleoperation approach used by the offshore industry in Remotely Operated Vehicles (ROVs), brings the need for a higher degree of automation in the intervention tasks. To meet this requirement, the Underwater Vehicle-Manipulator Systems (UVMSs) are intended to be used in an autonomous way to perform Inspection, Maintenance and Repair (IMR) operations in the next fell years. Also, there is an increasing demand for alternative means of transportation in the underwater environment to assist in construction, deep-sea mining and general dexterous manipulation, which a single UVMS cannot perform. This work focuses on the motion control and coordination of UVMSs during cooperative transportation. Among the theoretical developments, the main contribution is the introduction of the Modular Control Methodology (MCM) for general multibody systems, whose potential engineering applications go beyond the class of problems that originally motivated this thesis. This novel methodology simplifies the control synthesis with a hierarchical approach, using standard controllers for the subsystems in the lowest levels of the control hierarchy and enforcing the constraints *a posteriori*. It also enables control allocation in the case of over-actuation and optimal control synthesis. The MCM can also be used for coordination during cooperative transportation, since the prescribed formation can be treated as a set of constraints among the agents according to the established communication topology. The contributions made here are tested through numerical simulations in different scenarios.

Keywords: Mathematical modeling, Nonlinear control, Multibody systems.

RESUMO

DE OLIVEIRA, É. L. **Estratégias Modulares Aplicadas ao Controle de Sistemas do tipo Veículo-Manipulador Subaquático durante o Transporte Cooperativo.** 2023. 281 f. Tese (Doutorado em Ciências na área de Engenharia de Controle e Automação Mecânica) – Escola Politécnica, Universidade de São Paulo, São Paulo, 2023.

A demanda por recursos naturais (por exemplo, petróleo e gás, minerais, etc.), juntamente com o alto custo e fadiga dos operadores associados à abordagem clássica de teleoperação utilizada pela indústria offshore em Veículos Operados Remotamente (ROVs), traz a necessidade de um maior grau de automação nas tarefas de intervenção. Para atender a esse requisito, os Sistemas de Veículos-Manipuladores Subaquáticos (UVMSs) pretendem ser utilizados de forma autônoma para realizar operações de Inspeção, Manutenção e Reparo (IMR) nos próximos anos. Além disso, há uma demanda crescente por meios alternativos de transporte no ambiente subaquático para auxiliar na construção, mineração em alto mar e manipulação hábil geral, que um único UVMS não pode realizar. Este trabalho tem como foco o controle de movimento e coordenação de UVMSs durante o transporte cooperativo. Entre os desenvolvimentos teóricos, a principal contribuição é a introdução da Metodologia Modular de Controle (MCM) para sistemas multicorpos genéricos, cujas potenciais aplicações em engenharia vão além da classe de problemas que originalmente motivou esta tese. Essa nova metodologia simplifica a síntese do controle com uma abordagem hierárquica, usando controladores padrão para os subsistemas nos níveis mais baixos da hierarquia de controle e impondo os vínculos de modelagem *a posteriori*. Esta ainda permite realizar a alocação de controle em caso de redundância de atuação e a síntese dos controladores padrão. A MCM também pode ser utilizada para coordenação durante o transporte cooperativo, já que a formação prescrita pode ser tratada como um conjunto de restrições entre os agentes de acordo com a topologia de comunicação estabelecida. As contribuições aqui feitas são testadas através de simulações numéricas em diferentes cenários.

Palavras chave: Modelagem matemática, Controle não-linear, Sistemas multicorpos.

FIGURES

TABLES

ACRONYMS

AI-AUV	–	Articulated Intervention-Autonomous Underwater Vehicle
AM	–	Aerial Manipulator
ARL	–	Aerospace Robotics Laboratory
AUV	–	Autonomous Underwater Vehicle
CAPES	–	Coordenação de Aperfeiçoamento de Pessoal de Nível Superior
CTC	–	Computed Torque Control
DC	–	Direct Current
DoFs	–	Degrees of Freedom
DPT	–	Digital Pressure Transducer
DVL	–	Doppler Velocity Log
EKF	–	Extended Kalman Filter
EoMs	–	Equations of Motion
GPM	–	Gradient Projection Method
GSTA	–	Generalized Super Twisting Algorithm
I-AUV	–	Intervention-Autonomous Underwater Vehicle
IMR	–	Inspection, Maintenance and Repair
IMU	–	Inertial Measurement Unit
I-ROV	–	Intervention-Remotely Operated Vehicle
ISMC	–	Integral Sliding Mode Control
ITAE	–	Integral Time Absolute Error
LBL	–	Long BaseLine

MCM – Modular Control Methodology

MMM – Modular Modeling Methodology

MPC – Model Predictive Control

NMPC – Nonlinear Model Predictive Control

P – Proportional

PD – Proportional-Derivative

PI – Pseudo-Inverse

PID – Proportional-Integral-Derivative

QP – Quadratic Programming

RMSE – Root Mean Square Error

ROS – Robot Operating System

ROV – Remotely Operated Vehicle

RPM – Revolutions Per Minute

SMC – Sliding Mode Control

STA – Super Twisting Algorithm

TDC – Time Delay Control

UM – Underwater Manipulator

USBL – Ultra Short BaseLine

USP – University of São Paulo

UUV – Unmanned Underwater Vehicle

UVMS – Underwater Vehicle-Manipulator System

UWSim – UnderWater Simulator

VIV – Vortex Induced Vibration

VMS – Vehicle Manipulator-System

SYMBOLS

$a, b, \ldots$	–	Scalars, indexes and elements of vectors or matrices
$\mathrm{A}, \mathrm{B}, \ldots$	–	Points
$\vec{\mathbf{a}}, \vec{\mathbf{b}}, \ldots$	–	Vectors
$\mathbf{a}, \mathbf{b}, \ldots$	–	Column-vectors
$\mathbf{A}, \mathbf{B}, \ldots$	–	Matrices
$\mathsf{A}, \mathsf{B}, \ldots$	–	Bodies
$\mathcal{A}, \mathcal{B}, \ldots$	–	Subsystems
$\mathtt{a}, \mathtt{A}, \mathtt{b}, \mathtt{B}, \ldots$	–	Labels

SUMMARY

1 INTRODUCTION

Underwater Vehicle-Manipulator Systems (UVMSs) are robots composed of an Unmanned Underwater Vehicle (UUV) endowed with at least one underwater robotic manipulator. UUVs can be of two types: Remotely Operated Vehicles (ROVs) and Autonomous Underwater Vehicles (AUVs). The manipulators available on the market generally have an anthropomorphic structure, varying the number of active joints from three to seven, or even more, depending on the type of application. The drive can also vary between hydraulic and electric. When an ROV is combined with one or more manipulators capable of carrying out Inspection, Maintenance and Repair (IMR) operations, it is an Intervention-ROV (I-ROV), also known as work-class ROV. Similarly, an AUV equal equipped is called Intervention-AUV (I-AUV). In this taxonomy, shown in Fig. 1, both I-ROVs and I-AUVs are part of the UVMS class. Fig. 2 (a) shows an I-ROV used for deep-water IMR operations (WRIGHT'S, 2020) and Fig. 2 (b) shows a prototype of an I-AUV developed by the University of Girona, Spain (YOUAKIM et al., 2017).

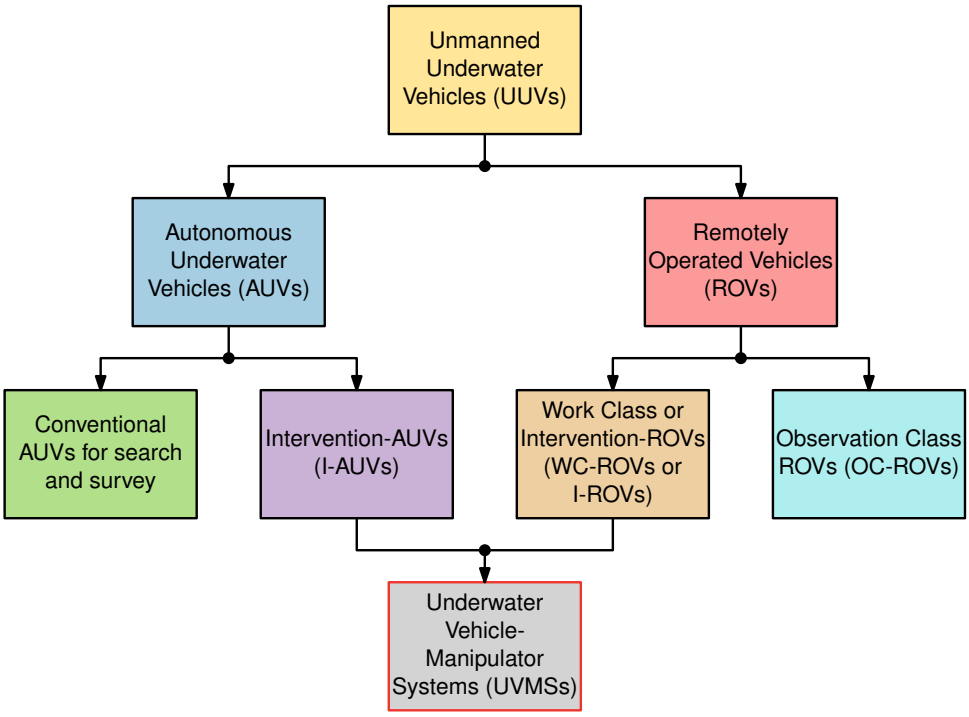

Figure 1: Taxonomy associated to UVMSs

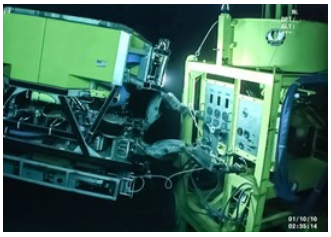

(a): I-ROV operating an underwater panel

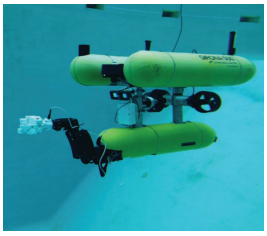

(b): I-AUV GIRONA 500 in pool experiment

Figure 2: Examples of UVMSs

Source: (a): Wright's (2020); (b): Youakim et al. (2017)

The offshore industry is the main application area for UVMSs. This is due to the need for underwater manipulation to perform dexterous tasks such as maintenance in sensors, valves and ducts, in addition to the transport of objects, e.g., tools or construction materials in this environment (SIMETTI et al., 2018), as illustrated in Fig. 3 (a)–(b). Nevertheless, the range of application for this type of equipment is not restricted to the offshore industry only. UVMSs have a high potential for application in the recovery of objects from the seabed, e.g., retrieving the black box of an aircraft, shown in Fig. 3 (c). Also the application in the marine archaeological research (RIDAO et al., 2014) or in the maintenance of pressurized water nuclear reactors, where UVMSs can be used to inspect and perform maintenance on pipelines that are susceptible to corrosion and that can put the nuclear plant functioning at risk (LEE et al., 2007; MAZUMDAR et al., 2012), as illustrated in Fig. 3 (d).

(a): IMR simulation with DexROV

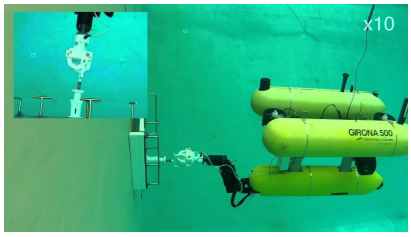

(b): I-AUV test for valve turn

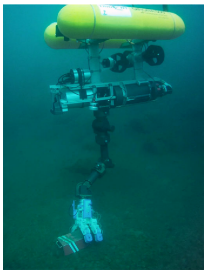

(c): I-AUV test in a black-box recovery

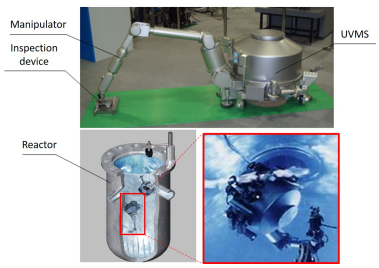

(d): UVMS for IMR in nuclear reactor

Figure 3: Examples of underwater manipulation

Source: (a): Simetti, Galeano and Casalino (2016); (b): Youakim et al. (2017);
(c): MIR (2020); (d): MHI (2011)

1.1 MOTIVATION

The demand for UVMSs has been growing due to the increase in oil and gas exploration in deep waters (RIDAO et al., 2014). However, current IMR operations at these depths are carried out with I-ROVs on the classical teleoperation scheme, where one operator takes care of the umbilical and steers the vehicle, while the other operates the manipulator (YOUAKIM et al., 2017). Despite this scheme being widely used in the offshore industry, it requires a large structure on the Support Surface Vessel (SSV), which turns the operation very expensive (SIVČEV et al., 2018). For example, the cost for ROV with SSV to perform an acoustic inspection of a pipeline can reach 50 k€ per day (SIMETTI, 2020). Other disadvantages of this kind of operation are the fatigue exposure that the operators are subjected to during the positioning and manipulation activities and the communication delays between the SSV and ROV, which can severely degrade the performance of whole operation (SIVČEV et al., 2018).

These problems can be solved by increasing the autonomy level of underwater manipulation tasks. One way to do this is to replace the I-ROVs by the I-AUVs, since they are seen as the natural evolution of the work-class ROVs, not requiring an expensive support structure due its autonomy and possibility to be operate from cheap vessels. Such a modification can reduce the operational costs associated with the classical teleoperation scheme and eliminate the human burden, since the operator will be responsible for high-level tasks as the assistance on task planning and operation management/supervision. For instance, the economy can reach 85% for the previous acoustic inspection, if it is performed by AUVs operating in tandem configuration (SIMETTI, 2020). Beyond the presented applications, recent works (CONTI et al., 2015; NIELSEN et al., 2016; SIMETTI; CASALINO, 2017; HESHMATI-ALAMDARI, 2018; HESHMATI-ALAMDARI et al., 2018; HESHMATI-ALAMDARI; KARRAS; KYRIAKOPOULOS, 2019; VERGINIS; MASTELLARO; DIMAROGONAS, 2019; HESHMATI-ALAMDARI et al., 2021a; HESHMATI-ALAMDARI et al., 2021b) highlighted that I-AUVs also could be used to perform cooperative manipulation tasks, in cases where more agents are needed to execute a single operation. In this context, they can be used to transport objects that cannot be carried by a single UVMS, due to their shape and weight restrictions, to carry and replace pipelines and cables lying on the ocean floor or on assembly tasks such as building and repairing underwater structures. Furthermore, underwater search, such as resource exploration, as the search for mineral deposits, and rescue tasks, could be more efficient and effective if multiple I-AUVs are used.

Looking for the presented possibilities and for the important role that AUVs and I-AUVs will play in the exploration of the sea in the future, many research projects focused on the development

of underwater autonomous manipulation systems. The list is long, including AMADEUS (LANE et al., 1997), UNION (RIGAUD et al., 1998), SAUVIM (MARANI; CHOI; YUH, 2009), TRIDENT (PRATS et al., 2012a; PRATS et al., 2012c; SANZ et al., 2012; FERNANDEZ et al., 2013; SIMETTI et al., 2014; RIBAS et al., 2015), PANDORA (LANE et al., 2012; CARRERA et al., 2014; CARRERA et al., 2015), DexROV (GANCET et al., 2016; SIMETTI; GALEANO; CASALINO, 2016) and ROBUST (SIMETTI et al., 2018; SIMETTI et al., 2020) and many others. All projects presented important developments on their scope of work and some of them being considered as milestones, nevertheless there is a long way to go until the I-AUVs can be used in the operational environment (RIDAO et al., 2014; SIVČEV et al., 2018). This is due to the strong constraints imposed on this kind of system that challenges its control.

For example, the vehicle has large inertia compared to the manipulator, which makes it adequate for slow and low precision motions (i.e., high amplitude displacements). In contrast, the manipulator is used in short-range tasks (e.g., picking and placing an object, turning a valve, or connecting a plug) due to its fast response and high precision. This heterogeneous behavior almost decouples the manipulator dynamics from vehicle motion. On the other hand, the vehicle is still prone to respond to the disturbances induced by the motion of the manipulator, which may severely affect its attitude (DUNNIGAN; RUSSELL, 1998; BARBALATA, 2017), depending on the ratio between the vehicle and manipulator masses (SIVČEV et al., 2018). There is also kinematic coupling since the position of the end-effector depends on the motion of the vehicle. Thus, any error in the vehicle positioning influences the end-effector, even if the manipulator is assumed to be dynamically decoupled from the vehicle.

In addition, the dynamics of this system is complex, highly nonlinear and time-varying because the UVMS is a multibody system, subject to severe environmental forces associated with the hydrodynamic forces due to the added mass, drag, waves and current effects, and due to the hydrostatic restoring forces. Although the hydrostatic forces can be estimated based on the geometry of the bodies, this can be done only within a certain precision. As well, there is not exactly a model for hydrodynamic forces since the classical maneuvering models are established only for UUVs and for basic geometry (e.g., sphere, parallelepiped, cylinder, ellipsoid, etc.). Moreover, as pointed by Richard and Lévesque (1996), the stochasticity associated with the environmental conditions is a very important factor that is not always taken into account.

There is also the redundancy resolution problem, because the I-AUVs have more Degrees of Freedom (DoFs) than those required to perform a task on the operational workspace. Hence, an inverse kinematics approach needs to be applied to generate the references for the coordination control in the joint space based on the desired path for the end-effector (ANTONELLI, 2014).

This brings the possibility to use these redundant DoFs to achieve secondary task objectives (e.g., avoid joints limits, reduce energy consumption, minimize the restoring moments, etc.). Similarly, the coordination of multiple I-AUVs in cooperative tasks is an important feature associated with the kinematics, where the references should preserve the formation (e.g., regulating agents position and velocity) and guarantee security objectives (e.g., collision avoidance, loss of agents, etc.).

Regarding technological aspects, I-AUVs are powered by batteries, being fundamental to save energy, seeking higher autonomy for long-time missions and higher operation capacity (e.g., payload transportation). Another important restriction is on the available feedback information, which is restricted to the onboard sensors. This feedback may be inaccurate and limited (i.e., low bandwidth), where it is necessary to adopt some kind of sensor fusion scheme to produce reliable information (HESHMATI-ALAMDARI et al., 2021a; HESHMATI-ALAMDARI et al., 2021b).

Besides that, there are problems related to the actuation system, since in general UUVs are propelled by thrusters, while the manipulators are actuated by electric motors. Although the electric motors have a fast response with a negligible influence in the global dynamics, this is not the case for thrusters, whose coupling effects can result in limit cycles on the closed-loop positioning when not compensated (YOERGER; COOKE; SLOTINE, 1990; BESSA et al., 2004; BESSA, 2005; BESSA; DUTRA; KREUZER, 2006; BESSA; DUTRA; KREUZER, 2013; ANTONELLI, 2014). Thus, based on the comments made above, one can summarize the main problems associated with the control of I-AUVs as below:

1. kinematic/dynamic coupling between the vehicle and manipulator;
2. complex dynamic model with several sources of uncertainty;
3. unstructured operating environment subjected to disturbances;
4. kinematic redundancy;
5. coordination of multiple agents in cooperative tasks;
6. thrusters dynamics;
7. limited operational capacity defined by its batteries;
8. restricted feedback information and low sensors bandwidth.

Moreover, the UVMSs are a part of the robotic field of mobile systems with manipulation capabilities, such as Vehicle-Manipulator Systems (VMSs), Aerial Manipulators (AMs), Underwater Manipulators (UMs) and I-AUVs. The research interest in these topics has been increasing

over the last years, as seen in the normalized scientific production factor of the previous decade raised by the author from Scopus (2022) and shown in Fig. 4 with the total number of publications indicated in the legend. Therefore, it is essential to contribute to developing such a field, presenting new approaches and techniques for modeling and control.

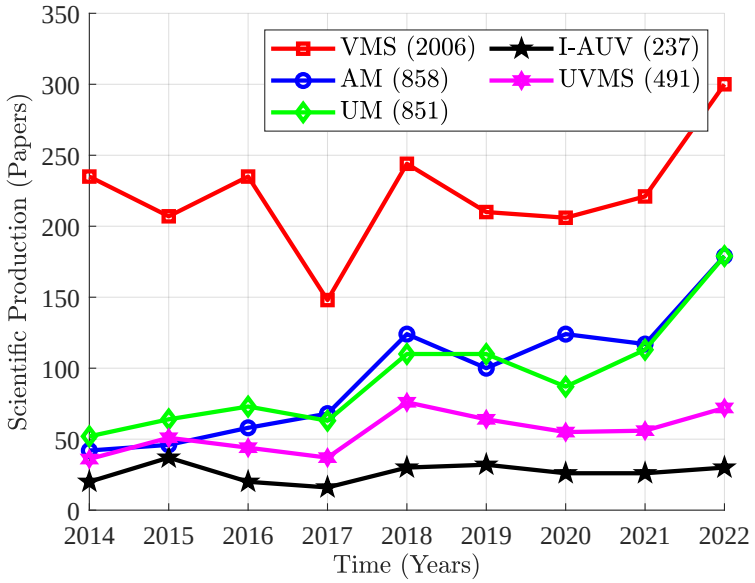

Figure 4: Scientific production of the last decade.

1.2 OBJECTIVES

The main objective of this thesis is to develop strategies for modeling and control of I-AUVs. To address this issue, the novel Modular Control Methodology (MCM), applicable to multibody dynamic systems in general and particularly to the class of I-AUVs, is introduced. The secondary objective is to test the approaches developed during a cooperative transportation.

The specific objectives are as below:

1. Create a generalized modeling approach for underwater multibody systems, where the models on the literature for submerged bodies can be used. This new approach enables a structured process and reduces the possibility of misleading actions during the modeling;

2. Develop the MCM for multibody systems, applicable to both in- and off-the-shelf systems, to reduce the control synthesis to the syntheses of sub-controllers and its coupling. This new methodology allows the utilization of already validated control algorithms for the sub-controllers, which may reduce the complexity of the design process;

3. Test the developed approaches by means of numerical simulations of operational tasks (e.g., station-keeping, coordinate control and cooperative transportation).

1.3 THESIS ORGANIZATION

Chapter 2 presents the literature review. The mathematical modeling approach, including several simulation studies considering benchmark models to validate the modeling, is presented in chapter 3. Chapter 4 is reserved for the formulation of the MCM and highlights the method features through numerical simulations with classical benchmark models for robotic systems. Chapter 5 applies the MCM of chapter 4 in simulation studies of cooperative transportation task performed by teams I-AUVs and modular ROVs. Finally, chapter 6 brings the conclusions and further works.

2 LITERATURE REVIEW

The state-of-the-art review is divided into: (i) dynamic modeling; (ii) inverse kinematics; (iii) coordinated control and (vi) cooperative control.

2.1 DYNAMIC MODELING

Over the years, many works have focused on developing dynamic models for UVMSs. Below, the items that we consider most important for this work were reviewed.

Ioi and Itoh (1990) derived a dynamic model for an underwater manipulator through the recursive Newton-Euler algorithm considering the influence of added mass, drag and lift forces on the links. As example, the inverse dynamics problem is treated considering and a 9-DoFs dual-arm manipulator. In addition, they investigated the inverse dynamics problem, considering a hybrid control for force and position regulation of a 6-DoFs manipulator. Schjolberg and Fossen (1994) developed a dynamic model of a UVMS through the same approach of Ioi and Itoh (1990) and proposed a feedback linearization control law for the coordinated control of the system. Despite the consistent modeling and detailed control synthesis presented by Schjolberg and Fossen (1994), there are no simulations or experiments in this work to show the applicability of the proposed control law.

Lévesque and Richard (1994) proposed a mathematical model for the drag forces on an underwater manipulator. The model considers the local variation of the velocity profile through the cross-flow principle for the drag force calculation. Due to this dependency, it is necessary numerically evaluate the drag forces, increasing the operations by 2-3 times compared to a standard algorithm without hydrodynamic forces evaluation. Lévesque and Richard (1994) also presented a method for the computation of the buoyance forces in fully or partially submerged bodies. Moreover, in Richard and Lévesque (1996), the importance of the stochastic effects between the fluid environment and manipulator is highlighted. According to the authors, such effects can be taken into account writing the relative velocity as the sum of a deterministic

component (mean value) associated with the manipulator motion and a stochastic component (zero-mean Gaussian white noise) related to the fluid velocity with respect to the links.

McMillan, Orin and McGhee (1994) presented a simulation algorithm for a UUV endowed with a robotic manipulator. This model is based on a modified version of the O(N) algorithm adapted for the inclusion of moving base effects and environmental forces, e.g., added mass, viscous drag, fluid acceleration and buoyance forces. McMillan, Orin and McGhee (1994) highlighted that despite the efficiency of the O (N) algorithm, the computations increased almost two times, when the environmental forces are added, in comparison with the case for an on-land moving base manipulator. Another interesting observation is that the computations grew linearly with the number of links of the manipulator.

McLain and Rock (1998) developed a model for the hydrodynamic forces on a single-link underwater manipulator of cylindrical geometry. Firstly, the model is constructed based on the two-dimensional potential-flow theory taking into account the effects of vortices in the wake, and then it is extended to include 3-D flow effects through the strip theory. Furthermore, the model counts with state-dependent coefficients for the inertial (added mass) and drag forces, written for each strip as functions (cubic-splines) of the diameters traveled along the longitudinal axis of the cylinder through the regression of hydrodynamic torque measurements. These data come from the experiments conducted with a circular PVC cylinder of ratio aspect (L/D) of 9.1, swinging with angles less than 120 degrees. Experimental tests validated the predictions of torque evaluation of the cylinder under different motion conditions. In this comparison, the state-dependent model showed to be very accurate, providing a significant improvement over the constant coefficients model.

Tarn, Shoults and Yang (1996) derived a dynamic model for a UVMS with an n-link manipulator through Kane's method, considering the major hydrodynamic effects such as added mass, profile drag, fluid acceleration and buoyancy forces. Kane's method made possible the direct incorporation of external environmental forces into the model, which simplified its derivation. Tarn, Shoults and Yang (1996) also present a modeling example of a 6-DoFs UUV with a 3-DoFs manipulator in a tutorial approach. The model developed by Tarn, Shoults and Yang (1996) is considered as a closed-form solution suitable for model-based control strategies.

Based on McLain's model (MCLAIN; ROCK, 1998), Leabourne and Rock (1998) developed a hydrodynamic model for an underwater two-link manipulator. The objective was to create a suitable representation of the hydrodynamic coupling between an UUV and a two-link manipulator, used for the coordinated control. This model can be interpreted as an extension of the one proposed by McLain and Rock (1998) for a single link manipulator. However, the model

of Leabourne and Rock (1998) does not consider the added mass effects, modeling only the drag torques experimented on the joints during the manipulator motion. This model considers a cylindrical-shaped links, fixed elbow angle and different drag coefficients for each link. The drag torque on the joints is determined by applying the strip theory on the links, considering only the in-line forces (those on the same plane of the cylinder motion) for the calculation. In addition, to include the 3-D flow effects, the drag coefficients are empirically determined as functions of joints angles. Compared with experimental results produced with a 2-DoFs planar manipulator (Fig. 5) mounted on the Stanford Aerospace Robotics Laboratory (ARL) test tank, the model with empirically determined coefficients had excellent results for estimating the drag torques, which were two times more accurate than those of the version for fixed coefficients. However, the model with fixed coefficients still produced good results, precise enough for use in the modeling and control synthesis.

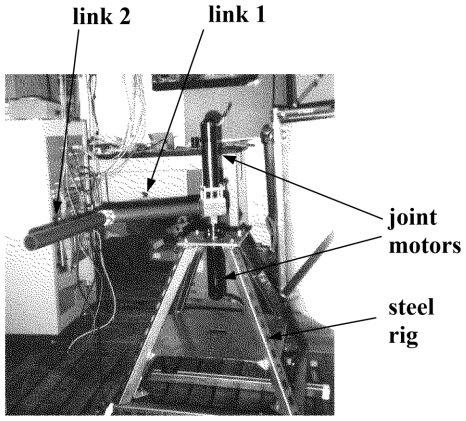

Figure 5: Two-link manipulator prototype
Source: Leabourne and Rock (1998)

Sagara et al. (2001) developed a dynamic model for a UVMS on the horizontal plane with a structure very similar to the previous works (IOI; ITOH, 1990; SCHJOLBERG; FOSSEN, 1994; MCMILLAN; ORIN; MCGHEE, 1994; TARN; SHOULTS; YANG, 1996). They validated the model through experimental tests in a water tank using a 5-DoFs prototype of the UVMS. The prototype was composed of a 3-DoFs cylindrical base and a 2-DoFs manipulator with rectangular-shaped links. In the experiments, the base only reacted to disturbances induced by the motion of the servo-controlled manipulator. They used the recording of the end-effector displacements caused by the motion of the manipulator at constant angular velocities and compared it with the results obtained with the mathematical model. Model and experiments showed good agreement for the path made by the end-effector. This is the only work found that tries to perform experimental tests to validate a mathematical model. In fact, the work of Sagara

et al. (2001) is very important since it also validates the modeling approaches adopted in previous works.

Dunnigan and Russell (1998) carried out a study on the dynamic coupling present in UVMSs. The numerical simulations have shown that the reaction forces generated by the manipulator movement are very harmful to the station-keeping of the UUV. This effect, in turn, directly affects the positioning of the end-effector of the manipulator, as it is kinematic coupled to the UUV. Dunnigan and Russell (1998) also synthesized a Sliding Mode Control (SMC) for the yaw angle of the UVMS considering the reaction moment generated by the manipulator as a feedforward term of the control law. This combination significantly improved the station-keeping of the UUV during underwater manipulation. Periasamy, Asokan and Singaperumal (2012) applied the bond graph method to study the dynamics of a UVMS composed of a 6-DoFs AUV with a 3-DoFs manipulator. To perform the modeling, the UVMS was divided into two individual modules, one for the AUV and the other for the manipulator, connected through the energy ports. Similarly simulation results of Dunnigan and Russell (1998) have shown that reaction forces due to the manipulator motion act like induced disturbances on the AUV, affecting its position and attitude. An important observation made by Periasamy, Asokan and Singaperumal (2012) is about the attitude DoFs of the AUV, described by the Euler angles – yaw, pitch and roll, which are more disturbed compared to the translational DoFs. In fact, Dunnigan and Russell (1998) also verified a stronger coupling influence for the attitude DoFs, which was credited to the restorative moments and reactions induced by the manipulator, as in Periasamy, Asokan and Singaperumal (2012).

The dynamic coupling in a lightweight UVMS was studied by Barbalata (2017). In this work, the pitch angle was the most affected DoF, corroborating previous research observations. The key point raised by Barbalata (2017) is the ratio manipulator/vehicle masses, once the dynamic coupling is intensified when the manipulator mass is similar to the vehicle mass. A practical rule given by Sivčev et al. (2018) says that the mass ratio should be less than 10%, meaning that for a lighter manipulator, the dynamic coupling effects are negligible. Xiong et al. (2022) proposed a method to evaluate the dynamic coupling intensity during manipulation tasks. This method is based on the calculation of coupling coefficients using the EoMs. These coefficients are associated with linear and angular motions. As expected, the angular coupling factor is much higher than the linear during manipulation. Vehicle motion is neglected during the analysis under the hypothesis of slow velocities. In Kolano and Davidson (2023), a recurrent neural network was proposed to predict the pitch motion of a small ROV during a manipulation task. The network was trained based on the simulated data from a mathematical model building in Julia. In the numerical simulations, the network learned the dynamics, predicted the pitch motion 4 seconds

in advance, and was robust to uncertainties in the hydrodynamic coefficients.

Gümüşel and Özmen (2011) presented the modeling and control of a horizontal two-link robot manipulator for on-land and underwater conditions. The modeling performed through Hamilton's Principle and differential eigenvalue problem, assumes the first link is a rigid body and the second is a flexible link. The inclusion of drag torques modeled the underwater case, described by the classical strip theory. The system response was evaluated and compared with three control methods (Proportional (P), Proportional-Derivative (PD) and integral augmented fuzzy control) through numerical simulations. The results show that the classical P control is not enough for set-point regulation on the underwater environment, especially when a payload is considered. Despite the similar performance between the PD and augmented fuzzy control on the land scenario, the PD control performed better on the underwater case. The author believes that the derivative control action better compensates the drag torques.

Huang et al. (2022) presented a dynamic model of a two-link underwater flexible manipulator based on the assumed mode method for flexibility and on Morrison's equation for the hydrodynamics forces. The singular perturbation method was adopted to decompose the dynamic model into two subsystems (i.e., slow and fast subsystems) and a composite controller was designed. An adaptive fuzzy sliding mode control was designed for the slow subsystem to compensate for the disturbances and suppress vibration. A PD controller was proposed to suppress residual vibration at the end-effector for the fast subsystem. The Lyapunov theory was used to prove the controller stability. Numerical simulations were performed with MSC ADAMS® and MATLAB/Simulink® to test the controller during trajectory tracking. The proposed controller performed better than a composite SMC and a standard PID. In the simulations, they verified that the effect of hydrodynamic force changes the flexible deformation and further interferes with the joints motion. Similarly, Shang et al. (2023) developed a mathematical model for a single-link flexible underwater manipulator. The model is based on the assumed mode method considering two modes, i.e., flexional and torsional. In the modeling, hydrodynamics forces and frictions were treated as disturbances. Shang et al. (2023) also presented an adaptive PI controller with a disturbance observer to compensate for lumped disturbances and suppress vibration. Numerical simulations and experiments with a physical prototype have shown the improved performance of the proposed controller compared to simpler PI controllers.

Nielsen, Blanke and Schjølberg (2016) presented a methodology for the modeling of reconfigurable underwater robots, according to the Udwadia-Kalaba equation for constrained mechanical systems. The main idea is to model the moduli separated, using some previously available models and then calculate the coupling forces between the moduli *a posteriori*, with the

Udwadia-Kalaba equation. This approach is further validated in Nielsen et al. (2016), where its effectiveness is accessed through experimental tests considering an underwater robot composed of two spherical-shaped moduli. Moreover, the analyses are extended in Nielsen et al. (2018), where they used the approach to model a reconfigurable ROV composed of two units of the BlueROV. This work also brings details about the identification of the parameters used in the model. They reported also some open-loop tests to verify the identified model.

Ingrosso et al. (2020) also presented a modeling approach for modular and reconfigurable UUVs. However, in the method of Ingrosso et al. (2020) the constraints are imposed *a priori* in the mathematical model. They applied the idea to the 4-Folaga cluster multi-hull system obtained from single-vehicle Folaga-AUV.

Sharma et al. (2019) developed a dynamic model for a UVMS with a structure similar to the previous ones in the literature, considering the rigid body dynamics and environmental hydrostatic and hydrodynamic forces. They based the modeling on a recursive approach using the decoupled natural orthogonal complement matrices of Saha (1999), which is advantageous for systems with many DoFs. Sharma et al. (2019) also proposed a simplified model for the hydrodynamic drag in an underwater manipulator. Despite not explicitly cited, the model employs the strip theory and assumes the profile drag as the most relevant part of the drag forces. Even with this simple structure, the model can capture variations on the drag coefficient, if adopting some identification scheme. This model also considers the dependency of the drag center in the UVMS configuration. To validate the proposed model, Sharma et al. (2019) performed experiments with a cylindrical-shaped underwater pendulum in free fall, considering two configurations (single and 2-links). In this comparison, the model results for the joints displacements were in good agreement with the experimental ones, despite some difference in the oscillation amplitude, attributed to the constant drag coefficient used in the simulation. In Sharma and Saha (2019), the previous model is reformulated, expressing the velocity distribution of a link with a constant cross-section as a function of its endpoints velocities. With such a modification, Sharma and Saha (2019) could express the drag coefficient as a function of the endpoints velocities and the aspect ratio of the link (link length/circular cross-section diameter). Thereby, the drag coefficient leaves the integrand for the calculation of the drag force, leading to the development of an analytical expression, which eliminates the need for numerical integration or discretization. However, the expression developed by Sharma and Saha (2019) is valid only if the endpoints velocities have the same sign; otherwise, the integration will need to be performed in two parts, considering the point with the null velocity of the link as the intermediate point of integration. Sharma and Saha (2019) used the proposed model to simulate the free fall of the 2-link underwater pendulum in different initial conditions. The obtained results were compared with those from

experiments, part of them already presented in Sharma et al. (2019). In this comparison, the authors found a good agreement between the simulation results and experimental ones concerning the joints displacements, velocities and accelerations. Sharma and Saha (2019) also made a comparison between the proposed model and a drag model based on the strip theory. In the comparison, despite the results being similar for both models, the one of Sharma and Saha (2019) was computationally more efficient than the result from the strip theory, due to the analytical expression for the drag force calculation. Sharma and Saha (2019) also shown the versatility of the proposed drag model combining it with the decoupled natural orthogonal complement matrices of Saha (1999) for the inverse dynamics simulation of a 10-DoFs UVMS (6-DoFs AUV and 4-DoFs manipulator).

Razzanelli et al. (2020) developed a hybrid simulator for UVMSs based on V-REP[1] with the Bullet Real-Time Physics Simulation engine for the rigid body dynamics and on the MATLAB/Simulink for computation of the hydrodynamics effects and implementation of guidance, navigation, control and machine interface. Numerical simulations were performed with a 6-DoFs work-class ROV endowed with a 3-DoFs manipulator. The dynamic coupling and collision effects on the vehicle body during a manipulation task could be verified in the results.

Shah et al. (2021) presented the mathematical modeling and the dynamic analysis of a UVMS composed of an AUV with 6-DoFs and a 2-link flexible manipulator. The modeling uses the quasi-Lagrange formulation on the AUV fixed-frame, considering joints friction, hysteresis in the coupling between the manipulators joints and links, hydrodynamic and hydrostatic forces acting on the system, including the lift forces associated with vortex shedding effects. Shah et al. (2021) performed a numerical simulation campaign to demonstrate the influence of the various effects on the precision of the end-effector positioning. Despite interesting results showing the impact of joints flexibility and Vortex-Induced Vibration (VIV) forces on the end-effector positioning, there is no comment about effects of the dynamics of the thrusters on the system response. McLain and Rock (1998) reported that the VIV forces in an underwater manipulator can be significant only in specific conditions, when the motion frequency coincides with the structural frequency of the manipulator. Even in such a case, VIV can still be suppressed if the trajectory performed by the manipulator disturbs the vortex shedding pattern, e.g., in the case of oscillatory motion. Another point in the analysis presented by Shah et al. (2021) is the dynamic coupling representation, which does not show influence of the manipulator motion on the vehicle pose, because the ratio between the manipulator and vehicle mass is low, around 5%.

Figure 6 presents the timeline and the main topics covered in the publications associated

[1]The robotics simulator CoppeliaSim.

with mathematical modeling[2].

Figure 6: Timeline of publications related to modeling

2.2 INVERSE KINEMATICS

The kinematic redundancy may allow multiple coordination strategies of the manipulators end-effector, while achieving secondary task objectives (e.g., minimize energy, avoid singularities, improve manipulability, etc.). To this end, many works focus on developing redundancy resolution algorithms for UVMSs.

Antonelli and Chiaverini (1998) proposed a task-priority inverse kinematics approach for the redundancy resolution of a UVMS considering additional secondary objectives, such as

[2]Although this review section is focus on floating base UVMSs, one can find interesting works about modeling and experimentation with articulated UVMSs (i.e., snake-type robots) in the research of Kelasidi (KELASIDI; PETTERSEN; GRAVDAHL, 2014; KELASIDI et al., 2014; KELASIDI et al., 2015; KELASIDI et al., 2016; KELASIDI et al., 2016; KOHL et al., 2016; KELASIDI et al., 2017; KELASIDI et al., 2018; KELASIDI et al., 2019) and in Schmidt-Didlaukies, Sørensen and Pettersen (2018).

energy-saving and the increase of the system manipulability. The energy-saving objective is achieved by minimizing the UVMS velocities, while the manipulability measured is used to avoid singular configurations during the manipulator motion. Numerical simulations tested the approach, considering a UVMS composed of the NPS-AUV II and 3-DoFs manipulator. The study considering only the horizontal plane (i.e., considering surge, sway and yaw motions of the AUV) incorporates the action of a time-constant ocean current. In the simulations, the approach of Antonelli and Chiaverini (1998) generated the references for the UVMS to align the AUV motion and current directions, to minimize the drag forces due to the relative velocity profile induced by the ocean current. The approach of Antonelli and Chiaverini (1998) also provides less energy consumption for long-term tasks compared to the case of fixed AUV orientation. The task-priority approach developed by Antonelli and Chiaverini (1998) is one of the first works dedicated to redundancy resolution in UVMSs.

Sarkar and Podder (2001) developed a motion planning algorithm for redundancy resolution and drag minimization of a UVMS. The redundancy resolution performs on the acceleration level, augmented with the UVMS dynamics. Sarkar and Podder (2001) also present the mathematical modeling of a UVMS with an n-link manipulator through the quasi-Lagrangian approach, which permits the direct derivation of the EoMs in the vehicle frame. The thrusters dynamics are also included in the mathematical modeling with the four-quadrant mapping for lift and drag forces proposed by Healey et al. (1995). The drag minimization requirements are expressed through a quadratic cost function, written in terms of the drag forces obtained from the mathematical modeling. The motion-planning algorithm was tested through numerical simulations considering a UVMS made of a 6-DoFs AUV and 3-DoFs planar manipulator. The simulations were performed considering a torque computed control law to track the references generated by the motion planning algorithm. Results reveal a significant minimization of the control forces, obtained with the references generated by the scheme of Sarkar and Podder (2001) compared to the classical Pseudo-Inverse (PI) approach. Moreover, Podder and Sarkar (2004) extended this work with a dynamic-based motion planning for UVMSs, to solve the inverse kinematics problem considering the different bandwidth characteristics of both subsystems. This scheme employs Fourier series expansion, to distribute the slow and fast parts of the trajectory on the UUV and manipulator, respectively, resulting in a significant reduction of the dynamic coupling intensity.

Santos et al. (2006) developed a redundancy resolution approach to UVMSs using the screw representation of the differential kinematics of rigid bodies, the Davies' method and a virtual kinematic chain model and it is based on explicitly applying kinematic constraints inherent to this type of system. Santos et al. (2006) conducted numerical simulations in the same simulation

scenario presented in Antonelli and Chiaverini (1998) to test the proposed approach. The results show that the undesirable motion that arises on the vehicle with the usual methods based on minimizing a cost function associated with the secondary objectives can be avoided with the approach developed by Santos et al. (2006). One should point that such result is due to the constraints imposed to the vehicle and that similar results can be obtained using a weighting matrix to allocate the motion in the active DoFs.

Soylu, Buckham and Podhorodeski (2010) presented a fault-tolerant redundancy resolution scheme for an I-ROV. The redundancy resolution happens through the Moore-Penrose PI on the velocity level. For secondary objectives achievement, the Gradient Projection Method (GPM) is used with a low-level fuzzy-rule-based artificial pilot, which determines the weighting factor for each secondary objectives, including joints limits, manipulability measurement for singularity avoidance, camera pose to keep the end-effector in the camera sight and drag minimization performed as in Antonelli and Chiaverini (1998). Fault management use a weighting matrix with adjustable gains that permits to choose the DoFs where the motion is allocated. Numerical simulations test the scheme, considering an I-ROV composed of a 6-DoFs Saab Seaeye FALCONTM-ROV and 4-DoFs HydrolekTM manipulator. The results reveal superior performance for this scheme during a manipulation operation with fault in joints, compared to simple versions of this scheme, without an artificial pilot and a fault management algorithm. Despite the promising results, the approach of Soylu, Buckham and Podhorodeski (2010) depends on the definition of fuzzy rules set to manage the secondary objectives, which can be a very time dispending task.

Han and Chung (2014) develop a task planning algorithm for redundancy resolution of a UVMS, which uses the extra DoFs for optimizing the restoring moments through a modified version of GPM with a variable gradient gain, calculated by comparing the task direction with the restoring moments one. Han and Chung (2014) also presented a robust adaptive coordinated control for UVMSs with an online update of the restoring moments based on the regressor method. The whole scheme developed and tested through numerical simulations by Han and Chung (2014) in the trajectory tracking problem considers a UVMS composed of the 6-DoFs PETUS-AUV and the 5-DoFs PUM-manipulator. In the simulations, the redundancy resolution algorithm of Han and Chung (2014) generated improved references to minimize the restoring moments compared to the classical PI approach. The coordinated control of Han and Chung (2014) performed better than the two versions of the classical Proportional-Integral-Derivative (PID) control tested, one without restoring moments information and the other considering the nominal restoring moments in a feedforward term. The algorithms of Han and Chung (2014) use many *ad-hoc* solutions, which can compromise the reliability of the framework. Moreover, the

hydrodynamic forces are neglected in the coordinated control, which justifies the assumption of using a robust PID control, another *ad-hoc* solution. However, the hydrodynamic forces are negligible in the conditions of slow UVMS motion and no current effects were simulated by Han and Chung (2014). These assumptions lead to a false sense of robustness.

Wang et al. (2017) presented a redundancy resolution method on the velocity level for a UVMS that take into account the payload transported by the manipulator as a secondary task objective to improve the system stability. As done in Soylu, Buckham and Podhorodeski (2010), Wang et al. (2017) used a set of fuzzy rules to manage the secondary task objectives. The numerical simulations considering a UVMS composed of a 4-DoFs AUV and a 5-DoFs manipulator reveals that with the secondary objective proposed by Wang et al. (2017) the manipulator motion is restricted, when operating with a payload. In practice, this can result in smaller pitch and roll angles for the UUV and improve the overall stability of the vehicle. Moreover, Tang et al. (2017) investigated a task-priority redundancy resolution scheme for UVMSs with restoring moments optimization on the acceleration level. Despite the similarity with the algorithm of Sarkar and Podder (2001) and Wang et al. (2017), the scheme of Tang et al. (2017) includes feedback terms to prevent numerical drift during the integration, which makes the algorithm more robust and suitable for real implementation in this sense. Also, to produce feasible references for pitch and roll angles, constraints are imposed for these DoFs in the primary task of the approach of Tang et al. (2017). The numerical simulations with a UVMS made of a 6-DoFs AUV and a 3-DoFs manipulator show that the scheme proposed by Tang et al. (2017) provides smaller restoring moments compared to two other approaches, one on the velocity level and the other acceleration one, but both using the generalized inertia matrix as weighting matrix.

Kang et al. (2017) developed a redundancy resolution method based on the GPM for the minimization of the relative distance between the UVMS center of gravity and the point where the moments summation generated by all active forces is equal to zero, namely zero moment point. As in previous works, the minimization was performed as a secondary objective considering a quadratic cost function written in terms of the relative distance. The penalization of the manipulator joints limits was also considered in the secondary objectives with an *ad-hoc* cost function. To verify the proposed approach, Kang et al. (2017) performed numerical simulations and experimental tests with a 6-DoFs UVMS prototype (Fig. 7) composed of a 3-DoFs floating base and a 3-DoFs manipulator on the vertical plane during the manipulation experiment. The results showed a significant improvement in the UVMS stability with the new secondary objective compared to the standard approach based on the PI during the manipulation experiment. Moreover, in Nguyen et al. (2018) these analysis were extended with new simulations

and experiments. The results obtained with a Inertial Measurement Unit (IMU) placed on the floating base showed a pitch acceleration two times smaller for the redundancy resolution scheme of Kang et al. (2017) compared to the PI approach. This is due to the reduction in the active moments generated by minimizing the distance between the center of gravity and zero moment point.

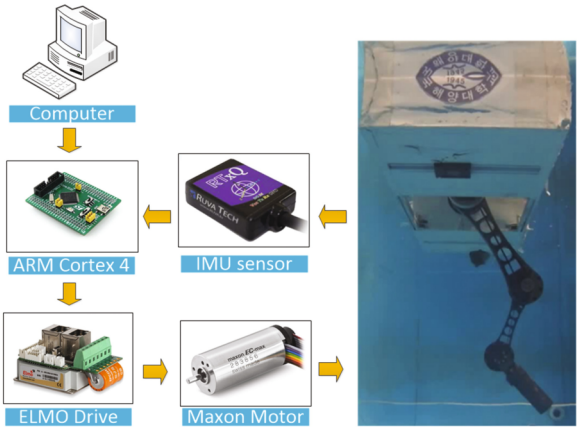

Figure 7: Hardware structure of UVMS
Source: Nguyen et al. (2018)

Simetti et al. (2014) presented an extension of the task-priority approach for achieving a dexterous object grasping with a UVMS while satisfying inequality constraints for safety and/or operational-enabling conditions, such as respecting joint limits and keeping the object centered in the camera system. Simulations and experimental trials with the TRIDENT I-AUV validate this approach. Simetti et al. (2015) extended the previous work to a dual-arm manipulator with the inclusion of multidimensional inequality control objectives. This modified version of the task-priority approach presented in Simetti et al. (2014) is tested through numerical simulations considering a UVMS within the scope of the project MARIS. More recently, Simetti et al. (2018) extended the previous works, which were limited to the grasping actions, to different applications in the scope of the DexROV and ROBUST projects. The simulation results show the applicability of this new framework to pipeline inspection and deep-sea mining.

A kinematic control approach for the coordination of a UVMS was presented by Haugaløkken, Jørgensen and Schjølberg (2018). This scheme generates the velocity references taking into account the velocity tracking errors, which eliminates the hypotheses of perfect tracking on the kinematic control. Haugaløkken, Jørgensen and Schjølberg (2018) applied this scheme to stabilizing the manipulator end-effector when the UVMS is under the action of a slow time-varying disturbance force emulating the ocean current effects. Also, a SMC with integral action is used to track the velocity references. This scheme is verified experimentally with a UVMS

composed of the SeaArm manipulator with 3-joints mounted under a BlueROV 2. The results obtained show a lower Root Mean Square Error (RMSE) for the end-effector error with the kinematic control proposed by Haugaløkken, Jørgensen and Schjølberg (2018) compared to two other approaches, one based on a decoupled control, disregarding the influence of the vehicle motion on the end-effector positioning and another considering the coupled kinematics.

Dai, Yu and Yan (2019) addressed the redundancy resolution of a UVMS during moving target tracking through an Extended Kalman Filter (EKF) based fast tube Model Predictive Control (MPC) algorithm. Authors formulated the scheme as a control problem, where the kinematic constraints are used to derive the dynamic model. The fast tube MPC is composed of an online fast nominal MPC and an auxiliary nonlinear controller to treat uncertainties and disturbances on the redundancy resolution level. This scheme could improve the performance of the low-level control generating controller references that are consistent with the physical constraints and closed-loop dynamics. The EKF was used to estimate the moving target trajectory through sensor measurements generally corrupted by measurement noises, thus, eliminating the assumption of precisely know tracking reference trajectory. The effectiveness of the prosed control scheme was verified through numerical simulation on the UnderWater Simulator (UWSim) software (PRATS et al., 2012b; FERNANDEZ et al., 2015) considering an I-AUV composed of a 6-DoFs AUV with a 5-DoFs manipulator based on the GIRONA 500 UVMS. The simulation results have shown the fast computation time and robustness of the EKF-based fast tube MPC to uncertainties and external disturbances while satisfying the physical constraints. This work was extended in Dai et al. (2020) with a motion controller and an EKF to estimate the lumped disturbances. In Dai et al. (2022), the motion controller was modified using a fast tube MPC formulation based on a nominal model and an SMC. Numerical simulations validated the schemes presented in Dai et al. (2020) and Dai et al. (2022).

Li et al. (2019) developed an uncalibrated IBVS with an eye-in-hand configuration camera. This approach also accounts with the restoring moments optimization in the redundancy resolution on the velocity level by the GPM. An adaptative control was developed to handle the parameters uncertainties in the camera model. Li et al. (2019) also addressed the motion control problem with a composite controller based on the nominal model, an SMC term and the disturbances estimates provided by a high-order disturbance observer. The Lyapunov theory was used to perform the stability proof. Simulations with a 9-DoFs UVMS composed of a 6-DoFs UUV and a 3-DoFs manipulator validated the scheme. Gao et al. (2021) proposed an Image-Based Visual Servoing (IBVS) with an eye-in-hand configuration camera. The redundancy resolution problem is solved on the velocity level using an MPC based on the camera model and its relationship with the end-effector kinematics. Gao et al. (2021) also presented a motion

control composed of a nonlinear PD augmented with the disturbance estimates provided by an extended state observer. In the control synthesis, the dynamic coupling between the vehicle and the manipulator was treated as an external disturbance, estimated by the extended state observer. Also, a UKF is used to estimate the UUV velocities based on visual measurements. Numerical simulations with a 12-DoFs UVMS composed of a 6-DoFs NPS Phoenix UUV and a 6-DoFs SMART-3S manipulator proved the effectiveness of the presented scheme. Karras et al. (2022) also presented an IBVS with an eye-in-hand configuration camera. The redundancy resolution problem was solved on the velocity level using the PI approach based on the camera model and its relationship with the end-effector kinematics. Prescribed performance functions were added to the scheme to address the physical limits (e.g., the field of view, joints limits, etc.). A model-free motion control based on the prescribed performance functions was also presented. Simulations in the UWSim environment with an 8-DoFs UVMS composed of a 4-DoFs UUV and a 4-DoFs manipulator validated the approach.

Yu et al. (2023) proposed a task-priority control with motion coordination and inequality-based singularity avoidance for the redundancy resolution on the velocity level. In this scheme, a heuristic subset is added to specify the boundary of the desired position of the end-effector relative to the vehicle to avoid boundary singularities. Experimental tests were performed with a 12-DoFs UVMS composed of a 6-DoFs ROV and a 6-DoFs manipulator. Results reveal an improved performance for the scheme presented by Yu et al. (2023) compared to the conventional PI approach and the QP-problem formulation.

Figure 8 presents the timeline and the main topics covered in the publications related to the inverse kinematics problem.

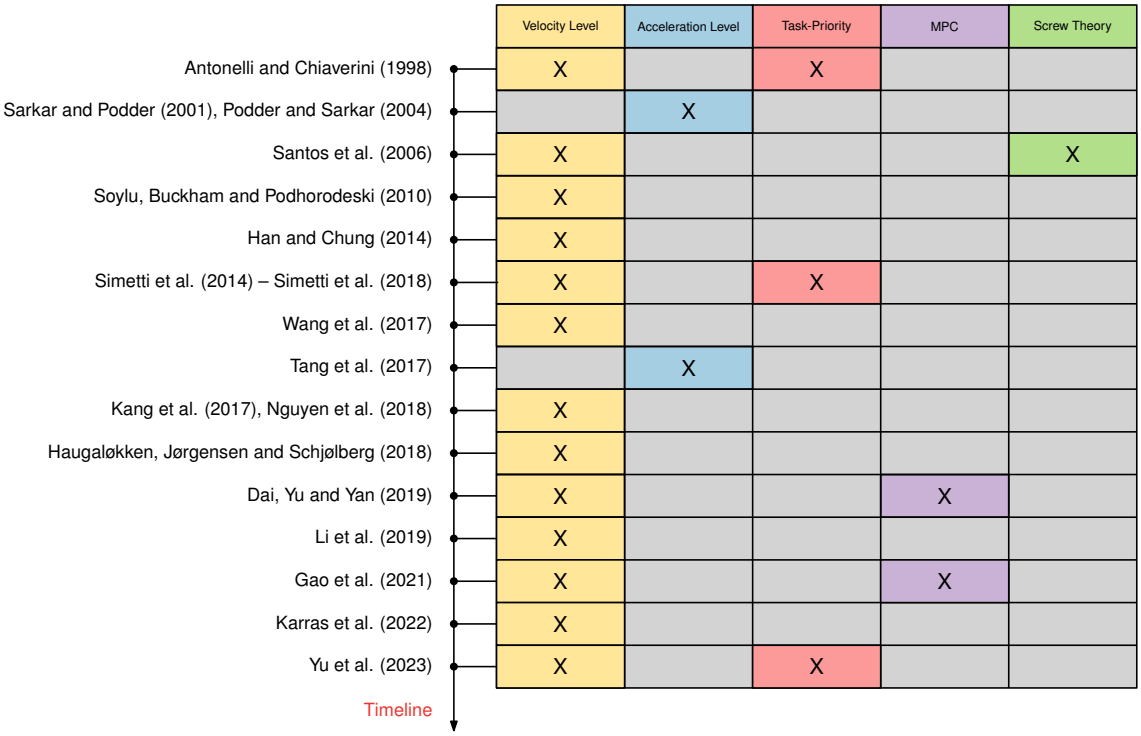

Figure 8: Timeline of publications related to inverse kinematics

2.3 COORDINATED CONTROL

The coordinated control refers to the motion control of the whole UVMS system simultaneously. This topic has received much attention over the years due to the difficulty to perform the control of the entire UVMS under dynamic coupling, modeling uncertainties and external disturbances. To treat this problem, many researchers developed their own coordination control approaches.

Practical experiments were conducted by McLain, Rock and Lee (1996) in the coordinate-control of a small AUV named OTTER with a single link underwater manipulator. The results have shown that the dynamic coupling can be very significant when the vehicle is not controlled. It was also noticed that the coordinate-control of the system, using the dynamic coupling forces as feedforward terms, provides a significant improvement in station-keeping with only a 5% increase in the total thrust when compared with a decentralized-control approach, where decoupled controllers are used for the vehicle and manipulator.

Canudas de Wit, Olguin Diaz and Perrier (1998) developed a non-model-based robust nonlinear decoupling control to a UVMS based on the singular perturbation theory. This control algorithm can decouple the UUV and manipulator dynamics due to the different bandwidth characteristics of the system while preserving the closed-loop stability. A critical remark made

by the authors says that only the UUV (slow subsystem) needs a robust control law since the manipulator response is too fast. According to the authors, the mass ratio between the vehicle and the manipulator is related to the bandwidth characteristics of the system, as in the previous works, which focus on the dynamic coupling, as in Dunnigan and Russell (1998), Periasamy, Asokan and Singaperumal (2012) and Barbalata, Dunnigan and Petillot (2014).

Chung et al. (2000) proposed a robust control algorithm based on a disturbance observer for UVMSs. In their scheme, the DoFs of the UUV are treated as passive joints, while the manipulator DoFs are taken as active joints. This idea comes from the fact that during manipulation the UUV should be as much stationary as possible. However, this cannot be totally achieved since there will be the disturbances induced by the manipulator motion. This trajectory-tracking was tested through numerical simulations considering a UVMS composed of 1-DoF translational passive base and a 3-DoFs planar manipulator. The simulations results reveal higher performance for the scheme of Chung et al. (2000) compared to the classic PID control. However, the most important drawback in the mathematical model considered by Chung et al. (2000) is the absence of attitude DoF in the base. As pointed before, the attitude DoFs are the most disturbed by the dynamic coupling between the vehicle and manipulator.

Sagara (2009) presented a continuous and a discrete version of the resolved acceleration control method for UVMSs. Unlike conventional approaches, this method obtains the desired values for the joints from kinematic and momentum equations with feedback of task-space signals. Sagara (2009) also presented two types of disturbance observers for the UUV, to improve the compensation provided by the resolved acceleration control method for the variation of hydrodynamic parameters and disturbances induced by the manipulator motion. He compared the control performance numerically and experimentally with the Computed Torque Control (CTC) technique on the trajectory tracking problem, considering a planar UVMS composed of a 3-DoFs AUV and a 2-DoFs manipulator (Fig. 9). Results confirm the superior performance of the resolved acceleration control over the CTC in compensating for the modeling errors and external disturbances during the trajectory tracking. The author believes this is due to the disturbance observers, which play an essential role in the UUV stabilization. The inclusion of task-space feedback terms in the reference acceleration also contributes to the improved performance. In fact, all the resolved acceleration control method has a structure very similar to the CTC technique, except for the reference acceleration.

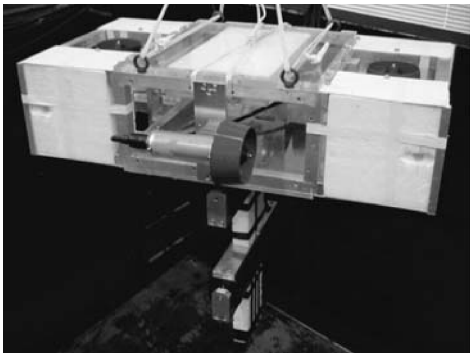

Figure 9: Vertical type 2-link underwater robot
Source: Sagara (2009)

Han, Park and Chung (2011) also proposed a robust coordination scheme for the control of a UVMS. Their approach exploits the problem of redundancy resolution to perform the minimizing of the restoring moments along with a nonlinear H-∞ control law and a disturbance observer for the motion control of the system. The minimization of the restoring moments is performed by penalizing the distance between the center of gravity and the center of buoyancy of the UVMS through the performance index presented in Han, Park and Chung (2011). The advantage of this index highlighted by Han, Park and Chung (2011) is that it generates a reduction in energy consumption without requiring knowledge of any hydrodynamic parameter. Han, Park and Chung (2011) achieved the synthesis of the nonlinear H-∞ control by solving the Riccati differential equation analytically. Then, they chose the disturbance observer so that the L2-norm conditions of the H-∞ are relaxed and the robustness of the control system is improved. The whole scheme is tested through numerical simulations in the trajectory-tracking problem considering a UVMS composed of a 6-DoFs PETUS-AUV and a 5-DoFs PUM-manipulator. In the simulations, the redundancy resolution scheme of Han, Park and Chung (2011) performed well, providing a significant reduction of the restoring moments compared to the classical PI approach. In addition, the nonlinear H-∞ control with disturbance observer provided enhanced tracking performance compared to a resolved acceleration control. This better tracking performance is due to the compensation provided by the nonlinear H-∞ control for parameters uncertainties and ocean current effects considered in the simulations. Han, Park and Chung (2011) also studied the trajectory tracking problem considering the thrusters dynamics in the mathematical model. To perform the control of the thrusters, a PD regulator is used to control the angular velocity of the motor shaft. The results obtained reveal a delay effect in the generated thrusts caused by the thrusters dynamics. However, the nonlinear H-∞ control still performed well but with tracking errors ten times greater compared to the case without the thrusters dynamics.

Mohan and Kim (2012) developed an indirect adaptive control scheme for UVMSs consider-

ing a CTC law combined with a disturbance observer based on the EKF algorithm. This approach permits the direct estimation of the disturbances without a proper structure on the mathematical model. However, the performance of this scheme depends on the disturbance observer accuracy, which can compromise the control performance when the estimations are not good enough. The coordination control can be performed on the task-space to avoid solving the inverse kinematics problem. Kim, Mohan and Kim (2014) proposed a coordination control for UVMSs on the task-space to the trajectory tracking in the presence of modeling errors and external disturbances. The control is based on a feedback linearization law. An EKF is used as a state observer to estimate the unmeasured states. The control was tested by numerical simulations considering a UVMS composed of a 6-DoFs AUV and a 3-DoFs manipulator. Experiments were also done with an ROV on the horizontal plane, i.e., considering surge, sway and yaw motions. The results are compared to those of a classical PID and of an indirect adaptive control Mohan and Kim (2012). The comparison showed improved tracking performance and less energy consumption with the control of Kim, Mohan and Kim (2014). Moreover, Mohan, Kim and Singh (2015) improved the previous scheme with a disturbance observer. To verify the effectiveness of this scheme, simulations of different tasks were conducted and compared with the indirect adaptive control of Mohan and Kim (2012). The results showed a better energy efficiency of the proposed control and less error in tracking the trajectory and good robustness in the presence of external disturbances and parametric uncertainties. Londhe et al. (2017) presented a robust nonlinear PID control algorithm with gain adjustment by fuzzy rules for the motion control of a UVMS. This algorithm has a structure similar to the scheme of Mohan and Kim (2012), including the use of a disturbance observer. However, despite Londhe et al. (2017) approach seems to be more robust to modeling uncertainties and external disturbances, it is also more complex due to the need to develop a set of fuzzy rules for tuning the gains of the PID. Dai and Yu (2018) synthesized an adaptive coordinated control for UVMSs composed of three terms: (i) an EKF for estimating external uncertainties and disturbances, (ii) a CTC term based on the nominal model, and (iii) an H-infinity control term. This scheme was tested through numerical simulations in different scenarios, e.g., nominal conditions, under parametric uncertainties and external disturbances, and considering a time-varying ocean current. The results were compared with other controllers (PID, SMC and the indirect adaptive control of Mohan and Kim (2012)), and greater precision in the trajectory tracking with the controller by Dai and Yu (2018) were verified.

Antonelli and Cataldi (2014) highlighted that off-the-self manipulators are often endowed with position or velocity controllers on the joints. In these cases, the coordinated control of the UVMS is limited to the regulation of the UUV, taking into account feedforward terms to counteract the reactions developed by the manipulator motion. To this end, Antonelli and Cataldi

(2014) developed an adaptative-recursive control approach with a minimal set of parameters based on the virtual decomposition control. A stability analysis using the Lyapunov theory was also presented. To evaluate the proposed controller, Antonelli and Cataldi (2014) performed numerical simulations in the Simurv 4.0 simulator considering a UVMS composed of a 6-DoFs Romeo-ROV with and a 7-DoFs manipulator from TRIDENT project. In the simulations, the adaptative-recursive control is used to control the Romeo-ROV, while a PID controller was used for the manipulators joints. The results obtained for the station-keeping of the vehicle and end-effector trajectory tracking showed improved performance for the controller of Antonelli and Cataldi (2014) in terms of the tracking errors of positioning and orientation compared to a benchmark controller (not specified).

Farivarnejad and Moosavian (2014) presented a recursive mathematical model based on the Lagrange equation for a dual-arm I-AUV considering the main effects (e.g., rigid body dynamics, added mass, drag and hydrostatic forces). Also, Farivarnejad and Moosavian (2014) compared the multiple impedance control and the augmented object model approaches for manipulation control. Simulations were performed considering an I-AUV composed of a 6-DoFs ellipsoidal-shaped AUV and two PUMA-type robotic manipulators. The multiple impedance control approach performed better in the numerical simulations concerning the tracking errors and energy dissipation during impact.

A hybrid cable-thruster control for UVMSs (Fig. 10) was proposed in El-Ghazaly, Gouttefarde and Creuze (2015). In this approach, a set of cables attached to the UUV allows the control through the regulation of the cables lengths and tension, which is performed with winches fixed on the offshore structure near UVMS workplace. This idea comes from the cable-driven parallel robots, which consist of a moving platform connected to a fixed base through a set of cables. This control approach permits some extra actuation on the UVMS since the thrusters are not the only elements able to generate control forces on the UUV. Beyond this new control approach, in El-Ghazaly, Gouttefarde and Creuze (2015) also focused on the determination of the force capability of the hybrid cable-thruster control. To do this, the available set of end-effector forces with the hybrid cable-thruster control was determined in a suitable mathematical representation. As a case study, the developed map was applied to a planar UVMS composed of a 3-DoFs UUV and 2-DoFs manipulator. The results of the analysis showed a significant improvement in the end-effector force with the hybrid tensioned cable-thruster control. Sacchi et al. (2022) studied the hybrid-cable thruster approach for the grasping operation in 6-DoFs accounting for the cable flexibility. In control, a QP-based algorithm was proposed for thrusters and cables forces allocation. Numerical simulations were performed in Vortex Studio considering the 6-DoFs Vortex Heavy Work Class ROV. Compared to the configuration with only thrusters, improved

performance was verified in peak, place, and hovering operations.

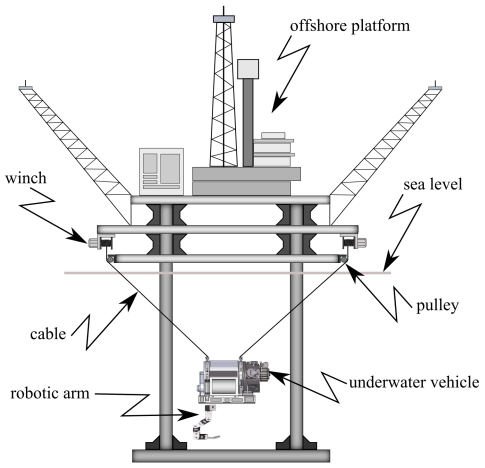

Figure 10: Hybrid cable-thruster control for UVMSs
Source: El-Ghazaly, Gouttefarde and Creuze (2015)

Esfahani, Azimirad and Danesh (2015) developed an improved Time Delay Control (TDC) approach for a UVMS. The controller is composed of an adaptative time-delay-estimation term, with fuzzy rules to tune its gains, to compensate for the system nonlinearities, a terminal SMC term to give a fast response and a PID term to reduce the tracking errors. In conventional TDC and terminal SMC, the tuning gains dependent on the system uncertainties, which is considered as a drawback for the need of some knowledge of the uncertainties. In the proposed approach this problem is fixed with fuzzy rules that adaptatively tune the gains. Numerical simulations were done to show the effectiveness of the proposed controller. The results showed that the proposed controller has high performance in the trajectory tracking and satisfactory robustness to external disturbances in comparison with a standard SMC.

Wang, Chen and Wu (2018) presented a continuous nonsingular fast terminal SMC with and TD estimation for UVMSs. The proposed controller was intended to be model-free due to TD estimation and ensure satisfactory control performance due to continuous nonsingular fast terminal SMC. The closed-loop stability proof was performed using the Lyapunov stability theory. The controller was tested through pool experiments using a 7-DoFs UVMS prototype composed of a 2-DoFs AUV and a 5-DoFs manipulator. An improved performance was obtained for the proposed controller on the trajectory tracking compared to a PD control with TD estimation and a standard PD control. However, the controller of Wang, Chen and Wu (2018) has many parameters, which can be challenging to tune.

Barbalata, Dunnigan and Petillot (2018) compared decoupled and coupled force/motion controllers for a lightweight UVMS. The decoupled controller was based on a task decomposition

technique and formulated on the vehicle and the manipulator task space. The coupled controller was fully synthesized in the task space. In the decoupled controller, the PILIM controller of Barbalata, Dunnigan and Petillot (2014) was adopted for vehicle positioning. Also, an integral SMC and a standard SMC were used for motion and force control of the manipulator, respectively. In the coupled controller, an integral SMC and a standard SMC were used for motion and force control, respectively. Numerical simulations were performed to test the controllers considering a 11-DoFs lightweight UVMS composed of a Nessie VII-AUV of 5-DoFs and a 6-DoFs HDT-MK3-M-manipulator. Better performance was verified for the coupled controller, especially during high-stiffness contact, due to the dynamic coupling considered in the control design.

Borlaug et al. (2019) study the trajectory tracking of an Articulated Intervention-Autonomous Underwater Vehicle (AI-AUV) with the Super Twisting Algorithm (STA) with adaptive gains and a higher-order sliding mode observer used when velocity measurements are not available. The ultimate boundedness of the tracking problem with the proposed scheme is proved by using the Lyapunov stability theory and the effectiveness of this controller is accessed through numerical simulations in the horizontal plane considering an AI-AUV with 16-links. In Borlaug, Pettersen and Gravdahl (2018), this approach is extended to the trajectory tracking in 6-DoFs and the simulations are performed considering an AI-AUV composed of 9-links and 7-thrusters. Next, a Generalized STA (GSTA) is proposed by Borlaug, Pettersen and Gravdahl (2019) for the previous problem of tracking in 6-DoFs. As before, the ultimate boundedness of the tracking errors is proved through the Lyapunov stability theory and the GSTA is compared with STA in the tracking problem presented in Borlaug, Pettersen and Gravdahl (2018). The simulations reveal an improved performance in terms of tracking errors and robustness to the GSTA. A modified version of the GTSA with adaptive gains is presented in Borlaug, Pettersen and Gravdahl (2020b). The analyses in Borlaug, Pettersen and Gravdahl (2019) are then extended in Borlaug, Pettersen and Gravdahl (2021) with simulations and experiments. Also, the observer presented in Borlaug et al. (2019) is used for the joint velocities estimation. Borlaug et al. (2019) proposed a kinematic/dynamic control for an AI-AUV, eliminating the assumption of perfect dynamic control in the kinematic stability analysis. In this approach, the velocity references are generated through a robust algorithm to solve the multiple task priority problem. A velocity controller based on the SMC is used to track the generated references. The simulations considering an AI-AUV of 5-links have shown the effectiveness of this approach in regulating all tasks to their respective set-point values. Moreover, Borlaug, Pettersen and Gravdahl (2020a) extended the previous work considering the GSTA and SMC technique to the velocity tracking problem and comparing it with standard control methods, as the classical PID control and the feedback linearization technique. Also, a detailed stability proof regarding the kinematic/dynamic control is presented

and the numerical simulations are performed considering AI-AUVs with different parameters.

A neural-adaptive network control for trajectory tracking of UVMSs was proposed by Wang and Perkins (2019). In this scheme, a feedback linearization law is used to compensate for the nominal dynamics, while a neural network is used to estimate the lumped disturbances, which are composed both by the modeling errors associated with parameter uncertainties and external disturbances. The control was tested through numerical simulations considering a UVMS composed of an ellipsoidal-shaped AUV with 6-DoFs endowed with a manipulator of 2-DoFs. The results showed improved performance for the neural control in the trajectory tracking compared to a standard PID control. However, there is no information about the accuracy of the estimates provided by the neural network, nether for the control efforts provided by both controllers, which compromises the comparison since one cannot attribute the improved tracking achieved with the control proposed by Wang and Perkins (2019) to the better compensation for the dynamics of the UVMS.

Taira, Sagara and Oya (2020) presented a model-based controller for the manipulator of a UVMS. This controller is developed considering one of the three types of servo subsystems, i.e., voltage-controlled, torque-controlled and velocity-controlled, for the manipulator and an independent controller for the UUV of poor performance. The motivation for the design of Taira, Sagara and Oya (2020) came from the practical observations. It is too difficult to obtain a good control performance for the UUV due to some factors, such as the greater body inertia compared to the manipulator one, inaccurate thrusters dynamics, inaccurate sensor information, etc. Therefore, to circumvent this problem, the approach of Taira, Sagara and Oya (2020) was made independent of the performance of the UUV control. This idea is very interesting and can help to solve many practical problems associated with the coordination of UVMSs. Also, this control can be used as a framework to design an end-effector control independent of the UUV motion. The controller was tested through numerical simulations in the trajectory tracking problem considering a UVMS prototype moving on the vertical plane composed of a 3-DoFs AUV and a 2-DoFs planar manipulator. However, the simulation results presented by Taira, Sagara and Oya (2020) are not appealing once only the tracking errors are shown. Also, there is no comparison with other control techniques, which difficult to access the real performance capabilities of the proposed controller. Moreover, the control synthesis presented by Taira, Sagara and Oya (2020) seems to be too complex and with many submodules in the control architecture, turning its applicability too tricky. In, Taira, Sagara and Oya (2022) this work was extended for motion and force control of a UVMS. This was done by adding a force error filter to allow force control and perform the stability proof. Numerical simulations validated the approach.

Han et al. (2020a) developed a fuzzy decoupling controller for a UVMS. This controller adapts the terms outside the main diagonal of the system inertia matrix through a fuzzy algorithm, which allows the decoupling between the UUV and the manipulator by means of a feedback linearization control law. Such a scheme was also tested through numerical simulation following a reference trajectory predefined by the final maker to reduce the effects of dynamic coupling. The results obtained confirmed the controller capability to estimate the terms outside the main diagonal of the inertia matrix, decoupling the system and ensuring that the reference trajectory is followed by the UVMS. Moreover, a coordination scheme composed of motion planning and a robust coordinated control was proposed by Han et al. (2020b) for UVMSs. In this scheme, a new secondary task objective is defined in inverse kinematics to minimize the energy consumption and dynamic coupling through the redundancy resolution. The energy minimization is performed penalizing the velocities of the UVMS through the GPM. However, it is not clear how the dynamic coupling is mitigated with the term proposed by Han et al. (2020b). Moreover, the coordinated control was constructed based on a feedback linearization law augmented with joint and task space feedback terms. A time-delay control was used to estimate the lumped disturbances and a fuzzy rule-based compensator was added to improve the robustness to external disturbances. An EKF was used to perform state estimation and attenuate sensor noise effects. Nonetheless, there is no much information about the sensors and parameters considered. This scheme was tested through numerical simulations in the trajectory tracking problem considering a UVMS composed of the REMUS-AUV with 5-DoFs endowed with a manipulator with 3-DoFs. The results were compared to another coordination scheme built on the robust coordinate control reported in Dai and Yu (2018), which was based on the H-∞ control technique augmented with an EKF to estimate the disturbances. The comparison revealed an improved tracking performance with less energy consumption for the scheme presented by Han et al. (2020b). However, despite the good results, the comparison seems to be not fair since there was no penalization for the velocities of the UVMS in the inverse kinematics modulus used in the scheme considered for comparison.

To overcome uncertainties and external disturbances while respecting the bounds of the control inputs of a UVMS, Dai et al. (2020) proposed a modified constrained H-infinity controller with a CTC and a nonlinear disturbance observer. The CTC provides the nominal model-based control and the disturbance observer designed based on the system dynamics estimates the lumped disturbances. The modified constrained H-infinity control was synthesized using a grey wolf optimizer to compensate for biased estimation, satisfy control input bounds and provide fast calculation. The Lyapunov theory was used to perform the closed-loop stability proof. Numerical simulations were performed with a 12-DoFs UVMS composed of a 6-DoFs AUV and a 6-DoFs

manipulator. Results reveal an improved tracking performance for the control proposed by Dai et al. (2020) compared to standard nonlinear H-infinity, nonlinear PID and nonlinear SMC.

Within the ROBUST project framework, Di Vito et al. (2021) presented the modeling and control of a multi-hull UVMS for sea mining (Fig. 11). Since the ROBUST base vehicle is seen as a composition of AUVs, the dynamic model is derived according to the modular approach presented in Ingrosso et al. (2020). The hydrodynamic parameters were calibrated experimentally. This model, together with the identified parameters, was used in a navigation filter based on the EKF algorithm used to provide the necessary feedback for the control scheme proposed by Di Vito et al. (2021), which was composed of a kinematic and a dynamic control layer. The kinematic control generated the references for the UVMS control. It was constructed based on the task-priority approach of Simetti et al. (2018), to accomplish several control objectives at the same time (e.g., bathymetric and optical survey, hold position, joint-space motion, etc.) but with a defined order priority. The dynamic control layer presented by Di Vito et al. (2021) only calculated the vehicle control forces needed to track the references generated by the kinematic control since the ROBUST manipulator had an embedded control on the motor joints to perform the tracking of the velocity references. Also, in this layer, one could choose between a standard PID control or a model-based adaptive control to the vehicle dynamic positioning. Di Vito et al. (2021) also reported remarkable results in the sea trials tests of this navigation-control architecture, where the UVMS successfully identified, tracked, landed and inspected a mock-up of a manganese nodule.

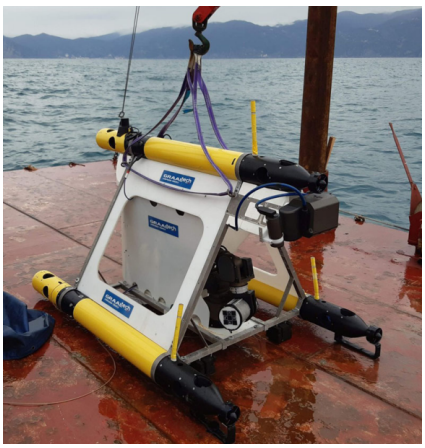

Figure 11: ROBUST UVMS

Source: Di Vito et al. (2021)

Cai et al. (2023) developed a composite controller based on NMPC and disturbance observer. The NMPC was synthesized using a prediction model network based on long short-term memory to estimate future disturbances and use these estimates on the prediction model to estimate

future states. The disturbance observer was formulated based on the radial basis function. The disturbance estimates provided by the disturbance observer were used as input in the prediction model network. Numerical simulations on the UWSim environment and water tank experiments with a 7-DoFs UVMS composed of a 3-DoFs AUV and a 4-DoFs manipulator were performed. Good results were obtained in autonomous grasping task validating the control proposed by Cai et al. (2023). However, there are no comparisons with other approaches.

Figure 12 presents the timeline and the main topics covered in the publications treating coordinated control.

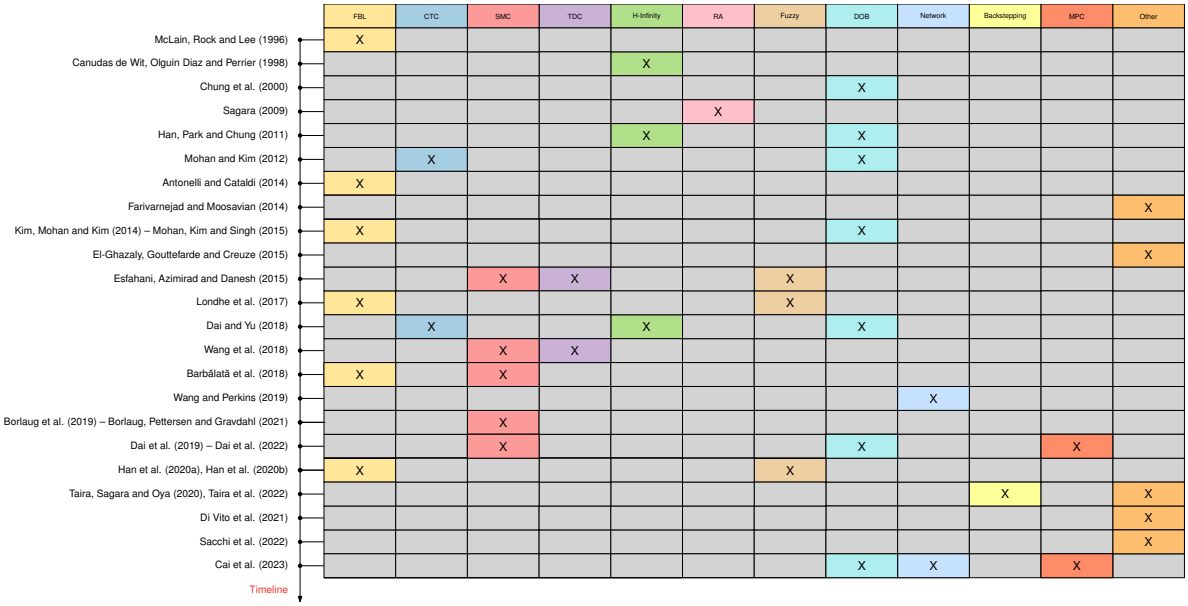

Figure 12: Timeline of publications related to coordinated control

2.4 COOPERATIVE CONTROL

Although cooperative control is a trending topic in dynamic systems control researches, it is still in an embryonic phase for UVMSs. Due to its intrinsic potential, coordination schemes have been developed over the last two decades.

Sun and Cheah (2004) developed two set-point regulators to perform the coordination of multiple UVMSs carrying a common object. The control stability proof was made by the Lyapunov stability theory, where sufficient conditions were established to guarantee the closed-loop stability even when the restoring forces are not exactly known. Despite the interesting controller formulations in Sun and Cheah (2004), the work lacks numerical simulations to test the developed algorithms.

Conti et al. (2015) proposed a very interesting decentralized approach for cooperative mobile

manipulation performed by I-AUVs. Such an approach was based on the use of the potential field method, which was employed in a multi-layer control structure to, in parallel, coordinate the swarm, guidance and navigation phases. Despite its low accuracy and robustness, the main advantage in the use of potential fields is the reduction of the transmitted data for navigation and control, which could be evaluated only with the distance vector between the vehicles, object and obstacles. This improvement was the core of this architecture because it also permitted the reduction of the onboard sensors and, consequently, the reduction of vehicle complexity while allowing operations with low bandwidth. The contribution of the work was also to use the manipulated object as the swarm reference system and the surface vehicle as the origin of the world reference system, that permitted the use of acoustic modems rather than an expensive Ultra Short Base Line (USBL) system. Due to the difficulty in performing a real experiment, the authors evaluated the proposed strategy only with numerical simulations. The simulation scenario established considered a swarm composed of four I-AUVs, each one with 7-DoFs. The objective was to transport an object of known geometry along the desired trajectory transmitted by the surface vessel through an unknown environment where some obstacles were placed. The results have shown that with this control strategy the swarm was able to keep the formation during the manipulation phase and to avoid collisions with the obstacles during the object transportation.

Cataldi, Chiaverini and Antonelli (2018) developed a cooperative control approach to perform the transportation of an object by two UVMSs. The proposed architecture was constituted by several control loops, each one with a specific goal, e.g., object pose control, end-effector force control, inverse kinematics resolution and UVMS low-level control. This structure permitted dealing with the constraints on each control loop, i.e., the uncertainties on the UVMS model, the sensors low bandwidth and limitations related to the manipulator control and the object pose estimation. The authors tested the proposed approach through numerical simulations on MATLAB/Simulink® environment with the Simscape™ package. In the scenario considered the two UVMSs (each one constituted of a fully actuated UUV and a 7-DoFs manipulator) transporting a cylindrical-shaped bar of unknown mass and known geometry over the desired trajectory. The results presented endorse the capacity of the proposed scheme to perform the task coordination with success and handle the limitations mentioned.

Heshmati-Alamdari (2018) proposed a distributed leader-following architecture based on impedance control for the object cooperative transportation by multiple UVMSs in a constrained workspace with static obstacles (Fig. 13). In this approach, to avoid explicit data exchange, the leading UVMS was the only one to know the object desired trajectory. So, the following UVMSs estimate the trajectory by a prescribed performance estimation considering that each UVMS is equipped with a force/torque sensor on its end-effector. The desired tracking behavior

was achieved through impedance control laws that linearize the dynamics and incorporate coefficients for load sharing among the UVMSs. To avoid the collisions with the obstacles, the work presented an obstacle-free path planning scheme based on Navigation Functions. The proposed architecture was tested through numerical simulation. In the scenario considered, a team of four UVMSs, each one composed by an AUV and a small 4-DoFs manipulator, was transporting an object on an unstructured environment with obstacles, represented by spheres and subjected to disturbances as slow time-varying water current. The simulations results have shown the feasibility of the proposed architecture for the transportation of the object from an initial position to the desired one, without collision with the obstacles, even with the disturbances considered in the simulation. Moreover, the analyses presented in Heshmati-Alamdari (2018) were extended in Heshmati-Alamdari et al. (2021b) with more simulation cases, considering a centralized cooperative scheme for comparison and more a complex scenario, where additional obstacles were placed.

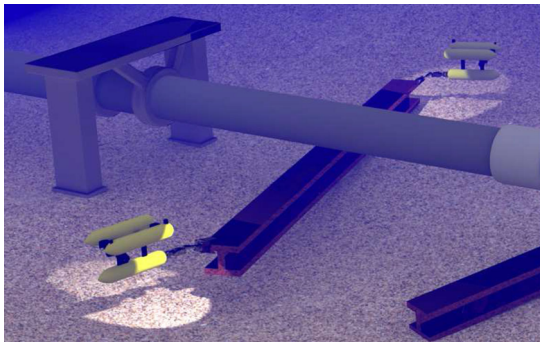

Figure 13: Cooperative transportation by two UVMSs
Source: Heshmati-Alamdari (2018)

Heshmati-Alamdari, Karras and Kyriakopoulos (2019) proposed a Nonlinear MPC (NMPC) scheme for coordination of a team of UVMS on the transportation of an object in a constrained workspace with static obstacles. In this approach, the coupled dynamics between the UVMSs and the object was penalized by load sharing coefficients according to the specific payload capabilities of each UVMS. The penalized model was used to design a distributed NMPC, which permits the inclusion of limits and constraints related to the operation (e.g., obstacles, joint limits, control input saturation and avoidance of singular configurations) in a unified way. A feedback scheme with no explicit exchange of information based on onboard measurements (e.g., sensor fusion based on sensors like IMU, USBL and Doppler Velocity Log (DVL)) was established to reduce bandwidth requirements and avoid intensive communication between the UVMSs. In addition, navigation functions were used to generate an obstacle-free path for object transportation. The proposed coordination scheme was tested through numerical simulations

with the UWSim simulator on the Robot Operating System (ROS) environment and by means of real-time experiments performed within a test tank. The case study considered for the numerical simulations consisted of two ROVs, each one with a 4-DoFs manipulator, transporting a bar over an unstructured environment (with obstacles). The results obtained confirmed the effectiveness of the proposed scheme for the coordination of cooperative transportation, while meeting the limitations and constraints imposed during the design processes. The experimental validation was performed with two small ROVs – a 4-DoFs Seabotix LBV and 3-DoFs VideoRay PRO – each one equipped with a custom-made underwater manipulator actuated by waterproof servomotors (Fig. 14). The experiments performed considered the transportation of an object (a plastic tube) in two distinct scenarios: 1) the stabilization of the object in the setpoint, and 2) the transportation of the object through various waypoints. Despite the simplifications, the experimental tests confirmed the validation of the scheme proposed by Heshmati-Alamdari, Karras and Kyriakopoulos (2019) on the scenarios tested. In the authors opinion, this work is a milestone in underwater cooperative transportation since they were the first to perform experimental validation.

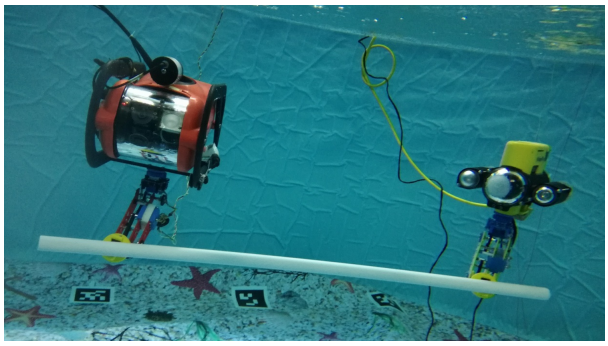

Figure 14: Small custom made UVMSs under cooperative transportation
Source: Heshmati-Alamdari, Karras and Kyriakopoulos (2019)

Pi et al. (2021) developed a decentralized task-priority kinematic control for cooperative transportation with I-AUVs adapted to the limited communication bandwidth. The control is based on the simultaneous coordination of the end-effectors velocities to achieve a common goal. In this scheme, an independent optimization of the task-priority hierarchies was performed for each I-AUV separately, with safety tasks at the top. Also, a normalization approach of the resulting velocities was considered to ensure that each agent can achieve end-effector velocity in all directions (i.e., linear and angular). Numerical simulations and pool experiments were performed with a team of two I-AUVs, each one with 8-DoFs and composed of the 4-DoFs GIRONA500-AUV and the 4-DoFs ECA 5E manipulator (mini and micro versions). The core simulation tool used was the open-source Stonefish C++ simulation library combined with the

ROS interface package called *stonefish_ros*. Promising results were obtained for a complex task comprising detection, pickup, transport, and placement operations.

Bae et al. (2022) presented a cooperative manipulation scheme for UVMSs with dual manipulators. This scheme was developed based on the assumption that the system can be treated as a parallel mechanism when fixed to a working structure. The PI approach was used to solve the redundancy resolution problem on the velocity level for motion coordination during task execution. The cooperation occurs with the UUV thrusters helping in the manipulation task and the manipulator motors helping compensate for disturbances (e.g., ocean current, thrusters fault, etc.). Numerical simulations and experiments with a prototype constructed with servo motors validated the proposed approach. Results reveal smaller errors and reduced energy consumption when the UUV and manipulator work cooperatively.

Kabanov et al. (2022) studied the cooperative transportation of a concentrated mass object by a team of UVMSs. The modeling was performed by coupling the individual models using the relationships between the end-effectors wrenches and those generated on the object. The redundancy resolution problem was solved using the PI approach with the kinematic relationships between the end-effectors and the object. Two motion control strategies were developed, centralized and decentralized, based on the state-dependent differential Riccati equation. A load-sharing approach was considered in control to distribute the object load between the agents. Numerical simulations were performed considering a team of two UVMSs, each one with 12-DoFs and composed of the 6-DoFs Sf-30k-ROV and the 6-DoFs Orion 7R manipulator. Good results were obtained on the trajectory tracking. However, the mathematical models and the simulation conditions are too simple, e.g., full-state feedback was considered available and the object dynamic was assumed to be known.

Figure 15 presents the timeline and the main topics covered in the publications of cooperative control[3].

[3]Despite not being the focus of this thesis, one can find interesting works about cooperative transportation with Unmanned Aerial Vehicles (UAVs) and general modular robots in Georgia Tech (2021) and ModLab (2023).

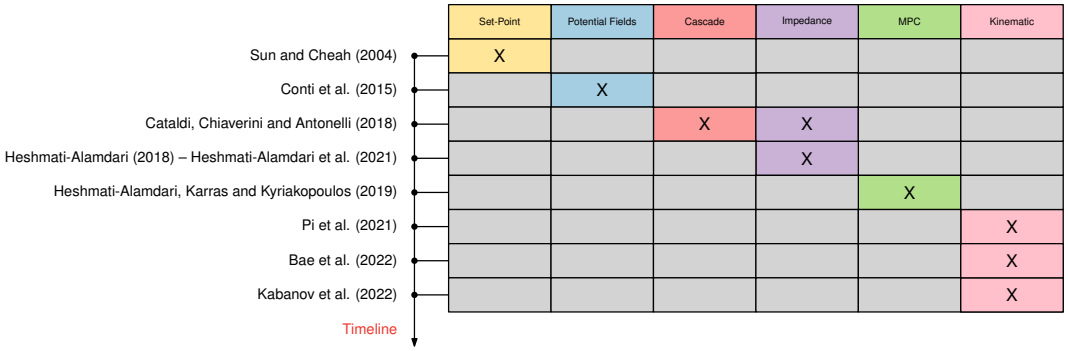

Figure 15: Timeline of publications related to coordinated control

2.5 COMMENTARIES

This chapter presented a literature review of UVMSs. Regarding the topics covered, i.e., mathematical modeling, inverse kinematics, coordinated and cooperative control, various approaches were developed, each one with particular features. However, except for Antonelli and Cataldi (2014), none of the reviewed works tried to create any unifying methodology where early developments already available can be used within a structured approach. Thus, the developments presented in the following chapters try to address this knowledge gap.

3 MATHEMATICAL MODELING

3.1 RECURSIVE MATHEMATICAL MODELING

This chapter presents a general modular and recursive mathematical modeling approach for a class of underwater multibody systems. Some experimental results from other authors are reproduced to verify the presented modeling approach.

3.1.1 Simplifying hypotheses

The mathematical model is derived under the following assumptions:

1. The bodies are rigid, symmetric and with uniform mass distribution;
2. The kinematic joints are ideal in the sense that there is no clearance;
3. The system is completely immersed on an unbounded fluid domain, thus, the invariance of the dynamics concerning rigid body transformation holds and boundary effects can be neglected (VIROZUB et al., 2019);
4. The free surface effects can be modeled as disturbances, which eliminates the frequency-dependent potential damping and making constant the local added mass and hydrodynamic damping matrices (NIELSEN et al., 2016);
5. The hydrodynamic interference between the bodies (i.e., vehicle and manipulator links) is neglected, thus the parasitic forces arising from proximity of other bodies are considered as second-order hydrodynamic effects (NIELSEN et al., 2016; VIROZUB et al., 2019);
6. The flow around the bodies is incompressible and irrotational and all the hydrodynamic effects can be directly superposed;
7. The ocean current is irrotational (FOSSEN, 1996; NIELSEN et al., 2016);

8. The dynamics of the actuators are independent of rigid body motions and can be described by active forces and moments described by *ad-hoc*[1] models (e.g., lookup-table);

9. The bodies mass and inertia proprieties are augmented with the actuators ones such that they are included together in the dynamics.

3.1.2 Hierarchical conception

A schematic representation of the modeled system, along with its hierarchical conception, is shown in Fig. 16. The AUV is denoted as body $i = 0$, the links of the manipulator are denoted as bodies $i = 1, \ldots, N-1$, while the end-effector as body $i = N$ (Fig. 16 (a)). Moreover, for each rigid body i a body-fixed coordinate system $\mathrm{O}_i\mathrm{x}_i\mathrm{y}_i\mathrm{z}_i$, along with the respective orthonormal vector basis $(\hat{\mathbf{x}}_i, \hat{\mathbf{y}}_i, \hat{\mathbf{z}}_i)$ is defined. The Earth-fixed coordinate system is denoted by Oxyz and its orthonormal vector basis is $(\hat{\mathbf{x}}, \hat{\mathbf{y}}, \hat{\mathbf{z}})$. Notice that the Earth is treated as an inertial reference frame. In the modeling hierarchy (Fig. 16 (b)), body A is the AUV, bodies denoted by B are the manipulator links, and body C is the end-effector. Also, $\mathcal{S}_r$ $(r = 1, \ldots, 4)$ represents the subsystems constructed during the modeling and $\mathcal{S}$ is the complete I-AUV constrained model. Also, active revolute joints (grey circles) connects the manipulator with the AUV, the manipulator links between them and the end-effector with the last manipulator link.

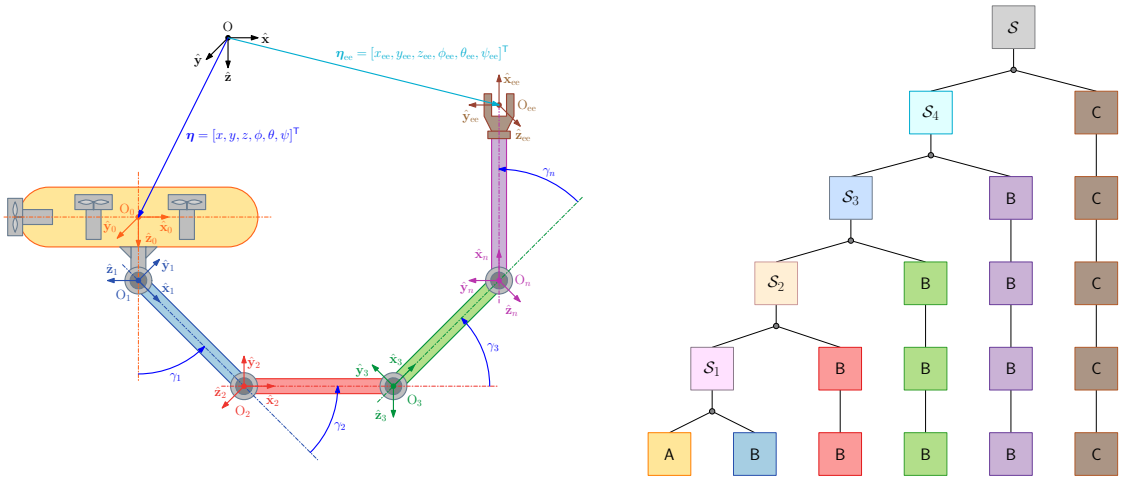

(a): I-AUV schematic diagram (b): Modeling hierarchy

Figure 16: I-AUV model with $(6 + n)$-DoFs

[1] An *ad-hoc* model is a mathematical representation developed for a specific purpose.

3.1.3 Kinematics

Let $\boldsymbol{\eta}_i = \left[\boldsymbol{\eta}_{i,1}^\mathsf{T}, \boldsymbol{\eta}_{i,2}^\mathsf{T}\right]^\mathsf{T}$ be the vector of generalized coordinates of the i-th body describing its configuration with respect to the Earth-fixed frame, with $\boldsymbol{\eta}_{i,1} = [x_i, y_i, z_i]^\mathsf{T}$ being the Cartesian coordinates and $\boldsymbol{\eta}_{i,2} = [\phi_i, \theta_i, \psi_i]^\mathsf{T}$ being the Euler angles ($i = 0, 1, \ldots, N$), as shown on the schematic diagram of the base model in Fig. 17. Also, let $\boldsymbol{\nu}_i = \left[\boldsymbol{\nu}_{i,1}^\mathsf{T}, \boldsymbol{\nu}_{i,2}^\mathsf{T}\right]^\mathsf{T}$ be the vector of quasi-velocities expressed in the body-fixed coordinate system, with $\boldsymbol{\nu}_{i,1} = [u_i, v_i, w_i]^\mathsf{T}$ being the components of the velocity of the origin O_i and $\boldsymbol{\nu}_{i,2} = [p_i, q_i, r_i]^\mathsf{T}$ being the components of the angular velocity of the body.

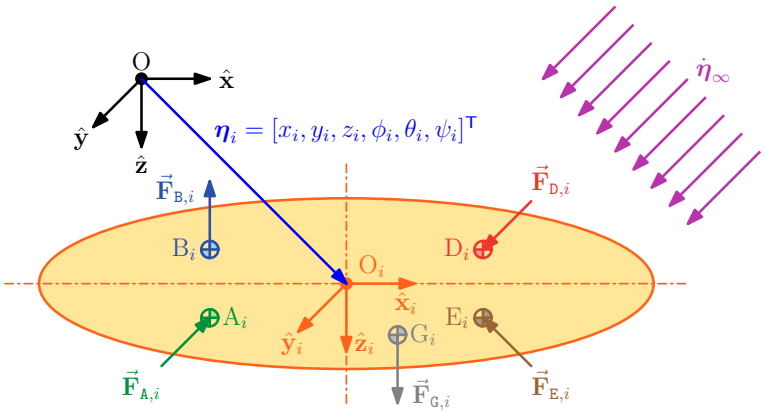

Figure 17: Base model schematic diagram

The following relations hold under the hypotheses 1 (FOSSEN, 1996):

$$\dot{\boldsymbol{\eta}}_i = \mathbf{J}_i \boldsymbol{\nu}_i; \quad \ddot{\boldsymbol{\eta}}_i = \mathbf{J}_i \dot{\boldsymbol{\nu}}_i + \dot{\mathbf{J}}_i \boldsymbol{\nu}_i, \tag{3.1}$$

where $\mathbf{J}_i$ is the transformation matrix between body-fixed and Earth-fixed coordinate systems, written as:

$$\mathbf{J}_i = \mathrm{blkdiag}\left(\mathbf{J}_{1,i}, \mathbf{J}_{2,i}\right), \tag{3.2}$$

with $\mathbf{J}_{1,i}$ and $\mathbf{J}_{2,i}$ satisfying (FOSSEN, 1996):

$$\begin{aligned} \dot{\boldsymbol{\eta}}_{1,i} &= \mathbf{J}_{1,i} \boldsymbol{\nu}_{1,i}; \quad \dot{\boldsymbol{\nu}}_{1,i} = \mathbf{J}_{1,i}^{-1} \boldsymbol{\eta}_{1,i} = \mathbf{J}_{1,i}^\mathsf{T} \boldsymbol{\eta}_{1,i}, \\ \dot{\boldsymbol{\eta}}_{2,i} &= \mathbf{J}_{2,i} \boldsymbol{\nu}_{2,i}; \quad \dot{\boldsymbol{\nu}}_{2,i} = \mathbf{J}_{2,i}^{-1} \boldsymbol{\eta}_{2,i}. \quad (\theta_i \neq \pm 90^\circ) \end{aligned} \tag{3.3}$$

If it is necessary to avoid singularities, i.e., when $\theta_i = \pm 90^\circ$, then, a 4-column-vector $\boldsymbol{\eta}_{2,i} = [e_{0,i}, e_{1,i}, e_{2,i}, e_{3,i}]^\mathsf{T}$ of Euler parameters (unit quaternions) is adopted instead of Euler angles $(\phi_i, \theta_i, \psi_i)$ to described the transformation matrix $\mathbf{J}_i$. To do this, let the normalizing factor be

given by (ORSINO, 2020):

$$\rho_i = \frac{2}{\boldsymbol{\eta}_{2,i}^{\mathsf{T}}\boldsymbol{\eta}_{2,i}} = \frac{2}{e_{0,i}^2 + e_{1,i}^2 + e_{2,i}^2 + e_{3,i}^2}. \tag{3.4}$$

In this case, the rotation matrices from body-fixed to Earth-fixed coordinates are expressed by (ORSINO, 2020):

$$\mathbf{J}_{1,i}(\boldsymbol{\eta}) = \mathbf{I} + \rho_i\left(e_{0,i}\mathbf{S}_i + \mathbf{S}_i^2\right); \quad \mathbf{J}_{2,i}(\boldsymbol{\eta}) = \rho_i\mathbf{L}_i, \tag{3.5}$$

where $\mathbf{S}_i$ is the skew-symmetric matrix representation of the 3-column-vector $[e_{1,i}, e_{2,i}, e_{3,i}]^{\mathsf{T}}$ and $\mathbf{L}_i$ comes from the skew-symmetric of $\boldsymbol{\nu}_{2,i}$ given by $\mathbf{J}_{1,i}^{\mathsf{T}}\dot{\mathbf{J}}_{1,i}$, such that (ORSINO, 2020):

$$\mathbf{S}_i = \begin{bmatrix} 0 & -e_{3,i} & e_{2,i} \\ e_{3,i} & 0 & -e_{1,i} \\ -e_{2,i} & e_{1,i} & 0 \end{bmatrix}; \quad \mathbf{L}_i = \begin{bmatrix} -e_{1,i} & e_{0,i} & e_{3,i} & -e_{2,i} \\ -e_{2,i} & -e_{3,i} & e_{0,i} & e_{1,i} \\ -e_{3,i} & e_{2,i} & -e_{1,i} & e_{0,i} \end{bmatrix}. \tag{3.6}$$

Due to the presence of the normalizing factor ρ_i in the former expressions, it can be verified that regardless of the value of the norm of $\boldsymbol{\eta}_{2,i}$, $\mathbf{J}_{1,i}$ is always an orthogonal matrix, i.e., $\mathbf{J}_{1,i}^{-1} = \mathbf{J}_{1,i}^{\mathsf{T}}$ (ORSINO, 2020).

3.1.4 Euler-Lagrange dynamics

Based on the Euler-Lagrange equation in terms of the quasi-velocities[2], the Equations of Motion (EoMs) of the i-th body can be written as (MEIROVITCH, 2003):

$$\frac{\mathrm{d}}{\mathrm{d}t}\left(\frac{\partial\mathcal{L}_i}{\partial\boldsymbol{\nu}_i}\right) + \mathbf{J}_i^{\mathsf{T}}\left(\boldsymbol{\gamma}_i\frac{\partial\mathcal{L}_i}{\partial\boldsymbol{\nu}_i} + \frac{\partial\mathcal{L}_i}{\partial\boldsymbol{\eta}_i}\right) + \frac{\partial\mathcal{R}_i}{\partial\boldsymbol{\nu}_i} = \mathbf{J}_i^{\mathsf{T}}\mathbf{Q}_i, \tag{3.7}$$

where $\mathcal{L}_i = \mathcal{T}_i - \mathcal{U}_i$ is the Lagrangian function, with $\mathcal{T}_i$ and $\mathcal{U}_i$ being the kinetic and potential energy functions, respectively, $\mathcal{R}_i$ is the Rayleigh dissipation function, $\mathbf{Q}_i$ is the column-vector of non-conservative generalized forces and $\boldsymbol{\gamma}_i$ is a matrix given by (MEIROVITCH, 2003):

$$\boldsymbol{\gamma}_i = \left[\boldsymbol{\nu}_i^{\mathsf{T}}\mathbf{J}_i^{\mathsf{T}}\left(\frac{\partial\boldsymbol{\alpha}_i}{\partial\boldsymbol{\eta}_i}\right)\right] - \left[\boldsymbol{\nu}_i^{\mathsf{T}}\mathbf{J}_i^{\mathsf{T}}\left[\frac{\partial\boldsymbol{\alpha}_i}{\partial\boldsymbol{\eta}_i}\right]\right], \tag{3.8}$$

where $\boldsymbol{\alpha}_i = \mathbf{J}_i^{-\mathsf{T}}$.

We must refer to Meirovitch (2003) for the correct interpretation of the matrix notation in Eq. (3.8). For example, let $\boldsymbol{\alpha}_i = \left[\alpha_{i,j,k}\right]$ $(j = 1, \ldots, m; k = 1, \ldots, n)$. Thus, the terms of the left

[2]Assuming that the quasi-velocities are defined as linear combinations of generalized velocities. The coefficients of this linear combination, given by the Jacobian $\mathbf{J}_i$, may depend explicitly on the configuration of the body.

matrix of Eq. (3.8) are calculated as follows (MEIROVITCH, 2003):

$$\boldsymbol{\nu}_i^{\mathsf{T}} \mathbf{J}_i^{\mathsf{T}} \left(\frac{\partial \boldsymbol{\alpha}_{i,j,k}}{\partial \boldsymbol{\eta}_i} \right) = \sum_{r=1}^{n} \frac{\partial \boldsymbol{\alpha}_{i,j,k}}{\partial \eta_{i,r}} \dot{\eta}_{i,r}, \tag{3.9}$$

which is a scalar. It must be stressed here that the above triple matrix product does not involve summation over the indices j and k.

Following the same pattern, we write (MEIROVITCH, 2003):

$$\boldsymbol{\nu}_i^{\mathsf{T}} \mathbf{J}_i^{\mathsf{T}} \left[\frac{\partial \boldsymbol{\alpha}_i}{\partial \eta_{i,k}} \right] = \sum_{j,k=1}^{n} \frac{\partial \boldsymbol{\alpha}_{i,j,k}}{\partial \eta_{i,r}} \dot{\eta}_{i,k}, \tag{3.10}$$

where the summations over both indices j and k are involved. However, there is no summation over the index r.

Eq. (3.7) can be rewritten in the canonical form of the EoMs:

$$\mathbf{M}_i \dot{\boldsymbol{\nu}}_i + \left(\mathbf{C}_i \left(\boldsymbol{\nu}_i \right) + \mathbf{D}_i \left(\boldsymbol{\nu}_i \right) \right) \boldsymbol{\nu}_i + \mathbf{g}_i \left(\boldsymbol{\eta}_i \right) = \boldsymbol{\tau}_i + \mathbf{d}_i, \tag{3.11}$$

where $\mathbf{M}_i$ is the generalized inertia matrix, $\mathbf{C}_i$ is the Coriolis and centrifugal forces matrix, $\mathbf{D}_i$ is the drag forces matrix, $\mathbf{g}_i$ is the column-vector of restoring forces, $\boldsymbol{\tau}_i$ is the column-vector of control forces, and $\mathbf{d}_i$ stands for the column-vector of externals disturbances forces.

3.1.4.1 Kinetic energy

The expression of the kinetic energy of a submerged body can be extended to directly include the inertial forces due to the added mass effects on the EoMs, as below:

$$\mathcal{T}_i = \frac{1}{2} \boldsymbol{\nu}_i^{\mathsf{T}} \mathbf{M}_i \boldsymbol{\nu}_i = \frac{1}{2} \boldsymbol{\nu}_i^{\mathsf{T}} \left(\mathbf{M}_{\mathtt{RB},i} + \mathbf{M}_{\mathtt{A},i} \right) \boldsymbol{\nu}_i, \quad (i = 0, 1, \ldots, N) \tag{3.12}$$

where $\mathbf{M}_{\mathtt{RB},i}$ and $\mathbf{M}_{\mathtt{A},i}$ are the mass matrices of rigid body and added mass expressed on the body-fixed frame, respectively, and calculated concerning the origin (O_i).

Calculating the right-hand-side terms of Eq. (3.7) for the quasi-velocities terms, disregarding the dissipation function, we get:

$$\frac{\partial \mathcal{L}_i}{\partial \boldsymbol{\nu}_i} = \frac{\partial \mathcal{T}_i}{\partial \boldsymbol{\nu}_i} = \mathbf{M}_i \boldsymbol{\nu}_i; \quad \frac{\mathrm{d}}{\mathrm{d}t} \left(\frac{\partial \mathcal{L}_i}{\partial \boldsymbol{\nu}_i} \right) = \frac{\mathrm{d}}{\mathrm{d}t} \left(\frac{\partial \mathcal{T}_i}{\partial \boldsymbol{\nu}_i} \right) = \mathbf{M}_i \dot{\boldsymbol{\nu}}_i, \quad (i = 0, 1, \ldots, N) \tag{3.13}$$

From Eq. (3.13), we can define the matrix of Coriolis and centrifugal forces matrix as:

$$\mathbf{C}_i \boldsymbol{\nu}_i = \mathbf{J}_i^{\mathsf{T}} \boldsymbol{\gamma}_i \mathbf{M}_i \boldsymbol{\nu}_i = \mathbf{J}_i^{\mathsf{T}} \boldsymbol{\gamma}_i \left(\mathbf{M}_{\mathtt{RB},i} + \mathbf{M}_{\mathtt{A},i} \right) \boldsymbol{\nu}_i = \left(\mathbf{C}_{\mathtt{RB},i} + \mathbf{C}_{\mathtt{A},i} \right) \boldsymbol{\nu}_i, \quad (i = 0, 1, \ldots, N) \tag{3.14}$$

where $\mathbf{C}_{\mathrm{RB},i}$ and $\mathbf{C}_{\mathrm{A},i}$ are the rigid body and added mass portions of the Coriolis and centrifugal forces matrix, respectively.

The terms of the added mass tensor can be identified from experimental results, or calculated with discrete methods (e.g., strip theory, panel method, etc.), or even with analytical formulations developed for regular geometries (e.g., cylinder, ellipsoid, parallelepiped, sphere, etc.). The former is especially suitable for the manipulator links since they are constructed based on those geometries. In this vein, McLain and Rock (1998) developed a very accurate model for the added mass forces experimented on cylindrical-shaped links through the strip theory and considering the local variation of the acceleration profile. The model of McLain and Rock (1998) can be adapted to the Lagrangian formulation exploring the relation between the strips velocities and the links generalized coordinates. To this end, let the added mass generalized forces be given by:

$$\mathbf{d}_{\mathrm{A},i} = \sum_{s=1}^{p} \vec{\mathbf{f}}^{i}_{\mathrm{A},s,i} \cdot \frac{\partial \boldsymbol{\nu}_{1,s,i}}{\partial \boldsymbol{\nu}_i}, \quad (i = 1, \ldots, N) \tag{3.15}$$

where $\boldsymbol{\nu}_{1,s,i} = [u_{s,i}, v_{s,i}, w_{s,i}]^{\mathsf{T}}$ is the velocity vector of the s-th strip ($s = 1, \ldots, p$) expressed in the body-fixed frame and $\vec{\mathbf{f}}^{i}_{\mathrm{A},s,i} = \left[X_{\mathrm{A},s,\mathrm{x}_i}, Y_{\mathrm{A},s,\mathrm{y}_i}, Z_{\mathrm{A},s,\mathrm{z}_i}\right]^{\mathsf{T}}$ is the added mass forces vector, with components given by (MCLAIN; ROCK, 1998):

$$\begin{aligned} X_{\mathrm{A},s,\mathrm{x}_i} &= \rho C_{\mathrm{A},\mathrm{x}_i} V_{s,\mathrm{x}_i} a_{s,\mathrm{x}_i}, \\ Y_{\mathrm{A},s,\mathrm{y}_i} &= \rho C_{\mathrm{A},\mathrm{y}_i} V_{s,\mathrm{y}_i} a_{s,\mathrm{y}_i}, \\ Z_{\mathrm{A},s,\mathrm{z}_i} &= \rho C_{\mathrm{A},\mathrm{z}_i} V_{s,\mathrm{z}_i} a_{s,\mathrm{z}_i}, \end{aligned} \tag{3.16}$$

where ρ is the water density; $V_{s,i}$ is the volume of s-th strip; $C_{\mathrm{A},\mathrm{x}_i}$, $C_{\mathrm{A},\mathrm{y}_i}$ and $C_{\mathrm{A},\mathrm{z}_i}$ are the added mass coefficients, adopting here a conservative approach and considering them as constants but who can be taken as function of the traveled distance along the links length (MCLAIN; ROCK, 1998); a_{s,x_i}, a_{s,y_i} and a_{s,z_i} are the acceleration components expressed in the body-fixed frame.

Introducing the relations:

$$\boldsymbol{\nu}_{1,s,i} = \mathbf{J}_{\boldsymbol{\nu}_{1,s,i}} \boldsymbol{\nu}_i; \quad \dot{\boldsymbol{\nu}}_{1,s,i} = \mathbf{J}_{\boldsymbol{\nu}_{1,s,i}} \dot{\boldsymbol{\nu}}_i + \dot{\mathbf{J}}_{\boldsymbol{\nu}_{1,s,i}} \boldsymbol{\nu}_i, \quad (i = 1, \ldots, N) \tag{3.17}$$

and after some algebraic manipulation, the generalized added mass forces can be rewrite as:

$$\mathbf{d}_{\mathrm{A},s,i} = \sum_{s=1}^{p} \mathbf{M}_{\mathrm{A},i} \dot{\boldsymbol{\nu}}_i + \mathbf{C}_{\mathrm{A},i} \boldsymbol{\nu}_i, \quad (i = 1, \ldots, N) \tag{3.18}$$

with $\mathbf{M}_{\mathrm{A},i}$ and $\mathbf{C}_{\mathrm{A},i}$ as the added mass matrix of the i-th link, given by:

$$\mathbf{M}_{\mathrm{A},i} = \sum_{s=1}^{p} \mathbf{M}_{\mathrm{A},s,i}; \quad \mathbf{C}_{\mathrm{A},i} = \sum_{s=1}^{p} \mathbf{C}_{\mathrm{A},s,i}, \quad (i = 1, \ldots, N) \tag{3.19}$$

$$\mathbf{M}_{\mathtt{A},s,i} = \mathbf{J}_{\boldsymbol{\nu}_{1,s,i}}^{\mathsf{T}} \boldsymbol{\Phi}_{\mathtt{A},s,i} \mathbf{J}_{\boldsymbol{\nu}_{1,s,i}}; \quad \mathbf{C}_{\mathtt{A},s,i} = \mathbf{J}_{\boldsymbol{\nu}_{1,s,i}}^{\mathsf{T}} \boldsymbol{\Phi}_{\mathtt{A},s,i} \dot{\mathbf{J}}_{\boldsymbol{\nu}_{1,s,i}}, \quad (i = 1, \ldots, N) \tag{3.20}$$

where

$$\boldsymbol{\Phi}_{\mathtt{A},s,i} = \rho V_{s,i} \operatorname{diag}\left(C_{\mathtt{A},\mathtt{x}_i}, C_{\mathtt{A},\mathtt{y}_i}, C_{\mathtt{A},\mathtt{z}_i}\right). \tag{3.21}$$

The kinetic energy function of the i-th link can be obtained with the added mass tensor of Eq. (3.12), considering the dynamic center velocity calculated as in Sharma et al. (2019) and Sharma and Saha (2019). Also, a discrete form of the kinetic energy function can be obtained considering the local variation of the velocity profile along with the link, as shown below:

$$\mathcal{T}_i = \frac{1}{2} \sum_{s=1}^{p} \boldsymbol{\nu}_i^{\mathsf{T}} \mathbf{J}_{\boldsymbol{\nu}_{1,s,i}}^{\mathsf{T}} \boldsymbol{\Phi}_{\mathtt{A},s,i} \mathbf{J}_{\boldsymbol{\nu}_{1,s,i}} \boldsymbol{\nu}_i = \frac{1}{2} \sum_{s=1}^{p} \boldsymbol{\nu}_i^{\mathsf{T}} \mathbf{M}_{\mathtt{A},s,i} \boldsymbol{\nu}_i = \frac{1}{2} \boldsymbol{\nu}_i^{\mathsf{T}} \mathbf{M}_{\mathtt{A},i} \boldsymbol{\nu}_i. \quad (i = 1, \ldots, N) \tag{3.22}$$

3.1.4.2 Potential energy

The restoring effects associated with the hydrostatic forces can be added on the model with a generalized potential related to the weight and buoyancy forces, as shown below:

$$\mathcal{U}_i = \mathcal{U}_i(0) + \vec{\mathbf{f}}_{\mathtt{W},i}^{\,i} \cdot \vec{\mathbf{p}}_{\mathtt{G}_i|\mathtt{O}_\mathtt{I}}^{\,i} + \vec{\mathbf{f}}_{\mathtt{B},i}^{\,i} \cdot \vec{\mathbf{p}}_{\mathtt{B}_i|\mathtt{O}_\mathtt{I}}^{\,i}, \quad (i = 0, 1, \ldots, N) \tag{3.23}$$

where $\vec{\mathbf{p}}_{\mathtt{G}_i|\mathtt{O}_\mathtt{I}}^{\,i} = \mathbf{J}_{1,i}^{\mathsf{T}} \vec{\mathbf{p}}_{\mathtt{G}_i|\mathtt{O}_i}^{\,\mathtt{I}}$ and $\vec{\mathbf{p}}_{\mathtt{B}_i|\mathtt{O}_\mathtt{I}}^{\,i} = \mathbf{J}_{1,i}^{\mathsf{T}} \vec{\mathbf{p}}_{\mathtt{B}_i|\mathtt{O}_i}^{\,\mathtt{I}}$ are the position vectors of the center of gravity and center of buoyancy of the i-th body and expressed on the body-fixed frame, respectively; $\vec{\mathbf{f}}_{\mathtt{W},i}^{\,i} = \mathbf{J}_{1,i}^{\mathsf{T}} \vec{\mathbf{f}}_{\mathtt{W},i}^{\,\mathtt{I}}$ with $\vec{\mathbf{f}}_{\mathtt{W},i}^{\,\mathtt{I}} = [0, 0, m_i g]^{\mathsf{T}}$ and $\vec{\mathbf{f}}_{\mathtt{B},i}^{\,i} = \mathbf{J}_{1,i}^{\mathsf{T}} \vec{\mathbf{f}}_{\mathtt{B},i}^{\,\mathtt{I}}$ with $\vec{\mathbf{f}}_{\mathtt{B},i}^{\,\mathtt{I}} = [0, 0, -\rho V_i g]^{\mathsf{T}}$ are the vectors of weight and buoyancy forces expressed on the body-fixed frame, in this order, with m_i as the mass, V_i as the displaced volume and g as the acceleration of gravity.

Let us introduce the following relations:

$$\boldsymbol{\nu}_{1,\mathtt{G}_i} = \dot{\vec{\mathbf{p}}}_{\mathtt{G}_i|\mathtt{O}_\mathtt{I}}^{\,i} = \mathbf{J}_{\boldsymbol{\nu}_{1,\mathtt{G}_i}} \boldsymbol{\nu}_i; \quad \boldsymbol{\nu}_{1,\mathtt{B}_i} = \dot{\vec{\mathbf{p}}}_{\mathtt{B}_i|\mathtt{O}_\mathtt{I}}^{\,i} = \mathbf{J}_{\boldsymbol{\nu}_{1,\mathtt{B}_i}} \boldsymbol{\nu}_i. \quad (i = 0, 1, \ldots, N) \tag{3.24}$$

Based on the Euler-Lagrange equation in terms of quasi-velocities and considering the relations of Eq. (3.24), the generalized restoring forces becomes:

$$\mathbf{g}_i = \mathbf{J}_i^{\mathsf{T}} \frac{\partial \mathcal{U}_i}{\partial \boldsymbol{\eta}_i} = \sum_{i=0}^{N} \mathbf{J}_{\boldsymbol{\nu}_{1,\mathtt{G}_i}}^{\mathsf{T}} \vec{\mathbf{f}}_{\mathtt{W},i}^{\,i} + \mathbf{J}_{\boldsymbol{\nu}_{1,\mathtt{B}_i}}^{\mathsf{T}} \vec{\mathbf{f}}_{\mathtt{B},i}^{\,i} = \sum_{i=0}^{N} \mathbf{J}_{\boldsymbol{\nu}_{1,\mathtt{G}_i}}^{\mathsf{T}} \mathbf{J}_{1,i}^{\mathsf{T}} \vec{\mathbf{f}}_{\mathtt{W},i}^{\,\mathtt{I}} + \mathbf{J}_{\boldsymbol{\nu}_{1,\mathtt{B}_i}}^{\mathsf{T}} \mathbf{J}_{1,i}^{\mathsf{T}} \vec{\mathbf{f}}_{\mathtt{B},i}^{\,\mathtt{I}}. \quad (i = 0, 1, \ldots, N) \tag{3.25}$$

3.1.4.3 Drag forces

Generalized drag forces arise due to the viscous effects associated to the relative velocity between the submerged bodies and the fluid medium. The model presented by Fossen (1996) for the hydrodynamic damping on UUVs can be used to model the linear and quadratic drag forces acting on the AUVs, as follows:

$$\frac{\partial \mathcal{R}_0}{\partial \boldsymbol{\nu}_0} = \vec{\mathbf{f}}^{0}_{\mathrm{D},0} \cdot \frac{\partial \boldsymbol{\nu}_{1,0}}{\partial \boldsymbol{\nu}_0} + \vec{\mathbf{n}}^{0}_{\mathrm{D},0} \cdot \frac{\partial \boldsymbol{\nu}_{2,0}}{\partial \boldsymbol{\nu}_0} = \mathbf{D}_0 \boldsymbol{\nu}_0, \tag{3.26}$$

where $\vec{\mathbf{f}}^{0}_{\mathrm{D},0}$ and $\vec{\mathbf{n}}^{0}_{\mathrm{D},0}$ are the vectors of drag forces and moments, respectively, expressed on the body-fixed frame whereas $\mathbf{D}_0$ is the associated hydrodynamic damping matrix, which can be divided into linear and quadratic parts:

$$\mathbf{D}_0 = \mathbf{D}_{\mathrm{L},0} + \mathbf{D}_{\mathrm{Q},0}, \tag{3.27}$$

where $\mathbf{D}_{\mathrm{L},0}$ and $\mathbf{D}_{\mathrm{Q},0}$ are the matrices of linear and quadratic hydrodynamic damping coefficients.

There are semi-empirical models based on Morison's equation that are more appropriate for the manipulator links. One of those is the model of Leabourne and Rock (1998), which is a multi-link version of the model of McLain and Rock (1998) for the drag forces developed on cylindrical-shaped bodies. This model is based on the links discretization into strips along its length, as shown by Fig. 18.

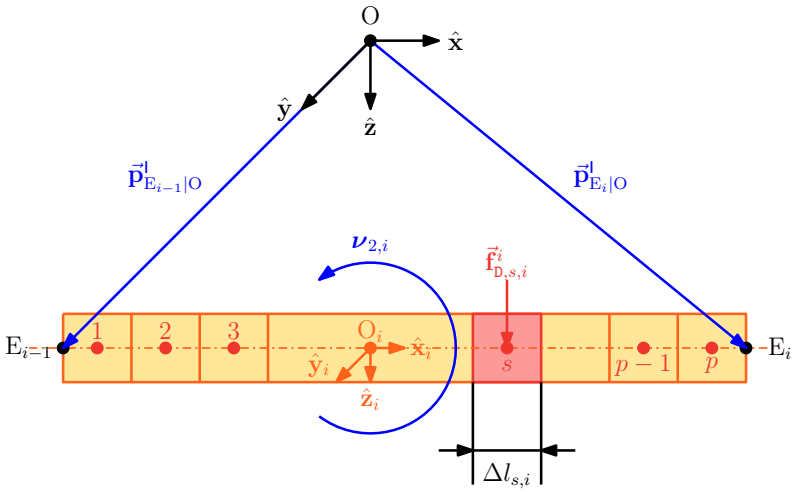

Figure 18: Discretization of the i-th link into strips

In this work, a modified version of the model of Leabourne and Rock (1998) is introduced by incorporating the generalized directions onto the drag forces calculation. The generalized drag forces are computed by taking the drag forces of each strip projected on the generalized directions. Following the same rationale of the added mass forces, the generalized drag forces

can be included on the EoMs as follows:

$$\frac{\partial \mathcal{R}_i}{\partial \boldsymbol{\nu}_i} = \sum_{s=1}^{p} \vec{\mathbf{f}}^{i}_{\mathrm{D},s,i} \cdot \frac{\partial \boldsymbol{\nu}_{1,s,i}}{\partial \boldsymbol{\nu}_i}, \quad (i = 1, \ldots, N) \tag{3.28}$$

where $\vec{\mathbf{f}}^{i}_{\mathrm{D},s,i} = \left[X_{\mathrm{D},s,\mathrm{x}_i}, Y_{\mathrm{D},s,\mathrm{y}_i}, Z_{\mathrm{D},s,\mathrm{z}_i}\right]^{\mathsf{T}}$ is the vector of drag forces of the s-th strip expressed in the body-fixed frame, with components given by:

$$\begin{aligned} X_{\mathrm{D},s,\mathrm{x}_i} &= \frac{1}{2}\rho C_{\mathrm{D},\mathrm{x}_i} |u_{s,\mathrm{x}_i}| u_{s,\mathrm{x}_i} A_{s,\mathrm{x}_i}, \\ Y_{\mathrm{D},s,\mathrm{y}_i} &= \frac{1}{2}\rho C_{\mathrm{D},\mathrm{y}_i} |v_{s,\mathrm{y}_i}| v_{s,\mathrm{y}_i} A_{s,\mathrm{y}_i}, \\ Z_{\mathrm{D},s,\mathrm{z}_i} &= \frac{1}{2}\rho C_{\mathrm{D},\mathrm{z}_i} |w_{s,\mathrm{z}_i}| w_{s,\mathrm{z}_i} A_{s,\mathrm{z}_i}, \end{aligned} \tag{3.29}$$

where A_{s,x_i}, A_{s,y_i} and A_{s,z_i} are the projected areas on the flow direction, while $C_{\mathrm{D},\mathrm{x}_i}$, $C_{\mathrm{D},\mathrm{y}_i}$ and $C_{\mathrm{D},\mathrm{z}_i}$ are the drag coefficients dependent on the flow conditions. If experimental results are available, these coefficients can be identified as a function of the links length (MCLAIN; ROCK, 1998) and in terms of the configuration of the system (LEABOURNE; ROCK, 1998). If not, as in this work, a more conservative approach is adopted, in which the drag coefficients are assumed to be constant, leading to an overestimation of the drag forces.

With the first relation of Eq. (3.17) and after some algebraic manipulation, the generalized drag forces becomes:

$$\frac{\partial \mathcal{R}_i}{\partial \boldsymbol{\nu}_i} = \mathbf{D}_i \boldsymbol{\nu}_i, \quad (i = 1, \ldots, N) \tag{3.30}$$

where $\mathbf{D}_i$ is the hydrodynamic damping matrix of the i-th link, calculated as:

$$\mathbf{D}_i = \sum_{s=1}^{p} \mathbf{J}^{\mathsf{T}}_{\boldsymbol{\nu}_{1,s,i}} \boldsymbol{\Phi}_{\mathrm{D},s,i} \mathbf{J}_{\boldsymbol{\nu}_{1,s,i}}, \quad (i = 1, \ldots, N) \tag{3.31}$$

with

$$\boldsymbol{\Phi}_{\mathrm{D},s,i} = \frac{1}{2}\rho \operatorname{diag}\left(C_{\mathrm{D},\mathrm{x}_i} A_{\mathrm{x}_i} |u_{r,\mathrm{x}_i}|, C_{\mathrm{D},\mathrm{y}_i} A_{\mathrm{y}_i} |v_{r,\mathrm{y}_i}|, C_{\mathrm{D},\mathrm{z}_i} A_{\mathrm{z}_i} |w_{r,\mathrm{z}_i}|\right). \tag{3.32}$$

The disadvantage of the model of Leabourne and Rock (1998) is the number of computations which should be performed for each strip. An alternative to reduce the computational effort is to use a continuous model, such as the one of Shah et al. (2021). However, the former has a significant limitation since it is assumed to be continuous velocity profile along the link during its derivation. To overcome these issues, this work introduces a novel model, alternative to the ones of Leabourne and Rock (1998) and of Shah et al. (2021), that is continuous but also able to handle discontinuities of the velocity profile along the link.

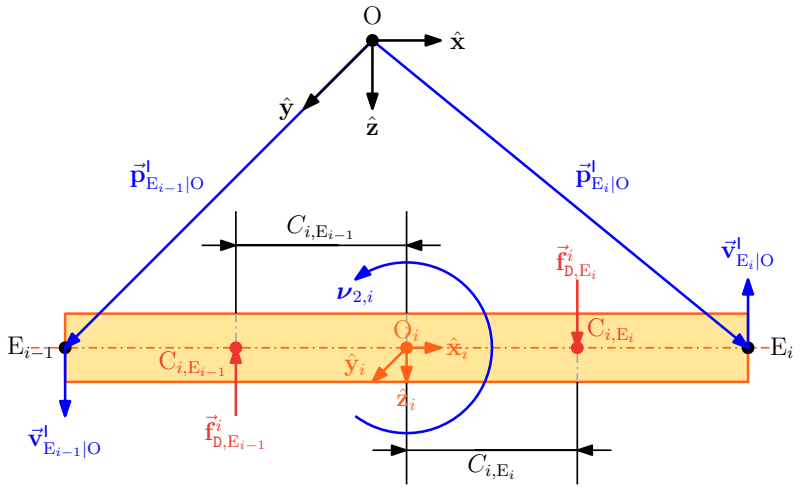

Figure 19: Schematic diagram of the continuous drag model for the i-th link

Based on Fig. 19 and considering the i-th link with length equal to $2l_i$, angular velocity q_i around y_i axis and transversal velocity w_i along the axis z_i and at O_i, then, let $a_i = q_i + \delta_i$ be the damped angular velocity, with $0 < \delta_i << 1$ as the numeric damping, $b_i = w_i - a_i l_i$ is the transversal velocity at extremity E_{i-1} and $w_i(\bar{x}_i) = b_i + a_i \bar{x}_i$ is the transversal velocity profile as a function of the longitudinal displacement $\bar{x}_i$ along the link measured from the extremity E_{i-1}.

The transversal drag force along the axis z_i of the i-th link can be written as:

$$\frac{\mathrm{d}f_{D,z_i}}{\mathrm{d}\bar{x}_i} = \frac{1}{2}\rho C_{D,z_i} d_i w_i(\bar{x}_i)\,|w_i(\bar{x}_i)|. \tag{3.33}$$

To handle the absolute value function inside the integral, consider the transformation of variables expressed by $\bar{u}_i = b_i + a_i \bar{x}_i$, with $\mathrm{d}\bar{u}_i = a_i \mathrm{d}\bar{x}_i$, such that Eq. (3.33) becomes:

$$a_i \frac{\mathrm{d}f_{D,z_i}}{\mathrm{d}\bar{u}_i} = \frac{1}{2}\rho C_{D,z_i} d_i \bar{u}_i|\bar{u}_i| \Rightarrow \mathrm{d}f_{D,z_i} = \frac{1}{2a_i}\rho C_{D,z_i} d_i \bar{u}_i|\bar{u}_i|\mathrm{d}\bar{u}_i. \tag{3.34}$$

Performing the integration along the link length, we obtain:

$$\begin{aligned}
f_{D,z_i} &= \int_0^{2l_i} \mathrm{d}f_{D,z_i}, \\
&= \int_{\bar{u}_i(0)}^{\bar{u}_i(2l_i)} \frac{1}{2a_i}\rho C_{D,z_i} d_i \bar{u}_i|\bar{u}_i|\mathrm{d}\bar{u}_i, \\
&= \int_{b_i}^{b_i+2a_i l_i} \frac{1}{2a_i}\rho C_{D,z_i} d_i \bar{u}_i|\bar{u}_i|\mathrm{d}\bar{u}_i, \\
&= \frac{1}{6a_i}\rho C_{D,z_i} d_i \bar{u}_i^3 \,\mathrm{sign}(\bar{u}_i)\Big|_{b_i}^{b_i+2a_i l_i}, \\
&= \frac{1}{6a_i}\rho C_{D,z_i} d_i \left(w_{i,2l_i}^3 \,\mathrm{sign}\left(w_{i,2l_i}\right) - w_{i,0}^3 \,\mathrm{sign}\left(w_{i,0}\right)\right),
\end{aligned} \tag{3.35}$$

where $w_{i,0} = w_i(0)$ and $w_{i,2l_i} = w_i(2l_i)$.

From Eq. (3.35), the following drag force expression arises:

$$f_{\mathrm{D},z_i}(\bar{x}_i) = \frac{1}{6a_i}\rho C_{\mathrm{D},z_i} d_i w_i^3(\bar{x}_i)\,\mathrm{sign}(w_i(\bar{x}_i)). \tag{3.36}$$

Eq. (3.35) can be rewritten in terms of two force components, as follows:

$$f_{\mathrm{D},z_i} = f_{\mathrm{D},z_i,2l_i} - f_{\mathrm{D},z_i,0}, \tag{3.37}$$

where $f_{\mathrm{D},z_i,0} = f_{\mathrm{D},z_i}(0)$ and $f_{\mathrm{D},z_i,2l_i} = f_{\mathrm{D},z_i}(2l_i)$.

The same procedure is used to calculate the drag moment, but now considering the force location inside the expression, as shown below:

$$\frac{\mathrm{d}n_{\mathrm{D},y_i}}{\mathrm{d}\bar{x}_i} = \frac{1}{2}\rho C_{\mathrm{D},z_i} d_i w_i(\bar{x}_i)|w_i(\bar{x}_i)|\bar{x}_i. \tag{3.38}$$

From the change of variables, we have:

$$a_i\frac{\mathrm{d}n_{\mathrm{D},y_i}}{\mathrm{d}\bar{u}_i} = \frac{1}{2}\rho C_{\mathrm{D},z_i} d_i \bar{u}_i|\bar{u}_i|\frac{\bar{u}_i - b_i}{a_i} \Rightarrow \mathrm{d}n_{\mathrm{D},y_i} = \frac{1}{2a_i}\rho C_{\mathrm{D},z_i} d_i \bar{u}_i|\bar{u}_i|\frac{\bar{u}_i - b_i}{a_i}\mathrm{d}\bar{u}_i. \tag{3.39}$$

Performing the integration of Eq. (3.37) along the link length, we get:

$$\begin{aligned}
n_{\mathrm{D},y_i} &= \int_0^{2l_i} \mathrm{d}n_{\mathrm{D},y_i}, \\
&= \int_{\bar{u}_i(0)}^{\bar{u}_i(2l_i)} \frac{1}{2a_i}\rho C_{\mathrm{D},z_i} d_i \bar{u}_i|\bar{u}_i|\frac{\bar{u}_i - b_i}{a_i}\mathrm{d}\bar{u}_i, \\
&= \int_{b_i}^{b_i+2a_il_i} \frac{1}{2a_i}\rho C_{\mathrm{D},z_i} d_i \bar{u}_i|\bar{u}_i|\frac{\bar{u}_i - b_i}{a_i}\mathrm{d}\bar{u}_i, \\
&= \frac{1}{6a_i}\rho C_{\mathrm{D},z_i} d_i \bar{u}_i^3\,\mathrm{sign}(\bar{u}_i)\frac{3\bar{u}_i - 4b_i}{4a_i}\Bigg|_{b_i}^{b_i+2a_il_i}, \\
&= \frac{1}{6a_i}\rho C_{\mathrm{D},z_i} d_i \left(w_{i,2l_i}^3\,\mathrm{sign}(w_{i,2l_i})\frac{3w_{i,2l_i} - 4b_i}{4a_i} - w_{i,0}^3\,\mathrm{sign}(w_{i,0})\frac{3w_{i,0} - 4b_i}{4a_i}\right),
\end{aligned} \tag{3.40}$$

Analyzing the drag moment expression we can identify the drag centers position along the longitudinal axis of the link, as follows:

$$\mathrm{C}_i(\bar{u}_i) = \frac{3\bar{u}_i - 4b_i}{4a_i} \Rightarrow \mathrm{C}_i(x_i) = \frac{3a_i\bar{x}_i - b_i}{4a_i}. \tag{3.41}$$

With Eq. (3.41), the drag moment of (3.40) can be rewritten as:

$$n_{\mathrm{D},y_i} = f_{\mathrm{D},z_i,2l_i}\mathrm{C}_{i,2l_i} - f_{\mathrm{D},z_i,0}\mathrm{C}_{i,0}. \tag{3.42}$$

where $\mathrm{C}_{i,0} = \mathrm{C}_i\,(0)$ and $\mathrm{C}_{i,2l_i} = \mathrm{C}_i\,(2l_i)$.

To extend the model given by Eqs. (3.33)–(3.38) to the 3D case, let $\vec{\mathbf{p}}^{\,i}_{\mathrm{E}_{i-1}|\mathrm{O}_i} = [-l_i, 0, 0]^\mathsf{T}$, $\vec{\mathbf{p}}^{\,i}_{\mathrm{E}_i|\mathrm{O}_i} = [l_i, 0, 0]^\mathsf{T}$ be the position vectors of E_{i-1} and E_i with respect to O_i on the body-fixed frame, such that $\boldsymbol{\nu}_{\mathrm{E}_{i-1}} = \boldsymbol{\nu}_{1,i} - \boldsymbol{\nu}_{2,i} \times \vec{\mathbf{p}}^{\,i}_{\mathrm{E}_{i-1}|\mathrm{O}_i} = [u_{\mathrm{E}_{i-1}}, v_{\mathrm{E}_{i-1}}, w_{\mathrm{E}_{i-1}}]^\mathsf{T}$ and $\boldsymbol{\nu}_{\mathrm{E}_i} = \boldsymbol{\nu}_{1,i} + \boldsymbol{\nu}_{2,i} \times \vec{\mathbf{p}}^{\,i}_{\mathrm{E}_i|\mathrm{O}_i} = [u_{\mathrm{E}_i}, v_{\mathrm{E}_i}, w_{\mathrm{E}_i}]^\mathsf{T}$ are the velocity vectors of E_{i-1} and E_i, in this order. Also, let $a_{\mathrm{y}_i} = r_i + \delta_i$ and $a_{\mathrm{z}_i} = \delta_i - q_i$ be the damped angular velocities along y_i and z_i axes, respectively, while $b_{\mathrm{y}_i} = v_{\mathrm{E}_{i-1},\mathrm{y}_i}$ and $b_{\mathrm{z}_i} = v_{\mathrm{E}_{i-1},\mathrm{z}_i}$ are the velocities components at the extremity E_{i-1}.

Defining $\vec{\mathbf{f}}^{\,i}_{\mathrm{D},\mathrm{G}_i} = [f_{\mathrm{D},\mathrm{x}_i,\mathrm{G}_i}, 0, 0]^\mathsf{T}$, $\vec{\mathbf{f}}^{\,i}_{\mathrm{D},\mathrm{E}_{i-1}} = \left[0, f_{\mathrm{D},\mathrm{y}_i,\mathrm{E}_{i-1}}, f_{\mathrm{D},\mathrm{z}_i,\mathrm{E}_{i-1}}\right]^\mathsf{T}$ and $\vec{\mathbf{f}}^{\,i}_{\mathrm{D},\mathrm{E}_i} = \left[0, f_{\mathrm{D},\mathrm{y}_i,\mathrm{E}_i}, f_{\mathrm{D},\mathrm{z}_i,\mathrm{E}_i}\right]^\mathsf{T}$ as the drag force vector on G_i, E_{i-1} and E_i, respectively, the generalized drag forces on the i-th link are given by:

$$\frac{\partial \mathcal{R}_i}{\partial \boldsymbol{\nu}_i} = \vec{\mathbf{f}}^{\,i}_{\mathrm{D},\mathrm{G}_i} \cdot \frac{\partial \boldsymbol{\nu}_{1,\mathrm{G}_i}}{\partial \boldsymbol{\nu}_i} + \vec{\mathbf{f}}^{\,i}_{\mathrm{D},\mathrm{E}_{i-1}} \cdot \frac{\partial \boldsymbol{\nu}_{\mathrm{E}_{i-1}}}{\partial \boldsymbol{\nu}_i} + \vec{\mathbf{f}}^{\,i}_{\mathrm{D},\mathrm{E}_i} \cdot \frac{\partial \boldsymbol{\nu}_{\mathrm{E}_i}}{\partial \boldsymbol{\nu}_i}, \quad (i = 1, \ldots, N) \tag{3.43}$$

with the velocity vectors $\boldsymbol{\nu}_{1,\mathrm{G}_i}$, $\boldsymbol{\nu}_{1,\mathrm{E}_{i-1}}$ and $\boldsymbol{\nu}_{1,\mathrm{E}_i}$ obeying the relations:

$$\boldsymbol{\nu}_{1,\mathrm{G}_i} = \mathbf{J}_{\boldsymbol{\nu}_{1,\mathrm{G}_i}} \boldsymbol{\nu}_i; \quad \boldsymbol{\nu}_{1,\mathrm{E}_{i-1}} = \mathbf{J}_{\boldsymbol{\nu}_{1,\mathrm{E}_{i-1}}} \boldsymbol{\nu}_i; \quad \boldsymbol{\nu}_{1,\mathrm{E}_i} = \mathbf{J}_{\boldsymbol{\nu}_{1,\mathrm{E}_i}} \boldsymbol{\nu}_i. \quad (i = 1, \ldots, N) \tag{3.44}$$

From Eq. (3.36), the drag components can be written as:

$$\begin{aligned}
f_{\mathrm{D},\mathrm{x}_i,\mathrm{G}_i} &= \frac{1}{2}\rho C_{\mathrm{D},\mathrm{x}_i} A_{\mathrm{x}_i} u_{\mathrm{G}_i} \operatorname{sign}(u_{\mathrm{G}_i}), \\
f_{\mathrm{D},\mathrm{y}_i,\mathrm{E}_{i-1}} &= \frac{1}{2}\rho C_{\mathrm{D},\mathrm{y}_i} d_i v_{\mathrm{E}_{i-1}}^2 \operatorname{sign}(v_{\mathrm{E}_{i-1}})\,/3a_{\mathrm{y}_i}, \\
f_{\mathrm{D},\mathrm{y}_i,\mathrm{E}_i} &= \frac{1}{2}\rho C_{\mathrm{D},\mathrm{y}_i} d_i v_{\mathrm{E}_i}^2 \operatorname{sign}(v_{\mathrm{E}_i})\,/3a_{\mathrm{y}_i}, \\
f_{\mathrm{D},\mathrm{z}_i,\mathrm{E}_{i-1}} &= \frac{1}{2}\rho C_{\mathrm{D},\mathrm{z}_i} d_i w_{\mathrm{E}_{i-1}}^2 \operatorname{sign}(w_{\mathrm{E}_{i-1}})\,/3a_{\mathrm{z}_i}, \\
f_{\mathrm{D},\mathrm{z}_i,\mathrm{E}_i} &= \frac{1}{2}\rho C_{\mathrm{D},\mathrm{z}_i} d_i w_{\mathrm{E}_i}^2 \operatorname{sign}(w_{\mathrm{E}_i})\,/3a_{\mathrm{z}_i}.
\end{aligned} \tag{3.45}$$

The drag centers associated to each drag component of Eq. (3.45) are written based on (3.41), as below:

$$\begin{aligned}
C_{\mathrm{y}_i,\mathrm{E}_{i-1}} &= \frac{3v_{\mathrm{E}_{i-1}} - 4b_{\mathrm{y}_i}}{4a_{\mathrm{y}_i}}; \quad C_{\mathrm{y}_i,\mathrm{E}_i} = \frac{3v_{\mathrm{E}_i} - 4b_{\mathrm{y}_i}}{4a_{\mathrm{y}_i}}, \\
C_{\mathrm{z}_i,\mathrm{E}_{i-1}} &= \frac{3w_{\mathrm{E}_{i-1}} - 4b_{\mathrm{z}_i}}{4a_{\mathrm{z}_i}}; \quad C_{\mathrm{z}_i,\mathrm{E}_i} = \frac{3w_{\mathrm{E}_i} - 4b_{\mathrm{z}_i}}{4a_{\mathrm{z}_i}}.
\end{aligned} \tag{3.46}$$

Moreover, the drag centers of Eq. (3.41) can be rewritten with respect to the gravity center of the i-link (see Fig. 20), as follows:

$$\begin{aligned}
G_{\mathrm{y}_i,\mathrm{E}_{i-1}} &= C_{\mathrm{y}_i,\mathrm{E}_{i-1}} - (l_i + x_{\mathrm{G}_i}); \quad G_{\mathrm{y}_i,\mathrm{E}_i} = C_{\mathrm{y}_i,\mathrm{E}_i} - (l_i + x_{\mathrm{G}_i}), \\
G_{\mathrm{z}_i,\mathrm{E}_{i-1}} &= C_{\mathrm{z}_i,\mathrm{E}_{i-1}} - (l_i + x_{\mathrm{G}_i}); \quad G_{\mathrm{z}_i,\mathrm{E}_i} = C_{\mathrm{z}_i,\mathrm{E}_i} - (l_i + x_{\mathrm{G}_i}).
\end{aligned} \tag{3.47}$$

where x_{G_i} is the longitudinal body-fixed coordinate of the center of gravity of the i-th link.

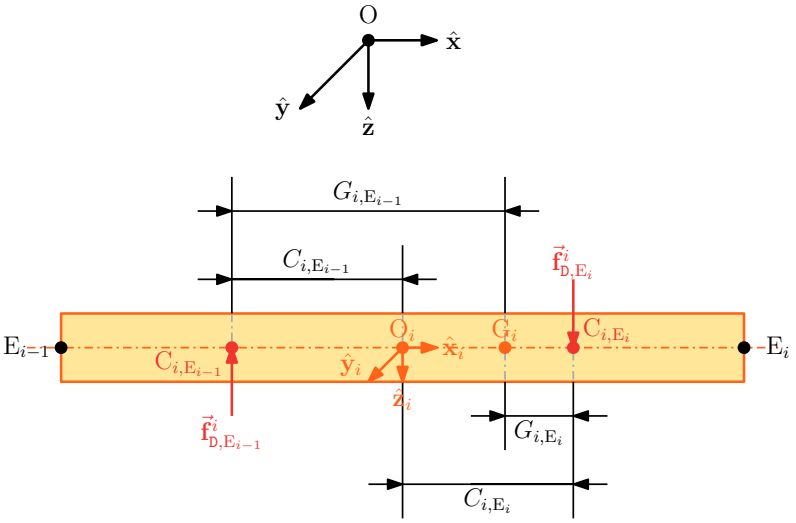

Figure 20: Relative centers of the continuous drag model for the i-th link

Developing Eq. (3.43), we obtain the following damping matrix of the i-th link:

$$\mathbf{D}_i = \mathbf{J}^{\mathsf{T}}_{\boldsymbol{\nu}_{1,\mathrm{G}_i}} \boldsymbol{\Phi}_{\mathrm{D},\mathrm{G}_i} \mathbf{J}_{\boldsymbol{\nu}_{1,i}} + \mathbf{J}^{\mathsf{T}}_{\boldsymbol{\nu}_{1,\mathrm{G}_i}} \boldsymbol{\Phi}_{\mathrm{D},\mathrm{E}_{i-1}} \mathbf{J}_{\boldsymbol{\nu}_{1,\mathrm{E}_{i-1}}} + \mathbf{J}^{\mathsf{T}}_{\boldsymbol{\nu}_{1,\mathrm{G}_i}} \boldsymbol{\Phi}_{\mathrm{D},\mathrm{E}_i} \mathbf{J}_{\boldsymbol{\nu}_{1,\mathrm{E}_i}} + \mathbf{I}^{\mathsf{T}}_{\mathrm{E}_{i-1}} \boldsymbol{\Gamma}_{\mathrm{D},\mathrm{E}_{i-1}} \bar{\mathbf{J}}_{\boldsymbol{\nu}_{1,\mathrm{E}_{i-1}}} + \mathbf{I}^{\mathsf{T}}_{\mathrm{E}_i} \boldsymbol{\Gamma}_{\mathrm{D},\mathrm{E}_i} \bar{\mathbf{J}}_{\boldsymbol{\nu}_{1,\mathrm{E}_i}}, \quad (3.48)$$

where

$$\begin{aligned}
\boldsymbol{\Phi}_{\mathrm{D},\mathrm{G}_i} &= -\operatorname{diag}\left(-f_{\mathrm{D},\mathrm{x}_i,\mathrm{G}_i}, 0, 0\right), \\
\boldsymbol{\Phi}_{\mathrm{D},\mathrm{E}_{i-1}} &= -\operatorname{diag}\left(0, f_{\mathrm{D},\mathrm{y}_i,\mathrm{E}_{i-1}}, f_{\mathrm{D},\mathrm{z}_i,\mathrm{E}_{i-1}}\right), \\
\boldsymbol{\Phi}_{\mathrm{D},\mathrm{E}_i} &= -\operatorname{diag}\left(0, -f_{\mathrm{D},\mathrm{y}_i,\mathrm{E}_i}, -f_{\mathrm{D},\mathrm{z}_i,\mathrm{E}_i}\right), \\
\boldsymbol{\Gamma}_{\mathrm{D},\mathrm{E}_{i-1}} &= -\operatorname{diag}\left(0, 0, 0, 0, -f_{\mathrm{D},\mathrm{z}_i,\mathrm{E}_{i-1}} G_{\mathrm{E}_{i-1},\mathrm{z}_i}, f_{\mathrm{D},\mathrm{y}_i,\mathrm{E}_{i-1}} G_{\mathrm{E}_{i-1},\mathrm{y}_i}\right), \\
\boldsymbol{\Gamma}_{\mathrm{D},\mathrm{E}_i} &= -\operatorname{diag}\left(0, 0, 0, 0, f_{\mathrm{D},\mathrm{z}_i,\mathrm{E}_i} G_{\mathrm{E}_i,\mathrm{z}_i}, -f_{\mathrm{D},\mathrm{y}_i,\mathrm{E}_i} G_{\mathrm{E}_i,\mathrm{y}_i}\right),
\end{aligned} \quad (3.49)$$

with "diag" indicating a diagonal matrix and

$$\begin{aligned}
&\mathbf{I}_{\mathrm{E}_{i-1}} = \begin{bmatrix} \mathbf{0} & \mathbf{0} \\ \mathbf{0} & \mathbf{I} \end{bmatrix}; \quad \mathbf{I}_{\mathrm{E}_i} = \mathbf{I}_{\mathrm{E}_{i-1}}, \\
&\bar{\mathbf{J}}_{\boldsymbol{\nu}_{1,\mathrm{E}_{i-1}}} = \begin{bmatrix} \mathbf{0} \\ \mathbf{A}_\mathbf{I} \mathbf{J}_{\boldsymbol{\nu}_{1,\mathrm{E}_{i-1}}} \end{bmatrix}; \quad \bar{\mathbf{J}}_{\boldsymbol{\nu}_{1,\mathrm{E}_i}} = \begin{bmatrix} \mathbf{0} \\ \mathbf{A}_\mathbf{I} \mathbf{J}_{\boldsymbol{\nu}_{1,\mathrm{E}_i}} \end{bmatrix}; \quad \mathbf{A}_\mathbf{I} = \begin{bmatrix} 0 & 0 & 1 \\ 0 & 1 & 0 \\ 1 & 0 & 0 \end{bmatrix}.
\end{aligned} \quad (3.50)$$

3.1.4.4 Generalized actuation forces

With respect to the actuation, the I-AUVs have two kinds of actuators, namely the thrusters of the AUV and the motors of the manipulator joints.

The generalized forces due to the action of the thrusters on the AUV are given by:

$$\boldsymbol{\tau}_0 = \vec{\mathbf{f}}^{0}_{\mathtt{M},0} \cdot \frac{\partial \boldsymbol{\nu}_{1,0}}{\partial \boldsymbol{\nu}_0} + \vec{\mathbf{n}}^{0}_{\mathtt{M},0} \cdot \frac{\partial \boldsymbol{\nu}_{2,0}}{\partial \boldsymbol{\nu}_0} = \mathbf{B}_0 \mathbf{t}_0, \tag{3.51}$$

where $\vec{\mathbf{f}}^{0}_{\mathtt{M},0}$ and $\vec{\mathbf{n}}^{0}_{\mathtt{M},0}$ are the vectors of forces and moments generated by the thrusters expressed on the body-fixed frame, respectively; $\mathbf{B}_0$ is the thrust allocation matrix that expresses the thrusters configuration on the AUV and $\mathbf{t}_0 = \left[T_j\right]^{\mathsf{T}}$ $(j = 1, \ldots, p)$ is the column-vector of the generated thrusts, whose dimension depends on the numbers of thrusters mounted on the AUV.

The generalized motor torques of the manipulators joints are written as:

$$\boldsymbol{\tau}_i = \vec{\mathbf{n}}^{i}_{\mathtt{M},i} \cdot \frac{\partial \boldsymbol{\nu}_{2,i}}{\partial \boldsymbol{\nu}_i} = \mathbf{J}_i \mathbf{n}^{i}_{i} - \mathbf{J}_{i+1} \mathbf{n}^{i+1}_{i+1}, \quad (i = 1, \ldots, N) \tag{3.52}$$

with $\mathbf{n}^{i}_{i} = [0, 0, 0, 0, 0, \tau_i]^{\mathsf{T}}$ being the torque generated by the motor located at O_i and $\mathbf{n}^{i+1}_{i+1} = [0, 0, 0, 0, 0, \tau_{i+1}]^{\mathsf{T}}$ as the reaction torque induced by the motor of the subsequent link on the kinematic chain, both expressed at the respective body-fixed frame (according to the Denavit-Hartenberg convention). Notice that $\tau_0 = 0$ $(i = 0)$ since there is no actuated joints on the AUV. Also, if there is no motors on the end-effector wrist, $\tau_N = 0$ $(i = N)$.

If the motors dynamic should be considered, its EoMs need be incorporated on the modeling. For sake of example, let us consider a model of a current controlled Direct Current (DC) brushless motor with a gearbox of reduction $N_{\mathtt{R},i}$ and efficiency $\eta_{\mathtt{M},i}$ expressed by:

$$\tau_{\mathtt{M},i} = N^2_{\mathtt{R},i} \eta_{\mathtt{M},i} I_{\mathtt{M},i} \ddot{\gamma}_i - N^2_{\mathtt{R},i} \eta_{\mathtt{M},i} b_{\mathtt{M},i} \dot{\gamma}_i - N_{\mathtt{R},i} \eta_{\mathtt{M},i} c_{\mathtt{M},i} \operatorname{sign}(\dot{\gamma}_i), \quad (i = 1, \ldots, N) \tag{3.53}$$

where γ_i is motor shaft angle, $I_{\mathtt{M},i}$ is the motor-shaft inertia moment, $b_{\mathtt{M},i}$ is the coefficient of back-emf and of viscous damping, and $c_{\mathtt{M},i}$ is the coefficient of Coulomb friction.

Eq. (3.53) can be rewritten in matrix form as follows:

$$\boldsymbol{\tau}_{\mathtt{M}} = \mathbf{I}_{\mathtt{M}} \ddot{\boldsymbol{\gamma}} - \mathbf{B}_{\mathtt{M}} \dot{\boldsymbol{\gamma}} - \mathbf{C}_{\mathtt{M}} \operatorname{sign}(\dot{\boldsymbol{\gamma}}), \tag{3.54}$$

where $\mathbf{I}_{\mathtt{M}}$, $\mathbf{B}_{\mathtt{M}}$ and $\mathbf{C}_{\mathtt{M}}$ are the matrices of motors equivalent inertia, viscous and Coulomb friction, respectively, given by:

$$\begin{aligned} \mathbf{I}_{\mathtt{M}} &= \operatorname{diag}\left(N^2_{\mathtt{R},1} \eta_{\mathtt{M},1} I_{\mathtt{M},1}, \ldots, N^2_{\mathtt{R},N} \eta_{\mathtt{M},N} I_{\mathtt{M},N}\right), \\ \mathbf{B}_{\mathtt{M}} &= \operatorname{diag}\left(N^2_{\mathtt{R},1} \eta_{\mathtt{M},1} b_{\mathtt{M},1}, \ldots, N^2_{\mathtt{R},N} \eta_{\mathtt{M},N} b_{\mathtt{M},N}\right), \\ \mathbf{C}_{\mathtt{M}} &= \operatorname{diag}\left(N_{\mathtt{R},1} \eta_{\mathtt{M},1} c_{\mathtt{M},1}, \ldots, N_{\mathtt{R},N} \eta_{\mathtt{M},N} c_{\mathtt{M},N}\right). \end{aligned} \tag{3.55}$$

3.1.4.5 Generalized disturbance forces

Let the column-vector of fluid-velocity expressed on the Earth-fixed frame be given by $\dot{\boldsymbol{\eta}}_\infty = [\dot{x}_\infty, \dot{y}_\infty, \dot{z}_\infty, 0, 0, 0]^\mathsf{T}$, where the last three components are under the hypothesis 7 of irrotational current. The current-induced disturbances can be written considering the approximated solution of Froude-Krylov and diffraction forces, as follows (FOSSEN, 1996):

$$\mathbf{d}_i = (\mathbf{M}_{\mathtt{FK,i}} + \mathbf{M}_{\mathtt{A},i})\,\dot{\boldsymbol{\nu}}_{\infty,i} + (\mathbf{C}_{\mathtt{A},i} + \mathbf{D}_i)\,\boldsymbol{\nu}_{\infty,i}, \quad (i = 0, 1, \ldots, N) \tag{3.56}$$

with $\mathbf{M}_{\mathtt{FK,i}}$ as the Froude-Krylov mass matrix associated with the displaced volume, expressed on the body-fixed frame and calculated concerning the origin (O_i), while $\boldsymbol{\nu}_\infty$ and $\dot{\boldsymbol{\nu}}_\infty$ are the column-vectors of fluid-velocity and acceleration on the body-fixed frame, written as:

$$\boldsymbol{\nu}_{\infty,i} = \mathbf{J}_i \dot{\boldsymbol{\eta}}_\infty; \quad \dot{\boldsymbol{\nu}}_{\infty,i} = \mathbf{J}_i \ddot{\boldsymbol{\eta}}_\infty + \dot{\mathbf{J}}_i \dot{\boldsymbol{\eta}}_\infty. \tag{3.57}$$

Other disturbances such as forces and moments induced during contact can be written as:

$$\mathbf{d}_i = \vec{\mathbf{f}}^{\,i}_{\mathrm{P},i} \cdot \frac{\partial \boldsymbol{\nu}_{1,i}}{\partial \boldsymbol{\nu}_i} + \vec{\mathbf{n}}^{\,i}_{\mathrm{P},i} \cdot \frac{\partial \boldsymbol{\nu}_{2,i}}{\partial \boldsymbol{\nu}_i} = \mathbf{P}_i \boldsymbol{\tau}_{\mathrm{P},i}, \quad (i = 0, 1, \ldots, N) \tag{3.58}$$

where $\vec{\mathbf{f}}^{\,i}_{\mathrm{P},0} = \mathbf{J}^\mathsf{T}_{1,i} \vec{\mathbf{f}}^{\,\mathrm{I}}_{\mathrm{P},0}$ with $\vec{\mathbf{f}}^{\,\mathrm{I}}_{\mathrm{P},0} = \left[f_{\mathrm{P,x},i}, f_{\mathrm{P,y},i}, f_{\mathrm{P,z},i}\right]^\mathsf{T}$ and $\vec{\mathbf{n}}^{\,i}_{\mathrm{P},0} = \mathbf{J}^{-1}_{2,i} \vec{\mathbf{n}}^{\,\mathrm{I}}_{\mathrm{P},0}$ with $\vec{\mathbf{n}}^{\,\mathrm{I}}_{\mathrm{P},0} = \left[n_{\mathrm{P,x},i}, n_{\mathrm{P,y},i}, n_{\mathrm{P,z},i}\right]^\mathsf{T}$ are the vectors of external forces and moments with respect to the origin (O_i) and expressed on body-fixed frame, respectively, while $\boldsymbol{\tau}_{\mathrm{P},i} = \left[\left(\vec{\mathbf{f}}^{\,i}_{\mathrm{P},0}\right)^\mathsf{T}, \left(\vec{\mathbf{n}}^{\,i}_{\mathrm{P},0}\right)^\mathsf{T}\right]^\mathsf{T}$ is the column-vector of external wrenches and $\mathbf{P}_i$ is the associated projection matrix, which is written as:

$$\mathbf{P}_i = \mathrm{blkdiag}\left(\mathbf{I}, \mathbf{J}^\mathsf{T}_{\boldsymbol{\nu}_{2,i}}\right), \quad (i = 0, 1, \ldots, N) \tag{3.59}$$

with $\mathbf{J}_{\boldsymbol{\nu}_{2,i}}$ satisfying $\boldsymbol{\nu}_{2,i} = \mathbf{J}_{\boldsymbol{\nu}_{2,i}} \boldsymbol{\nu}_i$ and "blkdiag" indicating a block-diagonal matrix[3].

3.1.5 Modular modeling

Let $\mathcal{S}$ be a v-DoFs system (v finite). Denote $\boldsymbol{\eta}$ as the n-column-vector ($n \geq v$) of generalized coordinates and $\boldsymbol{\nu}$ as the m-column vector ($m \geq v$) of quasi-velocities, such as:

$$\boldsymbol{\eta} = \left[\boldsymbol{\eta}_0^\mathsf{T}, \ldots, \boldsymbol{\eta}_N^\mathsf{T}, \boldsymbol{\gamma}^\mathsf{T}\right]^\mathsf{T}; \quad \boldsymbol{\nu} = \left[\boldsymbol{\nu}_0^\mathsf{T}, \ldots, \boldsymbol{\nu}_N^\mathsf{T}, \dot{\boldsymbol{\gamma}}^\mathsf{T}\right]^\mathsf{T}, \tag{3.60}$$

where $\boldsymbol{\eta}_i$ and $\boldsymbol{\nu}_i$ are the column-vectors of generalized coordinates and quasi-velocities of the i-th body, respectively, and $\boldsymbol{\gamma}$ is the column-vector of generalized motors displacements.

[3] A block diagonal matrix is a square matrix of other square matrices lying along the diagonal, and all the other entries of the matrix equal zero.

The relaxed dynamic model is written as a collection of EoMs for each body of the system $\mathcal{S}$ expressed in the following matrix form:

$$\begin{aligned} \dot{\boldsymbol{\eta}} &= \mathbf{J}(\boldsymbol{\eta})\,\boldsymbol{\nu}, \\ \mathbf{M}\dot{\boldsymbol{\nu}} + (\mathbf{C}(\boldsymbol{\nu}) + \mathbf{D}(\boldsymbol{\nu}))\,\boldsymbol{\nu} + \mathbf{g}(\boldsymbol{\eta}) &= \boldsymbol{\tau} + \mathbf{d}, \end{aligned} \tag{3.61}$$

where

$$\begin{aligned} \mathbf{g} &= \left[\mathbf{g}_0^{\mathsf{T}}, \ldots, \mathbf{g}_N^{\mathsf{T}}, \mathbf{0}^{\mathsf{T}}\right]^{\mathsf{T}}, \\ \boldsymbol{\tau} &= \left[\boldsymbol{\tau}_0^{\mathsf{T}}, \ldots, \boldsymbol{\tau}_N^{\mathsf{T}}, \boldsymbol{\tau}_{\mathtt{M}}^{\mathsf{T}}\right]^{\mathsf{T}}, \\ \mathbf{d} &= \left[\mathbf{d}_0^{\mathsf{T}}, \ldots, \mathbf{d}_N^{\mathsf{T}}, (\mathbf{C}_{\mathtt{M}}\,\mathrm{sign}\,(\dot{\boldsymbol{\gamma}}))^{\mathsf{T}}\right]^{\mathsf{T}}, \\ \mathbf{J} &= \mathrm{blkdiag}\,(\mathbf{J}_0, \ldots, \mathbf{J}_N, \mathbf{I}), \\ \mathbf{M} &= \mathrm{blkdiag}\,(\mathbf{M}_0, \ldots, \mathbf{M}_N, \mathbf{I}_{\mathtt{M}}), \\ \mathbf{C} &= \mathrm{blkdiag}\,(\mathbf{C}_0, \ldots, \mathbf{C}_N, \mathbf{0}), \\ \mathbf{D} &= \mathrm{blkdiag}\,(\mathbf{D}_0, \ldots, \mathbf{D}_N, \mathbf{B}_{\mathtt{M}}). \end{aligned} \tag{3.62}$$

Let $\boldsymbol{\varphi}$ be the r-column-vector ($r \geq n - v$) of bilateral[4] holonomic and nonholonomic material constraints of the system $\mathcal{S}$, such that:

$$\boldsymbol{\varphi}(\boldsymbol{\eta}, \dot{\boldsymbol{\eta}}, t) = \mathbf{0}. \tag{3.63}$$

Differentiating Eq. (3.63) with respect to time, results in:

$$\mathbf{A}_{\boldsymbol{\eta}}(\boldsymbol{\eta}, \dot{\boldsymbol{\eta}}, t)\,\ddot{\boldsymbol{\eta}} = \mathbf{b}_{\boldsymbol{\eta}}(\boldsymbol{\eta}, \dot{\boldsymbol{\eta}}, t), \tag{3.64}$$

where $\mathbf{A}_{\boldsymbol{\eta}}$ is the r by n Jacobian matrix of the constraints in terms of the generalized velocities with rank $\leq n - v$, with less than $n - v$ only in singular configurations and $\mathbf{b}_{\boldsymbol{\eta}}$ is the associated n-column-vector.

Using the relations of Eq. (3.1) in (3.64), the constraints can be written in terms of the quasi-velocities and quasi-accelerations, as follows:

$$\mathbf{A}(\boldsymbol{\eta}, \boldsymbol{\nu}, t)\,\dot{\boldsymbol{\nu}} = \mathbf{b}(\boldsymbol{\eta}, \boldsymbol{\nu}, t), \tag{3.65}$$

in which

$$\mathbf{A} = \mathbf{A}_{\boldsymbol{\eta}}\mathbf{J}; \quad \mathbf{b} = \mathbf{b}_{\boldsymbol{\eta}} - \mathbf{A}_{\boldsymbol{\eta}}\dot{\mathbf{J}}\boldsymbol{\nu}, \tag{3.66}$$

where $\mathbf{A}$ is the r by m Jacobian matrix of the constraints in terms of the quasi-velocities with

[4]Bilateral constraints take the form $\boldsymbol{\varphi}(\boldsymbol{\eta}, \dot{\boldsymbol{\eta}}, t) = \mathbf{0}$, such as internal constraints, which give rise to the constant distances between the points of a rigid body. Unilateral constraints take the form $\boldsymbol{\varphi}(\boldsymbol{\eta}, \dot{\boldsymbol{\eta}}, t) \leq \mathbf{0}$, such as the motion of a body suspended by a soft thread.

rank $\leq m - v$, with less than $m - v$ only in singular configurations and $\mathbf{b}$ is the corresponding m-column-vector.

Conceiving the system $\mathcal{S}$ as a hierarchy of subsystems (see Sec. 3.1.2) distributed into $r = 0, 1, \ldots, s - 1$ levels, the constraints at level $r + 1$ can be expressed as (ORSINO, 2017):

$$\mathbf{A}_{r+1} = \begin{bmatrix} \mathbf{A}_r \\ \tilde{\mathbf{A}}_{r+1} \end{bmatrix}; \quad \mathbf{b}_{r+1} = \begin{bmatrix} \mathbf{b}_r \\ \tilde{\mathbf{b}}_{r+1} \end{bmatrix}, \tag{3.67}$$

where $\mathbf{A}_r$ and $\mathbf{b}_r$ comes from the constraints at level r, while $\tilde{\mathbf{A}}_{r+1}$ and $\tilde{\mathbf{b}}_{r+1}$ are from the constraints at current level, $r + 1$.

Let the sum of active and inertial generalized forces acting on the system be written according to Eq. (3.61) as below:

$$\mathbf{f} = \boldsymbol{\tau} + \mathbf{d} - \mathbf{M}\dot{\boldsymbol{\nu}} - \mathbf{C}\boldsymbol{\nu} - \mathbf{D}\boldsymbol{\nu} - \mathbf{g}. \tag{3.68}$$

The Gauss's principle for reversible virtual displacements becomes:

$$\delta Z = \mathbf{f}(\boldsymbol{\eta}, \boldsymbol{\nu}) \cdot \delta\dot{\boldsymbol{\nu}} = \mathbf{0}, \tag{3.69}$$

which does not mean that $\mathbf{f} = \mathbf{0}$ since the quasi-velocities are not independent.

To solve this we need to introduce a set of independent quasi-velocities consistent with the constraints, such that:

$$\mathbf{A}\dot{\boldsymbol{\nu}} - \mathbf{b} = \mathbf{0} \Rightarrow \delta\ddot{\boldsymbol{\varphi}} = \mathbf{A}\delta\dot{\boldsymbol{\nu}} = \mathbf{0}, \forall\boldsymbol{\nu}. \tag{3.70}$$

Let $\mathbf{S}$ be a v-rank matrix representing the orthogonal complement of $\mathbf{A}$, such that:

$$\delta\dot{\boldsymbol{\nu}} = \mathbf{S}\delta\dot{\boldsymbol{\zeta}} \Rightarrow \mathbf{A}\mathbf{S}\delta\dot{\boldsymbol{\zeta}} = \mathbf{0}, \forall\dot{\boldsymbol{\zeta}} \therefore \mathbf{A}\mathbf{S} = \mathbf{0}, \tag{3.71}$$

where $\boldsymbol{\zeta}$ is v-column-vector of arbitrary quasi-velocities associated with the actuated coordinates.

Substituting the relation of Eq. (3.71) into (3.69), results in:

$$\mathbf{f} \cdot \delta\dot{\boldsymbol{\nu}} = \delta\dot{\boldsymbol{\nu}}^{\mathsf{T}}\mathbf{f} = \delta\dot{\boldsymbol{\zeta}}^{\mathsf{T}}\mathbf{S}^{\mathsf{T}}\mathbf{f} = \mathbf{0}, \forall\dot{\boldsymbol{\zeta}} \Rightarrow \mathbf{S}^{\mathsf{T}}\mathbf{f} = \mathbf{0}, \tag{3.72}$$

which is the forward dynamic equation.

The following relations come from Eq. (3.71):

$$\boldsymbol{\nu} = \mathbf{S}\boldsymbol{\zeta}; \quad \dot{\boldsymbol{\nu}} = \dot{\mathbf{S}}\boldsymbol{\zeta} + \mathbf{S}\dot{\boldsymbol{\zeta}}, \tag{3.73}$$

with $\mathbf{S} \in C_n$ for $n \geq 1$.

Using the Modular Modeling Methodology (MMM) framework presented in Orsino (2017), we can get at level $r+1$ that:

$$\begin{aligned} \boldsymbol{\nu}_{r+1} &= \mathbf{S}_{r+1}\boldsymbol{\zeta}_{r+1} = \mathbf{S}_r\tilde{\mathbf{S}}_{r+1}\boldsymbol{\zeta}_{r+1}, \\ \dot{\boldsymbol{\nu}}_{r+1} &= \dot{\mathbf{S}}_{r+1}\boldsymbol{\zeta}_{r+1} + \mathbf{S}_{r+1}\dot{\boldsymbol{\zeta}}_{r+1} = \left(\dot{\mathbf{S}}_r\tilde{\mathbf{S}}_{r+1} + \mathbf{S}_r\dot{\tilde{\mathbf{S}}}_{r+1}\right)\boldsymbol{\zeta}_{r+1} + \mathbf{S}_{r+1}\dot{\boldsymbol{\zeta}}_{r+1}, \end{aligned} \tag{3.74}$$

where $\tilde{\mathbf{S}}_{r+1}$ is the orthogonal complement of $\tilde{\mathbf{A}}_{r+1}\mathbf{S}_r$, thus (ORSINO, 2017):

$$\left(\tilde{\mathbf{A}}_{r+1}\mathbf{S}_r\right)\tilde{\mathbf{S}}_{r+1}\delta\boldsymbol{\zeta}_{r+1} = \mathbf{0}, \forall\delta\boldsymbol{\zeta}_{r+1} \therefore \left(\tilde{\mathbf{A}}_{r+1}\mathbf{S}_r\right)\tilde{\mathbf{S}}_{r+1} = \mathbf{0}. \tag{3.75}$$

Using Eq. (3.67), the modeling constraints of (3.65) can be rewritten as:

$$\begin{bmatrix} \mathbf{A}_r \\ \tilde{\mathbf{A}}_{r+1} \end{bmatrix}\mathbf{a}_{r+1} = \begin{bmatrix} \mathbf{b}_r \\ \tilde{\mathbf{b}}_{r+1} \end{bmatrix}. \tag{3.76}$$

Moreover, let the quasi-accelerations be rewritten as:

$$\mathbf{a}_{r+1} = \mathbf{Q}_{r+1}\mathbf{a}^{\#}_{r+1} + \mathbf{R}_{r+1}\mathbf{a}^{*}_{r+1}, \tag{3.77}$$

where $\mathbf{a}^{\#}_{r+1}$ and $\mathbf{a}^{*}_{r+1}$ are the quasi-accelerations parcels associated to the independent and dependent quasi-accelerations, respectively, while $\mathbf{Q}_{r+1}$ and $\mathbf{R}_{r+1}$ are identifications matrices related to these parcels, i.e., matrices of zeros and ones, written as follows:

$$\mathbf{Q}_{r+1} = \mathbf{Q}_r\tilde{\mathbf{Q}}_{r+1}; \quad \mathbf{R}_{r+1} = \begin{bmatrix} \mathbf{R}_r & \tilde{\mathbf{R}}_{r+1} \end{bmatrix}, \tag{3.78}$$

where $\mathbf{Q}_r$ and $\mathbf{R}_r$ comes from the constraints until level r, while $\tilde{\mathbf{Q}}_{r+1}$ and $\tilde{\mathbf{R}}_{r+1}$ comes from the constraints at current level, $r+1$. In a more practical sense, the matrices $\mathbf{Q}_r$ and $\mathbf{R}_r$ identifies the actuated and non-actuated quasi-velocities at level r, respectively. If constraints are added to the model at level $r+1$ such that the number of actuated quasi-velocities decrease, then, the identification matrices should be updated as shown in Eq. (3.78), i.e., $\mathbf{Q}_{r+1}$ lose columns with respect to $\mathbf{Q}_r$ while the same amount of columns are added to $\mathbf{R}_{r+1}$, when compared to $\mathbf{R}_r$.

Substituting Eqs. (3.77) and (3.78) into (3.76) and applying the Gauss's principle, we get:

$$\begin{aligned}\begin{bmatrix}\mathbf{A}_r\\ \tilde{\mathbf{A}}_{r+1}\end{bmatrix}\delta\mathbf{a}_{r+1} &= \mathbf{0},\\ &= \begin{bmatrix}\mathbf{A}_r\\ \tilde{\mathbf{A}}_{r+1}\end{bmatrix}\mathbf{Q}_{r+1}\delta\mathbf{a}^{\#}_{r+1} + \begin{bmatrix}\mathbf{A}_r\\ \tilde{\mathbf{A}}_{r+1}\end{bmatrix}\mathbf{R}_{r+1}\delta\mathbf{a}^{*}_{r+1} = \mathbf{0},\\ &= \begin{bmatrix}\mathbf{A}_r\\ \tilde{\mathbf{A}}_{r+1}\end{bmatrix}\mathbf{Q}_r\tilde{\mathbf{Q}}_{r+1}\delta\mathbf{a}^{\#}_{r+1} + \begin{bmatrix}\mathbf{A}_r\\ \tilde{\mathbf{A}}_{r+1}\end{bmatrix}\begin{bmatrix}\mathbf{R}_r & \tilde{\mathbf{R}}_{r+1}\end{bmatrix}\delta\mathbf{a}^{*}_{r+1} = \mathbf{0}.\end{aligned} \tag{3.79}$$

Let $\mathbf{a}^{*}_{r+1} = \left[\left(\mathbf{a}^{*\mathsf{T}}_{r}\right)^{\mathsf{T}}, \left(\tilde{\mathbf{a}}^{*}_{r+1}\right)^{\mathsf{T}}\right]^{\mathsf{T}}$. Eq. (3.79) can be rewritten as:

$$\mathbf{A}_r\mathbf{R}_r\delta\mathbf{a}^{*}_{r} = -\mathbf{A}_r\left(\mathbf{Q}_r\tilde{\mathbf{Q}}_{r+1}\delta\mathbf{a}^{\#}_{r+1} + \tilde{\mathbf{R}}_{r+1}\delta\tilde{\mathbf{a}}^{*}_{r+1}\right), \tag{3.80}$$

$$\tilde{\mathbf{A}}_{r+1}\mathbf{R}_r\delta\mathbf{a}^{*}_{r} + \tilde{\mathbf{A}}_{r+1}\tilde{\mathbf{R}}_{r+1}\delta\tilde{\mathbf{a}}^{*}_{r+1} = -\tilde{\mathbf{A}}_{r+1}\mathbf{Q}_r\tilde{\mathbf{Q}}_{r+1}\delta\mathbf{a}^{\#}_{r+1}. \tag{3.81}$$

Solving Eq. (3.81) for $\delta\tilde{\mathbf{a}}_{r+1}$, we get:

$$\delta\tilde{\mathbf{a}}^{*}_{r+1} = -\left(\tilde{\mathbf{A}}_{r+1}\mathbf{S}_r\tilde{\mathbf{R}}_{r+1}\right)^{\mathrm{g}}\tilde{\mathbf{A}}_{r+1}\mathbf{S}_r\mathbf{Q}_{r+1}\delta\mathbf{a}^{\#}_{r+1}, \tag{3.82}$$

where $\left(\tilde{\mathbf{A}}_{r+1}\mathbf{S}_r\tilde{\mathbf{R}}_{r+1}\right)^{\mathrm{g}}$ is any $\{1,4\}$-inverse of $\tilde{\mathbf{A}}_{r+1}\mathbf{S}_r\tilde{\mathbf{R}}_{r+1}$.

Substituting Eq. (3.82) into (3.80) and solving for $\delta\mathbf{a}^{*}_{r}$, results in:

$$\delta\mathbf{a}^{*}_{r} = -\left(\mathbf{A}_r\mathbf{R}_r\right)^{\mathrm{g}}\mathbf{A}_r\left(\mathbf{Q}_r\tilde{\mathbf{Q}}_{r+1}\delta\mathbf{a}^{\#}_{r+1} - \tilde{\mathbf{R}}_{r+1}\left(\tilde{\mathbf{A}}_{r+1}\mathbf{S}_r\tilde{\mathbf{R}}_{r+1}\right)^{\mathrm{g}}\tilde{\mathbf{A}}_{r+1}\mathbf{S}_r\mathbf{Q}_r\tilde{\mathbf{Q}}_{r+1}\delta\mathbf{a}^{\#}_{r+1}\right), \tag{3.83}$$

with $\left(\mathbf{A}_r\mathbf{R}_r\right)^{\mathrm{g}}$ as any $\{1,4\}$-inverse of $\mathbf{A}_r\mathbf{R}_r$.

Gathering Eqs. (3.82) and (3.83), we obtain:

$$\begin{bmatrix}\delta\mathbf{a}^{*}_{r}\\ \delta\tilde{\mathbf{a}}^{*}_{r+1}\end{bmatrix} = \begin{bmatrix}-\left(\mathbf{A}_r\mathbf{R}_r\right)^{\mathrm{g}}\mathbf{A}_r\left(\mathbf{Q}_{r+1} - \tilde{\mathbf{R}}_{r+1}\left(\tilde{\mathbf{A}}_{r+1}\mathbf{S}_r\tilde{\mathbf{R}}_{r+1}\right)^{\mathrm{g}}\tilde{\mathbf{A}}_{r+1}\mathbf{S}_r\mathbf{Q}_{r+1}\right)\\ -\left(\tilde{\mathbf{A}}_{r+1}\mathbf{S}_r\tilde{\mathbf{R}}_{r+1}\right)^{\mathrm{g}}\tilde{\mathbf{A}}_{r+1}\mathbf{S}_r\mathbf{Q}_{r+1}\end{bmatrix}\delta\mathbf{a}^{\#}_{r+1}. \tag{3.84}$$

Substituting Eq. (3.84) into (3.79), we get:

$$
\begin{aligned}
\delta\mathbf{a}_{r+1} &= \mathbf{Q}_{r+1}\delta\mathbf{a}^{\#}_{r+1} - \mathbf{R}_r\left(\mathbf{A}_r\mathbf{R}_r\right)^{\mathrm{g}}\tilde{\mathbf{A}}_r\left(\mathbf{Q}_{r+1} + \ldots\right.\\
&\left.-\tilde{\mathbf{R}}_{r+1}\left(\tilde{\mathbf{A}}_{r+1}\mathbf{S}_r\tilde{\mathbf{R}}_{r+1}\right)^{\mathrm{g}}\tilde{\mathbf{A}}_{r+1}\mathbf{S}_r\mathbf{Q}_{r+1}\right)\delta\mathbf{a}^{\#}_{r+1} - \tilde{\mathbf{R}}_{r+1}\left(\tilde{\mathbf{A}}_{r+1}\mathbf{S}_r\tilde{\mathbf{R}}_{r+1}\right)^{\mathrm{g}}\tilde{\mathbf{A}}_{r+1}\mathbf{S}_r\mathbf{Q}_{r+1}\delta\mathbf{a}^{\#}_{r+1},\\
&= \left(\mathbf{I} - \mathbf{A}^{\mathrm{g}}_r\mathbf{A}_r\left(\mathbf{I} - \tilde{\mathbf{R}}_{r+1}\left(\tilde{\mathbf{A}}_{r+1}\mathbf{S}_r\tilde{\mathbf{R}}_{r+1}\right)^{\mathrm{g}}\tilde{\mathbf{A}}_{r+1}\mathbf{S}_r\right)\mathbf{Q}_{r+1} + \ldots\right.\\
&\left.-\tilde{\mathbf{R}}_{r+1}\left(\tilde{\mathbf{A}}_{r+1}\mathbf{S}_r\tilde{\mathbf{R}}_{r+1}\right)^{\mathrm{g}}\tilde{\mathbf{A}}_{r+1}\mathbf{S}_r\right)\mathbf{Q}_{r+1}\delta\mathbf{a}^{\#}_{r+1},\\
&= \left(\mathbf{I} - \mathbf{A}^{\mathrm{g}}_r\mathbf{A}_r + \left(\mathbf{A}^{\mathrm{g}}_r\mathbf{A}_r - \mathbf{I}\right)\tilde{\mathbf{R}}_{r+1}\left(\tilde{\mathbf{A}}_{r+1}\mathbf{S}_r\tilde{\mathbf{R}}_{r+1}\right)^{\mathrm{g}}\tilde{\mathbf{A}}_{r+1}\mathbf{S}_r\right)\mathbf{Q}_{r+1}\delta\mathbf{a}^{\#}_{r+1},\\
&= \left(\mathbf{I} - \mathbf{A}^{\mathrm{g}}_r\mathbf{A}_r\right)\left(\mathbf{I} - \tilde{\mathbf{R}}_{r+1}\left(\tilde{\mathbf{A}}_{r+1}\mathbf{S}_r\tilde{\mathbf{R}}_{r+1}\right)^{\mathrm{g}}\tilde{\mathbf{A}}_{r+1}\mathbf{S}_r\right)\mathbf{Q}_{r+1}\delta\mathbf{a}^{\#}_{r+1},\\
&= \mathbf{S}_r\left(\mathbf{I} - \left(\tilde{\mathbf{A}}_{r+1}\mathbf{S}_r\right)^{\mathrm{g}}\tilde{\mathbf{A}}_{r+1}\mathbf{S}_r\right)\mathbf{Q}_{r+1}\delta\mathbf{a}^{\#}_{r+1},\\
&= \mathbf{S}_r\tilde{\mathbf{S}}_{r+1}\mathbf{Q}_{r+1}\delta\mathbf{a}^{\#}_{r+1},\\
&= \mathbf{S}_{r+1}\mathbf{Q}_{r+1}\delta\mathbf{a}^{\#}_{r+1},\\
&= \mathbf{E}_{r+1}\delta\mathbf{a}^{\#}_{r+1},\\
&= \mathbf{E}_r\tilde{\mathbf{E}}_{r+1}\delta\mathbf{a}^{\#}_{r+1},
\end{aligned}
\tag{3.85}
$$

where

$$
\begin{aligned}
\mathbf{A}^{\mathrm{g}}_r &= \mathbf{R}_r\left(\mathbf{A}_r\mathbf{R}_r\right)^{\mathrm{g}},\\
\left(\tilde{\mathbf{A}}_{r+1}\mathbf{S}_r\right)^{\mathrm{g}} &= \tilde{\mathbf{R}}_{r+1}\left(\tilde{\mathbf{A}}_{r+1}\mathbf{S}_r\tilde{\mathbf{R}}_{r+1}\right)^{\mathrm{g}},\\
\mathbf{S}_r &= \mathbf{I} - \mathbf{A}^{\mathrm{g}}_r\mathbf{A}_r = \mathbf{I} - \mathbf{R}_r\left(\mathbf{A}_r\mathbf{R}_r\right)^{\mathrm{g}}\mathbf{A}_r,\\
\tilde{\mathbf{S}}_{r+1} &= \mathbf{I} - \left(\tilde{\mathbf{A}}_{r+1}\mathbf{S}_r\right)^{\mathrm{g}}\tilde{\mathbf{A}}_{r+1}\mathbf{S}_r = \mathbf{I} - \tilde{\mathbf{R}}_{r+1}\left(\tilde{\mathbf{A}}_{r+1}\mathbf{S}_r\tilde{\mathbf{R}}_{r+1}\right)^{\mathrm{g}}\tilde{\mathbf{A}}_{r+1}\mathbf{S}_r,\\
\mathbf{S}_{r+1} &= \mathbf{S}_r\tilde{\mathbf{S}}_{r+1},\\
\mathbf{E}_r &= \left(\mathbf{I} - \mathbf{R}_r\left(\mathbf{A}_r\mathbf{R}_r\right)^{\mathrm{g}}\mathbf{A}_r\right)\mathbf{Q}_r,\\
\tilde{\mathbf{E}}_{r+1} &= \left(\mathbf{I} - \mathbf{Q}_r^{\mathsf{T}}\tilde{\mathbf{R}}_{r+1}\left(\tilde{\mathbf{A}}_{r+1}\mathbf{E}_r\mathbf{Q}_r^{\mathsf{T}}\tilde{\mathbf{R}}_{r+1}\right)^{\mathrm{g}}\tilde{\mathbf{A}}_{r+1}\mathbf{S}_r\right)\tilde{\mathbf{Q}}_{r+1},
\end{aligned}
\tag{3.86}
$$

which are the recursive expressions to calculate the orthogonal complement[5].

Gathering the Eqs. (3.60)–(3.86), the following algorithm arises.

[5]The detailed derivation of the expressions presented in Eq. (3.86) can be seen in Appendix A.1

Algorithm 1. (Modular EoMs): Considering the relaxed model of Eq. (3.60) and the relations of (3.74), the present algorithm can be applied to obtain the constrained EoMs of $\mathcal{S}$.

(a) Initialize at $r = 0$:

$$\mathbf{M} = \mathbf{M}(\boldsymbol{\eta});\ \mathbf{C} = \mathbf{C}(\boldsymbol{\nu});\ \mathbf{D} = \mathbf{D}(\boldsymbol{\nu}),$$
$$\mathbf{g} = \mathbf{g}(\boldsymbol{\eta});\ \boldsymbol{\tau} = \boldsymbol{\tau}(\boldsymbol{\eta});\ \mathbf{d} = \mathbf{d}(\boldsymbol{\eta}, \boldsymbol{\nu});\ \mathbf{S}_0 = \mathbf{I}.$$

(b) For $r = 0, \ldots, s-1$, do:

$$\tilde{\mathbf{A}}_{r+1} = \tilde{\mathbf{A}}_{r+1}(t, \boldsymbol{\eta}),$$
$$\tilde{\mathbf{S}}_{r+1},\ \text{such that,}\ \left(\tilde{\mathbf{A}}_{r+1}\mathbf{S}_r\right)\tilde{\mathbf{S}}_{r+1} = \mathbf{0},$$
$$\mathbf{M}_{r+1} = \tilde{\mathbf{S}}_{r+1}^{\mathsf{T}}\mathbf{M}_r\tilde{\mathbf{S}}_{r+1},$$
$$\mathbf{C}_{r+1} = \tilde{\mathbf{S}}_{r+1}^{\mathsf{T}}\mathbf{C}_r\tilde{\mathbf{S}}_{r+1} + \tilde{\mathbf{S}}_{r+1}^{\mathsf{T}}\mathbf{M}_r\dot{\tilde{\mathbf{S}}}_{r+1},$$
$$\mathbf{D}_{r+1} = \tilde{\mathbf{S}}_{r+1}^{\mathsf{T}}\mathbf{D}_r\tilde{\mathbf{S}}_{r+1},$$
$$\mathbf{g}_{r+1} = \tilde{\mathbf{S}}_{r+1}^{\mathsf{T}}\mathbf{g}_r,$$
$$\boldsymbol{\tau}_{r+1} = \tilde{\mathbf{S}}_{r+1}^{\mathsf{T}}\boldsymbol{\tau}_r,$$
$$\mathbf{d}_{r+1} = \tilde{\mathbf{S}}_{r+1}^{\mathsf{T}}\mathbf{d}_r.$$

(c) For $r = s$, compute the quasi-accelerations:

$$\dot{\boldsymbol{\zeta}}_s = \mathbf{M}_s^{-1}\left(\boldsymbol{\tau}_s + \mathbf{d}_s - \mathbf{C}_s\boldsymbol{\zeta}_s - \mathbf{D}_s\boldsymbol{\zeta}_s - \mathbf{g}_s\right).$$

(d) Propagate the model through numerical integration:

$$\dot{\boldsymbol{\xi}} = \boldsymbol{\phi}\left(\boldsymbol{\xi}, \boldsymbol{\zeta}\right),$$
$$\dot{\boldsymbol{\zeta}} = \dot{\boldsymbol{\zeta}}_s.$$

where $\boldsymbol{\phi}$ is the generalized velocities function.

3.2 MODEL VALIDATION

To validate the modeling approach some experiments reported in early works are reproduced through numerical simulations.

3.2.1 Experiments by Sharma and Saha (2019)

The first experiments reproduced are the ones of Sharma and Saha (2019), which consists of the free-falling test of underwater pendulums as shown in Fig. 21.

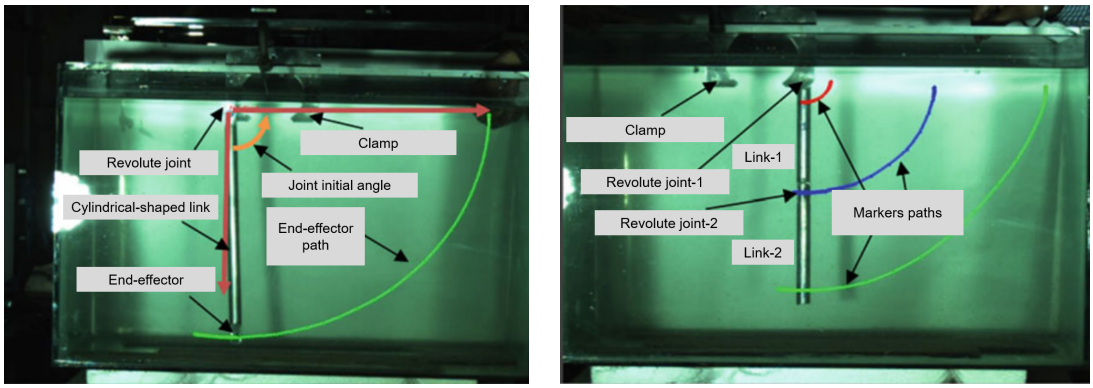

(a): Single pendulum (b): Double pendulum

Figure 21: Experiments performed by Sharma and Saha (2019)

The schematic diagram of the mathematical model used to reproduce the experiments and the adapted modeling hierarchy are shown in Fig. 22. The independent coordinates used in the comparison are indicated in Fig. 22 (a). The modeling is performed considering the mathematical model of an underwater body on the vertical plane presented by Fossen (1996) with the modified versions of the added mass and hydrodynamic damping matrices for the manipulator links (see Subsecs. 3.1.4.1 and 3.1.4.3) on the lowest level of the modeling hierarchy. In the modeling hierarchy of Fig. 22 (b), $\mathcal{G}$ is the ground, body A_1 is the first link, body A_2 is the second link, subsystem $\mathcal{S}_1$ is the underwater inverted pendulum subsystem and system $\mathcal{S}$ is the underwater double pendulum system. Passive revolute joints (with circles) connects the first link with the ground and the second link with the first one. At level 1, the constraints between the first link and ground are imposed. The model obtained in this level corresponds to the model of the first experiment with a single link underwater pendulum. Then, at the level 2, the constraints between the first and second links are imposed and the model of the second experiment is obtained.

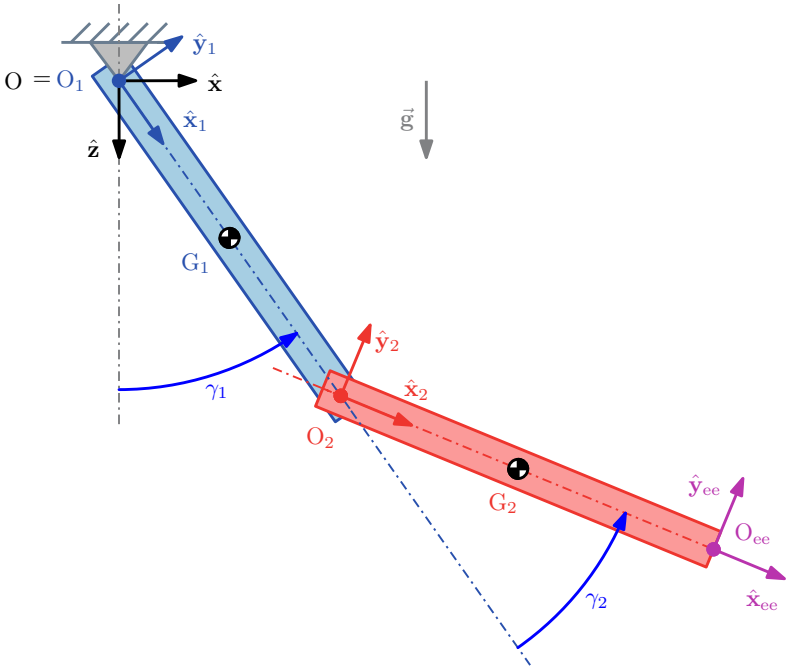

(a): Double pendulum schematic diagram

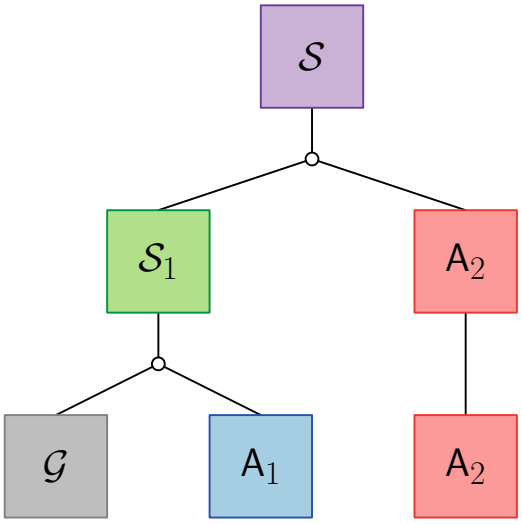

(b): Modeling hierarchy

Figure 22: Underwater double pendulum model

To demonstrate the modeling procedure, the terms of the relaxed model of the double pendulum are given below:

$$\begin{aligned}
\mathbf{J} &= \text{blkdiag}\left(\mathbf{J}_1, \mathbf{J}_2\right), \\
\mathbf{M} &= \text{blkdiag}\left(\mathbf{M}_1, \mathbf{M}_2\right), \\
\mathbf{C} &= \text{blkdiag}\left(\mathbf{C}_1, \mathbf{C}_2\right), \\
\mathbf{D} &= \text{blkdiag}\left(\mathbf{D}_1, \mathbf{D}_2\right), \\
\boldsymbol{\eta} &= \left[\boldsymbol{\eta}_1^\mathsf{T}, \boldsymbol{\eta}_2^\mathsf{T}\right]^\mathsf{T}, \\
\boldsymbol{\nu} &= \left[\boldsymbol{\nu}_1^\mathsf{T}, \boldsymbol{\nu}_2^\mathsf{T}\right]^\mathsf{T}, \\
\mathbf{g} &= \left[\mathbf{g}_1^\mathsf{T}, \mathbf{g}_2^\mathsf{T}\right]^\mathsf{T}, \\
\mathbf{d} &= \left[\mathbf{d}_1^\mathsf{T}, \mathbf{d}_2^\mathsf{T}\right]^\mathsf{T}, \\
\boldsymbol{\tau} &= \left[\boldsymbol{\tau}_1^\mathsf{T}, \boldsymbol{\tau}_2^\mathsf{T}\right]^\mathsf{T},
\end{aligned} \tag{3.87}$$

where $\boldsymbol{\eta}_i = [x_i, z_i, \theta_i]^\mathsf{T}$, $\boldsymbol{\nu}_i = [u_i, w_i, q_i]^\mathsf{T}$ and $\mathbf{d}_i = \boldsymbol{\tau}_i = \mathbf{0}$ $(i = 1, 2)$.

The constraints equations at the levels 1 and 2 and are written as:

$$\begin{aligned}
\boldsymbol{\varphi}_1\left(\boldsymbol{\eta}, t\right) &= \begin{bmatrix} x_1 - l_1 \cos\left(\theta_1\right) \\ z_1 + l_1 \sin\left(\theta_1\right) \end{bmatrix} = \mathbf{0}, \\
\boldsymbol{\varphi}_2\left(\boldsymbol{\eta}, t\right) &= \begin{bmatrix} x_1 + l_1 \cos\left(\theta_1\right) - \left(x_2 - l_2 \cos\left(\theta_2\right)\right) \\ z_1 - l_1 \sin\left(\theta_1\right) - \left(z_2 + l_2 \sin\left(\theta_2\right)\right) \end{bmatrix} = \mathbf{0}.
\end{aligned} \tag{3.88}$$

Their respective Jacobian matrices follows:

$$\begin{aligned}
\frac{\partial \boldsymbol{\varphi}_1}{\partial \boldsymbol{\eta}} &= \begin{bmatrix} 1 & 0 & l_1 \sin\left(\theta_1\right) & 0 & 0 & 0 \\ 0 & 1 & -l_1 \sin\left(\theta_1\right) & 0 & 0 & 0 \end{bmatrix}, \\
\frac{\partial \boldsymbol{\varphi}_2}{\partial \boldsymbol{\eta}} &= \begin{bmatrix} 1 & 0 & -l_1 \sin\left(\theta_1\right) & -1 & 0 & -l_2 \sin\left(\theta_2\right) \\ 0 & 1 & -l_1 \cos\left(\theta_1\right) & 0 & -1 & -l_2 \cos\left(\theta_2\right) \end{bmatrix}.
\end{aligned} \tag{3.89}$$

The identification matrices are given by:

$$\mathbf{Q} = \mathbf{Q}_1 \tilde{\mathbf{Q}}_2 = \begin{bmatrix} 0 & 0 \\ 0 & 0 \\ 1 & 0 \\ 0 & 0 \\ 0 & 0 \\ 0 & 1 \end{bmatrix}; \quad \mathbf{Q}_1 = \begin{bmatrix} 0 & 0 & 0 & 0 \\ 0 & 0 & 0 & 0 \\ 1 & 0 & 0 & 0 \\ 0 & 1 & 0 & 0 \\ 0 & 0 & 1 & 0 \\ 0 & 0 & 0 & 1 \end{bmatrix}; \quad \tilde{\mathbf{Q}}_2 = \mathbf{Q}_1^\mathsf{g} \mathbf{Q} = \begin{bmatrix} 1 & 0 \\ 0 & 0 \\ 0 & 0 \\ 0 & 1 \end{bmatrix}, \tag{3.90}$$

and

$$\mathbf{R} = \begin{bmatrix} \mathbf{R}_1 & \tilde{\mathbf{R}}_2 \end{bmatrix} = \left[\begin{array}{cc|cc} 1 & 0 & 0 & 0 \\ 0 & 1 & 0 & 0 \\ 0 & 0 & 0 & 0 \\ 0 & 0 & 1 & 0 \\ 0 & 0 & 0 & 1 \\ 0 & 0 & 0 & 0 \end{array}\right]. \tag{3.91}$$

With $\mathbf{A}_1 = \dfrac{\partial \boldsymbol{\varphi}_1}{\partial \boldsymbol{\eta}}\mathbf{J}$, $\mathbf{Q}_1$ and $\mathbf{R}_1$ the terms of the EoMs at level 1 are:

$$\begin{aligned} \mathbf{S}_1 &= \mathbf{I} - \mathbf{R}_1 \left(\mathbf{A}_1\mathbf{R}_1\right)^{\mathrm{g}} \mathbf{A}_1, \\ \mathbf{M}_1 &= \mathbf{S}_1^{\mathsf{T}}\mathbf{M}\mathbf{S}_1, \\ \mathbf{C}_1 &= \mathbf{S}_1^{\mathsf{T}}\mathbf{C}\mathbf{S}_1 + \mathbf{S}_1^{\mathsf{T}}\mathbf{M}\dot{\mathbf{S}}_1, \\ \mathbf{D}_1 &= \mathbf{S}_1^{\mathsf{T}}\mathbf{D}\mathbf{S}_1, \\ \mathbf{g}_1 &= \mathbf{S}_1^{\mathsf{T}}\mathbf{g}, \\ \boldsymbol{\tau}_1 &= \mathbf{S}_1^{\mathsf{T}}\boldsymbol{\tau}, \\ \mathbf{d}_1 &= \mathbf{S}_1^{\mathsf{T}}\mathbf{d}. \end{aligned} \tag{3.92}$$

Next, with $\tilde{\mathbf{A}}_2 = \dfrac{\partial \boldsymbol{\varphi}_2}{\partial \boldsymbol{\eta}}\mathbf{J}$, $\tilde{\mathbf{Q}}_2$ and $\tilde{\mathbf{R}}_2$ the terms of the EoMs[6] at level 2 are:

$$\begin{aligned} \tilde{\mathbf{S}}_2 &= \mathbf{I} - \tilde{\mathbf{R}}_2 \left(\tilde{\mathbf{A}}_2\mathbf{S}_1\tilde{\mathbf{R}}_2\right)^{\mathrm{g}} \tilde{\mathbf{A}}_2\mathbf{S}_1, \\ \mathbf{M}_2 &= \tilde{\mathbf{S}}_2^{\mathsf{T}}\mathbf{M}_1\tilde{\mathbf{S}}_2, \\ \mathbf{C}_2 &= \tilde{\mathbf{S}}_2^{\mathsf{T}}\mathbf{C}_1\tilde{\mathbf{S}}_2 + \tilde{\mathbf{S}}_2^{\mathsf{T}}\mathbf{M}_1\dot{\tilde{\mathbf{S}}}_2, \\ \mathbf{D}_2 &= \tilde{\mathbf{S}}_2^{\mathsf{T}}\mathbf{D}_1\tilde{\mathbf{S}}_2, \\ \mathbf{g}_2 &= \tilde{\mathbf{S}}_2^{\mathsf{T}}\mathbf{g}_1, \\ \boldsymbol{\tau}_2 &= \tilde{\mathbf{S}}_2^{\mathsf{T}}\boldsymbol{\tau}_1, \\ \mathbf{d}_2 &= \tilde{\mathbf{S}}_2^{\mathsf{T}}\mathbf{d}_1. \end{aligned} \tag{3.93}$$

The numerical simulations were conducted in MATLAB/Simulink® environment by integrating the dynamic model in a state-space form with the `ode8` function using a time step of 0.001 s. The parameters used in the simulations are shown in Tabs. 1 and 2. The initial states used in the simulations are indicated in Sharma and Saha (2019). The relations between the absolute

[6]The EoMs can also be obtained recursively with matrices $\mathbf{E}_r$ and $\tilde{\mathbf{E}}_{r+1}$ ($r = 0, 1, \ldots, s-1$) instead of $\mathbf{S}_r$ and $\tilde{\mathbf{S}}_{r+1}$. This modification will include $\mathbf{Q}_r$ and $\tilde{\mathbf{Q}}_{r+1}$ directly in the orthogonal complement, reducing the matrices size and the computational effort associated with its calculation.

angular coordinates used on the modeling and the relative ones are given by $\gamma_1 = \theta_1 + \pi/2$ and $\gamma_1 + \gamma_2 = \theta_2 + \pi/2$.

Table 1: Single pendulum parameters.

Symbols	Values	Units (SI)
$\mathbf{M}_{\mathrm{RB}}$	$\mathrm{diag}\,(0.3, 0.3, 0.004)$	$\mathrm{kg}, \mathrm{kgm}^2$
$C_{\mathrm{A,x}}, C_{\mathrm{A,y}}$	$0, 1$	–
W, B	$2.94, 0.13$	N
$C_{\mathrm{D,x}}, C_{\mathrm{D,y}}$	$0, 1.2$	–
$l_{\mathrm{O_2\vert O_1}}, d, \Delta l$	$0.4, 0.02, 0.04$	m
$\vec{\mathbf{p}}^{\,1}_{\mathrm{G_1\vert O_1}}$	$[0, 0.2, 0]^{\mathsf{T}}$	m
$\vec{\mathbf{p}}^{\,1}_{\mathrm{B_1\vert O_1}}$	$[0, 0.2, 0]^{\mathsf{T}}$	m

Table 2: Double pendulum parameters.

Symbols ($i = 1, 2$)	Values	Units (SI)
$\mathbf{M}_{\mathrm{RB},i}$	$\mathrm{diag}\,(0.17, 0.17, 0.0006)$	$\mathrm{kg}, \mathrm{kgm}^2$
$C_{\mathrm{A,x}_i}, C_{\mathrm{A,y}_i}$	$0, 1$	–
W_i, B_i	$1.66, 0.62$	N
$C_{\mathrm{D,x_1}}, C_{\mathrm{D,x_2}}, C_{\mathrm{D,y_1}}, C_{\mathrm{D,y_2}}$	$0, 0, 3.5, 1.3$	–
$l_{\mathrm{O}_{i+1}\vert\mathrm{O}_i}, D_i, \Delta l_i$	$0.2, 0.02, 0.02$	m
$\vec{\mathbf{p}}^{\,i}_{\mathrm{G}_i\vert\mathrm{O}_i}$	$[0, 0.1, 0]^{\mathsf{T}}$	m
$\vec{\mathbf{p}}^{\,i}_{\mathrm{B}_i\vert\mathrm{O}_i}$	$[0, 0.1, 0]^{\mathsf{T}}$	m

The comparison with the experimental results is shown by Figs. 23–25. Figure 23 shows the states in the single pendulum experiment. The end-effector path in the double pendulum experiment is shown in Fig. 24. The respective states are shown in Fig. 25. There is a good adherence between the experimental and the models results in all comparisons, which is achieved without parameters calibration. This is owed to the structure of the mathematical model that includes the most important dynamic effects.

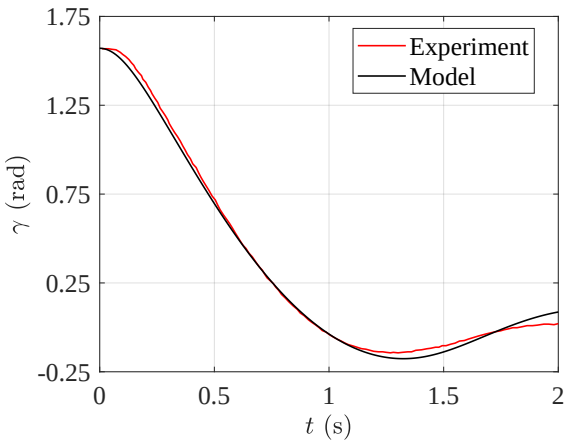

(a): Angular displacement

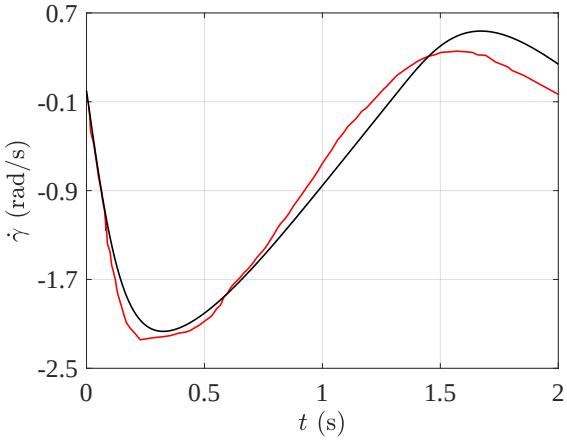

(b): Angular velocity

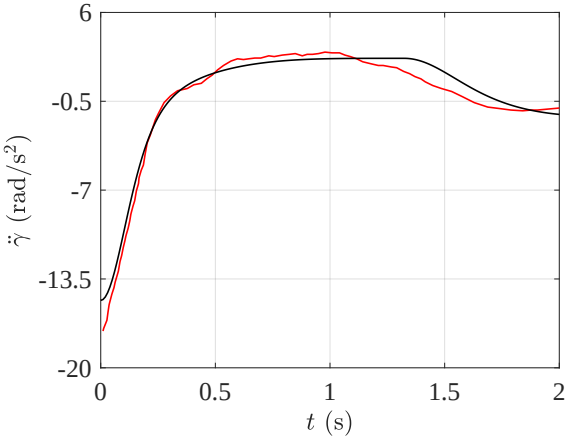

(c): Angular acceleration

Figure 23: Comparison with the underwater pendulum experiment

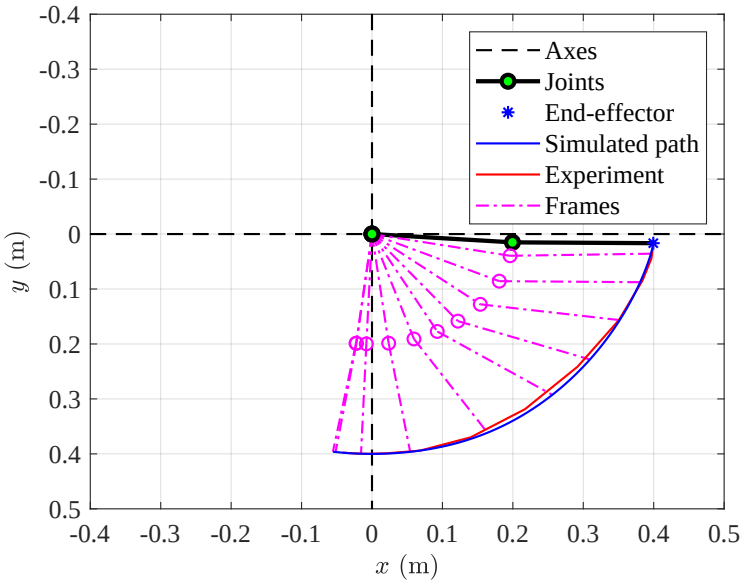

(a): First configuration

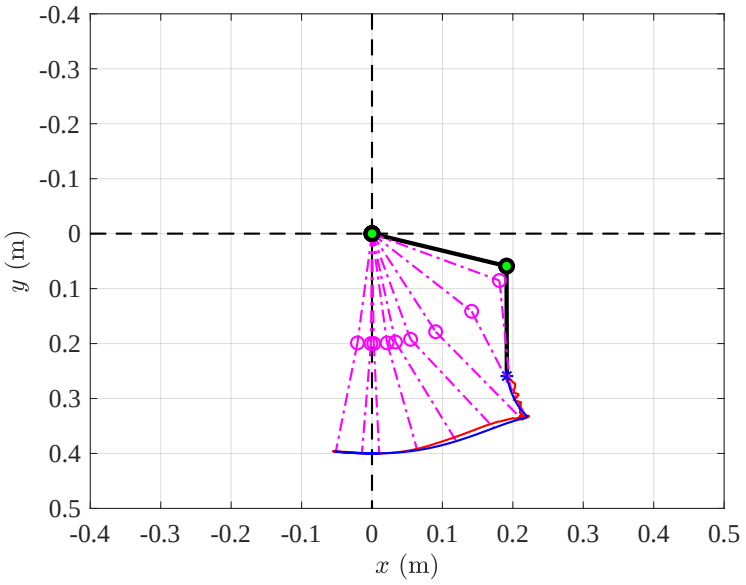

(b): Second configuration

Figure 24: End-effector path comparison during free fall motion

We will also use the underwater double pendulum to verify the added mass and drag forces models developed on Subsecs. 3.1.4.1 and 3.1.4.3, respectively. So, let us consider the double pendulum as a 2-link underwater manipulator, with reference trajectories given by (i) $\gamma_i = A_i \sin(\omega_i t)$ $(i = 1, 2)$ for the continuous velocity profile case, and (ii) $\gamma_1 = A_1 \sin(\omega_1 t)$,

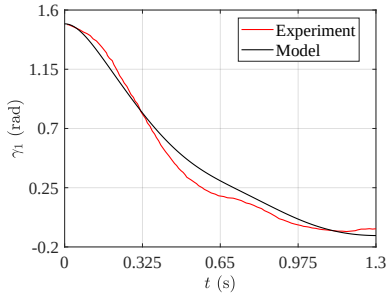

(a): Angular displacement of the 1-st joint

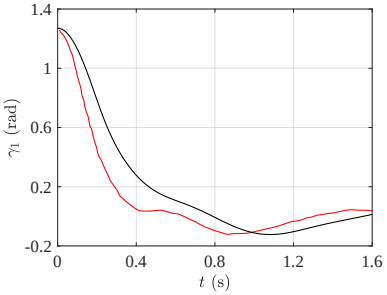

(e): Angular displacement of the 1-st joint

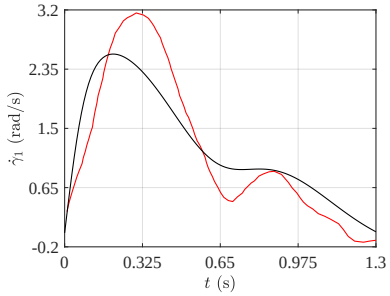

(b): Angular velocity of the 1-st joint

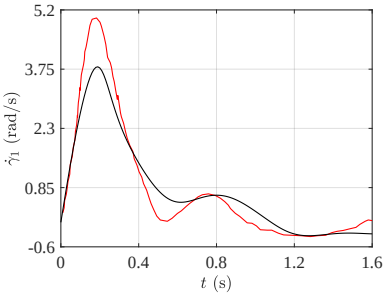

(f): Angular velocity of the 1-st joint

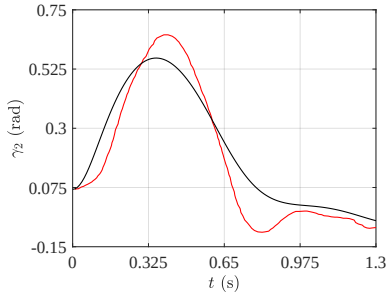

(c): Angular displacement of the 2-nd joint

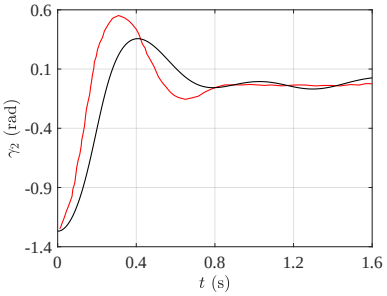

(g): Angular displacement of the 2-nd joint

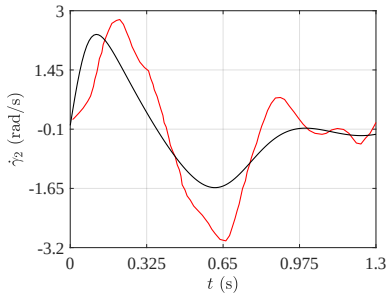

(d): Angular velocity of the 2-nd joint

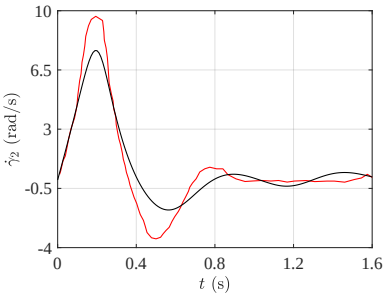

(h): Angular velocity of the 2-nd joint

(a)-(d): First configuration; (e)-(h): Second configuration

Figure 25: Comparison with the underwater double pendulum experiment

$\gamma_2 = A_2 \cos(\omega_2 t)$ for the discontinuous velocity profile case. In both case the trajectories parameters are given by $A_i = \pi/2$ rad and $\omega_i = 0.2\pi$ rad/s ($i = 1, 2$).

Figures 26-28 shows the results comparison of the proposed models with other ones from the literature. The added mass torque on each joint is shown by Fig. 26. As we can see, the continuous model early used by Tarn, Shoults and Yang (1996) and the discrete model developed by McLain and Rock (1998) present similar results. This is expected once these models do not consider the Coriolis and centrifugal effects induced by the added mass tensor, thus, treating it as a pure active force. On the other hand, the lumped model evaluated with the added mass tensor for high aspect ratio cylinders presented by Antonelli (2014) and the proposed one produce produces similar results. This is due to the fact that these models consider the Coriolis and centrifugal effects neglected by the other models. Moreover, once the proposed model is discrete, it can be calibrated to consider 3D flow effects on low aspect ratio cylinders.

Figure 27 shows the drag torque on each joint. We note that all the models produce similar results on the continuous velocity profile trajectory. However, on the discontinuous case, the model proposed by Sharma and Saha (2019) presents discontinuities on the torque profiles shown by Fig. 27 (b). These discontinuities are due to the hypothesis of continuous velocity profile adopted during the derivation of the model, as early commented. Also, the models of Tarn, Shoults and Yang (1996), McLain and Rock (1998) and the proposed one presented similar results on the discontinuous case too. A different behaviour is observed in Fig 28 when we compare the centers of drag calculated for each model, since the drag center calculated with the model of Sharma and Saha (2019) is continuous and the other ones are discontinuous. These results make sense once the model of Sharma and Saha (2019) does not capture the discontinuity on the velocity profile along the second link, resulting in the discontinuities on the joint torques. Moreover, the proposed model presents accurate results, comparable to the models of Tarn, Shoults and Yang (1996) and McLain and Rock (1998), while it is simple to implement, require no numerical integration or discretization, with a few number of algebraic computations.

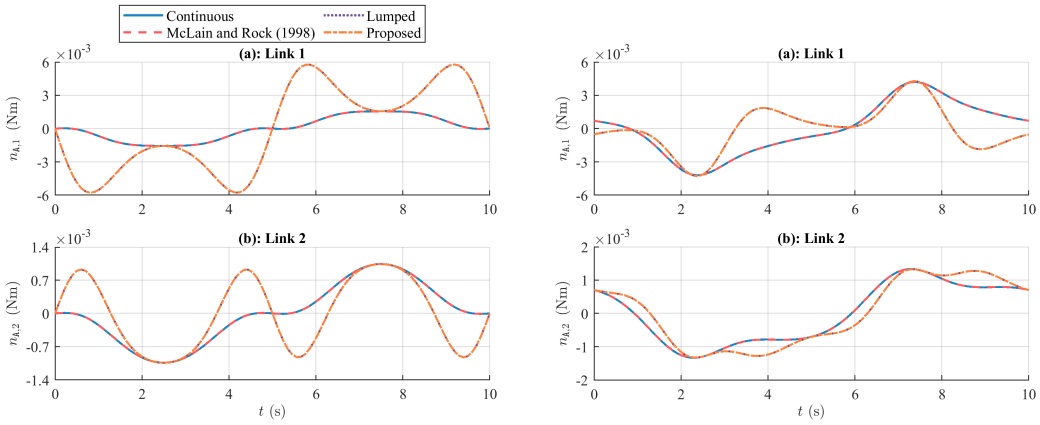

(a): First trajectory (b): Second trajectory

Figure 26: Manipulator added mass torques

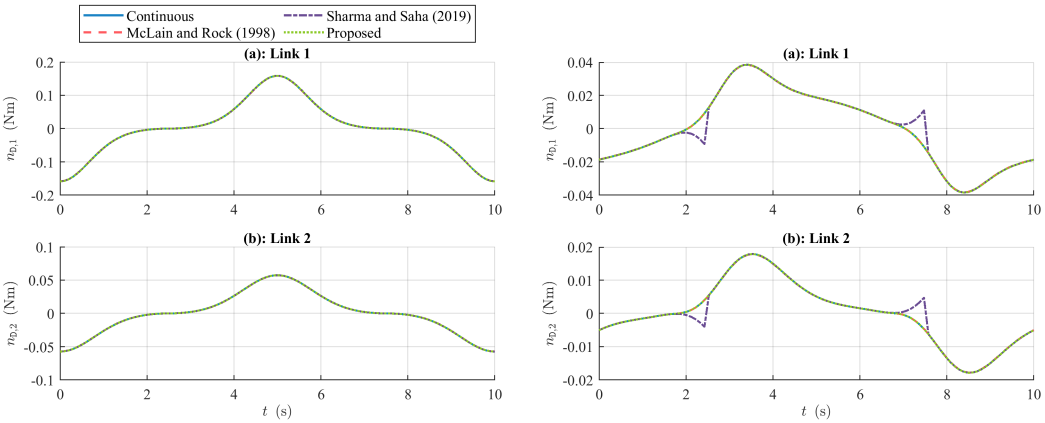

(a): First trajectory (b): Second trajectory

Figure 27: Manipulator drag torques

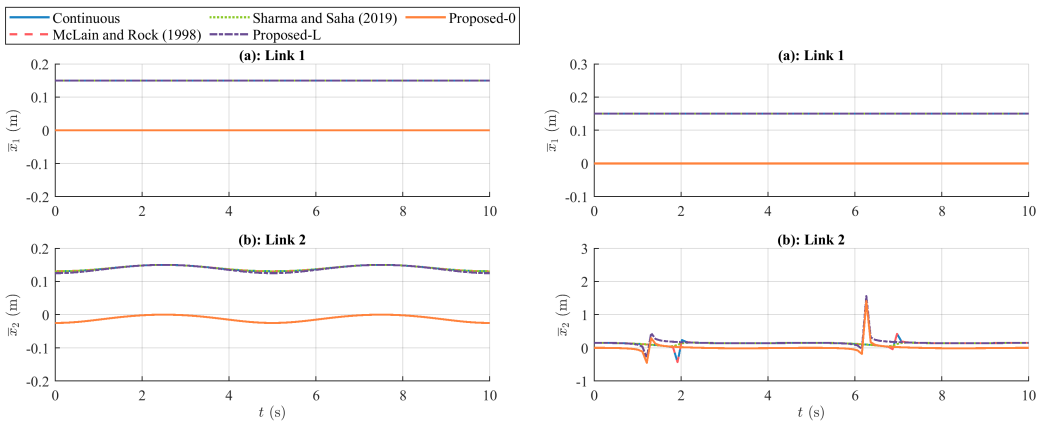

(a): First trajectory (b): Second trajectory

Figure 28: Manipulator drag centers with 0 and L referring to the lower and upper centers

3.2.2 Experiment by Sagara et al. (2001)

The second experiment reproduced here was made by Sagara et al. (2001) to verify the mathematical model developed for a UVMS. The objective was to reproduce the end-effector path of a 5-DoFs UVMS prototype generated by the rotation of the servo-controlled joints at a constant angular velocity. The idea is to verify if the mathematical model can reproduce the dynamic coupling effects between the floating base and manipulator observed in the experiment. The prototype and the experimental apparatus used by Sagara et al. (2001) in the experiments are shown in Fig. 29.

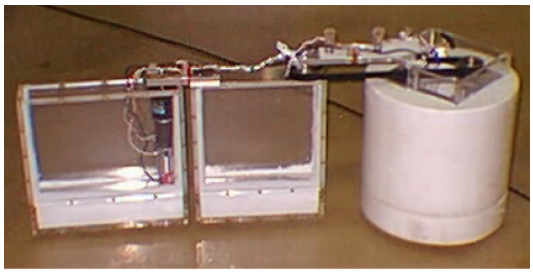

(a): 5-DoFs UVMS prototype

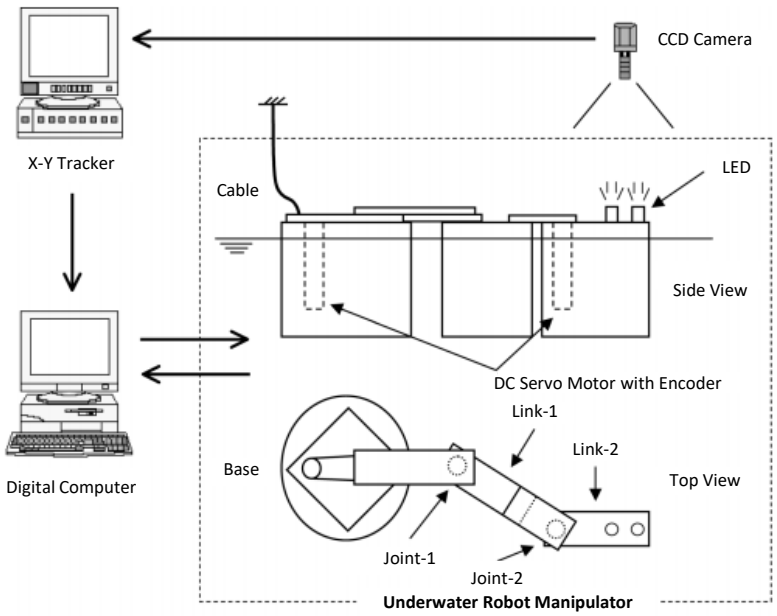

(b): Experimental apparatus

Figure 29: Prototype and experimental setup used by Sagara et al. (2001)

Figure 30 show the schematic diagram of the mathematical model and the modeling hierarchy adopted, composed on only two levels. Fig. 30 (a) show the independent coordinates used in the comparison. At the lowest level of the modeling hierarchy in Fig. 30 (b) is used the model of an underwater body on the horizontal plane presented by Fossen (1996) with the modified versions of the added mass and hydrodynamic damping matrices for the manipulators links. In the modeling hierarchy of Fig. 30 (b), body A is the AUV, bodies B_i ($i = 1, 2$) are the manipulator links and system $\mathcal{S}$ is the 5-DoFs UVMS. Active revolute joints (grey circles) connects the first link with the AUV and the second link with the first one. At level 1, the constraints between the joints are imposed and the mathematical model of the experiment is obtained.

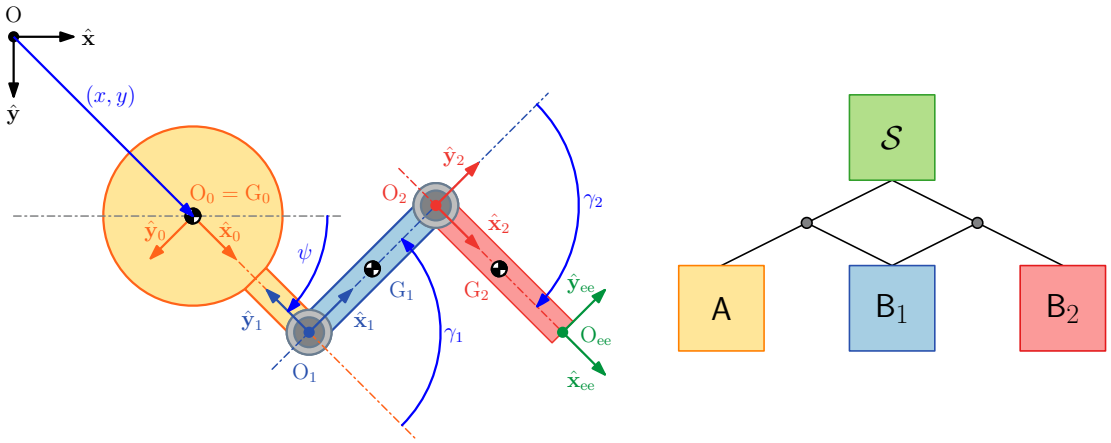

(a): 5-DoFs UVMS schematic diagram (b): Modeling hierarchy

Figure 30: 5-DoFs UVMS prototype model

The terms of the relaxed model of the 5-DoFs UVMS prototype are given below:

$$
\begin{aligned}
\mathbf{J} &= \text{blkdiag}\left(\mathbf{J}_0, \mathbf{J}_1, \mathbf{J}_2\right), \\
\mathbf{M} &= \text{blkdiag}\left(\mathbf{M}_0, \mathbf{M}_1, \mathbf{M}_2\right), \\
\mathbf{C} &= \text{blkdiag}\left(\mathbf{C}_0, \mathbf{C}_1, \mathbf{C}_2\right), \\
\mathbf{D} &= \text{blkdiag}\left(\mathbf{D}_0, \mathbf{D}_1, \mathbf{D}_2\right), \\
\boldsymbol{\eta} &= \left[\boldsymbol{\eta}_0^{\mathsf{T}}, \boldsymbol{\eta}_1^{\mathsf{T}}, \boldsymbol{\eta}_2^{\mathsf{T}}\right]^{\mathsf{T}}, \\
\boldsymbol{\nu} &= \left[\boldsymbol{\nu}_0^{\mathsf{T}}, \boldsymbol{\nu}_1^{\mathsf{T}}, \boldsymbol{\nu}_2^{\mathsf{T}}\right]^{\mathsf{T}}, \\
\mathbf{g} &= \left[\mathbf{g}_0^{\mathsf{T}}, \mathbf{g}_1^{\mathsf{T}}, \mathbf{g}_2^{\mathsf{T}}\right]^{\mathsf{T}}, \\
\mathbf{d} &= \left[\mathbf{d}_0^{\mathsf{T}}, \mathbf{d}_1^{\mathsf{T}}, \mathbf{d}_2^{\mathsf{T}}\right]^{\mathsf{T}}, \\
\boldsymbol{\tau} &= \left[\boldsymbol{\tau}_0^{\mathsf{T}}, \boldsymbol{\tau}_1^{\mathsf{T}}, \boldsymbol{\tau}_2^{\mathsf{T}}\right]^{\mathsf{T}},
\end{aligned}
\tag{3.94}
$$

where $\boldsymbol{\eta}_i = [x_i, y_i, \psi_i]^{\mathsf{T}}$, $\boldsymbol{\nu}_i = [u_i, v_i, r_i]^{\mathsf{T}}$ and $\mathbf{d}_i = \mathbf{0}$ ($i = 0, 1, 2$), while $\boldsymbol{\tau}_0 = \mathbf{0}$, $\boldsymbol{\tau}_1 = [0, 0, \tau_1]^{\mathsf{T}}$ and

$\boldsymbol{\tau}_2 = [0, 0, \tau_2]^\mathsf{T}$, with τ_1 and τ_2 being the motor torques of the first and second revolute joints, respectively.

The constraints equations are written as:

$$\boldsymbol{\varphi}(\boldsymbol{\eta}, t) = \begin{bmatrix} x_0 + l_0\cos(\psi_0) - (x_1 - l_1\cos(\psi_1)) \\ y_0 + l_0\sin(\psi_0) - (y_1 - l_1\sin(\psi_1)) \\ x_1 + l_1\cos(\psi_1) - (x_2 - l_2\cos(\psi_2)) \\ y_1 + l_1\sin(\psi_1) - (y_2 - l_2\sin(\psi_2)) \end{bmatrix} = \mathbf{0}. \tag{3.95}$$

Their Jacobian matrix follows:

$$\frac{\partial \boldsymbol{\varphi}}{\partial \boldsymbol{\eta}} = \begin{bmatrix} 1 & 0 & -l_0\sin(\psi_0) & -1 & 0 & -l_1\sin(\psi_1) & 0 & 0 & 0 \\ 0 & 1 & l_0\cos(\psi_0) & 0 & -1 & l_1\cos(\psi_1) & 0 & 0 & 0 \\ 0 & 0 & 0 & 1 & 0 & -l_1\sin(\psi_1) & -1 & 0 & -l_2\sin(\psi_2) \\ 0 & 0 & 0 & 0 & 1 & l_1\cos(\psi_1) & 0 & -1 & l_2\cos(\psi_2) \end{bmatrix}. \tag{3.96}$$

The identification matrices are given by:

$$\mathbf{Q} = \begin{bmatrix} 1 & 0 & 0 & 0 & 0 \\ 0 & 1 & 0 & 0 & 0 \\ 0 & 0 & 1 & 0 & 0 \\ 0 & 0 & 0 & 0 & 0 \\ 0 & 0 & 0 & 0 & 0 \\ 0 & 0 & 0 & 1 & 0 \\ 0 & 0 & 0 & 0 & 0 \\ 0 & 0 & 0 & 0 & 0 \\ 0 & 0 & 0 & 0 & 1 \end{bmatrix}; \quad \mathbf{R} = \begin{bmatrix} 0 & 0 & 0 & 0 \\ 0 & 0 & 0 & 0 \\ 0 & 0 & 0 & 0 \\ 1 & 0 & 0 & 0 \\ 0 & 1 & 0 & 0 \\ 0 & 0 & 0 & 0 \\ 0 & 0 & 1 & 0 \\ 0 & 0 & 0 & 1 \\ 0 & 0 & 0 & 0 \end{bmatrix}. \tag{3.97}$$

With $\mathbf{A} = \dfrac{\partial \boldsymbol{\varphi}}{\partial \boldsymbol{\eta}}\mathbf{J}$, $\mathbf{Q}$ and $\mathbf{R}$ the terms of the constrained EoMs of the 5-DoFs UVMS prototype can be written similarly to the terms of the level 1 of the EoMs of the double pendulum.

A second-order transfer function with a PID controller is used in each manipulator joint to reproduce the servomotors dynamics. The simulations were done for different joints velocities. Two configurations are considered for the manipulators in the simulations: (i) the second joint is blocked and the first one rotates, and (ii) the first joint is blocked and the second one rotates. The numerical simulations are performed considering the setup presented before. The parameters used in the simulations are shown in Tab. 3. The relation between the absolute angular coordinates

used on the modeling and the relative ones are given by $\gamma_1 = \psi_0 - \psi_1$ and $\gamma_2 = \psi_1 - \psi_2$.

Table 3: 5-DoFs UVMS prototype parameters

Symbols ($i = 1, 2$)	Values	Units (SI)
$\mathbf{M}_{\mathrm{RB},0}$	diag $(31.72, 31.72, 0.41)$	kg, kgm^2
$\mathbf{M}_{\mathrm{RB},1}$	diag $(7.48, 7.48, 0.2)$	kg, kgm^2
$\mathbf{M}_{\mathrm{RB},2}$	diag $(9.68, 9.68, 0.37)$	kg, kgm^2
$\mathbf{M}_{\mathrm{A},0}$	diag $(48.26, 48.26, 0)$	kg, kgm^2
$C_{\mathrm{A},\mathrm{x}_i}, C_{\mathrm{A},\mathrm{y}_i}$	$0, 1$	–
$\mathbf{D}_0$	diag $(53.76, 53.76, 0)$	Ns/m, Nms
$C_{\mathrm{D},\mathrm{x}_i}, C_{\mathrm{D},\mathrm{y}_i}$	$0, 2$	–
$l_{\mathrm{O}_i\mathrm{O}_{i+1}}, D_0, H_i, \Delta l_i$	$0.30, 0.16, 0.30, 0.03$	m
$\vec{\mathbf{p}}^{\,0}_{\mathrm{G}_0\mathrm{O}_0}$	$[0, 0, 0]^\mathsf{T}$	m
$\vec{\mathbf{p}}^{\,i}_{\mathrm{G}_i\mathrm{O}_i}$	$[0, 0.15, 0]^\mathsf{T}$	m

Figure 31 shows the UVMS motion and end-effector path comparison with the experimental results for the two configurations tested. The final configuration is defined by the total simulation time. At the first configuration there is no much agreement between the simulation and experiment for lower velocities ($\dot{\gamma} < 15\ ^\circ$/s), as seen in Figs. 31 (a) and (b). This can be attributed to some factors. For example, the servomotors dynamics were modeled by PI controllers since there is no information about that. The transmission made by a drive belt between the servomotor mounted in the floating base and the first link was not modeled. Moreover, the center of mass was approximated by the geometric center once there is no information about that. The friction torques in the mechanical joints were not considered and the three-dimensional flow effects and the hydrodynamic interference were neglected. Also, the prototype was not fully immersed in the water; thus, diffraction effects may occur, which was not considered in the model. When the angular velocity increases, the paths get closer, as seen in Fig. 31 (c). This happens because the drag forces are quadratic in the velocity, i.e., for low velocities, the model does not represent the experiment very well, as explained above. However, as the velocity increases ($\omega = 30\ ^\circ$/s), the drag forces become predominant and the prediction generated by the mathematical model gets closer to the experiment. The same can be said for the second configuration, but the agreement between the paths for lower velocities is much better than the first one. We believe this is due to the position of the second servo motor, which is mounted directly on the second link, without a drive belt transmission.

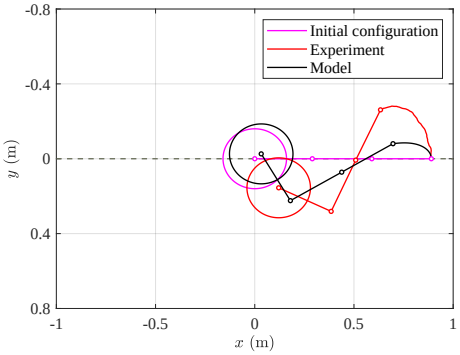

(a): $\dot{\gamma}_1 = 4.5\ ^\circ/\text{s}$

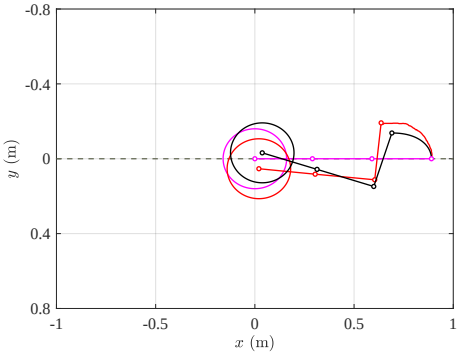

(d): $\dot{\gamma}_2 = 4.5\ ^\circ/\text{s}$

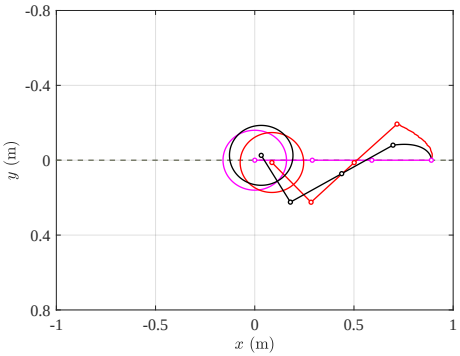

(b): $\dot{\gamma}_1 = 15\ ^\circ/\text{s}$

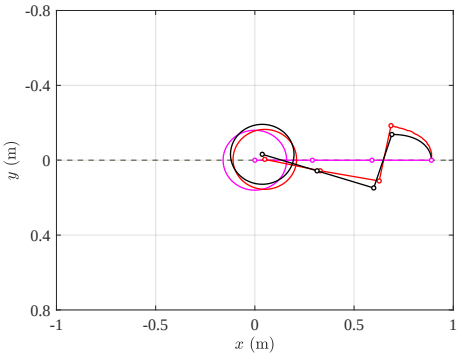

(e): $\dot{\gamma}_2 = 15\ ^\circ/\text{s}$

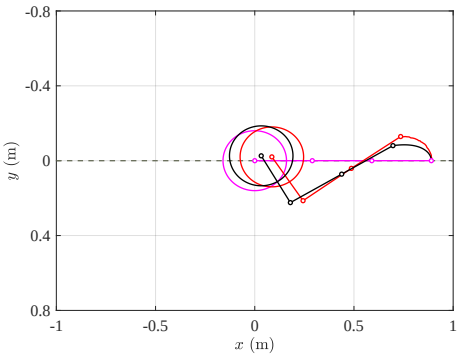

(c): $\dot{\gamma}_1 = 30\ ^\circ/\text{s}$

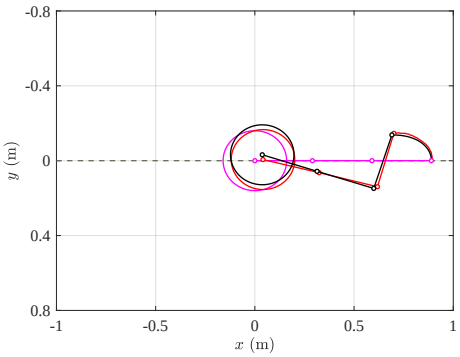

(f): $\dot{\gamma}_2 = 30\ ^\circ/\text{s}$

(a)-(c): First configuration; (d)-(f): Second configuration

Figure 31: UVMS motion on the horizontal plane

3.2.3 Experiment by McLain, Rock and Lee (1996)

The last experiment reproduced here was made by McLain, Rock and Lee (1996) to test a coordinated control scheme for a 4-DoFs I-AUV, composed of the 3-DoFs OTTER-AUV and a single link manipulator. Figure 32 shows the I-AUV prototype used in the experiment by McLain, Rock and Lee (1996). To induce the dynamic coupling effects in all AUV DoFs, the manipulator is mounted in front of the AUV on the horizontal plane and tilted down 60°. However, to simplify the modeling process and reduce the number of DoFs involved, the manipulator is considered tilted down by an angle of 90°, such that the modeling can be performed on the vertical plane. Such simplification showed to be reasonable since the coupling between the horizontal and vertical planes is weak for this application.

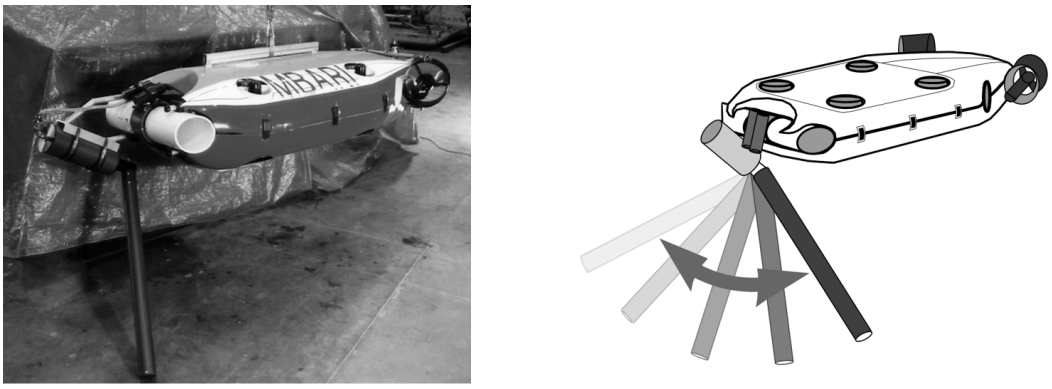

(a): 4-DoFs UVMS prototype (b): Swing motion performed during the experiment

Figure 32: Prototype and experimental setup used by McLain, Rock and Lee (1996)

The mathematical modeling was performed similar to the previous ones, as shown in the schematic diagram and modeling hierarchy in Fig. 33. The independent coordinates for the comparison are shown in Fig. 33 (a). As done before, in the lowest level of modeling hierarchy shown in Fig. 33 (b), we used the mathematical model of an underwater body on the vertical plane with the modified versions added mass and hydrodynamic damping matrices for the manipulator link. In the modeling hierarchy of Fig. 33 (b), body A is the AUV, body B is the manipulator link and system $\mathcal{S}$ is the 4-DoFs UVMS. An active revolute joint (grey circle) connects the manipulator link with the AUV. At level 1, the constraints between the AUV and manipulator are imposed and the mathematical model of the I-AUV prototype is obtained.

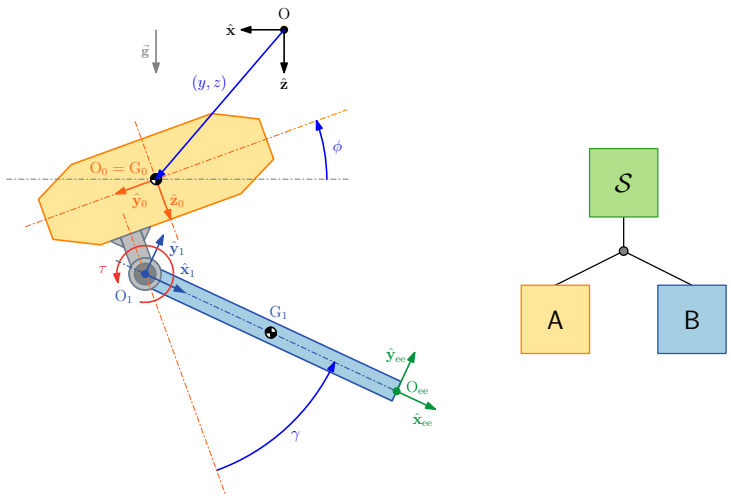

(a): 4-DoFs I-AUV schematic diagram (b): Modeling hierarchy

Figure 33: 4-DoFs UVMS prototype model

The terms of the relaxed model of the 4-DoFs UVMS prototype are presented below:

$$
\begin{aligned}
\mathbf{J} &= \text{blkdiag}\left(\mathbf{J}_0, \mathbf{J}_1\right), \\
\mathbf{M} &= \text{blkdiag}\left(\mathbf{M}_0, \mathbf{M}_1\right), \\
\mathbf{C} &= \text{blkdiag}\left(\mathbf{C}_0, \mathbf{C}_1\right), \\
\mathbf{D} &= \text{blkdiag}\left(\mathbf{D}_0, \mathbf{D}_1\right), \\
\boldsymbol{\eta} &= \left[\boldsymbol{\eta}_0^{\mathsf{T}}, \boldsymbol{\eta}_1^{\mathsf{T}}\right]^{\mathsf{T}}, \\
\boldsymbol{\nu} &= \left[\boldsymbol{\nu}_0^{\mathsf{T}}, \boldsymbol{\nu}_1^{\mathsf{T}}\right]^{\mathsf{T}}, \\
\mathbf{g} &= \left[\mathbf{g}_0^{\mathsf{T}}, \mathbf{g}_1^{\mathsf{T}}\right]^{\mathsf{T}}, \\
\mathbf{d} &= \left[\mathbf{d}_0^{\mathsf{T}}, \mathbf{d}_1^{\mathsf{T}}\right]^{\mathsf{T}}, \\
\boldsymbol{\tau} &= \left[\boldsymbol{\tau}_0^{\mathsf{T}}, \boldsymbol{\tau}_1^{\mathsf{T}}\right]^{\mathsf{T}},
\end{aligned}
\tag{3.98}
$$

where $\boldsymbol{\eta}_i = [y_i, z_i, \phi_i]^{\mathsf{T}}$, $\boldsymbol{\nu}_i = [v_i, w_i, p_i]^{\mathsf{T}}$ and $\mathbf{d}_i = \mathbf{0}$ $(i = 0, 1)$, while $\boldsymbol{\tau}_0 = \mathbf{0}$ and $\boldsymbol{\tau}_1 = [0, 0, \tau]^{\mathsf{T}}$ with τ being the motor torque of the revolute joint.

The constraints equations are written as:

$$
\boldsymbol{\varphi}\left(\boldsymbol{\eta}, t\right) = \begin{bmatrix} y_0 + b_0 \cos\left(\phi_0\right) - h_0 \sin\left(\phi_0\right) - \left(x_1 - l_1 \cos\left(\phi_1\right)\right) \\ z_0 - b_0 \sin\left(\phi_0\right) + h_0 \cos\left(\phi_0\right) - \left(z_1 - l_1 \sin\left(\phi_1\right)\right) \end{bmatrix} = \mathbf{0}, \tag{3.99}
$$

where b_0 and h_0 are body-fixed coordinates of the revolute joint center with respect to the AUV.

Their Jacobian matrix follows:

$$\frac{\partial \boldsymbol{\varphi}}{\partial \boldsymbol{\eta}} = \begin{bmatrix} 1 & 0 & -h_0 \cos(\phi_0) - b_0 \sin(\phi_0) & -1 & 0 & -l_1 \sin(\phi_1) \\ 0 & 1 & -b_0 \cos(\phi_0) - h_0 \sin(\phi_0) & 0 & -1 & l_1 \cos(\phi_1) \end{bmatrix}. \tag{3.100}$$

The identification matrices are given by:

$$\mathbf{Q} = \begin{bmatrix} 1 & 0 & 0 & 0 \\ 0 & 1 & 0 & 0 \\ 0 & 0 & 1 & 0 \\ 0 & 0 & 0 & 0 \\ 0 & 0 & 0 & 0 \\ 0 & 0 & 0 & 1 \end{bmatrix}; \quad \mathbf{R} = \begin{bmatrix} 0 & 0 \\ 0 & 0 \\ 0 & 0 \\ 1 & 0 \\ 0 & 1 \\ 0 & 0 \end{bmatrix}. \tag{3.101}$$

With $\mathbf{A} = \dfrac{\partial \boldsymbol{\varphi}}{\partial \boldsymbol{\eta}}\mathbf{J}$, $\mathbf{Q}$ and $\mathbf{R}$ the contrained terms of the EoMs of the 4-DoFs UVMS prototype can be written similarly to the previous examples.

The simulation performed reproduces the AUV open-loop response under the disturbances induced by the manipulator swing motion. This test is useful to verify if the dynamic model can reproduce the coupling effects between the AUV and manipulator on the vertical plane. In the experiment of McLain, Rock and Lee (1996), the manipulator performs a controlled swing motion described by a quasi-sinusoidal reference signal, shown in Fig. 34 (a). The reference derivatives used in the control are obtained through a filtering scheme. However, no bigger details are given about such a process. Therefore, in the simulation, the reference signal is approximated by a sinusoidal function with amplitude of 45° and period 5 s, as shown in Fig. 34 (a). A feedback linearization control law augmented with a PD regulator is used in the manipulator control, similar to the one used in McLain, Rock and Lee (1996). The numerical simulation was performed with the same set-up reported before. The tracking performance obtained in the simulation can be verified in Fig. 34 (a). The parameters used in the simulation are shown in Tab. 4. The relation between the absolute angular coordinates used on the modeling and the relative angular displacement of the manipulator is given by $\phi_0 + \gamma = \pi/2 - \phi_1$.

Table 4: 4-DoFs I-AUV prototype parameters

Symbols	Values	Units (SI)
$\mathbf{M}_{\mathrm{RB},0}$	diag (145, 145, 4.72)	kg, kgm^2
$\mathbf{M}_{\mathrm{RB},1}$	diag (0.84, 0.84, 0.07)	kg, kgm^2
$\mathbf{M}_{\mathrm{A},0}$	diag (1410, 3000, 33.44)	kg, kgm^2
$C_{\mathrm{A,x_1}}, C_{\mathrm{A,y_1}}$	0, 1	–
$\mathbf{D}_0$	diag (450, 1570, 36.7)	Ns/m, Nms
$C_{\mathrm{D,x_1}}, C_{\mathrm{D,y_1}}$	0, 1.2	–
$l_{\mathrm{O_1\|O_2}}, \Delta l$	1, 0.20	m
W_0, B_0, W_1, B_1	1422.5, 1422.2, 8.21, 8.42	N
$\vec{\mathbf{p}}^{\,0}_{\mathrm{G_0\|O_0}}$	$[0, 0.02, 0]^\mathsf{T}$	m
$\vec{\mathbf{p}}^{\,0}_{\mathrm{B_0\|O_0}}$	$[0, 0, 0]^\mathsf{T}$	m
$\vec{\mathbf{p}}^{\,1}_{\mathrm{G_1\|O_1}}$	$[0, 0.50, 0]^\mathsf{T}$	m
$\vec{\mathbf{p}}^{\,1}_{\mathrm{B_1\|O_1}}$	$[0, 0.50, 0]^\mathsf{T}$	m

The comparison with experimental results is shown in Fig. 34 (b) and (c). The time series for the UUV displacement on the lateral plane are shown in Fig. 34 (b). Good agreement is found between simulated and experimental displacements for all of them. However, in the roll angle, we can notice some phase shift between the displacements. We believe this is due to the approximation made in the manipulator reference displacement. Moreover, Fig. 34 (c) shows the hydrodynamic torque experienced on the manipulator joint during the swing motion. Again, despite some phase shift between the series and some dry friction effects not considered on the mathematical model, the series amplitudes and shape agreement is considered good. Finally, Fig. 35 shows the I-AUV motion comparison on the lateral plane for some instants. Fig. 35 also shows the end-effector path comparison. In those frames, we can see a good agreement between simulated motion and the experiment. The end-effector path is very well reproduced by the mathematical model.

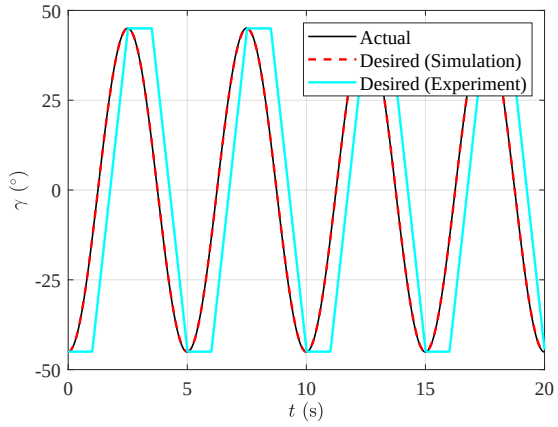

(a): Manipulator displacement

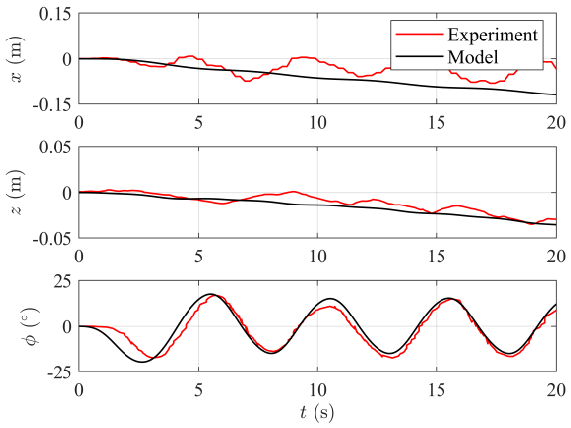

(b): Displacements

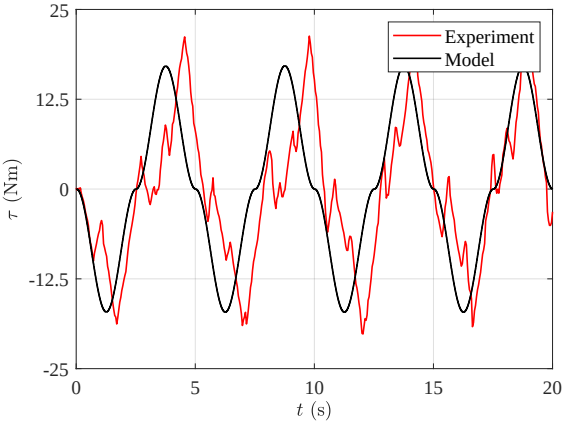

(c): Drag torque

Figure 34: 4-DoFs I-AUV results comparison

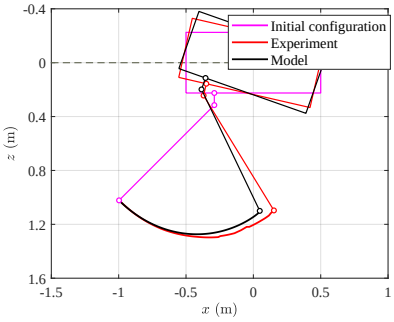

t = 2.5 s

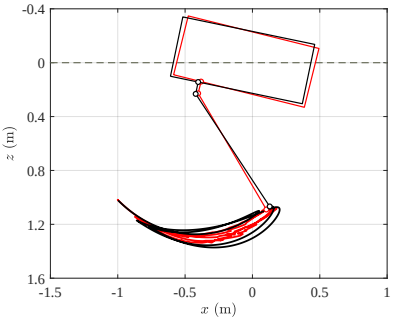

t = 12.5 s

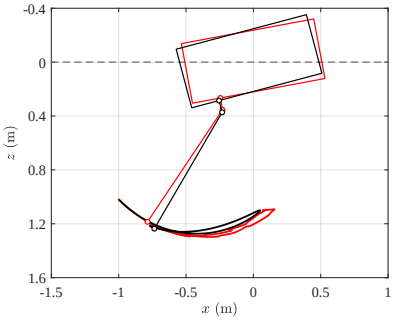

t = 5 s

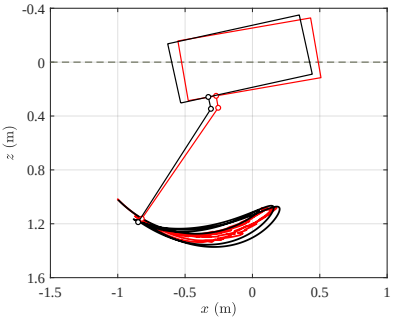

t = 15 s

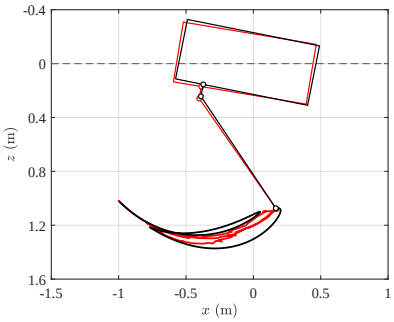

t = 7.5 s

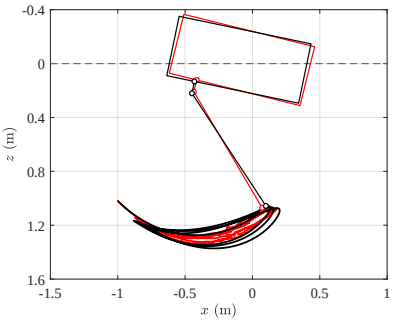

t = 17.5 s

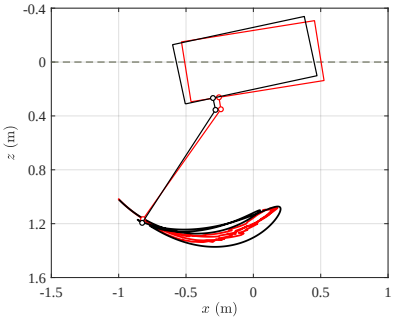

t = 10 s

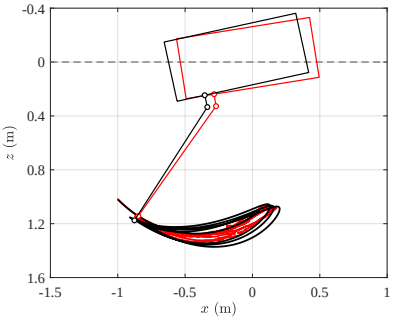

t = 20 s

Figure 35: I-AUV motion on the vertical plane

3.3 COMMENTARIES

This chapter presented a new modular mathematical modeling approach for multibody underwater systems, specifically for UVMSs. This approach permits the derivation of the mathematical model of any underwater multibody system in the classical EoMs form of UUVs, which turns the application direct of already synthesized control algorithms. Moreover, new mathematical models for the hydrodynamic loads on underwater manipulator links are also developed to overcome the limitations of previous models existent in the literature. Finally, the approaches presented in this chapter are validated by comparing the numerical simulation results with those of experiments reported by previous works.

4 MODULAR CONTROL METHODOLOGY

This chapter presents the MCM formulation. All the content presented here is original and is a part of the contributions of this thesis. Figure 36 shows a block diagram describing the contributions of this chapter.

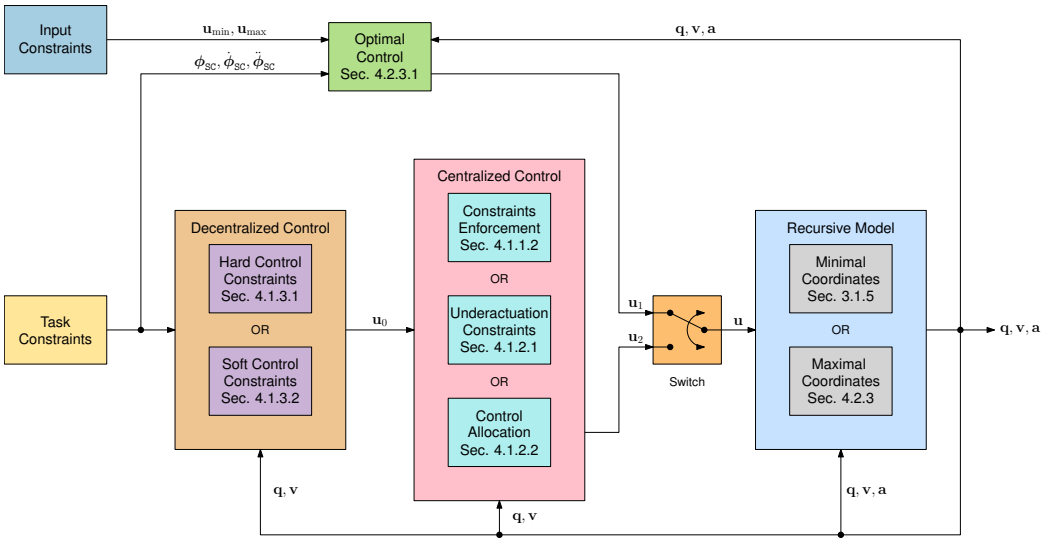

Figure 36: MCM block diagram

4.1 FORMULATION

4.1.1 Constraint enforcement based on the Gauss's principle

4.1.1.1 Closed-loop dynamic constraints

Let $\mathcal{S}$ be a v-DoFs system (v finite). Denote $\mathbf{q}$ as the n-column-vector ($n \geq v$) of generalized coordinates, $\mathbf{v}$ as the m-column vector ($m \geq v$) of quasi-velocities and $\mathbf{a}$ as the m-column vector of quasi-accelerations such that $\dot{\mathbf{v}} = \mathbf{a}$. Also, let $\boldsymbol{\varphi}$ be the r-column-vector ($r \geq m - v$) of bilateral holonomic and nonholonomic material modeling constraints of the system $\mathcal{S}$, such that:

$$\boldsymbol{\varphi}(\mathbf{v}, \mathbf{q}, t) = \mathbf{0}. \tag{4.1}$$

Differentiating Eq. (4.1) with respect to time results in:

$$\mathbf{A}\left(\mathbf{v},\mathbf{q},t\right)\mathbf{a}=\mathbf{b}\left(\mathbf{v},\mathbf{q},t\right), \tag{4.2}$$

where $\mathbf{A}$ is the r by m Jacobian matrix of the constraints with rank = $m-v$, with less than $m-v$ only in singular configurations, and $\mathbf{b}$ is the associated m-vector.

Let $\mathbf{M}$ be the m by m symmetric and positive semi-definite generalized inertia matrix and $\mathbf{f}$ the m-column-vector of active forces not associated to the control forces. With the extended definition of Gaussian deviation function proposed by Orsino (2020), the admissible substitutes for $\mathbf{M}$ and $\mathbf{f}$ are given, respectively, by:

$$\begin{aligned}\mathbf{N}\left(\mathbf{v},\mathbf{q},t\right)&=\mathbf{M}+\mathbf{A}^{\mathsf{T}}\mathbf{W}\mathbf{A},\\ \mathbf{g}\left(\mathbf{v},\mathbf{q},t\right)&=\mathbf{f}+\mathbf{A}^{\mathsf{T}}\mathbf{W}\mathbf{b},\end{aligned} \tag{4.3}$$

where $\mathbf{W}$ is a m by m symmetrical positive definite matrix. The substitutes of $\mathbf{M}$ and $\mathbf{f}$ are used in the case $\mathbf{M}^{-1}$ is singular. If $\mathbf{M}$ is already a positive definite matrix, then, $\mathbf{W}=\mathbf{0}$ is an appropriated choice (ORSINO, 2020).

Let $\mathbf{u}$ be a m-column-vector of generalized control forces associated with the quasi-velocities and consistent with the modeling constraints.

To obtain a stable closed-loop dynamic we propose the following constraints:

$$\mathbf{A}\left(\mathbf{a}+\mathbf{N}^{-1}\mathbf{u}\right)=\mathbf{b}, \tag{4.4}$$

$$\mathbf{A}\mathbf{N}^{-1}\mathbf{u}=\mathbf{0}, \tag{4.5}$$

where $\mathbf{A}\mathbf{N}^{-1}\mathbf{u}$ represents the acceleration parcel due to the control forces consistent with the modeling constraints.

The relaxed dynamic model is given by:

$$\mathbf{a}_0\left(\mathbf{v},\mathbf{q},t\right)=\mathbf{N}^{-1}\left(\mathbf{g}+\mathbf{c}\right), \tag{4.6}$$

where $\mathbf{c}$ is the m-column-vector of knowing functions of states related to the non-ideal constraints forces.

The constrained dynamic is given by the Udwadia-Kalaba equation, as follows:

$$\mathbf{a}=\mathbf{a}_0+\mathbf{N}^{-1}\mathbf{A}^{\mathsf{T}}\left(\mathbf{A}\mathbf{N}^{-1}\mathbf{A}^{\mathsf{T}}\right)^{\mathrm{g}}\left(\mathbf{b}-\mathbf{A}\mathbf{a}_0\right), \tag{4.7}$$

where the second term represents the modeling constraints accelerations. The superscript “g” indicates the generalized inverse matrix, which is classified according to the proprieties presented

in Orsino (2020). For example, a matrix $\mathbf{X}^{\mathrm{g}}$ is a generalized inverse of $\mathbf{X}$ if it satisfies at least property P_1 among the following:

$$\begin{aligned} &\mathrm{P}_1 : \mathbf{X}\mathbf{X}^{\mathrm{g}}\mathbf{X} = \mathbf{X}, \qquad \mathrm{P}_3 : (\mathbf{X}^{\mathrm{g}})^{\mathsf{T}}\mathbf{X}^{\mathsf{T}} = (\mathbf{X}\mathbf{X}^{\mathrm{g}})^{\mathsf{T}} = \mathbf{X}\mathbf{X}^{\mathrm{g}}, \\ &\mathrm{P}_2 : \mathbf{X}^{\mathrm{g}}\mathbf{X}\mathbf{X}^{\mathrm{g}} = \mathbf{X}^{\mathrm{g}}, \quad \mathrm{P}_4 : \mathbf{X}^{\mathsf{T}}(\mathbf{X}^{\mathrm{g}})^{\mathsf{T}} = (\mathbf{X}^{\mathrm{g}}\mathbf{X})^{\mathsf{T}} = \mathbf{X}^{\mathrm{g}}\mathbf{X}. \end{aligned} \tag{4.8}$$

The Moore-Penrose generalized inverse of $\mathbf{X}$, which is also denoted by $\mathbf{X}^{+}$, is the unique matrix $\mathbf{X}^{\mathrm{g}}$ that satisfies the four properties above. A generalized inverse which satisfies at least property P_1 is called a $\{1\}$-inverse, a generalized inverse which satisfies at least properties P_1 and P_4 is called a $\{1,4\}$-inverse, and so on.

From Eq. (4.7), the closed-loop dynamic[1] can be written as:

$$\mathbf{a} + \mathbf{N}^{-1}\mathbf{u} = \mathbf{a}_0 + \mathbf{N}^{-1}\mathbf{u}_0 + \mathbf{N}^{-1}\mathbf{A}^{\mathsf{T}}\left(\mathbf{A}\mathbf{N}^{-1}\mathbf{A}^{\mathsf{T}}\right)^{\mathrm{g}}\left(\mathbf{b} - \mathbf{A}\mathbf{a}_0 - \mathbf{A}\mathbf{N}^{-1}\mathbf{u}_0\right), \tag{4.9}$$

where $\left(\mathbf{A}\mathbf{N}^{-1}\mathbf{A}^{\mathsf{T}}\right)^{\mathrm{g}}$ is any $\{1,4\}$-inverse of $\mathbf{A}\mathbf{N}^{-1}\mathbf{A}^{\mathsf{T}}$ and $\mathbf{u}_0$ is the m-column vector of decentralized (relaxed) controllers.

Based on the feedback linearization technique and the relaxed dynamic model in Eq. (4.6), we get the following decentralized control:

$$\mathbf{u}_0 = \mathbf{N}\boldsymbol{\upsilon} - (\mathbf{g} + \mathbf{c}), \tag{4.10}$$

where $\boldsymbol{\upsilon}$ is the m-column-vector of injection terms that must be chosen to obtain stable closed-loop error dynamic.

Substituting Eqs. (4.10) and (4.9) into (4.4), results in:

$$\begin{aligned} \mathbf{A}\mathbf{a} + \mathbf{A}\mathbf{N}^{-1}\mathbf{u} &= \mathbf{A}\boldsymbol{\upsilon} + \mathbf{A}\mathbf{N}^{-1}\mathbf{A}^{\mathsf{T}}\left(\mathbf{A}\mathbf{N}^{-1}\mathbf{A}^{\mathsf{T}}\right)^{\mathrm{g}}(\mathbf{b} - \mathbf{A}\boldsymbol{\upsilon}), \\ \mathbf{A}\mathbf{a} - \mathbf{A}\boldsymbol{\upsilon} &= \mathbf{A}\mathbf{N}^{-1}\mathbf{A}^{\mathsf{T}}\left(\mathbf{A}\mathbf{N}^{-1}\mathbf{A}^{\mathsf{T}}\right)^{\mathrm{g}}(\mathbf{b} - \mathbf{A}\boldsymbol{\upsilon}). \end{aligned} \tag{4.11}$$

Let the desired closed-loop dynamic be described by a stable 2-nd order error dynamics:

$$\tilde{\mathbf{a}} + \mathbf{K}_{\mathrm{D}}\tilde{\mathbf{v}} + \mathbf{K}_{\mathrm{P}}\tilde{\mathbf{q}} = \mathbf{0}, \tag{4.12}$$

where the tracking errors are given by:

$$\tilde{\mathbf{q}} = \mathbf{q} - \mathbf{q}_{\mathrm{d}}; \quad \tilde{\mathbf{v}} = \mathbf{v} - \mathbf{v}_{\mathrm{d}}; \quad \tilde{\mathbf{a}} = \mathbf{a} - \mathbf{a}_{\mathrm{d}}, \tag{4.13}$$

with the subscript "d" indicating the desired states.

[1]The detailed derivation of the expression presented in Eq. (4.9) can be seen in Appendix A.2

Based on Eq. (4.12), the linear controllers are chosen as:

$$\boldsymbol{\upsilon} = \mathbf{a}_{\mathrm{d}} - \mathbf{K}_{\mathrm{D}}\tilde{\mathbf{v}} - \mathbf{K}_{\mathrm{P}}\tilde{\mathbf{q}}. \tag{4.14}$$

Substituting Eq. (4.14) into (4.11) and using the propriety P_2 with $\mathbf{X} = \mathbf{A}\mathbf{N}^{-1}\mathbf{A}^{\mathsf{T}}$, we get:

$$\begin{aligned} \mathbf{A}\mathbf{a} - \mathbf{A}\mathbf{a}_{\mathrm{d}} + \mathbf{A}\left(\mathbf{K}_{\mathrm{D}}\tilde{\mathbf{v}} + \mathbf{K}_{\mathrm{P}}\tilde{\mathbf{q}}\right) &= \mathbf{X}\mathbf{X}^{\mathrm{g}}\left(\mathbf{b} - \mathbf{A}\mathbf{a}_{\mathrm{d}} + \mathbf{A}\left(\mathbf{K}_{\mathrm{D}}\tilde{\mathbf{v}} + \mathbf{K}_{\mathrm{P}}\tilde{\mathbf{q}}\right)\right), \\ \mathbf{X}^{\mathrm{g}}\mathbf{A}\mathbf{a}_{\mathrm{d}} &= \mathbf{X}^{\mathrm{g}}\left(\mathbf{b} - \mathbf{A}\left(\mathbf{a} - \mathbf{a}_{\mathrm{d}}\right)\right), \\ \mathbf{X}^{\mathrm{g}}\mathbf{A}\mathbf{a}_{\mathrm{d}} &= \mathbf{X}^{\mathrm{g}}\left(\mathbf{b} - \mathbf{A}\tilde{\mathbf{a}}\right). \end{aligned} \tag{4.15}$$

From Eq. (4.12), the quasi-acceleration tracking error can be written as:

$$\tilde{\mathbf{a}} = -\mathbf{K}_{\mathrm{D}}\tilde{\mathbf{v}} - \mathbf{K}_{\mathrm{P}}\tilde{\mathbf{q}}. \tag{4.16}$$

Substituting Eq. (4.16) into (4.15) and using the modeling constraints in Eq. (4.2), we obtain:

$$\begin{aligned} \mathbf{X}\mathbf{X}^{\mathrm{g}}\left(\mathbf{A}\mathbf{a} + \mathbf{A}\left(\mathbf{K}_{\mathrm{D}}\tilde{\mathbf{v}} + \mathbf{K}_{\mathrm{P}}\tilde{\mathbf{q}}\right)\right) &= \mathbf{X}\mathbf{X}^{\mathrm{g}}\mathbf{A}\mathbf{a}_{\mathrm{d}}, \\ \mathbf{X}\mathbf{X}^{\mathrm{g}}\left(\mathbf{A}\left(\mathbf{a} - \mathbf{a}_{\mathrm{d}}\right) + \mathbf{A}\left(\mathbf{K}_{\mathrm{D}}\tilde{\mathbf{v}} + \mathbf{K}_{\mathrm{P}}\tilde{\mathbf{q}}\right)\right) &= \mathbf{0}, \\ \mathbf{X}\mathbf{X}^{\mathrm{g}}\mathbf{A}\left(\tilde{\mathbf{a}} + \mathbf{K}_{\mathrm{D}}\tilde{\mathbf{v}} + \mathbf{K}_{\mathrm{P}}\tilde{\mathbf{q}}\right) &= \mathbf{0}. \end{aligned} \tag{4.17}$$

Once $\mathbf{X}\mathbf{X}^{\mathrm{g}}\mathbf{A} = \mathbf{A}$, a stable closed-loop dynamic consistent with the modeling constraints can be obtained if the control forces are consistent with the modeling constraints, as follows:

$$\mathbf{A}\left(\tilde{\mathbf{a}} + \mathbf{K}_{\mathrm{D}}\tilde{\mathbf{v}} + \mathbf{K}_{\mathrm{P}}\tilde{\mathbf{q}}\right) = \mathbf{0}, \tag{4.18}$$

which completes our proof.

4.1.1.2 Generalized control forces

To obtain control forces consistent with the modeling constraints, let us define a Gaussian deviation function as follows:

$$Z(\mathbf{u}) = \frac{1}{2}\left(\mathbf{u} - \mathbf{u}_0\right)^{\mathsf{T}}\mathbf{N}^{-1}\left(\mathbf{u} - \mathbf{u}_0\right). \tag{4.19}$$

From the control constraints presented before, we have:

$$\mathbf{A}\mathbf{N}^{-1}\mathbf{u} = \mathbf{0}. \tag{4.20}$$

The consistent control forces are obtained by solving the minimization problem in Eq. (4.19)

subjected to the constraints in (4.20).

Let $\boldsymbol{\lambda}$ be a r-column-vector of Lagrange multipliers used in the following constrained optimization problem:

$$\overline{Z}(\mathbf{u}, \boldsymbol{\lambda}) = \frac{1}{2}(\mathbf{u} - \mathbf{u}_0)^{\mathsf{T}} \mathbf{N}^{-1}(\mathbf{u} - \mathbf{u}_0) - \boldsymbol{\lambda}^{\mathsf{T}} \mathbf{A}\mathbf{N}^{-1}\mathbf{u}. \tag{4.21}$$

The sufficient conditions to solve the optimization problem are obtained by calculating the stationary points, as follows:

$$\frac{\partial \overline{Z}}{\partial \mathbf{u}} = \mathbf{N}^{-1}(\mathbf{u} - \mathbf{u}_0) - \mathbf{N}^{-1}\mathbf{A}^{\mathsf{T}}\boldsymbol{\lambda} = \mathbf{0} \Leftrightarrow \mathbf{u} = \mathbf{u}_0 + \mathbf{A}^{\mathsf{T}}\boldsymbol{\lambda}, \tag{4.22}$$

$$\frac{\partial \overline{Z}}{\partial \boldsymbol{\lambda}} = \mathbf{A}\mathbf{N}^{-1}\mathbf{u} = \mathbf{0} \Leftrightarrow \mathbf{A}\mathbf{N}^{-1}\mathbf{u} = \mathbf{0}. \tag{4.23}$$

Introducing Eq. (4.22) into (4.23) and solving for the $\boldsymbol{\lambda}$, results in:

$$\boldsymbol{\lambda} = -\left(\mathbf{A}\mathbf{N}^{-1}\mathbf{A}^{\mathsf{T}}\right)^{\mathrm{g}} \mathbf{A}\mathbf{N}^{-1}\mathbf{u}_0 + \left(\mathbf{I} - \left(\mathbf{A}\mathbf{N}^{-1}\mathbf{A}^{\mathsf{T}}\right)^{\mathrm{g}} \mathbf{A}\mathbf{N}^{-1}\mathbf{A}^{\mathsf{T}}\right)\mathbf{w}, \tag{4.24}$$

where $\mathbf{w}$ is an arbitrary column-vector.

Multiplying Eq. (4.24) by $\mathbf{A}^{\mathsf{T}}$, we get:

$$\mathbf{A}^{\mathsf{T}}\boldsymbol{\lambda} = -\mathbf{A}^{\mathsf{T}}\left(\mathbf{A}\mathbf{N}^{-1}\mathbf{A}^{\mathsf{T}}\right)^{\mathrm{g}} \mathbf{A}\mathbf{N}^{-1}\mathbf{u}_0 + \mathbf{A}^{\mathsf{T}}\left(\mathbf{I} - \left(\mathbf{A}\mathbf{N}^{-1}\mathbf{A}^{\mathsf{T}}\right)^{\mathrm{g}} \mathbf{A}\mathbf{N}^{-1}\mathbf{A}^{\mathsf{T}}\right)\mathbf{w}. \tag{4.25}$$

Let us prove that $\mathbf{A}^{\mathsf{T}}\mathbf{U} = \mathbf{0}$, where $\mathbf{U}$ is given by:

$$\mathbf{U} = \mathbf{I} - \left(\mathbf{A}\mathbf{N}^{-1}\mathbf{A}^{\mathsf{T}}\right)^{\mathrm{g}} \mathbf{A}\mathbf{N}^{-1}\mathbf{A}^{\mathsf{T}}. \tag{4.26}$$

Multiplying Eq. (4.26) by $\mathbf{A}\mathbf{N}^{-1}\mathbf{A}^{\mathsf{T}}$ and developing, results in:

$$\begin{aligned} \mathbf{A}\mathbf{N}^{-1}\mathbf{A}^{\mathsf{T}}\mathbf{U} &= \mathbf{A}\mathbf{N}^{-1}\mathbf{A}^{\mathsf{T}}\left(\mathbf{I} - \left(\mathbf{A}\mathbf{N}^{-1}\mathbf{A}^{\mathsf{T}}\right)^{\mathrm{g}} \mathbf{A}\mathbf{N}^{-1}\mathbf{A}^{\mathsf{T}}\right), \\ &= \mathbf{A}\mathbf{N}^{-1}\mathbf{A}^{\mathsf{T}} - \mathbf{A}\mathbf{N}^{-1}\mathbf{A}^{\mathsf{T}}\left(\mathbf{A}\mathbf{N}^{-1}\mathbf{A}^{\mathsf{T}}\right)^{\mathrm{g}} \mathbf{A}\mathbf{N}^{-1}\mathbf{A}^{\mathsf{T}}, \\ &= \mathbf{A}\mathbf{N}^{-1}\mathbf{A}^{\mathsf{T}} - \mathbf{A}\mathbf{N}^{-1}\mathbf{A}^{\mathsf{T}}, \\ &= \mathbf{0}. \end{aligned} \tag{4.27}$$

Multiplying Eq. (4.27) by $\mathbf{U}^{\mathsf{T}}$ and developing, we get:

$$\begin{aligned} \mathbf{U}^{\mathsf{T}}\mathbf{A}\mathbf{N}^{-1}\mathbf{A}^{\mathsf{T}}\mathbf{U} &= \mathbf{0}, \\ \mathbf{U}^{\mathsf{T}}\mathbf{A}\mathbf{N}^{-1/2}\mathbf{N}^{-1/2}\mathbf{A}^{\mathsf{T}}\mathbf{U} &= \mathbf{0}, \\ \left(\mathbf{N}^{-1/2}\mathbf{A}^{\mathsf{T}}\mathbf{U}\right)^{\mathsf{T}} \mathbf{N}^{-1/2}\mathbf{A}^{\mathsf{T}}\mathbf{U} &= \mathbf{0}. \end{aligned} \tag{4.28}$$

From Eq. (4.28) we have $\mathbf{N}^{-1/2}\mathbf{A}^{\mathsf{T}}\mathbf{U} = \mathbf{0}$, that is equivalent to:

$$\begin{aligned} \mathbf{N}^{-1/2}\mathbf{A}^{\mathsf{T}}\mathbf{U} &= \mathbf{0}, \\ \mathbf{N}^{1/2}\mathbf{N}^{-1/2}\mathbf{A}^{\mathsf{T}}\mathbf{U} &= \mathbf{N}^{1/2}\mathbf{0}, \\ \mathbf{A}^{\mathsf{T}}\mathbf{U} &= \mathbf{0}, \end{aligned} \tag{4.29}$$

which completes our proof.

Substituting Eq. (4.24) into (4.22), we get:

$$\mathbf{u} = \mathbf{u}_0 - \mathbf{A}^{\mathsf{T}}\left(\mathbf{A}\mathbf{N}^{-1}\mathbf{A}^{\mathsf{T}}\right)^{\mathrm{g}}\mathbf{A}\mathbf{N}^{-1}\mathbf{u}_0. \tag{4.30}$$

Equation (4.30) represents a set of control forces consistent with the modeling constraints. The term $\mathbf{A}^{\mathsf{T}}\left(\mathbf{A}\mathbf{N}^{-1}\mathbf{A}^{\mathsf{T}}\right)^{\mathrm{g}}\mathbf{A}\mathbf{N}^{-1}\mathbf{u}_0$ in Eq. (4.30) can be interpreted as a feedforward term associated with the constraints forces when the control is turned on.

To simplify Eq. (4.30), let us introduce the scaled control as $\boldsymbol{\mu} = \mathbf{N}^{-1/2}\mathbf{u}$ and $\boldsymbol{\mu}_0 = \mathbf{N}^{-1/2}\mathbf{u}_0$. Also, let $\mathbf{H} = \mathbf{A}\mathbf{N}^{-1/2}$, such that Eq. (4.30) multiplied by $\mathbf{N}^{-1/2}$ becomes:

$$\begin{aligned} \mathbf{N}^{-1/2}\mathbf{u} &= \mathbf{N}^{-1/2}\mathbf{u}_0 - \mathbf{N}^{-1/2}\mathbf{A}^{\mathsf{T}}\left(\mathbf{A}\mathbf{N}^{-1/2}\mathbf{N}^{-1/2}\mathbf{A}^{\mathsf{T}}\right)^{\mathrm{g}}\mathbf{A}\mathbf{N}^{-1/2}\mathbf{N}^{-1/2}\mathbf{u}_0, \\ \boldsymbol{\mu} &= \boldsymbol{\mu}_0 - \mathbf{H}^{\mathsf{T}}\left(\mathbf{H}\mathbf{H}^{\mathsf{T}}\right)^{\mathrm{g}}\mathbf{H}\boldsymbol{\mu}_0, \\ &= \left(\mathbf{I} - \mathbf{H}^{\mathrm{g}}\mathbf{H}\right)\boldsymbol{\mu}_0, \end{aligned} \tag{4.31}$$

where $\mathbf{H}^{\mathrm{g}} = \mathbf{H}^{\mathsf{T}}\left(\mathbf{H}\mathbf{H}^{\mathsf{T}}\right)^{\mathrm{g}}$ is any $\{1,4\}$-inverse of $\mathbf{H}$.

Let $\mathbf{P} = \mathbf{I} - \mathbf{H}^{\mathrm{g}}\mathbf{H}$ be the orthogonal projector onto kernel of $\mathbf{H}$, such that $\mathbf{H}\mathbf{P} = \mathbf{H}\left(\mathbf{I} - \mathbf{H}^{\mathrm{g}}\mathbf{H}\right) = \mathbf{H} - \mathbf{H}\mathbf{H}^{\mathrm{g}}\mathbf{H} = \mathbf{0}$, and $\mathbf{P}^{\mathsf{T}}\mathbf{H}^{\mathsf{T}} = \left(\mathbf{I} - \mathbf{H}^{\mathsf{T}}\left(\mathbf{H}^{\mathrm{g}}\right)^{\mathsf{T}}\right)\mathbf{H}^{\mathsf{T}} = \mathbf{H}^{\mathsf{T}} - \left(\mathbf{H}\mathbf{H}^{\mathrm{g}}\mathbf{H}\right)^{\mathsf{T}} = \mathbf{0}$. Thus, Eq. (4.31) can be rewritten as:

$$\boldsymbol{\mu} = \left(\mathbf{I} - \mathbf{H}^{\mathrm{g}}\mathbf{H}\right)\boldsymbol{\mu}_0 = \mathbf{P}\boldsymbol{\mu}_0. \tag{4.32}$$

In terms of $\mathbf{u}$ and $\mathbf{u}_0$, we have:

$$\mathbf{u} = \mathbf{N}^{1/2}\mathbf{P}\mathbf{N}^{-1/2}\mathbf{u}_0. \tag{4.33}$$

4.1.1.3 Stability proof

To verify closed-loop asymptotic stability the Lyapunov theory is used.

Let $\boldsymbol{\sigma}$ be m-column-vector of like-error functions (e.g., tracking error derivative, sliding

surface variables, etc.) defined as follows:

$$\boldsymbol{\sigma}(\mathbf{v}, \mathbf{q}, t) = \mathbf{S}\mathbf{r} = \mathbf{0}, \tag{4.34}$$

where $\mathbf{S}$ is the m by v orthogonal complement matrix associated with the modeling constraints such that $\mathbf{A}\mathbf{S} = \mathbf{S}^{\mathsf{T}}\mathbf{A}^{\mathsf{T}} = \mathbf{0}$, and $\mathbf{r}$ is v-column-vector of like-error functions related to the DoFs of the system $\mathcal{S}$.

The semi-definite positive scalar function considered as Lyapunov candidate is:

$$V = \frac{1}{2}\boldsymbol{\sigma}^{\mathsf{T}}\mathbf{N}\boldsymbol{\sigma} = \frac{1}{2}\mathbf{r}^{\mathsf{T}}\mathbf{S}^{\mathsf{T}}\mathbf{N}\mathbf{S}\mathbf{r} = \frac{1}{2}\mathbf{r}^{\mathsf{T}}\tilde{\mathbf{N}}\mathbf{r}, \quad (V \geq 0) \tag{4.35}$$

where $\tilde{\mathbf{N}} = \mathbf{S}^{\mathsf{T}}\mathbf{N}\mathbf{S} = \mathbf{S}^{\mathsf{T}}\mathbf{M}\mathbf{S} + \mathbf{S}^{\mathsf{T}}\mathbf{A}^{\mathsf{T}}\mathbf{W}\mathbf{A}\mathbf{S} = \mathbf{S}^{\mathsf{T}}\mathbf{M}\mathbf{S}$ is the v by v generalized inertia matrix related to the DoFs of the system $\mathcal{S}$.

Performing the time-derivative of Eq. (4.35), we get:

$$\dot{V} = \mathbf{r}^{\mathsf{T}}\mathbf{S}^{\mathsf{T}}\mathbf{N}\dot{\mathbf{S}}\mathbf{r} + \mathbf{r}^{\mathsf{T}}\mathbf{S}^{\mathsf{T}}\mathbf{N}\mathbf{S}\dot{\mathbf{r}} = \mathbf{r}^{\mathsf{T}}\mathbf{S}^{\mathsf{T}}\mathbf{N}(\dot{\mathbf{S}}\mathbf{r} + \mathbf{S}\dot{\mathbf{r}}). \tag{4.36}$$

From Eq. (4.34) we note that $\dot{\boldsymbol{\sigma}} = \dot{\mathbf{S}}\mathbf{r} + \mathbf{S}\dot{\mathbf{r}}$ in (4.36). Moreover, since $\boldsymbol{\sigma}$ is chosen during the synthesis we can impose that $\dot{\boldsymbol{\sigma}} = \mathbf{a} - \mathbf{a}_{\mathrm{r}}$, with $\mathbf{a}_{\mathrm{r}}$ as the reference acceleration[2] vector. Therefore, we obtain:

$$\dot{V} = \mathbf{r}^{\mathsf{T}}\mathbf{S}^{\mathsf{T}}\mathbf{N}\dot{\boldsymbol{\sigma}} = \mathbf{r}^{\mathsf{T}}\mathbf{S}^{\mathsf{T}}\mathbf{N}\left(\mathbf{a} - \mathbf{a}_{\mathrm{r}}\right). \tag{4.37}$$

Substituting Eq. (4.6) into (4.9) and using (4.5), the closed-loop dynamic becomes:

$$\mathbf{a} = \mathbf{N}^{-1}\left(\mathbf{g} + \mathbf{c}\right) + \mathbf{N}^{-1}\mathbf{u}_0 + \mathbf{N}^{-1}\mathbf{A}^{\mathsf{T}}\left(\mathbf{A}\mathbf{N}^{-1}\mathbf{A}^{\mathsf{T}}\right)^{\mathrm{g}}\left(\mathbf{b} - \mathbf{A}\mathbf{N}^{-1}\left(\mathbf{g} + \mathbf{c}\right) - \mathbf{A}\mathbf{N}^{-1}\mathbf{u}_0\right). \tag{4.38}$$

Let the decentralized control be chosen as follows:

$$\mathbf{u}_0 = \mathbf{N}\mathbf{a}_{\mathrm{r}} - \left(\mathbf{g} + \mathbf{c}\right) - \mathbf{K}\boldsymbol{\sigma}, \tag{4.39}$$

where $\mathbf{K}$ is a m by m symmetric positive semi-definite control gains matrix.

Substituting Eq. (4.39) into (4.38), results in:

$$\mathbf{a} - \mathbf{a}_{\mathrm{r}} = -\mathbf{N}^{-1}\mathbf{K}\boldsymbol{\sigma} + \mathbf{N}^{-1}\mathbf{A}^{\mathsf{T}}\left(\mathbf{A}\mathbf{N}^{-1}\mathbf{A}^{\mathsf{T}}\right)^{\mathrm{g}}\left(\mathbf{b} - \mathbf{A}\left(\mathbf{a}_{\mathrm{r}} - \mathbf{N}^{-1}\mathbf{K}\boldsymbol{\sigma}\right)\right). \tag{4.40}$$

[2]The reference acceleration is written as a function of the desired acceleration such that its values are shifted according to the velocity and position errors.

Multiplying Eq. (4.40) by $\mathbf{S}^{\mathsf{T}}\mathbf{N}$, since $\mathbf{AS} = \mathbf{S}^{\mathsf{T}}\mathbf{A}^{\mathsf{T}} = \mathbf{0}$, it can be stated that:

$$\begin{aligned}\mathbf{S}^{\mathsf{T}}\mathbf{N}\left(\mathbf{a}-\mathbf{a}_{\mathrm{r}}\right) &= -\mathbf{S}^{\mathsf{T}}\mathbf{K}\boldsymbol{\sigma} + \mathbf{S}^{\mathsf{T}}\mathbf{A}^{\mathsf{T}}\left(\mathbf{A}\mathbf{N}^{-1}\mathbf{A}^{\mathsf{T}}\right)^{\mathrm{g}}\left(\mathbf{b}-\mathbf{A}\left(\mathbf{a}_{\mathrm{r}}-\mathbf{N}^{-1}\mathbf{K}\boldsymbol{\sigma}\right)\right),\\ &= -\mathbf{S}^{\mathsf{T}}\mathbf{K}\mathbf{S}\mathbf{r},\\ &= -\tilde{\mathbf{K}}\mathbf{r},\end{aligned} \tag{4.41}$$

where $\tilde{\mathbf{K}} = \mathbf{S}^{\mathsf{T}}\mathbf{K}\mathbf{S}$ is the v by v symmetric positive semi-definite control gains matrix related with the DoFs of the system $\mathcal{S}$.

Substituting Eq. (4.41) into (4.37), we obtain:

$$\dot{V} = \mathbf{r}^{\mathsf{T}}\mathbf{S}^{\mathsf{T}}\mathbf{N}\dot{\boldsymbol{\sigma}} = \mathbf{r}^{\mathsf{T}}\mathbf{S}^{\mathsf{T}}\mathbf{N}\left(\mathbf{a}-\mathbf{a}_{\mathrm{r}}\right) = -\mathbf{r}^{\mathsf{T}}\mathbf{S}^{\mathsf{T}}\mathbf{K}\mathbf{S}\mathbf{r} = -\mathbf{r}^{\mathsf{T}}\tilde{\mathbf{K}}\mathbf{r} = -\boldsymbol{\sigma}^{\mathsf{T}}\mathbf{K}\boldsymbol{\sigma}, \tag{4.42}$$

which guarantees the closed-loop stability in the Lyapunov sense for the system $\mathcal{S}$ since V is positive semi-definite ($V \geq 0$) and $\dot{V}$ is negative semi-definite ($\dot{V} \leq 0$).

The former result can be extended to prove that the closed-loop system is stable only if all the closed-loop subsystems are stable. To show that let us define $\boldsymbol{\sigma} = \left[\boldsymbol{\sigma}_i^{\mathsf{T}}\right]^{\mathsf{T}}$ and $\mathbf{K} = \mathrm{blkdiag}\left(\mathbf{K}_i\right)$ ($i = 1, \ldots, N$) in terms of the i-th sub-controller, as follows:

$$\boldsymbol{\sigma} = \left[\boldsymbol{\sigma}_1^{\mathsf{T}}, \ldots, \boldsymbol{\sigma}_N^{\mathsf{T}}\right]^{\mathsf{T}}; \quad \mathbf{K} = \mathrm{blkdiag}\left(\mathbf{K}_1, \ldots, \mathbf{K}_N\right). \tag{4.43}$$

The structure adopted for the column-vector $\boldsymbol{\sigma}$ and for the matrix $\mathbf{K}$ is consistent with the present formulation since there is no interaction between the control laws of the subsystems.

Substituting Eq. (4.43) into (4.42), we get:

$$\dot{V} = -\sum_{i=1}^{N}\boldsymbol{\sigma}_i^{\mathsf{T}}\mathbf{K}_i\boldsymbol{\sigma}_i = \sum_{i=1}^{N}\dot{V}_i \quad \therefore \quad V = \sum_{i=1}^{N}V_i. \quad (i = 1, \ldots, N) \tag{4.44}$$

Therefore, to guarantee that $V \geq 0$ and $\dot{V} \leq 0$ is enough to prove that each $V_i \geq 0$ and $\dot{V}_i \leq 0$. This result recovers the classical theorem of the virtual decomposition technique (ZHU, 2010).

4.1.2 General formulation

4.1.2.1 Consistent enforcement of underactuation constraints

The control forces of Eq. (4.25) are defined based on the set of quasi-velocities. However, the system $\mathcal{S}$ may be underactuated in the sense of the quasi-coordinates since, in practice, the number of actuators is limited. Therefore, we should allocate the control forces on the actuators coordinates to solve this problem.

To perform the allocation we propose the following modified control constraints:

$$\mathbf{A}\mathbf{N}^{-1}\mathbf{u} = \mathbf{e}, \tag{4.45}$$

where $\mathbf{e}$ is a m-column-vector, which should be determined to guarantee that the control forces are generated only in the actuators coordinates.

We need to make some definitions. Let $\mathbf{u}_{\#}$ be the v-column-vector of independent generalized control forces associated with the respective quasi-velocities of the actuators. Define $\mathbf{u}_{*}$ as the r-column-vector of generalized control forces related with the dependent coordinates. These forces are effective control efforts necessary for the individual subsystems to achieve the control objectives. Regarding the actual system, such forces are associated with the passive coordinates, where there is no actuation source. Thus, the control forces can be rewritten as follows:

$$\mathbf{u} = \mathbf{Q}\mathbf{u}_{\#} + \mathbf{R}\mathbf{u}_{*}, \tag{4.46}$$

where $\mathbf{Q}$ is a m by v symmetric matrix used to identify the independent control forces and $\mathbf{R}$ is a m by r symmetric matrix used to identify the dependent control forces.

The following equalities holds:

$$\mathbf{u}_{\#} = \mathbf{Q}^{\mathsf{T}}\mathbf{u}; \quad \mathbf{u}_{*} = \mathbf{R}^{\mathsf{T}}\mathbf{u}; \quad \mathbf{Q}\mathbf{Q}^{\mathsf{T}} + \mathbf{R}\mathbf{R}^{\mathsf{T}} = \mathbf{I}. \tag{4.47}$$

The actuators can generate only the independent control forces. Therefore, to perform the allocation we introduce the underactuation constraints as below:

$$\mathbf{u}_{*} = \mathbf{R}^{\mathsf{T}}\mathbf{u} = \mathbf{0}. \tag{4.48}$$

We must point-out that such constraints cannot be added directly on the constrained minimization since $\mathbf{R}$, by definition, has rows that are identically zero. In this case, the Lagrange multipliers method will not be effective for enforcing this particular type of constraints, as can be seen in Nunemacher (2003).

The constrained optimization, considering the control constraint in Eq. (4.45), becomes:

$$\overline{Z}(\mathbf{u}, \boldsymbol{\lambda}) = \frac{1}{2}(\mathbf{u} - \mathbf{u}_0)^{\mathsf{T}}\mathbf{N}^{-1}(\mathbf{u} - \mathbf{u}_0) - \boldsymbol{\lambda}^{\mathsf{T}}\left(\mathbf{A}\mathbf{N}^{-1}\mathbf{u} - \mathbf{e}\right). \tag{4.49}$$

The stationary points of Eq. (4.49) follows:

$$\frac{\partial \overline{Z}}{\partial \mathbf{u}} = \mathbf{N}^{-1}(\mathbf{u} - \mathbf{u}_0) - \mathbf{N}^{-1}\mathbf{A}^{\mathsf{T}}\boldsymbol{\lambda} = \mathbf{0} \Leftrightarrow \mathbf{u} = \mathbf{u}_0 + \mathbf{A}^{\mathsf{T}}\boldsymbol{\lambda}, \tag{4.50}$$

$$\frac{\partial \overline{Z}}{\partial \boldsymbol{\lambda}} = \mathbf{A}\mathbf{N}^{-1}\mathbf{u} - \mathbf{e} = \mathbf{0} \Leftrightarrow \mathbf{A}\mathbf{N}^{-1}\mathbf{u} = \mathbf{e}. \tag{4.51}$$

Substituting Eq. (4.50) into (4.51) and solving for $\boldsymbol{\lambda}$, results in:

$$\boldsymbol{\lambda} = \left(\mathbf{A}\mathbf{N}^{-1}\mathbf{A}^{\mathsf{T}}\right)^{\mathrm{g}}\left(\mathbf{e} - \mathbf{A}\mathbf{N}^{-1}\mathbf{u}_0\right) + \left(\mathbf{I} - \left(\mathbf{A}\mathbf{N}^{-1}\mathbf{A}^{\mathsf{T}}\right)^{\mathrm{g}}\mathbf{A}\mathbf{N}^{-1}\mathbf{A}^{\mathsf{T}}\right)\mathbf{w}_1. \tag{4.52}$$

where $\mathbf{w}_1$ is an arbitrary column-vector.

Multipliying Eq. (4.52) by $\mathbf{A}^{\mathsf{T}}$ and using the result $\mathbf{A}^{\mathsf{T}}\left(\mathbf{I} - \left(\mathbf{A}\mathbf{N}^{-1}\mathbf{A}^{\mathsf{T}}\right)^{\mathrm{g}}\mathbf{A}\mathbf{N}^{-1}\mathbf{A}^{\mathsf{T}}\right) = \mathbf{0}$ from Eq. (4.31), we get:

$$\mathbf{A}^{\mathsf{T}}\boldsymbol{\lambda} = \mathbf{A}^{\mathsf{T}}\left(\mathbf{A}\mathbf{N}^{-1}\mathbf{A}^{\mathsf{T}}\right)^{\mathrm{g}}\left(\mathbf{e} - \mathbf{A}\mathbf{N}^{-1}\mathbf{u}_0\right). \tag{4.53}$$

Introducing Eq. (4.52) into (4.50), we obtain:

$$\mathbf{u} = \mathbf{u}_0 + \mathbf{A}^{\mathsf{T}}\left(\mathbf{A}\mathbf{N}^{-1}\mathbf{A}^{\mathsf{T}}\right)^{\mathrm{g}}\left(\mathbf{e} - \mathbf{A}\mathbf{N}^{-1}\mathbf{u}_0\right). \tag{4.54}$$

Imposing the underactuation constraints of Eq. (4.48) on (4.54), we get:

$$\begin{aligned} \mathbf{R}^{\mathsf{T}}\mathbf{u} &= \mathbf{R}^{\mathsf{T}}\mathbf{u}_0 + \mathbf{R}^{\mathsf{T}}\mathbf{A}^{\mathsf{T}}\left(\mathbf{A}\mathbf{N}^{-1}\mathbf{A}^{\mathsf{T}}\right)^{\mathrm{g}}\left(\mathbf{e} - \mathbf{A}\mathbf{N}^{-1}\mathbf{u}_0\right), \\ \mathbf{0} &= \left(\mathbf{R}^{\mathsf{T}}\mathbf{A}^{\mathsf{T}}\right)^{\mathrm{g}}\mathbf{R}^{\mathsf{T}}\mathbf{u}_0 + \left(\mathbf{R}^{\mathsf{T}}\mathbf{A}^{\mathsf{T}}\right)^{\mathrm{g}}\mathbf{R}^{\mathsf{T}}\mathbf{A}^{\mathsf{T}}\left(\mathbf{A}\mathbf{N}^{-1}\mathbf{A}^{\mathsf{T}}\right)^{\mathrm{g}}\left(\mathbf{e} - \mathbf{A}\mathbf{N}^{-1}\mathbf{u}_0\right). \end{aligned} \tag{4.55}$$

Solving Eq. (4.55) for $\left(\mathbf{A}\mathbf{N}^{-1}\mathbf{A}^{\mathsf{T}}\right)^{\mathrm{g}}\left(\mathbf{e} - \mathbf{A}\mathbf{N}^{-1}\mathbf{u}_0\right)$, we obtain:

$$\left(\mathbf{A}\mathbf{N}^{-1}\mathbf{A}^{\mathsf{T}}\right)^{\mathrm{g}}\left(\mathbf{e} - \mathbf{A}\mathbf{N}^{-1}\mathbf{u}_0\right) = \left(\mathbf{I} - \left(\mathbf{R}^{\mathsf{T}}\mathbf{A}^{\mathsf{T}}\right)^{\mathrm{g}}\mathbf{R}^{\mathsf{T}}\mathbf{A}^{\mathsf{T}}\right)\mathbf{w}_2 - \left(\mathbf{R}^{\mathsf{T}}\mathbf{A}^{\mathsf{T}}\right)^{\mathrm{g}}\mathbf{R}^{\mathsf{T}}\mathbf{u}_0, \tag{4.56}$$

where $\mathbf{w}_2$ is an arbitrary column-vector.

Multiplying Eq. (4.56) by $\mathbf{A}\mathbf{N}^{-1}\mathbf{A}^{\mathsf{T}}$ and developing, results in:

$$\begin{aligned} \mathbf{A}\mathbf{N}^{-1}\mathbf{A}^{\mathsf{T}}\left(\mathbf{A}\mathbf{N}^{-1}\mathbf{A}^{\mathsf{T}}\right)^{\mathrm{g}}\left(\mathbf{e} - \mathbf{A}\mathbf{N}^{-1}\mathbf{u}_0\right) = \mathbf{A}\mathbf{N}^{-1}\mathbf{A}^{\mathsf{T}}\left(\mathbf{I} - \left(\mathbf{R}^{\mathsf{T}}\mathbf{A}^{\mathsf{T}}\right)^{\mathrm{g}}\mathbf{R}^{\mathsf{T}}\mathbf{A}^{\mathsf{T}}\right)\mathbf{w}_1 + \ldots \\ - \mathbf{A}\mathbf{N}^{-1}\mathbf{A}^{\mathsf{T}}\left(\mathbf{R}^{\mathsf{T}}\mathbf{A}^{\mathsf{T}}\right)^{\mathrm{g}}\mathbf{R}^{\mathsf{T}}\mathbf{u}_0, \end{aligned} \tag{4.57}$$

assuming $\mathbf{A}\mathbf{N}^{-1}\mathbf{A}^{\mathsf{T}}\left(\mathbf{I} - \left(\mathbf{R}^{\mathsf{T}}\mathbf{A}^{\mathsf{T}}\right)^{\mathrm{g}}\mathbf{R}^{\mathsf{T}}\mathbf{A}^{\mathsf{T}}\right) = \mathbf{0}$.

Solving Eq. (4.57) for $\mathbf{e}$, results in:

$$\mathbf{e} = \mathbf{A}\mathbf{N}^{-1}\mathbf{A}^{\mathsf{T}}\left(\mathbf{A}\mathbf{N}^{-1}\mathbf{A}^{\mathsf{T}}\right)^{\mathrm{g}}\mathbf{A}\mathbf{N}^{-1}\left(\mathbf{I} - \mathbf{A}^{\mathsf{T}}\left(\mathbf{R}^{\mathsf{T}}\mathbf{A}^{\mathsf{T}}\right)^{\mathrm{g}}\mathbf{R}^{\mathsf{T}}\right)\mathbf{u}_0 + \left(\mathbf{I} - \mathbf{A}\mathbf{N}^{-1}\mathbf{A}^{\mathsf{T}}\left(\mathbf{A}\mathbf{N}^{-1}\mathbf{A}^{\mathsf{T}}\right)^{\mathrm{g}}\right)\mathbf{w}_3, \tag{4.58}$$

where $\mathbf{w}_3$ is an arbitrary column-vector.

Multiplying Eq. (4.58) by $\left(\mathbf{A}\mathbf{N}^{-1}\mathbf{A}^{\mathsf{T}}\right)^{\mathrm{g}}$ and developing, we obtain:

$$\begin{aligned}\left(\mathbf{A}\mathbf{N}^{-1}\mathbf{A}^{\mathsf{T}}\right)^{\mathrm{g}}\mathbf{e} &= \left(\mathbf{A}\mathbf{N}^{-1}\mathbf{A}^{\mathsf{T}}\right)^{\mathrm{g}}\mathbf{A}\mathbf{N}^{-1}\mathbf{A}^{\mathsf{T}}\left(\mathbf{A}\mathbf{N}^{-1}\mathbf{A}^{\mathsf{T}}\right)^{\mathrm{g}}\mathbf{A}\mathbf{N}^{-1}\left(\mathbf{I}-\mathbf{A}^{\mathsf{T}}\left(\mathbf{R}^{\mathsf{T}}\mathbf{A}^{\mathsf{T}}\right)^{\mathrm{g}}\mathbf{R}^{\mathsf{T}}\right)\mathbf{u}_0+\ldots\\ &\quad\left(\mathbf{A}\mathbf{N}^{-1}\mathbf{A}^{\mathsf{T}}\right)^{\mathrm{g}}\left(\mathbf{I}-\mathbf{A}\mathbf{N}^{-1}\mathbf{A}^{\mathsf{T}}\left(\mathbf{A}\mathbf{N}^{-1}\mathbf{A}^{\mathsf{T}}\right)^{\mathrm{g}}\right)\mathbf{w}_3,\\ &= \left(\mathbf{A}\mathbf{N}^{-1}\mathbf{A}^{\mathsf{T}}\right)^{\mathrm{g}}\mathbf{A}\mathbf{N}^{-1}\left(\mathbf{I}-\mathbf{A}^{\mathsf{T}}\left(\mathbf{R}^{\mathsf{T}}\mathbf{A}^{\mathsf{T}}\right)^{\mathrm{g}}\mathbf{R}^{\mathsf{T}}\right)\mathbf{u}_0+\ldots\\ &\quad\left(\left(\mathbf{A}\mathbf{N}^{-1}\mathbf{A}^{\mathsf{T}}\right)^{\mathrm{g}}-\left(\mathbf{A}\mathbf{N}^{-1}\mathbf{A}^{\mathsf{T}}\right)^{\mathrm{g}}\mathbf{A}\mathbf{N}^{-1}\mathbf{A}^{\mathsf{T}}\left(\mathbf{A}\mathbf{N}^{-1}\mathbf{A}^{\mathsf{T}}\right)^{\mathrm{g}}\right)\mathbf{w}_3,\\ &= \left(\mathbf{A}\mathbf{N}^{-1}\mathbf{A}^{\mathsf{T}}\right)^{\mathrm{g}}\mathbf{A}\mathbf{N}^{-1}\left(\mathbf{I}-\mathbf{A}^{\mathsf{T}}\left(\mathbf{R}^{\mathsf{T}}\mathbf{A}^{\mathsf{T}}\right)^{\mathrm{g}}\mathbf{R}^{\mathsf{T}}\right)\mathbf{u}_0.\end{aligned}\tag{4.59}$$

Substituting Eq. (4.59) into (4.50), we get:

$$\begin{aligned}\mathbf{u} &= \mathbf{u}_0+\mathbf{A}^{\mathsf{T}}\left(\mathbf{A}\mathbf{N}^{-1}\mathbf{A}^{\mathsf{T}}\right)^{\mathrm{g}}\left(\mathbf{A}\mathbf{N}^{-1}\left(\mathbf{I}-\mathbf{A}^{\mathsf{T}}\left(\mathbf{R}^{\mathsf{T}}\mathbf{A}^{\mathsf{T}}\right)^{\mathrm{g}}\mathbf{R}^{\mathsf{T}}\right)-\mathbf{A}\mathbf{N}^{-1}\right)\mathbf{u}_0,\\ &= \mathbf{u}_0-\mathbf{A}^{\mathsf{T}}\left(\mathbf{A}\mathbf{N}^{-1}\mathbf{A}^{\mathsf{T}}\right)^{\mathrm{g}}\mathbf{A}\mathbf{N}^{-1}\mathbf{A}^{\mathsf{T}}\left(\mathbf{R}^{\mathsf{T}}\mathbf{A}^{\mathsf{T}}\right)^{\mathrm{g}}\mathbf{R}^{\mathsf{T}}\mathbf{u}_0.\end{aligned}\tag{4.60}$$

Multiplying Eq. (4.60) by $\mathbf{N}^{-1/2}$, results in:

$$\begin{aligned}\mathbf{N}^{-1/2}\mathbf{u} &= \mathbf{N}^{-1/2}\mathbf{u}_0-\mathbf{N}^{-1/2}\mathbf{A}^{\mathsf{T}}\left(\mathbf{A}\mathbf{N}^{-1/2}\mathbf{N}^{-1/2}\mathbf{A}^{\mathsf{T}}\right)^{\mathrm{g}}\mathbf{A}\mathbf{N}^{-1/2}\mathbf{N}^{-1/2}\mathbf{A}^{\mathsf{T}}\left(\mathbf{R}^{\mathsf{T}}\mathbf{A}^{\mathsf{T}}\right)^{\mathrm{g}}\mathbf{R}^{\mathsf{T}}\mathbf{u}_0,\\ &= \mathbf{N}^{-1/2}\mathbf{u}_0-\mathbf{H}^{\mathsf{T}}\left(\mathbf{H}\mathbf{H}^{\mathsf{T}}\right)^{\mathrm{g}}\mathbf{H}\mathbf{H}^{\mathsf{T}}\left(\mathbf{R}^{\mathsf{T}}\mathbf{A}^{\mathsf{T}}\right)^{\mathrm{g}}\mathbf{R}^{\mathsf{T}}\mathbf{u}_0,\\ &= \mathbf{N}^{-1/2}\mathbf{u}_0-\mathbf{H}^{\mathsf{T}}\left(\mathbf{H}\mathbf{H}^{\mathsf{T}}\right)^{\mathrm{g}}\mathbf{H}\mathbf{H}^{\mathsf{T}}\left(\mathbf{R}^{\mathsf{T}}\mathbf{A}^{\mathsf{T}}\right)^{\mathrm{g}}\mathbf{R}^{\mathsf{T}}\mathbf{u}_0,\\ &= \mathbf{N}^{-1/2}\mathbf{u}_0-\mathbf{H}^{\mathsf{T}}\left(\mathbf{H}^{\mathsf{T}}\right)^{\mathrm{g}}\mathbf{H}^{\mathsf{T}}\left(\mathbf{R}^{\mathsf{T}}\mathbf{A}^{\mathsf{T}}\right)^{\mathrm{g}}\mathbf{R}^{\mathsf{T}}\mathbf{u}_0,\\ &= \mathbf{N}^{-1/2}\mathbf{u}_0-\mathbf{H}^{\mathsf{T}}\left(\mathbf{R}^{\mathsf{T}}\mathbf{A}^{\mathsf{T}}\right)^{\mathrm{g}}\mathbf{R}^{\mathsf{T}}\mathbf{u}_0.\end{aligned}\tag{4.61}$$

Multiplying Eq. (4.61) by $\mathbf{N}^{1/2}$, we have:

$$\begin{aligned}\mathbf{N}^{1/2}\mathbf{N}^{-1/2}\mathbf{u} &= \mathbf{N}^{1/2}\mathbf{N}^{-1/2}\mathbf{u}_0-\mathbf{N}^{1/2}\mathbf{H}^{\mathsf{T}}\left(\mathbf{R}^{\mathsf{T}}\mathbf{A}^{\mathsf{T}}\right)^{\mathrm{g}}\mathbf{R}^{\mathsf{T}}\mathbf{u}_0,\\ \mathbf{N}^{1/2}\mathbf{N}^{-1/2}\mathbf{u} &= \mathbf{N}^{1/2}\mathbf{N}^{-1/2}\mathbf{u}_0-\mathbf{N}^{1/2}\mathbf{N}^{-1/2}\mathbf{A}^{\mathsf{T}}\left(\mathbf{R}^{\mathsf{T}}\mathbf{A}^{\mathsf{T}}\right)^{\mathrm{g}}\mathbf{R}^{\mathsf{T}}\mathbf{u}_0,\\ \mathbf{u} &= \left(\mathbf{I}-\mathbf{A}^{\mathsf{T}}\left(\mathbf{R}^{\mathsf{T}}\mathbf{A}^{\mathsf{T}}\right)^{\mathrm{g}}\mathbf{R}^{\mathsf{T}}\right)\mathbf{u}_0.\end{aligned}\tag{4.62}$$

Using the first relation of Eq. (4.47) on (4.62), we obtain:

$$\mathbf{u}_{\#} = \mathbf{Q}^{\mathsf{T}}\left(\mathbf{I}-\mathbf{A}^{\mathsf{T}}\left(\mathbf{R}^{\mathsf{T}}\mathbf{A}^{\mathsf{T}}\right)^{\mathrm{g}}\mathbf{R}^{\mathsf{T}}\right)\mathbf{u}_0,\tag{4.63}$$

which is the set of independent control forces.

Define $\mathbf{H}_{\mathbf{Q}} = \mathbf{Q}^{\mathsf{T}}$, $\mathbf{H}_{\mathbf{R}} = \mathbf{R}^{\mathsf{T}}$ and $\mathbf{H}_{\mathbf{A}} = \mathbf{A}$ such that Eq. (4.63) can be rewritten in a more compact form, as follows:

$$\mathbf{u}_{\#} = \mathbf{H}_{\mathbf{Q}}\left(\mathbf{I}-\mathbf{H}_{\mathbf{A}}^{\mathsf{T}}\left(\mathbf{H}_{\mathbf{R}}\mathbf{H}_{\mathbf{A}}^{\mathsf{T}}\right)^{\mathrm{g}}\mathbf{H}_{\mathbf{R}}\right)\mathbf{u}_0 = \mathbf{H}_{\mathbf{Q}}\left(\mathbf{I}-\mathbf{H}_{\mathbf{R}|\mathbf{A}}^{\mathrm{g}}\mathbf{H}_{\mathbf{R}}\right)\mathbf{u}_0,\tag{4.64}$$

where $\mathbf{H}^{g}_{\mathbf{R}|\mathbf{A}} = \mathbf{H}^{T}_{\mathbf{A}} \left(\mathbf{H}_{\mathbf{R}} \mathbf{H}^{T}_{\mathbf{A}}\right)^{g}$.

Let $\left(\mathbf{R}^{T}\mathbf{A}^{T}\right)^{g}$ be any $\{1,4\}$-inverse of $\mathbf{R}^{T}\mathbf{A}^{T}$. Thus, the following proprieties holds for $\mathbf{H}^{g}_{\mathbf{R}|\mathbf{A}}$:

$$\begin{aligned}
&P_1 : \mathbf{X}\mathbf{X}^{g}\mathbf{X}\mathbf{X}^{T} = \mathbf{X}\mathbf{X}^{T} \Leftrightarrow \mathbf{H}_{\mathbf{R}}\mathbf{H}^{g}_{\mathbf{R}|\mathbf{A}}\mathbf{H}_{\mathbf{R}}\mathbf{H}^{T}_{\mathbf{A}} = \mathbf{R}^{T}\mathbf{A}^{T}\left(\mathbf{R}^{T}\mathbf{A}^{T}\right)^{g}\mathbf{R}^{T}\mathbf{A}^{T} = \mathbf{H}_{\mathbf{R}}\mathbf{H}^{T}_{\mathbf{A}},\\
&P_2 : \mathbf{X}^{g}\mathbf{X}\mathbf{X}^{g} = \mathbf{X}^{g} \Leftrightarrow \mathbf{H}^{g}_{\mathbf{R}|\mathbf{A}}\mathbf{H}_{\mathbf{R}}\mathbf{H}^{g}_{\mathbf{R}|\mathbf{A}} = \mathbf{A}^{T}\left(\mathbf{R}^{T}\mathbf{A}^{T}\right)^{g}\mathbf{R}^{T}\mathbf{A}^{T}\left(\mathbf{R}^{T}\mathbf{A}^{T}\right)^{g} = \mathbf{H}^{g}_{\mathbf{R}|\mathbf{A}},\\
&P_4 : (\mathbf{X}^{g}\mathbf{X})^{T} = \mathbf{X}^{g}\mathbf{X} \Leftrightarrow \mathbf{H}^{T}_{\mathbf{R}}\left(\mathbf{H}^{g}_{\mathbf{R}|\mathbf{A}}\right)^{T} = \mathbf{R}\,(\mathbf{A}\mathbf{R})^{g}\,\mathbf{A} = \mathbf{H}^{T}_{\mathbf{R}}\left(\mathbf{H}_{\mathbf{A}}\mathbf{H}^{T}_{\mathbf{R}}\right)^{g}\mathbf{H}_{\mathbf{A}} = \mathbf{H}^{g}_{\mathbf{A}|\mathbf{R}}\mathbf{H}_{\mathbf{A}}.
\end{aligned} \tag{4.65}$$

Therefore, if $\left(\mathbf{R}^{T}\mathbf{A}^{T}\right)^{g}$ is any $\{1,4\}$-inverse of $\mathbf{R}^{T}\mathbf{A}^{T}$, then, $\mathbf{H}^{g}_{\mathbf{R}|\mathbf{A}}$ is a $\{1,2,4\}$-inverse of $\mathbf{H}_{\mathbf{R}|\mathbf{A}}$. Similarly, if $(\mathbf{A}\mathbf{R})^{g}$ is any $\{1,4\}$-inverse of $\mathbf{A}\mathbf{R}$, then, $\mathbf{H}^{g}_{\mathbf{A}|\mathbf{R}}$ is a $\{1,2,4\}$-inverse of $\mathbf{H}_{\mathbf{A}|\mathbf{R}}$.

Thus, from Eq. (4.64), we can write:

$$\mathbf{u}_{\#} = \mathbf{H}_{\mathbf{Q}}\left(\mathbf{I} - \mathbf{H}^{g}_{\mathbf{R}|\mathbf{A}}\mathbf{H}_{\mathbf{R}}\right)\mathbf{u}_0 = \mathbf{H}_{\mathbf{Q}}\mathbf{P}_{\mathbf{R}|\mathbf{A}}\mathbf{u}_0, \tag{4.66}$$

where $\mathbf{P}_{\mathbf{R}|\mathbf{A}} = \mathbf{I} - \mathbf{H}^{g}_{\mathbf{R}|\mathbf{A}}\mathbf{H}_{\mathbf{R}}$ is the orthogonal projector onto the kernel of $\mathbf{H}_{\mathbf{R}}$, such that $\mathbf{H}_{\mathbf{R}}\mathbf{P}_{\mathbf{R}|\mathbf{A}} = \mathbf{H}_{\mathbf{R}} - \mathbf{H}_{\mathbf{R}}\mathbf{H}^{g}_{\mathbf{R}|\mathbf{A}}\mathbf{H}_{\mathbf{R}} = \mathbf{0}$ and $\mathbf{P}^{T}_{\mathbf{R}|\mathbf{A}}\mathbf{H}^{T}_{\mathbf{R}} = \mathbf{H}^{T}_{\mathbf{R}} - \mathbf{H}^{T}_{\mathbf{R}}\left(\mathbf{H}^{g}_{\mathbf{R}|\mathbf{A}}\right)^{T}\mathbf{H}^{T}_{\mathbf{R}} = \mathbf{0}$. Moreover, $\mathbf{P}_{\mathbf{A}|\mathbf{R}} = \mathbf{I} - \mathbf{H}^{g}_{\mathbf{A}|\mathbf{R}}\mathbf{H}_{\mathbf{A}}$ is the orthogonal projector onto the kernel of $\mathbf{H}_{\mathbf{A}}$, i.e, $\mathbf{H}_{\mathbf{A}}\mathbf{P}_{\mathbf{A}|\mathbf{R}} = \mathbf{H}_{\mathbf{A}} - \mathbf{H}_{\mathbf{A}}\mathbf{H}^{g}_{\mathbf{A}|\mathbf{R}}\mathbf{H}_{\mathbf{A}} = \mathbf{0}$ and $\mathbf{P}^{T}_{\mathbf{A}|\mathbf{R}}\mathbf{H}^{T}_{\mathbf{A}} = \mathbf{H}^{T}_{\mathbf{A}} - \mathbf{H}^{T}_{\mathbf{A}}\left(\mathbf{H}^{g}_{\mathbf{A}|\mathbf{R}}\right)^{T}\mathbf{H}^{T}_{\mathbf{A}} = \mathbf{0}$.

4.1.2.2 Simultaneous constraint enforcement and control forces allocation

The overactuation problem can also be solved with the proposed methodology.

Consider the following modified Gaussian function:

$$Z(\mathbf{u}, \boldsymbol{\tau}) = \frac{1}{2}(\mathbf{u} - \mathbf{u}_0)^{T}\mathbf{N}^{-1}(\mathbf{u} - \mathbf{u}_0) + \frac{1}{2}\boldsymbol{\tau}^{T}\mathbf{L}\boldsymbol{\tau}, \tag{4.67}$$

where $\boldsymbol{\tau}$ is the p-column-vector of actuators forces and $\mathbf{L}$ is the p by p symmetric positive semi-definite weighting matrix.

The independent control forces should be distributed between the actuators. To do that, we propose a set of additional constraints, given by:

$$\mathbf{u}_{\#} = \mathbf{Q}^{T}\mathbf{u} = \mathbf{T}\boldsymbol{\tau}, \tag{4.68}$$

where $\mathbf{T}$ is the v by p matrix that expresses the actuators configuration in the system $\mathcal{S}$. The matrix $\mathbf{T}$ for allocating independent generalized control forces to the actuators efforts is supposed to be known *a priori* for problems with actuation redundancy.

Let $\boldsymbol{\mu}$ be a v-column-vector of additional Lagrange multipliers associated with the constraints

in Eq. (4.68). The new constrained optimization problem becomes:

$$\overline{Z}(\mathbf{u},\boldsymbol{\tau},\boldsymbol{\lambda},\boldsymbol{\mu}) = \frac{1}{2}(\mathbf{u}-\mathbf{u}_0)^{\mathsf{T}}\mathbf{N}^{-1}(\mathbf{u}-\mathbf{u}_0) + \frac{1}{2}\boldsymbol{\tau}^{\mathsf{T}}\mathbf{L}\boldsymbol{\tau} - \boldsymbol{\lambda}^{\mathsf{T}}\left(\mathbf{A}\mathbf{N}^{-1}\mathbf{u}-\mathbf{c}\right) - \boldsymbol{\mu}^{\mathsf{T}}\left(\mathbf{Q}^{\mathsf{T}}\mathbf{u}-\mathbf{T}\boldsymbol{\tau}\right). \quad (4.69)$$

The stationary points of Eq. (4.69) follow:

$$\frac{\partial Z}{\partial \mathbf{u}} = \mathbf{N}^{-1}(\mathbf{u}-\mathbf{u}_0) - \mathbf{N}^{-1}\mathbf{A}^{\mathsf{T}}\boldsymbol{\lambda} - \mathbf{Q}\boldsymbol{\mu} = \mathbf{0} \Leftrightarrow \mathbf{u} = \mathbf{u}_0 + \mathbf{A}^{\mathsf{T}}\boldsymbol{\lambda} + \mathbf{N}\mathbf{Q}\boldsymbol{\mu}, \quad (4.70)$$

$$\frac{\partial Z}{\partial \boldsymbol{\tau}} = \mathbf{L}\boldsymbol{\tau} + \mathbf{T}^{\mathsf{T}}\boldsymbol{\mu} = \mathbf{0} \Leftrightarrow \boldsymbol{\tau} = -\mathbf{L}^{-1}\mathbf{T}^{\mathsf{T}}\boldsymbol{\mu}, \quad (4.71)$$

$$\frac{\partial Z}{\partial \boldsymbol{\lambda}} = \mathbf{A}\mathbf{N}^{-1}\mathbf{u} - \mathbf{c} = \mathbf{0} \Leftrightarrow \mathbf{A}\mathbf{N}^{-1}\mathbf{u} = \mathbf{c}, \quad (4.72)$$

$$\frac{\partial Z}{\partial \boldsymbol{\mu}} = \mathbf{Q}^{\mathsf{T}}\mathbf{u} - \mathbf{T}\boldsymbol{\tau} = \mathbf{0} \Leftrightarrow \mathbf{Q}^{\mathsf{T}}\mathbf{u} = \mathbf{T}\boldsymbol{\tau}. \quad (4.73)$$

The underactuation constraints still holds:

$$\mathbf{u}_* = \mathbf{R}^{\mathsf{T}}\mathbf{u} = \mathbf{0}. \quad (4.74)$$

Substituting Eq. (4.71) into (4.73) and solving for $\boldsymbol{\mu}$, results in:

$$\boldsymbol{\mu} = \left(\mathbf{I} - \left(\mathbf{T}\mathbf{L}^{-1}\mathbf{T}^{\mathsf{T}}\right)^{\mathrm{g}}\mathbf{T}\mathbf{L}^{-1}\mathbf{T}^{\mathsf{T}}\right)\mathbf{w}_1 - \left(\mathbf{T}\mathbf{L}^{-1}\mathbf{T}^{\mathsf{T}}\right)^{\mathrm{g}}\mathbf{Q}^{\mathsf{T}}\mathbf{u}, \quad (4.75)$$

where $\left(\mathbf{T}\mathbf{L}^{-1}\mathbf{T}^{\mathsf{T}}\right)^{\mathrm{g}}$ is any $\{1,4\}$-inverse of $\mathbf{T}\mathbf{L}^{-1}\mathbf{T}^{\mathsf{T}}$ and $\mathbf{w}_1$ is an arbitrary column-vector.

Introducing Eq. (4.75) into (4.71), we get:

$$\boldsymbol{\tau} = \mathbf{L}^{-1}\mathbf{T}^{\mathsf{T}}\left(\mathbf{T}\mathbf{L}^{-1}\mathbf{T}^{\mathsf{T}}\right)^{\mathrm{g}}\mathbf{Q}^{\mathsf{T}}\mathbf{u} - \mathbf{L}^{-1}\mathbf{T}^{\mathsf{T}}\left(\mathbf{I} - \left(\mathbf{T}\mathbf{L}^{-1}\mathbf{T}^{\mathsf{T}}\right)^{\mathrm{g}}\mathbf{T}\mathbf{L}^{-1}\mathbf{T}^{\mathsf{T}}\right)\mathbf{w}_1, \quad (4.76)$$

with $\mathbf{L}^{-1}\mathbf{T}^{\mathsf{T}}\left(\mathbf{I} - \left(\mathbf{T}\mathbf{L}^{-1}\mathbf{T}^{\mathsf{T}}\right)^{\mathrm{g}}\mathbf{T}\mathbf{L}^{-1}\mathbf{T}^{\mathsf{T}}\right) = \mathbf{0}$, similar to Eq. (4.29).

Using Eq. (4.75) on (4.70), results in:

$$\left(\mathbf{I} + \mathbf{N}\mathbf{Q}\left(\mathbf{T}\mathbf{L}^{-1}\mathbf{T}^{\mathsf{T}}\right)^{\mathrm{g}}\mathbf{Q}^{\mathsf{T}}\right)\mathbf{u} = \mathbf{u}_0 + \mathbf{A}^{\mathsf{T}}\boldsymbol{\lambda} + \mathbf{N}\mathbf{Q}\left(\mathbf{I} - \left(\mathbf{T}\mathbf{L}^{-1}\mathbf{T}^{\mathsf{T}}\right)^{\mathrm{g}}\mathbf{T}\mathbf{L}^{-1}\mathbf{T}^{\mathsf{T}}\right)\mathbf{w}_1. \quad (4.77)$$

Let $\mathbf{Z}$ be a m by m symmetric positive semi-definite matrix, given by:

$$\mathbf{Z} = \mathbf{I} + \mathbf{N}\mathbf{Q}\left(\mathbf{T}\mathbf{L}^{-1}\mathbf{T}^{\mathsf{T}}\right)^{\mathrm{g}}\mathbf{Q}^{\mathsf{T}}. \quad (4.78)$$

Substituting Eq. (4.76) into (4.77) and solving for $\mathbf{u}$ (supposing that $\mathbf{Z}^{-1}$ exist), we get:

$$\mathbf{u} = \mathbf{Z}^{-1}\mathbf{u}_0 + \mathbf{Z}^{-1}\mathbf{A}^{\mathsf{T}}\boldsymbol{\lambda} + \mathbf{Z}^{-1}\mathbf{N}\mathbf{Q}\left(\mathbf{I} - \left(\mathbf{T}\mathbf{L}^{-1}\mathbf{T}^{\mathsf{T}}\right)^{\mathrm{g}}\mathbf{T}\mathbf{L}^{-1}\mathbf{T}^{\mathsf{T}}\right)\mathbf{w}_1. \quad (4.79)$$

with $\mathbf{Z}^{-1}\mathbf{N}\mathbf{Q}\left(\mathbf{I} - \left(\mathbf{T}\mathbf{L}^{-1}\mathbf{T}^{\mathsf{T}}\right)^{\mathrm{g}}\mathbf{T}\mathbf{L}^{-1}\mathbf{T}^{\mathsf{T}}\right)$ being the orthogonal projector associated with the actua-

tion redundancy. For simplicity, we will disregard this second part of the solution. However, this term can be used to achieve secondary objectives (e.g., reduce the control effort, penalize control inputs near the actuation limits, etc.).

Introducing Eq. (4.79) into (4.72) and solving for $\boldsymbol{\lambda}$, results in:

$$\boldsymbol{\lambda} = \left(\mathbf{A}\mathbf{N}^{-1}\mathbf{Z}^{-1}\mathbf{A}^{\mathsf{T}}\right)^{\mathrm{g}}\left(\mathbf{c} - \mathbf{A}\mathbf{N}^{-1}\mathbf{Z}^{-1}\mathbf{u}_0\right) + \left(\mathbf{I} - \left(\mathbf{A}\mathbf{N}^{-1}\mathbf{Z}^{-1}\mathbf{A}^{\mathsf{T}}\right)^{\mathrm{g}}\mathbf{A}\mathbf{N}^{-1}\mathbf{Z}^{-1}\mathbf{A}^{\mathsf{T}}\right)\mathbf{w}_2, \tag{4.80}$$

where $\left(\mathbf{A}\mathbf{N}^{-1}\mathbf{Z}^{-1}\mathbf{A}^{\mathsf{T}}\right)^{\mathrm{g}}$ is any $\{1,4\}$-inverse of $\mathbf{A}\mathbf{N}^{-1}\mathbf{Z}^{-1}\mathbf{A}^{\mathsf{T}}$ and $\mathbf{w}_2$ is an arbitrary column-vector.

Using Eq. (4.80) in (4.79), we obtain:

$$\begin{aligned}\mathbf{u} = \mathbf{Z}^{-1}\mathbf{u}_0 + \mathbf{Z}^{-1}\mathbf{A}^{\mathsf{T}}\left(\mathbf{A}\mathbf{N}^{-1}\mathbf{Z}^{-1}\mathbf{A}^{\mathsf{T}}\right)^{\mathrm{g}}\left(\mathbf{c} - \mathbf{A}\mathbf{N}^{-1}\mathbf{Z}^{-1}\mathbf{u}_0\right) + \ldots \\ \mathbf{Z}^{-1}\mathbf{A}^{\mathsf{T}}\left(\mathbf{I} - \left(\mathbf{A}\mathbf{N}^{-1}\mathbf{Z}^{-1}\mathbf{A}^{\mathsf{T}}\right)^{\mathrm{g}}\mathbf{A}\mathbf{N}^{-1}\mathbf{Z}^{-1}\mathbf{A}^{\mathsf{T}}\right)\mathbf{w}_2,\end{aligned} \tag{4.81}$$

with $\mathbf{Z}^{-1}\mathbf{A}^{\mathsf{T}}\left(\mathbf{I} - \left(\mathbf{A}\mathbf{N}^{-1}\mathbf{Z}^{-1}\mathbf{A}^{\mathsf{T}}\right)^{\mathrm{g}}\mathbf{A}\mathbf{N}^{-1}\mathbf{Z}^{-1}\mathbf{A}^{\mathsf{T}}\right) = \mathbf{0}$, similar to Eq. (4.29).

Imposing the underactuation constraint of Eq. (4.74) in (4.81) and multiplying the result by $\left(\mathbf{R}^{\mathsf{T}}\mathbf{Z}^{-1}\mathbf{A}^{\mathsf{T}}\right)^{\mathrm{g}}$, we obtain:

$$\begin{aligned}\mathbf{0} = \left(\mathbf{R}^{\mathsf{T}}\mathbf{Z}^{-1}\mathbf{A}^{\mathsf{T}}\right)^{\mathrm{g}}\mathbf{R}^{\mathsf{T}}\mathbf{Z}^{-1}\mathbf{u}_0 + \ldots \\ \left(\mathbf{R}^{\mathsf{T}}\mathbf{Z}^{-1}\mathbf{A}^{\mathsf{T}}\right)^{\mathrm{g}}\mathbf{R}^{\mathsf{T}}\mathbf{Z}^{-1}\mathbf{A}^{\mathsf{T}}\left(\mathbf{A}\mathbf{N}^{-1}\mathbf{Z}^{-1}\mathbf{A}^{\mathsf{T}}\right)^{\mathrm{g}}\left(\mathbf{c} - \mathbf{A}\mathbf{N}^{-1}\mathbf{Z}^{-1}\mathbf{u}_0\right).\end{aligned} \tag{4.82}$$

Solving Eq. (4.82) for $\left(\mathbf{A}\mathbf{N}^{-1}\mathbf{Z}^{-1}\mathbf{A}^{\mathsf{T}}\right)^{\mathrm{g}}\left(\mathbf{c} - \mathbf{A}\mathbf{N}^{-1}\mathbf{Z}^{-1}\mathbf{u}_0\right)$, we get:

$$\begin{aligned}\left(\mathbf{A}\mathbf{N}^{-1}\mathbf{Z}^{-1}\mathbf{A}^{\mathsf{T}}\right)^{\mathrm{g}}\left(\mathbf{c} - \mathbf{A}\mathbf{N}^{-1}\mathbf{Z}^{-1}\mathbf{u}_0\right) = \left(\mathbf{I} - \left(\mathbf{R}^{\mathsf{T}}\mathbf{Z}^{-1}\mathbf{A}^{\mathsf{T}}\right)^{\mathrm{g}}\mathbf{R}^{\mathsf{T}}\mathbf{Z}^{-1}\mathbf{A}^{\mathsf{T}}\right)\mathbf{w}_3 + \ldots \\ - \left(\mathbf{R}^{\mathsf{T}}\mathbf{Z}^{-1}\mathbf{A}^{\mathsf{T}}\right)^{\mathrm{g}}\mathbf{R}^{\mathsf{T}}\mathbf{Z}^{-1}\mathbf{u}_0,\end{aligned} \tag{4.83}$$

where $\mathbf{w}_3$ is an arbitrary column-vector.

Multiplying Eq. (4.83) by $\mathbf{A}\mathbf{N}^{-1}\mathbf{Z}^{-1}\mathbf{A}^{\mathsf{T}}$ and developing, we obtain:

$$\begin{aligned}\mathbf{A}\mathbf{N}^{-1}\mathbf{Z}^{-1}\mathbf{A}^{\mathsf{T}}\left(\mathbf{A}\mathbf{N}^{-1}\mathbf{Z}^{-1}\mathbf{A}^{\mathsf{T}}\right)^{\mathrm{g}}\left(\mathbf{c} - \mathbf{A}\mathbf{N}^{-1}\mathbf{Z}^{-1}\mathbf{u}_0\right) = \ldots \\ \mathbf{A}\mathbf{N}^{-1}\mathbf{Z}^{-1}\mathbf{A}^{\mathsf{T}}\left(\mathbf{I} - \left(\mathbf{R}^{\mathsf{T}}\mathbf{Z}^{-1}\mathbf{A}^{\mathsf{T}}\right)^{\mathrm{g}}\mathbf{R}^{\mathsf{T}}\mathbf{Z}^{-1}\mathbf{A}^{\mathsf{T}}\right)\mathbf{w}_3 - \mathbf{A}\mathbf{N}^{-1}\mathbf{Z}^{-1}\mathbf{A}^{\mathsf{T}}\left(\mathbf{R}^{\mathsf{T}}\mathbf{Z}^{-1}\mathbf{A}^{\mathsf{T}}\right)^{\mathrm{g}}\mathbf{R}^{\mathsf{T}}\mathbf{Z}^{-1}\mathbf{u}_0,\end{aligned} \tag{4.84}$$

assuming $\mathbf{A}\mathbf{N}^{-1}\mathbf{Z}^{-1}\mathbf{A}^{\mathsf{T}}\left(\mathbf{I} - \left(\mathbf{R}^{\mathsf{T}}\mathbf{Z}^{-1}\mathbf{A}^{\mathsf{T}}\right)^{\mathrm{g}}\mathbf{R}^{\mathsf{T}}\mathbf{Z}^{-1}\mathbf{A}^{\mathsf{T}}\right) = \mathbf{0}$.

Solving Eq. (4.84) for $\mathbf{c}$ and developing, results in:

$$\begin{aligned}\mathbf{c} = \left(\mathbf{I} - \mathbf{A}\mathbf{N}^{-1}\mathbf{Z}^{-1}\mathbf{A}^{\mathsf{T}}\left(\mathbf{A}\mathbf{N}^{-1}\mathbf{Z}^{-1}\mathbf{A}^{\mathsf{T}}\right)^{\mathrm{g}}\right)\mathbf{w}_4 + \ldots \\ \mathbf{A}\mathbf{N}^{-1}\mathbf{Z}^{-1}\mathbf{A}^{\mathsf{T}}\left(\mathbf{A}\mathbf{N}^{-1}\mathbf{Z}^{-1}\mathbf{A}^{\mathsf{T}}\right)^{\mathrm{g}}\mathbf{A}\mathbf{N}^{-1}\mathbf{Z}^{-1}\left(\mathbf{I} - \mathbf{A}^{\mathsf{T}}\left(\mathbf{R}^{\mathsf{T}}\mathbf{Z}^{-1}\mathbf{A}^{\mathsf{T}}\right)^{\mathrm{g}}\mathbf{R}^{\mathsf{T}}\mathbf{Z}^{-1}\right)\mathbf{u}_0,\end{aligned} \tag{4.85}$$

where $\mathbf{w}_4$ is an arbitrary column-vector.

Substituting Eq. (4.85) into (4.72) and developing, we obtain:

$$
\begin{aligned}
\mathbf{u} &= \mathbf{Z}^{-1}\mathbf{u}_0 + \ldots \\
&\quad \mathbf{Z}^{-1}\mathbf{A}^{\mathsf{T}}\left(\mathbf{A}\mathbf{N}^{-1}\mathbf{Z}^{-1}\mathbf{A}^{\mathsf{T}}\right)^{\mathrm{g}} \times \ldots \\
&\quad \left(\mathbf{A}\mathbf{N}^{-1}\mathbf{Z}^{-1}\mathbf{A}^{\mathsf{T}}\left(\mathbf{A}\mathbf{N}^{-1}\mathbf{Z}^{-1}\mathbf{A}^{\mathsf{T}}\right)^{\mathrm{g}}\mathbf{A}\mathbf{N}^{-1}\mathbf{Z}^{-1}\left(\mathbf{I} - \mathbf{A}^{\mathsf{T}}\left(\mathbf{R}^{\mathsf{T}}\mathbf{Z}^{-1}\mathbf{A}^{\mathsf{T}}\right)^{\mathrm{g}}\mathbf{R}^{\mathsf{T}}\mathbf{Z}^{-1}\right)\mathbf{u}_0 + \ldots \right. \\
&\quad \left.\left(\mathbf{I} - \mathbf{A}\mathbf{N}^{-1}\mathbf{Z}^{-1}\mathbf{A}^{\mathsf{T}}\left(\mathbf{A}\mathbf{N}^{-1}\mathbf{Z}^{-1}\mathbf{A}^{\mathsf{T}}\right)^{\mathrm{g}}\right)\mathbf{w}_4 - \mathbf{A}\mathbf{N}^{-1}\mathbf{Z}^{-1}\mathbf{u}_0\right), \\
&= \mathbf{Z}^{-1}\mathbf{u}_0 + \ldots \\
&\quad \mathbf{Z}^{-1}\mathbf{A}^{\mathsf{T}}\left(\left(\mathbf{A}\mathbf{N}^{-1}\mathbf{Z}^{-1}\mathbf{A}^{\mathsf{T}}\right)^{\mathrm{g}}\mathbf{A}\mathbf{N}^{-1}\mathbf{Z}^{-1}\mathbf{A}^{\mathsf{T}}\left(\mathbf{A}\mathbf{N}^{-1}\mathbf{Z}^{-1}\mathbf{A}^{\mathsf{T}}\right)^{\mathrm{g}} \times \ldots \right. \\
&\quad \mathbf{A}\mathbf{N}^{-1}\mathbf{Z}^{-1}\left(\mathbf{I} - \mathbf{A}^{\mathsf{T}}\left(\mathbf{R}^{\mathsf{T}}\mathbf{Z}^{-1}\mathbf{A}^{\mathsf{T}}\right)^{\mathrm{g}}\mathbf{R}^{\mathsf{T}}\mathbf{Z}^{-1}\right)\mathbf{u}_0 + \ldots \\
&\quad \left.\left(\mathbf{A}\mathbf{N}^{-1}\mathbf{Z}^{-1}\mathbf{A}^{\mathsf{T}}\right)^{\mathrm{g}}\left(\mathbf{I} - \mathbf{A}\mathbf{N}^{-1}\mathbf{Z}^{-1}\mathbf{A}^{\mathsf{T}}\left(\mathbf{A}\mathbf{N}^{-1}\mathbf{Z}^{-1}\mathbf{A}^{\mathsf{T}}\right)^{\mathrm{g}}\right)\mathbf{w}_4 - \left(\mathbf{A}\mathbf{N}^{-1}\mathbf{Z}^{-1}\mathbf{A}^{\mathsf{T}}\right)^{\mathrm{g}}\mathbf{A}\mathbf{N}^{-1}\mathbf{Z}^{-1}\mathbf{u}_0\right), \\
&= \mathbf{Z}^{-1}\mathbf{u}_0 + \ldots \\
&\quad \mathbf{Z}^{-1}\mathbf{A}^{\mathsf{T}}\left(\left(\mathbf{A}\mathbf{N}^{-1}\mathbf{Z}^{-1}\mathbf{A}^{\mathsf{T}}\right)^{\mathrm{g}}\mathbf{A}\mathbf{N}^{-1}\mathbf{Z}^{-1}\mathbf{A}^{\mathsf{T}}\left(\mathbf{A}\mathbf{N}^{-1}\mathbf{Z}^{-1}\mathbf{A}^{\mathsf{T}}\right)^{\mathrm{g}} \times \ldots \right. \\
&\quad \mathbf{A}\mathbf{N}^{-1}\mathbf{Z}^{-1}\left(\mathbf{I} - \mathbf{A}^{\mathsf{T}}\left(\mathbf{R}^{\mathsf{T}}\mathbf{Z}^{-1}\mathbf{A}^{\mathsf{T}}\right)^{\mathrm{g}}\mathbf{R}^{\mathsf{T}}\mathbf{Z}^{-1}\right)\mathbf{u}_0, \\
&\quad \left(\left(\mathbf{A}\mathbf{N}^{-1}\mathbf{Z}^{-1}\mathbf{A}^{\mathsf{T}}\right)^{\mathrm{g}} - \left(\mathbf{A}\mathbf{N}^{-1}\mathbf{Z}^{-1}\mathbf{A}^{\mathsf{T}}\right)^{\mathrm{g}}\mathbf{A}\mathbf{N}^{-1}\mathbf{Z}^{-1}\mathbf{A}^{\mathsf{T}}\left(\mathbf{A}\mathbf{N}^{-1}\mathbf{Z}^{-1}\mathbf{A}^{\mathsf{T}}\right)^{\mathrm{g}}\right)\mathbf{w}_4 + \ldots \\
&\quad \left. - \left(\mathbf{A}\mathbf{N}^{-1}\mathbf{Z}^{-1}\mathbf{A}^{\mathsf{T}}\right)^{\mathrm{g}}\mathbf{A}\mathbf{N}^{-1}\mathbf{Z}^{-1}\mathbf{u}_0\right), \qquad (4.86) \\
&= \mathbf{Z}^{-1}\mathbf{u}_0 + \ldots \\
&\quad \mathbf{Z}^{-1}\mathbf{A}^{\mathsf{T}}\left(\left(\mathbf{A}\mathbf{N}^{-1}\mathbf{Z}^{-1}\mathbf{A}^{\mathsf{T}}\right)^{\mathrm{g}}\mathbf{A}\mathbf{N}^{-1}\mathbf{Z}^{-1}\left(\mathbf{I} - \mathbf{A}^{\mathsf{T}}\left(\mathbf{R}^{\mathsf{T}}\mathbf{Z}^{-1}\mathbf{A}^{\mathsf{T}}\right)^{\mathrm{g}}\mathbf{R}^{\mathsf{T}}\mathbf{Z}^{-1}\right)\mathbf{u}_0 + \ldots \right. \\
&\quad \left.\left(\left(\mathbf{A}\mathbf{N}^{-1}\mathbf{Z}^{-1}\mathbf{A}^{\mathsf{T}}\right)^{\mathrm{g}} - \left(\mathbf{A}\mathbf{N}^{-1}\mathbf{Z}^{-1}\mathbf{A}^{\mathsf{T}}\right)^{\mathrm{g}}\right)\mathbf{w}_4 - \left(\mathbf{A}\mathbf{N}^{-1}\mathbf{Z}^{-1}\mathbf{A}^{\mathsf{T}}\right)^{\mathrm{g}}\mathbf{A}\mathbf{N}^{-1}\mathbf{Z}^{-1}\mathbf{u}_0\right), \\
&= \mathbf{Z}^{-1}\mathbf{u}_0 + \ldots \\
&\quad \mathbf{Z}^{-1}\mathbf{A}^{\mathsf{T}}\left(\left(\mathbf{A}\mathbf{N}^{-1}\mathbf{Z}^{-1}\mathbf{A}^{\mathsf{T}}\right)^{\mathrm{g}}\mathbf{A}\mathbf{N}^{-1}\mathbf{Z}^{-1}\left(\mathbf{I} - \mathbf{A}^{\mathsf{T}}\left(\mathbf{R}^{\mathsf{T}}\mathbf{Z}^{-1}\mathbf{A}^{\mathsf{T}}\right)^{\mathrm{g}}\mathbf{R}^{\mathsf{T}}\mathbf{Z}^{-1}\right)\mathbf{u}_0 + \ldots \right. \\
&\quad \left. - \left(\mathbf{A}\mathbf{N}^{-1}\mathbf{Z}^{-1}\mathbf{A}^{\mathsf{T}}\right)^{\mathrm{g}}\mathbf{A}\mathbf{N}^{-1}\mathbf{Z}^{-1}\mathbf{u}_0\right), \\
&= \mathbf{Z}^{-1}\mathbf{u}_0 + \ldots \\
&\quad \mathbf{Z}^{-1}\mathbf{A}^{\mathsf{T}}\left(\left(\mathbf{A}\mathbf{N}^{-1}\mathbf{Z}^{-1}\mathbf{A}^{\mathsf{T}}\right)^{\mathrm{g}}\mathbf{A}\mathbf{N}^{-1}\mathbf{Z}^{-1}\mathbf{u}_0 + \ldots \right. \\
&\quad - \left(\mathbf{A}\mathbf{N}^{-1}\mathbf{Z}^{-1}\mathbf{A}^{\mathsf{T}}\right)^{\mathrm{g}}\mathbf{A}\mathbf{N}^{-1}\mathbf{Z}^{-1}\mathbf{A}^{\mathsf{T}}\left(\mathbf{R}^{\mathsf{T}}\mathbf{Z}^{-1}\mathbf{A}^{\mathsf{T}}\right)^{\mathrm{g}}\mathbf{R}^{\mathsf{T}}\mathbf{Z}^{-1}\mathbf{u}_0, \\
&\quad \left. - \left(\mathbf{A}\mathbf{N}^{-1}\mathbf{Z}^{-1}\mathbf{A}^{\mathsf{T}}\right)^{\mathrm{g}}\mathbf{A}\mathbf{N}^{-1}\mathbf{Z}^{-1}\mathbf{u}_0\right), \\
&= \mathbf{Z}^{-1}\mathbf{u}_0 + \ldots \\
&\quad - \mathbf{Z}^{-1}\mathbf{A}^{\mathsf{T}}\left(\mathbf{A}\mathbf{N}^{-1}\mathbf{Z}^{-1}\mathbf{A}^{\mathsf{T}}\right)^{\mathrm{g}}\mathbf{A}\mathbf{N}^{-1}\mathbf{Z}^{-1}\mathbf{A}^{\mathsf{T}}\left(\mathbf{R}^{\mathsf{T}}\mathbf{Z}^{-1}\mathbf{A}^{\mathsf{T}}\right)^{\mathrm{g}}\mathbf{R}^{\mathsf{T}}\mathbf{Z}^{-1}\mathbf{u}_0.
\end{aligned}
$$

Multiplying Eq. (4.86) by $\mathbf{N}^{-1}$ and developing, we obtain:

$$\begin{aligned}
\mathbf{N}^{-1}\mathbf{u} &= \mathbf{N}^{-1}\mathbf{Z}^{-1}\mathbf{u}_0 + \dots \\
&\quad - \mathbf{N}^{-1}\mathbf{Z}^{-1}\mathbf{A}^\intercal \left(\mathbf{A}\mathbf{N}^{-1}\mathbf{Z}^{-1}\mathbf{A}^\intercal\right)^{\mathrm{g}} \times \dots \\
&\quad \mathbf{A}\mathbf{N}^{-1}\mathbf{Z}^{-1}\mathbf{A}^\intercal \left(\mathbf{R}^\intercal\mathbf{Z}^{-1}\mathbf{A}^\intercal\right)^{\mathrm{g}} \mathbf{R}^\intercal\mathbf{Z}^{-1}\mathbf{u}_0, \\
&= \mathbf{N}^{-1}\mathbf{Z}^{-1}\mathbf{u}_0 + \dots \\
&\quad - \mathbf{N}^{-1/2}\mathbf{N}^{-1/2}\mathbf{Z}^{-1/2}\mathbf{Z}^{-1/2}\mathbf{A}^\intercal \left(\mathbf{A}\mathbf{N}^{-1}\mathbf{Z}^{-1}\mathbf{A}^\intercal\right)^{\mathrm{g}} \times \dots \\
&\quad \mathbf{A}\mathbf{N}^{-1}\mathbf{Z}^{-1}\mathbf{A}^\intercal \left(\mathbf{R}^\intercal\mathbf{Z}^{-1}\mathbf{A}^\intercal\right)^{\mathrm{g}} \mathbf{R}^\intercal\mathbf{Z}^{-1}\mathbf{u}_0, \\
&= \mathbf{N}^{-1}\mathbf{Z}^{-1}\mathbf{u}_0 + \dots \\
&\quad - \mathbf{N}^{-1/2}\left(\mathbf{Z}^{-1/2}\right)^\intercal \mathbf{N}^{-1/2}\mathbf{Z}^{-1/2}\mathbf{A}^\intercal \left(\mathbf{A}\mathbf{N}^{-1}\mathbf{Z}^{-1}\mathbf{A}^\intercal\right)^{\mathrm{g}} \times \dots \\
&\quad \mathbf{A}\mathbf{N}^{-1}\mathbf{Z}^{-1}\mathbf{A}^\intercal \left(\mathbf{R}^\intercal\mathbf{Z}^{-1}\mathbf{A}^\intercal\right)^{\mathrm{g}} \mathbf{R}^\intercal\mathbf{Z}^{-1}\mathbf{u}_0.
\end{aligned} \tag{4.87}$$

Define $\mathbf{H} = \mathbf{A}\left(\mathbf{Z}^{-1/2}\right)^\intercal \mathbf{N}^{-1/2}$ such that Eq. (4.87) can be rewritten as:

$$\begin{aligned}
\mathbf{N}^{-1}\mathbf{u} &= \mathbf{N}^{-1}\mathbf{Z}^{-1}\mathbf{u}_0 + \dots \\
&\quad - \mathbf{N}^{-1/2}\left(\mathbf{Z}^{-1/2}\right)^\intercal \mathbf{H}^\intercal \left(\mathbf{H}\mathbf{H}^\intercal\right)^{\mathrm{g}} \mathbf{H}\mathbf{H}^\intercal \times \dots \\
&\quad \left(\mathbf{R}^\intercal\mathbf{Z}^{-1}\mathbf{A}^\intercal\right)^{\mathrm{g}} \mathbf{R}^\intercal\mathbf{Z}^{-1}\mathbf{u}_0, \\
&= \mathbf{N}^{-1}\mathbf{Z}^{-1}\mathbf{u}_0 + \dots \\
&\quad - \mathbf{N}^{-1/2}\left(\mathbf{Z}^{-1/2}\right)^\intercal \mathbf{H}^\intercal \left(\mathbf{H}^\intercal\right)^{\mathrm{g}} \mathbf{H}^{\mathrm{g}}\mathbf{H}\mathbf{H}^\intercal \times \dots \\
&\quad \left(\mathbf{R}^\intercal\mathbf{Z}^{-1}\mathbf{A}^\intercal\right)^{\mathrm{g}} \mathbf{R}^\intercal\mathbf{Z}^{-1}\mathbf{u}_0, \\
&= \mathbf{N}^{-1}\mathbf{Z}^{-1}\mathbf{u}_0 + \dots \\
&\quad - \mathbf{N}^{-1/2}\left(\mathbf{Z}^{-1/2}\right)^\intercal \mathbf{H}^\intercal \left(\mathbf{H}^\intercal\right)^{\mathrm{g}} \mathbf{H}^\intercal \left(\mathbf{H}^\intercal\right)^{\mathrm{g}} \mathbf{H}^\intercal \times \dots \\
&\quad \left(\mathbf{R}^\intercal\mathbf{Z}^{-1}\mathbf{A}^\intercal\right)^{\mathrm{g}} \mathbf{R}^\intercal\mathbf{Z}^{-1}\mathbf{u}_0, \\
&= \mathbf{N}^{-1}\mathbf{Z}^{-1}\mathbf{u}_0 + \dots \\
&\quad - \mathbf{N}^{-1/2}\left(\mathbf{Z}^{-1/2}\right)^\intercal \mathbf{H}^\intercal \left(\mathbf{H}^\intercal\right)^{\mathrm{g}} \mathbf{H}^\intercal \times \dots \\
&\quad \left(\mathbf{R}^\intercal\mathbf{Z}^{-1}\mathbf{A}^\intercal\right)^{\mathrm{g}} \mathbf{R}^\intercal\mathbf{Z}^{-1}\mathbf{u}_0, \\
&= \mathbf{N}^{-1}\mathbf{Z}^{-1}\mathbf{u}_0 + \dots \\
&\quad - \mathbf{N}^{-1/2}\left(\mathbf{Z}^{-1/2}\right)^\intercal \mathbf{H}^\intercal \left(\mathbf{R}^\intercal\mathbf{Z}^{-1}\mathbf{A}^\intercal\right)^{\mathrm{g}} \mathbf{R}^\intercal\mathbf{Z}^{-1}\mathbf{u}_0.
\end{aligned} \tag{4.88}$$

Expanding the terms $\mathbf{H}$ of Eq. (4.88) and developing, results in:

$$\begin{aligned}\mathbf{N}^{-1}\mathbf{u} &= \mathbf{N}^{-1}\mathbf{Z}^{-1}\mathbf{u}_0 + \ldots \\ &\quad - \mathbf{N}^{-1/2}\left(\mathbf{Z}^{-1/2}\right)^{\mathsf{T}}\mathbf{N}^{-1/2}\mathbf{Z}^{-1/2}\mathbf{A}^{\mathsf{T}}\left(\mathbf{R}^{\mathsf{T}}\mathbf{Z}^{-1}\mathbf{A}^{\mathsf{T}}\right)^{\mathrm{g}}\mathbf{R}^{\mathsf{T}}\mathbf{Z}^{-1}\mathbf{u}_0, \\ &= \mathbf{N}^{-1}\mathbf{Z}^{-1}\mathbf{u}_0 - \mathbf{N}^{-1}\mathbf{Z}^{-1}\mathbf{A}^{\mathsf{T}}\left(\mathbf{R}^{\mathsf{T}}\mathbf{Z}^{-1}\mathbf{A}^{\mathsf{T}}\right)^{\mathrm{g}}\mathbf{R}^{\mathsf{T}}\mathbf{Z}^{-1}\mathbf{u}_0.\end{aligned} \tag{4.89}$$

Multiplying Eq. (4.89) by $\mathbf{N}$, we obtain:

$$\mathbf{u} = \left(\mathbf{I} - \mathbf{Z}^{-1}\mathbf{A}^{\mathsf{T}}\left(\mathbf{R}^{\mathsf{T}}\mathbf{Z}^{-1}\mathbf{A}^{\mathsf{T}}\right)^{\mathrm{g}}\mathbf{R}^{\mathsf{T}}\right)\mathbf{Z}^{-1}\mathbf{u}_0. \tag{4.90}$$

To simplify the expressions, we can rewrite Eqs. (4.90) and (4.76) as follows:

$$\mathbf{u}_{\#} = \mathbf{Q}^{\mathsf{T}}\left(\mathbf{I} - \mathbf{Z}^{-1/2}\mathbf{Z}^{-1/2}\mathbf{A}^{\mathsf{T}}\left(\mathbf{R}^{\mathsf{T}}\mathbf{Z}^{-1/2}\mathbf{Z}^{-1/2}\mathbf{A}^{\mathsf{T}}\right)^{\mathrm{g}}\mathbf{R}^{\mathsf{T}}\right)\mathbf{Z}^{-1/2}\mathbf{Z}^{-1/2}\mathbf{u}_0, \tag{4.91}$$

$$\boldsymbol{\tau} = \mathbf{L}^{-1/2}\mathbf{L}^{-1/2}\mathbf{T}^{\mathsf{T}}\left(\mathbf{T}\mathbf{L}^{-1/2}\mathbf{L}^{-1/2}\mathbf{T}^{\mathsf{T}}\right)^{\mathrm{g}}\mathbf{u}_{\#}. \tag{4.92}$$

Let us define $\mathbf{H}_{\mathbf{Q}} = \mathbf{Q}^{\mathsf{T}}$, $\bar{\mathbf{H}}_{\mathbf{R}} = \mathbf{R}^{\mathsf{T}}\mathbf{Z}^{-1/2}$, $\bar{\mathbf{H}}_{\mathbf{A}}^{\mathsf{T}} = \mathbf{Z}^{-1/2}\mathbf{A}^{\mathsf{T}}$, $\boldsymbol{\mu}_0 = \mathbf{Z}^{-1/2}\mathbf{u}_0$ and $\bar{\mathbf{H}}_{\mathbf{T}} = \mathbf{T}\mathbf{L}^{-1/2}$. Thus, Eqs. (4.91) and (4.92) become:

$$\mathbf{u}_{\#} = \mathbf{H}_{\mathbf{Q}}\mathbf{Z}^{-1/2}\left(\mathbf{I} - \bar{\mathbf{H}}_{\mathbf{A}}^{\mathsf{T}}\left(\bar{\mathbf{H}}_{\mathbf{R}}\bar{\mathbf{H}}_{\mathbf{A}}^{\mathsf{T}}\right)^{\mathrm{g}}\bar{\mathbf{H}}_{\mathbf{R}}\right)\boldsymbol{\mu}_0 = \mathbf{H}_{\mathbf{Q}}\mathbf{Z}^{-1/2}\left(\mathbf{I} - \bar{\mathbf{H}}_{\mathbf{R}|\mathbf{A}}^{\mathrm{g}}\bar{\mathbf{H}}_{\mathbf{R}}\right)\boldsymbol{\mu}_0, \tag{4.93}$$

$$\boldsymbol{\tau} = \mathbf{L}^{-1/2}\bar{\mathbf{H}}_{\mathbf{T}}^{\mathsf{T}}\left(\bar{\mathbf{H}}_{\mathbf{T}}\bar{\mathbf{H}}_{\mathbf{T}}^{\mathsf{T}}\right)^{\mathrm{g}}\mathbf{u}_{\#} = \mathbf{L}^{-1/2}\bar{\mathbf{H}}_{\mathbf{T}}^{\mathrm{g}}\mathbf{u}_{\#}, \tag{4.94}$$

with $\bar{\mathbf{H}}_{\mathbf{R}|\mathbf{A}}^{\mathrm{g}} = \bar{\mathbf{H}}_{\mathbf{A}}^{\mathsf{T}}\left(\bar{\mathbf{H}}_{\mathbf{R}}\bar{\mathbf{H}}_{\mathbf{A}}^{\mathsf{T}}\right)^{\mathrm{g}}$ being a $\{1,2,4\}$-inverse of $\bar{\mathbf{H}}_{\mathbf{R}}$ and $\bar{\mathbf{H}}_{\mathbf{T}}^{\mathrm{g}} = \bar{\mathbf{H}}_{\mathbf{T}}^{\mathsf{T}}\left(\bar{\mathbf{H}}_{\mathbf{T}}\bar{\mathbf{H}}_{\mathbf{T}}^{\mathsf{T}}\right)^{\mathrm{g}}$ as any $\{1,4\}$-inverse of $\bar{\mathbf{H}}_{\mathbf{T}}$.

Using the definitions above, the matrix $\mathbf{Z}$ can also be rewrite in a more compact form, as shown below:

$$\begin{aligned}\mathbf{Z} &= \mathbf{I} + \mathbf{N}\mathbf{Q}\left(\mathbf{T}\mathbf{L}^{-1/2}\mathbf{L}^{-1/2}\mathbf{T}^{\mathsf{T}}\right)^{\mathrm{g}}\mathbf{Q}^{\mathsf{T}}, \\ &= \mathbf{I} + \mathbf{N}\mathbf{Q}\left(\mathbf{T}\mathbf{L}^{-1/2}\mathbf{L}^{-1/2}\mathbf{T}^{\mathsf{T}}\right)^{\mathrm{g}}\mathbf{Q}^{\mathsf{T}}, \\ &= \mathbf{I} + \mathbf{N}\mathbf{H}_{\mathbf{Q}}^{\mathsf{T}}\left(\bar{\mathbf{H}}_{\mathbf{T}}\bar{\mathbf{H}}_{\mathbf{T}}^{\mathsf{T}}\right)^{\mathrm{g}}\mathbf{H}_{\mathbf{Q}}, \\ &= \mathbf{I} + \mathbf{N}\mathbf{H}_{\mathbf{Q}}^{\mathsf{T}}\left(\bar{\mathbf{H}}_{\mathbf{T}}^{\mathsf{T}}\right)^{\mathrm{g}}\bar{\mathbf{H}}_{\mathbf{T}}^{\mathrm{g}}\mathbf{H}_{\mathbf{Q}}, \\ &= \mathbf{I} + \mathbf{N}\left(\bar{\mathbf{H}}_{\mathbf{T}}^{\mathrm{g}}\mathbf{H}_{\mathbf{Q}}\right)^{\mathsf{T}}\bar{\mathbf{H}}_{\mathbf{T}}^{\mathrm{g}}\mathbf{H}_{\mathbf{Q}}.\end{aligned} \tag{4.95}$$

4.1.3 Decentralized controllers synthesis

4.1.3.1 Hard control constraints

Instead of using an *ad-hoc* control algorithm for the decentralized controllers, we can use the proposed methodology to obtain such controllers to guarantee their consistency with the modeling constraints, while other control objectives are achieved.

Let $\boldsymbol{\varphi}_{\mathrm{SC}}$ be the l-column-vector of bilateral holonomic and nonholonomic material servo-constraints of the system $\mathcal{S}$, such that:

$$\boldsymbol{\varphi}_{\mathrm{SC}}\left(\mathbf{v}, \mathbf{q}, t\right) = \mathbf{0}. \tag{4.96}$$

Performing the time-derivative of Eq. (4.96), we get:

$$\mathbf{A}_{\mathrm{SC}}\mathbf{a}_{\mathrm{SC}} = \mathbf{b}_{\mathrm{SC}}, \tag{4.97}$$

where $\mathbf{A}_{\mathrm{SC}}$ is the l by m Jacobian matrix associated with the control constraints and $\mathbf{b}_{\mathrm{SC}}$ is the respective l-column-vector.

Let the servo controlled quasi-accelerations be defined as:

$$\mathbf{a}_{\mathrm{SC}} = \mathbf{a} + \mathbf{N}^{-1}\mathbf{u}. \tag{4.98}$$

Substituting Eqs. (4.7) and (4.25) into (4.98), we obtain:

$$\mathbf{a}_{\mathrm{SC}} = \mathbf{a}_0 + \mathbf{N}^{-1}\mathbf{u}_0 + \mathbf{N}^{-1}\mathbf{A}^{\mathsf{T}}\left(\mathbf{A}\mathbf{N}^{-1}\mathbf{A}^{\mathsf{T}}\right)^{\mathrm{g}}\left(\mathbf{b} - \mathbf{A}\mathbf{a}_0 - \mathbf{A}\mathbf{N}^{-1}\mathbf{u}_0\right). \tag{4.99}$$

Gathering the terms of Eq. (4.99) multiplied by $\mathbf{u}_0$, we get:

$$\begin{aligned}\mathbf{N}^{-1} - \mathbf{N}^{-1}\mathbf{A}^{\mathsf{T}}\left(\mathbf{A}\mathbf{N}^{-1}\mathbf{A}^{\mathsf{T}}\right)^{\mathrm{g}}\mathbf{A}\mathbf{N}^{-1} &= \mathbf{N}^{-1/2}\mathbf{N}^{-1/2} + \ldots \\ -\mathbf{N}^{-1/2}\mathbf{N}^{-1/2}\mathbf{A}^{\mathsf{T}}\left(\mathbf{A}\mathbf{N}^{-1/2}\mathbf{N}^{-1/2}\mathbf{A}^{\mathsf{T}}\right)^{\mathrm{g}}&\mathbf{A}\mathbf{N}^{-1/2}\mathbf{N}^{-1/2}.\end{aligned} \tag{4.100}$$

With $\mathbf{H} = \mathbf{A}\mathbf{N}^{-1/2}$, we can rewrite Eq. (4.100) as:

$$\begin{aligned}\mathbf{N}^{-1/2}\mathbf{N}^{-1/2} - \mathbf{N}^{-1/2}\mathbf{H}^{\mathsf{T}}\left(\mathbf{H}\mathbf{H}^{\mathsf{T}}\right)^{\mathrm{g}}\mathbf{H}\mathbf{N}^{-1/2} &= \mathbf{N}^{-1/2}\left(\mathbf{I} - \mathbf{H}^{\mathsf{T}}\left(\mathbf{H}\mathbf{H}^{\mathsf{T}}\right)^{\mathrm{g}}\mathbf{H}\right)\mathbf{N}^{-1/2}, \\ &= \mathbf{N}^{-1/2}\left(\mathbf{I} - \mathbf{H}^{\mathrm{g}}\mathbf{H}\right)\mathbf{N}^{-1/2}, \\ &= \mathbf{N}^{-1/2}\mathbf{P}\mathbf{N}^{-1/2},\end{aligned} \tag{4.101}$$

with $\mathbf{P} = \mathbf{I} - \mathbf{H}^{\mathrm{g}}\mathbf{H}$.

Substituting Eq. (4.101) into (4.99), results in:

$$\mathbf{a}_{\text{SC}} = \mathbf{a} + \mathbf{N}^{-1/2}\mathbf{P}\mathbf{N}^{-1/2}\mathbf{u}_0. \tag{4.102}$$

Let the Gaussian function be given by:

$$Z(\mathbf{u}_0) = \frac{1}{2}\mathbf{u}_0^{\mathsf{T}}\boldsymbol{\Gamma}\mathbf{u}_0, \tag{4.103}$$

where $\boldsymbol{\Gamma}$ is a m by m symmetric positive semi-definite weighting matrix related with the decentralized controllers.

Let $\boldsymbol{\lambda}$ be a l-column-vector of Lagrange multipliers related to the constraints in Eq. (4.97). The new constrained optimization problem becomes:

$$\overline{Z}(\mathbf{u}_0, \boldsymbol{\lambda}) = \frac{1}{2}\mathbf{u}_0^{\mathsf{T}}\boldsymbol{\Gamma}\mathbf{u}_0 - \boldsymbol{\lambda}^{\mathsf{T}}\left(\mathbf{A}_{\text{SC}}\mathbf{a}_{\text{SC}} - \mathbf{b}_{\text{SC}}\right). \tag{4.104}$$

Substituting Eq. (4.102) into (4.104), we get:

$$\overline{Z}(\mathbf{u}_0, \boldsymbol{\lambda}) = \frac{1}{2}\mathbf{u}_0^{\mathsf{T}}\boldsymbol{\Gamma}\mathbf{u}_0 - \boldsymbol{\lambda}^{\mathsf{T}}\left(\mathbf{A}_{\text{SC}}\mathbf{a} + \mathbf{A}_{\text{SC}}\mathbf{N}^{-1/2}\mathbf{P}\mathbf{N}^{-1/2}\mathbf{u}_0 - \mathbf{b}_{\text{SC}}\right). \tag{4.105}$$

The stationary points of Eq. (4.105) are given by:

$$\frac{\partial \overline{Z}}{\partial \mathbf{u}_0} = \boldsymbol{\Gamma}\mathbf{u}_0 - \mathbf{N}^{-1/2}\mathbf{P}^{\mathsf{T}}\mathbf{N}^{-1/2}\mathbf{A}_{\text{SC}}^{\mathsf{T}}\boldsymbol{\lambda} = \mathbf{0} \Leftrightarrow \mathbf{u}_0 = \boldsymbol{\Gamma}^{-1}\mathbf{N}^{-1/2}\mathbf{P}^{\mathsf{T}}\mathbf{N}^{-1/2}\mathbf{A}_{\text{SC}}^{\mathsf{T}}\boldsymbol{\lambda}, \tag{4.106}$$

$$\frac{\partial \overline{Z}}{\partial \boldsymbol{\lambda}} = \mathbf{A}_{\text{SC}}\mathbf{a} + \mathbf{A}_{\text{SC}}\mathbf{N}^{-1/2}\mathbf{P}\mathbf{N}^{-1/2}\mathbf{u}_0 - \mathbf{b}_{\text{SC}} = \mathbf{0} \Leftrightarrow \mathbf{A}_{\text{SC}}\mathbf{a} + \mathbf{A}_{\text{SC}}\mathbf{N}^{-1/2}\mathbf{P}\mathbf{N}^{-1/2}\mathbf{u}_0 = \mathbf{b}_{\text{SC}}. \tag{4.107}$$

Substituting Eq. (4.106) into (4.107), we obtain:

$$\mathbf{A}_{\text{SC}}\mathbf{N}^{-1/2}\mathbf{P}\mathbf{N}^{-1/2}\boldsymbol{\Gamma}^{-1}\mathbf{N}^{-1/2}\mathbf{P}^{\mathsf{T}}\mathbf{N}^{-1/2}\mathbf{A}_{\text{SC}}^{\mathsf{T}}\boldsymbol{\lambda} = \mathbf{b}_{\text{SC}} - \mathbf{A}_{\text{SC}}\mathbf{a}. \tag{4.108}$$

Eq. (4.108) can be rewritten as follows:

$$\bar{\mathbf{H}}_{\text{SC}}\bar{\mathbf{H}}_{\text{SC}}^{\mathsf{T}}\boldsymbol{\lambda} = \mathbf{b}_{\text{SC}} - \mathbf{A}_{\text{SC}}\mathbf{a}, \tag{4.109}$$

with $\bar{\mathbf{H}}_{\text{SC}} = \mathbf{A}_{\text{SC}}\mathbf{N}^{-1/2}\mathbf{P}\mathbf{N}^{-1/2}\boldsymbol{\Gamma}^{-1/2} = \mathbf{H}_{\mathbf{A}_{\text{SC}}}\bar{\mathbf{H}}_{\mathbf{P}}\boldsymbol{\Gamma}^{-1/2}$, where $\mathbf{H}_{\mathbf{A}_{\text{SC}}} = \mathbf{A}_{\text{SC}}$ and $\bar{\mathbf{H}}_{\mathbf{P}} = \mathbf{N}^{-1/2}\mathbf{P}\mathbf{N}^{-1/2}$.

Solving Eq. (4.109) for $\boldsymbol{\lambda}$, results in:

$$\boldsymbol{\lambda} = \left(\bar{\mathbf{H}}_{\text{SC}}\bar{\mathbf{H}}_{\text{SC}}^{\mathsf{T}}\right)^{\text{g}}\left(\mathbf{b}_{\text{SC}} - \mathbf{A}_{\text{SC}}\mathbf{a}\right) + \left(\mathbf{I} - \left(\bar{\mathbf{H}}_{\text{SC}}\bar{\mathbf{H}}_{\text{SC}}^{\mathsf{T}}\right)^{\text{g}}\bar{\mathbf{H}}_{\text{SC}}\bar{\mathbf{H}}_{\text{SC}}^{\mathsf{T}}\right)\mathbf{w}, \tag{4.110}$$

where $\left(\bar{\mathbf{H}}_{\text{SC}}\bar{\mathbf{H}}_{\text{SC}}^{\mathsf{T}}\right)^{\text{g}}$ is any $\{1,4\}$-inverse of $\bar{\mathbf{H}}_{\text{SC}}\bar{\mathbf{H}}_{\text{SC}}^{\mathsf{T}}$ and $\mathbf{w}$ is an arbitrary column-vector.

Multiplying Eq. (4.110) by $\boldsymbol{\Gamma}^{-1/2}\bar{\mathbf{H}}_{\mathrm{SC}}^{\mathsf{T}}$, we get:

$$\boldsymbol{\Gamma}^{-1/2}\bar{\mathbf{H}}_{\mathrm{SC}}^{\mathsf{T}}\boldsymbol{\lambda} = \boldsymbol{\Gamma}^{-1/2}\bar{\mathbf{H}}_{\mathrm{SC}}^{\mathsf{T}}\left(\bar{\mathbf{H}}_{\mathrm{SC}}\bar{\mathbf{H}}_{\mathrm{SC}}^{\mathsf{T}}\right)^{\mathrm{g}}(\mathbf{b}_{\mathrm{SC}} - \mathbf{A}_{\mathrm{SC}}\mathbf{a}) + \boldsymbol{\Gamma}^{-1/2}\bar{\mathbf{H}}_{\mathrm{SC}}^{\mathsf{T}}\left(\mathbf{I} - \left(\bar{\mathbf{H}}_{\mathrm{SC}}\bar{\mathbf{H}}_{\mathrm{SC}}^{\mathsf{T}}\right)^{\mathrm{g}}\bar{\mathbf{H}}_{\mathrm{SC}}\bar{\mathbf{H}}_{\mathrm{SC}}^{\mathsf{T}}\right)\mathbf{w}. \quad (4.111)$$

Let us prove that $\boldsymbol{\Gamma}^{-1/2}\bar{\mathbf{H}}_{\mathrm{SC}}^{\mathsf{T}}\mathbf{U}$, where $\mathbf{U}$ is given by:

$$\mathbf{U} = \mathbf{I} - \left(\bar{\mathbf{H}}_{\mathrm{SC}}\bar{\mathbf{H}}_{\mathrm{SC}}^{\mathsf{T}}\right)^{\mathrm{g}}\bar{\mathbf{H}}_{\mathrm{SC}}\bar{\mathbf{H}}_{\mathrm{SC}}^{\mathsf{T}}. \quad (4.112)$$

Multiplying Eq. (4.112) by $\boldsymbol{\Gamma}^{-1/2}\bar{\mathbf{H}}_{\mathrm{SC}}^{\mathsf{T}}$ and developing, results in:

$$\begin{aligned}
\bar{\mathbf{H}}_{\mathrm{SC}}^{\mathsf{T}}\mathbf{U} &= \bar{\mathbf{H}}_{\mathrm{SC}}^{\mathsf{T}}\left(\mathbf{I} - \left(\bar{\mathbf{H}}_{\mathrm{SC}}\bar{\mathbf{H}}_{\mathrm{SC}}^{\mathsf{T}}\right)^{\mathrm{g}}\bar{\mathbf{H}}_{\mathrm{SC}}\bar{\mathbf{H}}_{\mathrm{SC}}^{\mathsf{T}}\right), \\
&= \bar{\mathbf{H}}_{\mathrm{SC}}^{\mathsf{T}} - \bar{\mathbf{H}}_{\mathrm{SC}}^{\mathsf{T}}\left(\bar{\mathbf{H}}_{\mathrm{SC}}\bar{\mathbf{H}}_{\mathrm{SC}}^{\mathsf{T}}\right)^{\mathrm{g}}\bar{\mathbf{H}}_{\mathrm{SC}}\bar{\mathbf{H}}_{\mathrm{SC}}^{\mathsf{T}}, \\
&= \bar{\mathbf{H}}_{\mathrm{SC}}^{\mathsf{T}} - \bar{\mathbf{H}}_{\mathrm{SC}}^{\mathsf{T}}\left(\bar{\mathbf{H}}_{\mathrm{SC}}^{\mathsf{T}}\right)^{\mathrm{g}}\left(\bar{\mathbf{H}}_{\mathrm{SC}}\right)^{\mathrm{g}}\bar{\mathbf{H}}_{\mathrm{SC}}\bar{\mathbf{H}}_{\mathrm{SC}}^{\mathsf{T}}), \\
&= \bar{\mathbf{H}}_{\mathrm{SC}}^{\mathsf{T}} - \bar{\mathbf{H}}_{\mathrm{SC}}^{\mathsf{T}}\left(\bar{\mathbf{H}}_{\mathrm{SC}}^{\mathsf{T}}\right)^{\mathrm{g}}\bar{\mathbf{H}}_{\mathrm{SC}}^{\mathsf{T}}\left(\bar{\mathbf{H}}_{\mathrm{SC}}^{\mathsf{T}}\right)^{\mathrm{g}}\bar{\mathbf{H}}_{\mathrm{SC}}^{\mathsf{T}}, \\
&= \bar{\mathbf{H}}_{\mathrm{SC}}^{\mathsf{T}} - \bar{\mathbf{H}}_{\mathrm{SC}}^{\mathsf{T}}\left(\bar{\mathbf{H}}_{\mathrm{SC}}^{\mathsf{T}}\right)^{\mathrm{g}}\bar{\mathbf{H}}_{\mathrm{SC}}^{\mathsf{T}}, \\
&= \bar{\mathbf{H}}_{\mathrm{SC}}^{\mathsf{T}} - \bar{\mathbf{H}}_{\mathrm{SC}}^{\mathsf{T}}, \\
&= \mathbf{0}.
\end{aligned} \quad (4.113)$$

From Eq. (4.113) we have $\boldsymbol{\Gamma}^{-1/2}\bar{\mathbf{H}}_{\mathrm{SC}}^{\mathsf{T}} = \mathbf{0}$ which completes our proof.

Using Eq. (4.110) in (4.106) with $\tilde{\mathbf{a}}_{\mathrm{SC}} = \mathbf{b}_{\mathrm{SC}} - \mathbf{A}_{\mathrm{SC}}\mathbf{a}$, we get:

$$\mathbf{u}_0 = \boldsymbol{\Gamma}^{-1/2}\bar{\mathbf{H}}_{\mathrm{SC}}^{\mathsf{T}}\left(\bar{\mathbf{H}}_{\mathrm{SC}}\bar{\mathbf{H}}_{\mathrm{SC}}^{\mathsf{T}}\right)^{\mathrm{g}}(\mathbf{b}_{\mathrm{SC}} - \mathbf{A}_{\mathrm{SC}}\mathbf{a}) = \boldsymbol{\Gamma}^{-1/2}\bar{\mathbf{H}}_{\mathrm{SC}}^{\mathrm{g}}(\mathbf{b}_{\mathrm{SC}} - \mathbf{A}_{\mathrm{SC}}\mathbf{a}) = \boldsymbol{\Gamma}^{-1/2}\bar{\mathbf{H}}_{\mathrm{SC}}^{\mathrm{g}}\tilde{\mathbf{a}}_{\mathrm{SC}}, \quad (4.114)$$

where $\bar{\mathbf{H}}_{\mathrm{SC}}^{\mathrm{g}} = \bar{\mathbf{H}}_{\mathrm{SC}}^{\mathsf{T}}\left(\bar{\mathbf{H}}_{\mathrm{SC}}\bar{\mathbf{H}}_{\mathrm{SC}}^{\mathsf{T}}\right)^{\mathrm{g}}$ is any $\{1,4\}$-inverse of $\bar{\mathbf{H}}_{\mathrm{SC}}$.

Equation (4.114) is the solution for the decentralized controllers.

4.1.3.2 Soft control constraints

The constraints expressed by Eq. (4.96) are classified as hard constraints once it should be strictly equal to zero. If the initial error is relatively large, such constraints can result in actuators saturation in the beginning of the motion. To solve this, the time derivative of Eq. (4.96) can be used to be written as a soft control constraint, as follows:

$$\left|\dot{\boldsymbol{\varphi}}_{\mathrm{SC}}(\mathbf{a}, \mathbf{v}, \mathbf{q}, t)\right| = \boldsymbol{\varepsilon} \Leftrightarrow -\boldsymbol{\varepsilon} \leq \dot{\boldsymbol{\varphi}}_{\mathrm{SC}}(\mathbf{a}, \mathbf{v}, \mathbf{q}, t) \leq \boldsymbol{\varepsilon}, \quad (4.115)$$

where $\boldsymbol{\varepsilon}$ is a m-column-vector of a slack variable to be defined during the design.

The time-derivative of Eq. (4.96) can be written as:

$$\dot{\boldsymbol{\varphi}}_{\mathrm{SC}}\left(\mathbf{a},\mathbf{v},\mathbf{q},t\right)=\mathbf{A}_{\mathrm{SC}}\mathbf{a}_{\mathrm{SC}}-\mathbf{b}_{\mathrm{SC}}. \tag{4.116}$$

Substituting Eq. (4.101) into (4.116), we obtain:

$$\begin{aligned}\mathbf{A}_{\mathrm{SC}}\left(\mathbf{a}+\mathbf{N}^{-1/2}\mathbf{P}\mathbf{N}^{-1/2}\mathbf{u}_0\right)&=\mathbf{b}_{\mathrm{SC}},\\ \mathbf{A}_{\mathrm{SC}}\mathbf{a}+\mathbf{A}_{\mathrm{SC}}\mathbf{N}^{-1/2}\mathbf{P}\mathbf{N}^{-1/2}\mathbf{u}_0&=\mathbf{b}_{\mathrm{SC}},\\ \mathbf{A}_{\mathrm{SC}}\mathbf{N}^{-1/2}\mathbf{P}\mathbf{N}^{-1/2}\mathbf{u}_0&=\mathbf{b}_{\mathrm{SC}}-\mathbf{A}_{\mathrm{SC}}\mathbf{a}.\end{aligned} \tag{4.117}$$

The new set of control constraints is defined as follows:

$$\mathbf{H}_{\mathrm{SC}}\mathbf{u}_0=\tilde{\mathbf{a}}_{\mathrm{SC}}, \tag{4.118}$$

where $\mathbf{H}_{\mathrm{SC}}=\mathbf{H}_{\mathbf{A}_{\mathrm{SC}}}\bar{\mathbf{H}}_{\mathbf{P}}=\mathbf{A}_{\mathrm{SC}}\mathbf{N}^{-1/2}\mathbf{P}\mathbf{N}^{-1/2}$ and $\tilde{\mathbf{a}}_{\mathrm{SC}}=\mathbf{b}_{\mathrm{SC}}-\mathbf{A}_{\mathrm{SC}}\mathbf{a}$.

The soft control constraints become:

$$-\boldsymbol{\varepsilon}\leq\dot{\boldsymbol{\varphi}}_{\mathrm{SC}}\left(\mathbf{a},\mathbf{v},\mathbf{q},t\right)\leq\boldsymbol{\varepsilon}\Leftrightarrow-\boldsymbol{\varepsilon}\leq\mathbf{H}_{\mathrm{SC}}\mathbf{u}_0-\tilde{\mathbf{a}}_{\mathrm{SC}}\leq\boldsymbol{\varepsilon}. \tag{4.119}$$

Equation (4.119) can be solved as a QP-problem defining a quadratic cost function associated with the control energy subjected to the proposed form of soft control constraints, as below:

$$\begin{aligned}&\min_{\mathbf{u}_0(\cdot)}J=\frac{1}{2}\mathbf{u}_0^{\top}\boldsymbol{\Gamma}\mathbf{u}_0,\\ &\text{s.t. }\mathbf{G}_{\mathrm{SC}}\mathbf{u}_0\leq\boldsymbol{\sigma}_{\mathrm{SC}},\end{aligned} \tag{4.120}$$

where

$$\mathbf{G}_{\mathrm{SC}}=\begin{bmatrix}-\mathbf{H}_{\mathrm{SC}}\\ +\mathbf{H}_{\mathrm{SC}}\end{bmatrix};\quad\boldsymbol{\sigma}_{\mathrm{SC}}=\begin{bmatrix}\boldsymbol{\varepsilon}-\tilde{\mathbf{a}}_{\mathrm{SC}}\\ \boldsymbol{\varepsilon}+\tilde{\mathbf{a}}_{\mathrm{SC}}\end{bmatrix}. \tag{4.121}$$

4.2 RECURSIVE MODULAR CONTROL

4.2.1 Definitions

Let $\mathcal{S}$ be a generic mechanical system in which the control is conceived as a hierarchy of s levels for which the equations associated with the constraints enforced at level r can be expressed in matrix form as $\mathbf{A}_r\left(\mathbf{v},\mathbf{q},t\right)\mathbf{a}=\mathbf{e}_r\left(\mathbf{v},\mathbf{q},t\right)$ and $\mathbf{R}_r^{\top}\mathbf{u}_r=\mathbf{0}$. In this case, the control of $\mathcal{S}$ can be

expressed by the following system of equations:

$$\begin{cases} \mathbf{u} = \mathbf{u}_0(\mathbf{v},\mathbf{q},t) + \boldsymbol{\gamma}(\mathbf{v},\mathbf{q},t), \\ \tilde{\mathbf{A}}_1(\mathbf{v},\mathbf{q},t)\,\mathbf{N}^{-1}\mathbf{u} = \mathbf{e}_1(\mathbf{v},\mathbf{q},t), \\ \tilde{\mathbf{R}}_1^{\mathsf{T}}\mathbf{u} = \mathbf{0}, \\ \tilde{\mathbf{A}}_2(\mathbf{v},\mathbf{q},t)\,\mathbf{N}^{-1}\mathbf{u} = \mathbf{e}_2(\mathbf{v},\mathbf{q},t), \\ \tilde{\mathbf{R}}_2^{\mathsf{T}}\mathbf{u} = \mathbf{0}, \\ \vdots \\ \tilde{\mathbf{A}}_s(\mathbf{v},\mathbf{q},t)\,\mathbf{N}^{-1}\mathbf{u} = \mathbf{e}_s(\mathbf{v},\mathbf{q},t), \\ \tilde{\mathbf{R}}_s^{\mathsf{T}}\mathbf{u} = \mathbf{0}. \end{cases} \tag{4.122}$$

As an example, consider the conception of the three bars mechanism shown in Fig. 37 (a) and its control hierarchy shown in Fig. 37 (b). The decoupled controller for each bar A_i ($i = 1, 2, 3$) constitute the base components. As shown in Fig. 37 (b), the constraints of $\mathcal{S}$ are distributed in two levels. At level 1, the constraints between the ground $\mathcal{G}$ and A_1, indicated by the active revolute joint (grey circle), and between A_1 and A_2, indicated by the passive revolute joint (white circle), are enforced and the controller for the serial mechanism associated with the subsystem $\mathcal{S}_1$ is obtained. Still at level 1, the constraints between the ground $\mathcal{G}$ and A_3, indicated by the passive revolute joint (white circle), are enforced, and the controller for the link related to subsystem $\mathcal{S}_1$ is obtained. At level 2, the constraints among $\mathcal{S}_1$ and $\mathcal{S}_2$, indicated by the passive revolute joint (white circle), are enforced, providing the centralized controller for the three bars mechanism associated with the system $\mathcal{S}$.

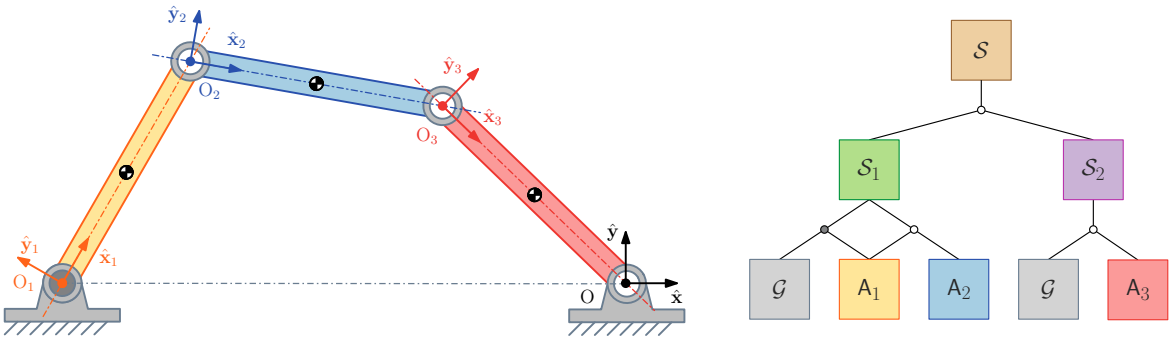

(a): Three-bar linkage (b): Control hierarchy

Figure 37: Hierarchical conception of a planar three-bar linkage mechanism constituted by a serial mechanism $\mathcal{S}_1$ and a single link $\mathcal{S}_2$.

Define for $r = 1, \ldots, s-1$:

$$\mathbf{A}_{r+1} = \begin{bmatrix} \mathbf{A}_r \\ \tilde{\mathbf{A}}_{r+1} \end{bmatrix}; \quad \mathbf{e}_{r+1} = \begin{bmatrix} \mathbf{e}_r \\ \tilde{\mathbf{e}}_{r+1} \end{bmatrix}. \tag{4.123}$$

The system Eqs. (4.122) can be rewritten in the form of (4.61) considering that all the constraint equations can be grouped in a single matrix form $\mathbf{A}(\mathbf{v}, \mathbf{q}, t)\,\mathbf{a} = \mathbf{e}(\mathbf{v}, \mathbf{q}, t)$ and $\mathbf{R}^{\mathsf{T}}\mathbf{u} = \mathbf{0}$, with $\mathbf{A}_s = \begin{bmatrix} \tilde{\mathbf{A}}_1^{\mathsf{T}} & \tilde{\mathbf{A}}_2^{\mathsf{T}} & \ldots & \tilde{\mathbf{A}}_s^{\mathsf{T}} \end{bmatrix}^{\mathsf{T}}$, $\mathbf{e}_s = \begin{bmatrix} \tilde{\mathbf{e}}_1^{\mathsf{T}} & \tilde{\mathbf{e}}_2^{\mathsf{T}} & \ldots & \tilde{\mathbf{e}}_s^{\mathsf{T}} \end{bmatrix}^{\mathsf{T}}$ and $\mathbf{R}_s = \begin{bmatrix} \tilde{\mathbf{R}}_1 & \tilde{\mathbf{R}}_2 & \ldots & \tilde{\mathbf{R}}_s \end{bmatrix}$.

Also, let $\mathbf{u}_r$ denote the m-vector of control that minimizes the Gaussian deviation function of the control design considering just the constraints enforced up to the hierarchical level r. The corresponding controller in this case can be expressed as follows:

$$\begin{cases} \mathbf{u}_r(\mathbf{v}, \mathbf{q}, t) = \mathbf{u}_0(\mathbf{v}, \mathbf{q}, t) + \boldsymbol{\gamma}_r, \\ \mathbf{A}_r(\mathbf{v}, \mathbf{q}, t)\,\mathbf{N}^{-1}\mathbf{u}_r = \mathbf{e}_r(\mathbf{v}, \mathbf{q}, t), \\ \mathbf{R}_r^{\mathsf{T}}\mathbf{u}_r = \mathbf{0}. \end{cases} \tag{4.124}$$

Set $\mathbf{W}(\mathbf{v}, \mathbf{q}, t)$, such that $\mathbf{N} = \mathbf{M} + \mathbf{A}^{\mathsf{T}}\mathbf{W}\mathbf{A}$ is a positive definite matrix and consider:

$$\mathbf{u}_0 = \mathbf{N}\boldsymbol{\nu} + (\mathbf{g} + \mathbf{c}) = \mathbf{N}\boldsymbol{\nu} + \left(\mathbf{f} + \mathbf{A}^{\mathsf{T}}\mathbf{W}\mathbf{b} + \mathbf{c}\right). \tag{4.125}$$

Also, define for $r = 1, \ldots, s$:

$$\tilde{\mathbf{H}}_r = \tilde{\mathbf{R}}_r^{\mathsf{T}}; \quad \mathbf{H}_r = \mathbf{R}_r^{\mathsf{T}}; \quad \tilde{\mathbf{C}}_r^{\mathsf{T}} = \tilde{\mathbf{A}}_r; \quad \mathbf{C}_r^{\mathsf{T}} = \mathbf{A}_r. \tag{4.126}$$

Since any control can be expressed as Eq. (4.61), considering the definitions provided above, Eq. (4.124) can be rewritten as:

$$\begin{cases} \mathbf{u}_r = \mathbf{u}_0 + \mathbf{C}_r^{\mathsf{T}}\boldsymbol{\lambda}_j, \\ \mathbf{H}_r\mathbf{C}_r^{\mathsf{T}}\boldsymbol{\lambda}_r = -\mathbf{H}_r\mathbf{u}_0. \end{cases} \tag{4.127}$$

The solution of Eq. (4.127) is given by:

$$\mathbf{u}_r = \left(\mathbf{I} - \mathbf{H}_r^{\mathrm{g}}\mathbf{H}_r\right)\mathbf{u}_0 = \mathbf{P}_r\mathbf{u}_0, \tag{4.128}$$

with $\mathbf{H}_r^{\mathrm{g}} = \mathbf{A}_r^{\mathsf{T}}\left(\mathbf{R}_r^{\mathsf{T}}\mathbf{A}_r^{\mathsf{T}}\right)^{\mathrm{g}} = \mathbf{C}_r^{\mathsf{T}}\left(\mathbf{H}_r\mathbf{C}_r^{\mathsf{T}}\right)^{\mathrm{g}}$ as the $\{1, 2, 4\}$-inverse of $\mathbf{H}_r$ and $\mathbf{P}_r = \mathbf{I} - \mathbf{H}_r^{\mathrm{g}}\mathbf{H}_r$ as the orthogonal projector onto the kernel of $\mathbf{H}_r$.

4.2.2 Recursive algorithm based on the orthogonal complement

In order to derive a recursive modular algorithm based on Eq. (4.61), consider the following definitions at the level $r+1$:

$$\tilde{\mathbf{H}}_{r+1} = \tilde{\mathbf{R}}_{r+1}^{\mathsf{T}}; \quad \mathbf{H}_{r+1} = \mathbf{R}_{r+1}^{\mathsf{T}} = \begin{bmatrix} \mathbf{R}_r^{\mathsf{T}} \\ \tilde{\mathbf{R}}_{r+1}^{\mathsf{T}} \end{bmatrix} = \begin{bmatrix} \mathbf{H}_r \\ \tilde{\mathbf{H}}_{r+1} \end{bmatrix}. \tag{4.129}$$

Also, let:

$$\tilde{\mathbf{C}}_{r+1}^{\mathsf{T}} = \tilde{\mathbf{A}}_{r+1}^{\mathsf{T}}; \quad \mathbf{C}_{r+1}^{\mathsf{T}} = \mathbf{A}_{r+1}^{\mathsf{T}} = \begin{bmatrix} \mathbf{A}_r^{\mathsf{T}} & \tilde{\mathbf{A}}_{r+1}^{\mathsf{T}} \end{bmatrix} = \begin{bmatrix} \mathbf{C}_r^{\mathsf{T}} & \tilde{\mathbf{C}}_{r+1}^{\mathsf{T}} \end{bmatrix}. \tag{4.130}$$

The gain matrix at the level $r+1$ is defined as follows:

$$\mathbf{K}_{r+1} = \mathbf{S}_r^{\mathsf{T}} \tilde{\mathbf{A}}_{r+1}^{\mathsf{T}} \left(\tilde{\mathbf{R}}_{r+1}^{\mathsf{T}} \mathbf{S}_r^{\mathsf{T}} \tilde{\mathbf{A}}_{r+1}^{\mathsf{T}} \right)^{\mathrm{g}} = \mathbf{P}_r \tilde{\mathbf{C}}_{r+1}^{\mathsf{T}} \left(\tilde{\mathbf{H}}_{r+1} \mathbf{P}_r \tilde{\mathbf{C}}_{r+1}^{\mathsf{T}} \right)^{\mathrm{g}}. \tag{4.131}$$

Moreover, consider the following equality:

$$\mathbf{H}_{r+1}^{\mathrm{g}} = \begin{bmatrix} \left(\mathbf{I} - \mathbf{K}_{r+1} \tilde{\mathbf{H}}_{r+1} \right) \mathbf{H}_r^{\mathrm{g}} & \mathbf{K}_{r+1} \end{bmatrix}. \tag{4.132}$$

From previous results derived, we have that $\mathbf{S}_{r+1} = \mathbf{S}_r \mathbf{E}_{r+1}$, with:

$$\begin{aligned} \mathbf{S}_r &= \mathbf{I} - \mathbf{R}_r \left(\mathbf{A}_r \mathbf{R}_r \right)^{\mathrm{g}} \tilde{\mathbf{A}}_r, \\ \mathbf{E}_{r+1} &= \mathbf{I} - \tilde{\mathbf{R}}_{r+1} \left(\tilde{\mathbf{A}}_{r+1} \mathbf{S}_r \tilde{\mathbf{R}}_{r+1} \right)^{\mathrm{g}} \tilde{\mathbf{A}}_{r+1} \mathbf{S}_r. \end{aligned} \tag{4.133}$$

Let $\mathbf{P}_r = \mathbf{S}_r^{\mathsf{T}} = \mathbf{I} - \mathbf{H}_r^{\mathrm{g}} \mathbf{H}_r$ and $\mathbf{P}_{r+1} = \mathbf{S}_{r+1}^{\mathsf{T}} = \mathbf{I} - \mathbf{H}_{r+1}^{\mathrm{g}} \mathbf{H}_{r+1}$, such that:

$$\begin{aligned} \mathbf{P}_{r+1} &= \left(\mathbf{I} - \mathbf{S}_r^{\mathsf{T}} \tilde{\mathbf{A}}_{r+1}^{\mathsf{T}} \left(\tilde{\mathbf{R}}_{r+1}^{\mathsf{T}} \mathbf{S}_r^{\mathsf{T}} \tilde{\mathbf{A}}_{r+1}^{\mathsf{T}} \right)^{\mathrm{g}} \tilde{\mathbf{R}}_{r+1}^{\mathsf{T}} \right) \mathbf{S}_r^{\mathsf{T}}, \\ &= \left(\mathbf{I} - \mathbf{K}_{r+1} \tilde{\mathbf{H}}_{r+1} \right) \mathbf{P}_r. \end{aligned} \tag{4.134}$$

We can proof that $\mathbf{P}_r$ and $\mathbf{P}_{r+1}$ are idempotent matrices, i.e., $\mathbf{P}_r \mathbf{P}_r = \mathbf{P}_r$ and $\mathbf{P}_{r+1} \mathbf{P}_{r+1} = \mathbf{P}_{r+1}$, as follows:

$$\begin{aligned} \mathbf{P}_r \mathbf{P}_r &= \left(\mathbf{I} - \mathbf{H}_r^{\mathrm{g}} \mathbf{H}_r \right) \left(\mathbf{I} - \mathbf{H}_r^{\mathrm{g}} \mathbf{H}_r \right), \\ &= \mathbf{I} - \mathbf{H}_r^{\mathrm{g}} \mathbf{H}_r - \mathbf{H}_r^{\mathrm{g}} \mathbf{H}_r + \mathbf{H}_r^{\mathrm{g}} \mathbf{H}_r \mathbf{H}_r^{\mathrm{g}} \mathbf{H}_r, \\ &= \mathbf{I} - \mathbf{H}_r^{\mathrm{g}} \mathbf{H}_r - \mathbf{H}_r^{\mathrm{g}} \mathbf{H}_r + \mathbf{C}_r^{\mathsf{T}} \left(\mathbf{H}_r \mathbf{C}_r^{\mathsf{T}} \right)^{\mathrm{g}} \mathbf{H}_r \mathbf{C}_r^{\mathsf{T}} \left(\mathbf{H}_r \mathbf{C}_r^{\mathsf{T}} \right)^{\mathrm{g}} \mathbf{H}_r, \\ &= \mathbf{I} - \mathbf{H}_r^{\mathrm{g}} \mathbf{H}_r - \mathbf{H}_r^{\mathrm{g}} \mathbf{H}_r + \mathbf{C}_r^{\mathsf{T}} \left(\mathbf{H}_r \mathbf{C}_r^{\mathsf{T}} \right)^{\mathrm{g}} \mathbf{H}_r, \\ &= \mathbf{I} - \mathbf{H}_r^{\mathrm{g}} \mathbf{H}_r - \mathbf{H}_r^{\mathrm{g}} \mathbf{H}_r + \mathbf{H}_r^{\mathrm{g}} \mathbf{H}_r, \\ &= \mathbf{I} - \mathbf{H}_r^{\mathrm{g}} \mathbf{H}_r, \\ &= \mathbf{P}_r. \end{aligned} \tag{4.135}$$

Similarly, for $\mathbf{P}_{r+1}$ and using Eq. (4.135), we have:

$$\begin{aligned}
\mathbf{P}_{r+1}\mathbf{P}_{r+1} &= \left(\mathbf{I} - \mathbf{K}_{r+1}\tilde{\mathbf{H}}_{r+1}\right)\mathbf{P}_r\left(\mathbf{I} - \mathbf{K}_{r+1}\tilde{\mathbf{H}}_{r+1}\right)\mathbf{P}_r, \\
&= \left(\mathbf{I} - \mathbf{K}_{r+1}\tilde{\mathbf{H}}_{r+1}\right)\mathbf{P}_r\left(\mathbf{I} - \mathbf{P}_r\tilde{\mathbf{C}}_{r+1}^{\mathsf{T}}\left(\tilde{\mathbf{H}}_{r+1}\mathbf{P}_r\tilde{\mathbf{C}}_{r+1}^{\mathsf{T}}\right)^{\mathrm{g}}\tilde{\mathbf{H}}_{r+1}\right)\mathbf{P}_r, \\
&= \left(\mathbf{I} - \mathbf{K}_{r+1}\tilde{\mathbf{H}}_{r+1}\right)\mathbf{P}_r - \mathbf{P}_r\tilde{\mathbf{C}}_{r+1}^{\mathsf{T}}\left(\tilde{\mathbf{H}}_{r+1}\mathbf{P}_r\tilde{\mathbf{C}}_{r+1}^{\mathsf{T}}\right)^{\mathrm{g}}\tilde{\mathbf{H}}_{r+1}\mathbf{P}_r + \ldots \\
&+ \mathbf{P}_r\tilde{\mathbf{C}}_{r+1}^{\mathsf{T}}\left(\tilde{\mathbf{H}}_{r+1}\mathbf{P}_r\tilde{\mathbf{C}}_{r+1}^{\mathsf{T}}\right)^{\mathrm{g}}\tilde{\mathbf{H}}_{r+1}\mathbf{P}_r\tilde{\mathbf{C}}_{r+1}^{\mathsf{T}}\left(\tilde{\mathbf{H}}_{r+1}\mathbf{P}_r\tilde{\mathbf{C}}_{r+1}^{\mathsf{T}}\right)^{\mathrm{g}}\tilde{\mathbf{H}}_{r+1}\mathbf{P}_r, \\
&= \left(\mathbf{I} - \mathbf{K}_{r+1}\tilde{\mathbf{H}}_{r+1}\right)\mathbf{P}_r - \mathbf{P}_r\tilde{\mathbf{C}}_{r+1}^{\mathsf{T}}\left(\tilde{\mathbf{H}}_{r+1}\mathbf{P}_r\tilde{\mathbf{C}}_{r+1}^{\mathsf{T}}\right)^{\mathrm{g}}\tilde{\mathbf{H}}_{r+1}\mathbf{P}_r + \ldots \\
&+ \mathbf{P}_r\tilde{\mathbf{C}}_{r+1}^{\mathsf{T}}\left(\tilde{\mathbf{H}}_{r+1}\mathbf{P}_r\tilde{\mathbf{C}}_{r+1}^{\mathsf{T}}\right)^{\mathrm{g}}\tilde{\mathbf{H}}_{r+1}\mathbf{P}_r, \\
&= \left(\mathbf{I} - \mathbf{K}_{r+1}\tilde{\mathbf{H}}_{r+1}\right)\mathbf{P}_r, \\
&= \mathbf{P}_{r+1},
\end{aligned} \tag{4.136}$$

which completes our proof.

Thus, with Eqs. (4.135) and (4.136), (4.134) can be rewritten as:

$$\mathbf{P}_{r+1} = \left(\mathbf{I} - \mathbf{K}_{r+1}\tilde{\mathbf{H}}_{r+1}\right)\mathbf{P}_r\left(\mathbf{I} - \mathbf{L}_{r+1}\tilde{\mathbf{C}}_{r+1}\right)^{\mathsf{T}}, \tag{4.137}$$

where $\mathbf{L}_{r+1} = \mathbf{P}_r^{\mathsf{T}}\tilde{\mathbf{H}}_{r+1}^{\mathsf{T}}\left(\tilde{\mathbf{C}}_{r+1}\mathbf{P}_r^{\mathsf{T}}\tilde{\mathbf{H}}_{r+1}^{\mathsf{T}}\right)^{\mathrm{g}}$.

From Eq. (4.134), we identify the following equality:

$$\mathbf{K}_{r+1}\tilde{\mathbf{H}}_{r+1}\mathbf{P}_r = \mathbf{P}_r - \mathbf{P}_{r+1}. \tag{4.138}$$

Using Eq. (4.138) we can prove that (4.132) is a valid expression for $\mathbf{H}_{r+1}^{\mathrm{g}}$, as follows:

$$\begin{aligned}
\mathbf{H}_{r+1}^{\mathrm{g}}\mathbf{H}_{r+1} &= \begin{bmatrix}\left(\mathbf{I} - \mathbf{K}_{r+1}\tilde{\mathbf{H}}_{r+1}\right)\mathbf{H}_r^{\mathrm{g}} & \mathbf{K}_{r+1}\end{bmatrix}\begin{bmatrix}\mathbf{H}_r \\ \tilde{\mathbf{H}}_{r+1}\end{bmatrix} \\
&= \left(\mathbf{I} - \mathbf{K}_{r+1}\tilde{\mathbf{H}}_{r+1}\right)\mathbf{H}_r^{\mathrm{g}}\mathbf{H}_r + \mathbf{K}_{r+1}\tilde{\mathbf{H}}_{r+1}, \\
&= \mathbf{I} - \mathbf{P}_r - \mathbf{K}_{r+1}\tilde{\mathbf{H}}_{r+1} + \mathbf{K}_{r+1}\tilde{\mathbf{H}}_{r+1}\mathbf{P}_r + \mathbf{K}_{r+1}\tilde{\mathbf{H}}_{r+1}, \\
&= \mathbf{I} - \mathbf{P}_r + \mathbf{P}_r - \mathbf{P}_{r+1}, \\
&= \mathbf{I} - \mathbf{P}_{r+1}, \\
&= \mathbf{H}_{r+1}^{\mathrm{g}}\mathbf{H}_{r+1},
\end{aligned} \tag{4.139}$$

which completes our proof.

Considering Eq. (4.128) with $\mathbf{u}_r^*$ being an additional m-column-vector of auxiliary control associated to the non-actuated quasi-velocities (e.g., an additional control term to compensate

for disturbances on the end-effector), we have:

$$\mathbf{u}_r^{\#} = \mathbf{u}_0 + \mathbf{H}_r^{\mathrm{g}} \left(\mathbf{u}_r^{*} - \mathbf{H}_r \mathbf{u}_0 \right). \tag{4.140}$$

Based on Eq. (4.140) and considering the relation of Eq. (4.132) for $\mathbf{H}_{r+1}$, we get:

$$\begin{aligned}
\mathbf{u}_{r+1}^{\#} &= \mathbf{u}_0 + \mathbf{H}_{r+1}^{\mathrm{g}} \left(\mathbf{u}_{r+1}^{*} - \mathbf{H}_{r+1} \mathbf{u}_0 \right), \\
\mathbf{u}_{r+1}^{\#} - \mathbf{u}_0 &= \left(\mathbf{I} - \mathbf{K}_{r+1} \tilde{\mathbf{H}}_{r+1} \right) \mathbf{H}_r^{\mathrm{g}} \left(\mathbf{u}_r^{*} - \mathbf{H}_r \mathbf{u}_0 \right) + \mathbf{K}_{r+1} \left(\tilde{\mathbf{u}}_{r+1}^{*} - \tilde{\mathbf{H}}_{r+1} \mathbf{u}_0 \right), \\
\mathbf{u}_{r+1}^{\#} - \mathbf{u}_0 &= \left(\mathbf{I} - \mathbf{K}_{r+1} \tilde{\mathbf{H}}_{r+1} \right) \left(\mathbf{u}_r^{\#} - \mathbf{u}_0 \right) + \mathbf{K}_{r+1} \left(\tilde{\mathbf{u}}_{r+1}^{*} - \tilde{\mathbf{H}}_{r+1} \mathbf{u}_0 \right), \\
\mathbf{u}_{r+1}^{\#} - \mathbf{u}_0 &= \mathbf{u}_k^{\#} - \mathbf{u}_0 - \mathbf{K}_{r+1} \tilde{\mathbf{H}}_{r+1} \left(\mathbf{u}_r^{\#} - \mathbf{u}_0 \right) + \mathbf{K}_{r+1} \left(\tilde{\mathbf{u}}_{r+1}^{*} - \tilde{\mathbf{H}}_{r+1} \mathbf{u}_0 \right), \\
\mathbf{u}_{r+1}^{\#} &= \mathbf{u}_r^{\#} + \mathbf{K}_{r+1} \left(\tilde{\mathbf{u}}_{r+1}^{*} - \tilde{\mathbf{H}}_{r+1} \mathbf{u}_r^{\#} \right).
\end{aligned} \tag{4.141}$$

Gathering the Eqs. (4.129)–(4.141), the following algorithm arises.

Algorithm 2. (Recursive modular control): Generalized recursive modular control algorithm based on Eq. (4.128).

(a) Initialize at $r = 0$:

$$\mathbf{P}_0 = \mathbf{I}; \quad \mathbf{u}_0^{\#} = \mathbf{u}_0.$$

(b) For $r = 0, \ldots, s-1$, do:

$$\begin{aligned}
\mathbf{K}_{r+1} &= \mathbf{P}_r \tilde{\mathbf{C}}_{r+1}^{\mathsf{T}} \left(\tilde{\mathbf{H}}_{r+1} \mathbf{P}_r \tilde{\mathbf{C}}_{r+1}^{\mathsf{T}} \right)^{\mathrm{g}}, \\
\mathbf{u}_{r+1}^{\#} &= \mathbf{u}_r^{\#} + \mathbf{K}_{r+1} \left(\tilde{\mathbf{u}}_{r+1}^{*} - \tilde{\mathbf{H}}_{r+1} \mathbf{u}_r^{\#} \right), \\
\mathbf{P}_{r+1} &= \left(\mathbf{I} - \mathbf{K}_{r+1} \tilde{\mathbf{H}}_{r+1} \right) \mathbf{P}_r.
\end{aligned}$$

(c) For $r = s$, compute the control:

$$\mathbf{u}_{\#} = \mathbf{Q}^{\mathsf{T}} \mathbf{u}_s^{\#}.$$

The algorithm 2 is analog to the Kalman filter for state estimation from a set of noiseless measurements. In this analogy, the constraint equations, $\tilde{\mathbf{u}}_{r+1}^{*} = \tilde{\mathbf{H}}_{r+1} \mathbf{u}_r^{\#}$, can be taken as the measurements, and the orthogonal projectors onto the kernel of $\mathbf{H}_r$, i.e., $\mathbf{P}_r$, as the updated estimate covariance matrix.

With algorithm 2 the computational implementations of the Kalman filter can be adapted to develop modular recursive control strategies. Moreover, measurement noises in the Kalman filter can provide an alternative approach to represent unmodeled dynamics or to improve the

numerical stability of the algorithm 2. However, these issues are intricate and will be properly addressed in future works.

For example, if $\mathbf{O}_{r+1}$ is the covariance matrix associated to the measurement noises, then, $\mathbf{K}_{r+1}$ and $\mathbf{P}_{r+1}$ are calculated as follows:

$$\mathbf{K}_{r+1} = \mathbf{P}_r \tilde{\mathbf{C}}_{r+1}^{\mathsf{T}} \left(\tilde{\mathbf{H}}_{r+1} \mathbf{P}_r \tilde{\mathbf{C}}_{r+1}^{\mathsf{T}} + \mathbf{O}_{r+1} \right)^{-1}, \tag{4.142}$$

and

$$\mathbf{P}_{r+1} = \left(\mathbf{I} - \mathbf{K}_{r+1} \tilde{\mathbf{H}}_{r+1} \right) \mathbf{P}_r \left(\mathbf{I} - \mathbf{L}_{r+1} \tilde{\mathbf{C}}_{r+1} \right)^{\mathsf{T}} + \mathbf{K}_{r+1} \mathbf{O}_{r+1} \mathbf{L}_{r+1}^{\mathsf{T}}. \tag{4.143}$$

4.2.3 Recursive algorithm based on the Udwadia-Kalaba equation

The classical form of the Udwadia-Kalaba equation can be seen as a closed-loop dynamic that is corrected according to a quasi-acceleration error weighting by a feedback gain. However, this structure can be better used for control purposes if written in a linear state-space-like form. Furthermore, such modification can enable the synthesis of optimal control techniques, which are generally challenging for multibody systems due to their nonlinearities. For this purpose, let us consider the linear closed-loop state-space system, as follows:

$$\begin{cases} \dot{\mathbf{x}} = \mathbf{E}\mathbf{x} + \mathbf{B}\left(\boldsymbol{\gamma} + \mathbf{u} + \mathbf{d} \right), \\ \mathbf{y} = \mathbf{C}\mathbf{x} + \mathbf{D}\boldsymbol{\gamma}, \\ \boldsymbol{\gamma} = \mathbf{K}\left(\mathbf{r} - \mathbf{y} \right), \end{cases} \tag{4.144}$$

where $\mathbf{x}$, $\boldsymbol{\gamma}$, $\mathbf{u}$, $\mathbf{d}$ and $\mathbf{y}$ are the m-column-vectors of states, constraints forces, control inputs, disturbances and measured outputs, respectively, while $\mathbf{E}$, $\mathbf{B}$, $\mathbf{C}$ and $\mathbf{D}$ are the m by m state-space matrices. Figure 38 shows the state-space block diagram associated with Eq. (4.144).

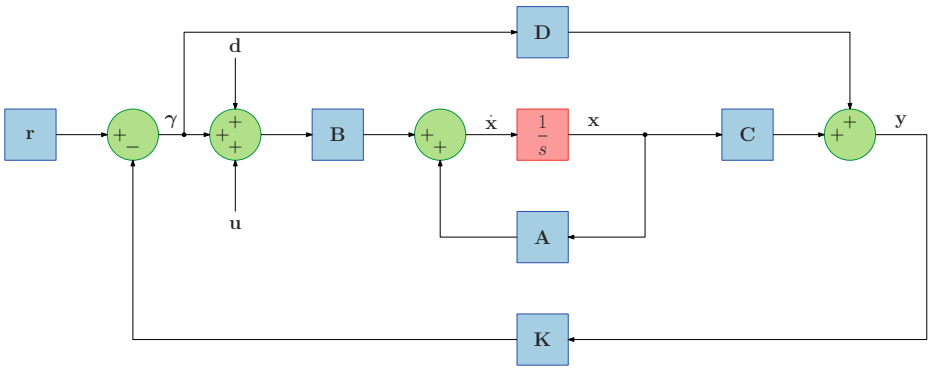

Figure 38: Closed-loop state-space block diagram

To show the existing analogy between the Udwadia-Kalaba equation and the state-space form presented in Eq. (4.144), let us consider the following modified version of the Udwadia-Kalaba equation where a first-order low-pass filter, for the sake of example, emulates a non-modeled dynamic (e.g., flexibility, actuators dynamics, delays, etc.) described by a m by m symmetric positive-definite cutoff frequency matrix $\boldsymbol{\Omega}_{\mathbf{a}}$:

$$\begin{cases} \mathbf{a}_0 = \mathbf{N}^{-1}\left(\mathbf{g}+\mathbf{c}\right), \\ \mathbf{A}\mathbf{a} = \mathbf{b}, \\ \dot{\mathbf{a}} + \boldsymbol{\Omega}_{\mathbf{a}}\mathbf{a} = \mathbf{a}_0 + \mathbf{N}^{-1}\mathbf{A}^{\mathsf{T}}\left(\mathbf{A}\mathbf{N}^{-1}\mathbf{A}^{\mathsf{T}}\right)^{\mathrm{g}}\left(\mathbf{b}-\mathbf{A}\mathbf{a}_0\right). \end{cases} \tag{4.145}$$

Also, consider that:

$$\dot{\mathbf{x}} = \dot{\mathbf{a}}; \quad \mathbf{x} = \mathbf{a}; \quad \mathbf{u} = \mathbf{Q}\mathbf{u}_{\#}; \quad \mathbf{d} = \mathbf{g}+\mathbf{c}; \quad \mathbf{r} = \mathbf{b}, \tag{4.146}$$

and

$$\begin{aligned} \mathbf{E} &= -\boldsymbol{\Omega}_{\mathbf{a}}, \\ \mathbf{B} &= \boldsymbol{\Omega}_{\mathbf{a}}\mathbf{N}^{-1}, \\ \mathbf{C} &= \mathbf{A}\boldsymbol{\Omega}_{\mathbf{a}}^{-1}, \\ \mathbf{D} &= -\mathbf{A}\mathbf{N}^{-1}, \\ \mathbf{K} &= \mathbf{A}^{\mathsf{T}}\left(\mathbf{A}\mathbf{N}^{-1}\mathbf{A}^{\mathsf{T}}\right)^{\mathrm{g}}. \end{aligned} \tag{4.147}$$

The constraint enforcement on the Udwadia-Kalaba equation is performed on the quasi-accelerations. Thus, to preserve constraints, the dynamic associated with the low-pass filter should be turned off to calculate the states to be used on the feedback control, as follows:

$$\dot{\mathbf{x}} = \mathbf{0} \Rightarrow \dot{\mathbf{x}} = \mathbf{E}\mathbf{x} + \mathbf{B}\left(\boldsymbol{\gamma}+\mathbf{u}+\mathbf{d}\right) \Rightarrow \mathbf{x} = \mathbf{B}\left(\boldsymbol{\gamma}+\mathbf{u}+\mathbf{d}\right). \tag{4.148}$$

Substituting the control expression of Eq. (4.144) into (4.148), we obtain:

$$\mathbf{x} = \mathbf{B}\mathbf{K}\left(\mathbf{r}-\mathbf{y}\right) + \mathbf{B}\left(\mathbf{u}+\mathbf{d}\right). \tag{4.149}$$

Introducing Eq. (4.149) in the output expression of (4.144), results in:

$$\begin{aligned} \mathbf{y} &= \mathbf{C}\mathbf{x} + \mathbf{D}\boldsymbol{\gamma}, \\ &= \mathbf{C}\mathbf{B}\mathbf{K}\left(\mathbf{r}-\mathbf{y}\right) + \mathbf{C}\mathbf{B}\left(\mathbf{u}+\mathbf{d}\right) + \mathbf{D}\mathbf{K}\left(\mathbf{r}-\mathbf{y}\right), \\ &= \mathbf{C}\mathbf{B}\left(\mathbf{u}+\mathbf{d}\right) - \mathbf{D}\mathbf{K}\left(\mathbf{r}-\mathbf{y}\right) + \mathbf{D}\mathbf{K}\left(\mathbf{r}-\mathbf{y}\right), \\ &= \mathbf{C}\mathbf{B}\left(\mathbf{u}+\mathbf{d}\right). \end{aligned} \tag{4.150}$$

Using Eq. (4.150) in the first expression of (4.144), we get:

$$\begin{aligned}\dot{\mathbf{x}} &= \mathbf{E}\mathbf{x} + \mathbf{B}\mathbf{K}\left(\mathbf{r} - \mathbf{C}\mathbf{B}\left(\mathbf{u} + \mathbf{d}\right)\right) + \mathbf{B}\left(\mathbf{u} + \mathbf{d}\right), \\ &= \mathbf{E}\mathbf{x} + \left(\mathbf{I} - \mathbf{B}\mathbf{K}\mathbf{C}\right)\mathbf{B}\left(\mathbf{u} + \mathbf{d}\right) + \mathbf{B}\mathbf{K}\mathbf{r}.\end{aligned} \tag{4.151}$$

Eq. (4.151) can be rewritten as:

$$\begin{aligned}\dot{\mathbf{x}} &= \mathbf{E}\mathbf{x} + \mathbf{L}\mathbf{z}_0 + \mathbf{H}\mathbf{r}, \\ &= \mathbf{E}\mathbf{x} + \mathbf{F}\mathbf{u}_{\#} + \mathbf{G}\mathbf{d} + \mathbf{H}\mathbf{r},\end{aligned} \tag{4.152}$$

where

$$\begin{aligned}\mathbf{L} &= \mathbf{I} - \mathbf{B}\mathbf{K}\mathbf{C}, \\ \mathbf{z}_0 &= \mathbf{B}\left(\mathbf{Q}\mathbf{u}_{\#} + \mathbf{d}\right), \\ \mathbf{F} &= \mathbf{L}\mathbf{B}\mathbf{Q}, \\ \mathbf{G} &= \mathbf{L}\mathbf{B}, \\ \mathbf{H} &= \mathbf{B}\mathbf{K}.\end{aligned} \tag{4.153}$$

Substituting Eqs. (4.147) and (4.153) into (4.152), we obtain:

$$\begin{aligned}\dot{\mathbf{x}} &= \mathbf{E}\mathbf{x} + \mathbf{F}\mathbf{u}_{\#} + \mathbf{G}\mathbf{d} + \mathbf{H}\mathbf{r}, \\ \dot{\mathbf{x}} &= \mathbf{E}\mathbf{x} + \left(\mathbf{I} - \mathbf{B}\mathbf{K}\mathbf{C}\right)\mathbf{B}\left(\mathbf{u} + \mathbf{d}\right) + \mathbf{B}\mathbf{K}\mathbf{r}, \\ \dot{\mathbf{a}} + \boldsymbol{\Omega}_{\mathbf{a}}\mathbf{a} &= \boldsymbol{\Omega}_{\mathbf{a}}\left(\mathbf{a}_0 + \mathbf{N}^{-1}\mathbf{A}^{\mathsf{T}}\left(\mathbf{A}\mathbf{N}^{-1}\mathbf{A}^{\mathsf{T}}\right)^{\mathrm{g}}\left(\mathbf{b} - \mathbf{A}\mathbf{a}_0\right)\right), \\ \mathbf{a} &= \left(\mathbf{I}s + \boldsymbol{\Omega}_{\mathbf{a}}\right)^{-1}\boldsymbol{\Omega}_{\mathbf{a}}\left(\mathbf{a}_0 + \mathbf{N}^{-1}\mathbf{A}^{\mathsf{T}}\left(\mathbf{A}\mathbf{N}^{-1}\mathbf{A}^{\mathsf{T}}\right)^{\mathrm{g}}\left(\mathbf{b} - \mathbf{A}\mathbf{a}_0\right)\right),\end{aligned} \tag{4.154}$$

which is the soft form of the Udwadia-Kalaba equation, completing the demonstration.

If we choose the cutoff frequency as $\|\boldsymbol{\Omega}_{\mathbf{a}}\| >> 0$, such that $\left(\mathbf{I}s + \boldsymbol{\Omega}_{\mathbf{a}}\right)^{-1}\boldsymbol{\Omega}_{\mathbf{a}} = \mathbf{I}$, then:

$$\begin{aligned}\mathbf{a} &= \left(\mathbf{I}s + \boldsymbol{\Omega}_{\mathbf{a}}\right)^{-1}\boldsymbol{\Omega}_{\mathbf{a}}\left(\mathbf{a}_0 + \mathbf{N}^{-1}\mathbf{A}^{\mathsf{T}}\left(\mathbf{A}\mathbf{N}^{-1}\mathbf{A}^{\mathsf{T}}\right)^{\mathrm{g}}\left(\mathbf{b} - \mathbf{A}\mathbf{a}_0\right)\right), \\ &= \mathbf{a}_0 + \mathbf{N}^{-1}\mathbf{A}^{\mathsf{T}}\left(\mathbf{A}\mathbf{N}^{-1}\mathbf{A}^{\mathsf{T}}\right)^{\mathrm{g}}\left(\mathbf{b} - \mathbf{A}\mathbf{a}_0\right),\end{aligned} \tag{4.155}$$

which is the classical form of the Udwadia-Kalaba equation.

Gathering the Eqs. (4.144)–(4.155) and using the recursive formulation developed in Subsec. 4.2.2, the following algorithm arises, which can be used for simulation purposes, calculating the constrained quasi-accelerations with the decoupled model and the modular control obtained with the formulations presented in this chapter.

Algorithm 3. (Recursive state-space model): Generalized recursive state-space model based on the soft Udwadia-Kalaba equation.

(a) Initialize at $r = 0$:

$$\mathbf{P}_0 = \mathbf{I}; \quad \mathbf{z}_0 = \mathbf{B}\left(\mathbf{Q}\mathbf{u}_{\#} + \mathbf{g} + \mathbf{c}\right).$$

(b) For $r = 0, \ldots, s-1$ do:

$$\begin{aligned}
\mathbf{K}_{r+1} &= \mathbf{P}_r \tilde{\mathbf{A}}_{r+1}^{\mathsf{T}} \left(\tilde{\mathbf{A}}_{r+1} \mathbf{B} \mathbf{P}_r \tilde{\mathbf{A}}_{r+1}^{\mathsf{T}}\right)^{\mathrm{g}}, \\
\mathbf{P}_{r+1} &= \left(\mathbf{I} - \mathbf{K}_{r+1} \tilde{\mathbf{A}}_{r+1} \mathbf{B}\right) \mathbf{P}_r, \\
\mathbf{L}_{r+1} &= \mathbf{I} - \mathbf{B}\mathbf{K}_{r+1} \tilde{\mathbf{A}}_{r+1}, \\
\mathbf{H}_{r+1} &= \mathbf{B}\mathbf{K}_{r+1}, \\
\mathbf{z}_{r+1} &= \mathbf{L}_{r+1} \mathbf{z}_r + \mathbf{H}_{r+1} \mathbf{r}_{r+1}.
\end{aligned}$$

(c) For $r = s$, compute the state-space model:

$$\dot{\mathbf{x}}_s = \mathbf{E}_s \mathbf{x}_s + \mathbf{z}_s.$$

4.2.3.1 Model predictive control

The analogy between the closed-loop state-space form and the Udwadia-Kalaba equation enables the application of linear control techniques to complex multibody systems. For example, let us consider the MPC formulation presented by Wang (2009) along with the discrete form of Eq. (4.152), as follows:

$$\begin{aligned}
\mathbf{x}(k+1) &= \mathbf{E}_{\mathrm{d}}(k)\,\mathbf{x}(k) + \mathbf{F}_{\mathrm{d}}(k)\,\mathbf{u}_{\#}(k) + \mathbf{G}_{\mathrm{d}}(k)\,\mathbf{d}(k) + \mathbf{H}_{\mathrm{d}}\mathbf{r}(k), \\
\mathbf{y}(k) &= \mathbf{C}_{\mathrm{d}}(k)\,\mathbf{x}(k),
\end{aligned} \tag{4.156}$$

where $\mathbf{x}(k)$, $\mathbf{u}_{\#}(k)$, $\mathbf{d}(k)$, $\mathbf{r}(k)$ and $\mathbf{y}(k)$ are the states, control inputs, disturbances, references and measured outputs column-vectors in the discrete form, respectively, while $\mathbf{E}_{\mathrm{d}}(k)$, $\mathbf{F}_{\mathrm{d}}(k)$, $\mathbf{G}_{\mathrm{d}}(k)$, $\mathbf{H}_{\mathrm{d}}(k)$ and $\mathbf{C}_{\mathrm{d}}(k)$ are the discrete version of the state matrices, calculated here through the Euler method considering a sample time T_{s}:

$$\begin{aligned}
\mathbf{E}_{\mathrm{d}}(k) &= \left(\mathbf{I} + \mathbf{E}(\mathbf{x})\,T_{\mathrm{s}}\right)\big|_{\mathbf{x}=\mathbf{x}(k)}, \\
\mathbf{F}_{\mathrm{d}}(k) &= \left(\mathbf{F}(\mathbf{x})\,T_{\mathrm{s}}\right)\big|_{\mathbf{x}=\mathbf{x}(k)}, \\
\mathbf{G}_{\mathrm{d}}(k) &= \left(\mathbf{G}(\mathbf{x})\,T_{\mathrm{s}}\right)\big|_{\mathbf{x}=\mathbf{x}(k)}, \\
\mathbf{H}_{\mathrm{d}}(k) &= \left(\mathbf{H}(\mathbf{x})\,T_{\mathrm{s}}\right)\big|_{\mathbf{x}=\mathbf{x}(k)}, \\
\mathbf{C}_{\mathrm{d}}(k) &= \mathbf{C}(\mathbf{x}).
\end{aligned} \tag{4.157}$$

Let p be the prediction horizon. The predicted states are given by the iteration of the discrete model in Eq. (4.156) at each prediction step, with $i = 1, 2, \ldots, p$ steps, as:

$$\mathbf{x}(k+i) = \mathbf{E}_{\mathrm{d}}^{i}(k)\,\mathbf{x}(k) + \sum_{j=1}^{i} \mathbf{E}_{\mathrm{d}}^{j-1}(k)\left(\mathbf{F}_{\mathrm{d}}(k)\,\mathbf{u}_{\#}(k+i-j) + \mathbf{G}_{\mathrm{d}}(k)\,\mathbf{d}(k) + \mathbf{H}_{\mathrm{d}}(k)\,\mathbf{r}(k)\right). \quad (4.158)$$

Also, let c be the control horizon, with $c \leq p$. Thus, based on Eq. (4.158) and considering $\mathbf{u}_{\#}(k+i) = \mathbf{u}_{\#}(k+c-1)\,; c \leq i \leq p-1$, i.e., admitting constant control inputs after reaching the control horizon, the predicted outputs vectors can be rearranged as follows, where the time step dependency is not used in the state matrices for the sake of notation simplicity:

$$\mathbf{Y} = \mathbf{S}_{\mathbf{x}}\mathbf{x}(k) + \mathbf{S}_{\mathbf{u}}\mathbf{U}_{\#} + \mathbf{S}_{\mathbf{d}}\mathbf{d} + \mathbf{S}_{\mathbf{r}}\mathbf{r}, \quad (4.159)$$

where

$$\begin{aligned}
\mathbf{Y} &= \left[\mathbf{y}^{\mathsf{T}}(k+1), \mathbf{y}^{\mathsf{T}}(k+2), \ldots, \mathbf{y}^{\mathsf{T}}(k+p)\right]^{\mathsf{T}}, \\
\mathbf{U}_{\#} &= \left[\mathbf{u}_{\#}^{\mathsf{T}}(k), \mathbf{u}_{\#}^{\mathsf{T}}(k+1), \ldots, \mathbf{u}_{\#}^{\mathsf{T}}(k+c-1)\right]^{\mathsf{T}}, \\
\mathbf{S}_{\mathbf{x}} &= \begin{bmatrix} \mathbf{C}_{\mathrm{d}}\mathbf{E}_{\mathrm{d}} \\ \mathbf{C}_{\mathrm{d}}\mathbf{E}_{\mathrm{d}}^{2} \\ \vdots \\ \mathbf{C}_{\mathrm{d}}\mathbf{E}_{\mathrm{d}}^{p} \end{bmatrix}, \\
\mathbf{S}_{\mathbf{U}_{\#}} &= \begin{bmatrix} \mathbf{C}_{\mathrm{d}}\mathbf{F}_{\mathrm{d}} & \mathbf{0} & \cdots & \mathbf{0} \\ \mathbf{C}_{\mathrm{d}}\mathbf{E}_{\mathrm{d}}\mathbf{F}_{\mathrm{d}} & \mathbf{C}_{\mathrm{d}}\mathbf{F}_{\mathrm{d}} & \cdots & \mathbf{0} \\ \vdots & \vdots & \ddots & \vdots \\ \mathbf{C}_{\mathrm{d}}\mathbf{E}_{\mathrm{d}}^{p-1}\mathbf{F}_{\mathrm{d}} & \mathbf{C}_{\mathrm{d}}\mathbf{E}_{\mathrm{d}}^{p-2}\mathbf{F}_{\mathrm{d}} & \cdots & \mathbf{C}_{\mathrm{d}}\mathbf{E}_{\mathrm{d}}^{p-c}\mathbf{F}_{\mathrm{d}} \end{bmatrix}, \\
\mathbf{S}_{\mathbf{d}} &= \begin{bmatrix} \mathbf{C}_{\mathrm{d}}\mathbf{G}_{\mathrm{d}} \\ \mathbf{C}_{\mathrm{d}}\mathbf{E}_{\mathrm{d}}\mathbf{G}_{\mathrm{d}} + \mathbf{C}_{\mathrm{d}}\mathbf{G}_{\mathrm{d}} \\ \vdots \\ \mathbf{C}_{\mathrm{d}}\mathbf{E}_{\mathrm{d}}^{p-1}\mathbf{G}_{\mathrm{d}} + \mathbf{C}_{\mathrm{d}}\mathbf{E}_{\mathrm{d}}^{p-2}\mathbf{G}_{\mathrm{d}} + \ldots + \mathbf{C}_{\mathrm{d}}\mathbf{G}_{\mathrm{d}} \end{bmatrix}, \\
\mathbf{S}_{\mathbf{r}} &= \begin{bmatrix} \mathbf{C}_{\mathrm{d}}\mathbf{H}_{\mathrm{d}} \\ \mathbf{C}_{\mathrm{d}}\mathbf{E}_{\mathrm{d}}\mathbf{H}_{\mathrm{d}} + \mathbf{C}_{\mathrm{d}}\mathbf{H}_{\mathrm{d}} \\ \vdots \\ \mathbf{C}_{\mathrm{d}}\mathbf{E}_{\mathrm{d}}^{p-1}\mathbf{H}_{\mathrm{d}} + \mathbf{C}_{\mathrm{d}}\mathbf{E}_{\mathrm{d}}^{p-2}\mathbf{H}_{\mathrm{d}} + \ldots + \mathbf{C}_{\mathrm{d}}\mathbf{H}_{\mathrm{d}} \end{bmatrix}.
\end{aligned} \quad (4.160)$$

We should note that in Eq. (4.160), the matrices $\mathbf{S}_{\mathbf{x}}$, $\mathbf{S}_{\mathbf{U}_{\#}}$, $\mathbf{S}_{\mathbf{d}}$ and $\mathbf{S}_{\mathbf{r}}$ are written in terms of the prediction and control horizons, p and c.

The objective of the MPC is to solve the following quadratic optimization problem:

$$\begin{aligned} \min_{\mathbf{U}_{\#}(\cdot)} J = \; & (\mathbf{Y} - \mathbf{Y}_{\mathrm{r}})^{\mathsf{T}} \tilde{\mathbf{Q}}_{\mathbf{Y}} (\mathbf{Y} - \mathbf{Y}_{\mathrm{r}}) + \mathbf{U}_{\#}^{\mathsf{T}} \tilde{\mathbf{R}}_{\mathbf{U}_{\#}} \mathbf{U}_{\#}, \\ \text{s.t. } & \mathbf{Y} = \mathbf{S}_{\mathbf{x}} \mathbf{x}(k) + \mathbf{S}_{\mathbf{U}_{\#}} \mathbf{U}_{\#} + \mathbf{S}_{\mathbf{d}} \mathbf{d} + \mathbf{S}_{\mathbf{r}} \mathbf{r}, \\ & \mathbf{U}_{\#,\min} \leq \mathbf{U}_{\#} \leq \mathbf{U}_{\#,\max}, \end{aligned} \tag{4.161}$$

with

$$\begin{aligned} \mathbf{Y}_{\mathrm{r}} &= \left[\mathbf{y}_{\mathrm{r}}^{\mathsf{T}}(k+1), \ldots, \mathbf{y}_{\mathrm{r}}^{\mathsf{T}}(k+p) \right]^{\mathsf{T}}, \\ \tilde{\mathbf{Q}}_{\mathbf{Y}} &= \mathrm{blkdiag}\left(\mathbf{Q}_{\mathbf{Y}}, \ldots, \mathbf{Q}_{\mathbf{Y}}, \mathbf{P}_{\mathbf{Y}} \right), \\ \tilde{\mathbf{R}}_{\mathbf{U}_{\#}} &= \mathrm{blkdiag}\left(\mathbf{R}_{\mathbf{U}_{\#}}, \ldots, \mathbf{R}_{\mathbf{U}_{\#}} \right), \end{aligned} \tag{4.162}$$

where $\mathbf{y}_{\mathrm{r}}(k+i)$ is the reference column-vector at the i-th prediction time step, $\mathbf{Q}_{\mathbf{Y}}$ and $\mathbf{R}_{\mathbf{U}_{\#}}$ are the weighting matrices for the tracking errors and control efforts, respectively, while $\mathbf{P}_{\mathbf{Y}}$ is the terminal weighting matrix used to enforce the closed-loop stability.

Inserting the predictive model of Eq. (4.158) into the cost function of (4.161) and after some algebraic manipulation neglecting the terms without $\mathbf{U}_{\#}$, comes:

$$\begin{aligned} \min_{\mathbf{U}_{\#}(\cdot)} J = \; & \mathbf{U}_{\#}^{\mathsf{T}} \left(\mathbf{S}_{\mathbf{U}_{\#}}^{\mathsf{T}} \tilde{\mathbf{Q}}_{\mathbf{Y}} \mathbf{S}_{\mathbf{U}_{\#}} + \tilde{\mathbf{R}}_{\mathbf{U}_{\#}} \right) \mathbf{U}_{\#} + \ldots \\ & 2 (\mathbf{S}_{\mathbf{x}} \mathbf{x} + \mathbf{S}_{\mathbf{d}} \mathbf{d} + \mathbf{S}_{\mathbf{r}} \mathbf{r} - \mathbf{Y}_{\mathrm{r}})^{\mathsf{T}} \tilde{\mathbf{Q}}_{\mathbf{Y}} \mathbf{S}_{\mathbf{U}_{\#}} \mathbf{U}_{\#}, \\ \text{s.t. } & \mathbf{U}_{\#,\min} \leq \mathbf{U}_{\#} \leq \mathbf{U}_{\#,\max}. \end{aligned} \tag{4.163}$$

The Quadratic Programming (QP) problem associated with Eq. (4.161) follows:

$$\begin{aligned} \min_{\mathbf{U}_{\#}(\cdot)} J = \; & \mathbf{U}_{\#}^{\mathsf{T}} \mathbf{H}_{\mathrm{QP}} \mathbf{U}_{\#} + \mathbf{f}_{\mathrm{QP}} \mathbf{U}_{\#}, \\ \text{s.t. } & \mathbf{G}_{\mathrm{QP}} \mathbf{U}_{\#} \leq \boldsymbol{\varphi}_{\mathrm{QP}}, \end{aligned} \tag{4.164}$$

where

$$\begin{aligned} \mathbf{H}_{\mathrm{QP}} &= \mathbf{S}_{\mathbf{U}_{\#}}^{\mathsf{T}} \tilde{\mathbf{Q}}_{\mathbf{Y}} \mathbf{S}_{\mathbf{U}_{\#}} + \tilde{\mathbf{R}}_{\mathbf{U}_{\#}}, \\ \mathbf{f}_{\mathrm{QP}} &= 2 (\mathbf{S}_{\mathbf{x}} \mathbf{x} + \mathbf{S}_{\mathbf{d}} \mathbf{d} + \mathbf{S}_{\mathbf{r}} \mathbf{r} - \mathbf{Y}_{\mathrm{r}})^{\mathsf{T}} \tilde{\mathbf{Q}}_{\mathbf{Y}} \mathbf{S}_{\mathbf{U}_{\#}}, \\ \mathbf{G}_{\mathrm{QP}} &= \mathrm{blkdiag}(-\mathbf{I}, +\mathbf{I}), \\ \boldsymbol{\varphi}_{\mathrm{QP}} &= \left[\mathbf{U}_{\#,\min}^{\mathsf{T}}, \mathbf{U}_{\#,\max}^{\mathsf{T}} \right]^{\mathsf{T}}, \\ \mathbf{U}_{\#,\min} &= \left[\mathbf{u}_{\#,\min}^{\mathsf{T}}, \ldots, \mathbf{u}_{\#,\min}^{\mathsf{T}} \right]^{\mathsf{T}}, \\ \mathbf{U}_{\#,\max} &= \left[\mathbf{u}_{\#,\max}^{\mathsf{T}}, \ldots, \mathbf{u}_{\#,\max}^{\mathsf{T}} \right]^{\mathsf{T}}. \end{aligned} \tag{4.165}$$

The block diagram of the MPC is shown in Fig. 39. The following steps summarize the MPC working process:

1. the controller receives the output reference, $\mathbf{y}_{\mathrm{r}}(k)$, at the time instant $t = kT_{\mathrm{s}}$;
2. based on the dynamic model of the system and on the current states, $\mathbf{x}(k)$, disturbances, $\mathbf{d}(k)$, and reference, $\mathbf{r}(k)$, an optimization process is performed over the prediction horizon, p, to minimize the cost function given in Eq. (4.161). The optimization is done through the calculation of an optimum control sequence, $\mathbf{U}_{\#}$, over the control horizon, c;
3. the first element of the control sequence is associated with the control input $\mathbf{u}_{\#}(k)$, and sent to the system;
4. this process is repeated until $k = N$.

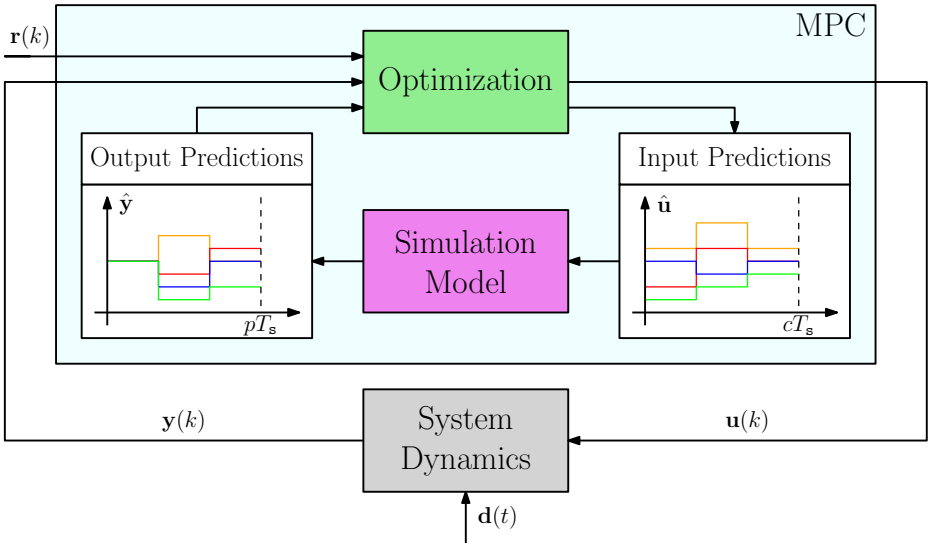

Figure 39: MPC block diagram

4.3 EXAMPLES

Some examples are presented to illustrate the application of the proposed methodology. The control objectives are to perform (1) set-point regulation and trajectory-tracking while ensuring (2) closed-loop stability and (3) disturbance rejection proprieties.

The control examples are implemented according to Fig. 40, where $\mathbf{y}$, $\mathbf{y}_\mathrm{d}$, $\mathbf{u}$ and $\mathbf{d}$ are the column-vectors of outputs, desired values, control and disturbances inputs, respectively. Also, in the block diagram of Fig. 40, the plants model is implemented using the recursive version of the Udwadia-Kalaba equation presented by Orsino (2020) and the controllers synthesis are performed with the MCM framework presented before.

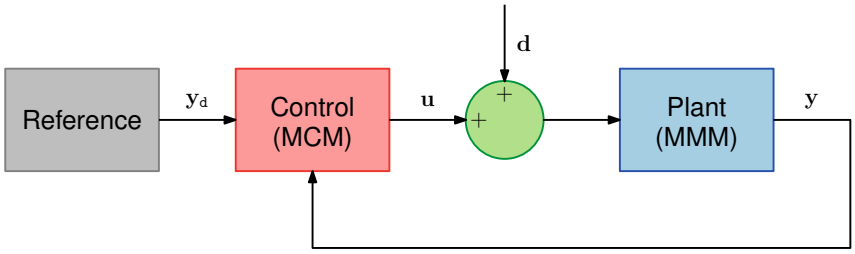

Figure 40: General control block diagram

4.3.1 Inverted pendulum

Figure 41 (a) shows the schematic diagram of the inverted pendulum physical model while Fig. 41 (b) shows the modeling/control hierarchy adopted.

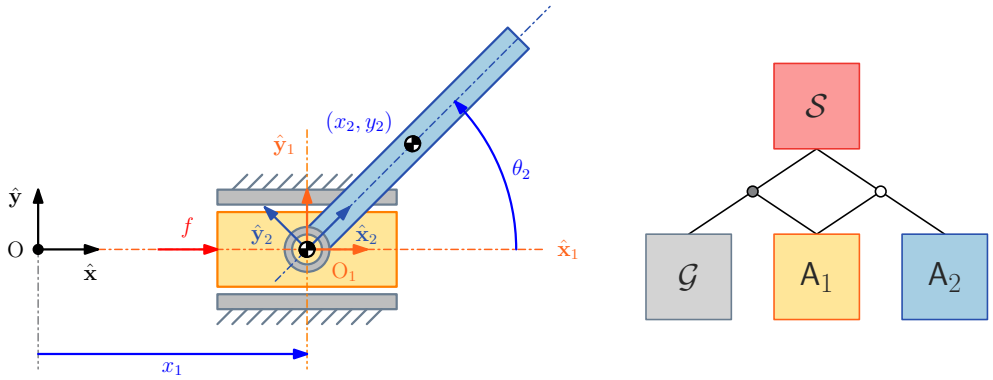

(a): Inverted pendulum physical model (b): Modeling/control hierarchy

Figure 41: Invented pendulum model

The generalized coordinates used in the modeling are given by $\mathbf{q} = \left[\mathbf{q}_1^\mathsf{T}, \mathbf{q}_2^\mathsf{T}\right]^\mathsf{T}$, with $\mathbf{q}_i = [x_i, y_i, \theta_i]^\mathsf{T}$ as the column-vector of generalized coordinates associated to the i-th body ($i = 1, 2$),

as shown in Fig. 41 (a). In the modeling hierarchy of Fig. 41 (b), $\mathcal{G}$ is the ground, body A_1 is the cart and body A_2 is the pendulum, while system $\mathcal{S}$ is the inverted pendulum. Also, an active prismatic joint (grey circle) connects the cart with the ground, and a passive revolute joint (white circle) connects the cart with the pendulum. A trivial set of quasi-velocities and accelerations is used on the synthesis, i.e., $\mathbf{v} = \dot{\mathbf{q}}$ and $\mathbf{a} = \dot{\mathbf{v}}$.

The relaxed dynamic model is given by:

$$\mathbf{N}\mathbf{a}_0 = \mathbf{g}, \tag{4.166}$$

where

$$\mathbf{N} = \mathbf{M}; \quad \mathbf{M} = \begin{bmatrix} \mathbf{M}_1 & \mathbf{0} \\ \mathbf{0} & \mathbf{M}_2 \end{bmatrix}; \quad \mathbf{g} = \mathbf{f}; \quad \mathbf{f} = \begin{bmatrix} \mathbf{f}_1 \\ \mathbf{f}_2 \end{bmatrix}. \tag{4.167}$$

The inertia matrix and active forces column-vectors related to the i-th body are written as:

$$\mathbf{M}_i = \begin{bmatrix} m_i & 0 & 0 \\ 0 & m_i & 0 \\ 0 & 0 & I_i \end{bmatrix}; \quad \mathbf{f}_i = \mathbf{f}_{\mathtt{A},i} + \mathbf{f}_{\mathtt{M},i}, \quad (i = 1, 2) \tag{4.168}$$

where m_i is the mass and I_i is the inertia moment, while $\mathbf{f}_{\mathtt{A},i}$ and $\mathbf{f}_{\mathtt{M},i}$ are the column-vectors of active forces due to the natural physical effects (e.g., weight, friction, etc.) and due to the motor forces, respectively. In this example, the active forces column-vectors are expressed by:

$$\begin{gathered} \mathbf{f}_{\mathtt{A},1} = \begin{bmatrix} -b_1\dot{x}_1 - c_1 \operatorname{sign}(\dot{x}_1) \\ -m_1 g \\ 0 \end{bmatrix}; \quad \mathbf{f}_{\mathtt{A},2} = \begin{bmatrix} 0 \\ -m_2 g \\ -b_2\dot{\theta}_2 - c_2 \operatorname{sign}\left(\dot{\theta}_2\right) \end{bmatrix}; \\ \mathbf{f}_{\mathtt{M},1} = \begin{bmatrix} f \\ 0 \\ 0 \end{bmatrix}; \quad \mathbf{f}_{\mathtt{M},2} = \begin{bmatrix} 0 \\ 0 \\ 0 \end{bmatrix}, \end{gathered} \tag{4.169}$$

where b_i and c_i $(i = 1, 2)$ are the coefficients of viscous and dry friction, respectively, and f is the horizontal control force on the cart.

The modeling constraints are written with respect to joints centers, as follows:

$$\boldsymbol{\varphi}(\mathbf{q}, t) = \begin{bmatrix} y_1 \\ \theta_1 \\ x_2 - x_1 - l\cos(\theta_2) \\ y_2 - l\sin(\theta_2) \end{bmatrix} = \mathbf{0}, \tag{4.170}$$

in which $2l$ is the pendulum length.

Performing the second time derivative of Eq. (4.170), we get:

$$\ddot{\boldsymbol{\varphi}}\left(\mathbf{a},\mathbf{v},\mathbf{q},t\right)=\mathbf{0}\Leftrightarrow\mathbf{A}\left(\mathbf{q},t\right)\mathbf{a}=\mathbf{b}\left(\mathbf{v},\mathbf{q},t\right), \tag{4.171}$$

where

$$\mathbf{A}=\begin{bmatrix}0&1&0&0&0&0\\0&0&1&0&0&0\\-1&0&0&1&0&l\sin\left(\theta_2\right)\\0&0&0&0&1&-l\cos\left(\theta_2\right)\end{bmatrix};\quad\mathbf{b}=\begin{bmatrix}0\\0\\-l\cos\left(\theta_2\right)\dot{\theta}_2^2\\-l\sin\left(\theta_2\right)\dot{\theta}_2^2\end{bmatrix}. \tag{4.172}$$

Since the cart horizontal displacement (x_1) is actuated, the identification matrices become:

$$\mathbf{Q}=\begin{bmatrix}1\\0\\0\\0\\0\\0\end{bmatrix};\quad\mathbf{R}=\begin{bmatrix}0&0&0&0&0\\1&0&0&0&0\\0&1&0&0&0\\0&0&1&0&0\\0&0&0&1&0\\0&0&0&0&1\end{bmatrix}. \tag{4.173}$$

The decentralized controllers are given by:

$$\mathbf{u}_0=\begin{bmatrix}\mathbf{u}_{0,1}\\\mathbf{u}_{0,2}\end{bmatrix}, \tag{4.174}$$

where

$$\mathbf{u}_{0,i}=\mathbf{N}_i\boldsymbol{\upsilon}_i+\mathbf{f}_{\mathrm{A},i}.\quad(i=1,2) \tag{4.175}$$

Let the cart sliding surface variable be given by:

$$\mathbf{s}_1\left(\mathbf{v}_1,\mathbf{q}_1,t\right)=\mathbf{v}_1+\boldsymbol{\Lambda}\tilde{\mathbf{q}}_1=\mathbf{0}, \tag{4.176}$$

where $\tilde{\mathbf{q}}_1=\mathbf{q}_1-\mathbf{q}_{\mathrm{d},1}$ is the tracking error column-vector and $\boldsymbol{\Lambda}=\boldsymbol{\Lambda}^{\mathsf{T}}\geq\mathbf{0}$ is a control gain matrix associated with the closed-loop bandwidth.

Based on Eq. (4.176), the following SMC[3] law is used for the cart:

$$\boldsymbol{\upsilon}_1=-\boldsymbol{\Lambda}\mathbf{v}_1-\mathbf{K}\,\mathrm{sign}\left(\mathbf{s}_1\right), \tag{4.177}$$

[3]To attenuate chattering effects in the SMC, the sign function will be replaced by tanh, i.e., $\mathrm{sign}\left(\mathbf{s}\right)\approx\tanh\left(\mathbf{s}/\epsilon\right)$, where $\epsilon>0$ regulates smoothness of such approximation. This procedure will be applied every time a SMC is used.

where $\mathbf{K} = \mathbf{K}^\mathsf{T} \geq \mathbf{0}$ is a control gain matrix.

For the pendulum we used a simple PD control, given by:

$$\boldsymbol{\upsilon}_2 = -\mathbf{K}_\mathrm{P}\tilde{\mathbf{q}}_2 - \mathbf{K}_\mathrm{D}\mathbf{v}_2, \tag{4.178}$$

where $\tilde{\mathbf{q}}_2 = \mathbf{q}_2 - \mathbf{q}_{\mathrm{d},2}$ is the tracking error column-vector, while $\mathbf{K}_\mathrm{P} = \mathbf{K}_\mathrm{P}^\mathsf{T} \geq \mathbf{0}$ and $\mathbf{K}_\mathrm{D} = \mathbf{K}_\mathrm{D}^\mathsf{T} \geq \mathbf{0}$ are the proportional and derivative control gain matrices, respectively.

Let $u_\# = f$. From Eq. (4.58), the control force is calculated as:

$$f = \mathbf{Q}^\mathsf{T}\left(\mathbf{I} - \mathbf{A}^\mathsf{T}\left(\mathbf{R}^\mathsf{T}\mathbf{A}^\mathsf{T}\right)^+\mathbf{R}^\mathsf{T}\right)\mathbf{u}_0, \tag{4.179}$$

where the superscript "+" denotes the Moore-Penrose PI.

The controller is tested for the set-point regulation/stabilization problem. The objective is to keep the pendulum on the upright position ($\theta_2 = \pi/2$) while the cart passes through a series of predefined set-points. The numerical simulations were performed in MATLAB/Simulink® environment. The dynamic model is numerically integrated with the `ode8` function using a fixed-time step of 0.001 s. The controller is implemented at a fixed rate frequency of 100 Hz. Table 5 shows the parameters used in the simulation.

Table 5: Inverted pendulum parameters

Symbols	Values	Units (SI)
m_1, m_2	2.70, 2.65	kg
I_1, I_2	0.01, 0.06	kgm^2
l	0.25	m
g	9.81	$\mathrm{m/s}^2$
$\mathbf{K}$	$\mathrm{diag}\,(40, 40, 40)$	$\mathrm{m/s}^2, \mathrm{rad/s}^2$
$\boldsymbol{\Lambda}$	$\mathrm{diag}\,(2, 2, 2)$	$1/\mathrm{s}$
ϵ	0.01	–
$\mathbf{K}_\mathrm{P}$	$\mathrm{diag}\,(400, 400, 400)$	$1/\mathrm{s}^2$
$\mathbf{K}_\mathrm{D}$	$\mathrm{diag}\,(800, 800, 800)$	$1/\mathrm{s}$

Figure 42 shows the set-point regulation/stabilization achieved with the proposed methodology. The horizontal control force is shown by Fig. 43. The set of control forces is shown by Fig. 43. We notice that the controller ensures the cart set-point regulation while stabilizing the inverted pendulum, bringing it from the bottom to an upright position and keeping it there. Moreover, the control forces consistency with the modeling constraints can be verified in Fig. 44 since the vertical control force and the control torque of the cart are null.

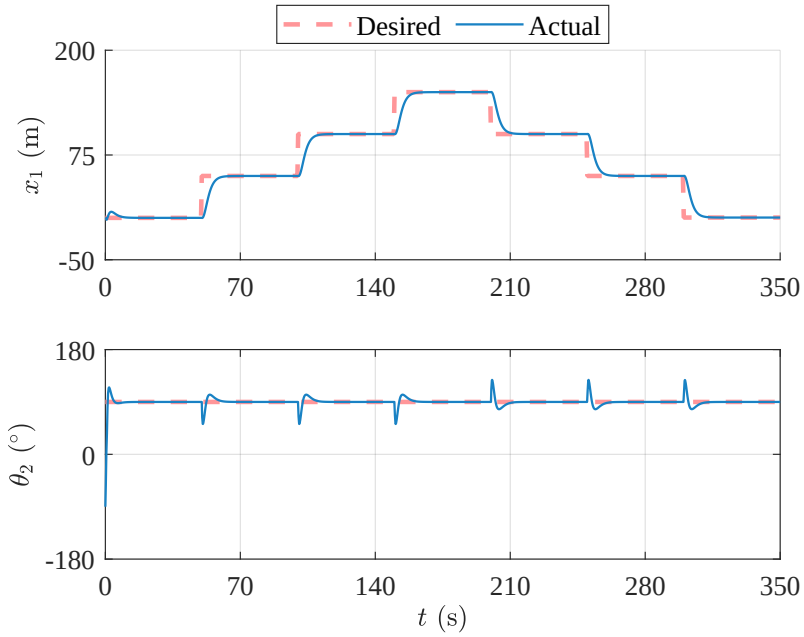

Figure 42: Set-point regulation of the inverted pendulum

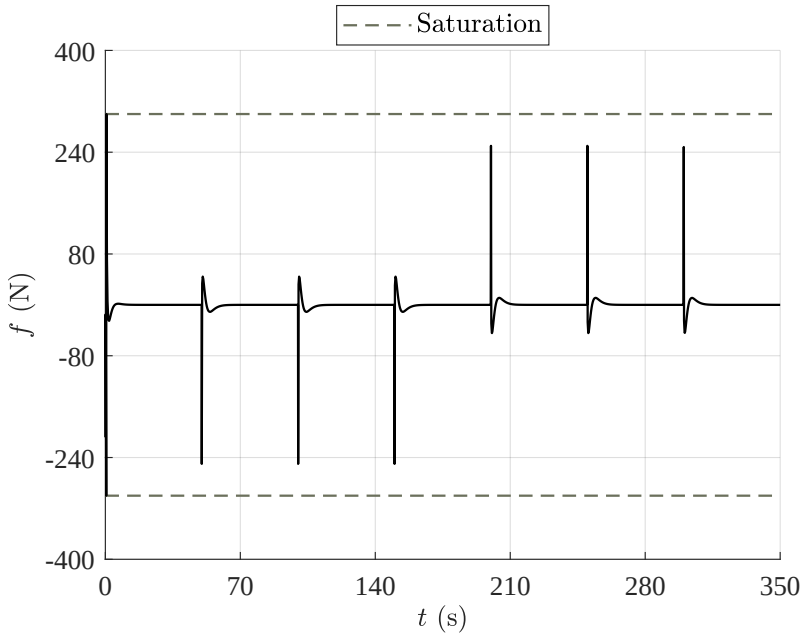

Figure 43: Horizontal control force of the inverted pendulum

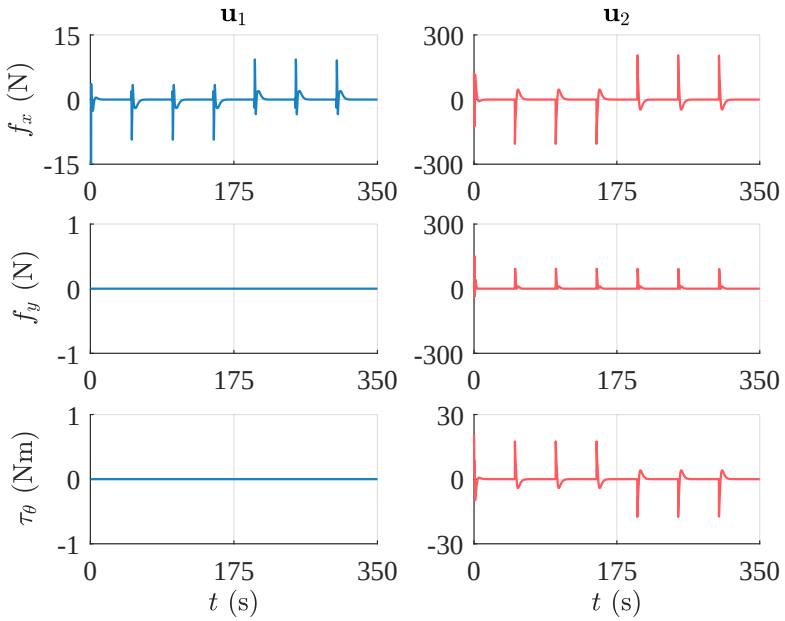

Figure 44: Control forces and torques of the inverted pendulum

4.3.2 Slider-crank mechanism

The schematic diagram of the slider-crank mechanism is shown in Fig. 45 (a), while the modeling/control hierarchy used in this example is shown in Fig. 45 (b).

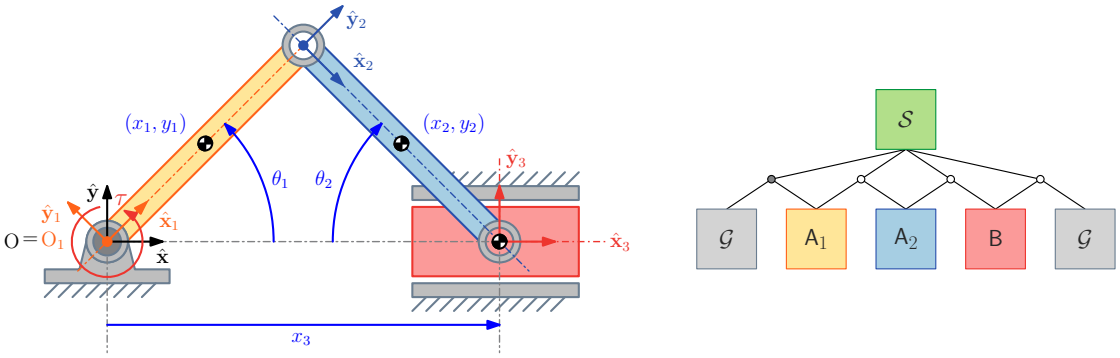

(a): Slider-crank schematic diagram (b): Modeling/control hierarchy

Figure 45: Slider-crank model

The generalized coordinates used on the synthesis are given by $\mathbf{q} = \left[\mathbf{q}_1^\mathsf{T}, \mathbf{q}_2^\mathsf{T}, \mathbf{q}_3^\mathsf{T}\right]^\mathsf{T}$, with $\mathbf{q}_i = [x_i, y_i, \theta_i]^\mathsf{T}$ as the column-vector of generalized coordinates associated with the i-th body ($i = 1, 2, 3$), as shown in Fig. 45 (a). In the modeling hierarchy of Fig. 45 (b), $\mathcal{G}$ is the ground, bodies A_i ($i = 1, 2$) are the links, body B is the slider block, and system $\mathcal{S}$ represents the slider-crank mechanism. Also, an active revolute joint (grey circle) connects the crank (first link) with the ground, two passive revolute joints (white circles) connect the crank with the rod (second link) and the rod with the slider, and a passive prismatic joint (white circle) connects the slider with the ground. The trivial set of quasi-velocities and quasi-accelerations is used again on the synthesis, i.e., $\mathbf{v} = \dot{\mathbf{q}}$ and $\mathbf{a} = \dot{\mathbf{v}}$.

The terms of the relaxed dynamic model for the slider-crank are given by:

$$\mathbf{N} = \mathbf{M}; \quad \mathbf{M} = \begin{bmatrix} \mathbf{M}_1 & \mathbf{0} & \mathbf{0} \\ \mathbf{0} & \mathbf{M}_2 & \mathbf{0} \\ \mathbf{0} & \mathbf{0} & \mathbf{M}_3 \end{bmatrix}; \quad \mathbf{g} = \mathbf{f}; \quad \mathbf{f} = \begin{bmatrix} \mathbf{f}_1 \\ \mathbf{f}_2 \\ \mathbf{f}_3 \end{bmatrix}, \tag{4.180}$$

where

$$\mathbf{M}_i = \begin{bmatrix} m_i & 0 & 0 \\ 0 & m_i & 0 \\ 0 & 0 & I_i \end{bmatrix}; \quad \mathbf{f}_i = \mathbf{f}_{\mathsf{A},i} + \mathbf{f}_{\mathsf{M},i}. \quad (i = 1, 2, 3) \tag{4.181}$$

The active forces due to natural physical effects are written as:

$$\begin{gathered}\mathbf{f}_{\mathrm{A},1}=\begin{bmatrix}0\\-m_1g\\-b_1\dot{\theta}_1-c_1\,\mathrm{sign}\left(\dot{\theta}_1\right)+b_2\left(\dot{\theta}_1+\dot{\theta}_2\right)+c_2\,\mathrm{sign}\left(\dot{\theta}_1+\dot{\theta}_2\right)\end{bmatrix},\\ \mathbf{f}_{\mathrm{A},2}=\begin{bmatrix}0\\-m_2g\\-b_2\left(\dot{\theta}_1+\dot{\theta}_2\right)-c_2\,\mathrm{sign}\left(\dot{\theta}_1+\dot{\theta}_2\right)\end{bmatrix};\quad \mathbf{f}_{\mathrm{A},3}=\begin{bmatrix}-b_3\dot{x}_3-c_3\,\mathrm{sign}\left(\dot{x}_3\right)\\-m_3g\\0\end{bmatrix},\end{gathered}\tag{4.182}$$

and the active motor forces are expressed by:

$$\mathbf{f}_{\mathrm{M},1}=\begin{bmatrix}0\\0\\\tau\end{bmatrix};\quad \mathbf{f}_{\mathrm{M},2}=\mathbf{f}_{\mathrm{M},3}=\begin{bmatrix}0\\0\\0\end{bmatrix},\tag{4.183}$$

in which τ is the control torque on the first link.

The modeling constraints are written with respect to the joints center, as follows:

$$\boldsymbol{\varphi}\left(\mathbf{q},t\right)=\begin{bmatrix}x_1-l\cos\left(\theta_1\right)\\y_1-l\sin\left(\theta_1\right)\\x_2-x_1-l\cos\left(\theta_1\right)-l\cos\left(\theta_2\right)\\y_2-y_1\\x_3-x_2-l\cos\left(\theta_2\right)\\y_3-y_2+l\sin\left(\theta_2\right)\\y_3\\\theta_3\end{bmatrix}=\mathbf{0}.\tag{4.184}$$

where l is half of the links length.

Performing the second time-derivative of Eq. (4.184), we get:

$$\mathbf{A} = \begin{bmatrix} 1 & 0 & l\sin(\theta_1) & 0 & 0 & 0 & 0 & 0 & 0 \\ 0 & 1 & -l\cos(\theta_1) & 0 & 0 & 0 & 0 & 0 & 0 \\ -1 & 0 & l\sin(\theta_1) & 1 & 0 & l\sin(\theta_2) & 0 & 0 & 0 \\ 0 & -1 & 0 & 0 & 1 & 0 & 0 & 0 & 0 \\ 0 & 0 & 0 & -1 & 0 & l\sin(\theta_2) & 1 & 0 & 0 \\ 0 & 0 & 0 & 0 & -1 & l\cos(\theta_2) & 0 & 1 & 0 \\ 0 & 0 & 0 & 0 & 0 & 0 & 0 & 1 & 0 \\ 0 & 0 & 0 & 0 & 0 & 0 & 0 & 0 & 1 \end{bmatrix},$$

$$\mathbf{b} = \begin{bmatrix} -l\cos(\theta_1)\,\dot{\theta}_1^2 \\ -l\sin(\theta_1)\,\dot{\theta}_1^2 \\ -l\cos(\theta_1)\,\dot{\theta}_1^2 - l\cos(\theta_2)\,\dot{\theta}_2^2 \\ 0 \\ -l\cos(\theta_2)\,\dot{\theta}_2^2 \\ l\sin(\theta_2)\,\dot{\theta}_2^2 \\ 0 \\ 0 \end{bmatrix}. \tag{4.185}$$

Only the angle of the first link (θ_1) is actuated, therefore we have:

$$\mathbf{Q} = \begin{bmatrix} 0 \\ 0 \\ 1 \\ 0 \\ 0 \\ 0 \\ 0 \\ 0 \\ 0 \end{bmatrix}; \quad \mathbf{R} = \begin{bmatrix} 1 & 0 & 0 & 0 & 0 & 0 & 0 & 0 & 0 \\ 0 & 1 & 0 & 0 & 0 & 0 & 0 & 0 & 0 \\ 0 & 0 & 0 & 0 & 0 & 0 & 0 & 0 & 0 \\ 0 & 0 & 0 & 1 & 0 & 0 & 0 & 0 & 0 \\ 0 & 0 & 0 & 0 & 1 & 0 & 0 & 0 & 0 \\ 0 & 0 & 0 & 0 & 0 & 1 & 0 & 0 & 0 \\ 0 & 0 & 0 & 0 & 0 & 0 & 1 & 0 & 0 \\ 0 & 0 & 0 & 0 & 0 & 0 & 0 & 1 & 0 \\ 0 & 0 & 0 & 0 & 0 & 0 & 0 & 0 & 1 \end{bmatrix}. \tag{4.186}$$

The decentralized controllers are given by:

$$\mathbf{u}_0 = \begin{bmatrix} \mathbf{u}_{0,1} \\ \mathbf{u}_{0,2} \\ \mathbf{u}_{0,3} \end{bmatrix}, \tag{4.187}$$

where

$$\mathbf{u}_{0,i} = \mathbf{N}_i \boldsymbol{\upsilon}_i + \mathbf{f}_{\mathrm{A},i}. \quad (i = 1, 2, 3) \tag{4.188}$$

Let the tracking errors be defined as:

$$\tilde{\mathbf{q}}_i = \mathbf{q}_i - \mathbf{q}_{\mathrm{d},i}; \quad \tilde{\mathbf{v}}_i = \mathbf{v}_i - \mathbf{v}_{\mathrm{d},i}; \quad \tilde{\mathbf{a}}_i = \mathbf{a}_i - \mathbf{a}_{\mathrm{d},i}. \quad (i = 1, 2, 3) \tag{4.189}$$

A CTC law is used in each sub-controller as follows:

$$\boldsymbol{\upsilon}_i = \mathbf{a}_{\mathrm{d},i} - \mathbf{K}_{\mathrm{P},i}\tilde{\mathbf{q}}_i - \mathbf{K}_{\mathrm{D},i}\tilde{\mathbf{v}}_i, \quad (i = 1, 2, 3) \tag{4.190}$$

with $\mathbf{K}_{\mathrm{P},i} = \mathbf{K}_{\mathrm{P},i}^{\mathsf{T}} \geq \mathbf{0}$ and $\mathbf{K}_{\mathrm{D},i} = \mathbf{K}_{\mathrm{D},i}^{\mathsf{T}} \geq \mathbf{0}$ as the proportional and derivative control gain matrices, respectively.

Let $u_{\#} = \tau$. From Eq. (4.63), the control torque is as follows:

$$\tau = \mathbf{Q}^{\mathsf{T}} \left(\mathbf{I} - \mathbf{A}^{\mathsf{T}} \left(\mathbf{R}^{\mathsf{T}} \mathbf{A}^{\mathsf{T}} \right)^{+} \mathbf{R}^{\mathsf{T}} \right) \mathbf{u}_0. \tag{4.191}$$

The controller of Eq. (4.191) is tested for the trajectory tracking problem.

The desired trajectory used in the simulation is given by (in radians):

$$\theta_{\mathrm{d},1}(t) = \frac{\pi}{4} + \sin(0.2\pi t). \tag{4.192}$$

The other desired coordinates are calculated using Eq. (4.192) on the modeling constraints in (4.184) and solving it for the other displacements.

The numerical simulations were performed with the same previous setup. Table 6 show the simulation parameters.

Table 6: Slider-crank parameters

Symbols ($i = 1, 2, 3$)	Values	Units (SI)
m_1, m_2, m_3	2.65, 2.65, 5.40	kg
I_1, I_2, I_3	0.06, 0.06, 0.01	kgm^2
b_1, b_2, b_3	0.1, 0.1, 0.1	Nms, Nms, Ns/m
c_1, c_2, c_3	0.01, 0.01, 0.01	Nm, Nm, N
l	0.25	m
g	9.81	m/s^2
$\mathbf{K}_{\mathrm{P},i}$	diag (10, 10, 10)	1/s^2
$\mathbf{K}_{\mathrm{D},i}$	diag (20, 20, 20)	1/s

Figure 46 shown the tracking achieved for θ_1 and x_3. The control torque is shown by Fig. 47 while the set of control forces is shown by Fig. 48. We can see a good tracking performance for the displacements in Fig. 46. Also, the control forces in Fig. 48 are consistent with the modeling constraints since the vertical control force and the control torque of the slider are null.

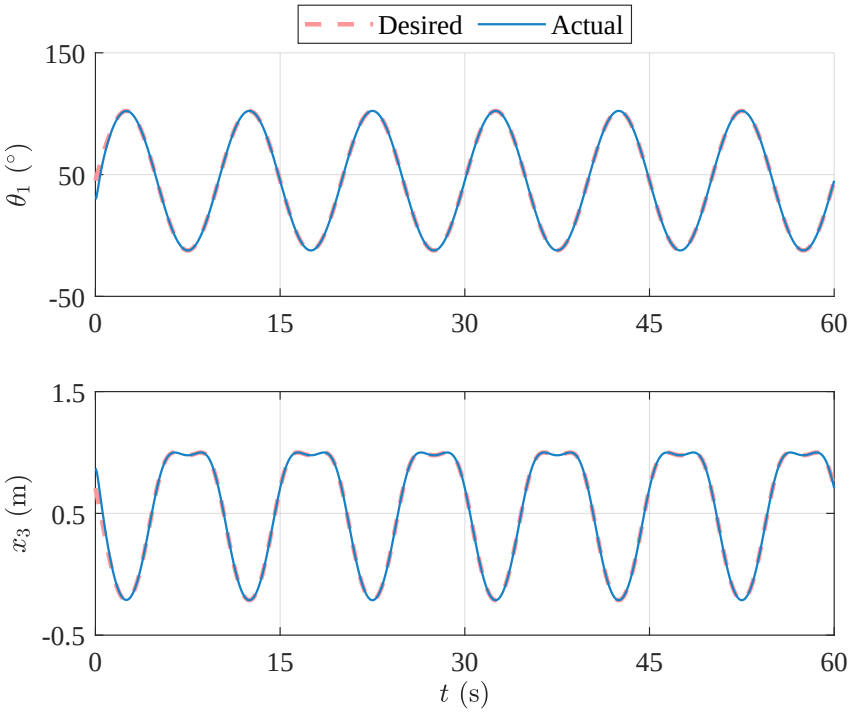

Figure 46: States tracking of the slider-crank mechanism

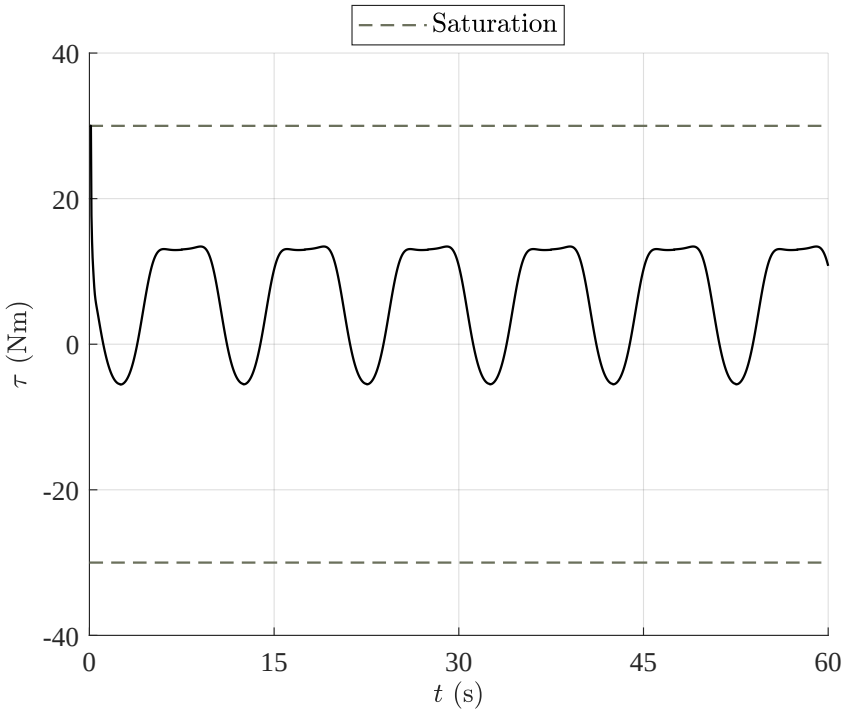

Figure 47: Control torque of the slider-crank mechanism

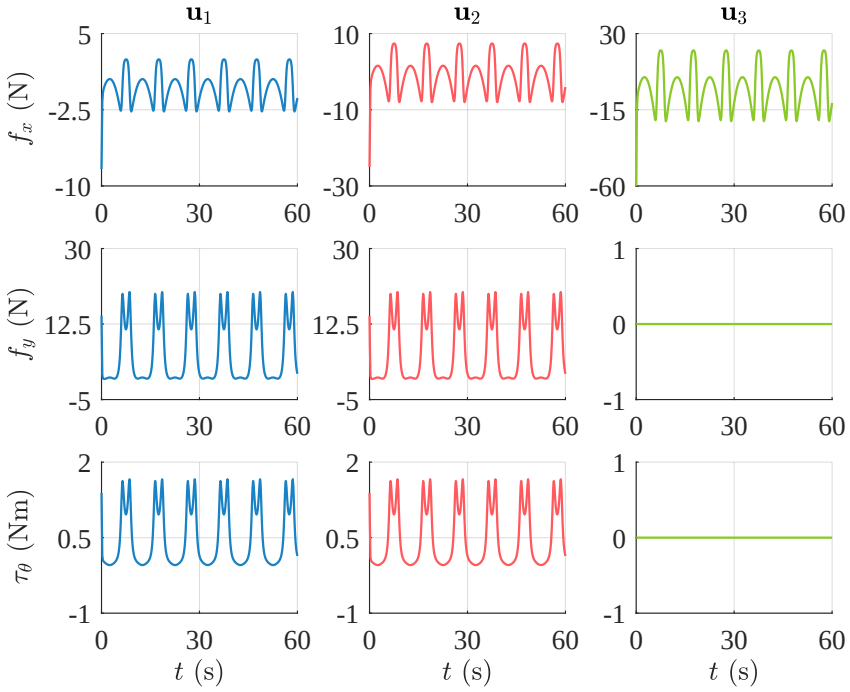

Figure 48: Control forces and torques of the slider-crank mechanism

4.3.3 RR-manipulator

Figure 49 (a) show the schematic diagram of the 2-link RR-manipulator and Fig. 49 (b) show the modeling/control hierarchy adopted in this example.

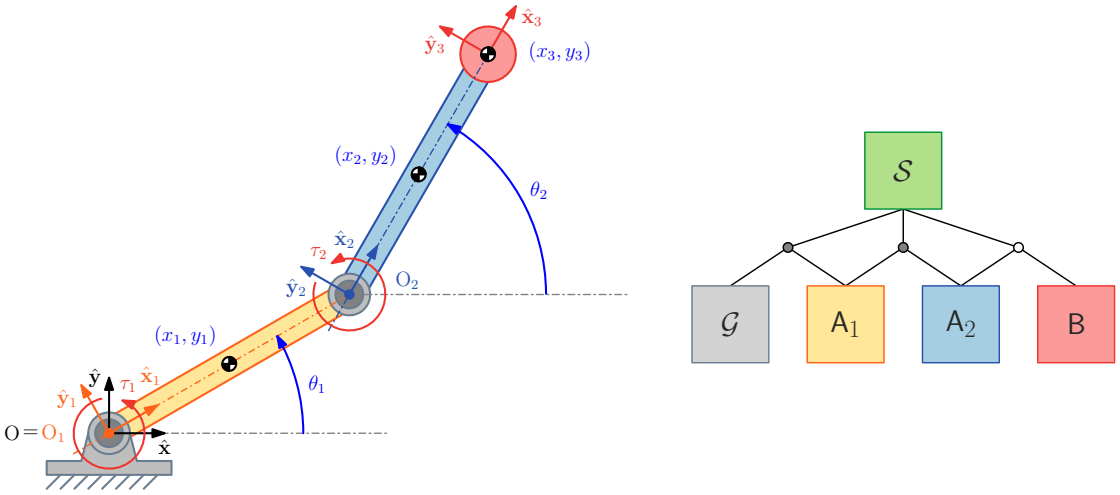

(a): RR-manipulator schematic diagram (b): Modeling/control hierarchy

Figure 49: RR-manipulator model

In this example we used the same set of generalized coordinates, quasi-velocities and quasi-accelerations of the slider-crank mechanism. The only differences between the dynamic model of the RR-manipulator and the slider-crank are the active forces of each subsystem and the modeling constraints. For example, in the modeling hierarchy of Fig. 49 (b), $\mathcal{G}$ is the ground, bodies A_i ($i = 1, 2$) are the links, body B is the end-effector, and system $\mathcal{S}$ represents the RR-manipulator. Regarding the constraints, two active revolute joints (grey circles) connect the first link with the ground and the second link with the first one, while a rigid joint connects the second link with the end-effector (white circle).

The active forces for the RR-manipulator are written as:

$$\begin{aligned}
\mathbf{f}_{\mathsf{A},1} &= \begin{bmatrix} 0 \\ -m_1 g \\ -b_1 \dot{\gamma}_1 - c_1 \operatorname{sign}(\dot{\gamma}_1) + b_2 (\dot{\gamma}_2) + c_2 \operatorname{sign}(\dot{\gamma}_2) \end{bmatrix}, \\
\mathbf{f}_{\mathsf{A},2} &= \begin{bmatrix} 0 \\ -m_2 g \\ -b_2 (\dot{\gamma}_2) - c_2 \operatorname{sign}(\dot{\gamma}_2) \end{bmatrix}; \quad \mathbf{f}_{\mathsf{A},3} = \begin{bmatrix} 0 \\ -m_3 g \\ 0 \end{bmatrix},
\end{aligned} \tag{4.193}$$

where $\gamma_1 = \theta_1$ and $\gamma_2 = \theta_2 - \theta_1$.

The active motor forces for the RR-manipulator are given by:

$$\mathbf{f}_{\mathrm{M},1} = \begin{bmatrix} 0 \\ 0 \\ \tau_1 - \tau_2 \end{bmatrix}; \quad \mathbf{f}_{\mathrm{M},2} = \begin{bmatrix} 0 \\ 0 \\ \tau_2 \end{bmatrix}; \quad \mathbf{f}_{\mathrm{M},3} = \begin{bmatrix} 0 \\ 0 \\ 0 \end{bmatrix}, \tag{4.194}$$

where τ_1 and τ_2 are the total motor torques on the first and second joint, respectively.

In this problem, we introduce actuation redundancy as an artificial hypothesis to test the presented methodology. Thus, let us considers that are two actuators in each revolute joint acting simultaneously, such that:

$$\tau_1 = \tau_{1,1} + \tau_{1,2}; \quad \tau_2 = \tau_{2,1} + \tau_{2,2}, \tag{4.195}$$

where $\tau_{i,1}$ and $\tau_{i,2}$ $(i = 1, 2)$ are the motor torques in the i-th joint.

The modeling constraints for the RR-manipulator are given by:

$$\boldsymbol{\varphi}(\mathbf{q}, t) = \begin{bmatrix} x_1 - l\cos(\theta_1) \\ y_1 - l\sin(\theta_1) \\ x_2 - x_1 - l\cos(\theta_1) - l\cos(\theta_2) \\ y_2 - y_1 - l\sin(\theta_1) - l\sin(\theta_2) \\ x_3 - x_2 - l\cos(\theta_2) \\ y_3 - y_2 - l\sin(\theta_2) \\ \theta_3 \end{bmatrix} = \mathbf{0}. \tag{4.196}$$

where l is half of the links length.

Performing the second time-derivative of Eq. (4.196), we get:

$$\mathbf{A} = \begin{bmatrix} 1 & 0 & l\sin(\theta_1) & 0 & 0 & 0 & 0 & 0 & 0 \\ 0 & 1 & -l\cos(\theta_1) & 0 & 0 & 0 & 0 & 0 & 0 \\ -1 & 0 & l\sin(\theta_1) & 1 & 0 & l\sin(\theta_2) & 0 & 0 & 0 \\ 0 & -1 & -l\cos(\theta_1) & 0 & 1 & -l\cos(\theta_2) & 0 & 0 & 0 \\ -1 & 0 & l\sin(\theta_1) & 0 & 0 & 2l\sin(\theta_2) & 1 & 0 & 0 \\ 0 & -1 & -l\cos(\theta_1) & 0 & 0 & -2l\cos(\theta_2) & 0 & 1 & 0 \\ 0 & 0 & 0 & 0 & 0 & 0 & 0 & 0 & 1 \end{bmatrix},$$

$$\mathbf{b} = \begin{bmatrix} -l\cos(\theta_1)\,\dot{\theta}_1^2 \\ -l\sin(\theta_1)\,\dot{\theta}_1^2 \\ -l\cos(\theta_1)\,\dot{\theta}_1^2 - l\cos(\theta_2)\,\dot{\theta}_2^2 \\ -l\sin(\theta_1)\,\dot{\theta}_1^2 - l\sin(\theta_2)\,\dot{\theta}_2^2 \\ -l\cos(\theta_1)\,\dot{\theta}_1^2 - 2l\cos(\theta_2)\,\dot{\theta}_2^2 \\ -l\sin(\theta_1)\,\dot{\theta}_1^2 - 2l\sin(\theta_2)\,\dot{\theta}_2^2 \\ 0 \end{bmatrix}. \tag{4.197}$$

The control torques are defined as follows:

$$\boldsymbol{\tau} = \left[\tau_{1,1}, \tau_{1,2}, \tau_{2,1}, \tau_{2,2}\right]^{\mathsf{T}}. \tag{4.198}$$

Let $\mathbf{u}_{\#} = [\tau_1 - \tau_2, \tau_2]^{\mathsf{T}}$ such that $\mathbf{u}_{\#} = \mathbf{T}\boldsymbol{\tau}$. From Eq. (4.194), we get:

$$\mathbf{T} = \begin{bmatrix} 1 & 1 & -1 & -1 \\ 0 & 0 & 1 & 1 \end{bmatrix}. \tag{4.199}$$

The weighting matrix is chosen as:

$$\mathbf{L} = \begin{bmatrix} 1 & 0 & 0 & 0 \\ 0 & 2 & 0 & 0 \\ 0 & 0 & 1 & 0 \\ 0 & 0 & 0 & 2 \end{bmatrix}. \tag{4.200}$$

Only the angle of the first and second links are actuated ($\theta_i;\ i = 1, 2$). Thus, the identification matrices become:

$$\mathbf{Q} = \begin{bmatrix} 0 & 0 \\ 0 & 0 \\ 1 & 0 \\ 0 & 0 \\ 0 & 0 \\ 0 & 1 \\ 0 & 0 \\ 0 & 0 \\ 0 & 0 \end{bmatrix}; \quad \mathbf{R} = \begin{bmatrix} 1 & 0 & 0 & 0 & 0 & 0 & 0 \\ 0 & 1 & 0 & 0 & 0 & 0 & 0 \\ 0 & 0 & 0 & 0 & 0 & 0 & 0 \\ 0 & 0 & 1 & 0 & 0 & 0 & 0 \\ 0 & 0 & 0 & 1 & 0 & 0 & 0 \\ 0 & 0 & 0 & 0 & 0 & 0 & 0 \\ 0 & 0 & 0 & 0 & 1 & 0 & 0 \\ 0 & 0 & 0 & 0 & 0 & 1 & 0 \\ 0 & 0 & 0 & 0 & 0 & 0 & 1 \end{bmatrix}. \tag{4.201}$$

Let us consider the same decentralized controllers used in the slider-crank mechanism. From Eq. (4.90), the control forces are as follows:

$$\mathbf{u}_{\#} = \mathbf{Q}^{\mathsf{T}} \left(\mathbf{I} - \mathbf{Z}^{-1} \mathbf{A}^{\mathsf{T}} \left(\mathbf{R}^{\mathsf{T}} \mathbf{Z}^{-1} \mathbf{A}^{\mathsf{T}} \right)^{+} \mathbf{R}^{\mathsf{T}} \right) \mathbf{Z}^{-1} \mathbf{u}_0, \tag{4.202}$$

where

$$\mathbf{Z} = \mathbf{I} + \mathbf{N}\mathbf{Q} \left(\mathbf{T}\mathbf{L}^{-1}\mathbf{T}^{\mathsf{T}} \right)^{+} \mathbf{Q}^{\mathsf{T}}. \tag{4.203}$$

According to Eq. (4.76), the motor torques becomes:

$$\boldsymbol{\tau} = \mathbf{L}^{-1}\mathbf{T}^{\mathsf{T}} \left(\mathbf{T}\mathbf{L}^{-1}\mathbf{T}^{\mathsf{T}} \right)^{+} \mathbf{u}_{\#}. \tag{4.204}$$

The controller of Eq. (4.204) is tested for the trajectory tracking problem.

The desired trajectory used in the simulation are written in terms of the end-effector coordinates as below (in meters):

$$\begin{aligned} x_{3,\mathrm{d}}(t) &= -0.3 \sin(0.2\pi t), \\ y_{3,\mathrm{d}}(t) &= 0.5 - 0.3 \cos(0.2\pi t). \end{aligned} \tag{4.205}$$

The numerical simulations were performed with the same previous setup. Table 7 shows the parameters used in the simulation.

Table 7: RR-manipulator parameters

Symbols	Values	Units (SI)
m_1, m_2, m_3	2.65, 2.65, 5.40	kg
I_1, I_2, I_3	0.06, 0.06, 0.01	kgm^2
b_1, b_2	0.1, 0.1	Nms
c_1, c_2	0.01, 0.01	Nm
l	0.25	m
g	9.81	$\mathrm{m/s}^2$
$\mathbf{K}_{\mathrm{P},1}, \mathbf{K}_{\mathrm{P},2}, \mathbf{K}_{\mathrm{P},3}$	$\mathbf{0}, \mathbf{0}, \mathrm{diag}\,(1000, 1000, 0)$	$1/\mathrm{s}^2$
$\mathbf{K}_{\mathrm{D},1}, \mathbf{K}_{\mathrm{D},2}, \mathbf{K}_{\mathrm{D},3}$	$\mathbf{0}, \mathbf{0}, \mathrm{diag}\,(2000, 2000, 0)$	$1/\mathrm{s}$

The end-effector tracking is shown by Figs. 50 and 51. The control torques are shown by Figs. 52 and 53. Concerning the control performance, the tracking achieved is good, both for the coordinates in Fig. 50 and for the path in Fig. 51. Moreover, the effect of using different weights on the control allocation can be seen in Fig. 48 since we have different motors in the same joint.

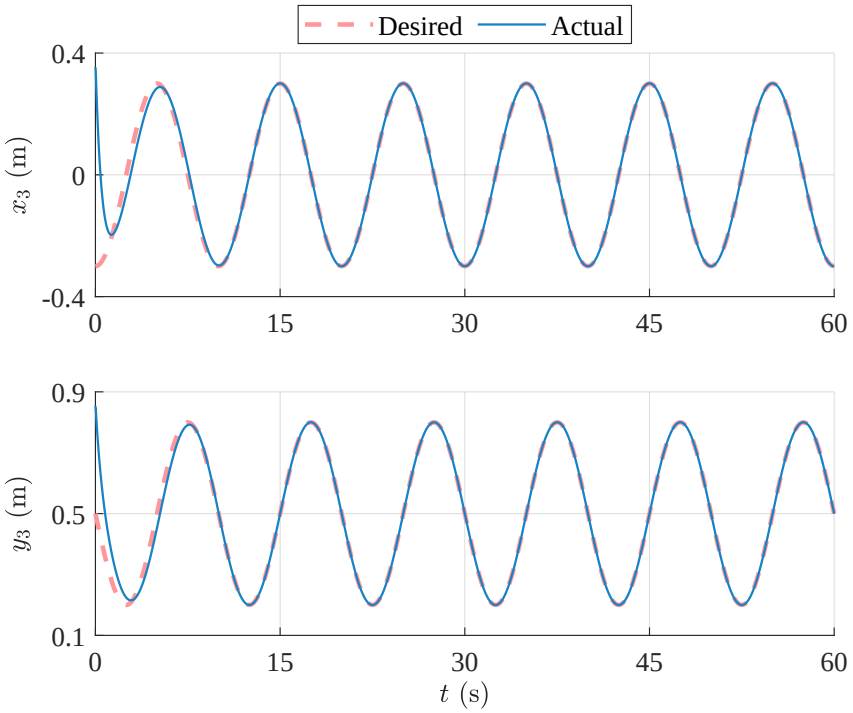

Figure 50: End-effector coordinates tracking of the RR-manipulator

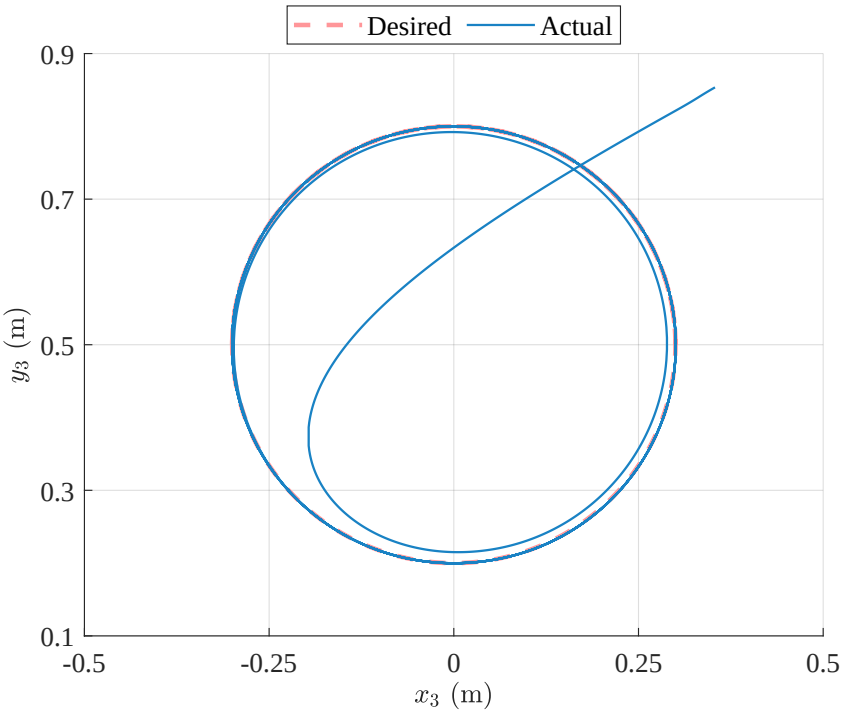

Figure 51: End-effector path tracking of the RR-manipulator

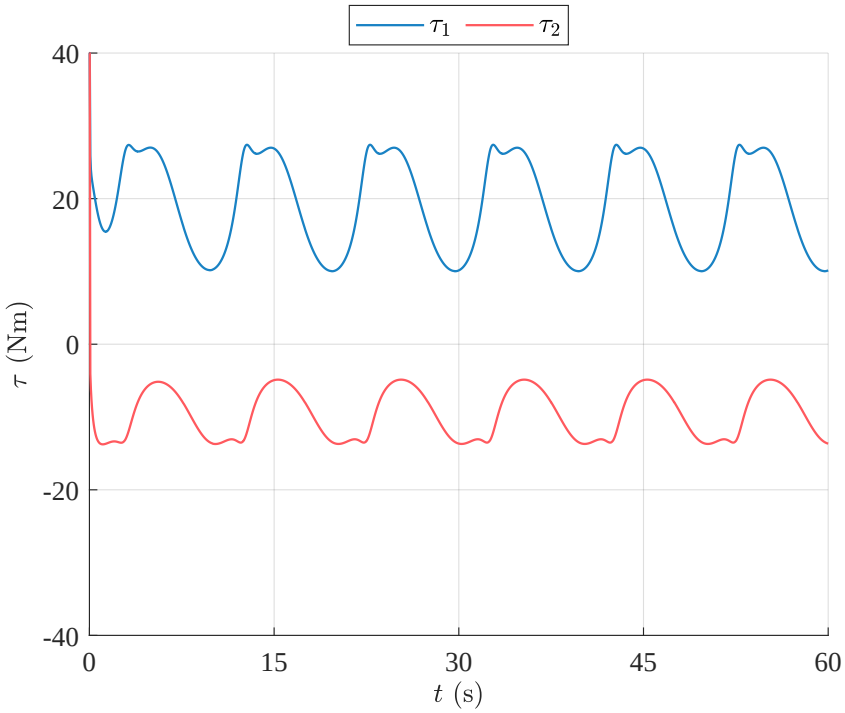

Figure 52: Total control torques of the RR-manipulator

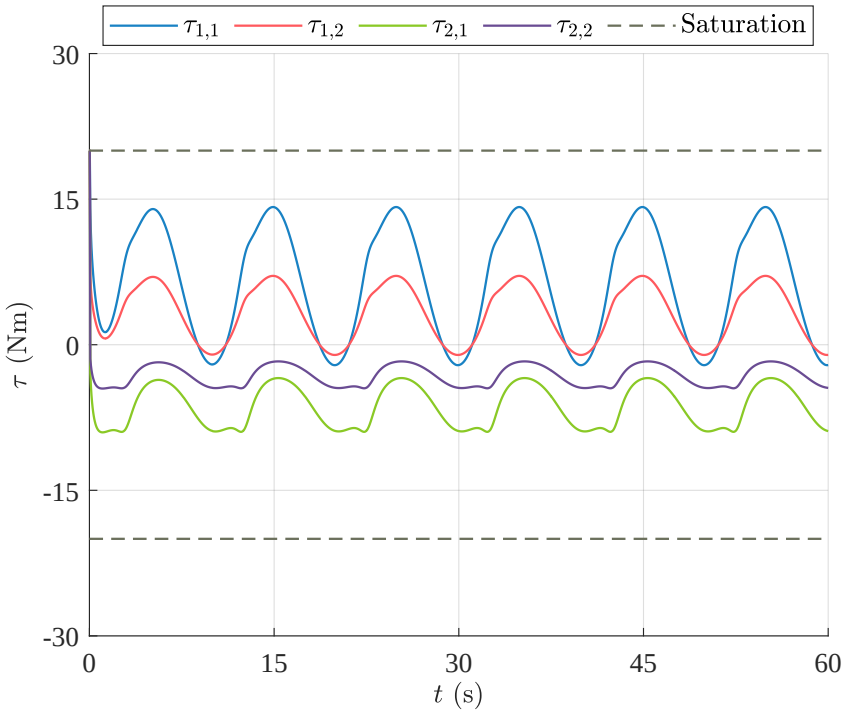

Figure 53: Control torques of the RR-manipulator

4.3.4 5R-manipulator

Figure 54 (a) shows the schematic diagram of the 5R-manipulator on the horizontal plane and Fig. 54 (b) shows the modeling/control hierarchy adopted to this example. Due to the parallel structure, this manipulator is used for high precision tasks, such as pick an place, printing, etc. We should point that this example is based on the prototype of the parallel manipulator CLARA constructed by Coutinho (2019) during his Ph.D.

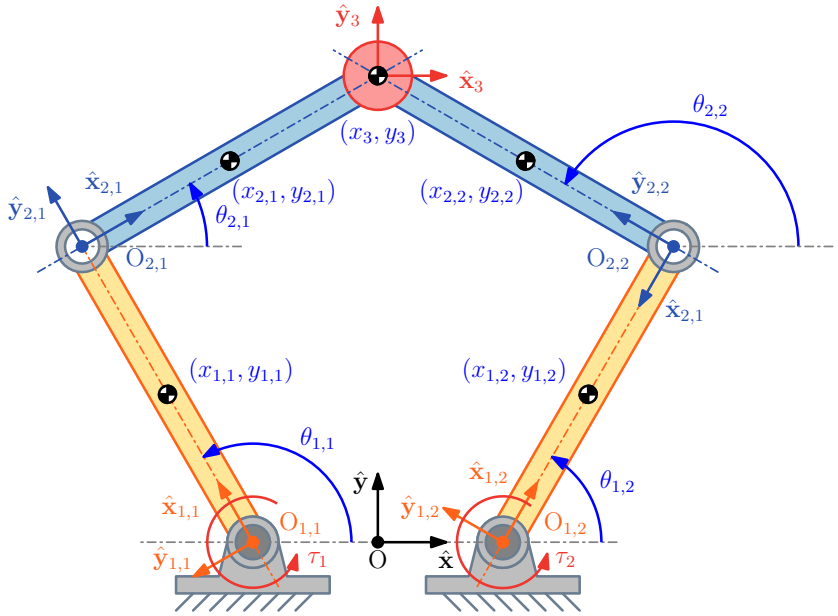

(a): 5R-manipulator schematic diagram

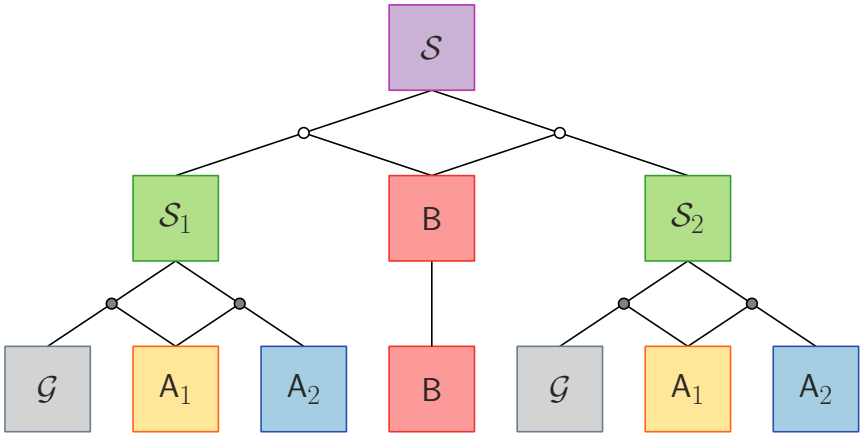

(b): Modeling/control hierarchy

Figure 54: 5R-manipulator model

In the modeling hierarchy of Fig. 54 (b), $\mathcal{G}$ is the ground, bodies A_i $(i = 1, 2)$ are the manipulator links, body B is the end-effector, considered in this example as a massless point, subsystems $\mathcal{S}_i$ $(i = 1, 2)$ are the RR-manipulators, while system $\mathcal{S}$ represents the 5R-manipulator.

In the subsystems $\mathcal{S}_i$ $(i = 1, 2)$, two active revolute joints (grey circles) connect the ground with the first link and the second link with the first one. In the system $\mathcal{S}$, passive revolute joints (white circles) connect the RR-manipulators with the end-effector. In this example, the control synthesis is performed from two sub-controllers originally made for the RR-manipulators. Therefore, the generalized coordinates of the synthesis are given by $\mathbf{q} = \left[\mathbf{q}_1^\mathsf{T}, \mathbf{q}_2^\mathsf{T}\right]^\mathsf{T}$, where $\mathbf{q}_i = [\theta_{1,i}, \theta_{2,i}]^\mathsf{T}$ is the column-vector of generalized coordinates of the i-th RR-manipulator $(i = 1, 2)$, as seen in Fig. 54 (a). The trivial set of quasi-velocities and quasi-accelerations is used once again, i.e., $\mathbf{v} = \dot{\mathbf{q}}$ and $\mathbf{a} = \dot{\mathbf{v}}$.

The dynamic model of the i-th RR-manipulator is written as:

$$\mathbf{N}_i \mathbf{a}_i = \mathbf{g}_i; \quad \mathbf{N}_i = \mathbf{M}_i; \quad \mathbf{g}_i = \mathbf{f}_i, \quad (i = 1, 2) \tag{4.206}$$

with the generalized inertia matrix given by:

$$\mathbf{N}_i = \begin{bmatrix} I_{1,i} + l_{1,i}^2 \left(m_{1,i} + 4\left(m_{2,i} + m_{3,i}\right)\right) & 2\cos\left(\theta_{12,i}\right) l_{1,i} \left(l_{\mathrm{G}_2,i} m_{2,i} + l_{2,i} m_{3,i}\right) \\ 2\cos\left(\theta_{12,i}\right) l_{1,i} \left(l_{\mathrm{G}_2,i} m_{2,i} + l_{2,i} m_{3,i}\right) & I_{2,i} + l_{\mathrm{G}_2,i}^2 m_{2,i} + 4 l_{2,i}^2 m_{3,i} \end{bmatrix}, \tag{4.207}$$

and the active forces expressed as:

$$\mathbf{f}_i = \mathbf{f}_{\mathtt{A},i} + \mathbf{f}_{\mathtt{M},i}, \quad (i = 1, 2) \tag{4.208}$$

where

$$\mathbf{f}_{\mathtt{A},i} = \begin{bmatrix} -\tau_{\mathtt{D},i} - 2\sin\left(\theta_{12,i}\right) l_{1,i} l_{\mathrm{G}_2,i} m_{2,i} \dot{\theta}_{2,i}^2 - 4\sin\left(\theta_{12,i}\right) l_{1,i} l_{2,i} m_{3,i} \dot{\theta}_{2,i}^2 \\ 2\sin\left(\theta_{12,i}\right) l_{1,i} \left(l_{\mathrm{G}_2,i} m_{2,i} + 2 l_{2,i} m_{3,i}\right) \dot{\theta}_{1,i}^2 \end{bmatrix}; \quad \mathbf{f}_{\mathtt{M},i} = \begin{bmatrix} \tau_{12,i} \\ \tau_{2,i} \end{bmatrix}, \tag{4.209}$$

in which $\theta_{12,i} = \theta_{1,i} - \theta_{2,i}$, $\tau_{12,i} = \tau_{1,i} - \tau_{2,i}$ and $\tau_{\mathtt{D},i} = b_{1,i}\dot{\theta}_{1,i} + c_{1,i}\,\mathrm{sign}\left(\dot{\theta}_{1,i}\right)$.

Let the coordinates of the i-th end-effector and their references be defined as follows:

$$\mathbf{p}_{3,i} = \begin{bmatrix} x_{3,i} \\ y_{3,i} \end{bmatrix}; \quad \mathbf{p}_{3,\mathtt{d},i} = \mathbf{p}_{3,\mathtt{d}} = \begin{bmatrix} x_{3,\mathtt{d}} \\ y_{3,\mathtt{d}} \end{bmatrix}, \quad (i = 1, 2) \tag{4.210}$$

with $x_{3,i}$ and $y_{3,i}$ written as:

$$\begin{aligned} x_{3,i} &= 2l_{1,i}\cos\left(\theta_{1,i}\right) + 2l_{2,i}\cos\left(\theta_{2,i}\right) \pm l_3, \\ y_{3,i} &= 2l_{1,i}\sin\left(\theta_{1,i}\right) + 2l_{2,i}\sin\left(\theta_{2,i}\right). \end{aligned} \tag{4.211}$$

Also, let the sliding surface for the i-th end-effector be given by:

$$\mathbf{s}_{3,i}\left(\mathbf{v}_i, \mathbf{q}_i, t\right) = \dot{\tilde{\mathbf{p}}}_{3,i} + \mathbf{\Lambda}_i \tilde{\mathbf{p}}_{3,i} = \mathbf{0}, \quad (i = 1, 2) \tag{4.212}$$

where $\tilde{\mathbf{p}}_{3,i} = \mathbf{p}_{3,i} - \mathbf{p}_{3,\mathrm{d}}$ is the tracking error column-vector and $\mathbf{\Lambda}_i = \mathbf{\Lambda}_i^{\mathsf{T}} \geq \mathbf{0}$ is a control gain matrix associated to the closed-loop bandwidth.

Based on Eq. (4.212), the following control constraint is defined:

$$\boldsymbol{\varphi}_{\mathrm{SC},i}\left(\mathbf{v}_i, \mathbf{q}_i, t\right) = \mathbf{s}_{3,i}\left(\mathbf{v}_i, \mathbf{q}_i, t\right) = \mathbf{0}. \quad (i = 1, 2) \tag{4.213}$$

Performing the time-derivative of Eq. (4.213) and imposing the sliding condition, we get:

$$\dot{\boldsymbol{\varphi}}_{\mathrm{SC},i} = -\mathbf{L}_i \mathbf{s}_{3,i} - \mathbf{K}_i \operatorname{sign}\left(\mathbf{s}_{3,i}\right), \quad (i = 1, 2) \tag{4.214}$$

where $\mathbf{L}_i = \mathbf{L}_i^{\mathsf{T}} \geq \mathbf{0}$ and $\mathbf{K}_i = \mathbf{K}_i^{\mathsf{T}} \geq \mathbf{0}$ are control gains matrices.

Moreover, Eq. (4.214) can be rewritten as:

$$\mathbf{A}_{\mathrm{SC},i}\left(\mathbf{q}_i, t\right) \mathbf{a}_{\mathrm{SC},i} = \mathbf{b}_{\mathrm{SC},i}\left(\mathbf{v}_i, \mathbf{q}_i, t\right), \quad (i = 1, 2) \tag{4.215}$$

where

$$\mathbf{A}_{\mathrm{SC},i} = \begin{bmatrix} -2\sin\left(\theta_{1,i}\right) l_{1,i} & -2\sin\left(\theta_{2,i}\right) l_{2,i} \\ 2\cos\left(\theta_{1,i}\right) l_{1,i} & 2\cos\left(\theta_{2,i}\right) l_{2,i} \end{bmatrix}, \tag{4.216}$$

$$\mathbf{b}_{\mathrm{SC},i} = \ddot{\mathbf{p}}_{3,\mathrm{d}} - \dot{\mathbf{A}}_{\mathrm{SC},i} \dot{\mathbf{q}}_i - \mathbf{\Lambda}_i \dot{\tilde{\mathbf{p}}}_{3,i} - \mathbf{L}_i \mathbf{s}_{3,i} - \mathbf{K}_i \operatorname{sign}\left(\mathbf{s}_{3,i}\right).$$

From Eq. (4.114), the decentralized control of the i-th RR-manipulator is given by:

$$\mathbf{u}_{0,i} = \mathbf{\Gamma}_i^{-1/2} \bar{\mathbf{H}}_{\mathrm{SC},i}^{+} \left(\mathbf{b}_{\mathrm{SC},i} - \mathbf{A}_{\mathrm{SC},i} \mathbf{a}_i\right). \quad (i = 1, 2) \tag{4.217}$$

In this case $\mathbf{P}_i = \mathbf{I}$ $(i = 1, 2)$ since the modeling constraints are already imposed on the RR-manipulator model. Moreover, taking $\mathbf{\Gamma}_i = \mathbf{I}$, we get:

$$\bar{\mathbf{H}}_{\mathrm{SC},i} = \mathbf{A}_{\mathrm{SC},i} \mathbf{N}_i^{-1/2} \mathbf{P}_i \mathbf{N}_i^{-1/2} \mathbf{\Gamma}_i^{-1/2} = \mathbf{A}_{\mathrm{SC},i} \mathbf{N}_i^{-1}. \tag{4.218}$$

The decentralized control of the 5R-manipulator is written as:

$$\mathbf{u}_0 = \begin{bmatrix} \mathbf{u}_{0,1} \\ \mathbf{u}_{0,2} \end{bmatrix}. \tag{4.219}$$

The modeling constraints of the 5R-manipulator are written concerning the center of the end-effectors, as follows:

$$\boldsymbol{\varphi}\left(\mathbf{q}, t\right) = \begin{bmatrix} x_{3,1} - x_{3,2} \\ y_{3,1} - y_{3,2} \end{bmatrix} = \mathbf{0}. \tag{4.220}$$

Performing the second time-derivative of Eq. (4.220), we get:

$$\begin{aligned}\mathbf{A} &= 2\begin{bmatrix} -l_{1,1}\sin(\theta_{1,1}) & -l_{2,1}\sin(\theta_{2,1}) & l_{1,2}\sin(\theta_{1,1}) & l_{2,2}\sin(\theta_{2,2}) \\ l_{1,1}\cos(\theta_{1,1}) & l_{2,1}\cos(\theta_{2,1}) & -l_{1,2}\cos(\theta_{1,1}) & -l_{2,2}\cos(\theta_{2,2}) \end{bmatrix}, \\ \mathbf{b} &= 2\begin{bmatrix} l_{1,1}\cos(\theta_{1,1})\,\dot{\theta}_{1,1}^2 + l_{2,1}\cos(\theta_{2,1})\,\dot{\theta}_{2,1}^2 - l_{1,2}\cos(\theta_{1,2})\,\dot{\theta}_{1,2}^2 - l_{2,2}\cos(\theta_{2,2})\,\dot{\theta}_{2,2}^2 \\ l_{1,1}\sin(\theta_{1,1})\,\dot{\theta}_{1,1}^2 + l_{2,1}\sin(\theta_{2,1})\,\dot{\theta}_{2,1}^2 - l_{1,2}\sin(\theta_{1,2})\,\dot{\theta}_{1,2}^2 - l_{2,2}\sin(\theta_{2,2})\,\dot{\theta}_{2,2}^2 \end{bmatrix}. \end{aligned} \tag{4.221}$$

Since only $\theta_{1,i}$ $(i = 1, 2)$ are actuated, the identification matrices becomes:

$$\mathbf{Q} = \begin{bmatrix} 1 & 0 \\ 0 & 0 \\ 0 & 1 \\ 0 & 0 \end{bmatrix}; \quad \mathbf{R} = \begin{bmatrix} 0 & 0 \\ 1 & 0 \\ 0 & 0 \\ 0 & 1 \end{bmatrix}. \tag{4.222}$$

Let $\mathbf{u}_{\#} = \boldsymbol{\tau} = [\tau_1, \tau_2]^{\mathsf{T}}$. From Eq. (4.58) the controller of the 5R-manipulator becomes:

$$\boldsymbol{\tau} = \mathbf{Q}^{\mathsf{T}}\left(\mathbf{I} - \mathbf{A}^{\mathsf{T}}\left(\mathbf{R}^{\mathsf{T}}\mathbf{A}^{\mathsf{T}}\right)^{+}\mathbf{R}^{\mathsf{T}}\right)\mathbf{u}_0. \tag{4.223}$$

The controller of Eq. (4.223) is tested on the trajectory tracking problem of a triangular trajectory with vertices coordinates given by (in meters):

$$\vec{\mathbf{p}}_1 = \begin{bmatrix} 0 \\ 0.11 \end{bmatrix}; \quad \vec{\mathbf{p}}_2 = \begin{bmatrix} 0.05 \\ 0.26 \end{bmatrix}; \quad \vec{\mathbf{p}}_3 = \begin{bmatrix} -0.05 \\ 0.26 \end{bmatrix}. \tag{4.224}$$

Each side of the triangle is parameterized as a polynomial trajectory of 7-th to impose zero velocity, acceleration and jerk at the beginning and end of each segment. The polynomial is expressed by:

$$r(t) = r(t_{\mathtt{i}}) + (r(t_{\mathtt{f}}) - r(t_{\mathtt{i}}))\left(35\delta t^4 - 84\delta t^5 + 70\delta t^6 - 20\delta t^7\right), \tag{4.225}$$

where $r(t_{\mathtt{i}})$ is the initial position, $r(t_{\mathtt{f}})$ is the final position and δt is the fraction of time, defined with respect to the actual time instant.

The numerical simulations were performed with the same previous setup. Table 8 show the parameters used in the simulation.

Table 8: 5R-manipulator parameters

Symbols ($i = 1, 2$)	Values	Units (SI)
$m_{1,1}, m_{2,1}, m_{1,2}, m_{2,2}, m_3$	0.062, 0.097, 0.062, 0.0124, 0.001	kg
$I_{1,1}, I_{2,1}, I_{1,2}, I_{2,2}, I_3$	0.0003, 0.001, 0.0001, 0.0004, 0	kgm^2
b_1, b_2	0.0002, 0.0001	Nms
c_1, c_2	0.05, 0.04	Nm
$l_{1,1}, l_{2,1}, l_{1,2}, l_{2,2}, l_{G_{2,1}}, l_{G_{2,2}}, l_3$	0.06, 0.08, 0.06, 0.08, 0.058, 0.078, 0.05	m
$\mathbf{\Lambda}_i$	diag (5, 5)	1/s
$\mathbf{L}_i$	diag (100, 100)	1/s
$\mathbf{K}_i$	diag (50, 50)	m/s^2

The results obtained are shown by Figs. 55 to 59. Figs. 55 and 56 show the end-effector tracking. The tracking achieved is good and the motion is smooth, which is due to the polynomial used to parameterize the triangle sides. The control torques are shown by Fig. 57. We can notice the dry friction effects in Fig. 57. The decentralized control torques are shown by Fig. 58. The constraints are shown by Fig. 59. The modeling constraints order is 10^{-4} and the control constraints order is 10^{-3}.

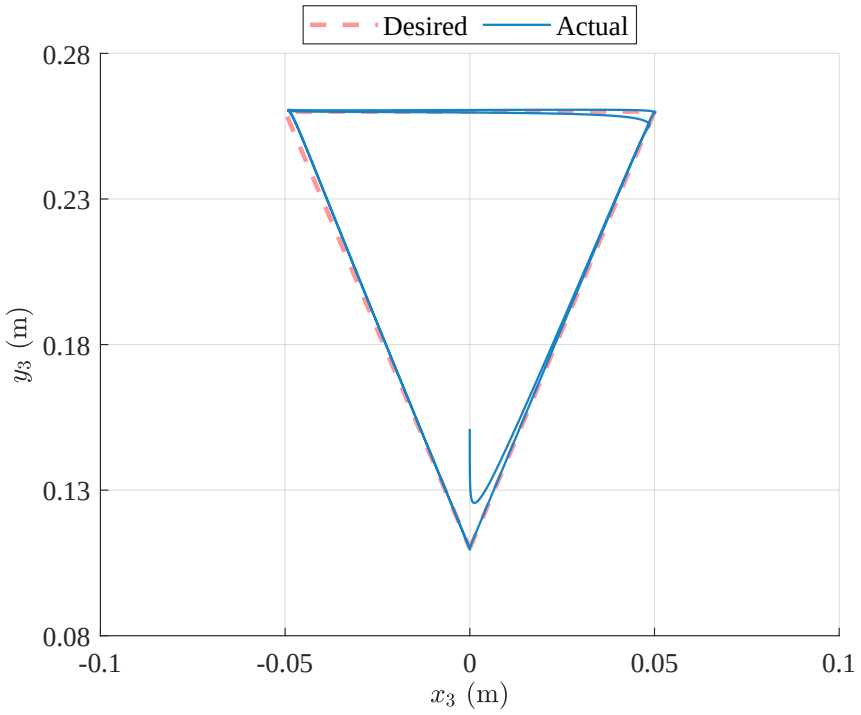

Figure 55: End-effector path tracking of the 5R-manipulator

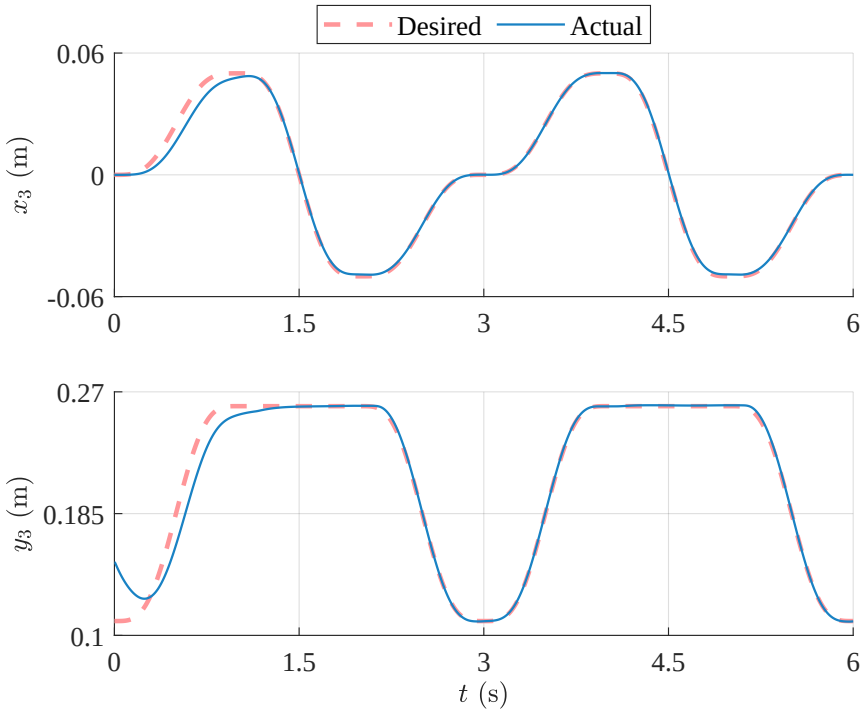

Figure 56: End-effector coordinates tracking of the 5R-manipulator

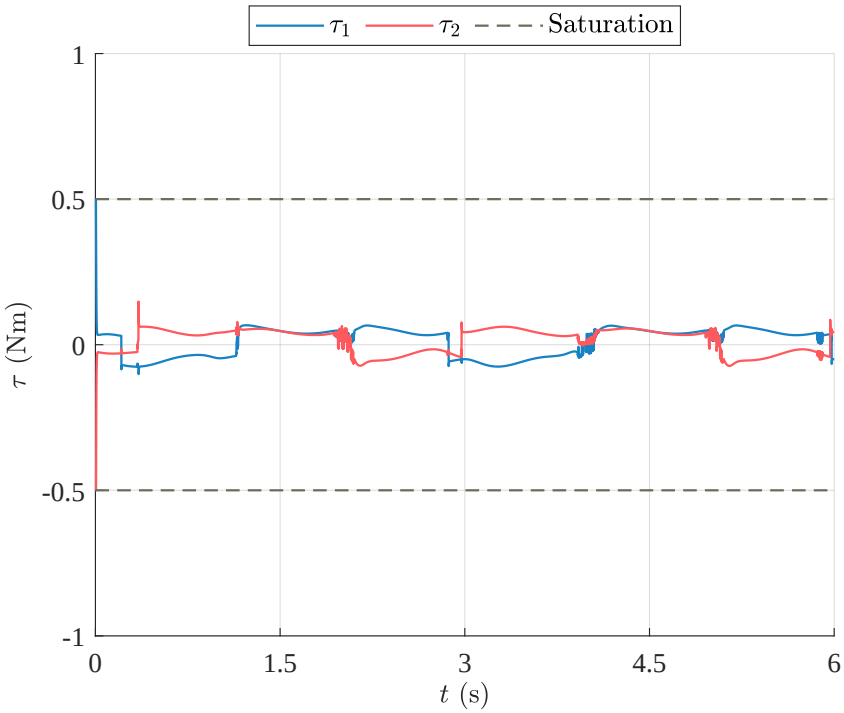

Figure 57: Control torques of the 5R-manipulator

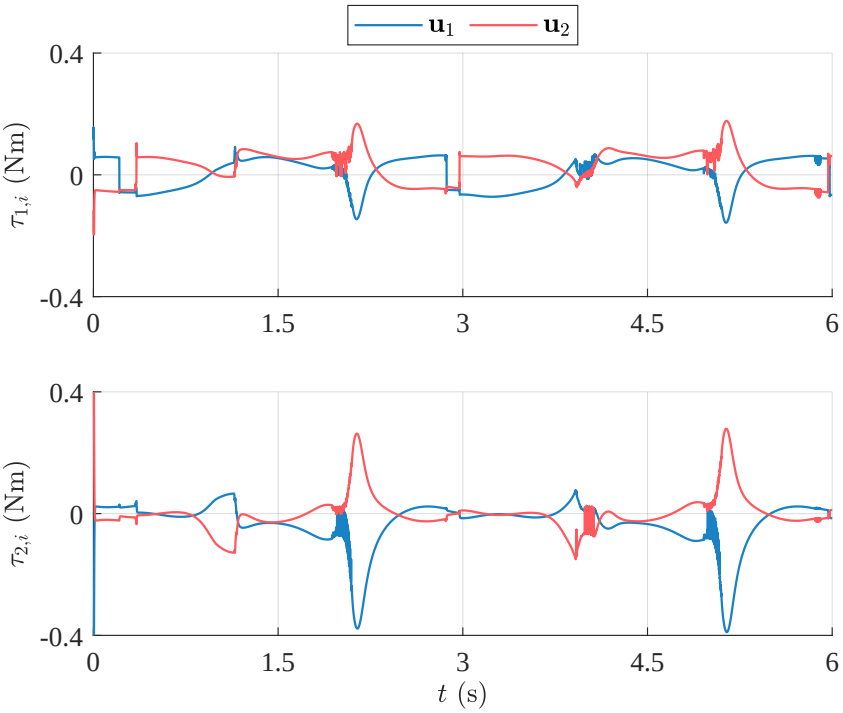

Figure 58: Decentralized control forces of the 5R-manipulator

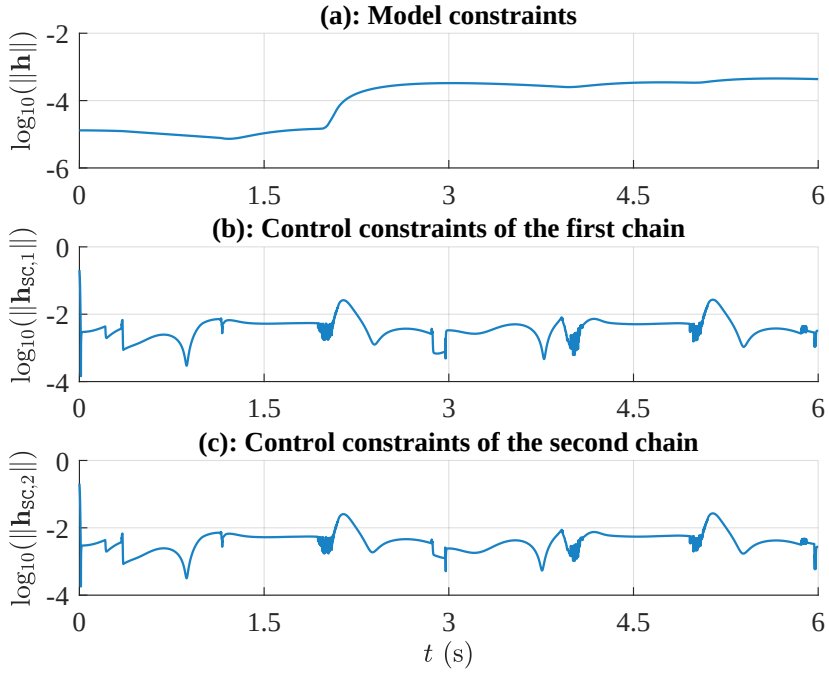

Figure 59: Constraints of the 5R-manipulator

4.3.5 4×RR-mechanism

Figure 60 (a) show the 4×RR-mechanism. This parallel mechanism is similar to the previous example of the 5R-manipulator in the kinematic structure once it is composed of open chains connected to the end-effector. However, the improved rigidity of the 4×RR-mechanism enables the execution of more complex tasks, such as high precision machining, grinding, etc. Also, it should be emphasized that there is an actuation redundancy (non-kinematic) once the system has more actuators than those required to perform the planar motion.

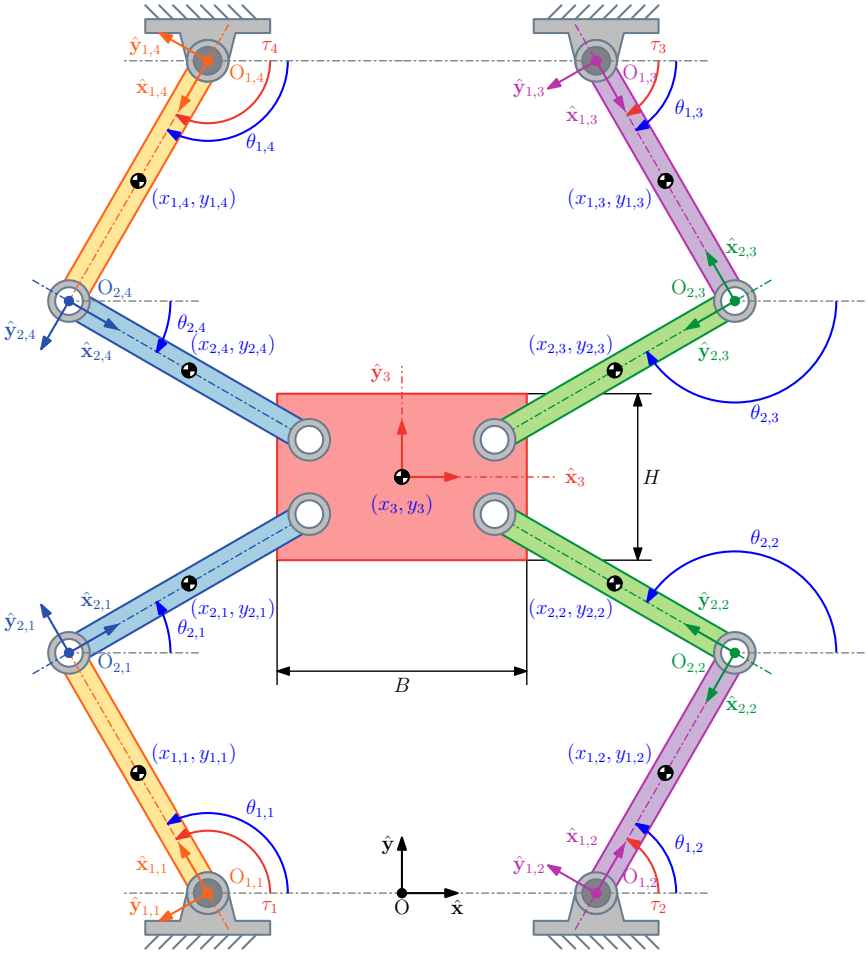

(a): 4×RR-mechanism schematic diagram

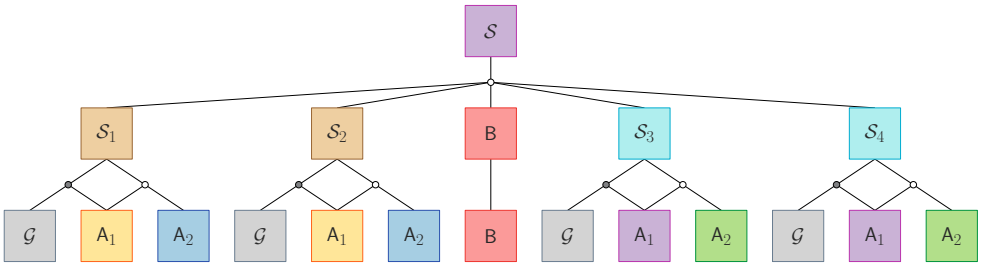

(b): Modeling/control hierarchy

Figure 60: 4×RR-mechanism model

In the modeling hierarchy of Fig. 60 (b), $\mathcal{G}$ is the ground, bodies A_i ($i = 1, 2$) are the manipulator links, and body B is the end-effector. In the subsystems $\mathcal{S}_i$, an active revolute joint (grey circle) connects the first link with the ground and a passive revolute joint connects the second link with the first one. In the system $\mathcal{S}$, four passive revolute joints (white circle) connects the chains with the end-effector. In this example, the control synthesis is performed from five sub-controllers, i.e., one controller four each chain and one for the end-effector. The generalized coordinates of the synthesis are given by $\mathbf{q} = \left[\mathbf{q}_{12,1}^{\mathsf{T}}, \ldots, \mathbf{q}_{12,4}^{\mathsf{T}}, \mathbf{q}_3^{\mathsf{T}}\right]^{\mathsf{T}}$, where $\mathbf{q}_{12,i} = [\theta_{1,i}, \theta_{2,i}]^{\mathsf{T}}$ ($i = 1, \ldots, 4$) and $\mathbf{q}_3 = [x_3, y_3, \theta_3]^{\mathsf{T}}$ as seen in Fig. 60 (a). The trivial set of quasi-velocities and quasi-accelerations is used once again, i.e., $\mathbf{v} = \dot{\mathbf{q}}$ and $\mathbf{a} = \dot{\mathbf{v}}$.

For this example, we synthesized the decentralized controllers using the soft control constraints formulation of Eq. (4.120). Due to the kinematic structure, we can use the same control constraints initially made for the RR-manipulators of the previous example on the chains of the 4×RR-mechanism. First, however, we should add a new set of control constraints for the end-effector. For this sake, let the sliding surface for the end-effector be given by:

$$\mathbf{s}_3\left(\mathbf{v}_3, \mathbf{q}_3, t\right) = \dot{\tilde{\mathbf{q}}}_3 + \boldsymbol{\Lambda}\tilde{\mathbf{q}}_3 = \mathbf{0}, \tag{4.226}$$

where $\tilde{\mathbf{q}}_3 = \mathbf{q}_3 - \mathbf{q}_{\mathrm{d},3}$ is the tracking error column-vector and $\boldsymbol{\Lambda}_3 = \boldsymbol{\Lambda}_3^{\mathsf{T}} \geq \mathbf{0}$ is a control gain matrix associated to the closed-loop bandwidth.

Based on Eq. (4.226), the following servo-constraints are defined:

$$\boldsymbol{\varphi}_{\mathrm{SC},3}\left(\mathbf{v}_3, \mathbf{q}_3, t\right) = \mathbf{s}_3\left(\mathbf{v}_3, \mathbf{q}_3, t\right) = \mathbf{0}. \tag{4.227}$$

Performing the time-derivative of Eq. (4.227) and imposing the sliding condition, we get:

$$\dot{\boldsymbol{\varphi}}_{\mathrm{SC},3} = -\mathbf{L}_3\mathbf{s}_3 - \mathbf{K}_3 \operatorname{sign}\left(\mathbf{s}_3\right), \tag{4.228}$$

where $\mathbf{L}_3 = \mathbf{L}_3^{\mathsf{T}} \geq \mathbf{0}$ and $\mathbf{K}_3 = \mathbf{K}_3^{\mathsf{T}} \geq \mathbf{0}$ are control gains matrices.

Moreover, Eq. (4.228) can be rewritten as:

$$\mathbf{A}_{\mathrm{SC},3}\mathbf{a}_{\mathrm{SC},3} = \mathbf{b}_{\mathrm{SC},3}\left(\mathbf{v}_3, \mathbf{q}_3, t\right), \tag{4.229}$$

where

$$\mathbf{A}_{\mathrm{SC},3} = \begin{bmatrix} 1 & 0 & 0 \\ 0 & 1 & 0 \\ 0 & 0 & 1 \end{bmatrix}; \quad \mathbf{b}_{\mathrm{SC},3} = \ddot{\mathbf{q}}_{3,\mathrm{d}} - \boldsymbol{\Lambda}_3\dot{\tilde{\mathbf{q}}}_3 - \mathbf{L}_3\mathbf{s}_3 - \mathbf{K}_3 \operatorname{sign}\left(\mathbf{s}_3\right). \tag{4.230}$$

The decentralized controllers are obtained with the constraints of Eqs. (4.215) and (4.229), solving the following QP-problem based on Eq. (4.120):

$$\begin{aligned} &\min_{\mathbf{u}_0} J_i = \frac{1}{2}\mathbf{u}_{0,i}^{\mathsf{T}}\mathbf{R}\mathbf{u}_{0,i}, \\ &\text{s.t.} \begin{bmatrix} -\mathbf{J}_{\mathsf{SC},i} \\ +\mathbf{J}_{\mathsf{SC},i} \end{bmatrix} \mathbf{u}_{0,i} \leq \begin{bmatrix} \boldsymbol{\varepsilon}_i - \mathbf{x}_{\mathsf{SC},i} \\ \boldsymbol{\varepsilon}_i + \mathbf{x}_{\mathsf{SC},i} \end{bmatrix}, \quad (i = 1, \ldots, 5) \end{aligned} \tag{4.231}$$

where $\boldsymbol{\varepsilon}_i = \left[\varepsilon_{i,j}\right]^{\mathsf{T}}$ $(i = 1, \ldots, 5;\, j = 1, \ldots, n)$ with components $\varepsilon_{i,j}$. A possible choose of smooth function presented in Heshmati-Alamdari et al. (2021b) is:

$$\varepsilon_{i,j}(t) = \left(\varepsilon_{i,j,0} - \varepsilon_{i,j,\infty}\right) \exp\left(-\lambda t\right) + \rho_{i,j,\infty}, \tag{4.232}$$

where the constant λ dictates the exponential convergence rate, $\varepsilon_{i,j,\infty}$ denotes the ultimate bound and $\varepsilon_{i,j,0}$ is chosen to satisfy $\rho_{i,j,0} \geq \left|\dot{h}_{\mathsf{SC},i,j}(0)\right|$.

The decentralized controllers are given by:

$$\mathbf{u}_0 = \begin{bmatrix} \mathbf{u}_{0,1} \\ \mathbf{u}_{0,2} \\ \mathbf{u}_{0,3} \\ \mathbf{u}_{0,4} \\ \mathbf{u}_{0,5} \end{bmatrix}. \tag{4.233}$$

To enforce the modeling constraints on the decentralized controllers of Eq. (4.233) with the recursive Algorithm 2, let the constraint equation between each end-effector and the platform be given by:

$$\tilde{\boldsymbol{\varphi}}_i(\mathbf{q}, t) = \vec{\mathbf{p}}^{\,\mathsf{I}}_{\mathrm{O}_{3,i}|\mathcal{S}_i}(\mathbf{q}, t) - \vec{\mathbf{p}}^{\,\mathsf{I}}_{\mathrm{O}_{3,i}|\mathsf{B}}(\mathbf{q}, t) = \mathbf{0}, \quad (i = 1, \ldots, 4) \tag{4.234}$$

with

$$\begin{aligned} \vec{\mathbf{p}}^{\,\mathsf{I}}_{\mathrm{O}_{3,1}|\mathcal{S}_1} &= \begin{bmatrix} x_3 - B\cos(\theta_3) - H\sin(\theta_3) \\ y_3 - H\cos(\theta_3) + B\sin(\theta_3) \end{bmatrix}; \quad \vec{\mathbf{p}}^{\,\mathsf{I}}_{\mathrm{O}_{3,2}|\mathcal{S}_2} = \begin{bmatrix} x_3 + B\cos(\theta_3) - H\sin(\theta_3) \\ y_3 - H\cos(\theta_3) - B\sin(\theta_3) \end{bmatrix}, \\ \vec{\mathbf{p}}^{\,\mathsf{I}}_{\mathrm{O}_{3,3}|\mathcal{S}_3} &= \begin{bmatrix} x_3 + B\cos(\theta_3) + H\sin(\theta_3) \\ y_3 + H\cos(\theta_3) - B\sin(\theta_3) \end{bmatrix}; \quad \vec{\mathbf{p}}^{\,\mathsf{I}}_{\mathrm{O}_{3,4}|\mathcal{S}_4} = \begin{bmatrix} x_3 - B\cos(\theta_3) + H\sin(\theta_3) \\ y_3 + H\cos(\theta_3) + B\sin(\theta_3) \end{bmatrix}, \end{aligned} \tag{4.235}$$

and

$$\begin{aligned}
\vec{\mathbf{p}}^{\,\mathsf{I}}_{\mathrm{O}_{3,1}|\mathsf{B}} &= \begin{bmatrix} 2l_{1,1}\cos(\theta_{1,1}) - x_0 + 2l_{2,1}\cos(\theta_{1,1}+\theta_{2,1}) \\ 2l_{1,1}\sin(\theta_{1,1}) - y_0 + 2l_{2,1}\sin(\theta_{1,1}+\theta_{2,1}) \end{bmatrix}, \\
\vec{\mathbf{p}}^{\,\mathsf{I}}_{\mathrm{O}_{3,2}|\mathsf{B}} &= \begin{bmatrix} x_0 - 2l_{1,2}\cos(\theta_{1,2}) - 2l_{2,2}\cos(\theta_{1,2}+\theta_{2,2}) \\ 2l_{1,2}\sin(\theta_{1,2}) - y_0 + 2l_{2,2}\sin(\theta_{1,2}+\theta_{2,2}) \end{bmatrix}, \\
\vec{\mathbf{p}}^{\,\mathsf{I}}_{\mathrm{O}_{3,3}|\mathsf{B}} &= \begin{bmatrix} x_0 - 2l_{1,3}\cos(\theta_{1,3}) - 2l_{2,3}\cos(\theta_{1,3}+\theta_{2,3}) \\ y_0 - 2l_{1,3}\sin(\theta_{1,3}) - 2l_{2,3}\sin(\theta_{1,3}+\theta_{2,3}) \end{bmatrix}, \\
\vec{\mathbf{p}}^{\,\mathsf{I}}_{\mathrm{O}_{3,4}|\mathsf{B}} &= \begin{bmatrix} 2l_{1,4}\cos(\theta_{1,4}) - x_0 + 2l_{2,4}\cos(\theta_{1,4}+\theta_{2,4}) \\ y_0 - 2l_{1,4}\sin(\theta_{1,4}) - 2l_{2,4}\sin(\theta_{1,4}+\theta_{2,4}) \end{bmatrix},
\end{aligned} \tag{4.236}$$

where B and H are the dimensions of the end-effector platform, $\pm x_0$ and $\pm y_0$ are the coordinates of the first revolute joint of each chain, while $2l_{i,j}$ ($i = 1, \ldots, 4$; $j = 1, \ldots, 4$) are the links lengths.

Performing the second time-derivative of Eq. (4.234), we get:

$$\ddot{\vec{\boldsymbol{\varphi}}}_i(\mathbf{a}, \mathbf{v}, \mathbf{q}, t) = \mathbf{0} \Leftrightarrow \tilde{\mathbf{A}}_i(\mathbf{q}, t)\,\mathbf{a} - \tilde{\mathbf{b}}_i(\mathbf{v}, \mathbf{q}, t) = \mathbf{0}, \quad (i = 1, \ldots, 4) \tag{4.237}$$

where

$$\begin{aligned}
\tilde{\mathbf{A}}_1 &= \begin{bmatrix} -2l_{1,1}\sin(\theta_{1,1}) - 2l_{2,1}\sin(\theta_{1,1}+\theta_{2,1}) & -2l_{2,1}\sin(\theta_{1,1}+\theta_{2,1}) & 0 & 0 & 0 & 0 & 0 & 0 & -1 & 0 & H\cos(\theta_3) - B\sin(\theta_3) \\ 2l_{1,1}\cos(\theta_{1,1}) + 2l_{2,1}\cos(\theta_{1,1}+\theta_{2,1}) & 2l_{2,1}\cos(\theta_{1,1}+\theta_{2,1}) & 0 & 0 & 0 & 0 & 0 & 0 & 0 & -1 & -B\cos(\theta_3) - H\sin(\theta_3) \end{bmatrix}, \\
\tilde{\mathbf{A}}_2 &= \begin{bmatrix} 0 & 0 & 2l_{1,2}\sin(\theta_{1,2}) + 2l_{2,2}\sin(\theta_{1,2}+\theta_{2,2}) & 2l_{2,2}\sin(\theta_{1,2}+\theta_{2,2}) & 0 & 0 & 0 & 0 & -1 & 0 & H\cos(\theta_3) + B\sin(\theta_3) \\ 0 & 0 & 2l_{1,2}\cos(\theta_{1,2}) + 2l_{2,2}\cos(\theta_{1,2}+\theta_{2,2}) & 2l_{2,2}\cos(\theta_{1,2}+\theta_{2,2}) & 0 & 0 & 0 & 0 & 0 & -1 & B\cos(\theta_3) - H\sin(\theta_3) \end{bmatrix}, \\
\tilde{\mathbf{A}}_3 &= \begin{bmatrix} 0 & 0 & 0 & 0 & 2l_{1,3}\sin(\theta_{1,3}) + 2l_{2,3}\sin(\theta_{1,3}+\theta_{2,3}) & 2l_{2,3}\sin(\theta_{1,3}+\theta_{2,3}) & 0 & 0 & -1 & 0 & B\sin(\theta_3) - H\cos(\theta_3) \\ 0 & 0 & 0 & 0 & -2l_{1,3}\cos(\theta_{1,3}) - 2l_{2,3}\cos(\theta_{1,3}+\theta_{2,3}) & -2l_{2,3}\cos(\theta_{1,3}+\theta_{2,3}) & 0 & 0 & 0 & -1 & B\cos(\theta_3) + H\sin(\theta_3) \end{bmatrix}, \\
\tilde{\mathbf{A}}_4 &= \begin{bmatrix} 0 & 0 & 0 & 0 & 0 & 0 & -2l_{1,4}\sin(\theta_{1,4}) - 2l_{2,4}\sin(\theta_{1,4}+\theta_{2,4}) & -2l_{2,4}\sin(\theta_{1,4}+\theta_{2,4}) & -1 & 0 & -H\cos(\theta_3) - B\sin(\theta_3) \\ 0 & 0 & 0 & 0 & 0 & 0 & -2l_{1,4}\cos(\theta_{1,4}) - 2l_{2,4}\cos(\theta_{1,4}+\theta_{2,4}) & -2l_{2,4}\cos(\theta_{1,4}+\theta_{2,4}) & 0 & -1 & H\sin(\theta_3) - B\cos(\theta_3) \end{bmatrix},
\end{aligned} \tag{4.238}$$

and

$$\begin{aligned}
\tilde{\mathbf{b}}_1 &= \begin{bmatrix} 2\dot{\theta}_{1,1}^2 l_{2,1}\cos(\theta_{1,1}+\theta_{2,1}) + 2\dot{\theta}_{2,1}^2 l_{2,1}\cos(\theta_{1,1}+\theta_{2,1}) + 2\dot{\theta}_{1,1}^2 l_{1,1}\cos(\theta_{1,1}) + B\dot{\theta}_3^2\cos(\theta_3) + H\dot{\theta}_3^2\sin(\theta_3) + 4\dot{\theta}_{1,1}\dot{\theta}_{2,1} l_{2,1}\cos(\theta_{1,1}+\theta_{2,1}) \\ 2\dot{\theta}_{1,1}^2 l_{2,1}\sin(\theta_{1,1}+\theta_{2,1}) + 2\dot{\theta}_{2,1}^2 l_{2,1}\sin(\theta_{1,1}+\theta_{2,1}) + 2\dot{\theta}_{1,1}^2 l_{1,1}\sin(\theta_{1,1}) + H\dot{\theta}_3^2\cos(\theta_3) - B\dot{\theta}_3^2\sin(\theta_3) + 4\dot{\theta}_{1,1}\dot{\theta}_{2,1} l_{2,1}\sin(\theta_{1,1}+\theta_{2,1}) \end{bmatrix}, \\
\tilde{\mathbf{b}}_2 &= \begin{bmatrix} H\dot{\theta}_3^2\sin(\theta_3) - 2\dot{\theta}_{2,2}^2 l_{2,2}\cos(\theta_{1,2}+\theta_{2,2}) - 2\dot{\theta}_{1,2}^2 l_{1,2}\cos(\theta_{1,2}) - B\dot{\theta}_3^2\cos(\theta_3) - 2\dot{\theta}_{1,2}^2 l_{2,2}\cos(\theta_{1,2}+\theta_{2,2}) - 4\dot{\theta}_{1,2}\dot{\theta}_{2,2} l_{2,2}\cos(\theta_{1,2}+\theta_{2,2}) \\ 2\dot{\theta}_{1,2}^2 l_{2,2}\sin(\theta_{1,2}+\theta_{2,2}) + 2\dot{\theta}_{2,2}^2 l_{2,2}\sin(\theta_{1,2}+\theta_{2,2}) + 2\dot{\theta}_{1,2}^2 l_{1,2}\sin(\theta_{1,2}) + H\dot{\theta}_3^2\cos(\theta_3) + B\dot{\theta}_3^2\sin(\theta_3) + 4\dot{\theta}_{1,2}\dot{\theta}_{2,2} l_{2,2}\sin(\theta_{1,2}+\theta_{2,2}) \end{bmatrix}, \\
\tilde{\mathbf{b}}_3 &= \begin{bmatrix} -2\dot{\theta}_{1,2}^2 l_{2,3}\cos(\theta_{1,3}+\theta_{2,3}) - 2\dot{\theta}_{2,3}^2 l_{2,3}\cos(\theta_{1,3}+\theta_{2,3}) - 2\dot{\theta}_{1,2}^2 l_{1,3}\cos(\theta_{1,3}) - B\dot{\theta}_3^2\cos(\theta_3) - H\dot{\theta}_3^2\sin(\theta_3) - 4\dot{\theta}_{1,3}\dot{\theta}_{2,3} l_{2,3}\cos(\theta_{1,3}+\theta_{2,3}) \\ B\dot{\theta}_3^2\sin(\theta_3) - 2\dot{\theta}_{2,3}^2 l_{2,3}\sin(\theta_{1,3}+\theta_{2,3}) - 2\dot{\theta}_{1,2}^2 l_{1,3}\sin(\theta_{1,3}) - H\dot{\theta}_3^2\cos(\theta_3) - 2\dot{\theta}_{1,2}^2 l_{2,3}\sin(\theta_{1,3}+\theta_{2,3}) - 4\dot{\theta}_{1,3}\dot{\theta}_{2,3} l_{2,3}\sin(\theta_{1,3}+\theta_{2,3}) \end{bmatrix}, \\
\tilde{\mathbf{b}}_4 &= \begin{bmatrix} 2\dot{\theta}_{1,4}^2 l_{2,4}\cos(\theta_{1,4}+\theta_{2,4}) + 2\dot{\theta}_{2,4}^2 l_{2,4}\cos(\theta_{1,4}+\theta_{2,4}) + 2\dot{\theta}_{1,4}^2 l_{1,4}\cos(\theta_{1,4}) + B\dot{\theta}_3^2\cos(\theta_3) - H\dot{\theta}_3^2\sin(\theta_3) + 4\dot{\theta}_{1,4}\dot{\theta}_{2,4} l_{2,4}\cos(\theta_{1,4}+\theta_{2,4}) \\ -2\dot{\theta}_{1,4}^2 l_{2,4}\sin(\theta_{1,4}+\theta_{2,4}) - 2\dot{\theta}_{2,4}^2 l_{2,4}\sin(\theta_{1,4}+\theta_{2,4}) - 2\dot{\theta}_{1,4}^2 l_{1,4}\sin(\theta_{1,4}) - H\dot{\theta}_3^2\cos(\theta_3) - B\dot{\theta}_3^2\sin(\theta_3) - 4\dot{\theta}_{1,4}\dot{\theta}_{2,4} l_{2,4}\sin(\theta_{1,4}+\theta_{2,4}) \end{bmatrix}.
\end{aligned} \tag{4.239}$$

The angle of the first link of each chain is actuated ($\theta_{1,i};\ i = 1, 2, 3, 4$). Thus, the identification matrices $\mathbf{Q}$ and $\mathbf{R}$ are given by:

$$\mathbf{Q} = \begin{bmatrix} 1 & 0 & 0 & 0 \\ 0 & 0 & 0 & 0 \\ 0 & 1 & 0 & 0 \\ 0 & 0 & 0 & 0 \\ 0 & 0 & 1 & 0 \\ 0 & 0 & 0 & 0 \\ 0 & 0 & 0 & 1 \\ 0 & 0 & 0 & 0 \\ 0 & 0 & 0 & 0 \\ 0 & 0 & 0 & 0 \\ 0 & 0 & 0 & 0 \end{bmatrix}; \quad \mathbf{R} = \begin{bmatrix} \tilde{\mathbf{R}}_1 & \tilde{\mathbf{R}}_2 & \tilde{\mathbf{R}}_3 & \tilde{\mathbf{R}}_4 \end{bmatrix} = \left[\begin{array}{cc|cc|cc|cc} 0 & 0 & 0 & 0 & 0 & 0 & 0 & 1 \\ 1 & 0 & 0 & 0 & 0 & 0 & 0 & 1 \\ 0 & 0 & 0 & 0 & 0 & 0 & 0 & 1 \\ 0 & 1 & 0 & 0 & 0 & 0 & 0 & 1 \\ 0 & 0 & 0 & 0 & 0 & 0 & 0 & 1 \\ 0 & 0 & 1 & 0 & 0 & 0 & 0 & 1 \\ 0 & 0 & 0 & 0 & 0 & 0 & 0 & 1 \\ 0 & 0 & 0 & 1 & 0 & 0 & 0 & 1 \\ 0 & 0 & 0 & 0 & 1 & 0 & 0 & 1 \\ 0 & 0 & 0 & 0 & 0 & 1 & 0 & 1 \\ 0 & 0 & 0 & 0 & 0 & 0 & 1 & 1 \end{array}\right]. \tag{4.240}$$

The terms of the last columns of $\mathbf{R}$ are set to one to handle actuation redundancy directly.

The controller of the 4×RR-mechanism is obtained using the decentralized controllers of Eq. (4.233) and the modeling constraints of Eqs. (4.234)–(4.240) as inputs into Algorithm 2.

The controller is tested on the trajectory tracking problem of the following circular trajectory (in meters):

$$\begin{aligned} x_{3,\mathrm{d}}(t) &= 0.55\cos(0.20\pi t), \\ y_{3,\mathrm{d}}(t) &= 0.55\sin(0.20\pi t), \\ \theta_{3,\mathrm{d}}(t) &= 0. \end{aligned} \tag{4.241}$$

The numerical simulations were performed with the same previous setup. Table 9 shows the parameters used in the simulation.

Table 9: 4×RR-mechanism parameters

Symbols ($i = 1, ..., 4$)	Values	Units (SI)
$m_{1,i}, m_{2,i}, m_3$	1, 1, 5	kg
$I_{1,i}, I_{2,i}, I_3$	1, 1, 5	kgm^2
$b_{1,i}, b_{2,i}, b_3$	1, 1, 1	Nms
$c_{1,i}, c_{2,i}, c_3$	1, 1, 1	Nm
$l_{1,i}, l_{2,i}, l_{\text{G}_1,i}, , l_{\text{G}_2,i}, l_3$	0.5, 0.5, 0.25, 0.25, 0.25	m
$\mathbf{\Lambda}_i, \mathbf{\Lambda}_5$	diag (1, 1), diag (1, 1, 1)	1/s
$\mathbf{L}_i, \mathbf{L}_5$	diag (5, 5), diag (5, 5, 5)	1/s
$\mathbf{K}_i, \mathbf{K}_5$	diag (2, 2), diag (2, 2, 2)	$\text{rad/s}^2, \text{m/s}^2$
$\epsilon_i = \epsilon_5$	0.1	–

The results are shown in Figs. 61 to 67. Figs. 61 and 62 show the end-effector tracking, while Fig. 63 show the associated angular displacements of the chains. The tracking achieved is good, and the motion obtained is smoother, especially on the reaching phase, which is due to soft control constraints formulation. The decentralized control torques and forces are shown in Figs. 64 and 65, while the control torques are shown in Fig. 66. We can notice the dry friction effects in Figs. 64 and 65, which is reflected on control torques of Fig. 65. Also, there is no control saturation since the soft control constraints relieve the feedback action during the early instant, as can be seen in Fig. 67, where the control constraints are around 2, at the beginning of the simulation, and about 0.1 at the end. The modeling constraints order is 10^{-4}.

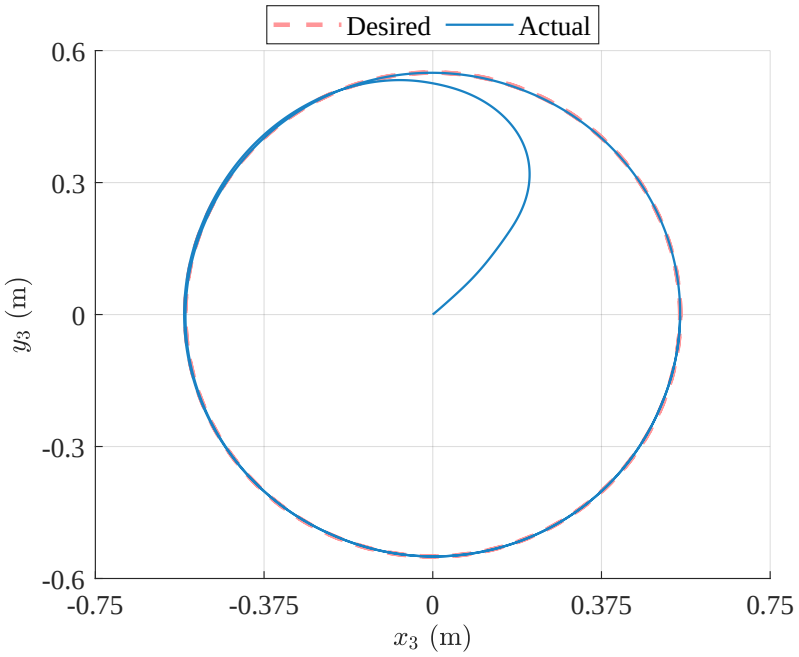

Figure 61: End-effector path tracking of the 4×RR-mechanism

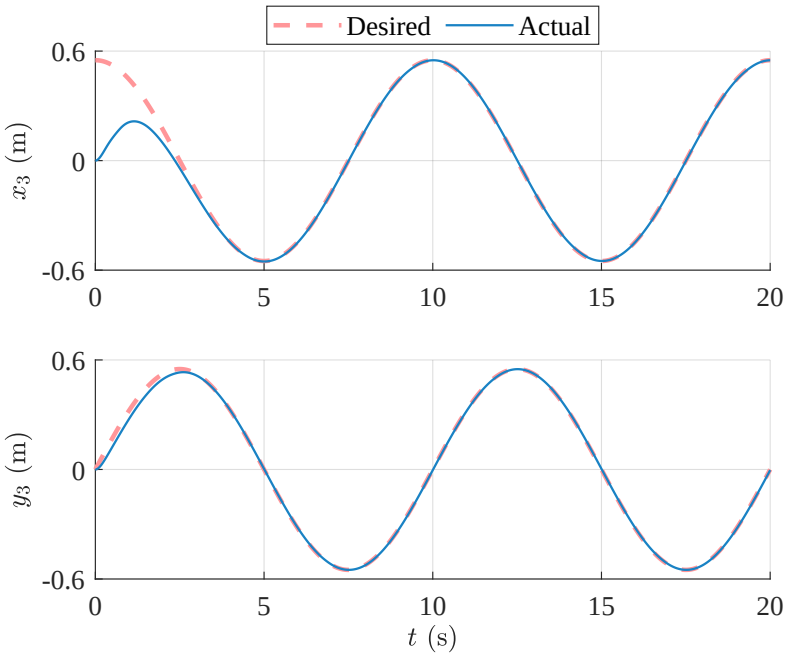

Figure 62: End-effector coordinates tracking of the 4×RR-mechanism

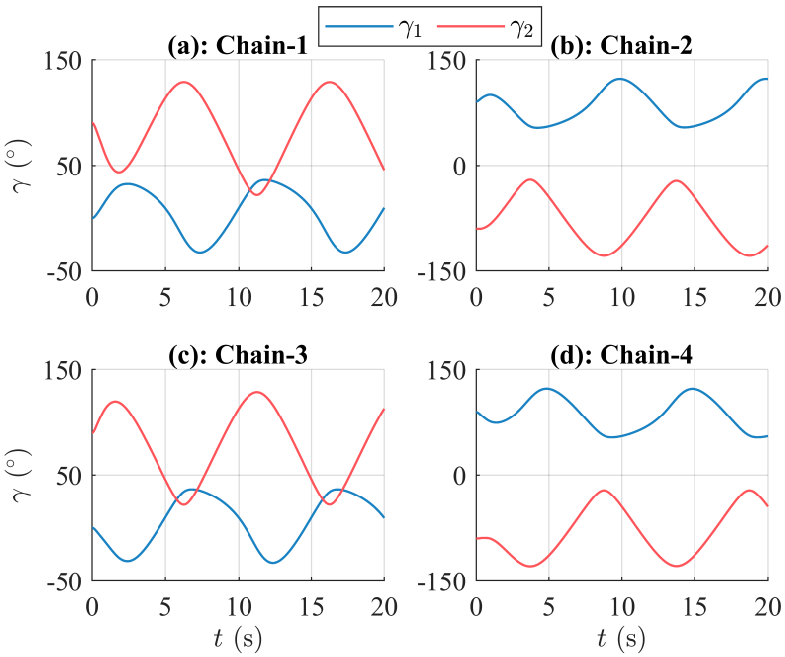

Figure 63: Displacements of the 4×RR-mechanism

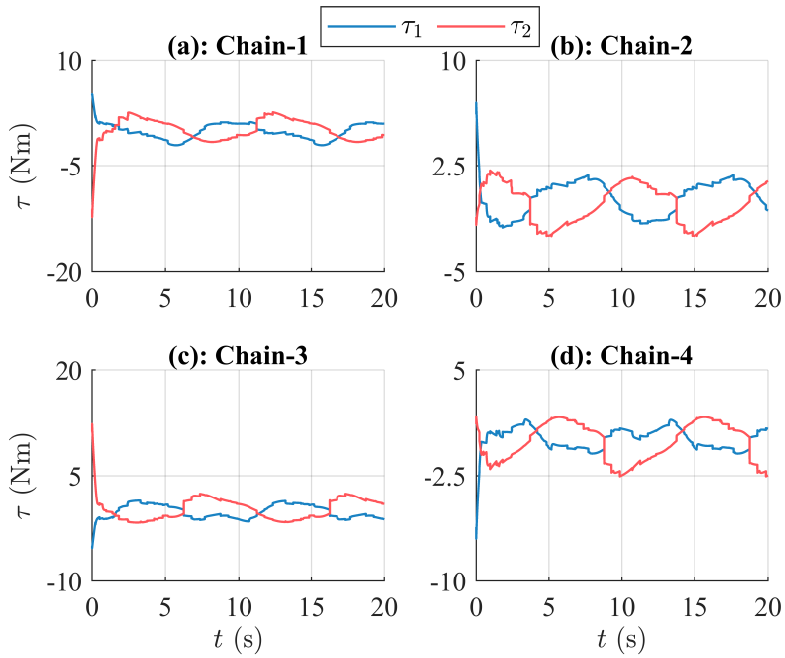

Figure 64: Decentralized control torques of the 4×RR-mechanism chains

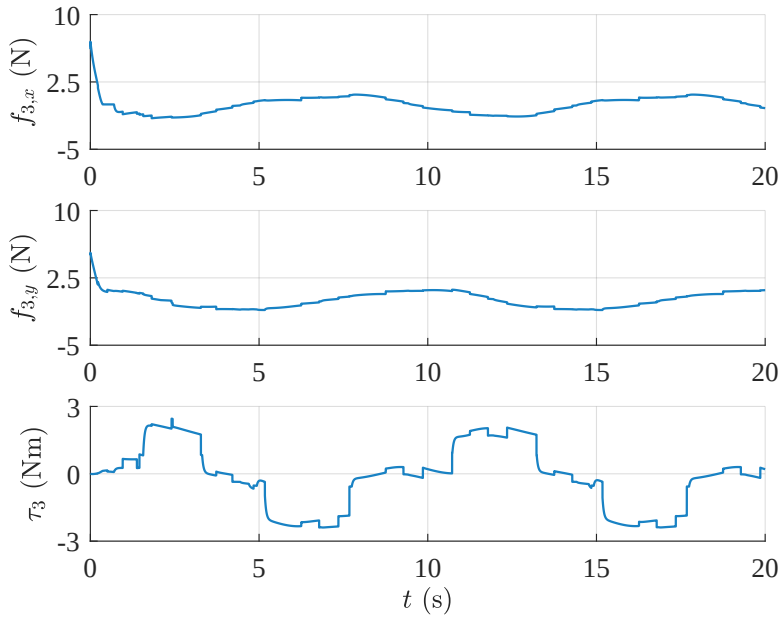

Figure 65: Decentralized control forces and torque of the 4×RR-mechanism load

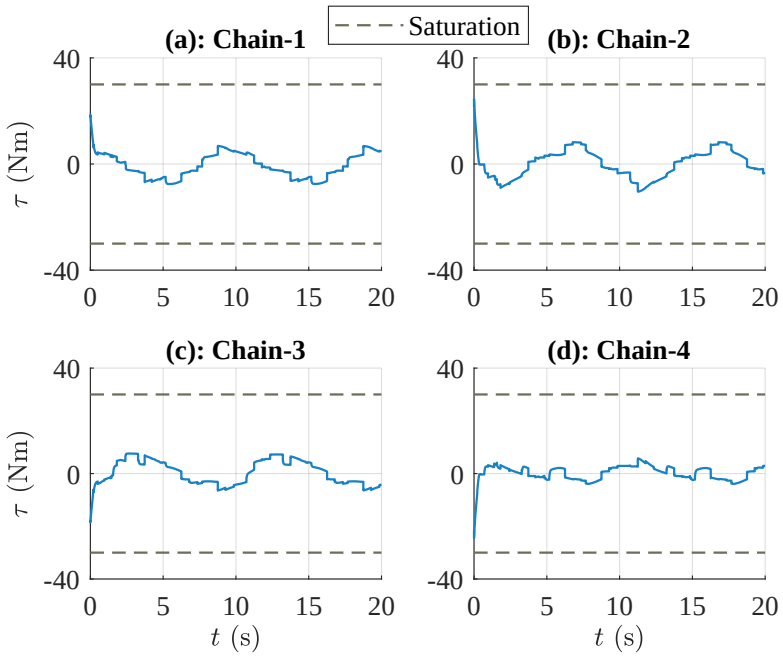

Figure 66: Control torques of the 4×RR-mechanism

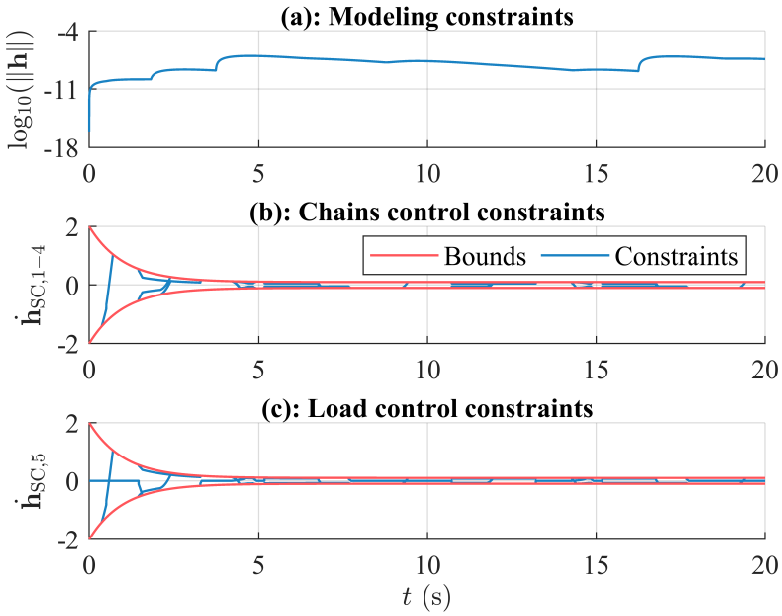

Figure 67: Constraints of the 4×RR-mechanism

4.3.6 2×PRR-manipulator

Figure 68 (a) show the 2×PRR-manipulator, which is another variation of the 5R-manipulator with kinematic redundancy once the system has more independent DoFs than those required to perform the planar motion. It comprises two open chains similar to the slider-crank mechanism but without prismatic constraints on the end-effector. This structure permits an increased workspace compared to the 5R-manipulator, which indicates its application for tasks involving long-range motion, such as machining or 3D printing.

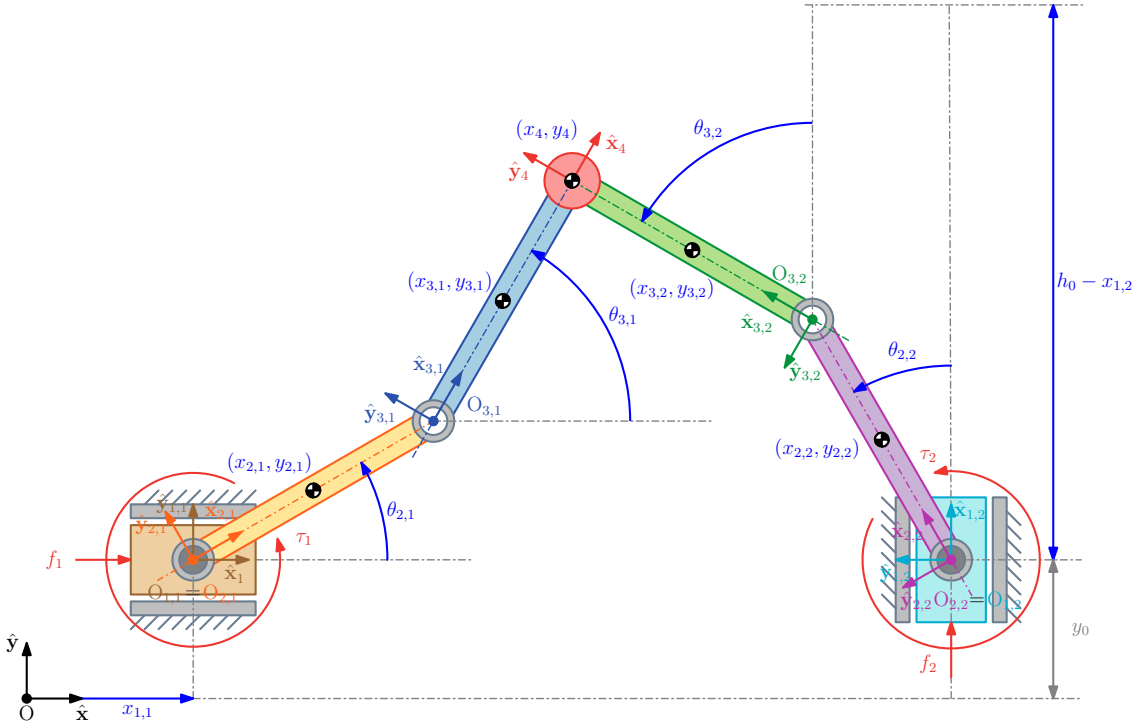

(a): 2×PRR-manipulator schematic diagram

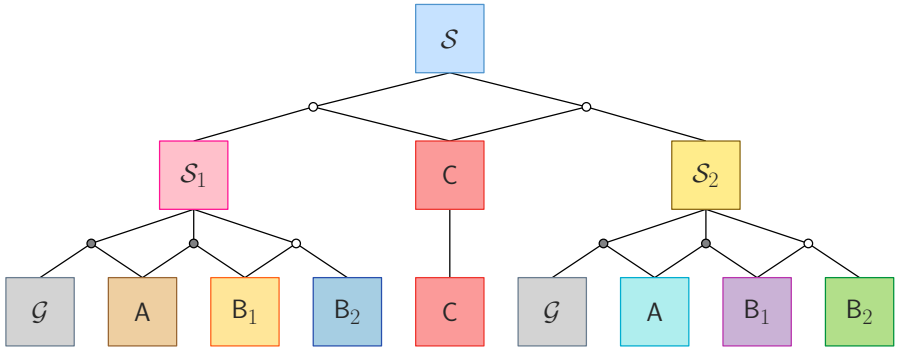

(b): Modeling/control hierarchy

Figure 68: 2×PRR-manipulator model

In the modeling hierarchy of Fig. 68 (b), $\mathcal{G}$ is the ground, body A is the sliding block, bodies B_i ($i = 1, 2$) are the manipulator links, and body C is the end-effector. The subsystems

S_i ($i = 1, 2$) are the chains and the system $\mathcal{S}$ represents the entire 2×PRR-manipulator. In the subsystems S_i ($i = 1, 2$), an active prismatic joint (grey circle) connects the sliding block with the ground, an active revolute joint (grey circle) connects the first link with the sliding block and a passive revolute joint (white circle) connects the second link with the first one. For the system $\mathcal{S}$, a passive revolute joint (white circle) connects chains and the end-effector. In this example, we perform the control synthesis from the sub-models of the PRR-manipulator. The independent generalized coordinates considered for the synthesis are given by $\mathbf{q}_{\#} = \left[\mathbf{q}_{\#,1}^{\mathsf{T}}, \mathbf{q}_{\#,2}^{\mathsf{T}}\right]^{\mathsf{T}}$, where $\mathbf{q}_{\#,i} = [x_{1,i}, \gamma_{1,i}, \gamma_{2,i}]^{\mathsf{T}}$ ($i = 1, 2$) as seen in Fig. 68 (a). The dependent generalized coordinates considered for the synthesis are given by $\mathbf{q}_{*} = \left[\mathbf{q}_{*,1}^{\mathsf{T}}, \mathbf{q}_{*,2}^{\mathsf{T}}\right]^{\mathsf{T}}$, where $\mathbf{q}_{*,i} = [y_{1,i}, \theta_{1,i}, \gamma_i, x_{2,i}, y_{2,i}, \theta_{2,i}, x_{3,i}, y_{3,i}, \theta_{3,i}]^{\mathsf{T}}$ ($i = 1, 2$) as seen in Fig. 68 (a). The generalized coordinates can be arranged as $\mathbf{q} = \mathbf{Q}\mathbf{q}_{\#} + \mathbf{R}\mathbf{q}_{*} = \left[\mathbf{q}_{j,i}^{\mathsf{T}}\right]$, with $\mathbf{q}_{j,i}^{\mathsf{T}} = \left[x_{j,i}, y_{j,i}, \theta_{j,i}, \gamma_{j,i}\right]^{\mathsf{T}}$ ($j = 1, 2, 3$). The trivial set of quasi-velocities and quasi-accelerations is used again, i.e., $\mathbf{v} = \dot{\mathbf{q}}$ and $\mathbf{a} = \dot{\mathbf{v}}$.

The terms of the relaxed dynamic model for the PRR-manipulator are given by:

$$\mathbf{M}_i = \begin{bmatrix} \mathbf{M}_{1,i} & \mathbf{0} & \mathbf{0} \\ \mathbf{0} & \mathbf{M}_{2,i} & \mathbf{0} \\ \mathbf{0} & \mathbf{0} & \mathbf{M}_{3,i} \end{bmatrix}; \quad \mathbf{f}_i = \begin{bmatrix} \mathbf{f}_{1,i} \\ \mathbf{f}_{2,i} \\ \mathbf{f}_{3,i} \end{bmatrix}, \quad (i = 1, 2) \tag{4.242}$$

where

$$\mathbf{M}_{j,i} = \begin{bmatrix} m_{j,i} & 0 & 0 & 0 \\ 0 & m_{j,i} & 0 & 0 \\ 0 & 0 & I_{j,i} & 0 \\ 0 & 0 & 0 & 0 \end{bmatrix}; \quad \mathbf{f}_i = \mathbf{f}_{\mathtt{A},i} + \mathbf{f}_{\mathtt{M},i}. \quad (i = 1, 2; j = 1, 2, 3) \tag{4.243}$$

The zero on the last diagonal term of $\mathbf{M}_{j,i}$ is due to the additional coordinated associated with the relative angular coordinate $\gamma_{j,i}$ ($i = 1, 2$; $j = 1, 2, 3$) of the rotational motor on the respective body.

The active forces due to natural psychical effects and motor forces are written as:

$$\mathbf{f}_{\mathtt{A},j,i} = \begin{bmatrix} 0 \\ -m_{j,i}g \\ 0 \\ 0 \end{bmatrix}; \quad \mathbf{f}_{\mathtt{M},1,i} = \begin{bmatrix} f_{1,i} \\ 0 \\ 0 \\ 0 \end{bmatrix}; \quad \mathbf{f}_{\mathtt{M},2,i} = \begin{bmatrix} 0 \\ 0 \\ 0 \\ \tau_{2,i} \end{bmatrix}; \quad \mathbf{f}_{\mathtt{M},3,i} = \begin{bmatrix} 0 \\ 0 \\ 0 \\ 0 \end{bmatrix}, \quad (i = 1, 2; j = 1, 2, 3) \tag{4.244}$$

where $f_{1,i}$ is the actuation force of the sliding block and $\tau_{2,i}$ is the motor torque on the second link of the i-th chain ($i = 1, 2$).

The modeling constraints of the i-th chain are given by:

$$\boldsymbol{\varphi}_i(\mathbf{q},t) = \begin{bmatrix} y_{1,i} \\ \theta_{1,i} - \gamma_i \\ \gamma_{1,i} - \phi_i \\ x_{2,i} - (x_{1,i} + l_i \cos(\theta_{2,i})) \\ y_{2,i} - (y_{1,i} + l_i \sin(\theta_{2,i})) \\ \gamma_{2,i} - \theta_{2,1} \\ x_{3,i} - (x_{2,i} + l_i \cos(\theta_{2,i}) + l_i \cos(\theta_{3,i})) \\ y_{3,i} - (y_{2,i} + l_i \sin(\theta_{2,i}) + l_i \sin(\theta_{3,i})) \\ \gamma_{3,i} - (\theta_{3,i} - \theta_{2,i}) \end{bmatrix} = \mathbf{0}. \quad (i = 1,2) \tag{4.245}$$

The Jacobian matrix and the associated column-vector of the constraints of Eq. (4.245), i.e., $\mathbf{A}_i$ and $\mathbf{b}_i$ ($i = 1,2$), respectively, follow:

$$\mathbf{A}_i = \begin{bmatrix} 0 & 1 & 0 & 0 & 0 & 0 & 0 & 0 & 0 & 0 & 0 & 0 \\ 0 & 0 & 1 & -1 & 0 & 0 & 0 & 0 & 0 & 0 & 0 & 0 \\ 0 & 0 & 0 & 1 & 0 & 0 & 0 & 0 & 0 & 0 & 0 & 0 \\ -1 & 0 & 0 & 0 & 1 & 0 & l_i \sin(\theta_{2,i}) & 0 & 0 & 0 & 0 & 0 \\ 0 & -1 & 0 & 0 & 0 & 1 & -l_i \cos(\theta_{2,i}) & 0 & 0 & 0 & 0 & 0 \\ 0 & 0 & 0 & 0 & 0 & 0 & -1 & 1 & 0 & 0 & 0 & 0 \\ 0 & 0 & 0 & 0 & -1 & 0 & l_i \sin(\theta_{2,i}) & 0 & 1 & 0 & l_i \sin(\theta_{3,i}) & 0 \\ 0 & 0 & 0 & 0 & 0 & -1 & -l_i \cos(\theta_{2,i}) & 0 & 0 & 1 & -l_i \cos(\theta_{3,i}) & 0 \\ 0 & 0 & 0 & 0 & 0 & 0 & 1 & 0 & 0 & 0 & -1 & 1 \end{bmatrix}, \tag{4.246}$$

$$\mathbf{b}_i = \begin{bmatrix} 0 \\ 0 \\ -l_i \cos(\theta_{2,i}) \dot{\theta}_{2,i}^2 \\ -l_i \sin(\theta_{2,i}) \dot{\theta}_{2,i}^2 \\ 0 \\ -l_i \left(\cos(\theta_{2,i}) \dot{\theta}_{2,i}^2 + \cos(\theta_{3,i}) \dot{\theta}_{3,i}^2 \right) \\ -l_i \left(\sin(\theta_{2,i}) \dot{\theta}_{2,i}^2 + \sin(\theta_{3,i}) \dot{\theta}_{3,i}^2 \right) \\ 0 \end{bmatrix}.$$

For $\mathbf{q}_{\#,i} = [x_{1,i}, \gamma_{2,i}, \gamma_{3,i}]^\mathsf{T}$ $(i = 1, 2)$, the identification matrices of the chains become:

$$\mathbf{Q}_i = \begin{bmatrix} 1 & 0 & 0 \\ 0 & 0 & 0 \\ 0 & 0 & 0 \\ 0 & 0 & 0 \\ 0 & 0 & 0 \\ 0 & 0 & 0 \\ 0 & 0 & 0 \\ 0 & 1 & 0 \\ 0 & 0 & 0 \\ 0 & 0 & 0 \\ 0 & 0 & 0 \\ 0 & 0 & 1 \end{bmatrix}; \quad \mathbf{R}_i = \begin{bmatrix} 0 & 0 & 0 & 0 & 0 & 0 & 0 & 0 & 0 \\ 1 & 0 & 0 & 0 & 0 & 0 & 0 & 0 & 0 \\ 0 & 1 & 0 & 0 & 0 & 0 & 0 & 0 & 0 \\ 0 & 0 & 1 & 0 & 0 & 0 & 0 & 0 & 0 \\ 0 & 0 & 0 & 1 & 0 & 0 & 0 & 0 & 0 \\ 0 & 0 & 0 & 0 & 1 & 0 & 0 & 0 & 0 \\ 0 & 0 & 0 & 0 & 0 & 1 & 0 & 0 & 0 \\ 0 & 0 & 0 & 0 & 0 & 0 & 0 & 0 & 0 \\ 0 & 0 & 0 & 0 & 0 & 0 & 1 & 0 & 0 \\ 0 & 0 & 0 & 0 & 0 & 0 & 0 & 1 & 0 \\ 0 & 0 & 0 & 0 & 0 & 0 & 0 & 0 & 1 \\ 0 & 0 & 0 & 0 & 0 & 0 & 0 & 0 & 0 \end{bmatrix}. \tag{4.247}$$

Using Eqs. (4.242)–(4.247) together with the relations $\dot{\mathbf{q}}_i = \mathbf{S}_i \dot{\mathbf{q}}_{\#,i}$ and $\ddot{\mathbf{q}}_i = \mathbf{S}_i \ddot{\mathbf{q}}_{\#,i} + \dot{\mathbf{S}}_i \dot{\mathbf{q}}_{\#,i}$ as inputs to the Algorithm 1, the modular model of the i-th chain in minimal coordinates is obtained as below:

$$\mathbf{N}_i = \mathbf{S}_i^\mathsf{T} \mathbf{M}_i \mathbf{S}_i + \mathbf{S}_i^\mathsf{T} \mathbf{A}_i^\mathsf{T} \mathbf{W}_i \mathbf{A}_i; \quad \mathbf{g}_i = \mathbf{S}_i^\mathsf{T} \left(\mathbf{f}_i - \mathbf{M}_i \dot{\mathbf{S}}_i \dot{\mathbf{q}}_{\#,i} + \mathbf{A}_i^\mathsf{T} \mathbf{b}_i + \mathbf{c}_i \right), \quad (i = 1, 2) \tag{4.248}$$

where $\mathbf{N}_i$ is the generalized inertia matrix and $\mathbf{g}_i$ is the column-vector of active forces of the i-th chain in minimal coordinates. Once $\mathbf{S}_i^\mathsf{T} \mathbf{A}_i^\mathsf{T} = \mathbf{A}_i \mathbf{S}_i = \mathbf{0}$, then, Eq. (4.248) becomes:

$$\mathbf{N}_i = \mathbf{S}_i^\mathsf{T} \mathbf{M}_i \mathbf{S}_i; \quad \mathbf{g}_i = \mathbf{S}_i^\mathsf{T} \left(\mathbf{f}_i - \mathbf{M}_i \dot{\mathbf{S}}_i \dot{\mathbf{q}}_{\#,i} \right). \quad (i = 1, 2) \tag{4.249}$$

The generalized inertia matrix of the i-th chain is written as:

$$\mathbf{N}_i = \begin{bmatrix} N_{11,i} & N_{12,i} & N_{13,i} \\ N_{21,i} & N_{22,i} & N_{23,i} \\ N_{31,i} & N_{32,i} & N_{33,i} \end{bmatrix}, \quad (i = 1, 2) \tag{4.250}$$

with

$$
\begin{aligned}
N_{11,i} &= m_{123,i}, \\
N_{12,i} &= -m_{3,i} 2 l_i s_{\gamma_{2,i}} - m_{2,i} l_i s_{\gamma_{2,i}} - m_{3,i} l_i s_{\gamma_{23,i}}, \\
N_{13,i} &= -m_{3,i} l_i s_{\gamma_{23,i}}, \\
N_{21,i} &= N_{12,i}, \\
N_{22,i} &= m_{3,i} 4 l_i^2 + 2 m_{3,i} c_{\gamma_{3,i}} 2 l_i^2 + m_{2,i} l_i^2 + m_{3,i} l_i^2 + I_{23,i}, \\
N_{23,i} &= m_{3,i} l_i^2 + m_{3,i} l_i c_{\gamma_{3,i}} l_i + I_{3,i}, \\
N_{31,i} &= N_{12,i}, \\
N_{32,i} &= N_{23,i}, \\
N_{33,i} &= m_{3,i} l_i^2 + I_{3,i}.
\end{aligned}
\tag{4.251}
$$

The column-vector of active forces of the i-th chain is written as:

$$
\mathbf{g}_i = \begin{bmatrix} g_{1,i} \\ g_{2,i} \\ g_{3,i} \end{bmatrix}, \quad (i = 1, 2)
\tag{4.252}
$$

where

$$
\begin{aligned}
g_{1,i} &= m_{3,i} l_i \dot{\gamma}_{2,i}^2 c_{\gamma_{23,i}} - m_{123,i} g s_{\phi_i} + m_{3,i} l_i \dot{\gamma}_{3,i}^2 c_{\gamma_{23,i}} + m_{3,i} l_i \dot{\gamma}_{2,i}^2 c_{\gamma_{2,i}} + \ldots \\
&\quad m_{2,i} l_i \dot{\gamma}_{2,i}^2 c_{\gamma_{2,i}} + 2 m_{3,i} l_i \dot{\gamma}_{2,i} \dot{\gamma}_{3,i} c_{\gamma_{23,i}}, \\
g_{2,i} &= m_{3,i} 2 l_i^2 \dot{\gamma}_{3,i} s_{\gamma_{3,i}} (2 \dot{\gamma}_{2,i} + \dot{\gamma}_{3,i}) - m_{3,i} g l_i c_{\phi_i + \gamma_{23,i}} - m_{3,i} g l_i c_{\phi_i + \gamma_{2,i}} - m_{2,i} g l_i c_{\phi_i + \gamma_{2,i}}, \\
g_{3,i} &= -m_{3,i} l_i^2 s_{\gamma_{3,i}} \dot{\gamma}_{2,i}^2 - m_{3,i} g l_i c_{\phi_i + \gamma_{23,i}}.
\end{aligned}
\tag{4.253}
$$

In Eqs. (4.251) and 4.253, we have:

$$
\begin{aligned}
s_{\gamma_{2,i}} &= \sin(\gamma_{2,i}); & c_{\gamma_{2,i}} &= \cos(\gamma_{2,i}), \\
s_{\gamma_{3,i}} &= \sin(\gamma_{3,i}); & c_{\gamma_{3,i}} &= \cos(\gamma_{3,i}), \\
s_{\gamma_{23,i}} &= \sin(\gamma_{2,i} + \gamma_{3,i}); & c_{\gamma_{23,i}} &= \cos(\gamma_{2,i} + \gamma_{3,i}), \\
s_{\phi_i} &= \sin(\phi_i); & c_{\phi_i} &= \cos(\phi_i), \\
s_{\phi_i + \gamma_{2,i}} &= \sin(\phi_i + \gamma_{2,i}); & c_{\phi_i + \gamma_{2,i}} &= \cos(\phi_i + \gamma_{2,i}), \\
s_{\phi_i + \gamma_{23,i}} &= \sin(\phi_i + \gamma_{2,i} + \gamma_{3,i}); & c_{\phi_i + \gamma_{23,i}} &= \cos(\phi_i + \gamma_{2,i} + \gamma_{3,i}),
\end{aligned}
\tag{4.254}
$$

where $\phi_1 = 0$ and $\phi_2 = \pi/2$ radians.

From Eqs. (4.250)–(4.253), the decoupled model of the 2×PRR-manipulator becomes:

$$\mathbf{N} = \begin{bmatrix} \mathbf{N}_1 & \mathbf{0} \\ \mathbf{0} & \mathbf{N}_2 \end{bmatrix}; \quad \mathbf{g} = \begin{bmatrix} \mathbf{g}_1 \\ \mathbf{g}_2 \end{bmatrix}. \tag{4.255}$$

The modeling constraints between the chains are given by the equality of the end-effectors position:

$$\boldsymbol{\varphi}(\mathbf{q}, t) = \vec{\mathbf{p}}^{\,\mathrm{I}}_{4,1}(\mathbf{q}, t) - \vec{\mathbf{p}}^{\,\mathrm{I}}_{4,2}(\mathbf{q}, t) = \mathbf{0}, \tag{4.256}$$

where

$$\begin{aligned} \vec{\mathbf{p}}^{\,\mathrm{I}}_{4,1} &= \begin{bmatrix} x_{4,1} \\ y_{4,1} \end{bmatrix} = \begin{bmatrix} r_{1,1}\cos(\phi_1) + 2l_1\cos(\phi_1 + \gamma_{2,1}) + 2l_1\cos(\phi_1 + \gamma_{23,1}) \\ r_{1,1}\sin(\phi_1) + 2l_1\sin(\phi_1 + \gamma_{2,1}) + 2l_1\sin(\phi_1 + \gamma_{23,1}) \end{bmatrix}, \\ \vec{\mathbf{p}}^{\,\mathrm{I}}_{4,2} &= \begin{bmatrix} x_{4,2} \\ y_{4,2} \end{bmatrix} = \begin{bmatrix} x_0 + r_{1,2}\cos(\phi_2) + 2l_2\cos(\phi_2 + \gamma_{2,2}) + 2l_2\cos(\phi_2 + \gamma_{23,2}) \\ y_0 + r_{1,2}\sin(\phi_2) + 2l_2\sin(\phi_2 + \gamma_{2,2}) + 2l_2\sin(\phi_2 + \gamma_{23,2}) \end{bmatrix}, \end{aligned} \tag{4.257}$$

with x_0 and y_0 are the initial coordinates of the sliding block of the second chain.

The second time-derivative of Eq. (4.256) results in:

$$\ddot{\boldsymbol{\varphi}}(\mathbf{a}, \mathbf{v}, \mathbf{q}, t) \Leftrightarrow \mathbf{A}(\mathbf{q}, t)\,\mathbf{a} - \mathbf{b}(\mathbf{v}, \mathbf{q}, t) = \mathbf{0}, \tag{4.258}$$

where

$$\mathbf{A} = 2\begin{bmatrix} \mathbf{A}_{1:2,1} & -\mathbf{A}_{1:2,2} \end{bmatrix}; \quad \mathbf{b} = 2\begin{bmatrix} b_1 \\ b_2 \end{bmatrix}, \tag{4.259}$$

with

$$\begin{aligned} \mathbf{A}_{1:2,1} &= \begin{bmatrix} 0.5\cos(\phi_1) & -l_1(\sin(\phi_1 + \gamma_{2,1}) + \sin(\phi_1 + \gamma_{23,1})) & -l_1\sin(\phi_1 + \gamma_{23,1}) \\ 0.5\sin(\phi_1) & l_1(\cos(\phi_1 + \gamma_{2,1}) + \cos(\phi_1 + \gamma_{23,1})) & l_1\cos(\phi_1 + \gamma_{23,1}) \end{bmatrix}, \\ \mathbf{A}_{1:2,2} &= \begin{bmatrix} 0.5\cos(\phi_2) & -l_2(\sin(\phi_2 + \gamma_{2,2}) + \sin(\phi_2 + \gamma_{23,2})) & -l_2\sin(\phi_2 + \gamma_{23,2}) \\ 0.5\sin(\phi_2) & l_2(\cos(\phi_2 + \gamma_{2,2}) + \cos(\phi_2 + \gamma_{23,2})) & l_2\cos(\phi_2 + \gamma_{23,2}) \end{bmatrix}, \end{aligned} \tag{4.260}$$

and

$$\begin{aligned} b_1 = {} & l_1\dot{\gamma}_{2,1}^2\cos(\phi_1 + \gamma_{2,1}) - l_2\dot{\gamma}_{2,2}^2\cos(\phi_2 + \gamma_{2,2}) + l_1\dot{\gamma}_{2,1}^2\cos(\phi_1 + \gamma_{23,1}) + \ldots \\ & l_1\dot{\gamma}_{3,1}^2\cos(\phi_1 + \gamma_{23,1}) - l_2\dot{\gamma}_{2,2}^2\cos(\phi_2 + \gamma_{23,2}) - l_2\dot{\gamma}_{3,2}^2\cos(\phi_2 + \gamma_{23,2}) + \ldots \\ & 2l_1\dot{\gamma}_{2,1}\dot{\gamma}_{3,1}\cos(\phi_1 + \gamma_{23,1}) - 2l_2\dot{\gamma}_{2,2}\dot{\gamma}_{3,2}\cos(\phi_2 + \gamma_{23,2}), \\ b_2 = {} & l_1\dot{\gamma}_{2,1}^2\sin(\phi_1 + \gamma_{2,1}) - l_2\dot{\gamma}_{2,2}^2\sin(\phi_2 + \gamma_{2,2}) + l_1\dot{\gamma}_{2,1}^2\sin(\phi_1 + \gamma_{23,1}) + \ldots \\ & l_1\dot{\gamma}_{3,1}^2\sin(\phi_1 + \gamma_{23,1}) - l_2\dot{\gamma}_{2,2}^2\sin(\phi_2 + \gamma_{23,2}) - l_2\dot{\gamma}_{3,2}^2\sin(\phi_2 + \gamma_{23,2}) + \ldots \\ & 2l_1\dot{\gamma}_{2,1}\dot{\gamma}_{3,1}\sin(\phi_1 + \gamma_{23,1}) - 2l_2\dot{\gamma}_{2,2}\dot{\gamma}_{3,2}\sin(\phi_2 + \gamma_{23,2}). \end{aligned} \tag{4.261}$$

With the actuated coordinates be given by $\mathbf{q}_{\#} = \left[\mathbf{q}_{\#,1}^{\mathsf{T}}, \mathbf{q}_{\#,2}^{\mathsf{T}}\right]^{\mathsf{T}}$, where $\mathbf{q}_{\#,i} = [x_{1,i}, \gamma_{2,i}]^{\mathsf{T}}$ $(i = 1, 2)$, the identification matrices become:

$$\mathbf{Q} = \begin{bmatrix}
1 & 0 & 0 & 0 \\ 0 & 0 & 0 & 0 \\ 0 & 0 & 0 & 0 \\ 0 & 0 & 0 & 0 \\ 0 & 0 & 0 & 0 \\ 0 & 0 & 0 & 0 \\ 0 & 0 & 0 & 0 \\ 0 & 1 & 0 & 0 \\ 0 & 0 & 0 & 0 \\ 0 & 0 & 0 & 0 \\ 0 & 0 & 0 & 0 \\ 0 & 0 & 0 & 0 \\ 0 & 0 & 1 & 0 \\ 0 & 0 & 0 & 0 \\ 0 & 0 & 0 & 0 \\ 0 & 0 & 0 & 0 \\ 0 & 0 & 0 & 0 \\ 0 & 0 & 0 & 0 \\ 0 & 0 & 0 & 1 \\ 0 & 0 & 0 & 0 \\ 0 & 0 & 0 & 0 \\ 0 & 0 & 0 & 0
\end{bmatrix}; \quad \mathbf{R} = \begin{bmatrix}
0 & 0 & 0 & 0 & 0 & 0 & 0 & 0 & 0 & 0 & 0 & 0 & 0 & 0 & 0 & 0 & 0 & 0 & 0 & 0 \\
1 & 0 & 0 & 0 & 0 & 0 & 0 & 0 & 0 & 0 & 0 & 0 & 0 & 0 & 0 & 0 & 0 & 0 & 0 & 0 \\
0 & 1 & 0 & 0 & 0 & 0 & 0 & 0 & 0 & 0 & 0 & 0 & 0 & 0 & 0 & 0 & 0 & 0 & 0 & 0 \\
0 & 0 & 1 & 0 & 0 & 0 & 0 & 0 & 0 & 0 & 0 & 0 & 0 & 0 & 0 & 0 & 0 & 0 & 0 & 0 \\
0 & 0 & 0 & 1 & 0 & 0 & 0 & 0 & 0 & 0 & 0 & 0 & 0 & 0 & 0 & 0 & 0 & 0 & 0 & 0 \\
0 & 0 & 0 & 0 & 1 & 0 & 0 & 0 & 0 & 0 & 0 & 0 & 0 & 0 & 0 & 0 & 0 & 0 & 0 & 0 \\
0 & 0 & 0 & 0 & 0 & 1 & 0 & 0 & 0 & 0 & 0 & 0 & 0 & 0 & 0 & 0 & 0 & 0 & 0 & 0 \\
0 & 0 & 0 & 0 & 0 & 0 & 0 & 0 & 0 & 0 & 0 & 0 & 0 & 0 & 0 & 0 & 0 & 0 & 0 & 0 \\
0 & 0 & 0 & 0 & 0 & 0 & 1 & 0 & 0 & 0 & 0 & 0 & 0 & 0 & 0 & 0 & 0 & 0 & 0 & 0 \\
0 & 0 & 0 & 0 & 0 & 0 & 0 & 1 & 0 & 0 & 0 & 0 & 0 & 0 & 0 & 0 & 0 & 0 & 0 & 0 \\
0 & 0 & 0 & 0 & 0 & 0 & 0 & 0 & 1 & 0 & 0 & 0 & 0 & 0 & 0 & 0 & 0 & 0 & 0 & 0 \\
0 & 0 & 0 & 0 & 0 & 0 & 0 & 0 & 0 & 1 & 0 & 0 & 0 & 0 & 0 & 0 & 0 & 0 & 0 & 0 \\
0 & 0 & 0 & 0 & 0 & 0 & 0 & 0 & 0 & 0 & 0 & 0 & 0 & 0 & 0 & 0 & 0 & 0 & 0 & 0 \\
0 & 0 & 0 & 0 & 0 & 0 & 0 & 0 & 0 & 0 & 1 & 0 & 0 & 0 & 0 & 0 & 0 & 0 & 0 & 0 \\
0 & 0 & 0 & 0 & 0 & 0 & 0 & 0 & 0 & 0 & 0 & 1 & 0 & 0 & 0 & 0 & 0 & 0 & 0 & 0 \\
0 & 0 & 0 & 0 & 0 & 0 & 0 & 0 & 0 & 0 & 0 & 0 & 1 & 0 & 0 & 0 & 0 & 0 & 0 & 0 \\
0 & 0 & 0 & 0 & 0 & 0 & 0 & 0 & 0 & 0 & 0 & 0 & 0 & 1 & 0 & 0 & 0 & 0 & 0 & 0 \\
0 & 0 & 0 & 0 & 0 & 0 & 0 & 0 & 0 & 0 & 0 & 0 & 0 & 0 & 1 & 0 & 0 & 0 & 0 & 0 \\
0 & 0 & 0 & 0 & 0 & 0 & 0 & 0 & 0 & 0 & 0 & 0 & 0 & 0 & 0 & 1 & 0 & 0 & 0 & 0 \\
0 & 0 & 0 & 0 & 0 & 0 & 0 & 0 & 0 & 0 & 0 & 0 & 0 & 0 & 0 & 0 & 1 & 0 & 0 & 0 \\
0 & 0 & 0 & 0 & 0 & 0 & 0 & 0 & 0 & 0 & 0 & 0 & 0 & 0 & 0 & 0 & 0 & 0 & 0 & 0 \\
0 & 0 & 0 & 0 & 0 & 0 & 0 & 0 & 0 & 0 & 0 & 0 & 0 & 0 & 0 & 0 & 0 & 1 & 0 & 0 \\
0 & 0 & 0 & 0 & 0 & 0 & 0 & 0 & 0 & 0 & 0 & 0 & 0 & 0 & 0 & 0 & 0 & 0 & 1 & 0 \\
0 & 0 & 0 & 0 & 0 & 0 & 0 & 0 & 0 & 0 & 0 & 0 & 0 & 0 & 0 & 0 & 0 & 0 & 0 & 1
\end{bmatrix}. \tag{4.262}$$

Also, let the sliding surface for the states of the 2×PRR-manipulator be given by:

$$\mathbf{s}(\mathbf{v}, \mathbf{q}, t) = \dot{\tilde{\mathbf{q}}} + \mathbf{\Lambda}\tilde{\mathbf{q}} = \mathbf{0}, \tag{4.263}$$

where $\tilde{\mathbf{q}} = \mathbf{q} - \mathbf{q}_{\mathrm{d}}$ is the column-vector of tracking error and $\mathbf{\Lambda} = \mathbf{\Lambda}^{\mathsf{T}} \geq \mathbf{0}$ is a control gain matrix associated to the closed-loop bandwidth. The reference states $(\mathbf{q}_{\mathrm{d}}, \dot{\mathbf{q}}_{\mathrm{d}}, \ddot{\mathbf{q}}_{\mathrm{d}})$ of the 2×PRR-manipulator are generated through the redundancy resolution approach on the acceleration level presented by Tang et al. (2017). This approach establishes a relation between the end-effector coordinates and the joints displacements by the direct kinematics. Performing the second-time derivative of this relation is possible to solve for the joints accelerations in terms of the end-effector variables. The joints accelerations are then numerically integrated with compatible initial conditions to obtain the associated velocities and displacements.

Based on Eq. (4.263), the following servo-constraints are defined:

$$\boldsymbol{\varphi}_{\mathrm{SC}}(\mathbf{v}, \mathbf{q}, t) = \mathbf{s}(\mathbf{v}, \mathbf{q}, t) = \mathbf{0}. \tag{4.264}$$

Performing the time-derivative of Eq. (4.264) and imposing the sliding condition, we get:

$$\dot{\boldsymbol{\varphi}}_{\mathrm{SC}} = -\mathbf{L}\mathbf{s} - \mathbf{K}\,\mathrm{sign}(\mathbf{s}), \tag{4.265}$$

where $\mathbf{L} = \mathbf{L}^{\mathsf{T}} \geq \mathbf{0}$ and $\mathbf{K} = \mathbf{K}^{\mathsf{T}} \geq \mathbf{0}$ are control gains matrices.

Moreover, Eq. (4.265) can be rewritten as:

$$\mathbf{A}_{\mathrm{SC}}\mathbf{a}_{\mathrm{SC}} = \mathbf{b}_{\mathrm{SC}}(\mathbf{v}, \mathbf{q}, t), \tag{4.266}$$

where

$$\mathbf{A}_{\mathrm{SC}} = \begin{bmatrix} 1 & 0 & 0 & 0 & 0 & 0 \\ 0 & 1 & 0 & 0 & 0 & 0 \\ 0 & 0 & 1 & 0 & 0 & 0 \\ 0 & 0 & 0 & 1 & 0 & 0 \\ 0 & 0 & 0 & 0 & 1 & 0 \\ 0 & 0 & 0 & 0 & 0 & 1 \end{bmatrix}; \quad \mathbf{b}_{\mathrm{SC}} = \ddot{\mathbf{q}}_{\mathrm{d}} - \boldsymbol{\Lambda}\dot{\tilde{\mathbf{q}}} - \mathbf{L}\mathbf{s} - \mathbf{K}\,\mathrm{sign}(\mathbf{s}). \tag{4.267}$$

Taking $\mathbf{y}_{\mathrm{r}} = \mathbf{b}_{\mathrm{SC}}$ and Eqs. (4.255)–(4.267) as inputs to the Algorithm 3, the MPC formulation can be used to obtain the controller of the 2×PRR-manipulator.

The controller is tested on the trajectory tracking problem of a linear trajectory with vertices coordinates given by (in meters):

$$\vec{\mathbf{p}}_1 = \begin{bmatrix} 0.40 \\ 1.60 \end{bmatrix}; \quad \vec{\mathbf{p}}_2 = \begin{bmatrix} 1.60 \\ 0.40 \end{bmatrix}. \tag{4.268}$$

The linear trajectory is parameterized as a polynomial trajectory of 5-th degree to impose zero velocity, acceleration and jerk at the beginning and end of the motion, as follows:

$$r_{\mathrm{d}}(t) = r(t_{\mathrm{i}}) + (r(t_{\mathrm{f}}) - r(t_{\mathrm{i}}))\left(6\delta t^5 - 15\delta t^4 + 10\delta t^3\right). \tag{4.269}$$

The numerical simulations were performed with the same previous setup. Table 10 show the parameters used in the simulation.

Table 10: 2×PRR-manipulator parameters

Symbols ($i = 1, 2$)	Values	Units (SI)
$m_{1,i}, m_{2,i}, m_{3,i}$	1, 1, 1	kg
$I_{1,i}, I_{2,i}, I_{3,i}$	0.25, 0.25, 0.25	kgm^2
$l_{2,i}, l_{3,i}, l_{\mathrm{G}_2,i}, l_{\mathrm{G}_3,i}$	0.25, 0.25, 0.25, 0.25	m
$\mathbf{\Lambda}_i$	diag (1, 1, 1)	1/s
$\mathbf{L}_i$	diag (100, 100, 100)	1/s
$\mathbf{K}_i$	diag (100, 100, 100)	$\mathrm{m/s}^2, \mathrm{rad/s}^2$
ϵ	0.1	–
$\mathbf{Q_Y}, \mathbf{P_Y}$	diag (10, 10, 10, 10, 10, 10)	–
$\mathbf{R}_{\mathrm{U}_\#}$	diag (0.10, 0.10, 0.10, 0.10)	–
$\mathbf{\Omega_a}$	diag (900, 900, 900, 900, 900, 900)	rad/s
p, c	20, 10	–
T_s	0.1	s

The results are shown in Figs. 69 to 73. Figs. 69 and 70 show the end-effector tracking, while Fig. 71 show the associated displacements of the chains. The tracking achieved is good, and the motion obtained is smooth. The control torques are shown in Fig. 72, where we can notice a discontinuity at the beginning of the simulation, which is induced by the reference states generated through the redundancy resolution approach of Tang et al. (2017). Also, a saturation at $t = 0.6$ s is intentionally induced during the simulation to verify control stability. As can be seen in Fig. 73, the saturation results in a peak in the cost function, which monotonically decreases the after that, ensuring the control stability. The modeling constraints order is 10^{-14}.

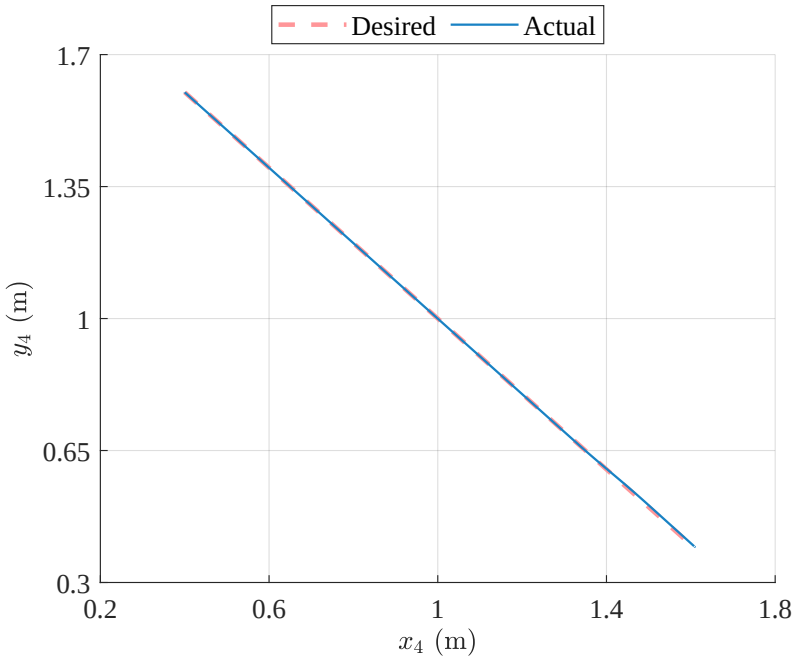

Figure 69: End-effector path tracking of the 2×PRR-manipulator

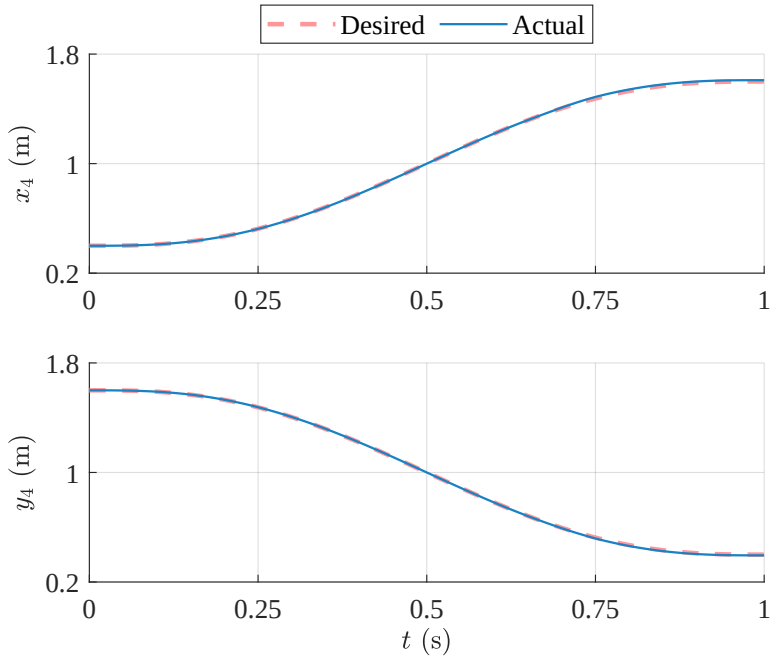

Figure 70: End-effector coordinates tracking of the 2×PRR-manipulator

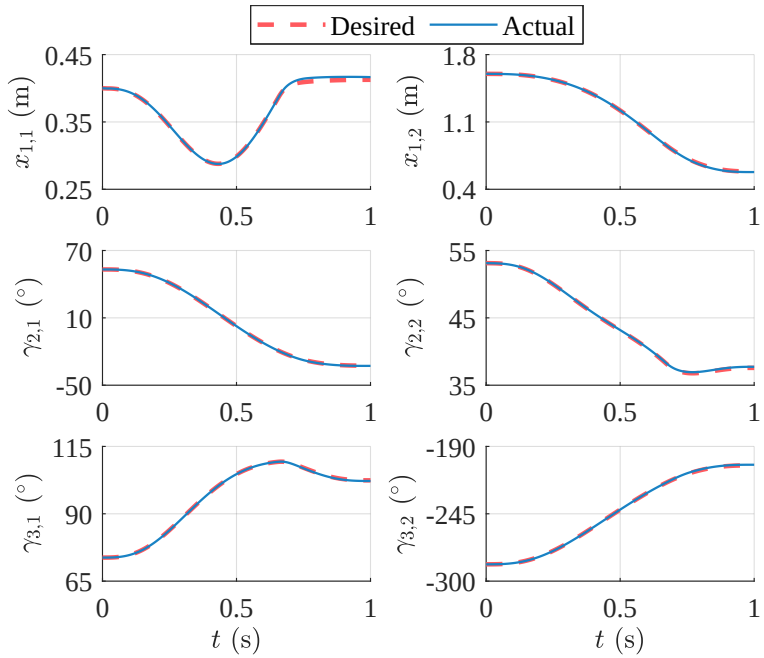

Figure 71: Displacements tracking of the 2×PRR-manipulator

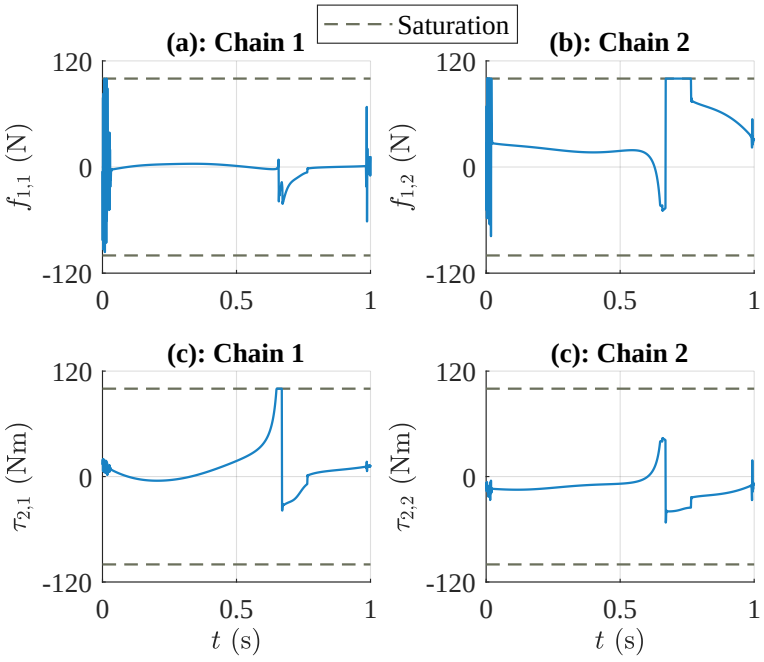

Figure 72: Control torques of the 2×PRR-manipulator

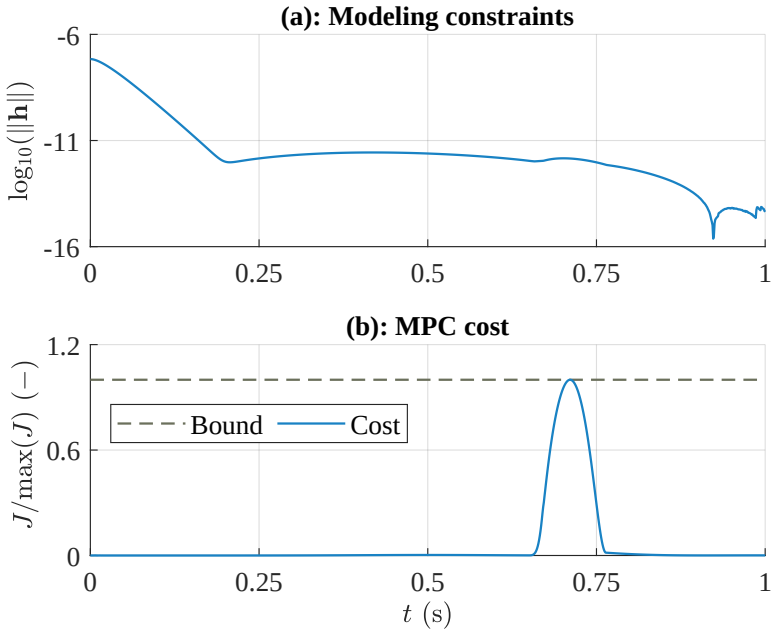

Figure 73: Cost function of the 2×PRR-manipulator

4.3.7 2-DoFs helicopter

Figure 74 show the Quanser AERO model, a 2-DoFs helicopter plant used as a standard platform for general control tests. It comprises two bodies connected by revolute joints. The pitch and yaw angles are actuated by the thrusters attached to the upper body.

Figure 74: Quanser AERO

The schematic diagram and modeling hierarchy adopted of this example are shown in Fig. 75.

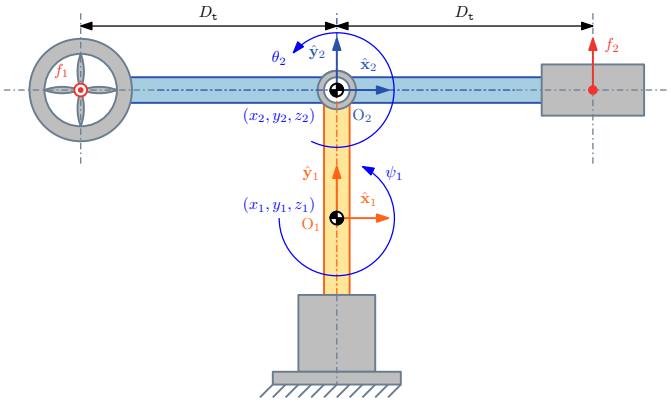

(a): 2-DoFs helicopter schematic diagram

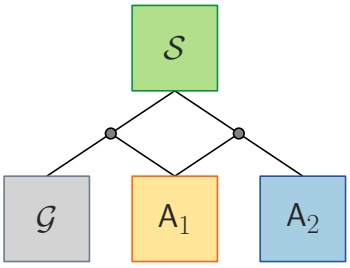

(b): Modeling/control hierarchy

Figure 75: 2-DoFs helicopter model

In this example the modeling is performed in the 3D space, thus, the generalized coordinates and quasi-velocities are given by $\mathbf{q} = \left[\mathbf{q}_1^\mathsf{T}, \mathbf{q}_2^\mathsf{T}\right]^\mathsf{T}$ and $\mathbf{v} = \left[\mathbf{v}_1^\mathsf{T}, \mathbf{v}_2^\mathsf{T}\right]^\mathsf{T}$, with $\mathbf{q}_i = [x_i, y_i, z_i, \phi_i, \theta_i, \psi_i]^\mathsf{T}$ and $\mathbf{v}_i = [u_i, v_i, w_i, p_i, q_i, r_i]^\mathsf{T}$ being the column-vectors of generalized coordinates and quasi-velocities, respectively, both associated to the i-th body ($i = 1, 2$), as shown in Fig. 75 (a). In the modeling hierarchy of Fig. 75 (b), $\mathcal{G}$ is the ground, body A_1 is the base and body A_2 is the helicopter, while system $\mathcal{S}$ is the 2-DoFs helicopter. Also, active revolute joints (grey circles) connect the base with the ground and the helicopter with the base. The relationship between generalized velocities and quasi-velocities and its time derivative are given, respectively, by $\dot{\mathbf{q}} = \mathbf{J}\mathbf{v}$ and $\ddot{\mathbf{q}} = \mathbf{J}\dot{\mathbf{v}} + \dot{\mathbf{J}}\mathbf{v}$, where $\mathbf{J}$ is the transformation matrix between body-fixed and Earth-fixed coordinate systems.

The relaxed dynamic model is given by:

$$\dot{\mathbf{q}} = \mathbf{J}\mathbf{v}; \quad \mathbf{N}\mathbf{a}_0 = \mathbf{g}, \tag{4.270}$$

where

$$\mathbf{J} = \begin{bmatrix} \mathbf{J}_1 & \mathbf{0} \\ \mathbf{0} & \mathbf{J}_2 \end{bmatrix}; \quad \mathbf{N} = \mathbf{M}; \quad \mathbf{M} = \begin{bmatrix} \mathbf{M}_1 & \mathbf{0} \\ \mathbf{0} & \mathbf{M}_2 \end{bmatrix}; \quad \mathbf{g} = \mathbf{f}; \quad \mathbf{f} = \begin{bmatrix} \mathbf{f}_1 \\ \mathbf{f}_2 \end{bmatrix}. \tag{4.271}$$

The transformation matrix related to the i-th body in terms of Euler angles is given by:

$$\mathbf{J}_i = \begin{bmatrix} \cos(\psi_i)\cos(\theta_i) & \cos(\psi_i)\sin(\phi_i)\sin(\theta_i) - \cos(\phi_i)\sin(\psi_i) & \sin(\phi_i)\sin(\psi_i) + \cos(\phi_i)\cos(\psi_i)\sin(\theta_i) & 0 & 0 & 0 \\ \cos(\theta_i)\sin(\psi_i) & \cos(\phi_i)\cos(\psi_i) + \sin(\phi_i)\sin(\psi_i)\sin(\theta_i) & \cos(\phi_i)\sin(\psi_i)\sin(\theta_i) - \cos(\psi_i)\sin(\phi_i) & 0 & 0 & 0 \\ -\sin(\theta_i) & \cos(\theta_i)\sin(\phi_i) & \cos(\phi_i)\cos(\theta_i) & 0 & 0 & 0 \\ 0 & 0 & 0 & i & \frac{\sin(\phi_i)\sin(\theta_i)}{\cos(\theta_i)} & \frac{\cos(\phi_i)\sin(\theta_i)}{\cos(\theta_i)} \\ 0 & 0 & 0 & 0 & \cos(\phi_i) & -\sin(\phi_i) \\ 0 & 0 & 0 & 0 & \frac{\sin(\phi_i)}{\cos(\theta_i)} & \frac{\cos(\phi_i)}{\cos(\theta_i)} \end{bmatrix}. \quad (i = 1, 2) \tag{4.272}$$

The inertia matrix and active forces column-vectors related to the i-th body are written as:

$$\mathbf{M}_i = \begin{bmatrix} m_i & 0 & 0 & 0 & m_i z_{\mathrm{G},i} & -m_i y_{\mathrm{G},i} \\ 0 & m_i & 0 & -m_i z_{\mathrm{G},i} & 0 & m_i x_{\mathrm{G},i} \\ 0 & 0 & m_i & m_i y_{\mathrm{G},i} & -m_i x_{\mathrm{G},i} & 0 \\ 0 & -m_i z_{\mathrm{G},i} & m_i y_{\mathrm{G},i} & I_{\mathrm{xx},i} & -\frac{I_{\mathrm{xy},i}}{2} - \frac{I_{\mathrm{yx},i}}{2} & -\frac{I_{\mathrm{xz},i}}{2} - \frac{I_{\mathrm{zx},i}}{2} \\ m_i z_{\mathrm{G},i} & 0 & -m_i x_{\mathrm{G},i} & -\frac{I_{\mathrm{xy},i}}{2} - \frac{I_{\mathrm{yx},i}}{2} & I_{\mathrm{yy},i} & -\frac{I_{\mathrm{yz},i}}{2} - \frac{I_{\mathrm{zy},i}}{2} \\ -m_i y_{\mathrm{G},i} & m_i x_{\mathrm{G},i} & 0 & -\frac{I_{\mathrm{xz},i}}{2} - \frac{I_{\mathrm{zx},i}}{2} & -\frac{I_{\mathrm{yz},i}}{2} - \frac{I_{\mathrm{zy},i}}{2} & I_{\mathrm{zz},i} \end{bmatrix}, \tag{4.273}$$

$$\mathbf{f}_i = \mathbf{f}_{\mathtt{A},i} + \mathbf{f}_{\mathtt{M},i}, \quad (i = 1, 2)$$

where m_i is the mass and I_i is the inertia moment, while $\mathbf{f}_{\mathtt{A},i}$ and $\mathbf{f}_{\mathtt{M},i}$ are the column-vectors of active forces due to the natural physical effects (e.g., weight, friction, etc.) and due to the motor

forces, respectively. In this example, the active forces column-vectors are expressed by:

$$\mathbf{f}_{\mathtt{A},i} = -\mathbf{V}_i\left(\mathbf{q}_i, \mathbf{v}_i\right) - \mathbf{D}_i\mathbf{v}_i - \mathbf{G}_i\left(\mathbf{q}_i\right); \quad \mathbf{f}_{\mathtt{M},1} = \begin{bmatrix} 0 \\ 0 \\ 0 \\ 0 \\ 0 \\ 0 \end{bmatrix}; \quad \mathbf{f}_{\mathtt{M},2} = \begin{bmatrix} 0 \\ 0 \\ 0 \\ 0 \\ \tau_\theta \\ \tau_\psi \end{bmatrix}, \tag{4.274}$$

with

$$\mathbf{V}_i = \begin{bmatrix} V_{1,i} \\ V_{2,i} \\ V_{3,i} \\ V_{4,i} \\ V_{5,i} \\ V_{6,i} \end{bmatrix}; \quad \mathbf{D}_i = \begin{bmatrix} b_{u,i} & 0 & 0 & 0 & 0 & 0 \\ 0 & b_{v,i} & 0 & 0 & 0 & 0 \\ 0 & 0 & b_{w,i} & 0 & 0 & 0 \\ 0 & 0 & 0 & b_{p,i} & 0 & 0 \\ 0 & 0 & 0 & 0 & b_{q,i} & 0 \\ 0 & 0 & 0 & 0 & 0 & b_{r,i} \end{bmatrix}; \quad \mathbf{G}_i = \begin{bmatrix} W_i \sin\left(\theta_i\right) \\ -W_i \cos\left(\theta_i\right) \sin\left(\phi_i\right) \\ -W_i \cos\left(\phi_i\right) \cos\left(\theta_i\right) \\ -W_i \cos\left(\theta_i\right)\left(y_{\mathrm{G},i} \cos\left(\phi_i\right) - z_{\mathrm{G},i} \sin\left(\phi_i\right)\right) \\ W_i\left(z_{\mathrm{G},i} \sin\left(\theta_i\right) + x_{\mathrm{G},i} \cos\left(\phi_i\right) \cos\left(\theta_i\right)\right) \\ -W_i\left(y_{\mathrm{G},i} \sin\left(\theta_i\right) + x_{\mathrm{G},i} \cos\left(\theta_i\right) \sin\left(\phi_i\right)\right) \end{bmatrix}, \tag{4.275}$$

and

$$\begin{aligned}
V_{1,i} &= m_i\left(q_i w_i - r_i v_i - q_i^2 x_{\mathrm{G},i} - r_i^2 x_{\mathrm{G},i} + p_i q_i y_{\mathrm{G},i} + p_i r_i z_{\mathrm{G},i}\right), \\
V_{2,i} &= -m_i\left(p_i w_i - r_i u_i + p_i^2 y_{\mathrm{G},i} + r_i^2 y_{\mathrm{G},i} - p_i q_i x_{\mathrm{G},i} - q_i r_i z_{\mathrm{G},i}\right), \\
V_{3,i} &= m_i\left(p_i v_i - q_i u_i - p_i^2 z_{\mathrm{G},i} - q_i^2 z_{\mathrm{G},i} + p_i r_i x_{\mathrm{G},i} + q_i r_i y_{\mathrm{G},i}\right), \\
V_{4,i} &= m_i p_i v_i y_{\mathrm{G},i} - m_i q_i u_i y_{\mathrm{G},i} + m_i p_i w_i z_{\mathrm{G},i} - m_i r_i u_i z_{\mathrm{G},i} - \frac{I_{\mathrm{yz},i} q_i^2}{2} - \frac{I_{\mathrm{zy},i} q_i^2}{2} + \ldots \\
&\quad \frac{I_{\mathrm{yz},i} r_i^2}{2} + \frac{I_{\mathrm{zy},i} r_i^2}{2} - \frac{I_{\mathrm{xz},i} p_i q_i}{2} - \frac{I_{\mathrm{zx},i} p_i q_i}{2} + \frac{I_{\mathrm{xy},i} p_i r_i}{2} + \frac{I_{\mathrm{yx},i} p_i r_i}{2} - I_{\mathrm{yy},i} q_i r_i + I_{\mathrm{zz},i} q_i r_i, \\
V_{5,i} &= -m_i p_i v_i x_{\mathrm{G},i} + m_i q_i u_i x_{\mathrm{G},i} + m_i q_i w_i z_{\mathrm{G},i} - m_i r_i v_i z_{\mathrm{G},i} - \frac{I_{\mathrm{xz},i} r_i^2}{2} + \frac{I_{\mathrm{xz},i} p_i^2}{2} + \ldots \\
&\quad \frac{I_{\mathrm{zx},i} p_i^2}{2} - \frac{I_{\mathrm{zx},i} r_i^2}{2} + \frac{I_{\mathrm{yz},i} p_i q_i}{2} + \frac{I_{\mathrm{zy},i} p_i q_i}{2} - \frac{I_{\mathrm{xy},i} q_i r_i}{2} - \frac{I_{\mathrm{yx},i} q_i r_i}{2} + I_{\mathrm{xx},i} p_i r_i - I_{\mathrm{zz},i} p_i r_i, \\
V_{6,i} &= -m_i p_i w_i x_{\mathrm{G},i} + m_i r_i u_i x_{\mathrm{G},i} - m_i q_i w_i y_{\mathrm{G},i} + m_i r_i v_i y_{\mathrm{G},i} - \frac{I_{\mathrm{xy},i} p_i^2}{2} - \frac{I_{\mathrm{yx},i} p_i^2}{2} + \ldots \\
&\quad \frac{I_{\mathrm{xy},i} q_i^2}{2} + \frac{I_{\mathrm{yx},i} q_i^2}{2} - \frac{I_{\mathrm{yz},i} p_i r_i}{2} - \frac{I_{\mathrm{zy},i} p_i r_i}{2} + \frac{I_{\mathrm{xz},i} q_i r_i}{2} + \frac{I_{\mathrm{zx},i} q_i r_i}{2} - I_{\mathrm{xx},i} p_i q_i + I_{\mathrm{yy},i} p_i q_i,
\end{aligned} \tag{4.276}$$

where b_i $(i = 1, 2)$ are the coefficients of viscous friction, while τ_θ and τ_ψ are the control torques generated by the thrusters with associated drive voltages u_θ and u_ψ.

Let $\boldsymbol{\tau} = \left[\tau_\theta, \tau_\psi\right]^\mathsf{T}$ and $\mathbf{u} = \left[u_\theta, u_\psi\right]^\mathsf{T}$ be the columns-vectors of control torques and associated drive voltages of the motors, respectively, such that $\boldsymbol{\tau} = \mathbf{T}\mathbf{u}$, where $\mathbf{T}$ is the thruster configuration

matrix, written as follows:

$$\mathbf{T} = \begin{bmatrix} k_{yy} & k_{yz} \\ k_{zy} & k_{zz} \end{bmatrix}, \tag{4.277}$$

where k_{yy}, k_{yz}, k_{zy} and k_{zz} are modeling parameters.

The modeling constraints are written with respect to joints centers, as follows:

$$\boldsymbol{\varphi}(\mathbf{q}, t) = \begin{bmatrix} x_1 \\ y_1 \\ z_1 \\ \phi_1 \\ \theta_1 \\ x_2 - x_1 \\ y_2 - y_1 \\ z_2 - z_1 \\ \phi_2 - \phi_1 \\ \psi_2 - \psi_1 \end{bmatrix} = \mathbf{0}. \tag{4.278}$$

Performing the second time derivative of Eq. (4.275), we get:

$$\ddot{\boldsymbol{\varphi}}(\mathbf{a}, \mathbf{v}, \mathbf{q}, t) = \mathbf{0} \Leftrightarrow \mathbf{A}(\mathbf{q}, t)\,\mathbf{a} = \mathbf{b}(\mathbf{v}, \mathbf{q}, t), \tag{4.279}$$

where

$$\mathbf{A} = \begin{bmatrix} \mathbf{A}_{1:2,1} & \mathbf{A}_{1:2,2} \end{bmatrix} \mathbf{J}; \quad \mathbf{b} = \begin{bmatrix} b_1 \\ b_2 \\ b_3 \\ b_4 \\ b_5 \\ b_6 \\ b_7 \\ b_8 \\ b_9 \\ b_{10} \end{bmatrix} - \mathbf{A}\dot{\mathbf{J}}\mathbf{v}, \tag{4.280}$$

with

$$\mathbf{A}_{1:2,1} = \begin{bmatrix} \cos(\psi_1)\cos(\theta_1) & \cos(\psi_1)\sin(\phi_1)\sin(\theta_1) - \cos(\phi_1)\sin(\psi_1) & \sin(\phi_1)\sin(\psi_1) + \cos(\phi_1)\cos(\psi_1)\sin(\theta_1) & 0 & 0 & 0 \\ \cos(\theta_1)\sin(\psi_1) & \cos(\phi_1)\cos(\psi_1) + \sin(\phi_1)\sin(\psi_1)\sin(\theta_1) & \cos(\phi_1)\sin(\psi_1)\sin(\theta_1) - \cos(\psi_1)\sin(\phi_1) & 0 & 0 & 0 \\ -\sin(\theta_1) & \cos(\theta_1)\sin(\phi_1) & \cos(\phi_1)\cos(\theta_1) & 0 & 0 & 0 \\ 0 & 0 & 0 & 1 & \frac{\sin(\phi_1)\sin(\theta_1)}{\cos(\theta_1)} & \frac{\cos(\phi_1)\sin(\theta_1)}{\cos(\theta_1)} \\ 0 & 0 & 0 & 0 & \cos(\phi_1) & -\sin(\phi_1) \\ -\cos(\psi_1)\cos(\theta_1) & \cos(\phi_1)\sin(\psi_1) - \cos(\psi_1)\sin(\phi_1)\sin(\theta_1) & -\sin(\phi_1)\sin(\psi_1) - \cos(\phi_1)\cos(\psi_1)\sin(\theta_1) & 0 & 0 & 0 \\ -\cos(\theta_1)\sin(\psi_1) & -\cos(\phi_1)\cos(\psi_1) - \sin(\phi_1)\sin(\psi_1)\sin(\theta_1) & \cos(\psi_1)\sin(\phi_1) - \cos(\phi_1)\sin(\psi_1)\sin(\theta_1) & 0 & 0 & 0 \\ \sin(\theta_1) & -\cos(\theta_1)\sin(\phi_1) & -\cos(\phi_1)\cos(\theta_1) & 0 & 0 & 0 \\ 0 & 0 & 0 & -1 & -\frac{\sin(\phi_1)\sin(\theta_1)}{\cos(\theta_1)} & -\frac{\cos(\phi_1)\sin(\theta_1)}{\cos(\theta_1)} \\ 0 & 0 & 0 & 0 & -\frac{\sin(\phi_1)}{\cos(\theta_1)} & -\frac{\cos(\phi_1)}{\cos(\theta_1)} \end{bmatrix}, \tag{4.281}$$

$$\mathbf{A}_{1:2,2} = \begin{bmatrix} 0 & 0 & 0 & 0 & 0 & 0 \\ 0 & 0 & 0 & 0 & 0 & 0 \\ 0 & 0 & 0 & 0 & 0 & 0 \\ 0 & 0 & 0 & 0 & 0 & 0 \\ 0 & 0 & 0 & 0 & 0 & 0 \\ \cos(\psi_2)\cos(\theta_2) & \cos(\psi_2)\sin(\phi_2)\sin(\theta_2) - \cos(\phi_2)\sin(\psi_2) & \sin(\phi_2)\sin(\psi_2) + \cos(\phi_2)\cos(\psi_2)\sin(\theta_2) & 0 & 0 & 0 \\ \cos(\theta_2)\sin(\psi_2) & \cos(\phi_2)\cos(\psi_2) + \sin(\phi_2)\sin(\psi_2)\sin(\theta_2) & \cos(\phi_2)\sin(\psi_2)\sin(\theta_2) - \cos(\psi_2)\sin(\phi_2) & 0 & 0 & 0 \\ -\sin(\theta_2) & \cos(\theta_2)\sin(\phi_2) & \cos(\phi_2)\cos(\theta_2) & 0 & 0 & 0 \\ 0 & 0 & 0 & 1 & \frac{\sin(\phi_2)\sin(\theta_2)}{\cos(\theta_2)} & \frac{\cos(\phi_2)\sin(\theta_2)}{\cos(\theta_2)} \\ 0 & 0 & 0 & 0 & \frac{\sin(\phi_2)}{\cos(\theta_2)} & \frac{\cos(\phi_2)}{\cos(\theta_2)} \end{bmatrix},$$

and

$$
\begin{aligned}
b_1 &= q_1 u_1 \sin(\phi_1)\sin(\psi_1) - p_1 v_1 \sin(\phi_1)\sin(\psi_1) - q_1 w_1 \cos(\psi_1)\cos(\theta_1) + \dots \\
&\quad r_1 v_1 \cos(\psi_1)\cos(\theta_1) - p_1 w_1 \cos(\phi_1)\sin(\psi_1) + r_1 u_1 \cos(\phi_1)\sin(\psi_1) + \dots \\
&\quad - p_1 v_1 \cos(\phi_1)\cos(\psi_1)\sin(\theta_1) + q_1 u_1 \cos(\phi_1)\cos(\psi_1)\sin(\theta_1) + \dots \\
&\quad p_1 w_1 \cos(\psi_1)\sin(\phi_1)\sin(\theta_1) - r_1 u_1 \cos(\psi_1)\sin(\phi_1)\sin(\theta_1), \\
b_2 &= r_1 v_1 \cos(\theta_1)\sin(\psi_1) - q_1 w_1 \cos(\theta_1)\sin(\psi_1) + p_1 w_1 \cos(\phi_1)\cos(\psi_1) + \dots \\
&\quad - r_1 u_1 \cos(\phi_1)\cos(\psi_1) + p_1 v_1 \cos(\psi_1)\sin(\phi_1) - q_1 u_1 \cos(\psi_1)\sin(\phi_1) + \dots \\
&\quad - p_1 v_1 \cos(\phi_1)\sin(\psi_1)\sin(\theta_1) + q_1 u_1 \cos(\phi_1)\sin(\psi_1)\sin(\theta_1) + \dots \\
&\quad p_1 w_1 \sin(\phi_1)\sin(\psi_1)\sin(\theta_1) - r_1 u_1 \sin(\phi_1)\sin(\psi_1)\sin(\theta_1), \\
b_3 &= q_1 w_1 \sin(\theta_1) - r_1 v_1 \sin(\theta_1) + p_1 w_1 \cos(\theta_1)\sin(\phi_1) - r_1 u_1 \cos(\theta_1)\sin(\phi_1) + \dots \\
&\quad - p_1 v_1 \cos(\phi_1)\cos(\theta_1) + q_1 u_1 \cos(\phi_1)\cos(\theta_1), \\
\cos(\theta_1)^2 b_4 &= \sin(\phi_1)\, q_1^2 \cos(\phi_1)\cos(\theta_1)^2 - \sin(2\phi_1)\, q_1^2 + 2 q_1 r_1 \cos(\phi_1)^2 \cos(\theta_1)^2 + \dots \\
&\quad - 4 q_1 r_1 \cos(\phi_1)^2 - q_1 r_1 \cos(\theta_1)^2 + 2 q_1 r_1 - p_1 \sin(\theta_1)\, q_1 \cos(\phi_1)\cos(\theta_1) + \dots \\
&\quad - \sin(\phi_1)\, r_1^2 \cos(\phi_1)\cos(\theta_1)^2 + \sin(2\phi_1)\, r_1^2 + p_1 \sin(\phi_1)\sin(\theta_1)\, r_1 \cos(\theta_1), \\
\cos(\theta_1)\, b_5 &= -\sin(\theta_1)\, q_1^2 \cos(\phi_1)^2 + \sin(\theta_1)\, q_1^2 + 2 \sin(\phi_1)\sin(\theta_1)\, q_1 r_1 \cos(\phi_1) + \dots \\
&\quad p_1 \cos(\theta_1)\sin(\phi_1)\, q_1 + \sin(\theta_1)\, r_1^2 \cos(\phi_1)^2 + p_1 \cos(\theta_1)\, r_1 \cos(\phi_1), \\
b_6 &= p_1 v_1 \sin(\phi_1)\sin(\psi_1) - q_1 u_1 \sin(\phi_1)\sin(\psi_1) - p_2 v_2 \sin(\phi_2)\sin(\psi_2) + \dots \\
&\quad q_2 u_2 \sin(\phi_2)\sin(\psi_2) + q_1 w_1 \cos(\psi_1)\cos(\theta_1) - r_1 v_1 \cos(\psi_1)\cos(\theta_1) + \dots \\
&\quad - q_2 w_2 \cos(\psi_2)\cos(\theta_2) + r_2 v_2 \cos(\psi_2)\cos(\theta_2) + p_1 w_1 \cos(\phi_1)\sin(\psi_1) + \dots \\
&\quad - r_1 u_1 \cos(\phi_1)\sin(\psi_1) - p_2 w_2 \cos(\phi_2)\sin(\psi_2) + r_2 u_2 \cos(\phi_2)\sin(\psi_2) + \dots \\
&\quad p_1 v_1 \cos(\phi_1)\cos(\psi_1)\sin(\theta_1) - q_1 u_1 \cos(\phi_1)\cos(\psi_1)\sin(\theta_1) + \dots \\
&\quad - p_2 v_2 \cos(\phi_2)\cos(\psi_2)\sin(\theta_2) + q_2 u_2 \cos(\phi_2)\cos(\psi_2)\sin(\theta_2) + \dots \\
&\quad - p_1 w_1 \cos(\psi_1)\sin(\phi_1)\sin(\theta_1) + r_1 u_1 \cos(\psi_1)\sin(\phi_1)\sin(\theta_1) + \dots \\
&\quad p_2 w_2 \cos(\psi_2)\sin(\phi_2)\sin(\theta_2) - r_2 u_2 \cos(\psi_2)\sin(\phi_2)\sin(\theta_2), \\
b_7 &= q_1 w_1 \cos(\theta_1)\sin(\psi_1) - r_1 v_1 \cos(\theta_1)\sin(\psi_1) - q_2 w_2 \cos(\theta_2)\sin(\psi_2) + \dots \\
&\quad r_2 v_2 \cos(\theta_2)\sin(\psi_2) - p_1 w_1 \cos(\phi_1)\cos(\psi_1) + r_1 u_1 \cos(\phi_1)\cos(\psi_1) + \dots \\
&\quad p_2 w_2 \cos(\phi_2)\cos(\psi_2) - r_2 u_2 \cos(\phi_2)\cos(\psi_2) - p_1 v_1 \cos(\psi_1)\sin(\phi_1) + \dots \\
&\quad q_1 u_1 \cos(\psi_1)\sin(\phi_1) + p_2 v_2 \cos(\psi_2)\sin(\phi_2) - q_2 u_2 \cos(\psi_2)\sin(\phi_2) + \dots \\
&\quad p_1 v_1 \cos(\phi_1)\sin(\psi_1)\sin(\theta_1) - q_1 u_1 \cos(\phi_1)\sin(\psi_1)\sin(\theta_1) + \dots \\
&\quad - p_2 v_2 \cos(\phi_2)\sin(\psi_2)\sin(\theta_2) + q_2 u_2 \cos(\phi_2)\sin(\psi_2)\sin(\theta_2) + \dots \\
&\quad - p_1 w_1 \sin(\phi_1)\sin(\psi_1)\sin(\theta_1) + r_1 u_1 \sin(\phi_1)\sin(\psi_1)\sin(\theta_1) + \dots \\
&\quad p_2 w_2 \sin(\phi_2)\sin(\psi_2)\sin(\theta_2) - r_2 u_2 \sin(\phi_2)\sin(\psi_2)\sin(\theta_2), \\
b_8 &= r_1 v_1 \sin(\theta_1) - q_1 w_1 \sin(\theta_1) + q_2 w_2 \sin(\theta_2) + \dots \\
&\quad - r_2 v_2 \sin(\theta_2) - p_1 w_1 \cos(\theta_1)\sin(\phi_1) + r_1 u_1 \cos(\theta_1)\sin(\phi_1) + \dots \\
&\quad p_2 w_2 \cos(\theta_2)\sin(\phi_2) - r_2 u_2 \cos(\theta_2)\sin(\phi_2) + p_1 v_1 \cos(\phi_1)\cos(\theta_1) + \dots \\
&\quad - q_1 u_1 \cos(\phi_1)\cos(\theta_1) - p_2 v_2 \cos(\phi_2)\cos(\theta_2) + q_2 u_2 \cos(\phi_2)\cos(\theta_2), \\
-\cos(\theta_1)^2 \cos(\theta_2)^2 b_9 &= \sin(\phi_1)\, q_1^2 \cos(\phi_1)\cos(\theta_1)^2 \cos(\theta_2)^2 - 2 \sin(\phi_1)\, q_1^2 \cos(\phi_1)\cos(\theta_2)^2 + \dots \\
&\quad 2 q_1 r_1 \cos(\phi_1)^2 \cos(\theta_1)^2 \cos(\theta_2)^2 - 4 q_1 r_1 \cos(\phi_1)^2 \cos(\theta_2)^2 - q_1 r_1 \cos(\theta_1)^2 \cos(\theta_2)^2 + \dots \\
&\quad 2 q_1 r_1 \cos(\theta_2)^2 - p_1 \sin(\theta_1)\, q_1 \cos(\phi_1)\cos(\theta_1)\cos(\theta_2)^2 - \sin(\phi_2)\, q_2^2 \cos(\phi_2)\cos(\theta_1)^2 \cos(\theta_2)^2 + \dots \\
&\quad 2 \sin(\phi_2)\, q_2^2 \cos(\phi_2)\cos(\theta_1)^2 - 2 q_2 r_2 \cos(\phi_2)^2 \cos(\theta_1)^2 \cos(\theta_2)^2 + 4 q_2 r_2 \cos(\phi_2)^2 \cos(\theta_1)^2 + \dots \\
&\quad q_2 r_2 \cos(\theta_1)^2 \cos(\theta_2)^2 - 2 q_2 r_2 \cos(\theta_1)^2 + p_2 \sin(\theta_2)\, q_2 \cos(\phi_2)\cos(\theta_1)^2 \cos(\theta_2) + \dots \\
&\quad - \sin(\phi_1)\, r_1^2 \cos(\phi_1)\cos(\theta_1)^2 \cos(\theta_2)^2 + 2 \sin(\phi_1)\, r_1^2 \cos(\phi_1)\cos(\theta_2)^2 + \dots \\
&\quad p_1 \sin(\phi_1)\sin(\theta_1)\, r_1 \cos(\theta_1)\cos(\theta_2)^2 + \sin(\phi_2)\, r_2^2 \cos(\phi_2)\cos(\theta_1)^2 \cos(\theta_2)^2 + \dots \\
&\quad - 2 \sin(\phi_2)\, r_2^2 \cos(\phi_2)\cos(\theta_1)^2 - p_2 \sin(\phi_2)\sin(\theta_2)\, r_2 \cos(\theta_1)^2 \cos(\theta_2), \\
-\cos(\theta_1)^2 \cos(\theta_2)^2 b_{10} &= -2 \sin(\phi_1)\sin(\theta_1)\, q_1^2 \cos(\phi_1)\cos(\theta_2)^2 - 4 \sin(\theta_1)\, q_1 r_1 \cos(\phi_1)^2 \cos(\theta_2)^2 + \dots \\
&\quad 2 \sin(\theta_1)\, q_1 r_1 \cos(\theta_2)^2 - p_1 q_1 \cos(\phi_1)\cos(\theta_1)\cos(\theta_2)^2 + 2 \sin(\phi_2)\sin(\theta_2)\, q_2^2 \cos(\phi_2)\cos(\theta_1)^2 + \dots \\
&\quad 4 \sin(\theta_2)\, q_2 r_2 \cos(\phi_2)^2 \cos(\theta_1)^2 - 2 \sin(\theta_2)\, q_2 r_2 \cos(\theta_1)^2 + p_2 q_2 \cos(\phi_2)\cos(\theta_1)^2 \cos(\theta_2) + \dots \\
&\quad 2 \sin(\phi_1)\sin(\theta_1)\, r_1^2 \cos(\phi_1)\cos(\theta_2)^2 + p_1 \sin(\phi_1)\, r_1 \cos(\theta_1)\cos(\theta_2)^2 + \dots \\
&\quad - 2 \sin(\phi_2)\sin(\theta_2)\, r_2^2 \cos(\phi_2)\cos(\theta_1)^2 - p_2 \sin(\phi_2)\, r_2 \cos(\theta_1)^2 \cos(\theta_2).
\end{aligned}
\tag{4.282}
$$

Once pitch (θ_2) and yaw (ψ_1) angles are actuated, the identification matrices become:

$$\mathbf{Q} = \begin{bmatrix} 0 & 0 \\ 0 & 0 \\ 0 & 0 \\ 0 & 0 \\ 0 & 0 \\ 0 & 1 \\ 0 & 0 \\ 0 & 0 \\ 0 & 0 \\ 0 & 0 \\ 1 & 0 \\ 0 & 0 \end{bmatrix}; \quad \mathbf{R} = \begin{bmatrix} 1 & 0 & 0 & 0 & 0 & 0 & 0 & 0 & 0 & 0 \\ 0 & 1 & 0 & 0 & 0 & 0 & 0 & 0 & 0 & 0 \\ 0 & 0 & 1 & 0 & 0 & 0 & 0 & 0 & 0 & 0 \\ 0 & 0 & 0 & 1 & 0 & 0 & 0 & 0 & 0 & 0 \\ 0 & 0 & 0 & 0 & 1 & 0 & 0 & 0 & 0 & 0 \\ 0 & 0 & 0 & 0 & 0 & 0 & 0 & 0 & 0 & 0 \\ 0 & 0 & 0 & 0 & 0 & 1 & 0 & 0 & 0 & 0 \\ 0 & 0 & 0 & 0 & 0 & 0 & 1 & 0 & 0 & 0 \\ 0 & 0 & 0 & 0 & 0 & 0 & 0 & 1 & 0 & 0 \\ 0 & 0 & 0 & 0 & 0 & 0 & 0 & 0 & 1 & 0 \\ 0 & 0 & 0 & 0 & 0 & 0 & 0 & 0 & 0 & 0 \\ 0 & 0 & 0 & 0 & 0 & 0 & 0 & 0 & 0 & 1 \end{bmatrix}. \tag{4.283}$$

The decentralized controllers are given by:

$$\mathbf{u}_0 = \begin{bmatrix} \mathbf{u}_{0,1} \\ \mathbf{u}_{0,2} \end{bmatrix}, \tag{4.284}$$

where

$$\mathbf{u}_{0,i} = \mathbf{N}_i \boldsymbol{\nu}_i + \mathbf{f}_{\mathrm{A},i}. \quad (i = 1, 2) \tag{4.285}$$

Four control types are tested, i.e., PID, SMC, Integral SMC (ISMC) and MPC.

The second-order error dynamic associated with the PID control is given by:

$$\dot{\tilde{\mathbf{v}}}_i + \mathbf{K}_{\mathrm{D},i}\tilde{\mathbf{v}}_i + \mathbf{K}_{\mathrm{P},i}\mathbf{J}_i^{-1}\tilde{\mathbf{q}}_i + \mathbf{K}_{\mathrm{I},i}\int_0^t \mathbf{J}_i^{-1}\tilde{\mathbf{q}}_i \mathrm{d}\tau = \mathbf{0}, \tag{4.286}$$

where $\tilde{\mathbf{q}}_i = \mathbf{q}_i - \mathbf{q}_{\mathrm{d},i}$ is the tracking error column-vector, while $\mathbf{K}_{\mathrm{P},i} = \mathbf{K}_{\mathrm{P},i}^{\mathsf{T}} \geq \mathbf{0}$, $\mathbf{K}_{\mathrm{I},i} = \mathbf{K}_{\mathrm{I},i}^{\mathsf{T}} \geq \mathbf{0}$ and $\mathbf{K}_{\mathrm{D},i} = \mathbf{K}_{\mathrm{D},i}^{\mathsf{T}} \geq \mathbf{0}$ are the proportional, integral and derivative control gain matrices, respectively.

The sliding surface variables are written as:

$$\begin{aligned} \mathbf{s}_{\mathrm{SMC},i}(\mathbf{v}_i, \mathbf{q}_i, t) &= \tilde{\mathbf{v}}_i + \boldsymbol{\Lambda}_i \mathbf{J}_i^{-1}\tilde{\mathbf{q}}_i = \mathbf{0}, \\ \mathbf{s}_{\mathrm{ISMC},i}(\mathbf{v}_i, \mathbf{q}_i, t) &= \tilde{\mathbf{v}}_i + 2\boldsymbol{\Lambda}_i \mathbf{J}_i^{-1}\tilde{\mathbf{q}}_i + \boldsymbol{\Lambda}^2 \int_0^t \mathbf{J}_i^{-1}\tilde{\mathbf{q}}_i \mathrm{d}\tau = \mathbf{0}, \end{aligned} \tag{4.287}$$

where $\boldsymbol{\Lambda}_i = \boldsymbol{\Lambda}_i^{\mathsf{T}} \geq \mathbf{0}$ is a control gain matrix associated with the closed-loop bandwidth.

Based on Eqs. (4.287) and (4.288), the following control laws are obtained:

$$\begin{aligned}
\boldsymbol{\upsilon}_{\mathtt{PID},i} &= \dot{\mathbf{v}}_{\mathtt{d},i} - \mathbf{K}_{\mathtt{P},i}\mathbf{J}_i^{-1}\tilde{\mathbf{q}}_i - \mathbf{K}_{\mathtt{I},i}\int_0^t \mathbf{J}_i^{-1}\tilde{\mathbf{q}}_i \mathrm{d}\tau - \mathbf{K}_{\mathtt{D},i}\tilde{\mathbf{v}}_i, \\
\boldsymbol{\upsilon}_{\mathtt{SMC},i} &= \dot{\mathbf{v}}_{\mathtt{d},i} - \boldsymbol{\Lambda}_i\tilde{\mathbf{v}}_i - \boldsymbol{\Lambda}_i\dot{\mathbf{J}}_i^{-1}\tilde{\mathbf{q}}_i - \mathbf{K}_i \operatorname{sign}(\mathbf{s}_i), \\
\boldsymbol{\upsilon}_{\mathtt{ISMC},i} &= \dot{\mathbf{v}}_{\mathtt{d},i} - 2\boldsymbol{\Lambda}_i\tilde{\mathbf{v}}_i - \left(2\boldsymbol{\Lambda}_i\dot{\mathbf{J}}_i^{-1} + \boldsymbol{\Lambda}_i^2\right)\tilde{\mathbf{q}}_i - \mathbf{K}_i \operatorname{sign}(\mathbf{s}_i),
\end{aligned} \tag{4.288}$$

where $\mathbf{K}_i = \mathbf{K}_i^{\mathsf{T}} \geq \mathbf{0}$ is a control gain matrix.

Let $\mathbf{u}_{\#} = \boldsymbol{\tau} = \left[\tau_\theta, \tau_\psi\right]^{\mathsf{T}}$. From Eq. (4.63), the control force is calculated as:

$$\boldsymbol{\tau} = \mathbf{Q}^{\mathsf{T}}\left(\mathbf{I} - \mathbf{A}^{\mathsf{T}}\left(\mathbf{R}^{\mathsf{T}}\mathbf{A}^{\mathsf{T}}\right)^{+}\mathbf{R}^{\mathsf{T}}\right)\mathbf{u}_0; \quad \mathbf{u} = \mathbf{T}^{-1}\boldsymbol{\tau}. \tag{4.289}$$

The MPC is synthesized using the derivative of the sliding surface variable of the SMC as reference signal, i.e., $\mathbf{y}_{\mathtt{r}} = \left[\boldsymbol{\upsilon}_{\mathtt{SMC},1}^{\mathsf{T}}, \boldsymbol{\upsilon}_{\mathtt{SMC},2}^{\mathsf{T}}\right]^{\mathsf{T}}$ and Eqs. (4.270)–(4.289) as inputs to the Algorithm 3.

The simulations were performed using the Digital Twin version of the Quanser AERO in MATLAB/Simulink® environment. This model considers highly fidelity dynamics (e.g., rigid body, motors and thrusters), sensors noise and communication limitations of the real plant. The simulations were done with `ode4` integrator using a fixed-time step of 0.001 s. The controller is implemented at a fixed rate frequency of 100 Hz.

The results are shown in Figs. 76 to 81. Figure 76 show the trajectory tracking achieved by all the controllers. The SMC and the MPC produced a faster response compared to the PID. The ISMC produced lower tracking errors at the price of some peaks at the beginning of each step. The control inputs are shown in Fig. 77, where we can notice the chattering effects, especially on the SMC and the MPC. The chattering is reduced on the ISMC due to the integral term. The normalized Integral Time Absolute Error (ITAE) indices for pitch and yaw angles are shown in Fig. 78. For the pitch angle, the ISMC performed better, followed by the MPC. The SMC produced a smaller yaw angle index trailed by the MPC. Other states recorded during the simulations, such as angular rates, motor velocities and electric currents, are shown in Figs. 79 to 81.

Table 11: 2-DoFs helicopter parameters

Symbols ($i = 1, 2$)	Values	Units (SI)
m_1, m_2	0, 1.075	kg
$I_{\mathrm{xx},1}, I_{\mathrm{xy},1}, I_{\mathrm{xz},1}$	0, 0, 0	kgm, kgm^2
$I_{\mathrm{yx},1}, I_{\mathrm{yy},1}, I_{\mathrm{yz},1}$	0, 0, 0	kgm, kgm^2
$I_{\mathrm{zx},1}, I_{\mathrm{zy},1}, I_{\mathrm{zz},1}$	0, 0, 0.0220	kgm, kgm^2
$I_{\mathrm{xx},2}, I_{\mathrm{xy},2}, I_{\mathrm{xz},2}$	0, 0, 0	kgm, kgm^2
$I_{\mathrm{yx},2}, I_{\mathrm{yy},2}, I_{\mathrm{yz},2}$	0, 0.0219, 0	kgm, kgm^2
$I_{\mathrm{zx},2}, I_{\mathrm{zy},2}, I_{\mathrm{zz},2}$	0, 0, 0	kgm, kgm^2
$x_{\mathrm{G},1}, y_{\mathrm{G},1}, z_{\mathrm{G},1}$	0, 0, 0	m
$x_{\mathrm{G},2}, y_{\mathrm{G},2}, z_{\mathrm{G},2}$	0, 0, 0.0076	m
$b_{u,1}, b_{v,1}, b_{w,1}$	0, 0, 0	Ns/m
$b_{p,1}, b_{q,1}, b_{r,1}$	0, 0, 0.0220	Nms
$b_{u,2}, b_{v,2}, b_{w,2}$	0, 0, 0	Ns/m
$b_{p,2}, b_{q,2}, b_{r,2}$	0, 0.0071, 0	Nms
W_1, W_2	0, 1.55	N
l_1, l_2	0, 0.158	m
$k_{\mathrm{yy}}, k_{\mathrm{yz}}, k_{\mathrm{zy}}, k_{\mathrm{zz}}$	0.0011, 0.0021, - 0.0027, 0.0022	Nm/V
$\mathbf{\Lambda}_{\mathtt{SMC},i}$	diag (1, 1, 1, 1, 1, 1)	1/s
$\mathbf{L}_{\mathtt{SMC},i}$	diag (10, 10, 10, 10, 10, 10)	1/s
$\mathbf{K}_{\mathtt{SMC},i}$	diag (10, 10, 10, 10, 10, 10)	m/s^2, rad/s^2
$\mathbf{\Lambda}_{\mathtt{ISMC},i}$	diag (0.3, 0.3, 0.3, 0.3, 0.3, 0.3)	1/s
$\mathbf{L}_{\mathtt{ISMC}i}$	diag (0, 0, 0, 0, 0, 0)	1/s
$\mathbf{K}_{\mathtt{ISMC}i}$	diag (10, 10, 10, 10, 10, 10)	m/s^2, rad/s^2
$\mathbf{K}_{\mathtt{P},i}$	diag (1, 1, 1, 1, 1, 1)	1/s^2
$\mathbf{K}_{\mathtt{I},i}$	diag (10, 10, 10, 10, 10, 10)	1/s^3
$\mathbf{K}_{\mathtt{D},i}$	diag (10, 10, 10, 10, 10, 10)	1/s
ϵ	0.001	–
$\mathbf{Q_Y}, \mathbf{P_Y}$	diag $(2, 2, 2, 2, 2, 2, 2, 2, 2, 2, 2, 2) \times 10^3$	–
$\mathbf{R}_{\mathbf{U}_\#}$	diag $(1, 1) \times 10^2$	–
$\mathbf{\Omega_a}$	diag $(1, 1, 1, 1, 1, 1, 1, 1, 1, 1, 1, 1) \times 10^2$	rad/s
p, c	30, 10	–
$T_{\mathtt{s}}$	0.01	s

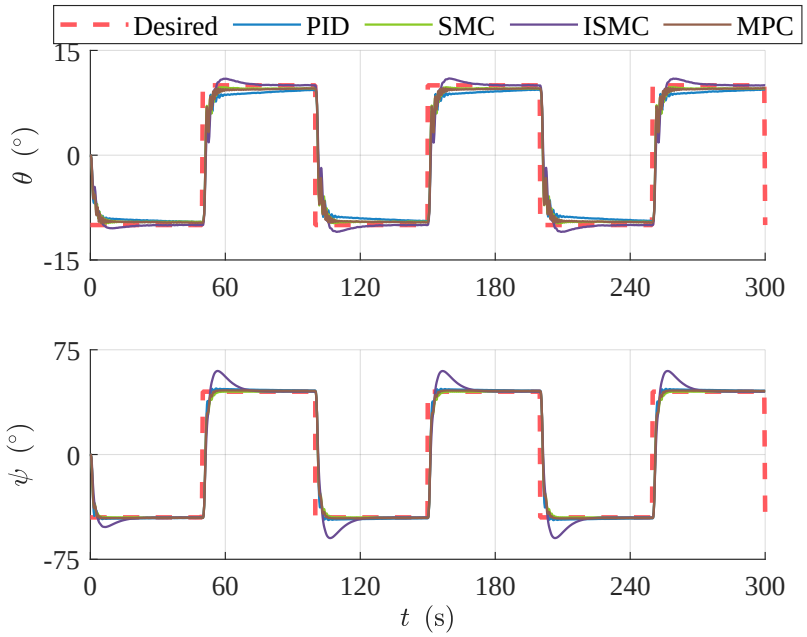

Figure 76: Displacements tracking of the 2-DoFs helicopter

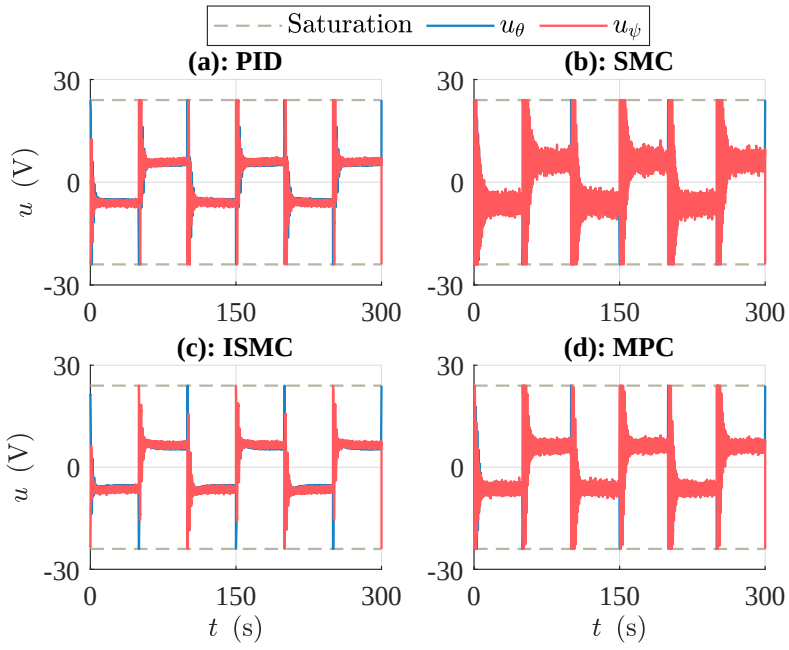

Figure 77: Control inputs of the 2-DoFs helicopter

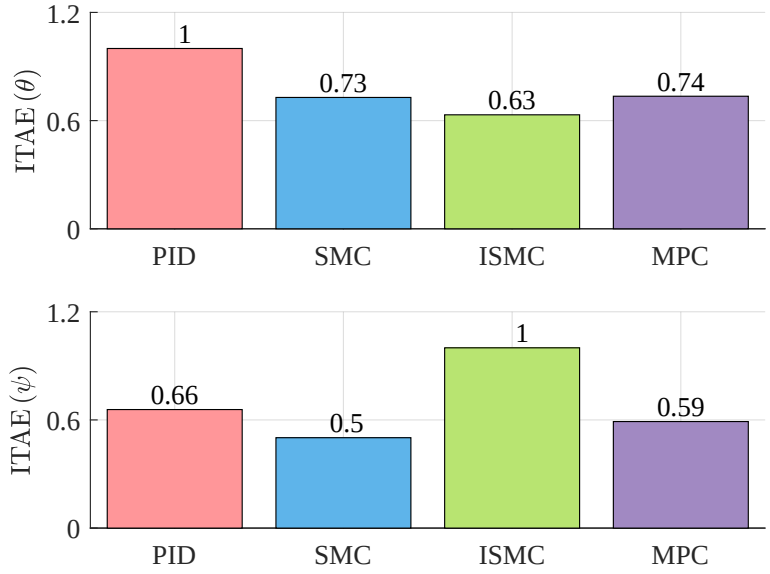

Figure 78: ITAE indices of the 2-DoFs helicopter

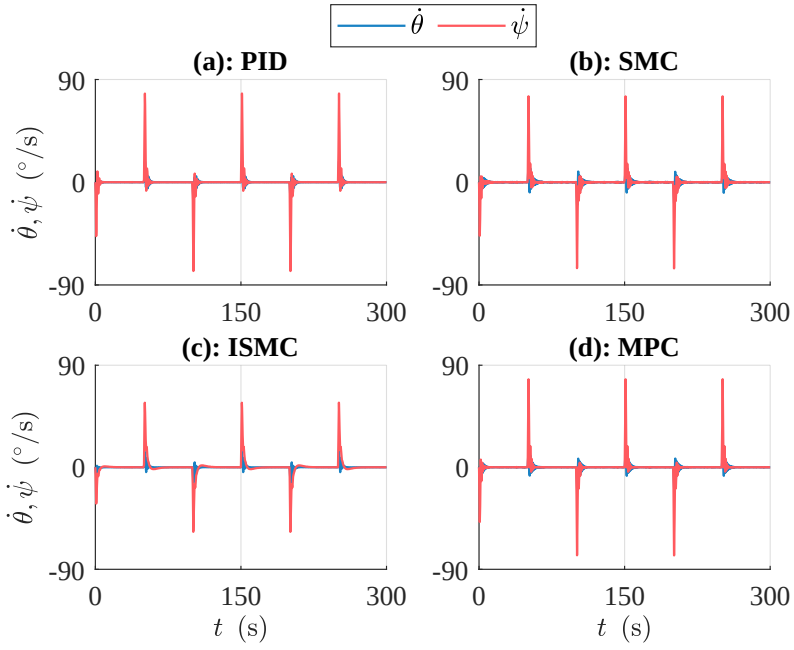

Figure 79: Angular rates of the 2-DoFs helicopter

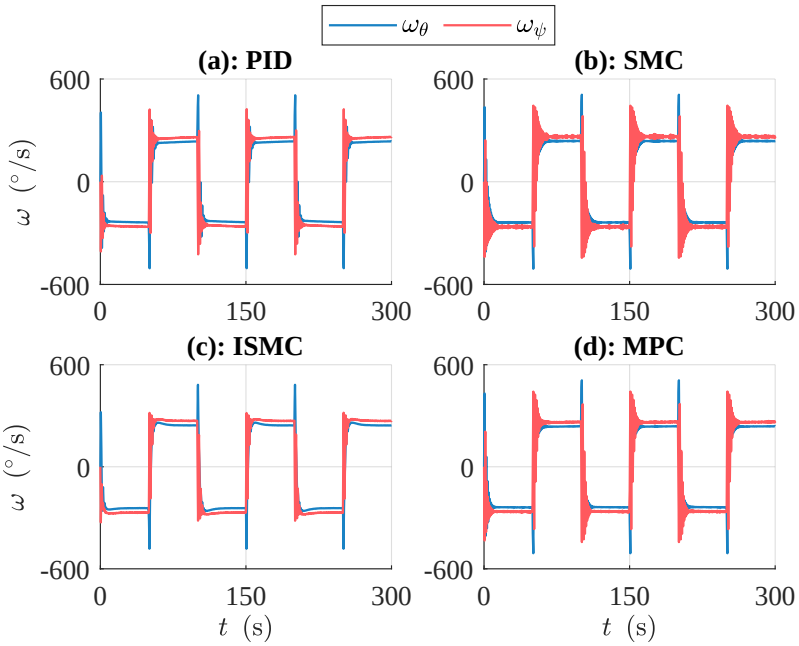

Figure 80: Motors velocities of the 2-DoFs helicopter

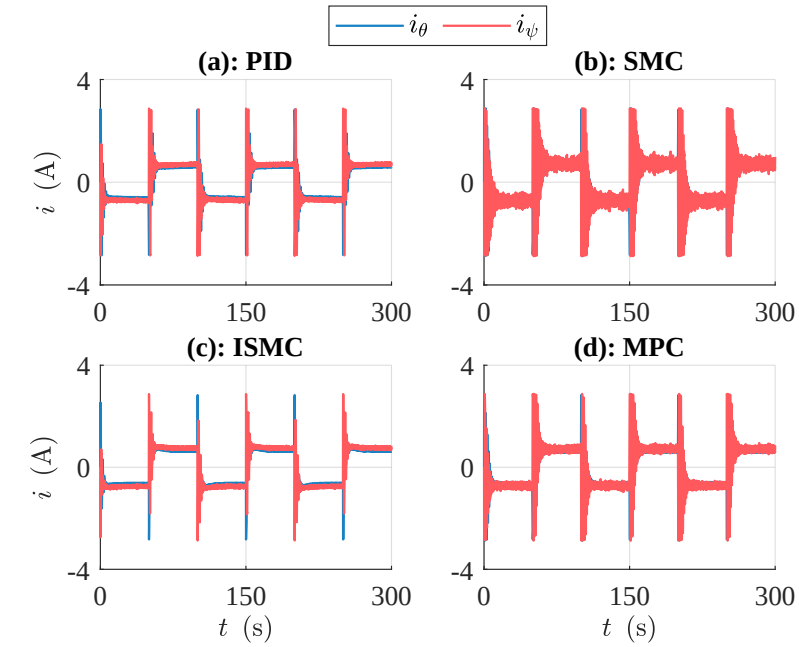

Figure 81: Motors currents of the 2-DoFs helicopter

4.3.8 Invented pendulum experiment

In this last example, the inverted pendulum is revisited. The intention is to test the MCM formulation in a physical prototype. Figure 82 show the inverted pendulum prototype and the hardware components used.

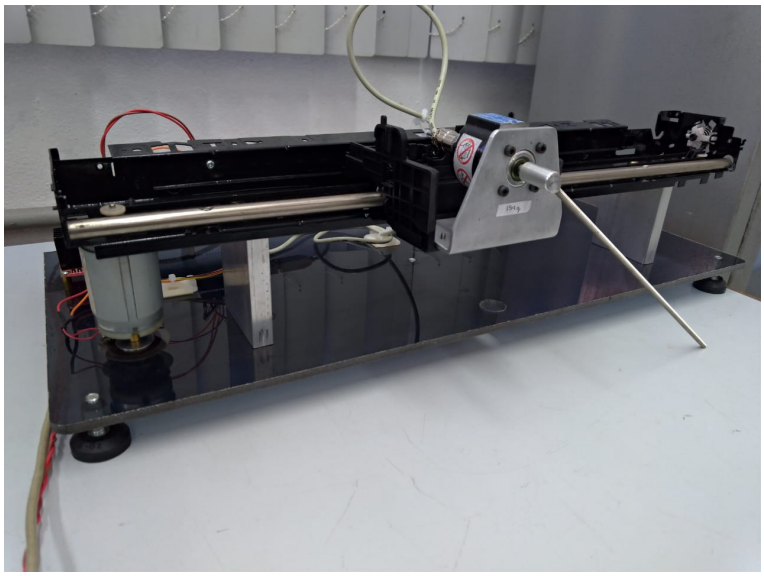

(a): Prototype

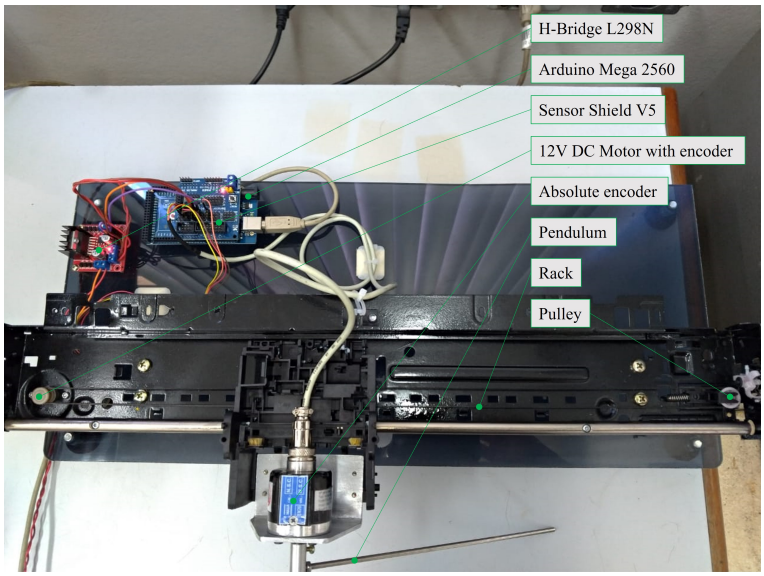

(b): Top view detailing

Figure 82: Inverted pendulum prototype

The inverted pendulum shown in Fig. 82 (a) was constructed based on the structure of an older paper printer. The main hardware components are indicated in Fig. 82 (b). The pendulum itself consists of a cylindrical rod mounted in bearing support. The 12V DC Motor with an

encoder commands the support through a pulley-rack system. The control hardware used in the experiment consists of Arduino Mega 2560 with H-Bridge L298N and Sensor Shield V5. The Arduino Mega 2560 drives the motor through the H-Bridge L298N. The readings from the motor encoder and the absolute encoder (used to measure the pendulum angle) are sent to the Sensor Shield V5 and then to the Arduino Mega 2560.

Figure 83 shown the schematic diagram and modeling hierarchy of the inverted pendulum system for the experiment.

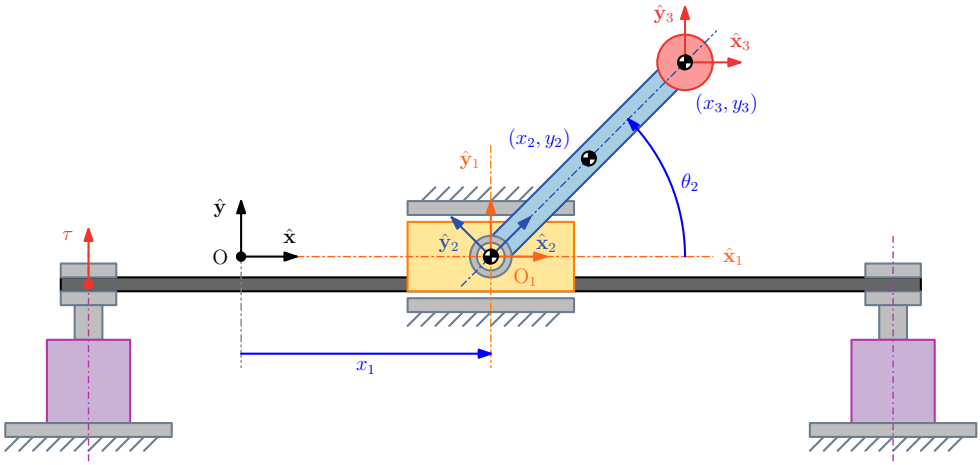

(a): Inverted pendulum prototype schematic diagram

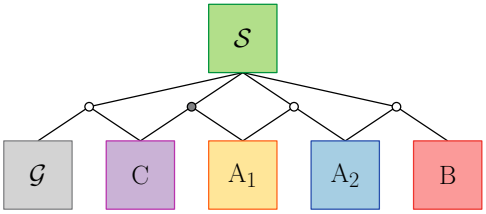

(b): Modeling/control hierarchy

Figure 83: Inverted pendulum prototype model

The generalized coordinates used in the modeling are given by $\mathbf{q} = \left[\mathbf{q}_1^\mathsf{T}, \mathbf{q}_2^\mathsf{T}, \mathbf{q}_3^\mathsf{T}, \gamma\right]^\mathsf{T}$, with $\mathbf{q}_i = [x_i, y_i, \theta_i]^\mathsf{T}$ as the column-vector of generalized coordinates associated with the i-th body ($i = 1, 2, 3$) and γ is the motor displacement, as shown in Fig. 83 (a). In the modeling hierarchy of Fig. 83 (b), $\mathcal{G}$ is the ground, body A_1 is the cart, body A_2 is the pendulum, body B is the end-effector and component C is the motor while system $\mathcal{S}$ is the inverted pendulum prototype. Also, an active prismatic joint (grey circle) connects the motor with the cart, a passive revolute joint (white circle) connects the cart with the pendulum and a fixed joint (white circle) connects the pendulum with the end-effector. A trivial set of quasi-velocities and accelerations is used on the synthesis, i.e., $\mathbf{v} = \dot{\mathbf{q}}$ and $\mathbf{a} = \dot{\mathbf{v}}$.

The relaxed dynamic model is given by:

$$\mathbf{N}\mathbf{a}_0 = \mathbf{g}, \tag{4.290}$$

where

$$\mathbf{N} = \mathbf{M} + \mathbf{A}^{\mathsf{T}}\mathbf{A}; \quad \mathbf{M} = \begin{bmatrix} \mathbf{M}_1 & \mathbf{0} & \mathbf{0} & 0 \\ \mathbf{0} & \mathbf{M}_2 & \mathbf{0} & 0 \\ \mathbf{0} & \mathbf{0} & \mathbf{M}_3 & 0 \\ 0 & 0 & 0 & I_4 \end{bmatrix}; \quad \mathbf{g} = \mathbf{f} + \mathbf{A}^{\mathsf{T}}\mathbf{b}; \quad \mathbf{f} = \begin{bmatrix} \mathbf{f}_1 \\ \mathbf{f}_2 \\ \mathbf{f}_3 \\ f_4 \end{bmatrix}. \tag{4.291}$$

The inertia matrix and active forces column-vectors related to the i-th body are written as:

$$\mathbf{M}_i = \begin{bmatrix} m_i & 0 & 0 \\ 0 & m_i & 0 \\ 0 & 0 & I_i \end{bmatrix}; \quad \mathbf{f}_i = \mathbf{f}_{\mathtt{A},i} + \mathbf{f}_{\mathtt{M},i}, \quad (i = 1, 2, 3) \tag{4.292}$$

where m_i is the mass and I_i is the inertia moment, while $\mathbf{f}_{\mathtt{A},i}$ and $\mathbf{f}_{\mathtt{M},i}$ are the column-vectors of active forces due to the natural physical effects (e.g., weight, friction, etc.) and due to the motor forces, respectively. In this example, the active forces column-vectors are expressed by:

$$\begin{gathered} \mathbf{f}_{\mathtt{A},1} = \begin{bmatrix} -b_1\dot{x}_1 - c_1 \operatorname{sign}(\dot{x}_1) \\ -m_1 g \\ 0 \end{bmatrix}; \quad \mathbf{f}_{\mathtt{A},2} = \begin{bmatrix} 0 \\ -m_2 g \\ -b_2\dot{\theta}_2 - c_2 \operatorname{sign}\left(\dot{\theta}_2\right) \end{bmatrix}; \quad \mathbf{f}_{\mathtt{A},3} = \begin{bmatrix} 0 \\ -m_3 g \\ 0 \end{bmatrix}, \\ f_{\mathtt{A},4} = -\left(\frac{K_4^2}{R_4} + b_4\right)\dot{\theta}_4 - c_4 \operatorname{sign}\left(\dot{\theta}_4\right); \quad \mathbf{f}_{\mathtt{M},1} = \mathbf{f}_{\mathtt{M},2} = \mathbf{f}_{\mathtt{M},3} = \begin{bmatrix} 0 \\ 0 \\ 0 \end{bmatrix}; \quad f_{\mathtt{M},4} = \tau_4, \end{gathered} \tag{4.293}$$

where b_i and c_i $(i = 1, 2, 3, 4)$ are the coefficients of viscous and dry friction, respectively, and $\tau_4 = (K_4/R_4)\, V_4$ is the motor, with K_4, R_4 and V_4 as the torque constant, electric resistance and drive voltage associated with the motor, respectively.

The modeling constraints are written with respect to joints centers, as follows:

$$\boldsymbol{\varphi}(\mathbf{q}, t) = \begin{bmatrix} y_1 \\ \theta_1 \\ x_1 - x_2 + l_2 \cos(\theta_2) \\ y_1 - y_2 + l_2 \sin(\theta_2) \\ x_3 - x_2 - l_2 \cos(\theta_2) \\ y_3 - y_2 - l_2 \sin(\theta_2) \\ \theta_3 - \theta_2 \\ x_1 - \theta_4 r_4 \end{bmatrix} = \mathbf{0}. \tag{4.294}$$

in which l_2 is half of the pendulum length and r_4 is the pulley radius.

Performing the second time-derivative of Eq. (4.294), we get:

$$\ddot{\boldsymbol{\varphi}}(\mathbf{a}, \mathbf{v}, \mathbf{q}, t) = \mathbf{0} \Leftrightarrow \mathbf{A}(\mathbf{q}, t)\,\mathbf{a} = \mathbf{b}(\mathbf{v}, \mathbf{q}, t), \tag{4.295}$$

where

$$\begin{aligned} \mathbf{A} &= \begin{bmatrix} 0 & 1 & 0 & 0 & 0 & 0 & 0 & 0 & 0 & 0 \\ 0 & 0 & 1 & 0 & 0 & 0 & 0 & 0 & 0 & 0 \\ 1 & 0 & 0 & -1 & 0 & -l_2 \sin(\theta_2) & 0 & 0 & 0 & 0 \\ 0 & 1 & 0 & 0 & -1 & l_2 \cos(\theta_2) & 0 & 0 & 0 & 0 \\ 0 & 0 & 0 & -1 & 0 & l_2 \sin(\theta_2) & 1 & 0 & 0 & 0 \\ 0 & 0 & 0 & 0 & -1 & -l_2 \cos(\theta_2) & 0 & 1 & 0 & 0 \\ 0 & 0 & 0 & 0 & 0 & -1 & 0 & 0 & 1 & 0 \\ 1 & 0 & 0 & 0 & 0 & 0 & 0 & 0 & 0 & -r_4 \end{bmatrix}, \\ \mathbf{b} &= \begin{bmatrix} 0 \\ 0 \\ l_2 \cos(\theta_2)\,\dot{\theta}_2^2 \\ l_2 \sin(\theta_2)\,\dot{\theta}_2^2 \\ -l_2 \cos(\theta_2)\,\dot{\theta}_2^2 \\ -l_2 \sin(\theta_2)\,\dot{\theta}_2^2 \\ 0 \\ 0 \end{bmatrix}. \end{aligned} \tag{4.296}$$

Since the motor displacement (γ) is actuated, the identification matrices become:

$$\mathbf{Q} = \begin{bmatrix} 0 \\ 0 \\ 0 \\ 0 \\ 0 \\ 0 \\ 0 \\ 0 \\ 0 \\ 1 \end{bmatrix}; \quad \mathbf{R} = \begin{bmatrix} 1 & 0 & 0 & 0 & 0 & 0 & 0 & 0 & 0 \\ 0 & 1 & 0 & 0 & 0 & 0 & 0 & 0 & 0 \\ 0 & 0 & 1 & 0 & 0 & 0 & 0 & 0 & 0 \\ 0 & 0 & 0 & 1 & 0 & 0 & 0 & 0 & 0 \\ 0 & 0 & 0 & 0 & 1 & 0 & 0 & 0 & 0 \\ 0 & 0 & 0 & 0 & 0 & 1 & 0 & 0 & 0 \\ 0 & 0 & 0 & 0 & 0 & 0 & 1 & 0 & 0 \\ 0 & 0 & 0 & 0 & 0 & 0 & 0 & 1 & 0 \\ 0 & 0 & 0 & 0 & 0 & 0 & 0 & 0 & 1 \\ 0 & 0 & 0 & 0 & 0 & 0 & 0 & 0 & 0 \end{bmatrix}. \tag{4.297}$$

The decentralized controllers are given by:

$$\mathbf{u}_0 = \begin{bmatrix} \mathbf{u}_{0,1} \\ \mathbf{u}_{0,2} \\ \mathbf{u}_{0,3} \\ u_{0,4} \end{bmatrix} = \mathbf{N}\boldsymbol{\upsilon} + \mathbf{f}_{\mathtt{A}} + \mathbf{A}^{\mathsf{T}}\mathbf{b}; \quad \boldsymbol{\upsilon} = \begin{bmatrix} \boldsymbol{\upsilon}_1 \\ \boldsymbol{\upsilon}_2 \\ \boldsymbol{\upsilon}_3 \\ \upsilon_4 \end{bmatrix}; \quad \mathbf{f}_{\mathtt{A}} = \begin{bmatrix} \mathbf{f}_{\mathtt{A},1} \\ \mathbf{f}_{\mathtt{A},2} \\ \mathbf{f}_{\mathtt{A},3} \\ f_{\mathtt{A},4} \end{bmatrix}. \tag{4.298}$$

For the pendulum we used a simple PD control, given by:

$$\boldsymbol{\upsilon}_i = -\mathbf{K}_{\mathtt{P},i}\tilde{\mathbf{q}}_i - \mathbf{K}_{\mathtt{D},i}\mathbf{v}_i; \quad \upsilon_4 = -k_{\mathtt{P},4}\tilde{\theta}_4 - k_{\mathtt{D},4}\dot{\theta}_4, \quad (i = 1, 2, 3) \tag{4.299}$$

where $\tilde{\mathbf{q}}_i = \mathbf{q}_i - \mathbf{q}_{\mathtt{d},i}$ is the tracking errors column-vector, while $\mathbf{K}_{\mathtt{P},i} = \mathbf{K}_{\mathtt{P},i}^{\mathsf{T}} \geq \mathbf{0}$ and $\mathbf{K}_{\mathtt{D},i} = \mathbf{K}_{\mathtt{D},i}^{\mathsf{T}} \geq \mathbf{0}$ are the proportional and derivative control gain matrices, respectively. Similarly, $\tilde{\theta}_4 = \theta_4 - \theta_{\mathtt{d},4}$ is the tracking error associated with the motor while $k_{\mathtt{P},4} \geq 0$ and $k_{\mathtt{D},4} \geq 0$ are the proportional and derivative control gains, respectively.

Let $u_{\#} = \tau_4$. From Eq. (4.63), the control torque is calculated as:

$$\tau_4 = \mathbf{Q}^{\mathsf{T}}\left(\mathbf{I} - \mathbf{A}^{\mathsf{T}}\left(\mathbf{R}^{\mathsf{T}}\mathbf{A}^{\mathsf{T}}\right)^{+}\mathbf{R}^{\mathsf{T}}\right)\mathbf{u}_0; \quad V_4 = (R_4/K_4)\,\tau_4. \tag{4.300}$$

Table 12: Inverted pendulum prototype parameters

Symbols	Values	Units (SI)
m_1, m_2, m_3	0.3, 0.02, 0	kg
I_1, I_2, I_3, I_4	0, 0.0004, 0, 0	kgm^2
b_1, b_2, b_3	0.1, 0, 0	Nms
c_1, c_2, c_3	0, 0, 0	Nm
l_1, l_2	0, 0.125	m
r_4	0.005	m
R_4	6.84	Ω
K_4	0.05	Nm/A
$\mathbf{K}_{\text{P},1}$	diag (1000, 1000, 1000)	$1/\text{s}^2$
$\mathbf{K}_{\text{P},2}$	diag (360, 360, 360)	$1/\text{s}^2$
$\mathbf{K}_{\text{P},3}$	diag (360, 360, 360)	$1/\text{s}^2$
$k_{\text{P},4}$	100	$1/\text{s}^2$
$\mathbf{K}_{\text{D},1}$	diag (1000, 1000, 1000)	1/s
$\mathbf{K}_{\text{D},2}$	diag (66, 66, 66)	1/s
$\mathbf{K}_{\text{D},3}$	diag (66, 66, 66)	1/s
$k_{\text{D},4}$	10	1/s

The experiment was performed with an initial condition corresponding to the pendulum misaligned with the vertical by 0.3 rad (unstable condition) and the cart displaced by 0.15 m from the origin. The control object is to stabilize the pendulum in the vertical position and bring the cart back to the origin. The desired displacements are (in meters and radians):

$$x_{\text{d},1} = 0; \quad \theta_{\text{d},2} = \pi/2. \tag{4.301}$$

The remain desired displacements were calculated with Eqs. (4.301) and (4.294). All the desired velocities were set to zero, as shown in Eq. (4.299). The controller was implemented using a rate frequency of 100 Hz.

The results are shown in Figs. 84 and 85. The states stabilization is shown in Fig. 84. The stabilization occurs with the pendulum reaching the vertical equilibrium position in less than 1.5 s. The drive voltage calculated with Eq. (4.300) is shown in Fig. 85. There is no control saturation, even at the beginning of the motion, where the positioning error is more significant.

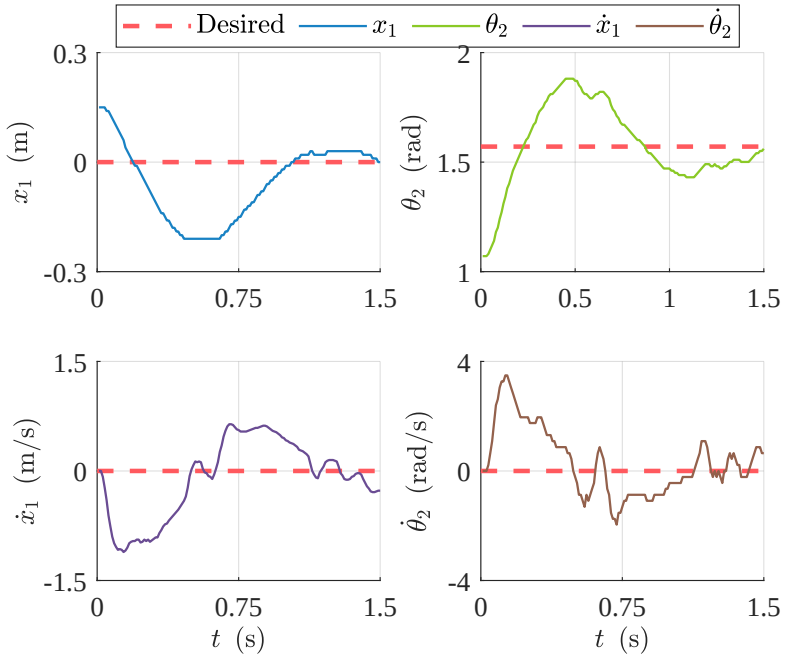

Figure 84: States stabilization of the inverted pendulum prototype

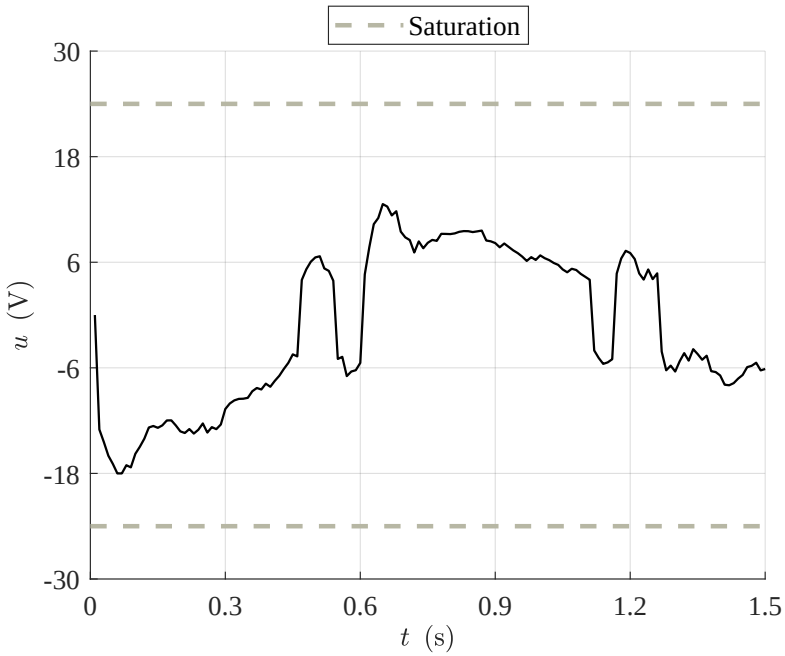

Figure 85: Control input of the inverted pendulum prototype

4.4 COMMENTARIES

This chapter presented the MCM for general multibody systems. This methodology permits the control synthesis through a hierarchical approach starting from already available decentralized controllers (or sub-controllers) and imposing the constraints *a posteriori*. This methodology is further extended considering the control allocation, decentralized controllers syntheses from prescribed servo-constraints and optimal control formulation. The methodology is validated through numerical simulation considering a series of problems presented in a tutorial approach, starting from classical mechanical systems and ending with more complex mechanisms of parallel kinematic structure. Also, some test are performed with a digital twin of a 2-DoFs helicopter and an inverted pendulum prototype.

5 CASES OF STUDY

This chapter presents three case studies with the MCM applied on the underwater cooperative transportation tasks. Some specific developments for each case of study regarding the formation-keeping are also presented. Numerical simulations are used to evaluate the presented approaches.

5.1 GENERAL INFORMATION

The case studies consist of 2D and 3D cooperative transportation tasks. General information regarding the common aspects between these cases (e.g., plant modeling, control, sensors, state estimation and simulation setup) is presented in the sequence.

Modeling

1. The models consider the inertial forces related to the mass and inertia of each body;
2. The manipulator and load links are cylindrical-shaped with high aspect ratio ($L/D > 10$);
3. The hydrodynamic forces (added mass and drag forces) are modeled with the lumped parameters model for the AUVs and by the discrete model based on the strip theory for the manipulator and load links. The hydrodynamic coefficients of the strips are calculated with the travel diameters relation along the length of the links (D/L) presented by McLain and Rock (1998) and shown in Fig. 86. To include 3D flow effects, the drag coefficients are corrected considering the stationary relation between two consecutive links raised by Leabourne and Rock (1998) and shown in Fig. 87. This correction is applicable in the 2D case once the relation between the stationary drag coefficients and the relative angle is only valid for a 2-link manipulator performing planar motion (LEABOURNE; ROCK, 1998);

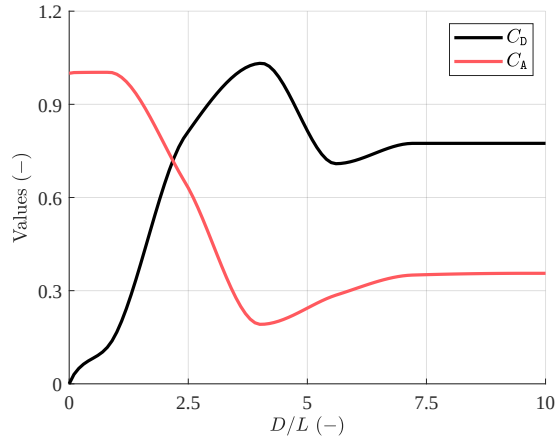

Figure 86: Added mass and drag coefficients of the 1-link manipulator

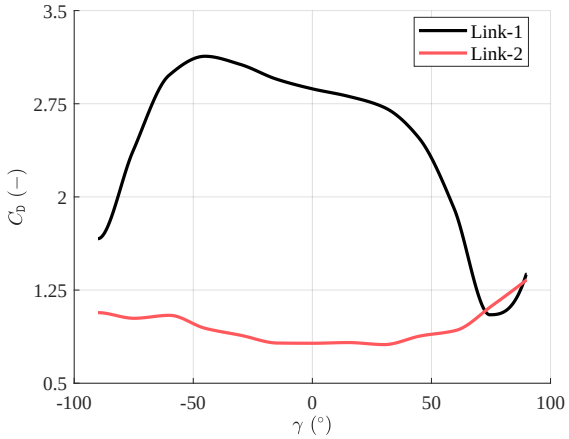

Figure 87: Drag coefficients of the 2-link manipulator

4. The hydrostatic forces, i.e., weight and buoyancy forces, are evaluated based on the mass and volumetric proprieties of each body;

5. The thrusters dynamic in the 2D cooperative transportation is modeled by the four quadrants model presented by Bachmayer, Whitcomb and Grosenbaugh (2000). For the other cases, a 3D table raised from the manufacturer experiments of the T560 thrusters (TECNADYNE, 2008) in series with a firs-order low-pass filter models the thrusters dynamic. The 3D table shown in Fig. 88 maps the gain of the low-pass filter as a function of the commanded motor velocity in Revolutions Per Minute (RPM) and the flow velocity along the propeller in m/s. A low-pass filter of unitary gain and time constant of 0.1 s models the delay associated with the dynamic response of the thrusters;

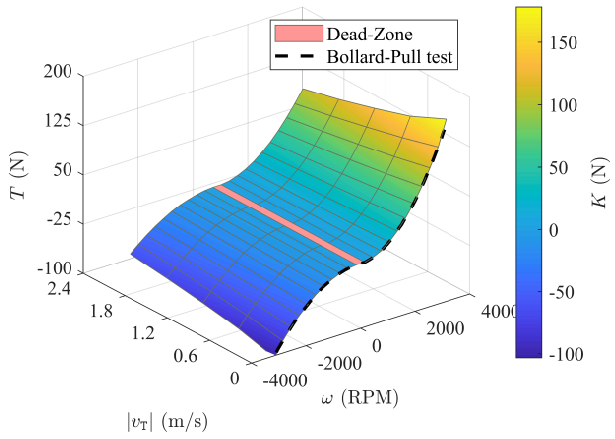

Figure 88: 3D model of the T560 thruster accounting for the losses due to the propeller flow

6. The manipulator motors are modeled with a second-order dynamic model, considering reduction and friction effects (viscous and Coulomb friction).

Control

1. The discrete models for the hydrodynamic forces of the manipulator are unsuitable for the control design since it needs many parameters and their estimation can be unfeasible in practice. Thus, for the control, the lumped model of the added mass matrix of Antonelli (2014) and the continuous drag model presented in chapter 3 are used (see Subsec. 3.1.4.3);

2. The control inputs are thrusts and torques generated by thrusters and motors. Thus, these inputs need to be converted into commanded signals. For example, the relation between the motors torque and current can be considered stationary, i.e., $\tau_{\mathtt{M}} = k_{\mathtt{M}} i_{\mathtt{M}}$, where $\tau_{\mathtt{M}}$ is the motor torque, $k_{\mathtt{M}}$ is the torque constant and $i_{\mathtt{M}}$ is the motor current. In the thrusters case, the calculated thrusts should be converted into commanded motor-shaft velocity with the inverse model of the thrusters raised in ideal condition (bollard-pull[1]). The thrusters curves used as inverse models for the 2D and 3D cooperative transportation problems are shown by Figs. 89 and 90, respectively;

[1]The bollard-pull test is performed by connecting a thruster with a measuring device and computing the force or tension developed in the connection using a load cell or similar component.

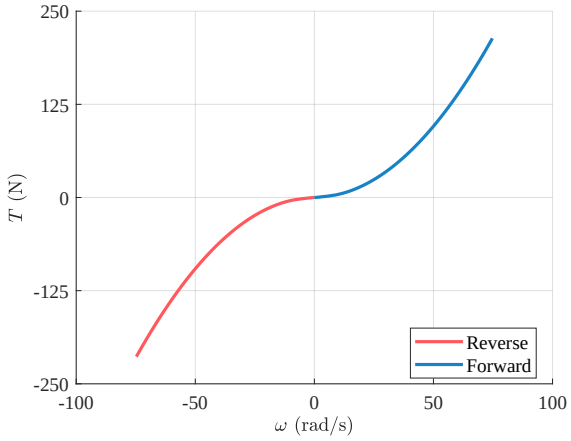

Figure 89: Twin-Burger 4-quadrant thruster model in bollard-pull condition

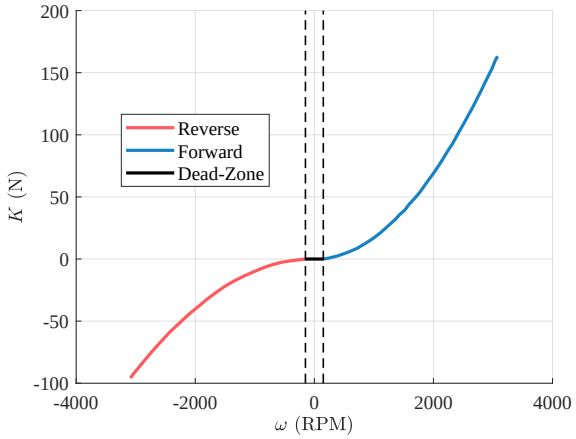

Figure 90: T560 thruster model in bollard-pull condition

3. The formation control is formulated as servo-constraints based on the graph theory. For sake of example, we adopted the sliding surface proposed by Ianagui (2019) as servo-constraint. However, any other type of formation error measurement based on the graph theory can be used (e.g., tracking error, second-order error dynamics, etc.). The formation topology is established based on Fig. 91 of an undirected graph, i.e., with bilateral connections, where a virtual leader is running on each agent to generate the desired load trajectory;

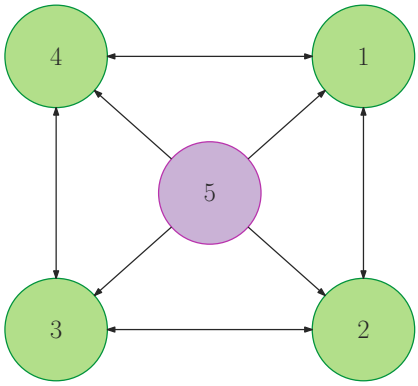

Figure 91: Formation topology

4. The reference trajectory of the load on the 2D and 3D cooperative transportation with I-AUVs is designed so that each segment is described by a cycloidal function. In this case, for a segment starting at the position $\mathbf{r}_{\mathrm{d}}(t_0)$ and ending in $\mathbf{r}_{\mathrm{d}}(t_1)$, for $t \in [t_0, t_1]$, it can be stated that:

$$\mathbf{r}_{\mathrm{d}}(t) = \mathbf{r}_{\mathrm{d}}(t_0) + (\mathbf{r}_{\mathrm{d}}(t_1) - \mathbf{r}_{\mathrm{d}}(t_0)) \frac{t - t_0}{t_1 - t_0} - \frac{1}{2\pi} \sin\left(2\pi \frac{t - t_0}{t_1 - t_0}\right); \tag{5.1}$$

5. For the 2D cooperative transportation with I-AUVs, the reference trajectory is described by horizontal, transversal and rotational segments with relative displacements of 10 m, 20 m and $\pm\pi/2$ rad, respectively, with a duration of 50 s. For the 3D cooperative transportation with I-AUVs, the reference trajectory is described by horizontal, transversal and vertical segments with relative displacements of 6 m, 6 m and 12 m, respectively, and by a final rotation with a relative displacement of $\pi/4$ rad. In this case, all segments have a duration of 30 s.

Sensors and state estimation

1. The proposed case studies assume an explicit communication between the agents at full state level (generalized coordinates, quasi-velocities and quasi-accelerations). To achieve explicit communication, some approaches can be adopted. For example, acoustic communication through onboard modems can be used to transmit information and image-based visual serving can be applied to estimate the relative distance between the agents. If the communication is too restrictive, the estimation schemes presented in Conti et al. (2015), Heshmati-Alamdari et al. (2021b) and Heshmati-Alamdari et al. (2021a) for cooperative transportation can be adopted. To handle broadcast information in discrete-time with limited information and time delays, an event-triggered communication algorithm

can be used (ALMEIDA; SILVESTRE; PASCOAL, 2017; BRIÑÓN-ARRANZ; SEURET; PASCOAL, 2019; HUNG; PASCOAL, 2022). Once efficient acoustic communications are still very challenging, depending on the agent configurations, a cable-guided system (e.g., to avoid interference on the thrusters and joints) can be used for communication among agents;

2. The vehicles measurements are provided by the onboard sensors. For the Twin-Burger and BlueROV 2, we considered:
   - a Long-Baseline (LBL) measures the linear displacements ($x_{\text{LBL}}, y_{\text{LBL}}, z_{\text{LBL}}$);
   - a Digital Pressure Transducer (DPT) measures the depth relative to the free surface (z_{DPT});
   - an Inertial Measurement Unit (IMU) measures the linear accelerations and angular velocities ($\dot{u}_{\text{IMU}}, \dot{v}_{\text{IMU}}, \dot{w}_{\text{IMU}}, p_{\text{IMU}}, q_{\text{IMU}}, r_{\text{IMU}}$);
   - a Doppler Velocity Log (DVL) measures the linear velocities ($u_{\text{DLV}}, v_{\text{DLV}}, w_{\text{DLV}}$);
   - a set of inclinometers and compass measures the attitude ($\phi_{\text{INC}}, \theta_{\text{INC}}, \psi_{\text{COM}}$).
3. Concerning the manipulator sensors, we considered that a set of encoders measures the joints displacements and velocities ($\boldsymbol{\gamma}_{\text{ENC}}, \dot{\boldsymbol{\gamma}}_{\text{ENC}}$);
4. A Kalman filter algorithm using a process (propagation) model established based on the kinematics of the agents are used to estimate the full state feedback, including the estimates of the quasi-accelerations. The kinematic model is formulated in minimal coordinates, therefore, to calculate the generalized coordinates, quasi-velocities and quasi-accelerations, the following relations are used: $\dot{\boldsymbol{\eta}} = \mathbf{J}\boldsymbol{\nu}$, $\boldsymbol{\nu} = \mathbf{S}\boldsymbol{\zeta}$ and $\dot{\boldsymbol{\nu}} = \mathbf{S}\dot{\boldsymbol{\zeta}} + \dot{\mathbf{S}}\boldsymbol{\zeta}$;
5. Details concerning the sensors parameters, the process and measurements models so as the Kalman filter algorithm can be found in Oliveira, Orsino and Donha (2021), Oliveira, Donha and Cardoso (2021), Oliveira, Orsino and Donha (2022) and Oliveira et al. (2022).

Disturbances

1. To reproduce realistic operation conditions, modeling errors and external disturbances are added on the simulation. Except for the 3D cooperative transport with modular ROVs, the modeling errors come from the transported load dynamics, since it is not considered on the design of the controllers. The external disturbances are modeled by a time-varying ocean current (on the 2D cooperative transportation problem) and by first-order wave forces (on the 3D cooperative transportation problems):

- As pointed out by Richard and Lévesque (1996), the stochasticity associated with the ocean current dynamic should be considered too. To this end, a first-order order Markov process is used to model its dynamics, as in Fossen (1996). The time history of the ocean current profile considering a mean value of 0.27 m/s, variance of a 0.15 m^2/s^2, saturation of ±0.3 m/s and incidence angle of $\pi/4$ rad is shown by Fig. 92;

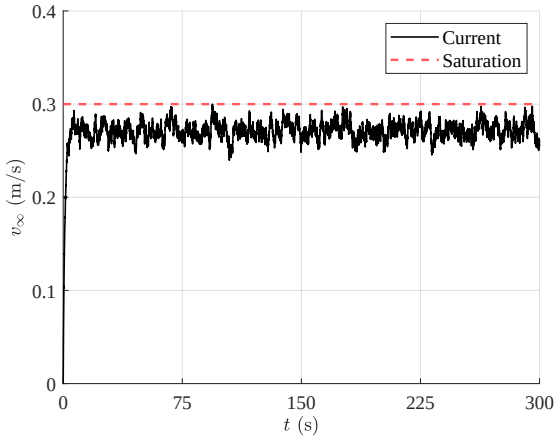

Figure 92: Ocean current velocity

- Wave forces are modeled by Morison's equations using the hydrodynamic coefficients previous defined. The sea state is defined by the wave velocity profile, which is calculated on the Earth-fixed frame through the summation of N sinusoidal components, where N is sufficiently large (PEREZ, 2005), as follows (LEWANDOWSKI, 2004):

$$
\begin{aligned}
\dot{x}_{\mathtt{w},i}\left(x_i, y_i, z_i, t\right) = & \sum_{j=1}^{N} \omega_j \cos\left(\chi_j\right) \frac{\cosh\left(k_j\left(h+z_i\right)\right)}{\sinh\left(k_j h\right)} A_j\left(\omega_j\right) \times \ldots \\
& \sin\left(\omega_j t + \epsilon_j - k_j x_i \cos\left(\chi_j\right) - k_j y_i \sin\left(\chi_j\right)\right), \\
\dot{y}_{\mathtt{w},i}\left(x_i, y_i, z_i, t\right) = & \sum_{j=1}^{N} \omega_j \cos\left(\chi_j\right) \frac{\cosh\left(k_j\left(h+z_i\right)\right)}{\sinh\left(k_j h\right)} A_j\left(\omega_j\right) \times \ldots \\
& \sin\left(\omega_j t + \epsilon_j - k_j x_i \cos\left(\chi_j\right) - k_j y_i \sin\left(\chi_j\right)\right), \\
\dot{z}_{\mathtt{w},i}\left(x_i, y_i, z_i, t\right) = & \sum_{j=1}^{N} \omega_j \frac{\sinh\left(k_j\left(h+z_i\right)\right)}{\sinh\left(k_j h\right)} A_j\left(\omega_j\right) \times \ldots \\
& \cos\left(\omega_j t + \epsilon_j - k_j x_i \cos\left(\chi_j\right) - k_j y_i \sin\left(\chi_j\right)\right),
\end{aligned}
\tag{5.2}
$$

where x_i, y_i and z_i are the i-th body coordinates, $A_j\left(\omega_j\right)$ is the wave amplitude at frequency ω_j, χ_j is the propagation angle, ϵ_j is the phase defined as independent identically distributed random variable with uniform distribution in the interval

$\epsilon_j \in [0, 2\pi]$. The choice of random phase ensures a Gaussian process (PEREZ, 2005). Also, each sinusoidal function is exponentially attenuated by the term $\exp\left(-k_j z_i\right)$ expressed by the hyperbolic identity, with k_j as the respective wave number and h as the local depth.

The wave height is obtained by the time integration of the wave velocity profile in Eq. (5.1) concerning the vertical component and $\zeta_{\mathrm{w},0}(0) = 0$ as the initial condition relative to the vehicle (LEWANDOWSKI, 2004):

$$\begin{aligned}\zeta_{\mathrm{w},0}(x_0, y_0, z_0, t) = \sum_{j=1}^{N} \frac{\sinh k_j(h+z)}{\sinh k_j h} A_j\left(\omega_j\right) \times \ldots \\ \cos\left(\omega_j t + \epsilon_j - k_j x_0 \cos\left(\chi_j\right) - k_j y_0 \sin\left(\chi_j\right)\right).\end{aligned} \tag{5.3}$$

According to Dantas, Cruz and Barros (2014), the wave amplitude is given by:

$$A_j\left(\omega_j\right) = \omega_{\mathrm{e},j} \sqrt{2S\left(\omega_j\right)\Delta\omega}, \tag{5.4}$$

where $\omega_{\mathrm{e},j}$ is the encounter frequency, $S\left(\omega_j\right)$ is the spectral energy density at the corresponding frequency and $\Delta\omega$ is the constant increment between two successive frequencies.

The encounter frequency follows (PEREZ, 2005; DANTAS; CRUZ; BARROS, 2014):

$$\omega_{\mathrm{e},j} = \omega_j + k_j u_i \cos(\beta), \tag{5.5}$$

where β is the wave heading angle.

Based on the static observation model, the DPT measure is modeled as the summation between the vehicle height, z_0, and the wave elevation, $\zeta_{\mathrm{w},0}$, as follows:

$$z_{\mathrm{DPT}} = z_0 + \zeta_{\mathrm{w},0}(x, z, t). \tag{5.6}$$

The spectral energy density is calculated according to the wave spectrum, $S\left(\omega_j\right)$. In this work, the Pierson–Moskowitz spectrum is used since it is appropriate to represent the sea conditions on the Brazilian southeast coast if the right parameters are used (DANTAS; CRUZ; BARROS, 2014):

$$\frac{S\left(\omega_j\right)}{H_{\mathrm{s}}^2 T_1} = \frac{0.11}{2\pi}\left(\frac{\omega_j T_1}{2\pi}\right)^{-5} \exp\left(-0.44\left(\frac{\omega_j T_1}{2\pi}\right)^{-4}\right), \tag{5.7}$$

where H_{s} is the significant wave height, defined as the average height of the highest one-third of all waves on the sea (CHAKRABARTI, 1987) and T_1 is the mean wave period.

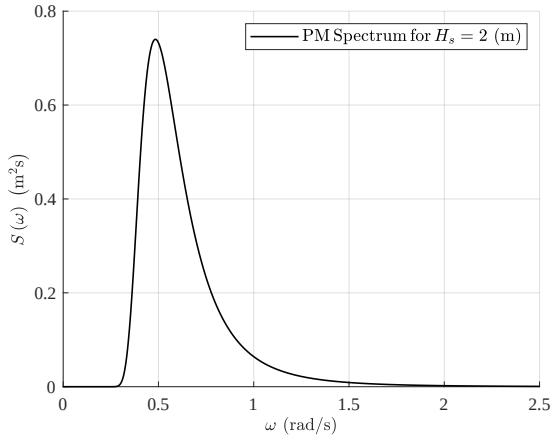

Figure 93: Pierson–Moskowitz spectrum for $H_{\mathtt{s}} = 2$ m

2. The disturbances are added into the models through the column-vectors $\mathbf{d}_i$ $(i = 1, \ldots, n)$.

Simulation

1. The constrained models are derived from the relaxed models and the modeling constraints in deferential form using the recursive version of the Udwadia-Kalaba equation developed by Orsino (2020) into the scope of the MMM;

2. To avoid numerical drift associated with the modeling during the numerical integration, the Baumgarte's stabilization coefficients (BAUMGARTE, 1972) are used such that during integration the differential constraints are replaced by:

$$\dot{\boldsymbol{\varphi}}(\boldsymbol{\eta}, \boldsymbol{\nu}, t) = \mathbf{0} \Rightarrow \mathbf{A}(\boldsymbol{\eta}, t)\,\dot{\boldsymbol{\nu}} = \mathbf{b}(\boldsymbol{\eta}, \boldsymbol{\nu}, t) \Rightarrow \mathbf{A}\dot{\boldsymbol{\nu}} = \mathbf{b} - 2\alpha_{\mathtt{B}}\dot{\boldsymbol{\varphi}} - \beta_{\mathtt{B}}^2\boldsymbol{\varphi}, \tag{5.8}$$

   where $\alpha_{\mathtt{B}} > 0$ and $\beta_{\mathtt{B}} > 0$ are the stabilization coefficients. For all the simulations, we have adopted $\alpha_{\mathtt{B}} = \beta_{\mathtt{B}} = 1$.

3. All the simulations are performed in MATLAB/Simulink® environment using the `ode5` function and a fixed time-step of 0.001 s for the numerical integration of the constrained models in state-space form. The reference generators (including the predictive-cooperative reference filter) are implemented with a rate frequency of 100 Hz; the low-level controllers (centralized and decentralized) and state estimators are implemented considering a rate frequency of 20 Hz; the sensors measurements are implemented with the associated noise variances and sample frequencies; the communication between the agents is performed considering a rate frequency of 10 Hz. Also, quantization effects (assuming the second decimal place for the hardware precision) are added to the simulation.

5.2 2D COOPERATIVE TRANSPORTATION WITH I-AUVs ON THE HORIZONTAL PLANE

5.2.1 Modeling

Figure 94 (a) show the 2D cooperative transportation with I-AUVs on the horizontal plane. The system comprises four I-AUVs transporting a rigid rectangular frame made of cylindrical-shaped links of aluminum. The I-AUV model is based on the Twin-Burger AUV equipped with a 2-DoFs manipulator with cylindrical-shaped links of stainless steel. This case of study is inspired by the works of Sagara (SAGARA et al., 2001; ISHITSUKA; SAGARA; ISHII, 2004; YATOH; SAGARA; TAMURA, 2008; SAGARA, 2009; TAIRA; SAGARA; OYA, 2018; TAIRA; SAGARA; OYA, 2020; SAGARA; AMBAR, 2020), who studied the motion control of I-AUVs using the Twin-Burger in some of them.

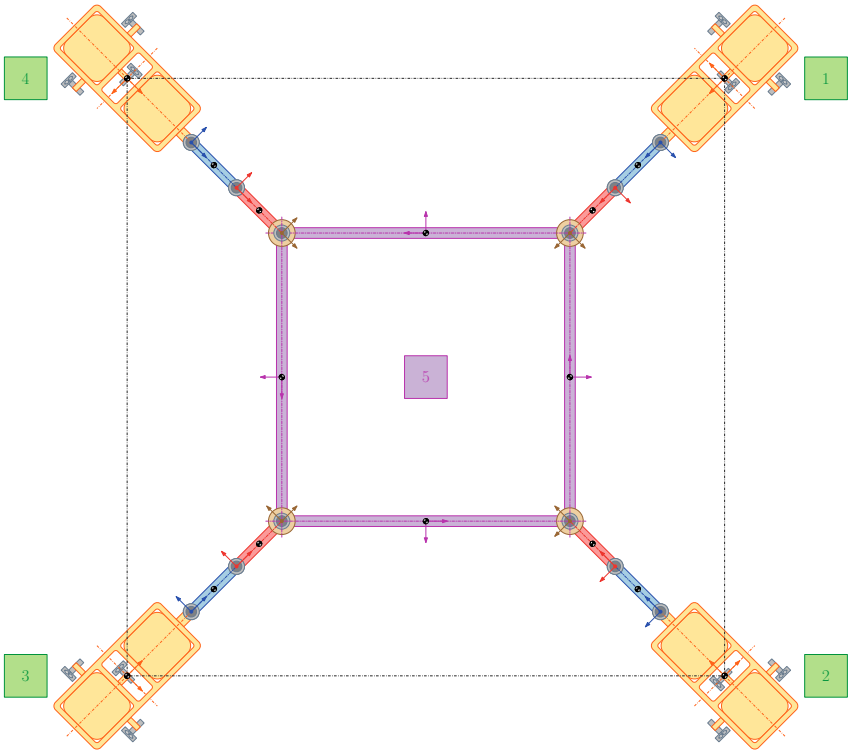

(a): 2D cooperative transportation system

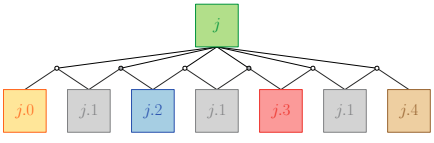

(b): Agent modeling hierarchy

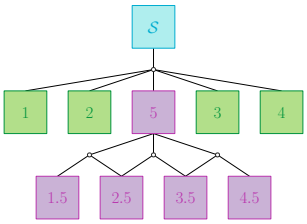

(c): Cooperative transportation modeling hierarchy

Figure 94: 2D cooperative transportation on the horizontal plane

In the modeling hierarchy of Fig. 94 (b), the j-th agent ($j = 1, \ldots, 4$) is constituted by the bodies 0, 1, 2, 3 and 4. In this hierarchy, the body $j.0$ is the vehicle, bodies $j.1$ are the motors, bodies $j.2$ and $j.3$ are the manipulator links, while body $j.4$ is the end-effector which is modeled as a sphere. Also, in Fig. 94 (c), agent 5 represents the load which is constituted by four other bodies, i.e., $j.5$ representing the frame links. In the j-th agent subsystems ($j = 1, \ldots, 4$), active revolute joints (grey circles) connect the motors with the links and passive revolute joints (white circles) connect the vehicle with the manipulator, the links between them and the end-effector with the second link. In the system $\mathcal{S}$, passive revolute joints (white circles) connect the end-effectors with the load.

5.2.1.1 I-AUV

The relaxed model of the j-th is written as follows:

$$\begin{aligned} \dot{\boldsymbol{\eta}}_j &= \mathbf{J}_j\left(\boldsymbol{\eta}_j\right)\boldsymbol{\nu}_j, \\ \mathbf{M}_j\dot{\boldsymbol{\nu}}_j &= \mathbf{f}_j\left(\boldsymbol{\eta}_j, \boldsymbol{\nu}_j\right), \end{aligned} \tag{5.9}$$

with

$$\begin{aligned} \mathbf{J}_j &= \text{blkdiag}\left(\mathbf{J}_{j.0}, \mathbf{J}_{j.1}, \mathbf{J}_{j.2}, \mathbf{J}_{j.3}, \mathbf{I}\right), \\ \mathbf{M}_j &= \text{blkdiag}\left(\mathbf{M}_{j.0}, \mathbf{M}_{j.1}, \mathbf{M}_{j.2}, \mathbf{M}_{j.3}, \mathbf{I}_{j.\mathtt{M}}\right), \\ \boldsymbol{\eta}_j &= \left[\boldsymbol{\eta}_{j.0}^{\mathsf{T}}, \boldsymbol{\eta}_{j.1}^{\mathsf{T}}, \boldsymbol{\eta}_{j.2}^{\mathsf{T}}, \boldsymbol{\eta}_{j.3}^{\mathsf{T}}, \boldsymbol{\gamma}_j^{\mathsf{T}}\right]^{\mathsf{T}}, \\ \boldsymbol{\nu}_j &= \left[\boldsymbol{\nu}_{j.0}^{\mathsf{T}}, \boldsymbol{\nu}_{j.1}^{\mathsf{T}}, \boldsymbol{\nu}_{j.2}^{\mathsf{T}}, \boldsymbol{\nu}_{j.3}^{\mathsf{T}}, \dot{\boldsymbol{\gamma}}_j^{\mathsf{T}}\right]^{\mathsf{T}}, \\ \mathbf{f}_j &= \begin{bmatrix} \boldsymbol{\tau}_{j.0} - \mathbf{C}_{j.0}\boldsymbol{\nu}_{j.0} - \mathbf{D}_{j.0}\boldsymbol{\nu}_{j.0} - \mathbf{g}_{j.0} + \mathbf{d}_{j.0} \\ \boldsymbol{\tau}_{j.1} - \mathbf{C}_{j.1}\boldsymbol{\nu}_{j.1} - \mathbf{D}_{j.1}\boldsymbol{\nu}_{j.1} - \mathbf{g}_{j.1} + \mathbf{d}_{j.1} \\ \boldsymbol{\tau}_{j.2} - \mathbf{C}_{j.2}\boldsymbol{\nu}_{j.2} - \mathbf{D}_{j.2}\boldsymbol{\nu}_{j.2} - \mathbf{g}_{j.2} + \mathbf{d}_{j.2} \\ \boldsymbol{\tau}_{j.3} - \mathbf{C}_{j.3}\boldsymbol{\nu}_{j.3} - \mathbf{D}_{j.3}\boldsymbol{\nu}_{j.3} - \mathbf{g}_{j.3} + \mathbf{d}_{j.3} \\ \boldsymbol{\tau}_{j.\mathtt{M}} - \mathbf{B}_{j.\mathtt{M}}\dot{\boldsymbol{\gamma}}_j - \mathbf{C}_{j.\mathtt{M}}\,\text{sign}\left(\dot{\boldsymbol{\gamma}}_j\right) \end{bmatrix}, \end{aligned} \tag{5.10}$$

where $\boldsymbol{\eta}_{j.i} = \left[x_{j.i}, y_{j.i}, \psi_{j.i}\right]^{\mathsf{T}}$ and $\boldsymbol{\nu}_{j.i} = \left[u_{j.i}, v_{j.i}, r_{j.i}\right]^{\mathsf{T}}$ ($i = 0, 1, 2, 3, 4$) are the column-vectors of generalized coordinates and quasi-velocities related to each body of the j-th agent and $\boldsymbol{\gamma}_j = \left[\gamma_{j.1}, \gamma_{j.2}, \gamma_{j.3}\right]^{\mathsf{T}}$ is the column-vector of motors displacements; $\boldsymbol{\tau}_{j.0} = \mathbf{T}_{j.0}\mathbf{u}_{j.0}$ is the column-vector of generalized control forces generated on the vehicle by the thrusters, with $\mathbf{T}_{j.0}$ being the thrusters configuration matrix and $\mathbf{u}_{j.0} = \left[T_{j.1}, T_{j.2}, T_{j.3}\right]^{\mathsf{T}}$ as the column-vector of thrusts; $\boldsymbol{\tau}_{j.\mathtt{M}} = \mathbf{T}_{j.\mathtt{M}}\mathbf{u}_{j.\mathtt{M}}$ is the column-vector of actuation torques generated by the motors on the manipulator joints, with $\mathbf{T}_{j.\mathtt{M}}$ as the gain matrix associated with the motors reduction and $\mathbf{u}_{j.\mathtt{M}} = \left[\tau_{j.1}, \tau_{j.2}\right]^{\mathsf{T}}$ is the column-vector of drive torques generated on the motors shaft which follows the stationary relation between motor current and torque constant; $\boldsymbol{\tau}_{j.i} = \mathbf{0}$ ($i = 1, 2, 3$) once the manipulator

links are actuated by the motors and the end-effector is non-actuated; $\mathbf{g}_{j.i} = \mathbf{0}$ $(i = 0, 1, 2, 3)$ since the motion is performed on the horizontal plane under the hypothesis of using the vertical thrusters of the AUVs to compensate for the forces out-off the horizontal plane.

The matrices $\mathbf{T}_{j.0}$ and $\mathbf{T}_{j.\mathtt{M}}$ follows:

$$\mathbf{T}_{j.0} = \begin{bmatrix} 1 & 1 & 0 \\ 0 & 0 & 1 \\ y_{j.\mathtt{T}} & -y_{j.\mathtt{T}} & 0 \end{bmatrix}; \quad \mathbf{T}_{j.\mathtt{M}} = \begin{bmatrix} N_{j.\mathtt{M}}\eta_{j.\mathtt{M}} & 0 \\ 0 & N_{j.\mathtt{M}}\eta_{j.\mathtt{M}} \\ 0 & 0 \end{bmatrix}, \tag{5.11}$$

where $y_{j.\mathtt{T}}$ is the distance between the thrusters line of action and vehicle center. We should point out that the zero line in $\mathbf{T}_{j.\mathtt{M}}$ is because the motor $j.3$ is non-actuated, acting as a pin used to connect the end-effector with the load.

The constraint associated to the revolute joints of the j-th agent are given by:

$$\boldsymbol{\varphi}_{\mathtt{I},j}\left(\boldsymbol{\eta}_j, t\right) = \begin{bmatrix} x_{j.0} + l_{j.0}\cos\left(\psi_{j.0}\right) - \left(x_{j.1} - l_{j.1}\cos\left(\psi_{j.1}\right)\right) \\ y_{j.0} + l_{j.0}\sin\left(\psi_{j.0}\right) - \left(y_{j.1} - l_{j.1}\sin\left(\psi_{j.1}\right)\right) \\ x_{j.1} + l_{j.1}\cos\left(\psi_{j.1}\right) - \left(x_{j.2} - l_{j.2}\cos\left(\psi_{j.2}\right)\right) \\ y_{j.1} + l_{j.1}\sin\left(\psi_{j.1}\right) - \left(y_{j.2} - l_{j.2}\sin\left(\psi_{j.2}\right)\right) \\ x_{j.2} + l_{j.2}\cos\left(\psi_{j.2}\right) - x_{j.3} \\ y_{j.2} + l_{j.2}\sin\left(\psi_{j.2}\right) - y_{j.3} \\ \psi_{j.3} - \psi_{j.2} \\ \psi_{j.1} - \left(\psi_{j.0} - \gamma_{j.1}\right) \\ \psi_{j.2} - \left(\psi_{j.1} - \gamma_{j.2}\right) \end{bmatrix} = \mathbf{0}, \tag{5.12}$$

where $l_{j.i}$ $(i = 0, 1, 2, 3)$ are the lengths of the bodies of the j-th agent.

5.2.1.2 Load frame

The relaxed model of the load can be written as follows:

$$\begin{aligned} \dot{\boldsymbol{\eta}}_5 &= \mathbf{J}_5\left(\boldsymbol{\eta}_5\right)\boldsymbol{\nu}_5, \\ \mathbf{M}_5\dot{\boldsymbol{\nu}}_5 &= \mathbf{f}_5\left(\boldsymbol{\eta}_5, \boldsymbol{\nu}_5\right), \end{aligned} \tag{5.13}$$

with

$$\begin{aligned} \mathbf{J}_5 &= \text{blkdiag}\left(\mathbf{J}_{1.5}, \mathbf{J}_{2.5}, \mathbf{J}_{3.5}, \mathbf{J}_{4.5}\right), \\ \mathbf{M}_5 &= \text{blkdiag}\left(\mathbf{M}_{1.5}, \mathbf{M}_{2.5}, \mathbf{M}_{3.5}, \mathbf{M}_{4.5}\right), \\ \boldsymbol{\eta}_5 &= \left[\boldsymbol{\eta}_{1.5}^{\mathsf{T}}, \boldsymbol{\eta}_{2.5}^{\mathsf{T}}, \boldsymbol{\eta}_{3.5}^{\mathsf{T}}, \boldsymbol{\eta}_{4.5}^{\mathsf{T}}\right]^{\mathsf{T}}, \\ \boldsymbol{\nu}_5 &= \left[\boldsymbol{\nu}_{1.5}^{\mathsf{T}}, \boldsymbol{\nu}_{2.5}^{\mathsf{T}}, \boldsymbol{\nu}_{3.5}^{\mathsf{T}}, \boldsymbol{\nu}_{4.5}^{\mathsf{T}}\right]^{\mathsf{T}}, \\ \mathbf{f}_5 &= \begin{bmatrix} \boldsymbol{\tau}_{1.5} - \mathbf{C}_{1.5}\boldsymbol{\nu}_{1.5} - \mathbf{D}_{1.5}\boldsymbol{\nu}_{1.5} - \mathbf{g}_{1.5} + \mathbf{d}_{1.5} \\ \boldsymbol{\tau}_{2.5} - \mathbf{C}_{2.5}\boldsymbol{\nu}_{2.5} - \mathbf{D}_{2.5}\boldsymbol{\nu}_{2.5} - \mathbf{g}_{2.5} + \mathbf{d}_{2.5} \\ \boldsymbol{\tau}_{3.5} - \mathbf{C}_{3.5}\boldsymbol{\nu}_{3.5} - \mathbf{D}_{3.5}\boldsymbol{\nu}_{3.5} - \mathbf{g}_{3.5} + \mathbf{d}_{3.5} \\ \boldsymbol{\tau}_{4.5} - \mathbf{C}_{4.5}\boldsymbol{\nu}_{4.5} - \mathbf{D}_{4.5}\boldsymbol{\nu}_{4.5} - \mathbf{g}_{4.5} + \mathbf{d}_{4.5} \end{bmatrix}, \end{aligned} \tag{5.14}$$

where $\boldsymbol{\eta}_{j.5} = \left[x_{j.5}, y_{j.5}, \psi_{j.5}\right]^{\mathsf{T}}$ and $\boldsymbol{\nu}_{j.5} = \left[u_{j.5}, v_{j.5}, r_{j.5}\right]^{\mathsf{T}}$ $(j = 1, \ldots, 4)$ as the column-vectors of generalized coordinates and quasi-velocities associated to each body of the load; $\boldsymbol{\tau}_{j.5} = \mathbf{0}$ and $\mathbf{g}_{j.5} = \mathbf{0}$ since the load is non-actuated and the motion is performed on the horizontal plane.

The constraints related to rigid connections between the load bodies are given by:

$$\boldsymbol{\varphi}_{\text{I},5}\left(\boldsymbol{\eta}_5, t\right) = \begin{bmatrix} x_{1.5} + l_{1.5}\cos\left(\psi_{1.5}\right) - \left(x_{2.5} - l_{2.5}\cos\left(\psi_{2.5}\right)\right) \\ y_{1.5} + l_{1.5}\sin\left(\psi_{1.5}\right) - \left(y_{2.5} - l_{2.5}\sin\left(\psi_{2.5}\right)\right) \\ x_{2.5} + l_{2.5}\cos\left(\psi_{2.5}\right) - \left(x_{3.5} - l_{3.5}\cos\left(\psi_{3.5}\right)\right) \\ y_{2.5} + l_{2.5}\sin\left(\psi_{2.5}\right) - \left(y_{3.5} - l_{3.5}\sin\left(\psi_{3.5}\right)\right) \\ x_{3.5} + l_{3.5}\cos\left(\psi_{3.5}\right) - \left(x_{4.5} - l_{4.5}\cos\left(\psi_{4.5}\right)\right) \\ y_{3.5} + l_{3.5}\sin\left(\psi_{3.5}\right) - \left(y_{4.5} - l_{4.5}\sin\left(\psi_{4.5}\right)\right) \\ x_{4.5} + l_{4.5}\cos\left(\psi_{4.5}\right) - \left(x_{1.5} - l_{1.5}\cos\left(\psi_{1.5}\right)\right) \\ y_{4.5} + l_{4.5}\sin\left(\psi_{4.5}\right) - \left(y_{1.5} - l_{1.5}\sin\left(\psi_{1.5}\right)\right) \\ \psi_{1.5} - \psi_{4.5} - \pi/2 \end{bmatrix} = \mathbf{0}, \tag{5.15}$$

where $l_{j.5}$ are the load lengths.

5.2.1.3 Cooperative transportation

The relaxed model of the 2D cooperative transportation performed with I-AUVs follows:

$$\begin{aligned} \dot{\boldsymbol{\eta}} &= \mathbf{J}(\boldsymbol{\eta})\,\boldsymbol{\nu}, \\ \mathbf{M}\dot{\boldsymbol{\nu}} &= \mathbf{f}(\boldsymbol{\eta}, \boldsymbol{\nu}), \end{aligned} \tag{5.16}$$

with

$$\begin{aligned} \mathbf{J} &= \text{blkdiag}\left(\mathbf{J}_1, \mathbf{J}_2, \mathbf{J}_3, \mathbf{J}_4, \mathbf{J}_5\right), \\ \mathbf{M} &= \text{blkdiag}\left(\mathbf{M}_1, \mathbf{M}_2, \mathbf{M}_3, \mathbf{M}_4, \mathbf{M}_5\right), \\ \boldsymbol{\eta} &= \left[\boldsymbol{\eta}_1^{\mathsf{T}}, \boldsymbol{\eta}_2^{\mathsf{T}}, \boldsymbol{\eta}_3^{\mathsf{T}}, \boldsymbol{\eta}_4^{\mathsf{T}}, \boldsymbol{\eta}_5^{\mathsf{T}}\right]^{\mathsf{T}}, \\ \boldsymbol{\nu} &= \left[\boldsymbol{\nu}_1^{\mathsf{T}}, \boldsymbol{\nu}_2^{\mathsf{T}}, \boldsymbol{\nu}_3^{\mathsf{T}}, \boldsymbol{\nu}_4^{\mathsf{T}}, \boldsymbol{\nu}_5^{\mathsf{T}}\right]^{\mathsf{T}}, \\ \mathbf{f} &= \left[\mathbf{f}_1^{\mathsf{T}}, \mathbf{f}_2^{\mathsf{T}}, \mathbf{f}_3^{\mathsf{T}}, \mathbf{f}_4^{\mathsf{T}}, \mathbf{f}_5^{\mathsf{T}}\right]^{\mathsf{T}}. \end{aligned} \tag{5.17}$$

The constraints between the end-effectors and load are given by:

$$\boldsymbol{\varphi}_{\text{II}}(\boldsymbol{\eta}, t) = \begin{bmatrix} x_{1.3} - (x_{1.5} + l_{1.5}\cos(\psi_{1.5})) \\ y_{1.3} - (y_{1.5} + l_{1.5}\sin(\psi_{1.5})) \\ x_{2.3} - (x_{2.5} + l_{2.5}\cos(\psi_{2.5})) \\ y_{2.3} - (y_{2.5} + l_{2.5}\sin(\psi_{2.5})) \\ x_{3.3} - (x_{3.5} + l_{3.5}\cos(\psi_{3.5})) \\ y_{3.3} - (y_{3.5} + l_{3.5}\sin(\psi_{3.5})) \\ x_{4.3} - (x_{4.5} + l_{4.5}\cos(\psi_{4.5})) \\ y_{4.3} - (y_{4.5} + l_{4.5}\sin(\psi_{4.5})) \\ \gamma_{1.3} - (\psi_{1.3} - \psi_{1.5}) \\ \gamma_{2.3} - (\psi_{2.3} - \psi_{2.5}) \\ \gamma_{3.3} - (\psi_{3.3} - \psi_{3.5}) \\ \gamma_{4.3} - (\psi_{4.3} - \psi_{4.5}) \end{bmatrix} = \mathbf{0}. \tag{5.18}$$

5.2.2 Formation filter based on the servo-constraints formulation

The formation control is applied to the kinematic model of each agent independently, assuming that the formation-keeping objectives correspond to servo-constraints from which the reference values for the control inputs could be directly computed using formulation presented in chapter 4. Thus, let us consider a cooperative system for which a sliding surface variable $\boldsymbol{\sigma}_{\mathrm{sc},j}$ ($j = 1, \ldots, 4$) as proposed by Ianagui (2019) is defined for each agent as a set of servo-constraints, as follows:

$$\boldsymbol{\sigma}_{\mathrm{sc},j} = d_{j,j}\left(\dot{\boldsymbol{\eta}}_j^{\mathrm{L}} + \boldsymbol{\Lambda}_j \boldsymbol{\eta}_j^{\mathrm{L}}\right) - \sum_{k=1}^{n} a_{j,k}\left(\dot{\boldsymbol{\eta}}_k^{\mathrm{L}} + \dot{\boldsymbol{\delta}}_{j,k} + \boldsymbol{\Lambda}_j\left(\boldsymbol{\eta}_k^{\mathrm{L}} + \boldsymbol{\delta}_{j,k}\right)\right) = \mathbf{0}, \tag{5.19}$$

where $d_{j,j}$ is a diagonal entry of the in-degree matrix, standing for the number of vehicles from which the j-th agent receives some communication signal and $a_{j,k}$ is an entry of the adjacency matrix, i.e., $a_{j,k} = 1$ if the j-th agent receives a communication signal from the k-th agent, and $a_{j,k} = 0$, otherwise; $\boldsymbol{\delta}_{j,k}$ stands from the desired offset between the j-th and k-th agents and $\boldsymbol{\Lambda}_j$ is a diagonal matrix whose terms are chosen to control the convergence towards the desired sliding surface. The superscript "L" indicate that the current variable is expressed on the leader body-fixed frame. Let the time derivative of Eq. (5.19) be written as:

$$\dot{\boldsymbol{\sigma}}_{\mathrm{sc},j} = \mathbf{A}_{\mathrm{sc},\boldsymbol{\eta}_j}\ddot{\boldsymbol{\eta}}_j - \mathbf{b}_{\mathrm{sc},\boldsymbol{\eta}_j}, \tag{5.20}$$

with $\mathbf{A}_{\mathrm{sc},\boldsymbol{\eta}_j} = \dfrac{\partial \dot{\boldsymbol{\sigma}}_{\mathrm{sc},j}}{\partial \ddot{\boldsymbol{\eta}}_j}$ and $\mathbf{b}_{\mathrm{sc},\boldsymbol{\eta}_j}$ standing for all the terms in the expression of $\dot{\boldsymbol{\sigma}}_{\mathrm{sc},j}$ which do not depend explicitly on $\boldsymbol{\eta}_j$. Thus, imposing the sliding condition on $\boldsymbol{\sigma}_{\mathrm{sc},j}$, we obtain:

$$\dot{\boldsymbol{\sigma}}_{\mathrm{sc},j} = -\mathbf{L}_j \boldsymbol{\sigma}_{\mathrm{sc},j} - \mathbf{K}_j \operatorname{sign}\left(\boldsymbol{\sigma}_{\mathrm{sc},j}\right) \Rightarrow \mathbf{A}_{\mathrm{sc},j}\ddot{\boldsymbol{\eta}}_j = \mathbf{b}_{\mathrm{sc},j} - \mathbf{L}_j \boldsymbol{\sigma}_{\mathrm{sc},j} - \mathbf{K}_j \operatorname{sign}\left(\boldsymbol{\sigma}_{\mathrm{sc},j}\right). \tag{5.21}$$

Using the kinematic relations between body-fixed and Earth-fixed frames, i.e., $\dot{\boldsymbol{\eta}}_j = \mathbf{J}_j \boldsymbol{\nu}_j$ and $\ddot{\boldsymbol{\eta}}_j = \mathbf{J}_j \dot{\boldsymbol{\nu}}_j + \dot{\mathbf{J}}_j \boldsymbol{\nu}_j$, into Eq. (5.21), we get:

$$\mathbf{A}_{\mathrm{sc},j}\dot{\boldsymbol{\nu}}_j = \mathbf{b}_{\mathrm{sc},j}, \tag{5.22}$$

where $\mathbf{A}_{\mathrm{sc},j} = \mathbf{A}_{\mathrm{sc},\boldsymbol{\eta}_j}\mathbf{J}_j$ and $\mathbf{b}_{\mathrm{sc},j} = \mathbf{b}_{\mathrm{sc},\boldsymbol{\eta}_j} - \mathbf{A}_{\mathrm{sc},\boldsymbol{\eta}_j}\dot{\mathbf{J}}_j\boldsymbol{\nu}_j - \mathbf{L}_j\boldsymbol{\sigma}_{\mathrm{sc},j} - \mathbf{K}_j \operatorname{sign}\left(\boldsymbol{\sigma}_{\mathrm{sc},j}\right)$.

Based on Eq. (4.149), the cooperative reference filter of the j-th can be written as:

$$\begin{aligned} \dot{\boldsymbol{\eta}}_{\mathrm{d},j} &= \mathbf{J}_j \boldsymbol{\nu}_{\mathrm{d},j}, \\ \dot{\boldsymbol{\nu}}_{\mathrm{d},j} &= \mathbf{E}_{\mathrm{sc},j}\dot{\boldsymbol{\nu}}_{0,j} + \mathbf{H}_{\mathrm{sc},j}\mathbf{b}_{\mathrm{sc},j}, \end{aligned} \tag{5.23}$$

where the subscript "d" refers to the desired states and $\dot{\boldsymbol{\nu}}_{0,j}$ is the kinematic model of j-th agent expressed on the body-fixed frame which will be derived in the sequence.

Considers the reference filter of Fossen (1996) expressed on the Earth-fixed frame:

$$\ddot{\boldsymbol{\eta}}_{0,j} = \boldsymbol{\Omega}_j^2 \mathbf{r}_j - 2\mathbf{Z}_j \boldsymbol{\Omega}_j \mathbf{J}_j \boldsymbol{\nu}_{\mathrm{d},j} - \boldsymbol{\Omega}_j^2 \boldsymbol{\eta}_{\mathrm{d},j}, \tag{5.24}$$

where $\boldsymbol{\Omega}_j$ is the matrix of shaping natural frequencies, $\mathbf{Z}_j$ is the matrix of shaping damping factors and $\mathbf{r}_j$ is the column-vector of input references.

Again, using the relations between body-fixed and Earth-fixed frames into Eq. (5.24), we obtain the kinematic model of j-th agent expressed the body-fixed frame as follows:

$$\dot{\boldsymbol{\nu}}_{0,j} = \mathbf{J}_j^{\mathsf{T}} \boldsymbol{\Omega}_j^2 \mathbf{r}_j - \mathbf{J}_j^{\mathsf{T}} \left(\left(2\mathbf{Z}_j \boldsymbol{\Omega}_j \mathbf{J}_j + \dot{\mathbf{J}}_j \right) \boldsymbol{\nu}_{\mathrm{d},j} + \boldsymbol{\Omega}_j^2 \boldsymbol{\eta}_{\mathrm{d},j} \right). \tag{5.25}$$

Substituting Eq. (5.25) into (5.23), we get:

$$\begin{aligned} \dot{\boldsymbol{\eta}}_{\mathrm{d},j} &= \mathbf{J}_j \boldsymbol{\nu}_{\mathrm{d},j}, \\ \dot{\boldsymbol{\nu}}_{\mathrm{d},j} &= \mathbf{F}_{\mathrm{SC},j} \mathbf{J}_j^{\mathsf{T}} \boldsymbol{\Omega}_j^2 \mathbf{r}_j + \mathbf{G}_{\mathrm{SC},j} \mathbf{d}_{0,j} + \mathbf{H}_{\mathrm{SC},j} \mathbf{b}_{\mathrm{SC},j}, \end{aligned} \tag{5.26}$$

where $\mathbf{d}_{0,j} = -\mathbf{J}_j^{\mathsf{T}} \left(\left(2\mathbf{Z}_j \boldsymbol{\Omega}_j \mathbf{J}_j + \dot{\mathbf{J}}_j \right) \boldsymbol{\nu}_{\mathrm{d},j} + \boldsymbol{\Omega}_j^2 \boldsymbol{\eta}_{\mathrm{d},j} \right)$.

From Eqs. (4.146) and (4.150), we have:

$$\begin{aligned} \mathbf{F}_{\mathrm{SC},j} &= \mathbf{G}_{\mathrm{SC},j}, \\ \mathbf{G}_{\mathrm{SC},j} &= \left(\mathbf{I} - \mathbf{K}_{\mathrm{SC},j} \mathbf{C}_{\mathrm{SC},j} \right), \\ \mathbf{H}_{\mathrm{SC},j} &= \mathbf{K}_{\mathrm{SC},j}, \\ \mathbf{C}_{\mathrm{SC},j} &= \mathbf{A}_{\mathrm{SC},j}, \\ \mathbf{K}_{\mathrm{SC},j} &= \mathbf{A}_{\mathrm{SC},j}^{\mathsf{T}} \left(\mathbf{A}_{\mathrm{SC},j} \mathbf{A}_{\mathrm{SC},j}^{\mathsf{T}} \right)^{\mathrm{g}} = \mathbf{A}_{\mathrm{SC},j}^{\mathrm{g}}, \end{aligned} \tag{5.27}$$

with $\mathbf{A}_{\mathrm{SC},j}^{\mathrm{g}}$ being any $\{1, 4\}$-inverse of $\mathbf{A}_{\mathrm{SC},j}$.

Gathering Eqs. (5.19)–(5.27), we get the cooperative reference filter of the j-th agent as follows:

$$\begin{bmatrix} \dot{\boldsymbol{\eta}}_{\mathrm{d},j} \\ \dot{\boldsymbol{\nu}}_{\mathrm{d},j} \end{bmatrix} = \begin{bmatrix} \mathbf{0} & \mathbf{J}_j \\ -\mathbf{G}_{\mathrm{SC},j} \boldsymbol{\Omega}_j^2 & -\mathbf{G}_{\mathrm{SC},j} \mathbf{J}_j^{\mathsf{T}} \left(2\mathbf{Z}_j \boldsymbol{\Omega}_j \mathbf{J}_j + \dot{\mathbf{J}}_j \right) \end{bmatrix} \begin{bmatrix} \boldsymbol{\eta}_{\mathrm{d},j} \\ \boldsymbol{\nu}_{\mathrm{d},j} \end{bmatrix} + \begin{bmatrix} \mathbf{0} \\ \mathbf{F}_{\mathrm{SC},j} \mathbf{J}_j^{\mathsf{T}} \boldsymbol{\Omega}_j^2 \end{bmatrix} \mathbf{r}_j + \begin{bmatrix} \mathbf{0} \\ \mathbf{H}_{\mathrm{SC},j} \end{bmatrix} \mathbf{b}_{\mathrm{SC},j}. \tag{5.28}$$

Let $\mathbf{x}_{\mathrm{d},j} = \left[\boldsymbol{\eta}_{\mathrm{d},j}^{\mathsf{T}}, \boldsymbol{\nu}_{\mathrm{d},j}^{\mathsf{T}} \right]^{\mathsf{T}}$ and $\mathbf{r}_j$ be the states and the control input column-vectors, respectively. Thus, the following state-space model can be written based on Eq (5.28):

$$\begin{aligned} \dot{\mathbf{x}}_{\mathrm{d},j} &= \mathbf{E}_j \mathbf{x}_{\mathrm{d},j} + \mathbf{F}_j \mathbf{r}_j + \mathbf{H}_j \mathbf{b}_{\mathrm{SC},j}, \\ \mathbf{y}_{\mathrm{d},j} &= \mathbf{x}_{\mathrm{d},j}, \end{aligned} \tag{5.29}$$

where

$$\mathbf{E}_j = \begin{bmatrix} \mathbf{0} & \mathbf{J}_j \\ -\mathbf{G}_{\mathrm{SC},j}\boldsymbol{\Omega}_j^2 & -\mathbf{G}_{\mathrm{SC},j}\mathbf{J}_j^{\intercal}\left(2\mathbf{Z}_j\boldsymbol{\Omega}_j\mathbf{J}_j + \dot{\mathbf{J}}_j\right) \end{bmatrix}; \quad \mathbf{F}_j = \begin{bmatrix} \mathbf{0} \\ \mathbf{F}_{\mathrm{SC},j}\mathbf{J}_j^{\intercal}\boldsymbol{\Omega}_j^2 \end{bmatrix}; \quad \mathbf{H}_j = \begin{bmatrix} \mathbf{0} \\ \mathbf{H}_{\mathrm{SC},j} \end{bmatrix}. \tag{5.30}$$

The state-space model of Eq. (5.29) is the input into the MPC of Eq. (4.164) to obtain the predictive-cooperative reference filter. Furthermore, the state-space model of Eq. (5.29) can be numerical integrated directly to generate the reference for the j-th agent without a predictive action.

5.2.3 Results

The predictive-cooperative reference filter developed for the 2D cooperative transportation with I-AUVs was tested on the trajectory tracking problem. The block diagram of the complete coordination scheme is shown by Fig. 95.

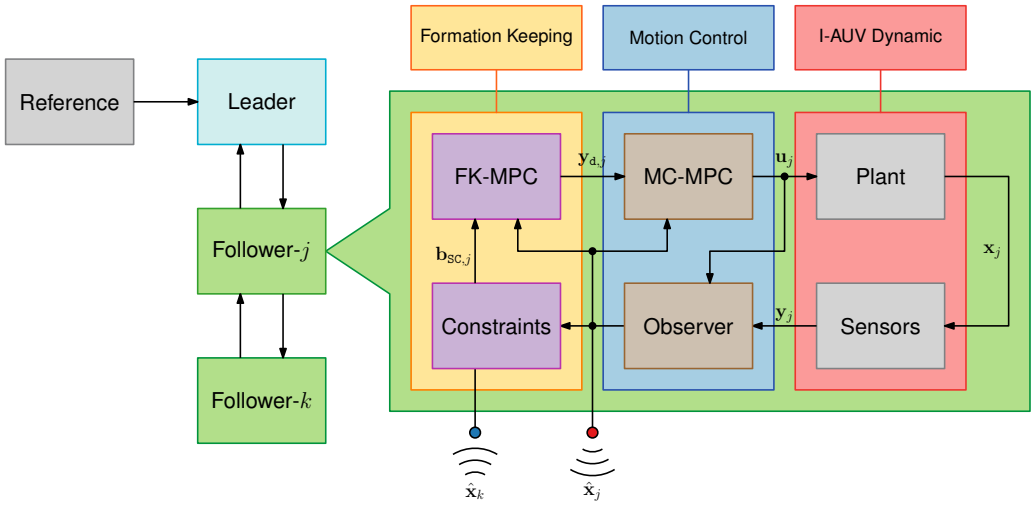

Figure 95: Cooperative MPC block diagram

In Fig. 95, the block diagram of the j-th agent is comprised by three sub-blocks:

- **Formation keeping**: constituted by the predictive-cooperative reference filter to generates the desired states to be tracked according to the formation requirements;
- **Motion control**: referring to the low-level MPC with augmented observer, similar to one presented by Oliveira, Orsino and Donha (2021), which is used to generate the commanded thrusts and torques in order to track the filter references and compensate for modeling errors and disturbances;

- **I-AUV dynamics**: representing the model of the 2D cooperative transportation and the sensor measurements specified before.

The simulation is performed using the previous specified setup. The modeling and control parameters are shown by Tabs. 13–15.

The formations matrices referring to the undirected graph of Fig. 91 follow:

$$\mathbf{A}_{\text{FK}} = \begin{bmatrix} 0 & 0 & 0 & 0 & 0 \\ 1 & 0 & 1 & 0 & 1 \\ 1 & 1 & 0 & 1 & 0 \\ 1 & 0 & 1 & 0 & 1 \\ 1 & 1 & 0 & 1 & 0 \end{bmatrix}; \quad \mathbf{D}_{\text{FK}} = \begin{bmatrix} 0 & 0 & 0 & 0 & 0 \\ 0 & 3 & 0 & 0 & 0 \\ 0 & 0 & 3 & 0 & 0 \\ 0 & 0 & 0 & 3 & 0 \\ 0 & 0 & 0 & 0 & 3 \end{bmatrix}. \tag{5.31}$$

The off-sets between the j-th and the k-th agent, $\boldsymbol{\delta}_{j,k}$ ($j = 1, \ldots, 4; k = 1, \ldots, 4$), are grouped as follows:

$$\begin{aligned} \boldsymbol{\delta}_1 &= [\boldsymbol{\delta}_{1,\text{L}}, \boldsymbol{\delta}_{1,1}, \boldsymbol{\delta}_{1,2}, \boldsymbol{\delta}_{1,3}, \boldsymbol{\delta}_{1,4}]; \quad \boldsymbol{\delta}_2 = [\boldsymbol{\delta}_{2,\text{L}}, \boldsymbol{\delta}_{2,1}, \boldsymbol{\delta}_{2,2}, \boldsymbol{\delta}_{2,3}, \boldsymbol{\delta}_{2,4}], \\ \boldsymbol{\delta}_3 &= [\boldsymbol{\delta}_{3,\text{L}}, \boldsymbol{\delta}_{3,1}, \boldsymbol{\delta}_{3,2}, \boldsymbol{\delta}_{3,3}, \boldsymbol{\delta}_{3,4}]; \quad \boldsymbol{\delta}_4 = [\boldsymbol{\delta}_{4,\text{L}}, \boldsymbol{\delta}_{4,1}, \boldsymbol{\delta}_{4,2}, \boldsymbol{\delta}_{4,3}, \boldsymbol{\delta}_{4,4}], \end{aligned} \tag{5.32}$$

where the subscript "L" refers to the virtual leader.

The off-sets values in the form of Eq. (5.32) are given by (in meters and radians):

$$\begin{aligned} \boldsymbol{\delta}_1 &= \begin{bmatrix} 2 & 0 & 4 & 0 & 0 \\ -2 & 0 & 0 & 0 & -4 \\ 3\pi/4 & 0 & 0 & 0 & 0 \end{bmatrix}; \quad \boldsymbol{\delta}_2 = \begin{bmatrix} -2 & -4 & 0 & 0 & 0 \\ -2 & 0 & 0 & -4 & 0 \\ \pi/4 & 0 & 0 & 0 & 0 \end{bmatrix}, \\ \boldsymbol{\delta}_3 &= \begin{bmatrix} -2 & 0 & 0 & 0 & -4 \\ 2 & 0 & 4 & 0 & 0 \\ -\pi/4 & 0 & 0 & 0 & 0 \end{bmatrix}; \quad \boldsymbol{\delta}_4 = \begin{bmatrix} 2 & 0 & 0 & 4 & 0 \\ 2 & 4 & 0 & 0 & 0 \\ 5\pi/4 & 0 & 0 & 0 & 0 \end{bmatrix}. \end{aligned} \tag{5.33}$$

Let $\mathbf{q}_{\text{E},j}\left(\boldsymbol{\eta}_{j.0}, \boldsymbol{\gamma}_j\right)$ be a function to calculate the end-effector coordinates of the j-th agent on the Earth-fixed frame using the vehicle coordinates and the manipulator joints angles. Also, let $\mathbf{q}_{\text{E},j.5}\left(\boldsymbol{\eta}_{j.5}\right)$ be a function to calculate the coordinates of the load vertices connected to the j-th agent with the load coordinates such that $\tilde{\mathbf{q}}_{\text{E},j}\left(\boldsymbol{\eta}_{j.0}, \boldsymbol{\gamma}_j, \boldsymbol{\eta}_{j.5}\right) = \mathbf{q}_{\text{E},j}\left(\boldsymbol{\eta}_{j.0}, \boldsymbol{\gamma}_j\right) - \mathbf{q}_{\text{E},j.5}\left(\boldsymbol{\eta}_{j.5}\right) = \mathbf{0}$. To actively use the manipulator during the transportation, the following set of servo-constraints are added on the sliding surface of the formation control:

$$\dot{\boldsymbol{\varphi}}_{\text{SC},j}\left(\ddot{\mathbf{q}}_{\text{E},j}, \dot{\mathbf{q}}_{\text{E},j}, \mathbf{q}_{\text{E},j}, t\right) = \ddot{\tilde{\mathbf{q}}}_{\text{E},j} + \lambda_j \dot{\tilde{\mathbf{q}}}_{\text{E},j} + k_j \tilde{\mathbf{q}}_{\text{E},j} = \mathbf{0}, \tag{5.34}$$

where $\lambda_j > 0$ and $k_j > 0$ are stabilization coefficients.

Table 13: 5-DoFs Twin-Burger I-AUVs and load model parameters

Symbols ($i = 1, 2$)	Values	Units (SI)
$\mathbf{M}_{\mathrm{RB},0}$	diag (120, 120, 1.33)	kg, kgm^2
$\mathbf{M}_{\mathrm{RB},1}$	diag (6, 6, 0.19)	kg, kgm^2
$\mathbf{M}_{\mathrm{RB},2}$	diag (6, 6, 0.012)	kg, kgm^2
$\mathbf{M}_{\mathrm{RB},3}$	diag (38.34, 38.34, 0.35)	kg, kgm^2
$\mathbf{M}_{\mathrm{RB},5}$	diag (38.34, 38.34, 0.35)	kg, kgm^2
$\mathbf{M}_{\mathrm{A},0}$	diag (191.90, 320.10, 29.40)	kg, kgm^2
$\mathbf{M}_{\mathrm{A},1}$	diag (2, 5.6, 0.45)	kg, kgm^2
$\mathbf{M}_{\mathrm{A},2}$	diag (4, 5.6, 0.024)	kg, kgm^2
$\mathbf{M}_{\mathrm{A},3}$	diag (7.07, 7.07, 0)	kg, kgm^2
$\mathbf{M}_{\mathrm{A},5}$	diag (7.07, 7.07, 0)	kg, kgm^2
$\mathbf{D}_0$	diag (150.30, 338.40, 1.56)	Ns/m, Nms
$C_{\mathrm{D},\mathrm{x}_1}, C_{\mathrm{D},\mathrm{y}_1}, \delta_1$	0, 1.2, 0.001	–
$C_{\mathrm{D},\mathrm{x}_2}, C_{\mathrm{D},\mathrm{y}_2}, \delta_2$	0, 1.2, 0.001	–
$\mathbf{D}_3$	diag(17.67, 17.67, 0)	Ns/m, Nms
$2l_1, d_1, \Delta l_1$	0.5, 0.12, 0.025	m
$2l_2, d_2, \Delta l_2$	0.5, 0.12, 0.025	m
$2l_5, d_5, \Delta l_5$	4, 0.20, 0.20	m
$\vec{\mathbf{p}}^{0}_{\mathrm{G}_0\vert\mathrm{O}_0}$	$[0, 0, 0]^{\mathsf{T}}$	m
$\vec{\mathbf{p}}^{1}_{\mathrm{G}_1\vert\mathrm{O}_1}$	$[0, 0, 0]^{\mathsf{T}}$	m
$\vec{\mathbf{p}}^{2}_{\mathrm{G}_2\vert\mathrm{O}_2}$	$[0, 0, 0]^{\mathsf{T}}$	m
$\vec{\mathbf{p}}^{3}_{\mathrm{G}_3\vert\mathrm{O}_3}$	$[0, 0, 0]^{\mathsf{T}}$	m
$\vec{\mathbf{p}}^{5}_{\mathrm{G}_5\vert\mathrm{O}_5}$	$[0, 0, 0]^{\mathsf{T}}$	m
$N_{\mathtt{M}}, \eta_{\mathtt{M}}$	10, 0.9	–
$b_{\mathtt{M}}, c_{\mathtt{M}}$	1, 0.1	Nms, Nm

Table 14: 5-DoFs Twin-Burger I-AUVs formation filter parameters

Symbols	Values	Units (SI)
$\mathbf{M}$	diag(1000, 1000, 1, 1, 1)	kg, kgm^2
$\mathbf{\Omega}$	diag(0.20π, 0.20π, 0.20π, 0.20π, 0.20π)	rad/s
$\mathbf{Z}$	diag(1, 1, 1, 1, 1)	-
$\mathbf{T}$	diag(0.1, 0.1, 0.1, 0.1, 0.1)	1/s
$\mathbf{\Lambda}$	diag(0.1, 0.1, 0.1, 0.1, 0.1)	1/s
$\mathbf{K}$	diag(10, 10, 10, 10, 10)	m/s^2, rad/s^2
$\mathbf{L}$	diag(100, 100, 100, 100, 100)	1/s
ϵ	1	-
$\mathbf{Q}_{\mathbf{Y}}$	blkdiag($\mathbf{Q}_{\mathbf{Y},\boldsymbol{\eta}}$, $\mathbf{Q}_{\mathbf{Y},\boldsymbol{\nu}}$, $\mathbf{Q}_{\mathbf{Y},\dot{\boldsymbol{\nu}}}$)	-
$\mathbf{Q}_{\mathbf{Y},\boldsymbol{\eta}}$	diag(0, 0, 0, 0, 0)	-
$\mathbf{Q}_{\mathbf{Y},\boldsymbol{\nu}}$	diag(1000, 1000, 1000, 1000, 1000)	-
$\mathbf{Q}_{\mathbf{Y},\dot{\boldsymbol{\nu}}}$	diag(10000, 10000, 10000, 10000, 10000)	-
$\mathbf{R}_{\mathbf{U}_{\#}}$	diag(1, 1, 1, 1, 1)	-
T_{s}	0.01	s
p, c	100, 20	-
λ, k	10, 100	1/s, 1/s^2

Table 15: 5-DoFs Twin-Burger I-AUVs low-level control parameters

Symbols	Values	Units (SI)
$\mathbf{Q}_{\mathbf{Y}}$	diag (1000, 1000, 1000, 1000, 1000)	-
$\mathbf{R}_{\mathbf{U}_{\#,j}}$	diag (1, 1, 1, 1, 1)	-
T_{s}	0.1	s
p, c	20, 10	-

Figure 96 shows the reference displacements, velocities and accelerations generated by the predictive-cooperative reference filters. As we can see, the references are smooth and continuous due to the velocities penalization on the optimization and the choice of shaping parameters for the kinematic filter. The commanded control inputs generated during the trajectory tracking are shown in Fig. 97. The noisy profiles for the thrusts and torques calculated by the low-level MPC are due to the sensors noise and sampling effects. Also, some saturation is due to the modeling errors and disturbances associated with the load dynamics and ocean current effects. Despite this, the control remains stable during the simulation, even when the load should be stopped on the final instants and the dry friction arises on the manipulator joints due to the velocity switch. Fig. 98 shows the trajectory tracking of the load. In Fig. 98 (a), we can see the path tracking obtained. Despite some significant errors in the medium of the trajectory due to modeling errors and disturbances, the track performance remains acceptable. The same behavior is observed on the coordinates tracking shown by Fig. 98 (b). Figure 99 shows a couple of animation frames of the 2D cooperative transportation with I-AUVs to illustrate the motion performed during the trajectory tracking.

The modeling and servo-constraints are shown in Fig. 100. These results are significant once they are related to the modeling and to the predictive-cooperative reference filter consistency. For example, the modeling and the servo-constraints order are 10^{-7} and 10^{-6}, respectively. These small values are due to the numerical stability of the model and of the predictive-cooperative reference filter, even in the presence of modeling errors and disturbances.

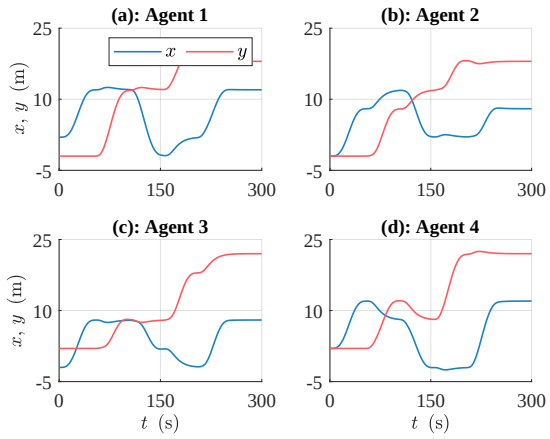

(a): Linear displacements

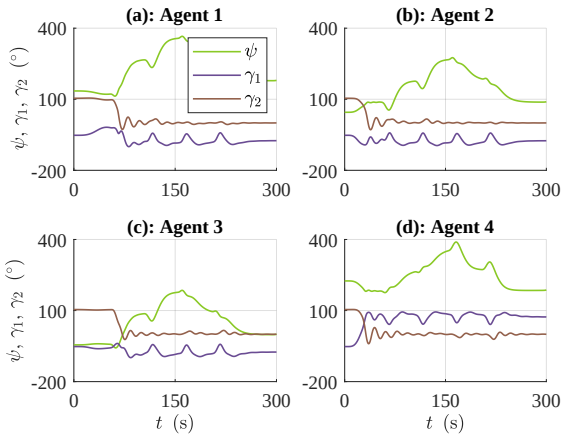

(b): Angular displacements

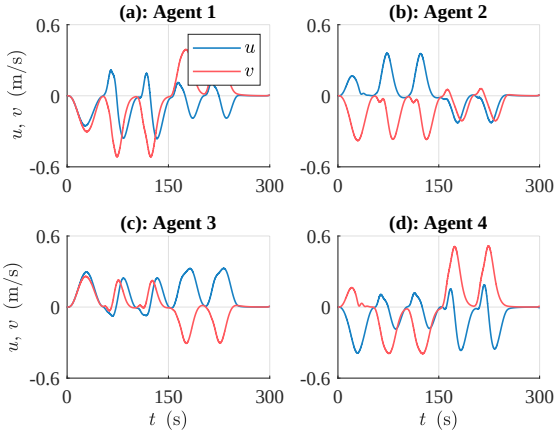

(c): Linear velocities

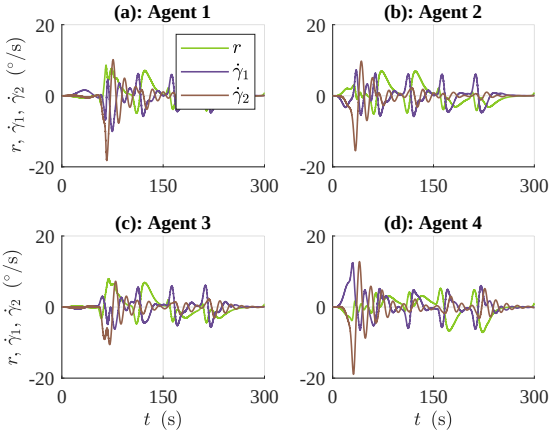

(d): Angular velocities

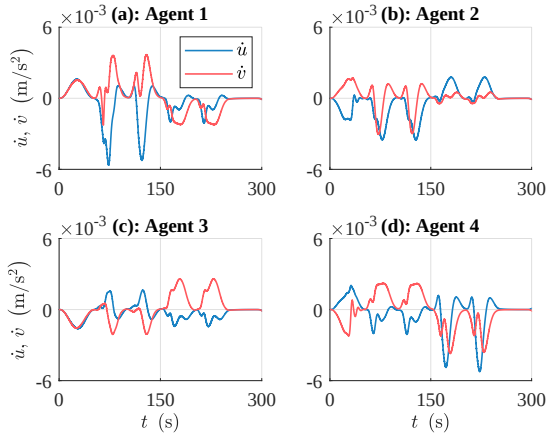

(e): Linear accelerations

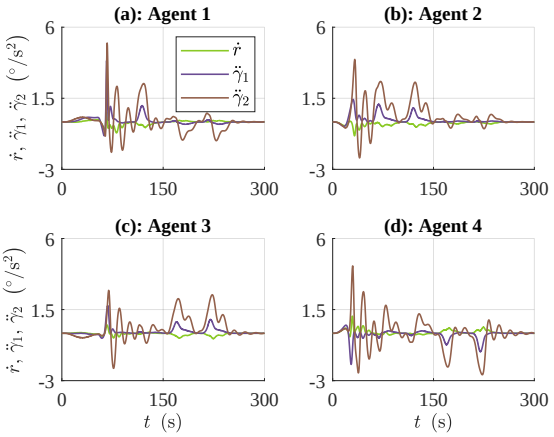

(f): Angular accelerations

Figure 96: Agents references on the 2D horizontal transportation with I-AUVs

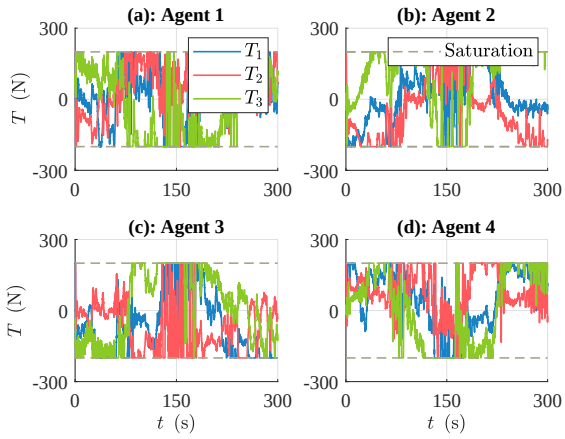

(a): Thrusts

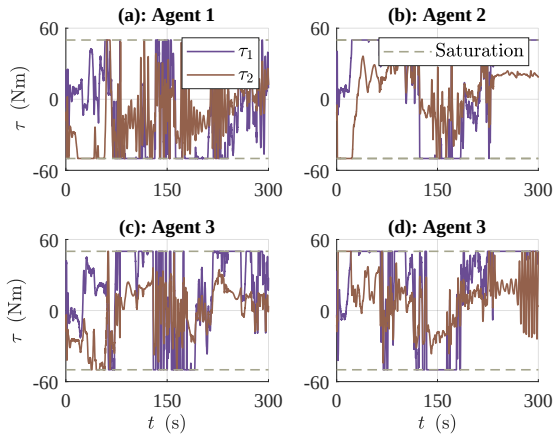

(b): Torques

Figure 97: Agents control on the 2D horizontal cooperative transportation with I-AUVs

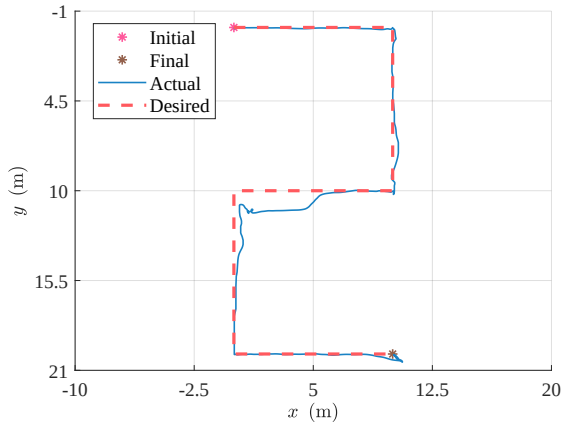

(a): Path

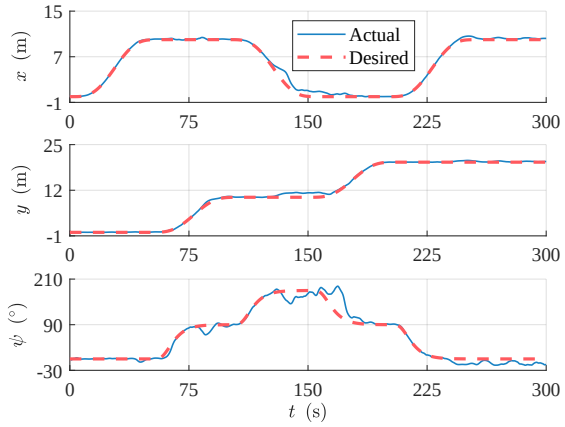

(b): Displacements

Figure 98: Load tracking on the 2D cooperative transportation with I-AUVs

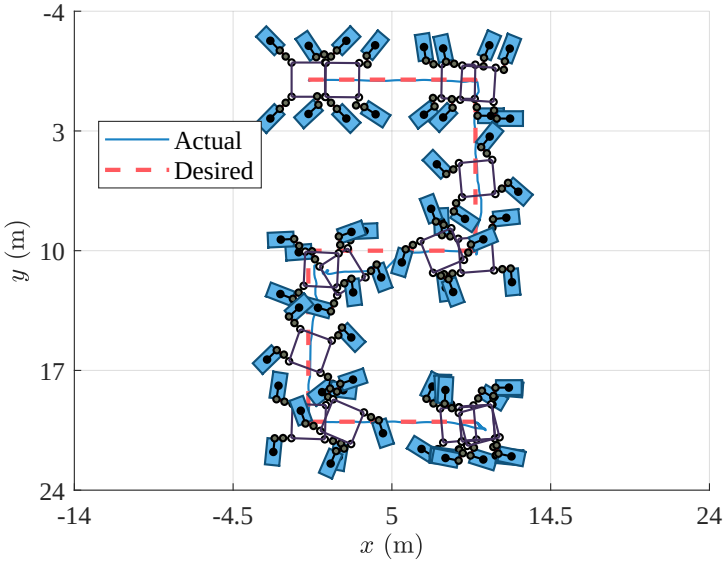

Figure 99: Frames of the 2D horizontal cooperative transportation with I-AUVs

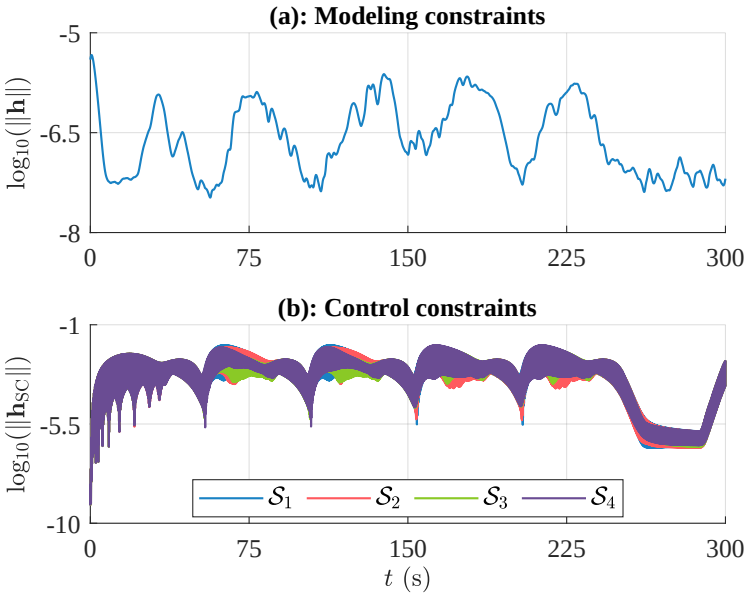

Figure 100: Constraints of the 2D horizontal cooperative transportation with I-AUVs

5.3 3D COOPERATIVE TRANSPORTATION WITH MODULAR ROVs

5.3.1 Modeling

Figure 101 (a) show the model of the 3D cooperative transportation with modular ROVs. The system comprises four modular ROVs transporting a rigid block of aluminum. The ROVs are based on the BlueROV 2 equipped with a support frame of stainless steel to attach the load. This case is inspired by the works of Nielsen (NIELSEN et al., 2016; NIELSEN; BLANKE; SCHJØLBERG, 2016; NIELSEN; JOHANSEN; BLANKE, 2018; NIELSEN et al., 2018), who studied the application of the Udwadia-Kalaba equation on the modeling of modular UUVs.

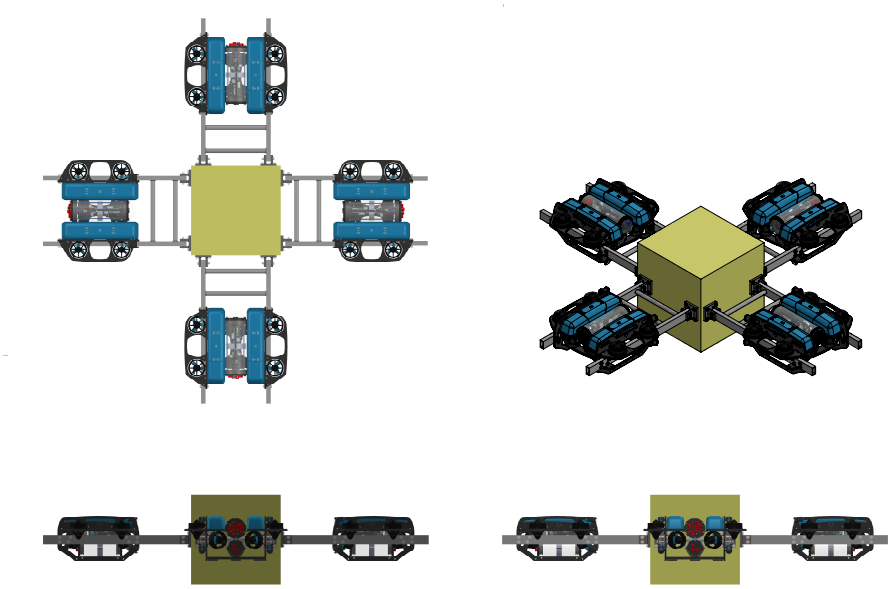

(a): 3D cooperative transportation system

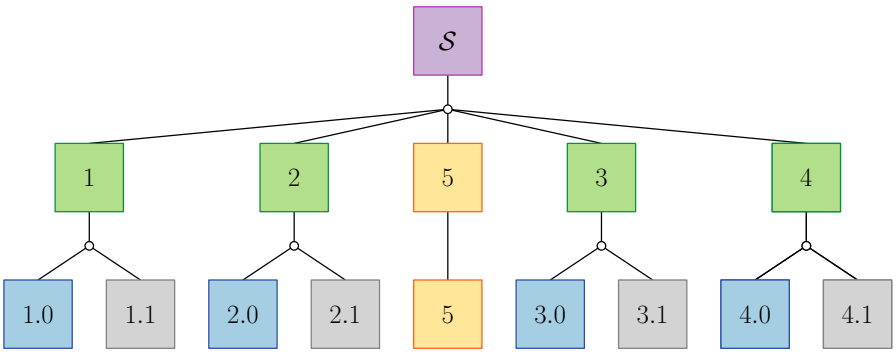

(b): Modeling hierarchy

Figure 101: 3D cooperative transportation with modular ROVs

In the modeling hierarchy of Fig. 101 (b), the j-th agent ($j = 1, \ldots, 4$) is constituted by the bodies 0 and 1, where the body $j.0$ is the ROV and body $j.1$ stands for the support. The agent 5 represents the load which is constituted by one single body. For the j-th agent ($j = 1, \ldots, 4$) subsystems, rigid joints (white circles) connect the ROV with the support. In system $\mathcal{S}$, rigid joints (white circle) are used again to connect the agents with the load.

5.3.1.1 Modular ROV

The relaxed model of the j-th can be written as follows:

$$\begin{aligned} \dot{\boldsymbol{\eta}}_j &= \mathbf{J}_j\left(\boldsymbol{\eta}_j\right)\boldsymbol{\nu}_j, \\ \mathbf{M}_j\dot{\boldsymbol{\nu}}_j &= \mathbf{f}_j\left(\boldsymbol{\eta}_j, \boldsymbol{\nu}_j\right), \end{aligned} \tag{5.35}$$

where

$$\begin{aligned} \mathbf{J}_j &= \text{blkdiag}\left(\mathbf{J}_{j.0}, \mathbf{J}_{j.1}\right), \\ \mathbf{M}_j &= \text{blkdiag}\left(\mathbf{M}_{j.0}, \mathbf{M}_{j.1}\right), \\ \boldsymbol{\eta}_j &= \left[\boldsymbol{\eta}_{j.0}^{\mathsf{T}}, \boldsymbol{\eta}_{j.1}^{\mathsf{T}}\right]^{\mathsf{T}}, \\ \boldsymbol{\nu}_j &= \left[\boldsymbol{\nu}_{j.0}^{\mathsf{T}}, \boldsymbol{\nu}_{j.1}^{\mathsf{T}}\right]^{\mathsf{T}}, \\ \mathbf{f}_j &= \begin{bmatrix} \boldsymbol{\tau}_{j.0} - \mathbf{C}_{j.0}\boldsymbol{\nu}_{j.0} - \mathbf{D}_{j.0}\boldsymbol{\nu}_{j.0} - \mathbf{g}_{j.0} + \mathbf{d}_{j.0} \\ \boldsymbol{\tau}_{j.1} - \mathbf{C}_{j.1}\boldsymbol{\nu}_{j.1} - \mathbf{D}_{j.1}\boldsymbol{\nu}_{j.1} - \mathbf{g}_{j.1} + \mathbf{d}_{j.1} \end{bmatrix}, \end{aligned} \tag{5.36}$$

where $\boldsymbol{\eta}_{j.i} = \left[\boldsymbol{\eta}_{1,j.i}^{\mathsf{T}}, \boldsymbol{\eta}_{2,j.i}^{\mathsf{T}}\right]^{\mathsf{T}}$ and $\boldsymbol{\nu}_{j.i} = \left[\boldsymbol{\nu}_{1,j.i}^{\mathsf{T}}, \boldsymbol{\nu}_{2,j.i}^{\mathsf{T}}\right]^{\mathsf{T}}$ ($i = 0, 1$) are the column-vectors of generalized coordinates and quasi-velocities related to each body of the j-th agent, with $\boldsymbol{\eta}_{1,j.i} = \left[x_{j.i}, y_{j.i}, z_{j.i}\right]^{\mathsf{T}}$, $\boldsymbol{\eta}_{2,j.i} = \left[\phi_{j.i}, \theta_{j.i}, \psi_{j.i}\right]^{\mathsf{T}}$, $\boldsymbol{\nu}_{1,j.i} = \left[u_{j.i}, v_{j.i}, w_{j.i}\right]^{\mathsf{T}}$ and $\boldsymbol{\nu}_{2,j.i} = \left[p_{j.i}, q_{j.i}, r_{j.i}\right]^{\mathsf{T}}$; $\boldsymbol{\tau}_{j.0} = \mathbf{T}_{j.0}\mathbf{u}_{j.0}$ is the column-vector of generalized control forces generated on the vehicle by the thrusters, with $\mathbf{T}_{j.0}$ as the thrusters configuration matrix and $\mathbf{u}_{j.0} = \left[T_{j.1}, \ldots, T_{j.8}\right]^{\mathsf{T}}$ as the column-vector of thrusts.

According to Wu (2018), the matrix $\mathbf{T}_{j.0}$ of the BlueROV 2 is (in SI units):

$$\mathbf{T}_{j.0} = \begin{bmatrix} 0.71 & 0.71 & -0.71 & -0.71 & 0 & 0 & 0 & 0 \\ -0.71 & 0.71 & -0.71 & 0.71 & 0 & 0 & 0 & 0 \\ 0 & 0 & 0 & 0 & -1 & 1 & 1 & -1 \\ 0.06 & -0.06 & 0.06 & -0.06 & -0.22 & -0.22 & 0.22 & 0.22 \\ 0.06 & 0.06 & -0.06 & -0.06 & 0.12 & -0.12 & 0.12 & -0.12 \\ -0.19 & 0.19 & 0.19 & -0.19 & 0 & 0 & 0 & 0 \end{bmatrix}. \tag{5.37}$$

The constraints related to the rigid joints of the j-th agent are written as:

$$
\begin{aligned}
\boldsymbol{\varphi}_{\mathrm{I},1}\left(\boldsymbol{\eta}_1, t\right) &= \begin{bmatrix} x_{1.0} - x_{1.1} - l_1 \cos\left(\psi_{1.0}\right) \cos\left(\theta_{1.0}\right) \\ y_{1.0} - y_{1.1} - l_1 \cos\left(\theta_{1.0}\right) \sin\left(\psi_{1.0}\right) \\ z_{1.0} - z_{1.1} + l_1 \sin\left(\theta_{1.0}\right) \\ \phi_{1.0} - \phi_{1.1} \\ \theta_{1.0} - \theta_{1.1} \\ \psi_{1.0} - \psi_{1.1} \end{bmatrix} = \mathbf{0}, \\
\boldsymbol{\varphi}_{\mathrm{I},2}\left(\boldsymbol{\eta}_2, t\right) &= \begin{bmatrix} x_{2.0} - x_{2.1} - l_2 \left(\cos\left(\phi_{2.0}\right) \sin\left(\psi_{2.0}\right) - \cos\left(\psi_{2.0}\right) \sin\left(\phi_{2.0}\right) \sin\left(\theta_{2.0}\right)\right) \\ y_{2.0} - y_{2.1} + l_2 \left(\cos\left(\phi_{2.0}\right) \cos\left(\psi_{2.0}\right) + \sin\left(\phi_{2.0}\right) \sin\left(\psi_{2.0}\right) \sin\left(\theta_{2.0}\right)\right) \\ z_{2.0} - z_{2.1} + l_2 \cos\left(\theta_{2.0}\right) \sin\left(\phi_{2.0}\right) \\ \phi_{2.0} - \phi_{2.1} \\ \theta_{2.0} - \theta_{2.1} \\ \psi_{2.0} - \psi_{2.1} \end{bmatrix} = \mathbf{0}, \\
\boldsymbol{\varphi}_{\mathrm{I},3}\left(\boldsymbol{\eta}_3, t\right) &= \begin{bmatrix} x_{3.0} - x_{3.1} + l_3 \cos\left(\psi_{3.0}\right) \cos\left(\theta_{3.0}\right) \\ y_{3.0} - y_{3.1} + l_3 \cos\left(\theta_{3.0}\right) \sin\left(\psi_{3.0}\right) \\ z_{3.0} - z_{3.1} - l_3 \sin\left(\theta_{3.0}\right) \\ \phi_{3.0} - \phi_{3.1} \\ \theta_{3.0} - \theta_{3.1} \\ \psi_{3.0} - \psi_{3.1} \end{bmatrix} = \mathbf{0}, \\
\boldsymbol{\varphi}_{\mathrm{I},4}\left(\boldsymbol{\eta}_4, t\right) &= \begin{bmatrix} x_{4.0} - x_{4.1} + l_4 \left(\cos\left(\phi_{4.0}\right) \sin\left(\psi_{4.0}\right) - \cos\left(\psi_{4.0}\right) \sin\left(\phi_{4.0}\right) \sin\left(\theta_{4.0}\right)\right) \\ y_{4.0} - y_{4.1} - l_4 \left(\cos\left(\phi_{4.0}\right) \cos\left(\psi_{4.0}\right) + \sin\left(\phi_{4.0}\right) \sin\left(\psi_{4.0}\right) \sin\left(\theta_{4.0}\right)\right) \\ z_{4.0} - z_{4.1} - l_4 \cos\left(\theta_{4.0}\right) \sin\left(\phi_{4.0}\right) \\ \phi_{4.0} - \phi_{4.1} \\ \theta_{4.0} - \theta_{4.1} \\ \psi_{4.0} - \psi_{4.1} \end{bmatrix} = \mathbf{0},
\end{aligned}
\tag{5.38}
$$

where l_j are the lengths defined between the centers of the bodies (ROVs and supports).

5.3.1.2 Cooperative transportation

The relaxed model of the 3D cooperative transportation with modular ROVs is written as:

$$
\begin{aligned}
\dot{\boldsymbol{\eta}} &= \mathbf{J}\left(\boldsymbol{\eta}\right) \boldsymbol{\nu}, \\
\mathbf{M}\dot{\boldsymbol{\nu}} &= \mathbf{f}\left(\boldsymbol{\eta}, \boldsymbol{\nu}\right),
\end{aligned}
\tag{5.39}
$$

with

$$\begin{aligned}
\mathbf{J} &= \text{blkdiag}\left(\mathbf{J}_1, \mathbf{J}_2, \mathbf{J}_3, \mathbf{J}_4, \mathbf{J}_5\right), \\
\mathbf{M} &= \text{blkdiag}\left(\mathbf{M}_1, \mathbf{M}_2, \mathbf{M}_3, \mathbf{M}_4, \mathbf{M}_5\right), \\
\boldsymbol{\eta} &= \left[\boldsymbol{\eta}_1^\mathsf{T}, \boldsymbol{\eta}_2^\mathsf{T}, \boldsymbol{\eta}_3^\mathsf{T}, \boldsymbol{\eta}_4^\mathsf{T}, \boldsymbol{\eta}_5^\mathsf{T}\right]^\mathsf{T}, \\
\boldsymbol{\nu} &= \left[\boldsymbol{\nu}_1^\mathsf{T}, \boldsymbol{\nu}_2^\mathsf{T}, \boldsymbol{\nu}_3^\mathsf{T}, \boldsymbol{\nu}_4^\mathsf{T}, \boldsymbol{\nu}_5^\mathsf{T}\right]^\mathsf{T}, \\
\mathbf{f} &= \left[\mathbf{f}_1^\mathsf{T}, \mathbf{f}_2^\mathsf{T}, \mathbf{f}_3^\mathsf{T}, \mathbf{f}_4^\mathsf{T}, \mathbf{f}_5^\mathsf{T}\right]^\mathsf{T}, \\
\boldsymbol{\varphi}_{\text{II}} &= \left[\boldsymbol{\varphi}_{\text{II},1}^\mathsf{T}, \boldsymbol{\varphi}_{\text{II},2}^\mathsf{T}, \boldsymbol{\varphi}_{\text{II},3}^\mathsf{T}, \boldsymbol{\varphi}_{\text{II},4}^\mathsf{T}\right]^\mathsf{T},
\end{aligned} \tag{5.40}$$

where $\boldsymbol{\eta}_5 = \left[\boldsymbol{\eta}_{1,5}^\mathsf{T}, \boldsymbol{\eta}_{2,5}^\mathsf{T}\right]^\mathsf{T}$ and $\boldsymbol{\nu}_5 = \left[\boldsymbol{\nu}_{1,5}^\mathsf{T}, \boldsymbol{\nu}_{2,5}^\mathsf{T}\right]^\mathsf{T}$ are the column-vectors of generalized coordinates and quasi-velocities associated to the load, with $\boldsymbol{\eta}_{1,5} = [x_5, y_5, z_5]^\mathsf{T}$, $\boldsymbol{\eta}_{2,5} = [\phi_5, \theta_5, \psi_5]^\mathsf{T}$, $\boldsymbol{\nu}_{1,5} = [u_5, v_5, w_5]^\mathsf{T}$ and $\boldsymbol{\nu}_{2,5} = [p_5, q_5, r_5]^\mathsf{T}$, while $\mathbf{f}_5 = \boldsymbol{\tau}_5 - \mathbf{C}_5\boldsymbol{\nu}_5 - \mathbf{D}_5\boldsymbol{\nu}_5 - \mathbf{g}_5 + \mathbf{d}_5$ with $\boldsymbol{\tau}_5 = \mathbf{0}$ once the load is non-actuated.

The constraints related to the rigid joints between the supports and load are given by:

$$
\begin{aligned}
\boldsymbol{\varphi}_{\mathrm{II},1}(\boldsymbol{\eta},t) &= \begin{bmatrix} x_{1.1} - x_5 - l_5\cos(\psi_{1.1})\cos(\theta_{1.1}) \\ y_{1.1} - y_5 - l_5\cos(\theta_{1.1})\sin(\psi_{1.1}) \\ z_{1.1} - z_5 + l_5\sin(\theta_{1.1}) \\ \phi_{1.1} - \phi_5 \\ \theta_{1.1} - \theta_5 \\ \psi_{1.1} - \psi_5 \end{bmatrix} = \mathbf{0}, \\
\boldsymbol{\varphi}_{\mathrm{II},2}(\boldsymbol{\eta},t) &= \begin{bmatrix} x_{2.1} - x_5 - l_6(\cos(\phi_{2.1})\sin(\psi_{2.1}) - \cos(\psi_{2.1})\sin(\phi_{2.1})\sin(\theta_{2.1})) \\ y_{2.1} - y_5 + l_6(\cos(\phi_{2.1})\cos(\psi_{2.1}) + \sin(\phi_{2.1})\sin(\psi_{2.1})\sin(\theta_{2.1})) \\ z_{2.1} - z_5 + l_6\cos(\theta_{2.1})\sin(\phi_{2.1}) \\ \phi_{2.1} - \phi_5 \\ \theta_{2.1} - \theta_5 \\ \psi_{2.1} - \psi_5 \end{bmatrix} = \mathbf{0}, \\
\boldsymbol{\varphi}_{\mathrm{II},3}(\boldsymbol{\eta},t) &= \begin{bmatrix} x_{3.1} - x_5 + l_7\cos(\psi_{3.1})\cos(\theta_{3.1}) \\ y_{3.1} - y_5 + l_7\cos(\theta_{3.1})\sin(\psi_{3.1}) \\ z_{3.1} - z_5 - l_7\sin(\theta_{3.1}) \\ \phi_{3.1} - \phi_5 \\ \theta_{3.1} - \theta_5 \\ \psi_{3.1} - \psi_5 \end{bmatrix} = \mathbf{0}, \\
\boldsymbol{\varphi}_{\mathrm{II},4}(\boldsymbol{\eta},t) &= \begin{bmatrix} x_{4.1} - x_5 + l_8(\cos(\phi_{4.1})\sin(\psi_{4.1}) - \cos(\psi_{4.1})\sin(\phi_{4.1})\sin(\theta_{4.1})) \\ y_{4.1} - y_5 - l_8(\cos(\phi_{4.1})\cos(\psi_{4.1}) + \sin(\phi_{4.1})\sin(\psi_{4.1})\sin(\theta_{4.1})) \\ z_{4.1} - z_5 - l_8\cos(\theta_{4.1})\sin(\phi_{4.1}) \\ \phi_{4.1} - \phi_5 \\ \theta_{4.1} - \theta_5 \\ \psi_{4.1} - \psi_5 \end{bmatrix} = \mathbf{0},
\end{aligned}
\tag{5.41}
$$

where l_{4+j} are the lengths defined between the bodies (supports and load).

5.3.2 Centralized cooperative control

The centralized cooperative control is formulated imposing the modeling constraints into the decentralized controllers and performing the control allocation together. The decentralized controllers are synthesized as sliding mode controllers to handle the modeling errors and external disturbances. The references used by the controllers are generated from the desired trajectory of

the load, solving the IK-problem on the acceleration level for each control sub-system with the Jacobians matrices of the modeling constraints. The approach used to solve the IK-problem is based on Tang et al. (2017).

5.3.2.1 Decentralized controllers

Let the sliding surface of the j-th agent be given by:

$$\mathbf{s}_j\left(\boldsymbol{\eta}_j, \dot{\boldsymbol{\eta}}_j\right) = \dot{\tilde{\boldsymbol{\eta}}}_j + \boldsymbol{\Lambda}_j \tilde{\boldsymbol{\eta}}_j = \mathbf{0}, \quad (j = 1, \ldots, 5) \tag{5.42}$$

where $\tilde{\boldsymbol{\eta}}_j = \boldsymbol{\eta}_{j.5} - \boldsymbol{\eta}_{\mathrm{d},5}$ is the tracking error column-vector and $\boldsymbol{\Lambda}_j = \boldsymbol{\Lambda}_j^{\mathsf{T}} \geq \mathbf{0}$ is a control gain matrix associated to the closed-loop bandwidth.

Based on Eq. (5.42), the following control constraint is defined:

$$\boldsymbol{\varphi}_{\mathrm{SC},j}\left(\boldsymbol{\eta}_j, \dot{\boldsymbol{\eta}}_j\right) = \mathbf{s}_j\left(\boldsymbol{\eta}_i, \dot{\boldsymbol{\eta}}_j\right) = \mathbf{0}. \quad (j = 1, \ldots, 5) \tag{5.43}$$

Performing the time-derivative of Eq. (5.43) and imposing the sliding condition, we get:

$$\dot{\boldsymbol{\varphi}}_{\mathrm{SC},j} = -\mathbf{L}_j \mathbf{s}_j - \mathbf{K}_j \operatorname{sign}\left(\mathbf{s}_j\right), \quad (j = 1, \ldots, 5) \tag{5.44}$$

where $\mathbf{L}_j = \mathbf{L}_j^{\mathsf{T}} \geq \mathbf{0}$ and $\mathbf{K}_j = \mathbf{K}_j^{\mathsf{T}} \geq \mathbf{0}$ are control gains matrices.

Moreover, Eq. (5.44) can be rewritten as:

$$\mathbf{A}_{\mathrm{SC},j} \dot{\boldsymbol{\nu}}_{\mathrm{SC},j} = \mathbf{b}_{\mathrm{SC},j}, \quad (j = 1, \ldots, 5) \tag{5.45}$$

where $\mathbf{A}_{\mathrm{SC},j} = \dfrac{\partial \boldsymbol{\varphi}_{\mathrm{SC},j}}{\partial \boldsymbol{\eta}_j} \mathbf{J}_j$ and $\mathbf{b}_{\mathrm{SC},j} = -\dot{\mathbf{A}}_{\mathrm{SC},j} \mathbf{J}_j \boldsymbol{\nu}_j - \mathbf{A}_{\mathrm{SC},j} \dot{\mathbf{J}}_j \boldsymbol{\nu}_j + \ddot{\boldsymbol{\eta}}_{\mathrm{d},5} - \boldsymbol{\Lambda}_j \tilde{\boldsymbol{\eta}}_j - \mathbf{L}_j \mathbf{s}_j - \mathbf{K}_j \operatorname{sign}\left(\mathbf{s}_j\right)$.

From Eq.(4.110), the decentralized control of the j-th agent is given by:

$$\mathbf{u}_{0,j} = \mathbf{F}_j^{-1/2} \bar{\mathbf{H}}_{\mathrm{SC},j}^{+} \left(\mathbf{b}_{\mathrm{SC},j} - \mathbf{A}_{\mathrm{SC},j} \dot{\boldsymbol{\nu}}_j\right). \quad (j = 1, \ldots, 5) \tag{5.46}$$

Moreover, taking $\mathbf{F}_j = \mathbf{M}_j^{-2}$, we get from Eq. (4.108):

$$\bar{\mathbf{H}}_{\mathrm{SC},j} = \mathbf{A}_{\mathrm{SC},j} \mathbf{P}_j \mathbf{M}_j^{-1} \mathbf{F}_j^{-1/2} = \mathbf{A}_{\mathrm{SC},j} \mathbf{P}_j. \quad (j = 1, \ldots, 4) \tag{5.47}$$

where $\mathbf{P}_j = \mathbf{I} - \mathbf{H}_j^{\mathrm{g}} \mathbf{H}_j$, with $\mathbf{H}_j = \mathbf{A}_j \mathbf{M}_j^{-1}$ and $\mathbf{A}_j = \dfrac{\partial \boldsymbol{\varphi}_{\mathrm{I},j}}{\partial \boldsymbol{\eta}_j} \mathbf{J}_j$ $(j = 1, \ldots, 4)$ related to the modeling constraints between the ROVs and the supports (1-st level of the modeling hierarchy). Concerning the load, we have $\mathbf{P}_5 = \mathbf{I}$ since no modeling constraints need to be included. Thus, from Eq. (4.108) and with $\mathbf{F}_5 = \mathbf{M}_5^{-2}$, we get $\bar{\mathbf{H}}_{\mathrm{SC},5} = \mathbf{A}_{\mathrm{SC},5} \mathbf{M}_5^{-1} \mathbf{F}_5^{-1/2} = \mathbf{A}_{\mathrm{SC},5}$.

5.3.2.2 Centralized controller with thrust allocation

From Eq. (5.46), $\mathbf{u}_0 = \left[\mathbf{u}_{0,1}^\mathsf{T}, \ldots, \mathbf{u}_{0,5}^\mathsf{T}\right]^\mathsf{T}$ is the column-vector of decentralized controllers.

The thrusters configuration matrix of the system is written as:

$$\mathbf{T} = \text{blkdiag}\left(\mathbf{T}_1, \mathbf{T}_2, \mathbf{T}_3, \mathbf{T}_4, \mathbf{T}_5\right), \tag{5.48}$$

where $\mathbf{T}_j = \text{blkdiag}\left(\mathbf{T}_{j.0}, \mathbf{T}_{j.1}\right)$, $\mathbf{T}_{j.1} = \mathbf{0}$ $(j = 1, \ldots, 4)$ and $\mathbf{T}_5 = \mathbf{0}$ once the supports and load are non-actuated.

With Eqs. (4.93) and (4.94), the centralized cooperative control becomes:

$$\begin{aligned} \mathbf{u}_\# &= \mathbf{H}_\mathbf{Q}\mathbf{Z}^{-1/2}\left(\mathbf{I} - \bar{\mathbf{H}}_{\mathbf{R}|\mathbf{A}}^\text{g}\bar{\mathbf{H}}_\mathbf{R}\right)\boldsymbol{\mu}_0, \\ \boldsymbol{\tau} &= \mathbf{L}^{-1/2}\bar{\mathbf{H}}_\mathbf{T}^\text{g}\mathbf{u}_\#, \end{aligned} \tag{5.49}$$

where

$$\begin{aligned} \mathbf{H}_\mathbf{Q} &= \mathbf{Q}^\mathsf{T}, \\ \bar{\mathbf{H}}_\mathbf{R} &= \mathbf{R}^\mathsf{T}\mathbf{Z}^{-1/2}, \\ \bar{\mathbf{H}}_\mathbf{A}^\mathsf{T} &= \mathbf{Z}^{-1/2}\mathbf{A}^\mathsf{T}, \\ \mathbf{Z} &= \mathbf{I} + \mathbf{M}\left(\bar{\mathbf{H}}_\mathbf{T}^\text{g}\mathbf{H}_\mathbf{Q}\right)^\mathsf{T}\bar{\mathbf{H}}_\mathbf{T}^\text{g}\mathbf{H}_\mathbf{Q}, \\ \boldsymbol{\mu}_0 &= \mathbf{Z}^{-1/2}\mathbf{u}_0, \\ \bar{\mathbf{H}}_\mathbf{T} &= \mathbf{T}\mathbf{L}^{-1/2}, \\ \bar{\mathbf{H}}_\mathbf{T}^\text{g} &= \bar{\mathbf{H}}_\mathbf{T}^\mathsf{T}\left(\bar{\mathbf{H}}_\mathbf{T}\bar{\mathbf{H}}_\mathbf{T}^\mathsf{T}\right)^\text{g}. \end{aligned} \tag{5.50}$$

In Eq. (5.50), $\mathbf{Q}$ and $\mathbf{R}$ are calculated considering the actuated and non-actuated quasi-velocities, i.e., $\mathbf{Q} = \dfrac{\partial \boldsymbol{\nu}_\#}{\partial \boldsymbol{\nu}}$ and $\mathbf{R} = \dfrac{\partial \boldsymbol{\nu}_*}{\partial \boldsymbol{\nu}}$, with $\boldsymbol{\nu}_\# = \left[\boldsymbol{\nu}_{1.0}^\mathsf{T}, \ldots, \boldsymbol{\nu}_{4.0}^\mathsf{T}\right]^\mathsf{T}$ and $\boldsymbol{\nu}_* = \left[\boldsymbol{\nu}_{1.1}^\mathsf{T}, \ldots, \boldsymbol{\nu}_{4.1}^\mathsf{T}, \boldsymbol{\nu}_5^\mathsf{T}\right]^\mathsf{T}$.

5.3.3 Results

The centralized cooperative control is tested on the tracking problem of a circular trajectory close to the free surface. The load desired trajectory are described by (in meters and radians):

$$\begin{aligned} x_\text{d}(t) &= 10\sin(0.063t), \\ y_\text{d}(t) &= 10\cos(0.063t), \\ z_\text{d}(t) &= 2, \\ \phi_\text{d}(t) &= \theta_\text{d}(t) = \psi_\text{d}(t) = 0. \end{aligned} \tag{5.51}$$

The simulation is performed using the previous specified setup. The modeling and control

parameters are shown in Tabs. 16 and 17. The wave parameters used to model the wave forces are found in Oliveira et al. (2022).

Table 16: Modular ROVs, supports and load model parameters

Symbols	Values	Units (SI)
$\mathbf{M}_{\mathrm{RB},0}$	diag (11.5, 11.5, 11.5, 0.16, 0.16, 0.16)	$\mathrm{kg}, \mathrm{kgm}^2$
$\mathbf{M}_{\mathrm{RB},1}$	diag (4.7, 4.7, 4.7, 0.15, 0.30, 0.44)	$\mathrm{kg}, \mathrm{kgm}^2$
$\mathbf{M}_{\mathrm{RB},5}$	diag (175, 175, 175, 7.29, 7.29, 7.29)	$\mathrm{kg}, \mathrm{kgm}^2$
$\mathbf{M}_{\mathrm{A},0}$	diag (5.5, 12.7, 14.6, 0.12, 0.12, 0.12)	$\mathrm{kg}, \mathrm{kgm}^2$
$\mathbf{M}_{\mathrm{A},1}$	diag (0, 0, 0, 0, 0, 0)	$\mathrm{kg}, \mathrm{kgm}^2$
$\mathbf{M}_{\mathrm{A},5}$	diag (112.25, 112.25, 112.25, 1.09, 1.09, 1.09)	$\mathrm{kg}, \mathrm{kgm}^2$
$\mathbf{D}_0$	diag (18.18, 21.66, 36.99, 1.55, 1.55, 1.55)	$\mathrm{Ns/m}, \mathrm{Nms}$
$\mathbf{D}_1$	diag (0, 0, 0, 0, 0, 0)	$\mathrm{Ns/m}, \mathrm{Nms}$
$\mathbf{D}_5$	diag (143.75, 143.75, 143.75, 0.84, 0.84, 0.84)	$\mathrm{Ns/m}, \mathrm{Nms}$
l_1, l_2, l_3, l_4	0.08	m
l_5, l_6, l_7, l_8	0.66	m
W_0, B_0	112.82, 114.78	N
W_1, B_1	46.11, 166.77	N
W_5, B_5	1716.70, 1226.30	N
$\vec{\mathbf{p}}^{0}_{\mathrm{G}_0\mid\mathrm{O}_0}$	$[0, 0, 0]^\mathsf{T}$	m
$\vec{\mathbf{p}}^{0}_{\mathrm{B}_0\mid\mathrm{O}_0}$	$[0, 0, -0.2]^\mathsf{T}$	m
$\vec{\mathbf{p}}^{1}_{\mathrm{G}_1\mid\mathrm{O}_1}$	$[0.23, 0, 0]^\mathsf{T}$	m
$\vec{\mathbf{p}}^{1}_{\mathrm{B}_1\mid\mathrm{O}_1}$	$[0, 0, 0]^\mathsf{T}$	m
$\vec{\mathbf{p}}^{5}_{\mathrm{G}_5\mid\mathrm{O}_5}$	$[0, 0, 0]^\mathsf{T}$	m
$\vec{\mathbf{p}}^{5}_{\mathrm{B}_5\mid\mathrm{O}_5}$	$[0, 0, 0]^\mathsf{T}$	m

Table 17: Modular ROVs and load control parameters

Symbols	Values	Units (SI)
$\mathbf{\Lambda}$	diag (1, 1, 1, 1, 1, 1)	1/s
$\mathbf{K}$	diag (5, 5, 5, 5, 5, 5)	$\mathrm{m/s}^2, \mathrm{rad/s}^2$
$\mathbf{L}$	diag (10, 10, 10, 10, 10, 10)	1/s

Figure 102 shows the control block diagram for the 3D cooperative transportation with modular ROVs.

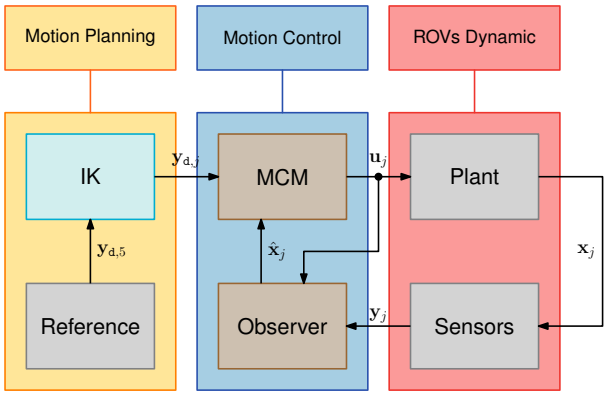

Figure 102: Cooperative centralized control block diagram

Figure 103 shows the displacements of each agent. Despite some oscillations on the height and on the Euler angles, the motion performed is continuous and smooth. These oscillations are due to the relative velocity effects on the thrusters propeller caused by the wave velocity profile and the system motion. As previously mentioned, the relative velocity effects on the thrusters propeller are included in the model through a 3D interpolation table. The commanded thrusts and associated motor velocities are shown in Fig. 104. There is a saturation at the beginning of the simulation for the thrusts and motor velocities profiles. This saturation is due to the additional control effort needed to reach the desired trajectory, as shown on the trajectory tracking shown in Fig. 105. Regarding the task quality, the control keeps the system stable and performs the tracking with acceptable performance as shown by the path and coordinates tracking in Fig. 105 (a) and (b), respectively. However, for higher significant wave heights ($H_s > 2$ m), the wave effects can comprise the task execution. Figure 106 shows some animation frames of the 3D cooperative transportation with modular ROVs to illustrate the motion performed during the trajectory tracking.

The modeling and servo-constraints orders are 10^{-9} and 10^{-1} as shown in Fig. 107.

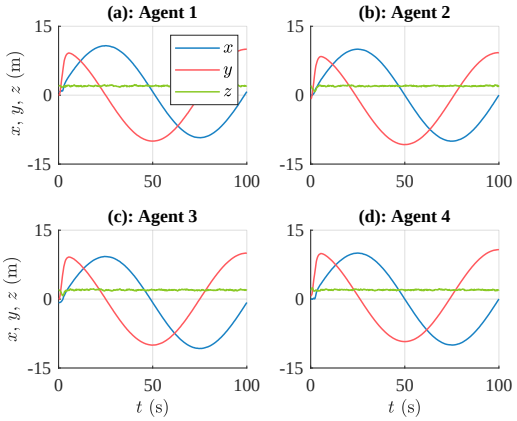

(a): Linear displacements

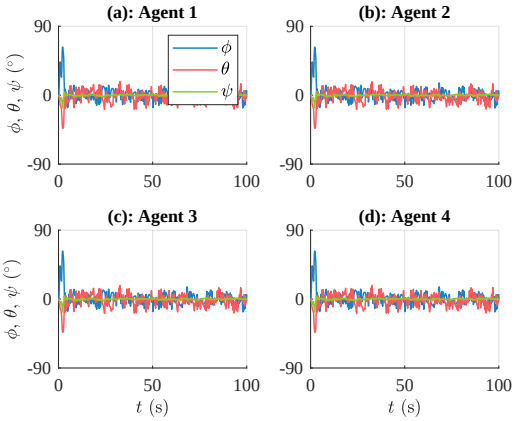

(b): Angular displacements

Figure 103: Agents displacements on the 3D cooperative transportation with modular ROVs

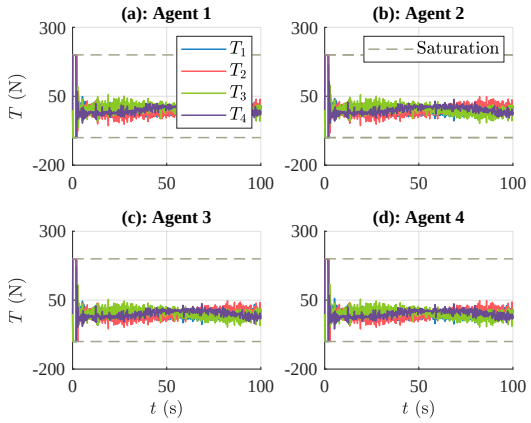

(a): Thrusts $(T_1, \ldots, T_4)$

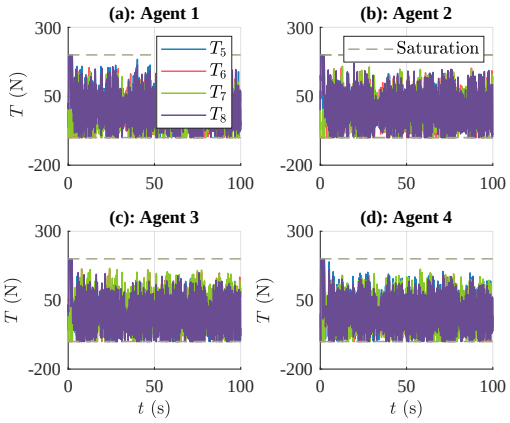

(b): Thrusts $(T_5, \ldots, T_8)$

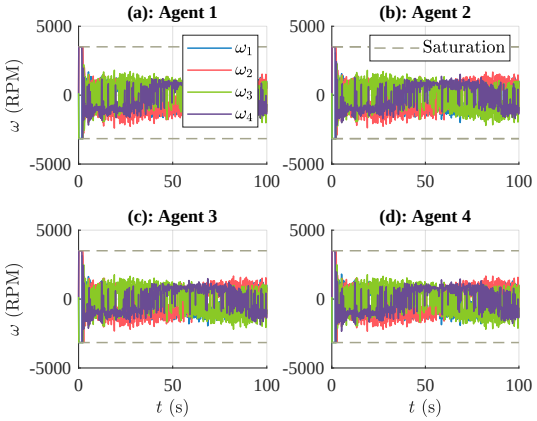

(c): Velocities $(\omega_1, \ldots, \omega_4)$

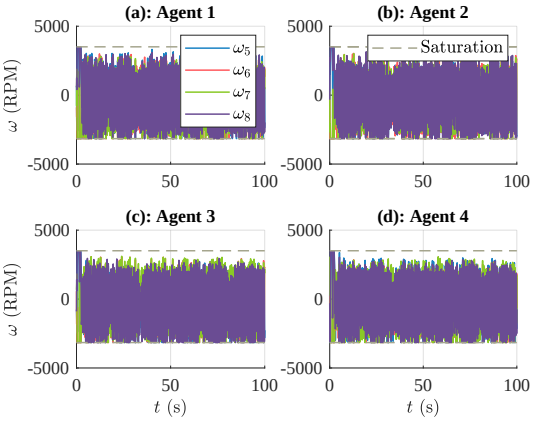

(d): Velocities $(\omega_5, \ldots, \omega_8)$

Figure 104: Control inputs on the 3D cooperative transportation with modular ROVs

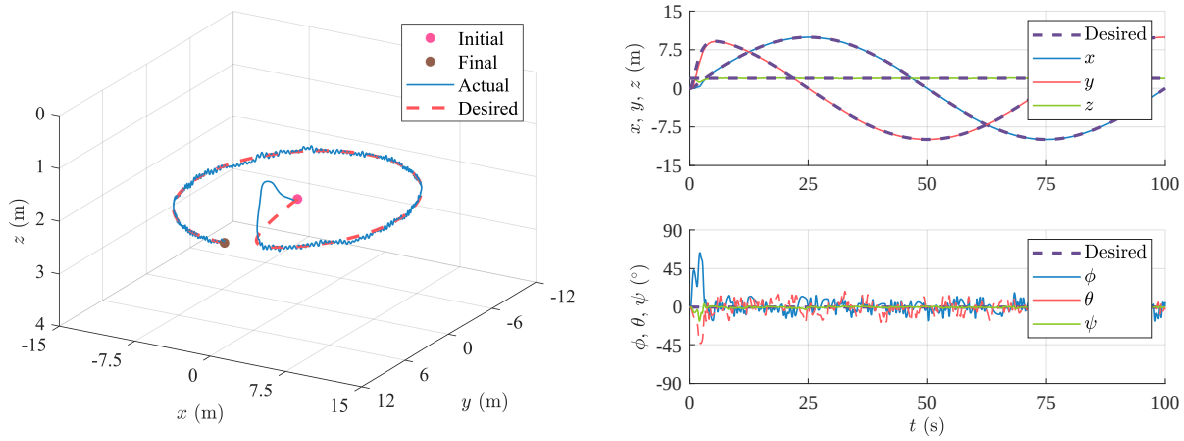

(a): Path (b): Displacements

Figure 105: Load tracking on the 3D cooperative transportation with modular ROVs

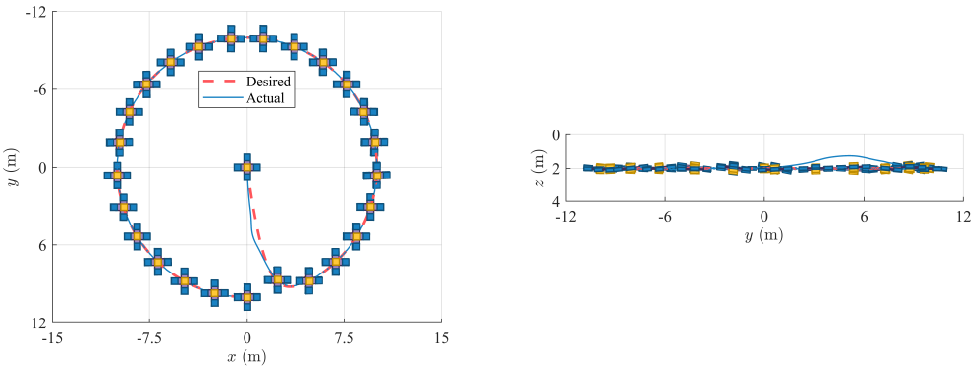

(a): *xy*-plane (b): *yz*-plane

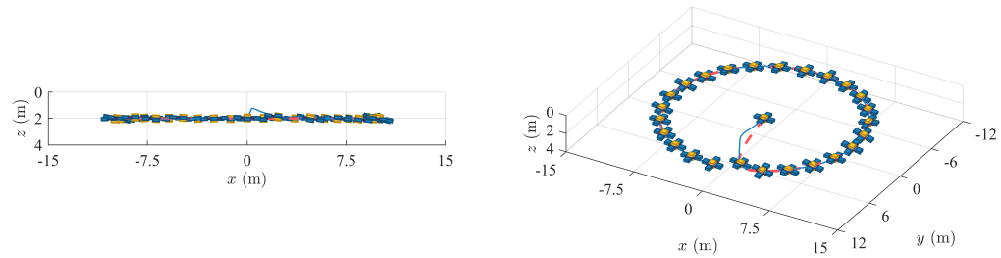

(a): *xz*-plane (b): 3D plot

Figure 106: Frames of the 3D cooperative transportation with modular ROVs

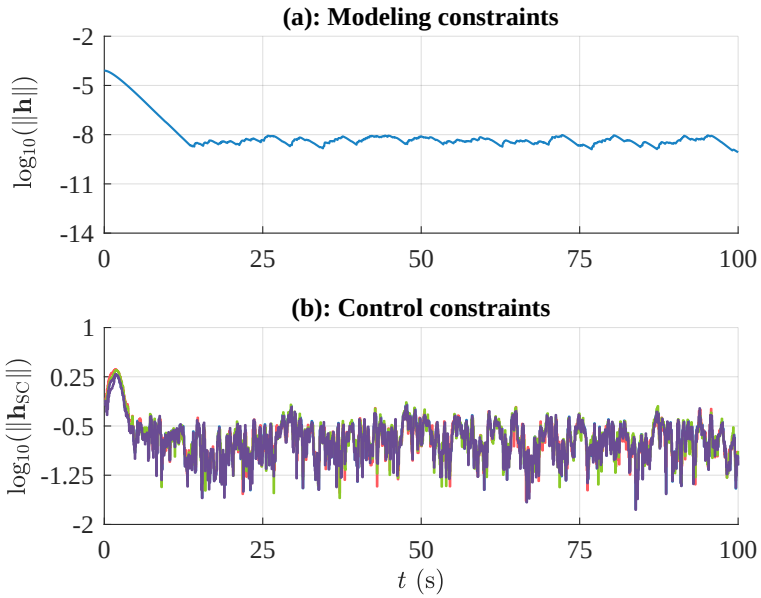

Figure 107: Constraints of the 3D cooperative transportation with modular ROVs

5.4 3D COOPERATIVE TRANSPORTATION WITH I-AUVs

5.4.1 Modeling

Figure 108 (a) shows the 3D cooperative transportation performed with I-AUVs. The system comprises four I-AUVs transporting a rigid rectangular frame made of cylindrical-shaped links of polyethylene. The I-AUV model is based on the BlueROV 2 equipped with a 3-DoFs manipulator of anthropomorphic structure made of cylindrical-shaped links also made of polyethylene. This case of study is inspired by the works of Heshmati-Alamdari (HESHMATI-ALAMDARI et al., 2017; HESHMATI-ALAMDARI, 2018; HESHMATI-ALAMDARI et al., 2018; HESHMATI-ALAMDARI; KARRAS; KYRIAKOPOULOS, 2019; HESHMATI-ALAMDARI et al., 2021a; HESHMATI-ALAMDARI et al., 2021b), who studied the cooperative transportation performed by groups of I-AUVs.

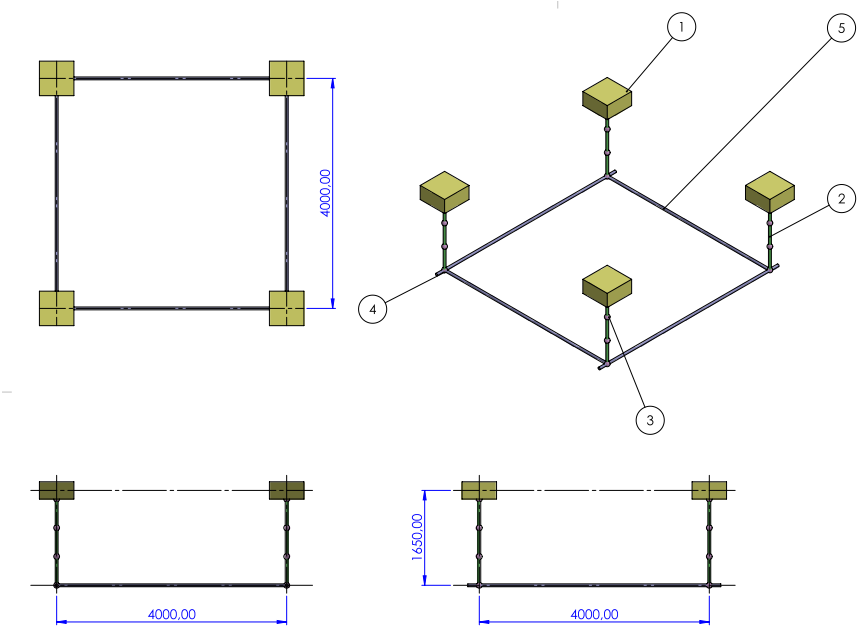

(a): 3D cooperative transportation system (main dimensions in millimeters) where (1) is the AUV, (2) is the link, (3) is the motor, (4) is the end-effector and (5) is the load

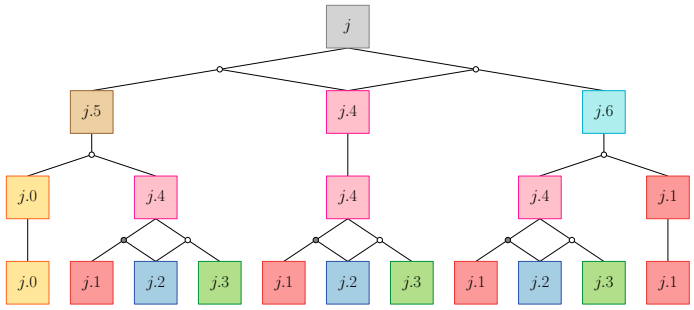

(b): Agent modeling hierarchy

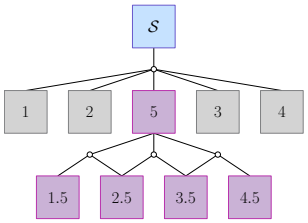

(c): Cooperative transportation modeling hierarchy

Figure 108: 3D cooperative transportation with I-AUVs

In the modeling hierarchy of Fig. 108 (b), the j-th agent ($j = 1, \ldots, 4$) is constituted by the bodies 0, 1, 2 and 3. The body $j.0$ is the vehicle, bodies $j.1$ are spheres used to model the motors house and the end-effector, bodies $j.2$ are the motors and bodies $j.3$ are the manipulator links. Also, in Fig. 108 (c), agent 5 represents the load and is constituted by four other bodies, i.e., $j.5$ representing the frame links. In the j-th agent subsystems ($j = 1, \ldots, 4$), active revolute joints (grey circles) connect the motors with the houses and rigid joints (white circles) connect the

vehicle with the motor house, the motor house with the manipulator links, the manipulator links with the motors and the end-effector with third manipulator link. For system $\mathcal{S}$, passive spherical joints (white circle) connect the end-effectors with the load.

We should point out that in this case of study, the use of Euler angles (ϕ, θ, ψ) to describe the rotations result in numerical problems once the initial position of the manipulator links represents a singular configuration ($\theta = \pm 90°$). To avoid these problems, in this system, the rotations are parameterized with the Euler parameters (e_0, e_1, e_2, e_3), as described in Subsec. 3.1.3.

5.4.1.1 I-AUV

The relaxed model of the j-th agent is written as follows:

$$\begin{aligned} \dot{\boldsymbol{\eta}}_j &= \mathbf{J}_j\left(\boldsymbol{\eta}_j\right)\boldsymbol{\nu}_j, \\ \mathbf{M}_j\dot{\boldsymbol{\nu}}_j &= \mathbf{f}_j\left(\boldsymbol{\eta}_j, \boldsymbol{\nu}_j\right), \end{aligned} \tag{5.52}$$

with

$$\begin{aligned} \mathbf{J}_j &= \text{blkdiag}\left(\mathbf{J}_{j.0}, \mathbf{J}_{j.1}, \mathbf{J}_{j.2}, \mathbf{J}_{j.3}, \mathbf{J}_{j.4}, \mathbf{J}_{j.5}, \mathbf{J}_{j.6}, \mathbf{J}_{j.7}, \mathbf{I}\right), \\ \mathbf{M}_j &= \text{blkdiag}\left(\mathbf{M}_{j.0}, \mathbf{M}_{j.1}, \mathbf{M}_{j.2}, \mathbf{M}_{j.3}, \mathbf{M}_{j.4}, \mathbf{M}_{j.5}, \mathbf{M}_{j.6}, \mathbf{M}_{j.7}, \mathbf{I}_{j.\mathtt{M}}\right), \\ \boldsymbol{\eta}_j &= \left[\boldsymbol{\eta}_{j.0}^{\mathsf{T}}, \boldsymbol{\eta}_{j.1}^{\mathsf{T}}, \boldsymbol{\eta}_{j.2}^{\mathsf{T}}, \boldsymbol{\eta}_{j.3}^{\mathsf{T}}, \boldsymbol{\eta}_{j.4}^{\mathsf{T}}, \boldsymbol{\eta}_{j.5}^{\mathsf{T}}, \boldsymbol{\eta}_{j.6}^{\mathsf{T}}, \boldsymbol{\eta}_{j.7}^{\mathsf{T}}, \boldsymbol{\gamma}_j^{\mathsf{T}}\right]^{\mathsf{T}}, \\ \boldsymbol{\nu}_j &= \left[\boldsymbol{\nu}_{j.0}^{\mathsf{T}}, \boldsymbol{\nu}_{j.1}^{\mathsf{T}}, \boldsymbol{\nu}_{j.2}^{\mathsf{T}}, \boldsymbol{\nu}_{j.3}^{\mathsf{T}}, \boldsymbol{\nu}_{j.4}^{\mathsf{T}}, \boldsymbol{\nu}_{j.5}^{\mathsf{T}}, \boldsymbol{\nu}_{j.6}^{\mathsf{T}}, \boldsymbol{\nu}_{j.7}^{\mathsf{T}}, \dot{\boldsymbol{\gamma}}_j^{\mathsf{T}}\right]^{\mathsf{T}}, \\ \mathbf{f}_j &= \begin{bmatrix} \boldsymbol{\tau}_{j.0} - \mathbf{C}_{j.0}\boldsymbol{\nu}_{j.0} - \mathbf{D}_{j.0}\boldsymbol{\nu}_{j.0} - \mathbf{g}_{j.0} + \mathbf{d}_{j.0} \\ \boldsymbol{\tau}_{j.1} - \mathbf{C}_{j.1}\boldsymbol{\nu}_{j.1} - \mathbf{D}_{j.1}\boldsymbol{\nu}_{j.1} - \mathbf{g}_{j.1} + \mathbf{d}_{j.1} \\ \boldsymbol{\tau}_{j.2} - \mathbf{C}_{j.2}\boldsymbol{\nu}_{j.2} - \mathbf{D}_{j.2}\boldsymbol{\nu}_{j.2} - \mathbf{g}_{j.2} + \mathbf{d}_{j.2} \\ \boldsymbol{\tau}_{j.3} - \mathbf{C}_{j.3}\boldsymbol{\nu}_{j.3} - \mathbf{D}_{j.3}\boldsymbol{\nu}_{j.3} - \mathbf{g}_{j.3} + \mathbf{d}_{j.3} \\ \boldsymbol{\tau}_{j.4} - \mathbf{C}_{j.4}\boldsymbol{\nu}_{j.4} - \mathbf{D}_{j.4}\boldsymbol{\nu}_{j.4} - \mathbf{g}_{j.4} + \mathbf{d}_{j.4} \\ \boldsymbol{\tau}_{j.5} - \mathbf{C}_{j.5}\boldsymbol{\nu}_{j.5} - \mathbf{D}_{j.5}\boldsymbol{\nu}_{j.5} - \mathbf{g}_{j.5} + \mathbf{d}_{j.5} \\ \boldsymbol{\tau}_{j.6} - \mathbf{C}_{j.6}\boldsymbol{\nu}_{j.6} - \mathbf{D}_{j.6}\boldsymbol{\nu}_{j.6} - \mathbf{g}_{j.6} + \mathbf{d}_{j.6} \\ \boldsymbol{\tau}_{j.7} - \mathbf{C}_{j.7}\boldsymbol{\nu}_{j.7} - \mathbf{D}_{j.7}\boldsymbol{\nu}_{j.7} - \mathbf{g}_{j.7} + \mathbf{d}_{j.7} \\ \boldsymbol{\tau}_{j.\mathtt{M}} - \mathbf{B}_{j.\mathtt{M}}\dot{\boldsymbol{\gamma}}_j - \mathbf{C}_{j.\mathtt{M}}\,\text{sign}\left(\dot{\boldsymbol{\gamma}}_j\right) \end{bmatrix}, \end{aligned} \tag{5.53}$$

with $\boldsymbol{\eta}_{j.i} = \left[\boldsymbol{\eta}_{1,j.i}^{\mathsf{T}}, \boldsymbol{\eta}_{2,j.i}^{\mathsf{T}}\right]^{\mathsf{T}}$ and $\boldsymbol{\nu}_{j.i} = \left[\boldsymbol{\nu}_{1,j.i}^{\mathsf{T}}, \boldsymbol{\nu}_{2,j.i}^{\mathsf{T}}\right]^{\mathsf{T}}$ $(i = 0, 1, \ldots, 7)$ as the column-vectors of generalized coordinates and quasi-velocities associated to each body of the j-th agent, where $\boldsymbol{\eta}_{1,j.i} = \left[x_{j.i}, y_{j.i}, z_{j.i}\right]^{\mathsf{T}}$, $\boldsymbol{\eta}_{2,j.i} = \left[e_{0,j.i}, e_{1,j.i}, e_{2,j.i}, e_{3,j.i}\right]^{\mathsf{T}}$, $\boldsymbol{\nu}_{1,j.i} = \left[u_{j.i}, v_{j.i}, w_{j.i}\right]^{\mathsf{T}}$ and $\boldsymbol{\nu}_{2,j.i} = \left[p_{j.i}, q_{j.i}, r_{j.i}\right]^{\mathsf{T}}$; $\boldsymbol{\gamma}_j = \left[\gamma_{j.1}, \gamma_{j.2}, \gamma_{j.3}\right]^{\mathsf{T}}$ is the column-vector of motors displacements; $\boldsymbol{\tau}_{j.0} = \mathbf{T}_{j.0}\mathbf{u}_{j.0}$ is the column-vector of generalized control forces generated on the vehicle by the thrusters, with $\mathbf{T}_{j.0}$ as the thrusters configuration matrix and $\mathbf{u}_{j.0} = \left[T_{j.1}, \ldots, T_{j.8}\right]^{\mathsf{T}}$ as the column-vector of

thrusts; $\boldsymbol{\tau}_{j.\mathtt{M}} = \mathbf{T}_{j.\mathtt{M}}\mathbf{u}_{j.\mathtt{M}}$ is the column-vector of actuation torques generated by the motors on the manipulator joints, with $\mathbf{T}_{j.\mathtt{M}}$ as the gain matrix associated with the motors reduction and $\mathbf{u}_{j.\mathtt{M}} = \left[\tau_{j.1}, \tau_{j.2}, \tau_{j.3}\right]^{\mathsf{T}}$ is the column-vector of drive torques generated on the motors shaft which follows the stationary relation between motor current and torque constant.

The constraints related to the joints of the j-th agent are given by:

$$\boldsymbol{\varphi}_{\mathtt{I},j}\left(\boldsymbol{\eta}_j, t\right) = \begin{bmatrix} \boldsymbol{\eta}_{1,j.0} + \mathbf{J}_{1,j.0}\vec{\mathbf{p}}^{\,j.0}_{\mathrm{O}_{j.1}|\mathrm{O}_{j.0}} - \left(\boldsymbol{\eta}_{1,j.1} - \mathbf{J}_{1,j.1}\vec{\mathbf{p}}^{\,j.1}_{\mathrm{C}_{j.1}|\mathrm{O}_{j.1}}\right) \\ \boldsymbol{\eta}_{1,j.1} + \mathbf{J}_{1,j.1}\vec{\mathbf{p}}^{\,j.1}_{\mathrm{O}_{j.2}|\mathrm{C}_{j.1}} - \left(\boldsymbol{\eta}_{1,j.2} - \mathbf{J}_{1,j.2}\vec{\mathbf{p}}^{\,j.2}_{\mathrm{C}_{j.2}|\mathrm{O}_{j.2}}\right) \\ \boldsymbol{\eta}_{1,j.2} + \mathbf{J}_{1,j.2}\vec{\mathbf{p}}^{\,j.2}_{\mathrm{O}_{j.3}|\mathrm{C}_{j.2}} - \left(\boldsymbol{\eta}_{1,j.3} - \mathbf{J}_{1,j.3}\vec{\mathbf{p}}^{\,j.3}_{\mathrm{C}_{j.3}|\mathrm{O}_{j.3}}\right) \\ \boldsymbol{\eta}_{1,j.0} + \mathbf{J}_{1,j.0}\vec{\mathbf{p}}^{\,j.0}_{\mathrm{O}_{j.1}|\mathrm{O}_{j.0}} - \boldsymbol{\eta}_{1,j.4} \\ \boldsymbol{\eta}_{1,j.1} + \mathbf{J}_{1,j.1}\vec{\mathbf{p}}^{\,j.1}_{\mathrm{O}_{j.2}|\mathrm{C}_{j.1}} - \boldsymbol{\eta}_{1,j.5} \\ \boldsymbol{\eta}_{1,j.2} + \mathbf{J}_{1,j.2}\vec{\mathbf{p}}^{\,j.2}_{\mathrm{O}_{j.3}|\mathrm{C}_{j.2}} - \boldsymbol{\eta}_{1,j.6} \\ \boldsymbol{\eta}_{1,j.3} + \mathbf{J}_{1,j.3}\vec{\mathbf{p}}^{\,j.3}_{\mathrm{O}_{j.4}|\mathrm{C}_{j.3}} - \boldsymbol{\eta}_{1,j.7} \\ \boldsymbol{\eta}^{*}_{2,j.0} \otimes \boldsymbol{\eta}_{2,j.1} - \boldsymbol{\eta}_{2,\gamma_{j.1}} \\ \boldsymbol{\eta}^{*}_{2,j.1} \otimes \boldsymbol{\eta}_{2,j.2} - \boldsymbol{\eta}_{2,\gamma_{j.2}} \\ \boldsymbol{\eta}^{*}_{2,j.2} \otimes \boldsymbol{\eta}_{2,j.3} - \boldsymbol{\eta}_{2,\gamma_{j.3}} \\ \boldsymbol{\eta}^{*}_{2,j.0} \otimes \boldsymbol{\eta}_{2,j.4} - \boldsymbol{\eta}_{2,0^{\circ}} \\ \boldsymbol{\eta}^{*}_{2,j.1} \otimes \boldsymbol{\eta}_{2,j.5} - \boldsymbol{\eta}_{2,0^{\circ}} \\ \boldsymbol{\eta}^{*}_{2,j.2} \otimes \boldsymbol{\eta}_{2,j.6} - \boldsymbol{\eta}_{2,0^{\circ}} \\ \boldsymbol{\eta}^{*}_{2,j.3} \otimes \boldsymbol{\eta}_{2,j.7} - \boldsymbol{\eta}_{2,0^{\circ}} \end{bmatrix} = \mathbf{0}, \tag{5.54}$$

where

- $\mathbf{J}_{1,j.i}$ $(i = 0, 1, \ldots, 7)$ is the rotation matrix from body-fixed to Earth-fixed frame;
- $\vec{\mathbf{p}}^{\,j.0}_{\mathrm{O}_{j.1}|\mathrm{O}_{j.0}} = \left[0, 0, l_{j.0}\right]^{\mathsf{T}}$ is the position vector defined between the points $\mathrm{O}_{j.1}$ (first joint center) and $\mathrm{O}_{j.0}$ (vehicle origin) expressed on the body-fixed frame;
- $\vec{\mathbf{p}}^{\,j.i}_{\mathrm{C}_{j.i}|\mathrm{O}_{j.i}} = \left[l_{j.i}, 0, 0\right]^{\mathsf{T}}$ $(i = 1, \ldots, 7)$ is the position vector defined between the points $\mathrm{C}_{j.i}$ (body center) and $\mathrm{O}_{j.i}$ (joint origin) expressed on the body-fixed frame;
- $\vec{\mathbf{p}}^{\,j.i}_{\mathrm{O}_{j.i+1}|\mathrm{C}_{j.i}} = \left[l_{j.i}, 0, 0\right]^{\mathsf{T}}$ $(i = 1, \ldots, 3)$ is the position vector defined between the points $\mathrm{O}_{j.1+1}$ (joint centers) and $\mathrm{C}_{j.i}$ (body centers) expressed on the body-fixed frame;
- $l_{j.0}$ is the length between the points $\mathrm{O}_{j.1}$ and $\mathrm{O}_{j.0}$;
- $l_{j.i}$ is the length between the points $\mathrm{C}_{j.i}$ and $\mathrm{O}_{j.i}$ as the points $\mathrm{O}_{j.i+1}$ and $\mathrm{C}_{j.i}$;

- $\boldsymbol{\eta}_{2,\gamma_{j.i}} = \left[\cos\left(\gamma_{j.i}/2\right), \sin\left(\gamma_{j.i}/2\right), 0, 0\right]^{\mathsf{T}}$ $(i = 1, \ldots, 3)$ are the relative quaternions associated to the manipulator displacements;
- $\boldsymbol{\eta}_{2,0^\circ} = [1, 0, 0, 0]^{\mathsf{T}}$ is the unity quaternion.

In Eq. (5.54), the superscript "$*$" indicates the quaternion conjugate and "$\otimes$" represents the Hamiltonian product.

5.4.1.2 Load frame

The relaxed model of the load is written as follows:

$$\begin{aligned} \dot{\boldsymbol{\eta}}_5 &= \mathbf{J}_5\left(\boldsymbol{\eta}_5\right)\boldsymbol{\nu}_5, \\ \mathbf{M}_5\dot{\boldsymbol{\nu}}_5 &= \mathbf{f}_5\left(\boldsymbol{\eta}_5, \boldsymbol{\nu}_5\right), \end{aligned} \tag{5.55}$$

with

$$\begin{aligned} \mathbf{J}_5 &= \text{blkdiag}\left(\mathbf{J}_{1.5}, \mathbf{J}_{2.5}, \mathbf{J}_{3.5}, \mathbf{J}_{4.5}\right), \\ \mathbf{M}_5 &= \text{blkdiag}\left(\mathbf{M}_{1.5}, \mathbf{M}_{2.5}, \mathbf{M}_{3.5}, \mathbf{M}_{4.5}\right), \\ \boldsymbol{\eta}_5 &= \left[\boldsymbol{\eta}_{1.5}^{\mathsf{T}}, \boldsymbol{\eta}_{2.5}^{\mathsf{T}}, \boldsymbol{\eta}_{3.5}^{\mathsf{T}}, \boldsymbol{\eta}_{4.5}^{\mathsf{T}}\right]^{\mathsf{T}}, \\ \boldsymbol{\nu}_5 &= \left[\boldsymbol{\nu}_{1.5}^{\mathsf{T}}, \boldsymbol{\nu}_{2.5}^{\mathsf{T}}, \boldsymbol{\nu}_{3.5}^{\mathsf{T}}, \boldsymbol{\nu}_{4.5}^{\mathsf{T}}\right]^{\mathsf{T}}, \\ \mathbf{f}_5 &= \begin{bmatrix} \boldsymbol{\tau}_{1.5} - \mathbf{C}_{1.5}\boldsymbol{\nu}_{1.5} - \mathbf{D}_{1.5}\boldsymbol{\nu}_{1.5} - \mathbf{g}_{1.5} + \mathbf{d}_{1.5} \\ \boldsymbol{\tau}_{2.5} - \mathbf{C}_{2.5}\boldsymbol{\nu}_{2.5} - \mathbf{D}_{2.5}\boldsymbol{\nu}_{2.5} - \mathbf{g}_{2.5} + \mathbf{d}_{2.5} \\ \boldsymbol{\tau}_{3.5} - \mathbf{C}_{3.5}\boldsymbol{\nu}_{3.5} - \mathbf{D}_{3.5}\boldsymbol{\nu}_{3.5} - \mathbf{g}_{3.5} + \mathbf{d}_{3.5} \\ \boldsymbol{\tau}_{4.5} - \mathbf{C}_{4.5}\boldsymbol{\nu}_{4.5} - \mathbf{D}_{4.5}\boldsymbol{\nu}_{4.5} - \mathbf{g}_{4.5} + \mathbf{d}_{4.5} \end{bmatrix}, \end{aligned} \tag{5.56}$$

where $\boldsymbol{\eta}_{j.5} = \left[\boldsymbol{\eta}_{1,j.5}^{\mathsf{T}}, \boldsymbol{\eta}_{2,j.5}^{\mathsf{T}}\right]^{\mathsf{T}}$ and $\boldsymbol{\nu}_{j.5} = \left[\boldsymbol{\nu}_{1,j.5}^{\mathsf{T}}, \boldsymbol{\nu}_{2,j.5}^{\mathsf{T}}\right]^{\mathsf{T}}$ are the column-vectors of generalized coordinates and quasi-velocities associated to each body of the load, with $\boldsymbol{\eta}_{1,j.5} = \left[x_{j.5}, y_{j.5}, z_{j.5}\right]^{\mathsf{T}}$, $\boldsymbol{\eta}_{2,j.5} = \left[e_{j.5,0}, e_{j.5,1}, e_{j.5,2}, e_{j.5,3}\right]^{\mathsf{T}}$, $\boldsymbol{\nu}_{1,j.5} = \left[u_{j.5}, v_{j.5}, w_{j.5}\right]^{\mathsf{T}}$ and $\boldsymbol{\nu}_{2,j.5} = \left[p_{j.5}, q_{j.5}, r_{j.5}\right]^{\mathsf{T}}$; $\boldsymbol{\tau}_{j.5} = \mathbf{0}$ once the load is non-actuated.

The constraints associated to the vertices position of the load are given by:

$$\boldsymbol{\varphi}_{\mathrm{I},5}\left(\boldsymbol{\eta}_5, t\right) = \begin{bmatrix} \boldsymbol{\eta}_{1,1.5} - \mathbf{J}_{1,1.5}\vec{\mathbf{p}}^{1.5}_{\mathrm{C}_{1.5}|\mathrm{O}_{1.5}} - \left(\boldsymbol{\eta}_{1,2.5} + \mathbf{J}_{1,2.5}\vec{\mathbf{p}}^{2.5}_{\mathrm{C}_{2.5}|\mathrm{O}_{2.5}}\right) \\ \boldsymbol{\eta}_{1,2.5} - \mathbf{J}_{1,2.5}\vec{\mathbf{p}}^{2.5}_{\mathrm{C}_{2.5}|\mathrm{O}_{2.5}} - \left(\boldsymbol{\eta}_{1,3.5} - \mathbf{J}_{1,3.5}\vec{\mathbf{p}}^{3.5}_{\mathrm{C}_{3.5}|\mathrm{O}_{3.5}}\right) \\ \boldsymbol{\eta}_{1,3.5} + \mathbf{J}_{1,3.5}\vec{\mathbf{p}}^{3.5}_{\mathrm{O}_{3.5}|\mathrm{C}_{3.5}} - \left(\boldsymbol{\eta}_{1,4.5} - \mathbf{J}_{1,4.5}\vec{\mathbf{p}}^{4.5}_{\mathrm{C}_{4.5}|\mathrm{O}_{4.5}}\right) \\ \boldsymbol{\eta}_{1,4.5} + \mathbf{J}_{1,4.5}\vec{\mathbf{p}}^{4.5}_{\mathrm{O}_{4.5}|\mathrm{C}_{4.5}} - \left(\boldsymbol{\eta}_{1,1.5} + \mathbf{J}_{1,1.5}\vec{\mathbf{p}}^{1.5}_{\mathrm{C}_{1.5}|\mathrm{O}_{1.5}}\right) \\ \boldsymbol{\eta}^{*}_{2,1.5} \otimes \boldsymbol{\eta}_{2,3.5} - \boldsymbol{\eta}_{2,0^\circ} \\ \boldsymbol{\eta}^{*}_{2,2.5} \otimes \boldsymbol{\eta}_{2,4.5} - \boldsymbol{\eta}_{2,0^\circ} \\ \boldsymbol{\eta}^{*}_{2,3.5} \otimes \boldsymbol{\eta}_{2,4.5} - \boldsymbol{\eta}_{2,90^\circ} \end{bmatrix} = \mathbf{0}, \tag{5.57}$$

where $\boldsymbol{\eta}_{2,90^\circ} = \left[\cos\left(\pi/4\right), 0, 0, \sin\left(\pi/4\right)\right]^{\mathsf{T}}$ is the relative quaternion associated with the fixed orientation between the frame links.

5.4.1.3 Cooperative transportation

The relaxed model of the 3D cooperative transportation with I-AUVs is written as:

$$\begin{aligned} \dot{\boldsymbol{\eta}} &= \mathbf{J}\left(\boldsymbol{\eta}\right)\boldsymbol{\nu}, \\ \mathbf{M}\dot{\boldsymbol{\nu}} &= \mathbf{f}\left(\boldsymbol{\eta}, \boldsymbol{\nu}\right), \end{aligned} \tag{5.58}$$

where

$$\begin{aligned} \mathbf{J} &= \mathrm{blkdiag}\left(\mathbf{J}_1, \mathbf{J}_2, \mathbf{J}_3, \mathbf{J}_4, \mathbf{J}_5\right), \\ \mathbf{M} &= \mathrm{blkdiag}\left(\mathbf{M}_1, \mathbf{M}_2, \mathbf{M}_3, \mathbf{M}_4, \mathbf{M}_5\right), \\ \boldsymbol{\eta} &= \left[\boldsymbol{\eta}_1^{\mathsf{T}}, \boldsymbol{\eta}_2^{\mathsf{T}}, \boldsymbol{\eta}_3^{\mathsf{T}}, \boldsymbol{\eta}_4^{\mathsf{T}}, \boldsymbol{\eta}_5^{\mathsf{T}}\right]^{\mathsf{T}}, \\ \boldsymbol{\nu} &= \left[\boldsymbol{\nu}_1^{\mathsf{T}}, \boldsymbol{\nu}_2^{\mathsf{T}}, \boldsymbol{\nu}_3^{\mathsf{T}}, \boldsymbol{\nu}_4^{\mathsf{T}}, \boldsymbol{\nu}_5^{\mathsf{T}}\right]^{\mathsf{T}}, \\ \mathbf{f} &= \left[\mathbf{f}_1^{\mathsf{T}}, \mathbf{f}_2^{\mathsf{T}}, \mathbf{f}_3^{\mathsf{T}}, \mathbf{f}_4^{\mathsf{T}}, \mathbf{f}_5^{\mathsf{T}}\right]^{\mathsf{T}}. \end{aligned} \tag{5.59}$$

The constraints associated to the spherical joints connecting the end-effectors with the load vertices are written as:

$$\boldsymbol{\varphi}_{\mathrm{II}}\left(\boldsymbol{\eta}, t\right) = \begin{bmatrix} \boldsymbol{\eta}_{1,1.5} - \mathbf{J}_{1,1.5}\vec{\mathbf{p}}^{1.5}_{\mathrm{C}_{1.5}|\mathrm{O}_{1.5}} - \boldsymbol{\eta}_{1,1.7} \\ \boldsymbol{\eta}_{1,2.5} - \mathbf{J}_{1,2.5}\vec{\mathbf{p}}^{2.5}_{\mathrm{C}_{2.5}|\mathrm{O}_{2.5}} - \boldsymbol{\eta}_{1,2.7} \\ \boldsymbol{\eta}_{1,3.5} + \mathbf{J}_{1,3.5}\vec{\mathbf{p}}^{3.5}_{\mathrm{O}_{3.5}|\mathrm{C}_{3.5}} - \boldsymbol{\eta}_{1,3.7} \\ \boldsymbol{\eta}_{1,4.5} + \mathbf{J}_{1,4.5}\vec{\mathbf{p}}^{4.5}_{\mathrm{O}_{4.5}|\mathrm{C}_{4.5}} - \boldsymbol{\eta}_{1,4.7} \end{bmatrix} = \mathbf{0}. \tag{5.60}$$

5.4.2 Decentralized cooperative control

To handle the modeling and control constraints while considering the control inputs bounds, the cooperative control of the j-th agent is synthesized as a MPC using the QP-problem formulation presented in chapter 3 (see Subsec. 4.2.3.1).

Thus, let us consider the predictive model of the j-th agent written in the form of Eq. (4.159) and defined along the prediction and control horizons, p and c.

Based on Eq. (5.22), the formation constrains along the prediction horizon can be written as (the agent index is committed here to simplify the notation):

$$\tilde{\mathbf{A}}_{\text{SC}} = \text{blkdiag}\left(\mathbf{A}_{\text{SC}}, \ldots, \mathbf{A}_{\text{SC}}\right); \quad \tilde{\mathbf{b}}_{\text{SC}} = \left[\mathbf{b}_{\text{SC}}^{\mathsf{T}}, \ldots, \mathbf{b}_{\text{SC}}^{\mathsf{T}}\right]^{\mathsf{T}}. \tag{5.61}$$

With Eqs. (4.161), (4.159) and (5.61), the QP-problem of the j-th agent becomes:

$$\begin{aligned} \min_{\mathbf{U}_{\#}(\cdot)} J = \; & \left(\mathbf{Y} - \mathbf{Y}_{\mathbf{r}}\right)^{\mathsf{T}} \tilde{\mathbf{Q}}_{\mathbf{Y}} \left(\mathbf{Y} - \mathbf{Y}_{\mathbf{r}}\right) + \mathbf{U}_{\#}^{\mathsf{T}} \tilde{\mathbf{R}}_{\mathbf{U}_{\#}} \mathbf{U}_{\#}, \\ \text{s.t. } & \mathbf{Y} = \mathbf{S}_{\mathbf{x}}\mathbf{x} + \mathbf{S}_{\mathbf{U}_{\#}}\mathbf{U}_{\#} + \mathbf{S}_{\mathbf{d}}\mathbf{d} + \mathbf{S}_{\mathbf{r}}\mathbf{r}, \\ & \tilde{\mathbf{A}}_{\text{SC}}\mathbf{Y} = \tilde{\mathbf{b}}_{\text{SC}}, \\ & \mathbf{U}_{\#,\min} \leq \mathbf{U}_{\#} \leq \mathbf{U}_{\#,\max}. \end{aligned} \tag{5.62}$$

Let $\tilde{\boldsymbol{\lambda}}$ be a column-vector of Lagrange multipliers associated with the formation constraints along the prediction horizon, such that $\tilde{\boldsymbol{\lambda}} = \left[\boldsymbol{\lambda}_1^{\mathsf{T}}, \ldots, \boldsymbol{\lambda}_p^{\mathsf{T}}\right]^{\mathsf{T}}$. Thus, the modified QP-problem of the j-th agent becomes:

$$\begin{aligned} \min_{\mathbf{U}_{\#}(\cdot),\, \tilde{\boldsymbol{\lambda}}(\cdot)} J = \; & \left(\mathbf{Y} - \mathbf{Y}_{\mathbf{r}}\right)^{\mathsf{T}} \tilde{\mathbf{Q}}_{\mathbf{Y}} \left(\mathbf{Y} - \mathbf{Y}_{\mathbf{r}}\right) + \mathbf{U}_{\#}^{\mathsf{T}} \tilde{\mathbf{R}}_{\mathbf{U}_{\#}} \mathbf{U}_{\#} - \tilde{\boldsymbol{\lambda}}^{\mathsf{T}} \left(\tilde{\mathbf{A}}_{\text{SC}}\mathbf{Y} - \tilde{\mathbf{b}}_{\text{SC}}\right), \\ \text{s.t. } & \mathbf{Y} = \mathbf{S}_{\mathbf{x}}\mathbf{x} + \mathbf{S}_{\mathbf{U}_{\#}}\mathbf{U}_{\#} + \mathbf{S}_{\mathbf{d}}\mathbf{d} + \mathbf{S}_{\mathbf{r}}\mathbf{r}. \end{aligned} \tag{5.63}$$

Inserting the predictive model of Eq. (4.159) into the cost function of (5.63), we get:

$$\begin{aligned} \min_{\mathbf{U}_{\#}(\cdot),\, \tilde{\boldsymbol{\lambda}}(\cdot)} J = & \mathbf{U}_{\#}^{\mathsf{T}} \left(\mathbf{S}_{\mathbf{U}_{\#}}^{\mathsf{T}} \tilde{\mathbf{Q}}_{\mathbf{Y}} \mathbf{S}_{\mathbf{U}_{\#}} + \tilde{\mathbf{R}}_{\mathbf{U}_{\#}}\right) \mathbf{U}_{\#} + 2\left(\mathbf{S}_{\mathbf{x}}\mathbf{x} + \mathbf{S}_{\mathbf{d}}\mathbf{d} + \mathbf{S}_{\mathbf{r}}\mathbf{r} - \mathbf{Y}_{\mathbf{r}}\right)^{\mathsf{T}} \tilde{\mathbf{Q}}_{\mathbf{Y}} \mathbf{S}_{\mathbf{U}_{\#}} \mathbf{U}_{\#} + \ldots \\ & - \left(\tilde{\mathbf{A}}_{\text{SC}} \left(\mathbf{S}_{\mathbf{x}}\mathbf{x} + \mathbf{S}_{\mathbf{U}_{\#}}\mathbf{U}_{\#} + \mathbf{S}_{\mathbf{d}}\mathbf{d} + \mathbf{S}_{\mathbf{r}}\mathbf{r}\right) - \tilde{\mathbf{b}}_{\text{SC}}\right)^{\mathsf{T}} \tilde{\boldsymbol{\lambda}}. \end{aligned} \tag{5.64}$$

The conditions related to the stationary points of Eq. (5.64) follow:

$$\begin{aligned} \frac{\delta J}{\delta \mathbf{U}_{\#}} &= 2\left(\mathbf{S}_{\mathbf{U}_{\#}}^{\mathsf{T}} \tilde{\mathbf{Q}}_{\mathbf{Y}} \mathbf{S}_{\mathbf{U}_{\#}} + \tilde{\mathbf{R}}_{\mathbf{U}_{\#}}\right) \mathbf{U}_{\#} + 2\mathbf{S}_{\mathbf{U}_{\#}}^{\mathsf{T}} \tilde{\mathbf{Q}}_{\mathbf{Y}} \left(\mathbf{S}_{\mathbf{x}}\mathbf{x} + \mathbf{S}_{\mathbf{d}}\mathbf{d} + \mathbf{S}_{\mathbf{r}}\mathbf{r} - \mathbf{Y}_{\mathbf{r}}\right) - \mathbf{S}_{\mathbf{U}_{\#}}^{\mathsf{T}} \tilde{\mathbf{A}}_{\text{SC}}^{\mathsf{T}} \tilde{\boldsymbol{\lambda}} = \mathbf{0}, \\ \frac{\delta J}{\delta \tilde{\boldsymbol{\lambda}}} &= \tilde{\mathbf{A}}_{\text{SC}} \left(\mathbf{S}_{\mathbf{x}}\mathbf{x} + \mathbf{S}_{\mathbf{U}_{\#}}\mathbf{U}_{\#} + \mathbf{S}_{\mathbf{d}}\mathbf{d} + \mathbf{S}_{\mathbf{r}}\mathbf{r}\right) - \tilde{\mathbf{b}}_{\text{SC}} = \mathbf{0}. \end{aligned} \tag{5.65}$$

We can define $\mathbf{\Phi}_{\mathbf{U}_\#} = 2\left(\mathbf{S}_{\mathbf{U}_\#}^\top \tilde{\mathbf{Q}}_\mathbf{Y} \mathbf{S}_{\mathbf{U}_\#} + \tilde{\mathbf{R}}_{\mathbf{U}_\#}\right)$ as the inverse of the Hessian matrix and $\mathbf{H}_{\mathbf{U}_\#} = \tilde{\mathbf{A}}_{\mathrm{SC}} \mathbf{S}_{\mathbf{U}_\#} \mathbf{\Phi}_{\mathbf{U}_\#}^{-1/2}$. Then, Eq. (5.65) becomes:

$$\begin{aligned} \mathbf{U}_\# &= \mathbf{\Phi}_{\mathbf{U}_\#}^{-1/2}\left(\mathbf{H}_{\mathbf{U}_\#}^\top \tilde{\boldsymbol{\lambda}} - 2\mathbf{\Phi}_{\mathbf{U}_\#}^{-1/2} \mathbf{S}_{\mathbf{U}_\#}^\top \tilde{\mathbf{Q}}_\mathbf{Y}\left(\mathbf{S}_\mathbf{x}\mathbf{x} + \mathbf{S}_\mathbf{d}\mathbf{d} + \mathbf{S}_\mathbf{r}\mathbf{r} - \mathbf{Y}_\mathbf{r}\right)\right), \\ \mathbf{H}_{\mathbf{U}_\#}\mathbf{H}_{\mathbf{U}_\#}^\top \tilde{\boldsymbol{\lambda}} &= 2\mathbf{H}_{\mathbf{U}_\#}\mathbf{\Phi}_{\mathbf{U}_\#}^{-1/2} \mathbf{S}_{\mathbf{U}_\#}^\top \tilde{\mathbf{Q}}_\mathbf{Y}\left(\mathbf{S}_\mathbf{x}\mathbf{x} + \mathbf{S}_\mathbf{d}\mathbf{d} + \mathbf{S}_\mathbf{r}\mathbf{r} - \mathbf{Y}_\mathbf{r}\right) + \tilde{\mathbf{b}}_{\mathrm{SC}} - \tilde{\mathbf{A}}_{\mathrm{SC}}\left(\mathbf{S}_\mathbf{x}\mathbf{x} + \mathbf{S}_\mathbf{d}\mathbf{d} + \mathbf{S}_\mathbf{r}\mathbf{r}\right). \end{aligned} \tag{5.66}$$

Let $\tilde{\mathbf{a}}_{\mathbf{U}_\#,\mathbf{Y}} = \mathbf{S}_{\mathbf{U}_\#}^\top \tilde{\mathbf{Q}}_\mathbf{Y}\left(\mathbf{S}_\mathbf{x}\mathbf{x} + \mathbf{S}_\mathbf{d}\mathbf{d} + \mathbf{S}_\mathbf{r}\mathbf{r} - \mathbf{Y}_\mathbf{r}\right)$ be the weighted column-vector of tracking errors associated with the secondary objectives and $\tilde{\mathbf{a}}_{\mathrm{SC}} = \tilde{\mathbf{b}}_{\mathrm{SC}} - \tilde{\mathbf{A}}_{\mathrm{SC}}\left(\mathbf{S}_\mathbf{x}\mathbf{x} + \mathbf{S}_\mathbf{d}\mathbf{d} + \mathbf{S}_\mathbf{r}\mathbf{r}\right)$ the column-vector of tracking errors related to the formation. Thus, Eq. (5.66) can be rewritten as:

$$\begin{aligned} \mathbf{U}_\# &= \mathbf{\Phi}_{\mathbf{U}_\#}^{-1/2}\left(\mathbf{H}_{\mathbf{U}_\#}^\top \tilde{\boldsymbol{\lambda}} - 2\mathbf{\Phi}_{\mathbf{U}_\#}^{-1/2} \tilde{\mathbf{a}}_{\mathbf{U}_\#,\mathbf{Y}}\right), \\ \mathbf{H}_{\mathbf{U}_\#}\mathbf{H}_{\mathbf{U}_\#}^\top \tilde{\boldsymbol{\lambda}} &= 2\mathbf{H}_{\mathbf{U}_\#}\mathbf{\Phi}_{\mathbf{U}_\#}^{-1/2} \tilde{\mathbf{a}}_{\mathbf{U}_\#,\mathbf{Y}} + \tilde{\mathbf{a}}_{\mathrm{SC}}. \end{aligned} \tag{5.67}$$

The unconstrained solution (disregarding the control inputs bounds) of the QP-problem of Eq. (5.62) is given by:

$$\mathbf{U}_\# = \mathbf{\Phi}_{\mathbf{U}_\#}^{-1/2}\left(\mathbf{H}_{\mathbf{U}_\#}^{\mathrm{g}} \tilde{\mathbf{a}}_{\mathrm{SC}} - 2\left(\mathbf{I} - \mathbf{H}_{\mathbf{U}_\#}^{\mathrm{g}}\mathbf{H}_{\mathbf{U}_\#}\right)\mathbf{\Phi}_{\mathbf{U}_\#}^{-1/2} \tilde{\mathbf{a}}_{\mathbf{U}_\#,\mathbf{Y}}\right). \tag{5.68}$$

Let $\mathbf{P}_{\mathbf{U}_\#} = \mathbf{I} - \mathbf{H}_{\mathbf{U}_\#}^{\mathrm{g}}\mathbf{H}_{\mathbf{U}_\#}$ be the orthogonal projector onto the kernel of $\mathbf{H}_{\mathbf{U}_\#}$ such that $\mathbf{H}_{\mathbf{U}_\#}\mathbf{P}_{\mathbf{U}_\#} = \mathbf{P}_{\mathbf{U}_\#}^\top \mathbf{H}_{\mathbf{U}_\#}^\top = \mathbf{0}$. Then, Eq. (5.68) can be rewritten as:

$$\mathbf{U}_\# = \mathbf{\Phi}_{\mathbf{U}_\#}^{-1/2}\mathbf{H}_{\mathbf{U}_\#}^{\mathrm{g}} \tilde{\mathbf{a}}_{\mathrm{SC}} - 2\mathbf{\Phi}_{\mathbf{U}_\#}^{-1/2}\mathbf{P}_{\mathbf{U}_\#}\mathbf{\Phi}_{\mathbf{U}_\#}^{-1/2} \tilde{\mathbf{a}}_{\mathbf{U}_\#,\mathbf{Y}}. \tag{5.69}$$

For numerical implementation, Eq. (5.69) should be saturated to consider the control inputs bounds, as below:

$$\mathbf{U}_\# = \mathrm{sat}\left(\mathbf{\Phi}_{\mathbf{U}_\#}^{-1/2}\mathbf{H}_{\mathbf{U}_\#}^{\mathrm{g}} \tilde{\mathbf{a}}_{\mathrm{SC}} - 2\mathbf{\Phi}_{\mathbf{U}_\#}^{-1/2}\mathbf{P}_{\mathbf{U}_\#}\mathbf{\Phi}_{\mathbf{U}_\#}^{-1/2} \tilde{\mathbf{a}}_{\mathbf{U}_\#,\mathbf{Y}}, \mathbf{U}_{\#,\min}, \mathbf{U}_{\#,\max}\right). \tag{5.70}$$

To simplify the implementation, Eq. (5.70) control can be rewritten as a two-loop controller, as follows:

$$\mathbf{U}_\# = \mathrm{sat}\left(\mathbf{C}_1 \tilde{\mathbf{a}}_{\mathrm{SC}} + \mathbf{C}_2 \tilde{\mathbf{a}}_{\mathbf{U}_\#,\mathbf{Y}}, \mathbf{U}_{\#,\min}, \mathbf{U}_{\#,\max}\right), \tag{5.71}$$

where $\mathbf{C}_1 = \mathbf{\Phi}_{\mathbf{U}_\#}^{-1/2}\mathbf{H}_{\mathbf{U}_\#}^{\mathrm{g}}$ and $\mathbf{C}_2 = -2\mathbf{\Phi}_{\mathbf{U}_\#}^{-1/2}\mathbf{P}_{\mathbf{U}_\#}\mathbf{\Phi}_{\mathbf{U}_\#}^{-1/2}$.

The block diagram of the two-loop control structure of the j-th agent is shown by Fig. 109. The first controller, $\mathbf{C}_1$, is associated with the formation-keeping and the second one, $\mathbf{C}_2$, is related to the secondary objectives.

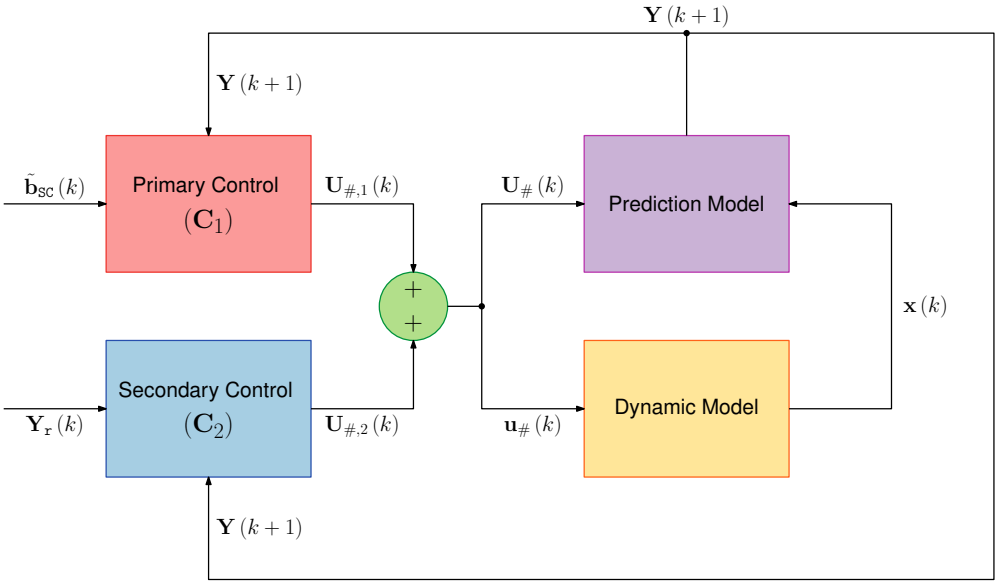

Figure 109: Two-Loop MPC block diagram

In order to consider the control inputs bounds direct on the optimization, the QP-problem of Eq. (5.62) can be rewritten as:

$$\begin{aligned}
\min_{\mathbf{U}_{\#}(\cdot),\,\tilde{\boldsymbol{\lambda}}(\cdot)} \; J &= \frac{1}{2}\mathbf{U}_{\#}^{\mathsf{T}}\boldsymbol{\Phi}_{\mathbf{U}_{\#}}\mathbf{U}_{\#} + 2\tilde{\mathbf{a}}_{\mathbf{U}_{\#},\mathbf{Y}}^{\mathsf{T}}\mathbf{U}_{\#} - \mathbf{U}_{\#}^{\mathsf{T}}\boldsymbol{\Phi}_{\mathbf{U}_{\#}}^{1/2}\boldsymbol{\Phi}_{\mathbf{U}_{\#}}^{-1/2}\mathbf{S}_{\mathbf{U}_{\#}}^{\mathsf{T}}\tilde{\mathbf{A}}_{\text{SC}}^{\mathsf{T}}\tilde{\boldsymbol{\lambda}}, \\
&= \frac{1}{2}\mathbf{U}_{\#}^{\mathsf{T}}\boldsymbol{\Phi}_{\mathbf{U}_{\#}}\mathbf{U}_{\#} + 2\tilde{\mathbf{a}}_{\mathbf{U}_{\#},\mathbf{Y}}^{\mathsf{T}}\mathbf{U}_{\#} - \mathbf{U}_{\#}^{\mathsf{T}}\boldsymbol{\Phi}_{\mathbf{U}_{\#}}^{1/2}\mathbf{H}_{\mathbf{U}_{\#}}^{\mathsf{T}}\tilde{\boldsymbol{\lambda}}, \\
\text{s.t. } & \mathbf{H}_{\mathbf{U}_{\#}}\mathbf{H}_{\mathbf{U}_{\#}}^{\mathsf{T}}\tilde{\boldsymbol{\lambda}} = 2\mathbf{H}_{\mathbf{U}_{\#}}\boldsymbol{\Phi}_{\mathbf{U}_{\#}}^{-1/2}\tilde{\mathbf{a}}_{\mathbf{U}_{\#},\mathbf{Y}} + \tilde{\mathbf{a}}_{\text{SC}}, \\
& \mathbf{U}_{\#,\min} \leq \mathbf{U}_{\#} \leq \mathbf{U}_{\#,\max}.
\end{aligned} \tag{5.72}$$

Let $\mathbf{H}_{\mathbf{U}_{\#}}^{\text{g}}$ be any $\{1,4\}$-inverse of $\mathbf{H}_{\mathbf{U}_{\#}}$, such that inserting the equality constraints associated with the Lagrange multipliers related to the formation constraints into the cost function of Eq. (5.72), results in:

$$\begin{aligned}
\min_{\mathbf{U}_{\#}(\cdot)} J &= \frac{1}{2}\mathbf{U}_{\#}^{\mathsf{T}}\boldsymbol{\Phi}_{\mathbf{U}_{\#}}\mathbf{U}_{\#} + 2\tilde{\mathbf{a}}_{\mathbf{U}_{\#},\mathbf{Y}}^{\mathsf{T}}\mathbf{U}_{\#} - \left(2\mathbf{H}_{\mathbf{U}_{\#}}^{\text{g}}\mathbf{H}_{\mathbf{U}_{\#}}\boldsymbol{\Phi}_{\mathbf{U}_{\#}}^{-1/2}\tilde{\mathbf{a}}_{\mathbf{U}_{\#},\mathbf{Y}} + \mathbf{H}_{\mathbf{U}_{\#}}^{\text{g}}\tilde{\mathbf{a}}_{\text{SC}}\right)^{\mathsf{T}}\boldsymbol{\Phi}_{\mathbf{U}_{\#}}^{1/2}\mathbf{U}_{\#}, \\
&= \frac{1}{2}\mathbf{U}_{\#}^{\mathsf{T}}\boldsymbol{\Phi}_{\mathbf{U}_{\#}}\mathbf{U}_{\#} + 2\tilde{\mathbf{a}}_{\mathbf{U}_{\#},\mathbf{Y}}^{\mathsf{T}}\boldsymbol{\Phi}_{\mathbf{U}_{\#}}^{-1/2}\boldsymbol{\Phi}_{\mathbf{U}_{\#}}^{1/2}\mathbf{U}_{\#} - \left(2\mathbf{H}_{\mathbf{U}_{\#}}^{\text{g}}\mathbf{H}_{\mathbf{U}_{\#}}\boldsymbol{\Phi}_{\mathbf{U}_{\#}}^{-1/2}\tilde{\mathbf{a}}_{\mathbf{U}_{\#},\mathbf{Y}} + \mathbf{H}_{\mathbf{U}_{\#}}^{\text{g}}\tilde{\mathbf{a}}_{\text{SC}}\right)^{\mathsf{T}}\boldsymbol{\Phi}_{\mathbf{U}_{\#}}^{1/2}\mathbf{U}_{\#}, \\
&= \frac{1}{2}\mathbf{U}_{\#}^{\mathsf{T}}\boldsymbol{\Phi}_{\mathbf{U}_{\#}}\mathbf{U}_{\#} + \left(2\tilde{\mathbf{a}}_{\mathbf{U}_{\#},\mathbf{Y}}^{\mathsf{T}}\boldsymbol{\Phi}_{\mathbf{U}_{\#}}^{-1/2} - 2\tilde{\mathbf{a}}_{\mathbf{U}_{\#},\mathbf{Y}}^{\mathsf{T}}\boldsymbol{\Phi}_{\mathbf{U}_{\#}}^{-1/2}\left(\mathbf{H}_{\mathbf{U}_{\#}}^{\text{g}}\mathbf{H}_{\mathbf{U}_{\#}}\right)^{\mathsf{T}} + \tilde{\mathbf{a}}_{\text{SC}}^{\mathsf{T}}\left(\mathbf{H}_{\mathbf{U}_{\#}}^{\text{g}}\right)^{\mathsf{T}}\right)\boldsymbol{\Phi}_{\mathbf{U}_{\#}}^{1/2}\mathbf{U}_{\#}, \\
&= \frac{1}{2}\mathbf{U}_{\#}^{\mathsf{T}}\boldsymbol{\Phi}_{\mathbf{U}_{\#}}\mathbf{U}_{\#} + \left(2\tilde{\mathbf{a}}_{\mathbf{U}_{\#},\mathbf{Y}}^{\mathsf{T}}\boldsymbol{\Phi}_{\mathbf{U}_{\#}}^{-1/2}\left(\mathbf{I} - \left(\mathbf{H}_{\mathbf{U}_{\#}}^{\text{g}}\mathbf{H}_{\mathbf{U}_{\#}}\right)^{\mathsf{T}}\right) + \tilde{\mathbf{a}}_{\text{SC}}^{\mathsf{T}}\left(\mathbf{H}_{\mathbf{U}_{\#}}^{\text{g}}\right)^{\mathsf{T}}\right)\boldsymbol{\Phi}_{\mathbf{U}_{\#}}^{1/2}\mathbf{U}_{\#}, \\
&= \frac{1}{2}\mathbf{U}_{\#}^{\mathsf{T}}\boldsymbol{\Phi}_{\mathbf{U}_{\#}}\mathbf{U}_{\#} + \left(2\tilde{\mathbf{a}}_{\mathbf{U}_{\#},\mathbf{Y}}^{\mathsf{T}}\boldsymbol{\Phi}_{\mathbf{U}_{\#}}^{-1/2}\mathbf{P}_{\mathbf{U}_{\#}}^{\mathsf{T}} + \tilde{\mathbf{a}}_{\text{SC}}^{\mathsf{T}}\left(\mathbf{H}_{\mathbf{U}_{\#}}^{\text{g}}\right)^{\mathsf{T}}\right)\boldsymbol{\Phi}_{\mathbf{U}_{\#}}^{1/2}\mathbf{U}_{\#}, \\
\text{s.t. } & \mathbf{U}_{\#,\min} \leq \mathbf{U}_{\#} \leq \mathbf{U}_{\#,\max}.
\end{aligned} \tag{5.73}$$

Finally, Eq. (5.73) can be rewritten as follows:

$$\begin{aligned} \min_{\mathbf{U}_{\#}(\cdot)} J &= \mathbf{U}_{\#}^{\mathsf{T}}\mathbf{H}_{\mathrm{QP}}\mathbf{U}_{\#} + \mathbf{f}_{\mathrm{QP}}\mathbf{U}_{\#}, \\ \text{s.t. } \mathbf{G}_{\mathrm{QP}}\mathbf{U}_{\#} &\leq \boldsymbol{\varphi}_{\mathrm{QP}}, \end{aligned} \tag{5.74}$$

where

$$\begin{aligned} \mathbf{H}_{\mathrm{QP}} &= \frac{1}{2}\boldsymbol{\Phi}_{\mathbf{U}_{\#}} = \mathbf{S}_{\mathbf{U}_{\#}}^{\mathsf{T}}\tilde{\mathbf{Q}}_{\mathbf{Y}}\mathbf{S}_{\mathbf{U}_{\#}} + \tilde{\mathbf{R}}_{\mathbf{U}_{\#}}, \\ \mathbf{f}_{\mathrm{QP}} &= \left(2\tilde{\mathbf{a}}_{\mathbf{U}_{\#},\mathbf{Y}}^{\mathsf{T}}\boldsymbol{\Phi}_{\mathbf{U}_{\#}}^{-1/2}\mathbf{P}_{\mathbf{U}_{\#}}^{\mathsf{T}} + \tilde{\mathbf{a}}_{\mathrm{SC}}^{\mathsf{T}}\left(\mathbf{H}_{\mathbf{U}_{\#}}^{\mathrm{g}}\right)^{\mathsf{T}}\right)\boldsymbol{\Phi}_{\mathbf{U}_{\#}}^{1/2}, \\ \mathbf{G}_{\mathrm{QP}} &= \mathrm{blkdiag}\left(-\mathbf{I}, +\mathbf{I}\right), \\ \boldsymbol{\varphi}_{\mathrm{QP}} &= \left[\mathbf{U}_{\#,\min}^{\mathsf{T}}, \mathbf{U}_{\#,\max}^{\mathsf{T}}\right]^{\mathsf{T}}, \\ \mathbf{U}_{\#,\min} &= \left[\mathbf{u}_{\#,\min}^{\mathsf{T}}, \ldots, \mathbf{u}_{\#,\min}^{\mathsf{T}}\right]^{\mathsf{T}}, \\ \mathbf{U}_{\#,\max} &= \left[\mathbf{u}_{\#,\max}^{\mathsf{T}}, \ldots, \mathbf{u}_{\#,\max}^{\mathsf{T}}\right]^{\mathsf{T}}. \end{aligned} \tag{5.75}$$

5.4.3 Results

The decentralized cooperative control versions (saturated and QP-problem) are tested on the tracking problem of a cycloidal trajectory as described in Sec. 5.1.

The simulations are performed using the previously specified setup. The modeling and control parameters are shown in Tabs. 18 and 19.

The off-sets values in the form of Eq. (5.32) are given by (in meters and radians):

$$\begin{aligned} \boldsymbol{\delta}_1 &= \begin{bmatrix} 2 & 0 & 0 & 0 & 4 \\ 2 & 0 & 4 & 0 & 0 \\ 0 & 0 & 0 & 0 & 0 \\ 0 & 0 & 0 & 0 & 0 \\ 0 & 0 & 0 & 0 & 0 \\ 0 & 0 & 0 & 0 & 0 \end{bmatrix}; \qquad \boldsymbol{\delta}_2 = \begin{bmatrix} 2 & 0 & 0 & 4 & 0 \\ -2 & -4 & 0 & 0 & 0 \\ 0 & 0 & 0 & 0 & 0 \\ 0 & 0 & 0 & 0 & 0 \\ 0 & 0 & 0 & 0 & 0 \\ 0 & 0 & 0 & 0 & 0 \end{bmatrix}, \\ \boldsymbol{\delta}_3 &= \begin{bmatrix} -2 & 0 & -4 & 0 & 0 \\ -2 & 0 & 0 & 0 & -4 \\ 0 & 0 & 0 & 0 & 0 \\ 0 & 0 & 0 & 0 & 0 \\ 0 & 0 & 0 & 0 & 0 \\ 0 & 0 & 0 & 0 & 0 \end{bmatrix}; \quad \boldsymbol{\delta}_4 = \begin{bmatrix} -2 & -4 & 0 & 0 & 0 \\ 2 & 0 & 0 & 4 & 0 \\ 0 & 0 & 0 & 0 & 0 \\ 0 & 0 & 0 & 0 & 0 \\ 0 & 0 & 0 & 0 & 0 \\ 0 & 0 & 0 & 0 & 0 \end{bmatrix}. \end{aligned} \tag{5.76}$$

To keep the manipulator joints static during the transportation, the following servo-constraints are added on the sliding surfaces of the formation-keeping:

$$\dot{\boldsymbol{\varphi}}_{\mathrm{SC},j}\left(\ddot{\boldsymbol{\gamma}}_j, \dot{\boldsymbol{\gamma}}_j, \boldsymbol{\gamma}_j, t\right) = \ddot{\boldsymbol{\gamma}}_j + \lambda_j \dot{\boldsymbol{\gamma}}_j + k_j \boldsymbol{\gamma}_j = \mathbf{0}, \tag{5.77}$$

where $\lambda_j > 0$ and $k_j > 0$ are stabilization coefficients.

Table 18: 9-DoFs I-AUV and load model parameters

Symbols	Values	Units (SI)
$\mathbf{M}_{\mathrm{RB},1}$	diag(0.95, 0.95, 0.95, 0.001, 0.02, 0.02)	kg, kgm^2
$\mathbf{M}_{\mathrm{RB},2}$	diag(1.41, 1.41, 1.41, 0.0014, 0.0014, 0.0014)	kg, kgm^2
$\mathbf{M}_{\mathrm{RB},5}$	diag(7.58, 7.58, 7.58, 0.001, 10.11, 10.11)	kg, kgm^2
$\mathbf{M}_{\mathrm{A},1}$	diag(1410, 3000, 33.44, 1410, 3000, 33.44)	kg, kgm^2
$\mathbf{M}_{\mathrm{A},2}$	diag(1.41, 1.41, 1.41, 0, 0, 0)	kg, kgm^2
$\mathbf{M}_{\mathrm{A},5}$	diag(0.08, 4, 0.33, 0.08, 4, 0.33)	kg, kgm^2
$\mathbf{D}_1$	diag(1.96, 1.96, 1.96, 0, 0, 0)	Ns/m, Nms
$C_{\mathrm{D,x_2}}, C_{\mathrm{D,y_2}}, C_{\mathrm{D,z_2}}, \delta_2$	0, 1.2, 1.2, 0.001	–
$2l_2, d_2, \Delta l_2$	0.5, 0.05, 0.05	m
$2l_5, d_5, \Delta l_5$	4, 0.05, 0.40	m
W_1, B_1	9.29, 9.63	N
W_2, B_2	13.87, 5.14	N
W_5, B_5	74.35, 77.05	N
$\vec{\mathbf{p}}^{1}_{\mathrm{G}_1\mid\mathrm{O}_1}$	$[0, 0, 0]^{\mathsf{T}}$	m
$\vec{\mathbf{p}}^{1}_{\mathrm{B}_1\mid\mathrm{O}_1}$	$[0, 0, 0]^{\mathsf{T}}$	m
$\vec{\mathbf{p}}^{2}_{\mathrm{G}_2\mid\mathrm{O}_2}$	$[0, 0, 0]^{\mathsf{T}}$	m
$\vec{\mathbf{p}}^{2}_{\mathrm{B}_2\mid\mathrm{O}_2}$	$[0, 0, 0]^{\mathsf{T}}$	m
$\vec{\mathbf{p}}^{5}_{\mathrm{G}_5\mid\mathrm{O}_5}$	$[0, 0, 0]^{\mathsf{T}}$	m
$\vec{\mathbf{p}}^{5}_{\mathrm{B}_5\mid\mathrm{O}_5}$	$[0, 0, 0]^{\mathsf{T}}$	m
$N_{\mathrm{M}}, \eta_{\mathrm{M}}$	10, 0.9	–
$b_{\mathrm{M}}, c_{\mathrm{M}}$	1, 0.1	Nms, Nm

Table 19: 9-DoFs I-AUV control parameters

Symbols	Values	Units (SI)
$\mathbf{\Lambda}$	diag(1, 1, 1, 1, 1, 1, 1, 1, 1)	$1/s$
$\mathbf{K}$	diag(10, 10, 10, 10, 10, 10, 10, 10, 10)	$m/s^2, rad/s^2$
$\mathbf{L}$	diag(100, 100, 100, 100, 100, 100, 100, 100, 100)	$1/s$
ϵ	1	–
$\mathbf{Q_Y}$	diag(0, 0, 0, 0, 0, 0, 0, 0, 0)	–
$\mathbf{R_{U_\#}}$	diag(10, 10, 10, 10, 10, 10, 10, 10, 100, 100, 100)	–
$\mathbf{\Omega_a}$	diag (100, 100, 100, 100, 100, 100, 100, 100, 100)	rad/s
p, c	20, 20	–
T_s	0.01	s
λ, k	10, 100	$1/s, 1/s^2$

Figures 110 to 115 show the results for the saturated control of Eq. (5.74). Figure 110 shows the displacements of each agent. We can see that the motion performed by the agents is continuous and smooth. In this case, there are no oscillations due to the relative velocity effects on the thrusters propeller once the system goes down, thus, reducing the influence of the wave forces. The commanded thrusts and motor torques are shown in Fig. 111. In this case, there is no saturation at the beginning of the simulation since the motion starts at the desired trajectory, as shown on the trajectory tracking in Fig. 113. Concerning the task performance, the controller keeps the system stable and performs the tracking with good performance as shown by the path and coordinates tracking in Fig. 113 (a) and (b), respectively. Figure 114 shows some animation frames of the 3D cooperative transportation with I-AUVs to illustrate the motion performed during the trajectory tracking.

The modeling and servo-constraints orders are 10^{-6} and 10^{-1} as shown in Fig. 115.

Figures 116 to 121 show the results for the QP-problem control of Eq. (5.72). The tracking performance is similar to the saturated control, as can be seen in Figs. 116, 119 and 114. The modeling and servo-constraints orders are similar to the saturated control, as shown in Fig. 121. However, the control inputs calculated by Eq. (5.72) and shown in Figs. 117 and 118 are prone to chattering due to the sensitive of the QP to the measurements noises.

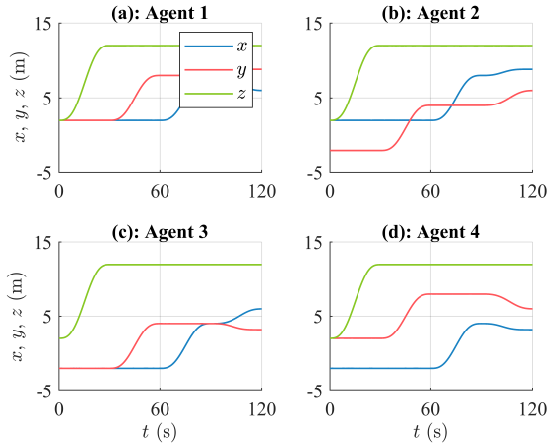

(a): Linear displacements

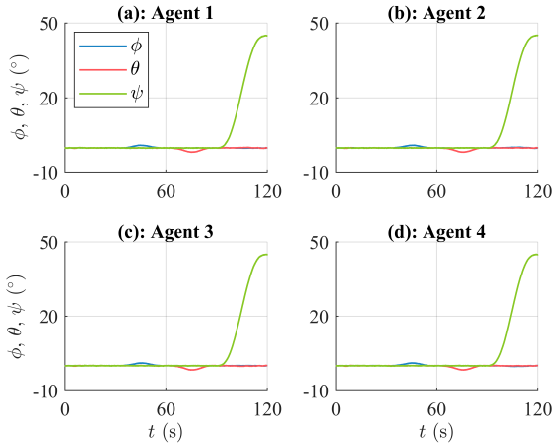

(b): Angular displacements

Figure 110: Agents displacements on the 3D cooperative transportation with I-AUVs (saturated)

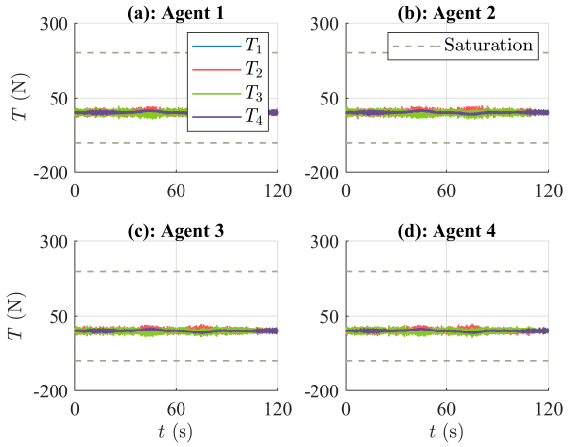

(a): Thrusts $(T_1, \ldots, T_4)$

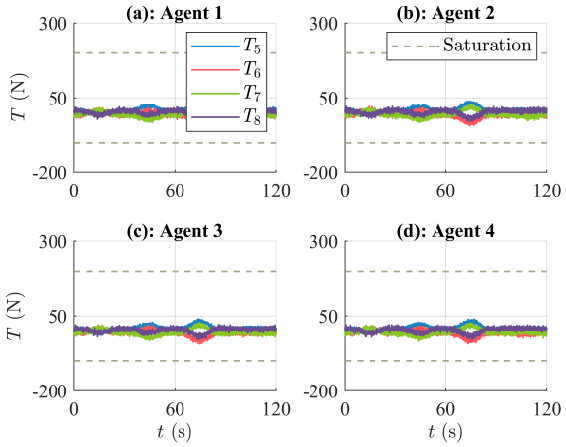

(b): Thrusts $(T_5, \ldots, T_8)$

Figure 111: Agents thrusts on the 3D cooperative transportation with I-AUVs (saturated)

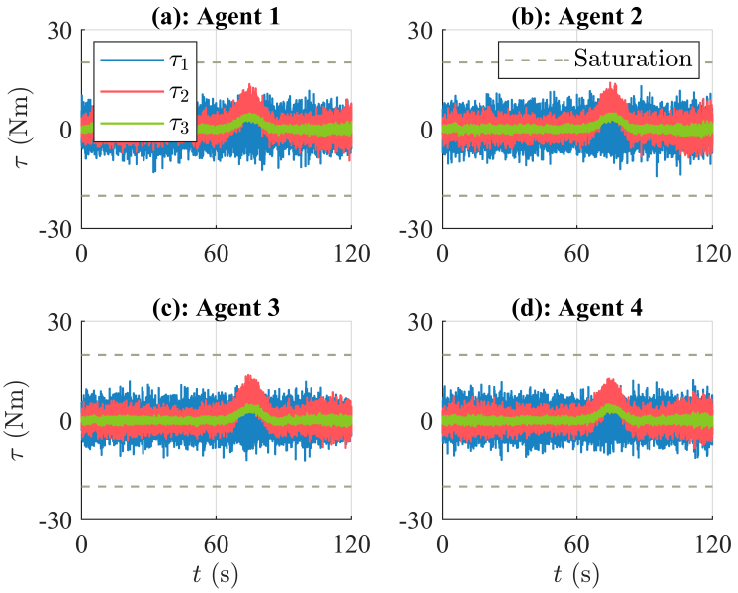

Figure 112: Agents torques on the 3D cooperative transportation with I-AUVs (saturated)

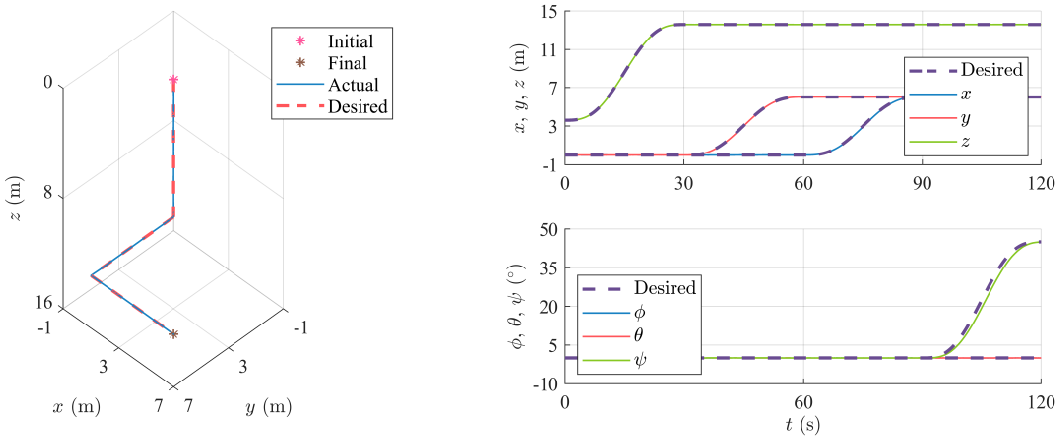

(a): Path tracking

(b): Load displacements

Figure 113: Load tracking on the 3D cooperative transportation with I-AUVs (saturated)

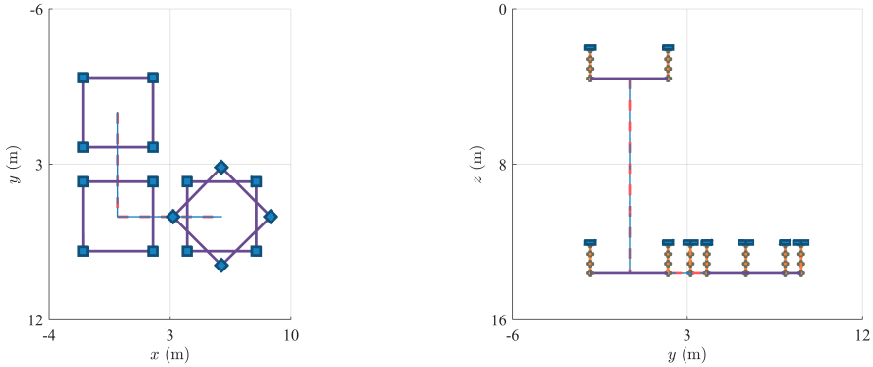

(a): *xy*-plane (b): *yz*-plane

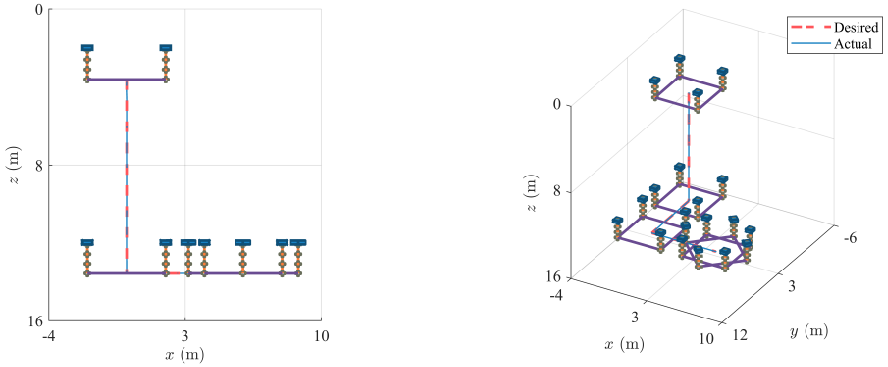

(a): *xz*-plane (b): 3D plot

Figure 114: Frames of the 3D cooperative transportation with I-AUVs (saturated)

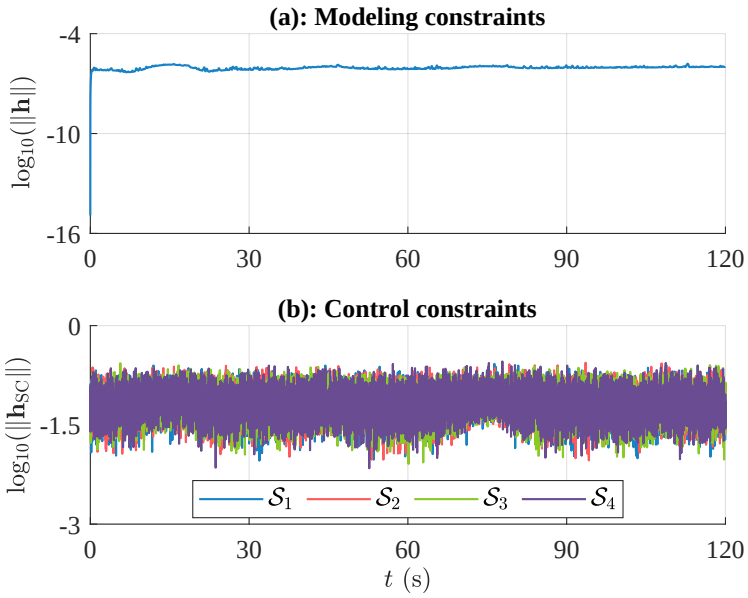

Figure 115: Constraints of the 3D cooperative transportation with I-AUVs (saturated)

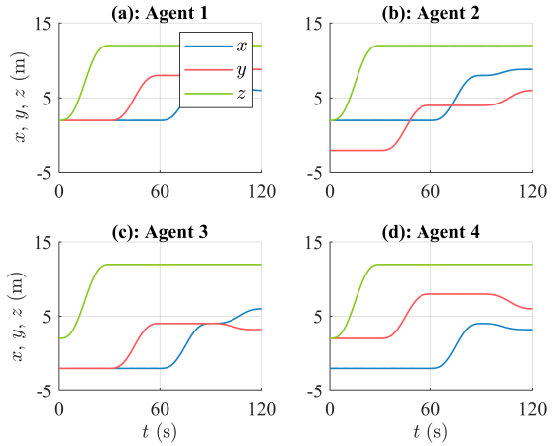

(a): Linear displacements

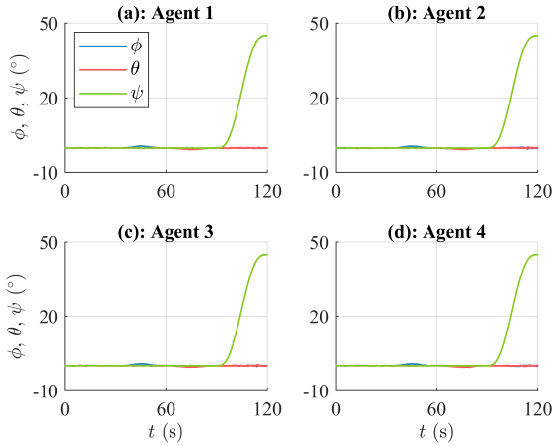

(b): Angular displacements

Figure 116: Agents displacements on the 3D cooperative transportation with I-AUVs (QP-problem)

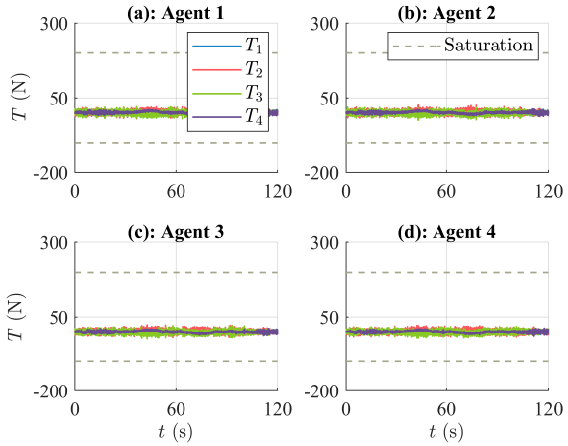

(a): Thrusts $(T_1, \ldots, T_4)$

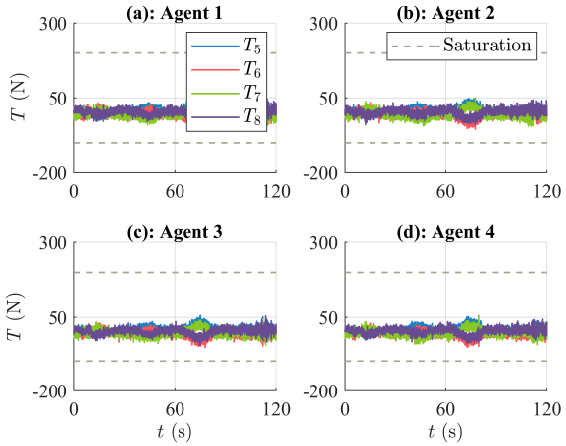

(b): Thrusts $(T_5, \ldots, T_8)$

Figure 117: Agents thrusts on the 3D cooperative transportation with I-AUVs (QP-problem)

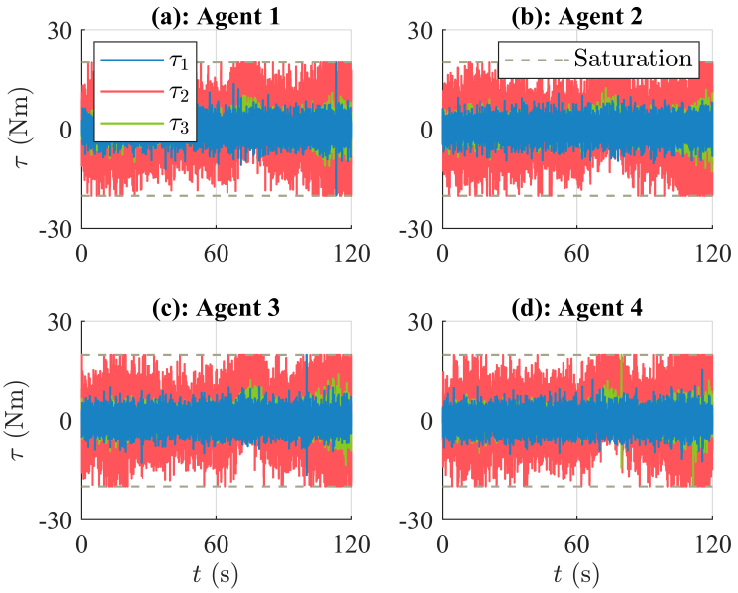

Figure 118: Agents torques on the 3D cooperative transportation with I-AUVs (QP-problem)

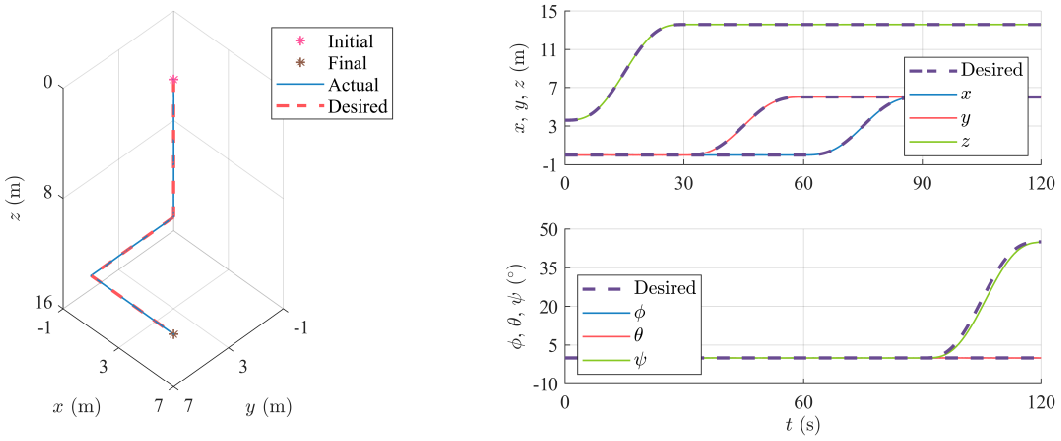

(a): Path tracking

(b): Load displacements

Figure 119: Load tracking on the 3D cooperative transportation with I-AUVs (QP-problem)

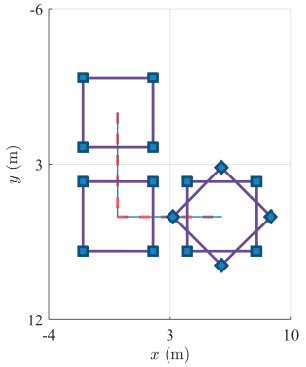

(a): *xy*-plane

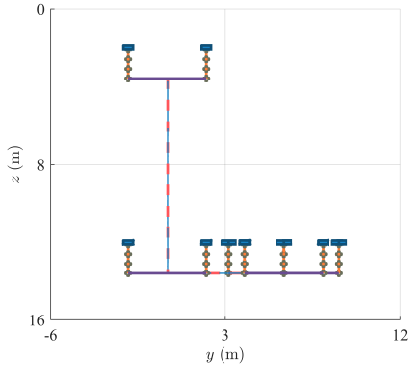

(b): *yz*-plane

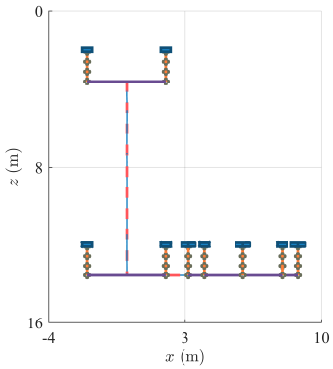

(a): *xz*-plane

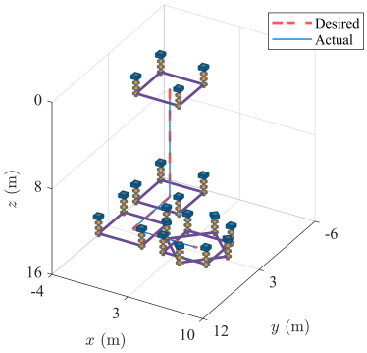

(b): 3D plot

Figure 120: Frames of the 3D cooperative transportation with I-AUVs (QP-problem)

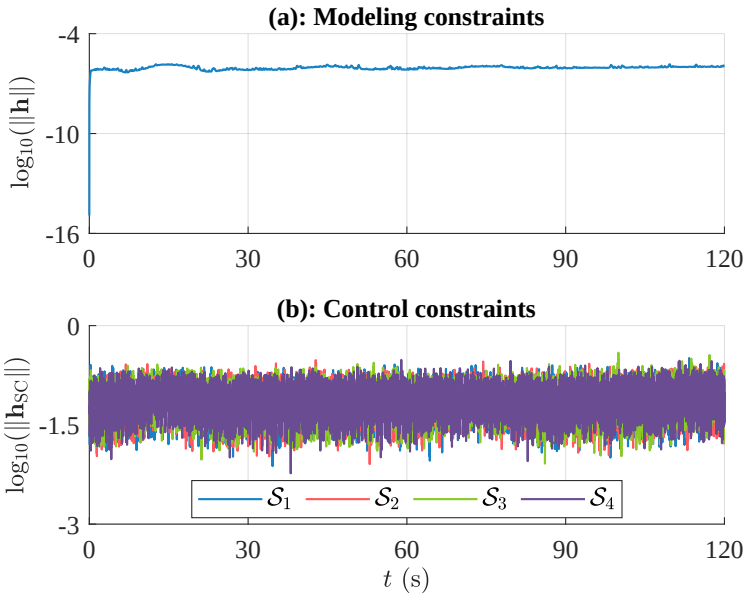

Figure 121: Constraints of the 3D cooperative transportation with I-AUVs (QP-problem)

5.5 COMMENTARIES

This chapter presented three cases of study of underwater cooperative transportation. The first case considered the 2D cooperative transportation performed by a group of I-AUVs on the horizontal plane. In this first example, we developed a predictive filter based on the state-space form of the Udwadia-Kalaba equation of chapter 4 to perform the agents coordination. The second case concerns the 3D cooperative transportation performed by a group of modular ROVs. In this example, we used the MCM formulated with control allocation to synthesize a centralized cooperative control. The third case concerns the 3D cooperative transportation performed by a group of I-AUVs. In this last example, we merged the agents coordination and control using the MPC and the servo-constraints approach presented in chapter 4. All cases of study are evaluated through detailed numerical simulations, considering disturbances, actuators dynamic, sensor measurements and sampling effects.

6 CONCLUSIONS

In this thesis, we presented modular methodologies for modeling and controlling UVMSs applied to cooperative transportation, which can also be used for general underwater or off-the-self multibody systems.

The modeling approach enables the derivation of the EoMs of any underwater multibody system starting from bases models, e.g., the 3D submerged body model, and then projecting the relaxed model in the directions compatible with the modeling constraints *a posteriori* and recursively, according to the modeling hierarchical defined. The constrained EoMs are obtained in the classical form of the UUVs dynamic, which permits the direct application of already existing algorithms for control, filtering, estimation, localization, etc. The modeling methodology is validated through numerical simulations, reproducing experiments of underwater multibody systems reported in the literature.

The modular control methodology permits the control synthesis through a hierarchical approach starting from already available decentralized controllers of the subsystems and imposing the constraints *a posteriori* according to the control hierarchy defined. The methodology also can handle the control allocation, decentralized controllers synthesis with prescribed servo-constraints and optimal control formulation. The modular control methodology is tested with classical robot systems used for control design (e.g., inverted pendulum, slider-crank mechanism, RR-manipulator) and more complex mechanisms with parallel kinematic structure. Some tests are also performed with a digital twin of a 2-DoFs helicopter and an inverted pendulum prototype. Moreover, the modular control methodology was then applied to underwater cooperative transportation problems performed by groups of I-AUVs and modular ROVs, resulting in the following developments:

- A decentralized predictive-cooperative reference filter based on the state-space form of the Udwadia-Kalaba equation to perform the agents coordination;
- A centralized cooperative control based on the servo-constraints formulation and with control allocation;

- A decentralized model predictive control that combines the agents coordination with its low-level control using the state-space form of the Udwadia-Kalaba equation and the servo constraints formulation.

All problems were evaluated through detailed numerical simulations, considering disturbances (e.g., modeling errors, ocean current, etc.), actuator dynamics (e.g., thrusters and motors dynamics), sensor measurements, noise and sampling effects. The results confirm the applicability of the proposed approaches for such complex multibody-multiagent systems. However, experimental tests still needed to be performed.

For future works, we suggest the following topics:

- Perform experimental tests with the modular control methodology in other standard robotic systems, e.g., double inverted pendulum, 3-DoFs helicopter, 3D gyroscopic, etc.;
- Explore the recursive modular formulation based on the Kalman filter algorithm to compensate for numerical instabilities, modeling errors, disturbances, etc.;
- Adapt the modular control methodology to other cooperative systems, such as aerial and ground vehicles, with manipulation capabilities or not.

REFERENCES

ALMEIDA, J.; SILVESTRE, C.; PASCOAL, A. Synchronization of Multiagent Systems Using Event-Triggered and Self-Triggered Broadcasts. *IEEE Transactions on Automatic Control*, v. 62, n. 9, p. 4741–4746, sep 2017. ISSN 0018-9286. Disponível em: <http://ieeexplore.ieee.org/document/7858661/>.

ANTONELLI, G. *Underwater Robots*. Cham: Springer International Publishing, 2014. v. 96. 595–622 p. (Springer Tracts in Advanced Robotics, v. 96). ISBN 978-3-319-02876-7. Disponível em: <http://link.springer.com/10.1007/978-3-319-32552-1_25>.

ANTONELLI, G.; CATALDI, E. Recursive adaptive control for an underwater vehicle carrying a manipulator. In: *22nd Mediterranean Conference on Control and Automation*. IEEE, 2014. p. 847–852. ISBN 978-1-4799-5901-3. Disponível em: <http://ieeexplore.ieee.org/document/6961479/>.

ANTONELLI, G.; CHIAVERINI, S. Task-priority redundancy resolution for underwater vehicle-manipulator systems. In: *Proceedings. 1998 IEEE International Conference on Robotics and Automation (Cat. No.98CH36146)*. IEEE, 1998. v. 1, n. May, p. 768–773. ISBN 0-7803-4300-X. Disponível em: <http://ieeexplore.ieee.org/document/677070/>.

BACHMAYER, R.; WHITCOMB, L.; GROSENBAUGH, M. An accurate four-quadrant nonlinear dynamical model for marine thrusters: theory and experimental validation. *IEEE Journal of Oceanic Engineering*, v. 25, n. 1, p. 146–159, jan 2000. ISSN 0364-9059. Disponível em: <http://ieeexplore.ieee.org/document/820747/>.

BAE, J. et al. Cooperative Underwater Vehicle-Manipulator Operation Using Redundant Resolution Method. *International Journal of Precision Engineering and Manufacturing*, Korean Society for Precision Engineering, v. 23, n. 9, p. 1003–1017, 2022. ISSN 20054602. Disponível em: <https://doi.org/10.1007/s12541-022-00685-4>.

BARBALATA, C. *Modelling and Control of Lightweight Underwater Vehicle-Manipulator Systems*. 206 p. Tese (Ph.D. Thesis) — Heriot-Watt University, 2017.

BARBALATA, C.; DUNNIGAN, M. W.; PETILLOT, Y. Dynamic coupling and control issues for a lightweight underwater vehicle manipulator system. In: *2014 Oceans - St. John's*. IEEE, 2014. p. 1–6. ISBN 978-1-4799-4918-2. Disponível em: <http://ieeexplore.ieee.org/document/7002989/>.

____. Coupled and Decoupled Force/Motion Controllers for an Underwater Vehicle-Manipulator System. *Journal of Marine Science and Engineering*, v. 6, n. 3, p. 96, aug 2018. ISSN 2077-1312. Disponível em: <http://www.mdpi.com/2077-1312/6/3/96>.

BAUMGARTE, J. Stabilization of constraints and integrals of motion in dynamical systems. *Computer Methods in Applied Mechanics and Engineering*, v. 1, n. 1, p. 1–16, jun 1972. ISSN 00457825. Disponível em: <https://linkinghub.elsevier.com/retrieve/pii/0045782572900187>.

BESSA, W.; DUTRA, M.; KREUZER, E. THRUSTER DYNAMICS COMPENSATION FOR THE POSITIONING OF UNDERWATER ROBOTIC VEHICLES THROUGH A FUZZY SLIDING MODE BASED APPROACH. In: *ABCM Symposium Series in Mechatronics*. [S.l.: s.n.], 2006. v. 2, n. 1990, p. 605–612.

BESSA, W. M. *CONTROLE POR MODOS DESLIZANTES DE SISTEMAS DINÂMICOS COM ZONA MORTA APLICADO AO POSICIONAMENTO DE ROVS*. 106 p. Tese (Ph.D. Thesis) — Federal University of Rio de Janeiro, 2005.

BESSA, W. M.; DUTRA, M. S.; KREUZER, E. Dynamic Positioning of Underwater Robotic Vehicles with Thruster Dynamics Compensation. *International Journal of Advanced Robotic Systems*, v. 10, n. 9, p. 325, sep 2013. ISSN 1729-8814. Disponível em: <http://journals.sagepub.com/doi/10.5772/56601>.

BESSA, W. M. et al. AVALIAÇÃO EXPERIMENTAL DA MODELAGEM MATEMÁTICA DOS PROPULSORES DE UM VEÍCULO ROBÓTICO SUBMARINO. In: *III Congresso Nacional de Engenharia Mecânica*. Belém, Brasil: [s.n.], 2004. p. 1–10.

BORLAUG, I.-L.; PETTERSEN, K.; GRAVDAHL, J. Trajectory tracking for an articulated intervention AUV using a super-twisting algorithm in 6 DOF. *IFAC-PapersOnLine*, Elsevier B.V., v. 51, n. 29, p. 311–316, 2018. ISSN 24058963. Disponível em: <https://doi.org/10.1016/j.ifacol.2018.09.506>.

BORLAUG, I.-L. G. et al. Trajectory Tracking for Underwater Swimming Manipulators using a Super Twisting Algorithm. *Asian Journal of Control*, v. 21, n. 1, p. 208–223, 2019. ISSN 19346093.

BORLAUG, I.-L. G.; PETTERSEN, K. Y.; GRAVDAHL, J. T. Tracking control of an articulated intervention AUV in 6DOF using the generalized super-twisting algorithm. In: *2019 American Control Conference (ACC)*. IEEE, 2019. v. 29, n. 1, p. 5705–5712. ISBN 978-1-5386-7926-5. ISSN 1063-6536. Disponível em: <https://ieeexplore.ieee.org/document/8815093/>.

____. Combined kinematic and dynamic control of vehicle-manipulator systems. *Mechatronics*, Elsevier Ltd, v. 69, n. October 2019, 2020. ISSN 09574158.

____. The generalized super-twisting algorithm with adaptive gains. In: *2020 European Control Conference (ECC)*. IEEE, 2020. p. 1624–1631. ISBN 978-3-90714-402-2. Disponível em: <https://ieeexplore.ieee.org/document/9143617/>.

____. Tracking Control of an Articulated Intervention Autonomous Underwater Vehicle in 6DOF Using Generalized Super-twisting: Theory and Experiments. *IEEE Transactions on Control Systems Technology*, IEEE, v. 29, n. 1, p. 353–369, jan 2021. ISSN 1063-6536. Disponível em: <https://ieeexplore.ieee.org/document/9032376/>.

BORLAUG, I.-L. G. et al. Combined kinematic and dynamic control of an underwater swimming manipulator. In: *12th IFAC Conference on Control Applications in Marine Systems, Robotics, and Vehicles CAMS 2019*. Elsevier Ltd, 2019. v. 52, n. 21, p. 8–13. ISSN 2405-8963. Disponível em: <https://doi.org/10.1016/j.ifacol.2019.12.275>.

BRIÑÓN-ARRANZ, L.; SEURET, A.; PASCOAL, A. Circular formation control for cooperative target tracking with limited information. *Journal of the Franklin Institute*, v. 356, n. 4, p. 1771–1788, mar 2019. ISSN 00160032. Disponível em: <https://linkinghub.elsevier.com/retrieve/pii/S0016003219300031>.

CAI, M. et al. Autonomous Manipulation of an Underwater Vehicle-Manipulator System by a Composite Control Scheme With Disturbance Estimation. *IEEE Transactions on Automation Science and Engineering*, IEEE, p. 1–11, 2023. ISSN 1545-5955. Disponível em: <https://ieeexplore.ieee.org/document/10016284/>.

Canudas de Wit, C.; Olguin Diaz, E.; PERRIER, M. Robust nonlinear control of an underwater vehicle/manipulator system with composite dynamics. In: *Proceedings. 1998 IEEE International Conference on Robotics and Automation (Cat. No.98CH36146)*. IEEE, 1998. v. 1, n. May, p. 452–457. ISBN 0-7803-4300-X. Disponível em: <http://ieeexplore.ieee.org/document/677015/>.

CARRERA, A. et al. Learning multiple strategies to perform a valve turning with underwater currents using an I-AUV. In: *OCEANS 2015 - Genova*. IEEE, 2015. p. 1–8. ISBN 978-1-4799-8736-8. Disponível em: <http://ieeexplore.ieee.org/document/7271609/>.

____. An Intervention-AUV learns how to perform an underwater valve turning. In: *OCEANS 2014 - TAIPEI*. IEEE, 2014. p. 1–7. ISBN 978-1-4799-3646-5. Disponível em: <http://ieeexplore.ieee.org/document/6964483/>.

CATALDI, E.; CHIAVERINI, S.; ANTONELLI, G. Cooperative Object Transportation by Two Underwater Vehicle-Manipulator Systems. In: *2018 26th Mediterranean Conference on Control and Automation (MED)*. IEEE, 2018. p. 161–166. ISBN 978-1-5386-7890-9. Disponível em: <https://ieeexplore.ieee.org/document/8442760/>.

CHAKRABARTI, S. K. *Hydrodynamics of Offshore Structures*. Dorchester: WIT Press, 1987. 439 p. ISBN 0-905451-66-X.

CHUNG, G. et al. Disturbance observer-based robust control for underwater robotic systems with passive joints. In: *Proceedings 2000 ICRA. Millennium Conference. IEEE International Conference on Robotics and Automation. Symposia Proceedings (Cat. No.00CH37065)*. IEEE, 2000. v. 2, n. April, p. 1775–1780. ISBN 0-7803-5886-4. ISSN 01691864. Disponível em: <http://ieeexplore.ieee.org/lpdocs/epic03/wrapper.htm?arnumber=844852http://ieeexplore.ieee.org/document/844852/>.

CONTI, R. et al. An innovative decentralized strategy for I-AUVs cooperative manipulation tasks. *Robotics and Autonomous Systems*, Elsevier B.V., v. 72, p. 261–276, oct 2015. ISSN 09218890. Disponível em: <https://linkinghub.elsevier.com/retrieve/pii/S0921889015001347>.

COUTINHO, A. G. *CONTRIBUIÇÕES À MODELAGEM DINÂMICA E AO CONTROLE DE MANIPULADORES PARALELOS*. 155 p. Tese (Ph.D. Thesis) — University of São Paulo (USP), 2019. Disponível em: <https://teses.usp.br/teses/disponiveis/3/3151/tde-18052020-092338/pt-br.php>.

DAI, Y. et al. A fast tube model predictive control scheme based on sliding mode control for underwater vehicle-manipulator system. *Ocean Engineering*, Elsevier Ltd, v. 254, n. September 2021, p. 111259, 2022. ISSN 00298018. Disponível em: <https://doi.org/10.1016/j.oceaneng.2022.111259>.

____. Robust Control of Underwater Vehicle-Manipulator System Using Grey Wolf Optimizer-Based Nonlinear Disturbance Observer and H-Infinity Controller. *Complexity*, v. 2020, 2020. ISSN 10990526.

DAI, Y.; YU, S. Design of an indirect adaptive controller for the trajectory tracking of UVMS. *Ocean Engineering*, Elsevier Ltd, v. 151, n. July 2017, p. 234–245, mar 2018. ISSN 00298018. Disponível em: <https://doi.org/10.1016/j.oceaneng.2017.12.070>.

DAI, Y.; YU, S.; YAN, Y. An Adaptive EKF-FMPC for the Trajectory Tracking of UVMS. *IEEE Journal of Oceanic Engineering*, IEEE, PP, p. 1–15, 2019. ISSN 0364-9059. Disponível em: <https://ieeexplore.ieee.org/document/8675963/>.

DANTAS, J. L.; CRUZ, J. J. da; BARROS, E. A. de. Study of autonomous underwater vehicle wave disturbance rejection in the diving plane. *Proceedings of the Institution of Mechanical Engineers, Part M: Journal of Engineering for the Maritime Environment*, v. 228, n. 2, p. 122–135, may 2014. ISSN 1475-0902. Disponível em: <http://journals.sagepub.com/doi/10.1177/1475090213501650>.

Di Vito, D. et al. Experimental validation of the modeling and control of a multibody underwater vehicle manipulator system for sea mining exploration. *Journal of Field Robotics*, v. 38, n. 2, p. 171–191, 2021. ISSN 15564967.

DUNNIGAN, M. W.; RUSSELL, G. T. Evaluation and reduction of the dynamic coupling between a manipulator and an underwater vehicle. *IEEE Journal of Oceanic Engineering*, v. 23, n. 3, p. 260–273, 1998. ISSN 03649059.

EL-GHAZALY, G.; GOUTTEFARDE, M.; CREUZE, V. Hybrid cable-thruster actuated underwater vehicle-manipulator systems: A study on force capabilities. In: *2015 IEEE/RSJ International Conference on Intelligent Robots and Systems (IROS)*. IEEE, 2015. p. 1672–1678. ISBN 978-1-4799-9994-1. Disponível em: <http://ieeexplore.ieee.org/document/7353592/>.

ESFAHANI, H. N.; AZIMIRAD, V.; DANESH, M. A Time Delay Controller included terminal sliding mode and fuzzy gain tuning for Underwater Vehicle-Manipulator Systems. *Ocean Engineering*, Elsevier, v. 107, p. 97–107, oct 2015. ISSN 00298018. Disponível em: <https://linkinghub.elsevier.com/retrieve/pii/S002980181500356X>.

FARIVARNEJAD, H.; MOOSAVIAN, S. A. A. Multiple Impedance Control for object manipulation by a dual arm underwater vehicle-manipulator system. *Ocean Engineering*, Elsevier, v. 89, p. 82–98, 2014. ISSN 00298018. Disponível em: <http://dx.doi.org/10.1016/j.oceaneng.2014.06.032>.

FERNANDEZ, J. J. et al. Benchmarking using UWSim, Simurv and ROS: An autonomous free floating dredging intervention case study. In: *OCEANS 2015 - Genova*. IEEE, 2015. p. 1–7. ISBN 978-1-4799-8736-8. Disponível em: <http://ieeexplore.ieee.org/document/7271514/>.

____. Grasping for the Seabed: Developing a New Underwater Robot Arm for Shallow-Water Intervention. *IEEE Robotics & Automation Magazine*, v. 20, n. 4, p. 121–130, dec 2013. ISSN 1070-9932. Disponível em: <http://ieeexplore.ieee.org/document/6627980/>.

FOSSEN, T. I. *Guidance and Control of Ocean Vehicles*. Chichester: John Wiley & Sons, 1996. 494 p. ISSN 00051098. Disponível em: <https://linkinghub.elsevier.com/retrieve/pii/0005109896823314>.

GANCET, J. et al. Dexterous Undersea Interventions with Far Distance Onshore Supervision: the DexROV Project. *IFAC-PapersOnLine*, Elsevier B.V., v. 49, n. 23, p. 414–419, 2016. ISSN 24058963. Disponível em: <https://linkinghub.elsevier.com/retrieve/pii/S2405896316320274>.

GAO, J. et al. Hierarchical image-based visual serving of underwater vehicle manipulator systems based on model predictive control and active disturbance rejection control. *Ocean Engineering*, Elsevier Ltd, v. 229, n. April, p. 108814, 2021. ISSN 00298018. Disponível em: <https://doi.org/10.1016/j.oceaneng.2021.108814>.

Georgia Tech. *Control System Helps Several Drones Team Up to Deliver Heavy Packages | News Center*. 2021. Disponível em: <https://news.gatech.edu/news/2021/03/22/control-system-helps-several-drones-team-deliver-heavy-packages>.

GÜMÜşEL, L.; ÖZMEN, N. G. Modelling and control of manipulators with flexible links working on land and underwater environments. *Robotica*, v. 29, n. 3, p. 461–470, 2011. ISSN 02635747.

HAN, H. et al. Modeling and Fuzzy Decoupling Control of an Underwater Vehicle-Manipulator System. *IEEE Access*, v. 8, p. 18962–18983, 2020. ISSN 21693536.

____. Motion Planning and Coordinated Control of Underwater Vehicle-Manipulator Systems with Inertial Delay Control and Fuzzy Compensator. *Applied Sciences*, v. 10, n. 11, p. 3944, jun 2020. ISSN 2076-3417. Disponível em: <https://www.mdpi.com/2076-3417/10/11/3944>.

HAN, J.; CHUNG, W. K. Active Use of Restoring Moments for Motion Control of an Underwater Vehicle-Manipulator System. *IEEE Journal of Oceanic Engineering*, v. 39, n. 1, p. 100–109, jan 2014. ISSN 0364-9059. Disponível em: <http://ieeexplore.ieee.org/document/6484197/>.

HAN, J.; PARK, J.; CHUNG, W. K. Robust coordinated motion control of an underwater vehicle-manipulator system with minimizing restoring moments. *Ocean Engineering*, Elsevier, v. 38, n. 10, p. 1197–1206, 2011. ISSN 00298018. Disponível em: <http://dx.doi.org/10.1016/j.oceaneng.2011.05.014>.

HAUGALØKKEN, B. O. A.; JØRGENSEN, E. K.; SCHJØLBERG, I. Experimental validation of end-effector stabilization for underwater vehicle-manipulator systems in subsea operations. *Robotics and Autonomous Systems*, Elsevier B.V., v. 109, p. 1–12, nov 2018. ISSN 09218890. Disponível em: <https://doi.org/10.1016/j.robot.2018.08.007>.

HEALEY, A. et al. Toward an improved understanding of thruster dynamics for underwater vehicles. *IEEE Journal of Oceanic Engineering*, v. 20, n. 4, p. 354–361, 1995. ISSN 03649059. Disponível em: <https://ieeexplore.ieee.org/document/518646>.

HESHMATI-ALAMDARI, S. *Cooperative and Interaction Control for Underwater Robotic Vehicles*. 253 p. Tese (Ph.D. Thesis) — National Technical University of Athens, 2018.

HESHMATI-ALAMDARI, S. et al. Decentralized Impedance Control for Cooperative Manipulation of Multiple Underwater Vehicle Manipulator Systems under Lean Communication. In: *2018 IEEE/OES Autonomous Underwater Vehicle Workshop (AUV)*. IEEE, 2018. p. 1–6. ISBN 978-1-7281-0253-5. Disponível em: <https://ieeexplore.ieee.org/document/8729687/>.

____. Cooperative Impedance Control for Multiple Underwater Vehicle Manipulator Systems Under Lean Communication. *IEEE Journal of Oceanic Engineering*, v. 46, n. 2, p. 447–465, apr 2021. ISSN 0364-9059. Disponível em: <https://ieeexplore.ieee.org/document/9118878/>.

____. Cooperative Impedance Control for Multiple Underwater Vehicle Manipulator Systems Under Lean Communication. *IEEE Journal of Oceanic Engineering*, v. 46, n. 2, p. 447–465, apr 2021. ISSN 0364-9059. Disponível em: <https://ieeexplore.ieee.org/document/9118878/>.

HESHMATI-ALAMDARI, S.; KARRAS, G. C.; KYRIAKOPOULOS, K. J. A Distributed Predictive Control Approach for Cooperative Manipulation of Multiple Underwater Vehicle Manipulator Systems. In: *2019 International Conference on Robotics and Automation (ICRA)*. IEEE, 2019. p. 4626–4632. ISBN 978-1-5386-6027-0. Disponível em: <https://ieeexplore.ieee.org/document/8793476/>.

HESHMATI-ALAMDARI, S. et al. A Robust Force Control Approach for Underwater Vehicle Manipulator Systems. *IFAC-PapersOnLine*, v. 50, n. 1, p. 11197–11202, jul 2017. ISSN 24058963. Disponível em: <https://linkinghub.elsevier.com/retrieve/pii/S2405896317317548>.

HUANG, H. et al. Dynamic Modeling and Vibration Suppression for Two-Link Underwater Flexible Manipulators. *IEEE Access*, IEEE, v. 10, p. 40181–40196, 2022. ISSN 2169-3536. Disponível em: <https://ieeexplore.ieee.org/document/9749078/>.

HUNG, N. T.; PASCOAL, A. M. Consensus/synchronisation of networked nonlinear multiple agent systems with event-triggered communications. *International Journal of Control*, v. 95, n. 5, p. 1305–1314, may 2022. ISSN 0020-7179. Disponível em: <https://www.tandfonline.com/doi/full/10.1080/00207179.2020.1849806>.

IANAGUI, A. S. S. *Robust System Design for Consensus Control in Dynamically Positioned Vessel Fleet*. 236 p. Tese (Ph.D. thesis) — University of São Paulo, 2019. Disponível em: <https://www.teses.usp.br/teses/disponiveis/3/3152/tde-07012020-155948/en.php>.

INGROSSO, R. et al. Dynamic Modeling of Underwater Multi-Hull Vehicles. *Robotica*, v. 38, n. 9, p. 1682–1702, sep 2020. ISSN 0263-5747. Disponível em: <https://www.cambridge.org/core/product/identifier/S0263574719001693/type/journal_article>.

IOI, K.; ITOH, K. Modelling and simulation of an underwater manipulator. *Advanced Robotics*, v. 4, n. 4, p. 303–317, 1990. ISSN 15685535. Disponível em: <https://www.tandfonline.com/doi/abs/10.1163/156855390X00152>.

ISHITSUKA, M.; SAGARA, S.; ISHII, K. Dynamics analysis and resolved acceleration control of an autonomous underwater vehicle equipped with a manipulator. In: *Proceedings of the 2004 International Symposium on Underwater Technology (IEEE Cat. No.04EX869)*. IEEE, 2004. p. 277–281. ISBN 0-7803-8541-1. Disponível em: <http://ieeexplore.ieee.org/document/1405575/>.

KABANOV, A. et al. Cooperative Control of Underwater Vehicle–Manipulator Systems Based on the SDC Method. *Sensors*, v. 22, n. 13, p. 5038, jul 2022. ISSN 1424-8220. Disponível em: <https://www.mdpi.com/1424-8220/22/13/5038>.

KANG, J. I. et al. EXPERIMENTAL STUDY OF DYNAMIC STABILITY OF UNDERWATER VEHICLE-MANIPULATOR SYSTEM USING ZERO MOMENT POINT. *Journal of Marine Science and Technology (Taiwan)*, v. 25, n. 6, p. 767–774, 2017. ISSN 10232796. Disponível em: <https://www.airitilibrary.com/Publication/alDetailedMesh?docid=10232796-201712-201801030003-201801030003-767-774>.

KARRAS, G. C. et al. Image Based Visual Servoing for Floating Base Mobile Manipulator Systems with Prescribed Performance under Operational Constraints. *Machines*, v. 10, n. 7, p. 547, jul 2022. ISSN 2075-1702. Disponível em: <https://www.mdpi.com/2075-1702/10/7/547>.

KELASIDI, E. et al. Multi-objective optimization for efficient motion of underwater snake robots. *Artificial Life and Robotics*, Springer Japan, v. 21, n. 4, p. 411–422, 2016. ISSN 16147456. Disponível em: <http://link.springer.com/10.1007/s10015-016-0332-3>.

____. Experimental investigation of locomotion efficiency and path-following for underwater snake robots with and without a caudal fin. *Annual Reviews in Control*, Elsevier Ltd, v. 46, n. 223254, p. 281–294, 2018. ISSN 13675788. Disponível em: <https://doi.org/10.1016/j.arcontrol.2018.10.001>.

____. Experimental investigation of efficient locomotion of underwater snake robots for lateral undulation and eel-like motion patterns. *Robotics and Biomimetics*, Springer Berlin Heidelberg, v. 2, n. 1, 2015. ISSN 2197-3768. Disponível em: <https://jrobio.springeropen.com/articles/10.1186/s40638-015-0029-4>.

____. Innovation in Underwater Robots: Biologically Inspired Swimming Snake Robots. *IEEE Robotics and Automation Magazine*, v. 23, n. 1, p. 44–62, 2016. ISSN 10709932. Disponível em: <http://ieeexplore.ieee.org/document/7426526/>.

____. Path Following, Obstacle Detection and Obstacle Avoidance for Thrusted Underwater Snake Robots. *Frontiers in Robotics and AI*, v. 6, n. July, p. 1–15, 2019. ISSN 22969144. Disponível em: <https://www.frontiersin.org/article/10.3389/frobt.2019.00057/full>.

KELASIDI, E.; PETTERSEN, K. Y.; GRAVDAHL, J. T. Modeling of underwater snake robots moving in a vertical plane in 3D. *IEEE International Conference on Intelligent Robots and Systems*, IEEE, n. Iros, p. 266–273, 2014. ISSN 21530866. Disponível em: <http://ieeexplore.ieee.org/document/6942571/>.

KELASIDI, E. et al. Modeling of underwater snake robots. *Proceedings - IEEE International Conference on Robotics and Automation*, IEEE, p. 4540–4547, 2014. ISSN 10504729. Disponível em: <http://ieeexplore.ieee.org/document/6907522/>.

____. Modeling and propulsion methods of underwater snake robots. *1st Annual IEEE Conference on Control Technology and Applications, CCTA 2017*, v. 2017-Janua, p. 819–826, 2017. Disponível em: <http://ieeexplore.ieee.org/document/8062561/>.

KIM, Y.; MOHAN, S.; KIM, J. Task space-based control of an underwater robotic system for position keeping in ocean currents. *Advanced Robotics*, v. 28, n. 16, p. 1109–1119, 2014. ISSN 15685535.

KOHL, A. M. et al. Planar maneuvering control of underwater snake robots using virtual holonomic constraints. *Bioinspiration and Biomimetics*, IOP Publishing, v. 11, n. 6, 2016. ISSN 17483190. Disponível em: <https://iopscience.iop.org/article/10.1088/1748-3190/11/6/065005>.

KOLANO, H.; DAVIDSON, J. R. Forecasting Vehicle Pitch of a Lightweight Underwater Vehicle Manipulator System with Recurrent Neural Networks. In: *Proceedings of the 2023 International Conference on Robotics and Automation*. [s.n.], 2023. Disponível em: <https://doi.org/10.48550/arXiv.2209.13577>.

LANE, D. et al. AMADEUS: advanced manipulation for deep underwater sampling. *IEEE Robotics & Automation Magazine*, v. 4, n. 4, p. 34–45, 1997. ISSN 10709932. Disponível em: <http://ieeexplore.ieee.org/document/637804/>.

LANE, D. M. et al. Persistent autonomy: the challenges of the PANDORA project. *IFAC Proceedings Volumes*, v. 45, n. 27, p. 268–273, 2012. ISSN 14746670. Disponível em: <https://linkinghub.elsevier.com/retrieve/pii/S147466701631240X>.

LEABOURNE, K.; ROCK, S. Model development of an underwater manipulator for coordinated arm-vehicle control. In: *IEEE Oceanic Engineering Society. OCEANS'98. Conference Proceedings (Cat. No.98CH36259)*. IEEE, 1998. v. 2, p. 941–946. ISBN 0-7803-5045-6. ISSN 01977385. Disponível em: <http://ieeexplore.ieee.org/document/724376/>.

LEE, S. U. et al. Development of an underwater manipulator for maintaining nuclear power reactor. *ICCAS 2007 - International Conference on Control, Automation and Systems*, p. 1006–1010, 2007.

LÉVESQUE, B.; RICHARD, M. J. Dynamic analysis of a manipulator in a fluid environment. *International Journal of Robotics Research*, v. 13, n. 3, p. 221–230, 1994. ISSN 02783649. Disponível em: <https://journals.sagepub.com/doi/abs/10.1177/027836499401300304>.

LEWANDOWSKI, E. M. *The Dynamics of Marine Craft*. Singapore: WORLD SCIENTIFIC, 2004. v. 22. 411 p. (Advanced Series on Ocean Engineering, v. 22). ISBN 978-981-02-4755-3. Disponível em: <https://www.worldscientific.com/worldscibooks/10.1142/4815>.

LI, J. et al. Uncalibrated Visual Servoing for Underwater Vehicle Manipulator Systems with an Eye in Hand Configuration Camera. *Sensors*, v. 19, n. 24, p. 5469, dec 2019. ISSN 1424-8220. Disponível em: <https://www.mdpi.com/1424-8220/19/24/5469>.

LONDHE, P. et al. Robust task-space control of an autonomous underwater vehicle-manipulator system by PID-like fuzzy control scheme with disturbance estimator. *Ocean Engineering*, Elsevier Ltd, v. 139, n. April, p. 1–13, jul 2017. ISSN 00298018. Disponível em: <https://linkinghub.elsevier.com/retrieve/pii/S0029801817302123>.

MARANI, G.; CHOI, S. K.; YUH, J. Underwater autonomous manipulation for intervention missions AUVs. *Ocean Engineering*, v. 36, n. 1, p. 15–23, jan 2009. ISSN 00298018. Disponível em: <https://linkinghub.elsevier.com/retrieve/pii/S002980180800173X>.

MAZUMDAR, A. et al. A compact, maneuverable, underwater robot for direct inspection of nuclear power piping systems. *Proceedings - IEEE International Conference on Robotics and Automation*, p. 2818–2823, 2012. ISSN 10504729.

MCLAIN, T. W.; ROCK, S. M. Development and Experimental Validation of an Underwater Manipulator Hydrodynamic Model. *The International Journal of Robotics Research*, v. 17, n. 7, p. 748–759, jul 1998. ISSN 0278-3649. Disponível em: <http://journals.sagepub.com/doi/10.1177/027836499801700705>.

MCLAIN, T. W.; ROCK, S. M.; LEE, M. J. Experiments in the coordinated control of an underwater arm/vehicle system. *Autonomous Robots*, v. 3, n. 2-3, p. 213–232, 1996. ISSN 0929-5593. Disponível em: <http://link.springer.com/10.1007/BF00141156>.

MCMILLAN, S.; ORIN, D.; MCGHEE, R. Efficient dynamic simulation of an unmanned underwater vehicle with a manipulator. In: *Proceedings of the 1994 IEEE International Conference on Robotics and Automation*. IEEE Comput. Soc. Press, 1994. p. 1133–1140. ISBN 0-8186-5330-2. ISSN 10504729. Disponível em: <http://ieeexplore.ieee.org/document/351208/>.

MEIROVITCH, L. *Methods of Analytical Dynamics*. New York: McGraw-Hill, 2003. 540 p.

MHI, L. *Robot Technologies of PWR for Nuclear Power Plant Maintenance*. 2011. Disponível em: <http://www.jsm.or.jp/ejam/Vol.5No.1/NT/NT54/NT54.html>.

MIR. *MIR – EMJMD IN MARINE AND MARITIME INTELLIGENT ROBOTICS*. 2020. Disponível em: <http://www.master-mir.eu/uji-description/>.

MODLAB. *ModLab – UPenn – the modular robotics laboratory at the university of pennsylvania*. 2023. Disponível em: <https://www.modlabupenn.org/>.

MOHAN, S.; KIM, J. Indirect adaptive control of an autonomous underwater vehicle-manipulator system for underwater manipulation tasks. *Ocean Engineering*, Elsevier, v. 54, p. 233–243, 2012. ISSN 00298018. Disponível em: <http://dx.doi.org/10.1016/j.oceaneng.2012.07.022>.

MOHAN, S.; KIM, J.; SINGH, Y. A robust task space position tracking control of an underwater vehicle manipulator system. In: *Proceedings of the 2015 Conference on Advances In Robotics - AIR '15*. New York, New York, USA: ACM Press, 2015. v. 02-04-July, p. 1–6. ISBN 9781450333566. Disponível em: <http://dl.acm.org/citation.cfm?doid=2783449.2783451>.

NGUYEN, N. D. et al. Simulation and Experiment of Underwater Vehicle Manipulator System Using Zero-Moment Point Method. *Lecture Notes in Electrical Engineering*, v. 465, p. 669–676, 2018. ISSN 18761119.

NIELSEN, M. et al. Validation of multi-body modelling methodology for reconfigurable underwater robots. In: *OCEANS 2016 MTS/IEEE Monterey*. IEEE, 2016. p. 1–8. ISBN 978-1-5090-1537-5. Disponível em: <http://ieeexplore.ieee.org/document/7761240/>.

NIELSEN, M. C.; BLANKE, M.; SCHJØLBERG, I. Efficient Modelling Methodology for Reconfigurable Underwater Robots. *IFAC-PapersOnLine*, Elsevier B.V., v. 49, n. 23, p. 74–80, 2016. ISSN 24058963. Disponível em: <http://dx.doi.org/10.1016/j.ifacol.2016.10.324>.

NIELSEN, M. C. et al. Constrained multi-body dynamics for modular underwater robots — Theory and experiments. *Ocean Engineering*, v. 149, n. July 2017, p. 358–372, 2018. ISSN 00298018. Disponível em: <https://www.sciencedirect.com/science/article/abs/pii/S0029801817307291>.

NIELSEN, M. C.; JOHANSEN, T. A.; BLANKE, M. Cooperative Rendezvous and Docking for Underwater Robots using Model Predictive Control and Dual Decomposition. In: *2018 European Control Conference (ECC)*. IEEE, 2018. p. 14–19. ISBN 978-3-9524-2698-2. Disponível em: <https://ieeexplore.ieee.org/document/8550366/>.

NUNEMACHER, J. Lagrange Multipliers Can Fail to Determine Extrema. *The College Mathematics Journal*, v. 34, n. 1, p. 60, jan 2003. ISSN 07468342. Disponível em: <http://www.jstor.org/stable/3595848?origin=crossref>.

OLIVEIRA, É. L. de; DONHA, D. C.; CARDOSO, R. Modeling and Station-Keeping Control of an Underwater Vehicle Manipulator System Through Reactions Wheels. In: *Volume 7B: Dynamics, Vibration, and Control*. American Society of Mechanical Engineers, 2021. ISBN 978-0-7918-8562-8. Disponível em: <https://asmedigitalcollection.asme.org/IMECE/proceedings/IMECE2021/85628/V07BT07A001/1132813>.

OLIVEIRA, É. L. de et al. Station-keeping of a ROV under wave disturbance: Modeling and control design. *Proceedings of the Institution of Mechanical Engineers, Part M: Journal of Engineering for the Maritime Environment*, p. 147509022211166, sep 2022. ISSN 1475-0902. Disponível em: <http://journals.sagepub.com/doi/10.1177/14750902221116673>.

OLIVEIRA, É. L. de; ORSINO, R. M.; DONHA, D. C. Disturbance-Observer-Based Model Predictive Control of Underwater Vehicle-Manipulator Systems. *IFAC-PapersOnLine*, v. 54, n. 16, p. 348–355, 2021. ISSN 24058963. Disponível em: <https://linkinghub.elsevier.com/retrieve/pii/S2405896321015172>.

OLIVEIRA, É. L. de; ORSINO, R. M. M.; DONHA, D. C. Modular modeling and coordination control scheme for an underwater cooperative transportation performed by two I-AUVs. *Control Engineering Practice*, Elsevier Ltd, v. 125, n. May, p. 105198, aug 2022. ISSN 09670661. Disponível em: <https://doi.org/10.1016/j.conengprac.2022.105198>.

ORSINO, R. M. M. Recursive modular modelling methodology for lumped-parameter dynamic systems. *Proceedings of the Royal Society A: Mathematical, Physical and Engineering Sciences*, v. 473, n. 2204, p. 16, aug 2017. ISSN 1364-5021. Disponível em: <https://royalsocietypublishing.org/doi/10.1098/rspa.2016.0891>.

____. Extended constraint enforcement formulations for finite-DOF systems based on Gauss's principle of least constraint. *Nonlinear Dynamics*, Springer Netherlands, v. 101, n. 4, p. 2577–2597, sep 2020. ISSN 0924-090X. Disponível em: <https://link.springer.com/10.1007/s11071-020-05924-9>.

PEREZ, T. *Ship Motion Control*. London: Springer-London, 2005. 300 p. (Advances in Industrial Control). ISSN 2193-1577. ISBN 978-1-85233-959-3. Disponível em: <https://link.springer.com/book/10.1007/1-84628-157-1>.

PERIASAMY, T.; ASOKAN, T.; SINGAPERUMAL, M. Investigations on the dynamic coupling in AUV-manipulator system and the manipulator trajectory errors using bond graph method. *International Journal of Systems Science*, v. 43, n. 6, p. 1104–1122, jun 2012. ISSN 0020-7721. Disponível em: <http://www.tandfonline.com/doi/abs/10.1080/00207721.2010.543488>.

PI, R. et al. TWINBOT: Autonomous underwater cooperative transportation. *IEEE Access*, v. 9, p. 37668–37684, 2021. ISSN 21693536.

PODDER, T. K.; SARKAR, N. *Unified Dynamics-based Motion Planning Algorithm for Autonomous Underwater VehicleManipulator Systems (UVMS)*. [s.n.], 2004. v. 22. 117–128 p. ISSN 02635747. ISBN 3866112831. Disponível em: <https://www.cambridge.org/core/product/identifier/S0263574703005368/type/journal_article>.

PRATS, M. et al. Multipurpose autonomous underwater intervention: A systems integration perspective. In: *2012 20th Mediterranean Conference on Control & Automation (MED)*. IEEE, 2012. v. 03, p. 1379–1384. ISBN 978-1-4673-2531-8. Disponível em: <http://ieeexplore.ieee.org/document/6265831/>.

____. An open source tool for simulation and supervision of underwater intervention missions. In: *2012 IEEE/RSJ International Conference on Intelligent Robots and Systems*. IEEE, 2012. p. 2577–2582. ISBN 978-1-4673-1736-8. ISSN 21530858. Disponível em: <http://ieeexplore.ieee.org/document/6385788/>.

____. Reconfigurable AUV for intervention missions: a case study on underwater object recovery. *Intelligent Service Robotics*, v. 5, n. 1, p. 19–31, jan 2012. ISSN 1861-2776. Disponível em: <http://link.springer.com/10.1007/s11370-011-0101-z>.

RAZZANELLI, M. et al. Development of a Hybrid Simulator for Underwater Vehicles With Manipulators. *IEEE Journal of Oceanic Engineering*, IEEE, v. 45, n. 4, p. 1235–1251, oct 2020. ISSN 0364-9059. Disponível em: <https://ieeexplore.ieee.org/document/8862914/>.

RIBAS, D. et al. I-AUV Mechatronics Integration for the TRIDENT FP7 Project. *IEEE/ASME Transactions on Mechatronics*, v. 20, n. 5, p. 2583–2592, oct 2015. ISSN 1083-4435. Disponível em: <http://ieeexplore.ieee.org/lpdocs/epic03/wrapper.htm?arnumber=7047908>.

RICHARD, M.; LÉVESQUE, B. STOCHASTIC DYNAMICAL MODELLING OF AN OPEN-CHAIN MANIPULATOR IN A FLUID ENVIRONMENT. *Mechanism and Machine Theory*, v. 31, n. 5, p. 561–572, jul 1996. ISSN 0094114X. Disponível em: <https://linkinghub.elsevier.com/retrieve/pii/0094114X95001058>.

RIDAO, P. et al. *Intervention AUVs: The next challenge*. IFAC, 2014. v. 19. 12146–12159 p. ISSN 14746670. ISBN 9783902823625. Disponível em: <http://dx.doi.org/10.3182/20140824-6-ZA-1003.02819>.

RIGAUD, V. et al. UNION: underwater intelligent operation and navigation. *IEEE Robotics & Automation Magazine*, v. 5, n. 1, p. 25–35, mar 1998. ISSN 10709932. Disponível em: <http://ieeexplore.ieee.org/document/667323/>.

SACCHI, N. et al. Analysis of Hybrid Cable-Thruster actuated ROV in heavy lifting interventions. In: *2022 IEEE/RSJ International Conference on Intelligent Robots and Systems (IROS)*. IEEE, 2022. v. 2022-Octob, p. 8430–8435. ISBN 978-1-6654-7927-1. ISSN 21530866. Disponível em: <https://ieeexplore.ieee.org/document/9981861/>.

SAGARA, S. MiResolved Acceleration Control for Underwater Vehicle-Manipulator Systems: Continuous and Discrete Time Approach. In: *Underwater Vehicles*. InTech, 2009. p. 23. ISBN 9789537619497. Disponível em: <https://www.intechopen.com/chapters/6225>.

SAGARA, S.; AMBAR, R. Performance comparison of control methods using a dual-arm underwater robot-Computed torque based control and resolved acceleration control for UVMS-. *Proceedings of the 2020 IEEE/SICE International Symposium on System Integration, SII 2020*, IEEE, p. 1094–1099, 2020.

SAGARA, S. et al. Experiments on a floating underwater robot with a two-link manipulator. *Artificial Life and Robotics*, v. 5, n. 4, p. 215–219, 2001. ISSN 1433-5298. Disponível em: <https://link.springer.com/article/10.1007/BF02481505>.

SAHA, S. K. Dynamics of serial multibody systems using the decoupled natural orthogonal complement matrices. *Journal of Applied Mechanics, Transactions ASME*, v. 66, n. 4, p. 986–996, 1999. ISSN 15289036.

SANTOS, C. H. F. dos et al. Virtual Kinematic Chains to Solve the Underwater Vehicle-Manipulator Systems Redundancy. *Journal of the Brazilian Society of Mechanical Sciences and Engineering*, v. 28, n. 3, p. 354–361, sep 2006. ISSN 1678-5878. Disponível em: <https://www.scielo.br/j/jbsmse/a/ygCQzfVXWtVLt89X9MZ6LjD/abstract/?lang=en>.

SANZ, P. J. et al. TRIDENT: Recent Improvements about Autonomous Underwater Intervention Missions. *IFAC Proceedings Volumes*, v. 45, n. 5, p. 355–360, 2012. ISSN 14746670. Disponível em: <https://linkinghub.elsevier.com/retrieve/pii/S1474667016306280>.

SARKAR, N.; PODDER, T. Coordinated motion planning and control of autonomous underwater vehicle-manipulator systems subject to drag optimization. *IEEE Journal of Oceanic Engineering*, v. 26, n. 2, p. 228–239, apr 2001. ISSN 03649059. Disponível em: <http://ieeexplore.ieee.org/document/922789/>.

SCHJOLBERG, I.; FOSSEN, T. I. Modelling and control of underwater vehicle manipulator systems. *Conf. on Marine Craft Maneuvering and Control*, p. 11, 1994.

SCHMIDT-DIDLAUKIES, H. M.; SøRENSEN, A. J.; PETTERSEN, K. Y. Modeling of Articulated Underwater Robots for Simulation and Control. *AUV 2018 - 2018 IEEE/OES Autonomous Underwater Vehicle Workshop, Proceedings*, IEEE, n. 2, p. 1–7, 2018. Disponível em: <https://ieeexplore.ieee.org/document/8729806/>.

SCOPUS. *Scopus - Articles Search*. 2022. 1–10 p. Disponível em: <https://www.scopus.com/standard/marketing.uri>.

SHAH, U. H. et al. Dynamic Analysis of the UVMS: Effect of Disturbances, Coupling, and Joint-Flexibility on End-Effector Positioning. *Robotica*, n. 19, p. 1–29, feb 2021. ISSN 0263-5747. Disponível em: <https://www.cambridge.org/core/product/identifier/S0263574721000072/type/journal_article>.

SHANG, D. et al. Vibration suppression method for flexible link underwater manipulator considering torsional flexibility based on adaptive PI controller with nonlinear disturbance observer. *Ocean Engineering*, Elsevier Ltd, v. 274, n. November 2022, p. 114111, 2023. ISSN 00298018. Disponível em: <https://doi.org/10.1016/j.oceaneng.2023.114111>.

SHARMA, A. K. et al. Dynamic Analysis of Underwater Vehicle-Manipulator Systems. In: BADODKAR, D. N.; DWARAKANATH, T. A. (Ed.). *Proceedings of iNaCoMM 2017*. Singapore: Springer Singapore, 2019, (Lecture Notes in Mechanical Engineering). p. 739–748. ISBN 978-981-10-8596-3. Disponível em: <https://link.springer.com/chapter/10.1007/978-981-10-8597-0_63>.

SHARMA, A. K.; SAHA, S. K. Simplified Drag Modeling for the Dynamics of an Underwater Manipulator. *IEEE Journal of Oceanic Engineering*, IEEE, PP, p. 1–16, 2019. ISSN 0364-9059. Disponível em: <https://ieeexplore.ieee.org/document/8915726/>.

SIMETTI, E. Autonomous Underwater Intervention. *Current Robotics Reports*, v. 1, n. 3, p. 117–122, sep 2020. ISSN 2662-4087. Disponível em: <https://link.springer.com/10.1007/s43154-020-00012-7>.

SIMETTI, E. et al. Sea Mining Exploration with an UVMS: Experimental Validation of the Control and Perception Framework. *IEEE/ASME Transactions on Mechatronics*, v. 14, n. 8, p. 1–1, 2020. ISSN 1083-4435. Disponível em: <https://ieeexplore.ieee.org/document/9204397/>.

SIMETTI, E.; CASALINO, G. Manipulation and Transportation With Cooperative Underwater Vehicle Manipulator Systems. *IEEE Journal of Oceanic Engineering*, v. 42, n. 4, p. 782–799, oct 2017. ISSN 0364-9059. Disponível em: <http://ieeexplore.ieee.org/document/7790865/>.

SIMETTI, E. et al. Cooperation between autonomous underwater vehicle manipulations systems with minimal information exchange. In: *OCEANS 2015 - Genova*. IEEE, 2015. p. 1–6. ISBN 978-1-4799-8736-8. Disponível em: <http://ieeexplore.ieee.org/document/7271700/>.

____. Floating Underwater Manipulation: Developed Control Methodology and Experimental Validation within the TRIDENT Project. *Journal of Field Robotics*, v. 31, n. 3, p. 364–385, may 2014. ISSN 15564959. Disponível em: <https://onlinelibrary.wiley.com/doi/abs/10.1002/rob.21497>.

____. Task priority control of underwater intervention systems: Theory and applications. *Ocean Engineering*, Elsevier Ltd, v. 164, n. June, p. 40–54, 2018. ISSN 00298018. Disponível em: <https://doi.org/10.1016/j.oceaneng.2018.06.026>.

SIMETTI, E.; GALEANO, S.; CASALINO, G. Underwater vehicle manipulator systems: Control methodologies for inspection and maintenance tasks. In: *OCEANS 2016 - Shanghai*. IEEE, 2016. p. 1–7. ISBN 978-1-4673-9724-7. Disponível em: <http://ieeexplore.ieee.org/document/7485690/>.

SIVČEV, S. et al. Underwater manipulators: A review. *Ocean Engineering*, v. 163, n. April, p. 431–450, sep 2018. ISSN 00298018. Disponível em: <https://linkinghub.elsevier.com/retrieve/pii/S0029801818310308>.

SOYLU, S.; BUCKHAM, B. J.; PODHORODESKI, R. P. Redundancy resolution for underwater mobile manipulators. *Ocean Engineering*, Elsevier, v. 37, n. 2-3, p. 325–343, feb 2010. ISSN 00298018. Disponível em: <https://linkinghub.elsevier.com/retrieve/pii/S0029801809002376>.

SUN, Y.; CHEAH, C. Coordinated control of multiple cooperative underwater vehicle-manipulator systems holding a common load. In: *Oceans '04 MTS/IEEE Techno-Ocean '04 (IEEE Cat. No.04CH37600)*. IEEE, 2004. v. 3, p. 1542–1547. ISBN 0-7803-8669-8. Disponível em: <http://ieeexplore.ieee.org/document/1406351/>.

TAIRA, Y.; SAGARA, S.; OYA, M. Motion and force control with a nonlinear force error filter for underwater vehicle-manipulator systems. *Artificial Life and Robotics*, Springer Japan, v. 23, n. 1, p. 103–117, 2018. ISSN 16147456.

____. Model-based motion control for underwater vehicle-manipulator systems with one of the three types of servo subsystems. *Artificial Life and Robotics*, Springer Japan, v. 25, n. 1, p. 133–148, 2020. ISSN 16147456. Disponível em: <https://doi.org/10.1007/s10015-019-00564-8>.

____. Motion and force control with a linear force error filter for the manipulator of an underwater vehicle-manipulator system. *Artificial Life and Robotics*, Springer Japan, v. 27, n. 1, p. 90–106, 2022. ISSN 16147456. Disponível em: <https://doi.org/10.1007/s10015-021-00708-9>.

TANG, Q. et al. Task-priority redundancy resolution on acceleration level for underwater vehicle-manipulator system. *International Journal of Advanced Robotic Systems*, v. 14, n. 4, p. 172988141771982, jul 2017. ISSN 1729-8814. Disponível em: <http://journals.sagepub.com/doi/10.1177/1729881417719825>.

TARN, T. J.; SHOULTS, G. a.; YANG, S. P. A dynamic model of an underwater vehicle with a robotic manipulator using Kane's method. *Autonomous Robots*, v. 3, n. 2-3, p. 269–283, 1996. ISSN 0929-5593. Disponível em: <http://link.springer.com/10.1007/BF00141159>.

TECNADYNE. *Dc Brushless Thruster Model 8020 Model 8020*. 2008. 1–7 p. Disponível em: <https://tecnadyne.com/wp-content/uploads/2017/06/Model-560-Brochure-1.pdf>.

VERGINIS, C. K.; MASTELLARO, M.; DIMAROGONAS, D. V. Robust Cooperative Manipulation Without Force/Torque Measurements: Control Design and Experiments. *IEEE Transactions on Control Systems Technology*, p. 1–17, 2019. ISSN 1063-6536.

VIROZUB, E. et al. Planar Multi-Link Swimmers: Experiments and Theoretical Investigation using Perfect Fluid Model. *Robotica*, v. 37, n. 8, p. 1289–1301, 2019. ISSN 14698668.

WANG, J.; PERKINS, E. Trajectory Tracking Control for an Underwater Vehicle Manipulator System Using a Neural-adaptive Network. n. December, 2019.

WANG, L. *Model Predictive Control System Design and Implementation Using MATLAB®*. London: Springer London, 2009. 403 p. (Advances in Industrial Control). ISSN 1430-9491. ISBN 978-1-84882-330-3. Disponível em: <http://link.springer.com/10.1007/978-1-84882-331-0>.

WANG, Y.; CHEN, B.; WU, H. Joint space tracking control of underwater vehicle-manipulator systems using continuous nonsingular fast terminal sliding mode. *Proceedings of the Institution of Mechanical Engineers Part M: Journal of Engineering for the Maritime Environment*, v. 232, n. 4, p. 448–458, 2018. ISSN 20413084.

WANG, Y. et al. A new redundancy resolution for underwater vehicle–manipulator system considering payload. *International Journal of Advanced Robotic Systems*, v. 14, n. 5, p. 172988141773393, sep 2017. ISSN 1729-8814. Disponível em: <http://journals.sagepub.com/doi/10.1177/1729881417733934>.

WRIGHT'S. *Pipeline Services*. 2020. Disponível em: <https://www.linkedin.com/company/wright's-well-control-services>.

WU, C.-j. *6-DoF Modelling and Control of a Remotely Operated Vehicle*. 99 p. Tese (Master thesis) — Flinders University, 2018. Disponível em: <https://flex.flinders.edu.au/file/27aa0064-9de2-441c-8a17-655405d5fc2e/1/ThesisWu2018.pdf>.

XIONG, X. et al. On dynamic coupling effects of underwater vehicle-dual-manipulator system. *Ocean Engineering*, Elsevier Ltd, v. 258, n. January, p. 111699, aug 2022. ISSN 00298018. Disponível em: <https://linkinghub.elsevier.com/retrieve/pii/S002980182201054X>.

YATOH, T.; SAGARA, S.; TAMURA, M. Digital type disturbance compensation control of a floating underwater robot with 2 link manipulator. *Artificial Life and Robotics*, v. 13, n. 1, p. 377–381, 2008. ISSN 14335298.

YOERGER, D.; COOKE, J.; SLOTINE, J.-J. The influence of thruster dynamics on underwater vehicle behavior and their incorporation into control system design. *IEEE Journal of Oceanic Engineering*, v. 15, n. 3, p. 167–178, jul 1990. ISSN 03649059. Disponível em: <http://ieeexplore.ieee.org/document/107145/>.

YOUAKIM, D. et al. MoveIt!: Autonomous Underwater Free-Floating Manipulation. *IEEE Robotics & Automation Magazine*, v. 24, n. 3, p. 41–51, sep 2017. ISSN 1070-9932. Disponível em: <http://ieeexplore.ieee.org/document/7906569/>.

YU, F. et al. Motion coordination and dexterous manipulation for underwater vehicle-manipulator systems. *ISA Transactions*, Elsevier Ltd, n. xxxx, 2023. ISSN 00190578. Disponível em: <https://doi.org/10.1016/j.isatra.2023.01.027>.

ZHU, W.-H. *Virtual Decomposition Control*. Berlin, Heidelberg: Springer Berlin Heidelberg, 2010. v. 60. 447 p. (Springer Tracts in Advanced Robotics, v. 60). ISSN 16107438. ISBN 978-3-642-10723-8. Disponível em: <http://link.springer.com/10.1007/978-3-642-10724-5>.

APPENDIX A

A.1 Recursive orthogonal complement

Applying the Gauss's principles in Eq. (3.76), we obtain:

$$\begin{bmatrix} \mathbf{A}_r \\ \tilde{\mathbf{A}}_{r+1} \end{bmatrix} \mathbf{a}_{r+1} = \begin{bmatrix} \mathbf{b}_r \\ \tilde{\mathbf{b}}_{r+1} \end{bmatrix} \Rightarrow \begin{bmatrix} \mathbf{A}_r \\ \tilde{\mathbf{A}}_{r+1} \end{bmatrix} \delta\mathbf{a}_{r+1} = \mathbf{0}. \tag{A.1}$$

Similarly, applying the Gauss's principles in Eq. (3.77), we get:

$$\mathbf{a}_{r+1} = \mathbf{Q}_{r+1}\mathbf{a}^{\#}_{r+1} + \mathbf{R}_{r+1}\mathbf{a}^{*}_{r+1} \Rightarrow \delta\mathbf{a}_{r+1} = \mathbf{Q}_{r+1}\delta\mathbf{a}^{\#}_{r+1} + \mathbf{R}_{r+1}\delta\mathbf{a}^{*}_{r+1}. \tag{A.2}$$

Substituting Eq. (A.2) into (A.1), results in:

$$\begin{aligned} \begin{bmatrix} \mathbf{A}_r \\ \tilde{\mathbf{A}}_{r+1} \end{bmatrix} \delta\mathbf{a}_{r+1} &= \begin{bmatrix} \mathbf{A}_r \\ \tilde{\mathbf{A}}_{r+1} \end{bmatrix} \mathbf{Q}_{r+1}\delta\mathbf{a}^{\#}_{r+1} + \begin{bmatrix} \mathbf{A}_r \\ \tilde{\mathbf{A}}_{r+1} \end{bmatrix} \mathbf{R}_{r+1}\delta\mathbf{a}^{*}_{r+1} = \mathbf{0}, \\ &= \begin{bmatrix} \mathbf{A}_r \\ \tilde{\mathbf{A}}_{r+1} \end{bmatrix} \mathbf{Q}_r\tilde{\mathbf{Q}}_{r+1}\delta\mathbf{a}^{\#}_{r+1} + \begin{bmatrix} \mathbf{A}_r \\ \tilde{\mathbf{A}}_{r+1} \end{bmatrix} \begin{bmatrix} \mathbf{R}_r & \tilde{\mathbf{R}}_{r+1} \end{bmatrix} \delta\mathbf{a}^{*}_{r+1} = \mathbf{0}. \end{aligned} \tag{A.3}$$

Developing Eq. (A.3), we obtain:

$$\begin{aligned} \begin{bmatrix} \mathbf{A}_r \\ \tilde{\mathbf{A}}_{r+1} \end{bmatrix} \begin{bmatrix} \mathbf{R}_r & \tilde{\mathbf{R}}_{r+1} \end{bmatrix} \delta\mathbf{a}^{*}_{r+1} &= -\begin{bmatrix} \mathbf{A}_r \\ \tilde{\mathbf{A}}_{r+1} \end{bmatrix} \mathbf{Q}_r\tilde{\mathbf{Q}}_{r+1}\delta\mathbf{a}^{\#}_{r+1}, \\ \begin{bmatrix} \mathbf{A}_r\mathbf{R}_r & \mathbf{A}_r\tilde{\mathbf{R}}_{r+1} \\ \tilde{\mathbf{A}}_{r+1}\mathbf{R}_r & \tilde{\mathbf{A}}_{r+1}\tilde{\mathbf{R}}_{r+1} \end{bmatrix} \begin{bmatrix} \delta\mathbf{a}^{*}_r \\ \delta\tilde{\mathbf{a}}^{*}_{r+1} \end{bmatrix} &= -\begin{bmatrix} \mathbf{A}_r \\ \tilde{\mathbf{A}}_{r+1} \end{bmatrix} \mathbf{Q}_r\tilde{\mathbf{Q}}_{r+1}\delta\mathbf{a}^{\#}_{r+1}, \end{aligned} \tag{A.4}$$

which can be rewritten as:

$$\mathbf{A}_r\mathbf{R}_r\delta\mathbf{a}^{*}_r + \mathbf{A}_r\tilde{\mathbf{R}}_{r+1}\delta\tilde{\mathbf{a}}^{*}_{r+1} = -\mathbf{A}_r\mathbf{Q}_r\tilde{\mathbf{Q}}_{r+r}\delta\mathbf{a}^{\#}_{r+1}, \tag{A.5}$$

$$\tilde{\mathbf{A}}_{r+1}\mathbf{R}_r\delta\mathbf{a}^{*}_r + \tilde{\mathbf{A}}_{r+1}\tilde{\mathbf{R}}_{r+1}\delta\tilde{\mathbf{a}}^{*}_{r+1} = -\tilde{\mathbf{A}}_{r+1}\mathbf{Q}_r\tilde{\mathbf{Q}}_{r+r}\delta\mathbf{a}^{\#}_{r+1}. \tag{A.6}$$

Solving Eq. (A.5) for $\delta\mathbf{a}^{*}_r$, we get:

$$\delta\mathbf{a}^{*}_r = -\left(\mathbf{A}_r\mathbf{R}_r\right)^{\mathrm{g}}\mathbf{A}_r\left(\tilde{\mathbf{R}}_{r+1}\delta\tilde{\mathbf{a}}^{*}_{r+1} + \mathbf{Q}_r\tilde{\mathbf{Q}}_{r+r}\delta\mathbf{a}^{\#}_{r+1}\right). \tag{A.7}$$

Substituting Eq. (A.7) into (A.6) and developing, results in:

$$\begin{aligned}
-\tilde{\mathbf{A}}_{r+1}\mathbf{R}_r\left(\mathbf{A}_r\mathbf{R}_r\right)^{\mathrm{g}}\mathbf{A}_r\left(\tilde{\mathbf{R}}_{r+1}\delta\tilde{\mathbf{a}}^*_{r+1}+\mathbf{Q}_r\tilde{\mathbf{Q}}_{r+1}\delta\mathbf{a}^{\#}_{r+1}\right)+\tilde{\mathbf{A}}_{r+1}\tilde{\mathbf{R}}_{r+1}\delta\tilde{\mathbf{a}}^*_{r+1} &= -\tilde{\mathbf{A}}_{r+1}\mathbf{Q}_r\tilde{\mathbf{Q}}_{r+1}\delta\mathbf{a}^{\#}_{r+1},\\
-\tilde{\mathbf{A}}_{r+1}\mathbf{A}^{\mathrm{g}}_r\mathbf{A}_r\left(\tilde{\mathbf{R}}_{r+1}\delta\tilde{\mathbf{a}}^*_{r+1}+\mathbf{Q}_r\tilde{\mathbf{Q}}_{r+1}\delta\mathbf{a}^{\#}_{r+1}\right)+\tilde{\mathbf{A}}_{r+1}\tilde{\mathbf{R}}_{r+1}\delta\tilde{\mathbf{a}}^*_{r+1} &= -\tilde{\mathbf{A}}_{r+1}\mathbf{Q}_r\tilde{\mathbf{Q}}_{r+1}\delta\mathbf{a}^{\#}_{r+1},\\
-\tilde{\mathbf{A}}_{r+1}\mathbf{A}^{\mathrm{g}}_r\mathbf{A}_r\tilde{\mathbf{R}}_{r+1}\delta\tilde{\mathbf{a}}^*_{r+1}-\tilde{\mathbf{A}}_{r+1}\mathbf{A}^{\mathrm{g}}_r\mathbf{A}_r\mathbf{Q}_r\tilde{\mathbf{Q}}_{r+1}\delta\mathbf{a}^{\#}_{r+1}+\tilde{\mathbf{A}}_{r+1}\tilde{\mathbf{R}}_{r+1}\delta\tilde{\mathbf{a}}^*_{r+1} &= -\tilde{\mathbf{A}}_{r+1}\mathbf{Q}_r\tilde{\mathbf{Q}}_{r+1}\delta\mathbf{a}^{\#}_{r+1}.
\end{aligned} \tag{A.8}$$

Equation (A.8) can be further simplified, as follows:

$$\begin{aligned}
-\tilde{\mathbf{A}}_{r+1}\mathbf{A}^{\mathrm{g}}_r\mathbf{A}_r\tilde{\mathbf{R}}_{r+1}\delta\tilde{\mathbf{a}}^*_{r+1}+\tilde{\mathbf{A}}_{r+1}\tilde{\mathbf{R}}_{r+1}\delta\tilde{\mathbf{a}}^*_{r+1} &= \tilde{\mathbf{A}}_{r+1}\mathbf{A}^{\mathrm{g}}_r\mathbf{A}_r\mathbf{Q}_r\tilde{\mathbf{Q}}_{r+1}\delta\mathbf{a}^{\#}_{r+1}-\tilde{\mathbf{A}}_{r+1}\mathbf{Q}_r\tilde{\mathbf{Q}}_{r+1}\delta\mathbf{a}^{\#}_{r+1},\\
-\tilde{\mathbf{A}}_{r+1}\left(\mathbf{A}^{\mathrm{g}}_r\mathbf{A}_r-\mathbf{I}\right)\tilde{\mathbf{R}}_{r+1}\delta\tilde{\mathbf{a}}^*_{r+1} &= \tilde{\mathbf{A}}_{r+1}\left(\mathbf{A}^{\mathrm{g}}_r\mathbf{A}_r-\mathbf{I}\right)\mathbf{Q}_r\tilde{\mathbf{Q}}_{r+1}\delta\mathbf{a}^{\#}_{r+1},\\
\tilde{\mathbf{A}}_{r+1}\left(\mathbf{I}-\mathbf{A}^{\mathrm{g}}_r\mathbf{A}_r\right)\tilde{\mathbf{R}}_{r+1}\delta\tilde{\mathbf{a}}^{\#}_{r+1} &= -\tilde{\mathbf{A}}_{r+1}\left(\mathbf{I}-\mathbf{A}^{\mathrm{g}}_r\mathbf{A}_r\right)\mathbf{Q}_r\tilde{\mathbf{Q}}_{r+1}\delta\mathbf{a}^{\#}_{r+1},\\
\tilde{\mathbf{A}}_{r+1}\mathbf{S}_r\tilde{\mathbf{R}}_{r+1}\delta\tilde{\mathbf{a}}^*_{r+1} &= -\tilde{\mathbf{A}}_{r+1}\mathbf{S}_r\mathbf{Q}_r\tilde{\mathbf{Q}}_{r+1}\delta\mathbf{a}^{\#}_{r+1},
\end{aligned} \tag{A.9}$$

where $\mathbf{S}_r=\mathbf{I}-\mathbf{A}^{\mathrm{g}}_r\mathbf{A}_r$.

Solving Eq. (A.9) for $\delta\tilde{\mathbf{a}}^*_{r+1}$, we obtain:

$$\delta\tilde{\mathbf{a}}^*_{r+1}=-\left(\tilde{\mathbf{A}}_{r+1}\mathbf{S}_r\tilde{\mathbf{R}}_{r+1}\right)^{\mathrm{g}}\tilde{\mathbf{A}}_{r+1}\mathbf{S}_r\mathbf{Q}_r\tilde{\mathbf{Q}}_{r+1}\delta\mathbf{a}^{\#}_{r+1}. \tag{A.10}$$

Substituting Eq. (A.10) into (A.7), we get:

$$\begin{aligned}
\delta\mathbf{a}^*_r &= -\left(\mathbf{A}_r\mathbf{R}_r\right)^{\mathrm{g}}\mathbf{A}_r\left(\tilde{\mathbf{R}}_{r+1}\delta\tilde{\mathbf{a}}^*_{r+1}+\mathbf{Q}_r\tilde{\mathbf{Q}}_{r+1}\delta\mathbf{a}^{\#}_{r+1}\right),\\
&= -\left(\mathbf{A}_r\mathbf{R}_r\right)^{\mathrm{g}}\mathbf{A}_r\left(\mathbf{Q}_r\tilde{\mathbf{Q}}_{r+1}\delta\mathbf{a}^{\#}_{r+1}-\tilde{\mathbf{R}}_{r+1}\left(\tilde{\mathbf{A}}_{r+1}\mathbf{S}_r\tilde{\mathbf{R}}_{r+1}\right)^{\mathrm{g}}\tilde{\mathbf{A}}_{r+1}\mathbf{S}_r\mathbf{Q}_r\tilde{\mathbf{Q}}_{r+1}\delta\mathbf{a}^{\#}_{r+1}\right).
\end{aligned} \tag{A.11}$$

Equations (A.7) and (A.10) can be rewritten as follows:

$$\begin{aligned}
\delta\mathbf{a}^*_{r+1} &= \begin{bmatrix}\delta\mathbf{a}^*_r\\ \delta\tilde{\mathbf{a}}^*_{r+1}\end{bmatrix},\\
&= \begin{bmatrix}-\left(\mathbf{A}_r\mathbf{R}_r\right)^{\mathrm{g}}\mathbf{A}_r\left(\mathbf{Q}_r\tilde{\mathbf{Q}}_{r+1}-\tilde{\mathbf{R}}_{r+1}\left(\tilde{\mathbf{A}}_{r+1}\mathbf{S}_r\tilde{\mathbf{R}}_{r+1}\right)^{\mathrm{g}}\tilde{\mathbf{A}}_{r+1}\mathbf{S}_r\mathbf{Q}_r\tilde{\mathbf{Q}}_{r+1}\right)\\ -\left(\tilde{\mathbf{A}}_{r+1}\mathbf{S}_r\tilde{\mathbf{R}}_{r+1}\right)^{\mathrm{g}}\tilde{\mathbf{A}}_{r+1}\mathbf{S}_r\mathbf{Q}_r\tilde{\mathbf{Q}}_{r+1}\end{bmatrix}\delta\mathbf{a}^{\#}_{r+1}.
\end{aligned} \tag{A.12}$$

Substituting Eq. (A.12) into (A.2) and developing, results in:

$$
\begin{aligned}
\delta\mathbf{a}_{r+1} &= \mathbf{Q}_r\tilde{\mathbf{Q}}_{r+1}\delta\mathbf{a}^{\#}_{r+1} + \mathbf{R}_{r+1}\delta\mathbf{a}^{*}_{r+1}, \\
&= \mathbf{Q}_r\tilde{\mathbf{Q}}_{r+1}\delta\mathbf{a}^{\#}_{r+1} + \begin{bmatrix} \mathbf{R}_r & \tilde{\mathbf{R}}_{r+1} \end{bmatrix} \times \ldots \\
&\begin{bmatrix} -(\mathbf{A}_r\mathbf{R}_r)^{\mathrm{g}}\,\mathbf{A}_r\left(\mathbf{Q}_r\tilde{\mathbf{Q}}_{r+1} - \tilde{\mathbf{R}}_{r+1}\left(\tilde{\mathbf{A}}_{r+1}\mathbf{S}_r\tilde{\mathbf{R}}_{r+1}\right)^{\mathrm{g}}\tilde{\mathbf{A}}_{r+1}\mathbf{S}_r\mathbf{Q}_r\tilde{\mathbf{Q}}_{r+1}\right) \\ -\left(\tilde{\mathbf{A}}_{r+1}\mathbf{S}_r\tilde{\mathbf{R}}_{r+1}\right)^{\mathrm{g}}\tilde{\mathbf{A}}_{r+1}\mathbf{S}_r\mathbf{Q}_r\tilde{\mathbf{Q}}_{r+1} \end{bmatrix}\delta\mathbf{a}^{\#}_{r+1}, \\
&= \mathbf{Q}_r\tilde{\mathbf{Q}}_{r+1}\delta\mathbf{a}^{\#}_{r+1} + \ldots \\
&- \mathbf{R}_r\,(\mathbf{A}_r\mathbf{R}_r)^{\mathrm{g}}\,\mathbf{A}_r\left(\mathbf{Q}_r\tilde{\mathbf{Q}}_{r+1} - \tilde{\mathbf{R}}_{r+1}\left(\tilde{\mathbf{A}}_{r+1}\mathbf{S}_r\tilde{\mathbf{R}}_{r+1}\right)^{\mathrm{g}}\tilde{\mathbf{A}}_{r+1}\mathbf{S}_r\mathbf{Q}_r\tilde{\mathbf{Q}}_{r+1}\right)\delta\mathbf{a}^{\#}_{r+1} + \ldots \\
&- \tilde{\mathbf{R}}_{r+1}\left(\tilde{\mathbf{A}}_{r+1}\mathbf{S}_r\tilde{\mathbf{R}}_{r+1}\right)^{\mathrm{g}}\tilde{\mathbf{A}}_{r+1}\mathbf{S}_r\mathbf{Q}_r\tilde{\mathbf{Q}}_{r+1}\delta\mathbf{a}^{\#}_{r+1}.
\end{aligned}
\tag{A.13}
$$

Equation (A.13) can be further simplified, as follows:

$$
\begin{aligned}
\delta\mathbf{a}_{r+1} &= \mathbf{Q}_r\tilde{\mathbf{Q}}_{r+1}\delta\mathbf{a}^{\#}_{r+1} - \mathbf{A}^{\mathrm{g}}_r\mathbf{A}_r\left(\mathbf{Q}_r\tilde{\mathbf{Q}}_{r+1} - \tilde{\mathbf{R}}_{r+1}\left(\tilde{\mathbf{A}}_{r+1}\mathbf{S}_r\tilde{\mathbf{R}}_{r+1}\right)^{\mathrm{g}}\tilde{\mathbf{A}}_{r+1}\mathbf{S}_r\mathbf{Q}_r\tilde{\mathbf{Q}}_{r+1}\right)\delta\mathbf{a}^{\#}_{r+1} + \ldots \\
&- \tilde{\mathbf{R}}_{r+1}\left(\tilde{\mathbf{A}}_{r+1}\mathbf{S}_r\tilde{\mathbf{R}}_{r+1}\right)^{\mathrm{g}}\tilde{\mathbf{A}}_{r+1}\mathbf{S}_r\mathbf{Q}_r\tilde{\mathbf{Q}}_{r+1}\delta\mathbf{a}^{\#}_{r+1}, \\
&= \left(\mathbf{Q}_r\tilde{\mathbf{Q}}_{r+1} - \mathbf{A}^{\mathrm{g}}_r\mathbf{A}_r\left(\mathbf{Q}_r\tilde{\mathbf{Q}}_{r+1} - \tilde{\mathbf{R}}_{r+1}\left(\tilde{\mathbf{A}}_{r+1}\mathbf{S}_r\tilde{\mathbf{R}}_{r+1}\right)^{\mathrm{g}}\tilde{\mathbf{A}}_{r+1}\mathbf{S}_r\mathbf{Q}_r\tilde{\mathbf{Q}}_{r+1}\right)\right)\delta\mathbf{a}^{\#}_{r+1} + \ldots \\
&- \tilde{\mathbf{R}}_{r+1}\left(\tilde{\mathbf{A}}_{r+1}\mathbf{S}_r\tilde{\mathbf{R}}_{r+1}\right)^{\mathrm{g}}\tilde{\mathbf{A}}_{r+1}\mathbf{S}_r\mathbf{Q}_r\tilde{\mathbf{Q}}_{r+1}\delta\mathbf{a}^{\#}_{r+1}, \\
&= \left(\mathbf{I} - \mathbf{A}^{\mathrm{g}}_r\mathbf{A}_r\left(\mathbf{I} - \tilde{\mathbf{R}}_{r+1}\left(\tilde{\mathbf{A}}_{r+1}\mathbf{S}_r\tilde{\mathbf{R}}_{r+1}\right)^{\mathrm{g}}\tilde{\mathbf{A}}_{r+1}\mathbf{S}_r\right)\right)\mathbf{Q}_r\tilde{\mathbf{Q}}_{r+1}\delta\mathbf{a}^{\#}_{r+1} + \ldots \\
&- \tilde{\mathbf{R}}_{r+1}\left(\tilde{\mathbf{A}}_{r+1}\mathbf{S}_r\tilde{\mathbf{R}}_{r+1}\right)^{\mathrm{g}}\tilde{\mathbf{A}}_{r+1}\mathbf{S}_r\mathbf{Q}_r\tilde{\mathbf{Q}}_{r+1}\delta\mathbf{a}^{\#}_{r+1}, \\
&= \left(\left(\mathbf{I} - \mathbf{A}^{\mathrm{g}}_r\mathbf{A}_r\left(\mathbf{I} - \tilde{\mathbf{R}}_{r+1}\left(\tilde{\mathbf{A}}_{r+1}\mathbf{S}_r\tilde{\mathbf{R}}_{r+1}\right)^{\mathrm{g}}\tilde{\mathbf{A}}_{r+1}\mathbf{S}_r\right)\right) + \ldots\right. \\
&\left.-\tilde{\mathbf{R}}_{r+1}\left(\tilde{\mathbf{A}}_{r+1}\mathbf{S}_r\mathbf{R}\right)^{\mathrm{g}}\tilde{\mathbf{A}}_{r+1}\mathbf{S}_r\right)\mathbf{Q}_r\tilde{\mathbf{Q}}_{r+1}\delta\mathbf{a}^{\#}_{r+1}, \\
&= \left(\mathbf{I} - \mathbf{A}^{\mathrm{g}}_r\mathbf{A}_r + \mathbf{A}^{\mathrm{g}}_r\mathbf{A}_r\tilde{\mathbf{R}}_{r+1}\left(\tilde{\mathbf{A}}_{r+1}\mathbf{S}_r\tilde{\mathbf{R}}_{r+1}\right)^{\mathrm{g}}\tilde{\mathbf{A}}_{r+1}\mathbf{S}_r \ldots\right. \\
&\left.-\tilde{\mathbf{R}}_{r+1}\left(\tilde{\mathbf{A}}_{r+1}\mathbf{S}_r\tilde{\mathbf{R}}_{r+1}\right)^{\mathrm{g}}\tilde{\mathbf{A}}_{r+1}\mathbf{S}_r\right)\mathbf{Q}_r\tilde{\mathbf{Q}}_{r+1}\delta\mathbf{a}^{\#}_{r+1}, \\
&= \left(\mathbf{I} - \mathbf{A}^{\mathrm{g}}_r\mathbf{A}_r + \left(\mathbf{A}^{\mathrm{g}}_r\mathbf{A}_r - \mathbf{I}\right)\tilde{\mathbf{R}}_{r+1}\left(\tilde{\mathbf{A}}_{r+1}\mathbf{S}_r\tilde{\mathbf{R}}_{r+1}\right)^{\mathrm{g}}\tilde{\mathbf{A}}_{r+1}\mathbf{S}_r\right)\mathbf{Q}_r\tilde{\mathbf{Q}}_{r+1}\delta\mathbf{a}^{\#}_{r+1}, \\
&= \left(\mathbf{I} - \mathbf{A}^{\mathrm{g}}_r\mathbf{A}_r - \left(\mathbf{I} - \mathbf{A}^{\mathrm{g}}_r\mathbf{A}_r\right)\tilde{\mathbf{R}}_{r+1}\left(\tilde{\mathbf{A}}_{r+1}\mathbf{S}_r\tilde{\mathbf{R}}_{r+1}\right)^{\mathrm{g}}\tilde{\mathbf{A}}_{r+1}\mathbf{S}_r\right)\mathbf{Q}_r\tilde{\mathbf{Q}}_{r+1}\delta\mathbf{a}^{\#}_{r+1}, \\
&= \left(\mathbf{I} - \mathbf{A}^{\mathrm{g}}_r\mathbf{A}_r\right)\left(\mathbf{I} - \tilde{\mathbf{R}}_{r+1}\left(\tilde{\mathbf{A}}_{r+1}\mathbf{S}_r\tilde{\mathbf{R}}_{r+1}\right)^{\mathrm{g}}\tilde{\mathbf{A}}_{r+1}\mathbf{S}_r\right)\mathbf{Q}_r\tilde{\mathbf{Q}}_{r+1}\delta\mathbf{a}^{\#}_{r+1}, \\
&= \mathbf{S}_r\left(\mathbf{I} - \left(\tilde{\mathbf{A}}_{r+1}\mathbf{S}_r\right)^{\mathrm{g}}\tilde{\mathbf{A}}_{r+1}\mathbf{S}_r\right)\mathbf{Q}_{r+1}\delta\mathbf{a}^{\#}_{r+1}, \\
&= \mathbf{S}_r\tilde{\mathbf{S}}_{r+1}\mathbf{Q}_{r+1}\delta\mathbf{a}^{\#}_{r+1}, \\
&= \mathbf{S}_{r+1}\mathbf{Q}_{r+1}\delta\mathbf{a}^{\#}_{r+1}, \\
&= \mathbf{E}_{r+1}\delta\mathbf{a}^{\#}_{r+1}, \\
&= \mathbf{E}_r\tilde{\mathbf{E}}_{r+1}\delta\mathbf{a}^{\#}_{r+1},
\end{aligned}
\tag{A.14}
$$

where

$$
\begin{aligned}
\mathbf{A}_r^{\mathrm{g}} &= \mathbf{R}_r \left(\mathbf{A}_r \mathbf{R}_r\right)^{\mathrm{g}}, \\
\left(\tilde{\mathbf{A}}_{r+1} \mathbf{S}_r\right)^{\mathrm{g}} &= \tilde{\mathbf{R}}_{r+1} \left(\tilde{\mathbf{A}}_{r+1} \mathbf{S}_r \tilde{\mathbf{R}}_{r+1}\right)^{\mathrm{g}}, \\
\mathbf{S}_r &= \mathbf{I} - \mathbf{A}_r^{\mathrm{g}} \mathbf{A}_r = \mathbf{I} - \mathbf{R}_r \left(\mathbf{A}_r \mathbf{R}_r\right)^{\mathrm{g}} \mathbf{A}_r, \\
\tilde{\mathbf{S}}_{r+1} &= \mathbf{I} - \left(\tilde{\mathbf{A}}_{r+1} \mathbf{S}_r\right)^{\mathrm{g}} \tilde{\mathbf{A}}_{r+1} \mathbf{S}_r = \mathbf{I} - \tilde{\mathbf{R}}_{r+1} \left(\tilde{\mathbf{A}}_{r+1} \mathbf{S}_r \tilde{\mathbf{R}}_{r+1}\right)^{\mathrm{g}} \tilde{\mathbf{A}}_{r+1} \mathbf{S}_r, \\
\mathbf{S}_{r+1} &= \mathbf{S}_r \tilde{\mathbf{S}}_{r+1}, \\
\mathbf{E}_r &= \left(\mathbf{I} - \mathbf{R}_r \left(\mathbf{A}_r \mathbf{R}_r\right)^{\mathrm{g}} \mathbf{A}_r\right) \mathbf{Q}_r, \\
\tilde{\mathbf{E}}_{r+1} &= \left(\mathbf{I} - \mathbf{Q}_r^{\mathsf{T}} \tilde{\mathbf{R}}_{r+1} \left(\tilde{\mathbf{A}}_{r+1} \mathbf{E}_r \mathbf{Q}_r^{\mathsf{T}} \tilde{\mathbf{R}}_{r+1}\right)^{\mathrm{g}} \tilde{\mathbf{A}}_{r+1} \mathbf{S}_r\right) \tilde{\mathbf{Q}}_{r+1},
\end{aligned}
\tag{A.15}
$$

are the expressions presented in Eq. (3.86) to the calculation of the recursive orthogonal complement.

A.2 Closed-loop dynamic

The modeling and control constraints are expressed as follows:

$$
\begin{aligned}
\mathbf{A}\mathbf{a} &= \mathbf{b}, \\
\mathbf{A}\mathbf{N}^{-1}\mathbf{u} &= \mathbf{0}.
\end{aligned}
\tag{A.16}
$$

To obtains the closed-loop dynamics, Eq. (A.16) can be rewritten as:

$$
\mathbf{A}\left(\mathbf{a} + \mathbf{N}^{-1}\mathbf{u}\right) = \mathbf{b}. \tag{A.17}
$$

To obtain the closed-loop dynamics consistent with the constraints of Eq. (A.17), let us define a Gaussian deviation function as follows:

$$
Z = \frac{1}{2}\left(\mathbf{a} - \mathbf{a}_0\right)^{\mathsf{T}} \mathbf{N} \left(\mathbf{a} - \mathbf{a}_0\right) + \frac{1}{2}\left(\mathbf{u} - \mathbf{u}_0\right)^{\mathsf{T}} \mathbf{N}^{-1} \left(\mathbf{u} - \mathbf{u}_0\right). \tag{A.18}
$$

Let $\boldsymbol{\lambda}_1$ and $\boldsymbol{\lambda}_2$ be r-column-vectors of Lagrange multipliers used in the following constrained optimization problem:

$$
\bar{Z} = Z - \boldsymbol{\lambda}_1^{\mathsf{T}} \left(\mathbf{A}\left(\mathbf{a} + \mathbf{N}^{-1}\mathbf{u}\right) - \mathbf{b}\right) - \boldsymbol{\lambda}_2^{\mathsf{T}} \mathbf{A}\mathbf{N}^{-1}\mathbf{u}. \tag{A.19}
$$

The sufficient conditions to solve the optimization problem are obtained by calculating the

stationary points, as follows:

$$\frac{\partial \bar{Z}}{\partial \mathbf{a}} = \mathbf{N}(\mathbf{a} - \mathbf{a}_0) - \mathbf{A}^\mathsf{T}\boldsymbol{\lambda}_1 = \mathbf{0} \Rightarrow \mathbf{a} = \mathbf{a}_0 + \mathbf{N}^{-1}\mathbf{A}^\mathsf{T}\boldsymbol{\lambda}_1, \tag{A.20}$$

$$\frac{\partial \bar{Z}}{\partial \mathbf{u}} = \mathbf{N}^{-1}(\mathbf{u} - \mathbf{u}_0) - \mathbf{N}^{-1}\mathbf{A}^\mathsf{T}(\boldsymbol{\lambda}_1 + \boldsymbol{\lambda}_2) \Rightarrow \mathbf{u} = \mathbf{u}_0 + \mathbf{A}^\mathsf{T}(\boldsymbol{\lambda}_1 + \boldsymbol{\lambda}_2), \tag{A.21}$$

$$\frac{\partial \bar{Z}}{\partial \boldsymbol{\lambda}_1} = \mathbf{A}\left(\mathbf{a} + \mathbf{N}^{-1}\mathbf{u}\right) - \mathbf{b} = \mathbf{0}, \tag{A.22}$$

$$\frac{\partial \bar{Z}}{\partial \boldsymbol{\lambda}_2} = \mathbf{A}\mathbf{N}^{-1}\mathbf{u} = \mathbf{0}. \tag{A.23}$$

Using Eq. (A.21) in (A.23), we obtain:

$$\mathbf{A}\mathbf{N}^{-1}\left(\mathbf{u}_0 + \mathbf{A}^\mathsf{T}(\boldsymbol{\lambda}_1 + \boldsymbol{\lambda}_2)\right) = \mathbf{0}. \tag{A.24}$$

Substituting Eqs. (A.20) and (A.21) into (A.22) and developing, we get:

$$\begin{aligned}
\mathbf{A}\left(\mathbf{a}_0 + \mathbf{N}^{-1}\mathbf{A}^\mathsf{T}\boldsymbol{\lambda}_1 + \mathbf{N}^{-1}\mathbf{u}_0 + \mathbf{N}^{-1}\mathbf{A}^\mathsf{T}(\boldsymbol{\lambda}_1 + \boldsymbol{\lambda}_2)\right) &= \mathbf{b}, \\
\mathbf{A}\mathbf{a}_0 + \mathbf{A}\mathbf{N}^{-1}\mathbf{A}^\mathsf{T}\boldsymbol{\lambda}_1 + \mathbf{A}\mathbf{N}^{-1}\mathbf{u}_0 + \mathbf{A}\mathbf{N}^{-1}\mathbf{A}^\mathsf{T}(\boldsymbol{\lambda}_1 + \boldsymbol{\lambda}_2) &= \mathbf{b}, \\
\mathbf{A}\mathbf{a}_0 + \mathbf{A}\mathbf{N}^{-1}\mathbf{A}^\mathsf{T}\boldsymbol{\lambda}_1 + \mathbf{A}\mathbf{N}^{-1}\mathbf{u}_0 - \mathbf{A}\mathbf{N}^{-1}\mathbf{u}_0 &= \mathbf{b}, \\
\mathbf{A}\mathbf{a}_0 + \mathbf{A}\mathbf{N}^{-1}\mathbf{A}^\mathsf{T}\boldsymbol{\lambda}_1 &= \mathbf{b}, \\
\mathbf{A}\mathbf{N}^{-1}\mathbf{A}^\mathsf{T}\boldsymbol{\lambda}_1 &= \mathbf{b} - \mathbf{A}\mathbf{a}_0.
\end{aligned} \tag{A.25}$$

Solving Eq. (A.25) for $\boldsymbol{\lambda}_1$, we obtain:

$$\boldsymbol{\lambda}_1 = \left(\mathbf{A}\mathbf{N}^{-1}\mathbf{A}^\mathsf{T}\right)^\mathrm{g}(\mathbf{b} - \mathbf{A}\mathbf{a}_0) + \left(\mathbf{I} - \left(\mathbf{A}\mathbf{N}^{-1}\mathbf{A}^\mathsf{T}\right)^\mathrm{g}\mathbf{A}\mathbf{N}^{-1}\mathbf{A}^\mathsf{T}\right)\mathbf{w}_1, \tag{A.26}$$

where $\mathbf{w}_1$ is an arbitrary column-vector.

Using Eq. (A.26) in (A.20) with $\mathbf{A}^\mathsf{T}\left(\mathbf{I} - \left(\mathbf{A}\mathbf{N}^{-1}\mathbf{A}^\mathsf{T}\right)^\mathrm{g}\mathbf{A}\mathbf{N}^{-1}\mathbf{A}^\mathsf{T}\right) = \mathbf{0}$ from Eq. (4.29), we get:

$$\mathbf{a} = \mathbf{a}_0 + \mathbf{N}^{-1}\mathbf{A}^\mathsf{T}\left(\mathbf{A}\mathbf{N}^{-1}\mathbf{A}^\mathsf{T}\right)^\mathrm{g}(\mathbf{b} - \mathbf{A}\mathbf{a}_0), \tag{A.27}$$

which is the Udwadia-Kalaba equation.

Using Eq. (A.25) in (A.24) and developing, results in:

$$\begin{aligned}
\mathbf{A}\mathbf{N}^{-1}\left(\mathbf{u}_0 + \mathbf{A}^{\mathsf{T}}\left(\boldsymbol{\lambda}_1 + \boldsymbol{\lambda}_2\right)\right) &= \mathbf{0}, \\
\mathbf{A}\mathbf{N}^{-1}\mathbf{A}^{\mathsf{T}}\left(\boldsymbol{\lambda}_1 + \boldsymbol{\lambda}_2\right) &= -\mathbf{A}\mathbf{N}^{-1}\mathbf{u}_0, \\
\mathbf{A}\mathbf{N}^{-1}\mathbf{A}^{\mathsf{T}}\boldsymbol{\lambda}_1 + \mathbf{A}\mathbf{N}^{-1}\mathbf{A}^{\mathsf{T}}\boldsymbol{\lambda}_2 &= -\mathbf{A}\mathbf{N}^{-1}\mathbf{u}_0, \\
\mathbf{b} - \mathbf{A}\mathbf{a}_0 + \mathbf{A}\mathbf{N}^{-1}\mathbf{A}^{\mathsf{T}}\boldsymbol{\lambda}_2 &= -\mathbf{A}\mathbf{N}^{-1}\mathbf{u}_0, \\
\mathbf{A}\mathbf{N}^{-1}\mathbf{A}^{\mathsf{T}}\boldsymbol{\lambda}_2 &= \mathbf{A}\mathbf{a}_0 - \mathbf{A}\mathbf{N}^{-1}\mathbf{u}_0 - \mathbf{b}.
\end{aligned} \tag{A.28}$$

Solving Eq. (A.28) for $\boldsymbol{\lambda}_2$, we obtain:

$$\boldsymbol{\lambda}_2 = \left(\mathbf{A}\mathbf{N}^{-1}\mathbf{A}^{\mathsf{T}}\right)^{\mathrm{g}}\left(\mathbf{A}\mathbf{a}_0 - \mathbf{A}\mathbf{N}^{-1}\mathbf{u}_0 - \mathbf{b}\right) + \left(\mathbf{I} - \left(\mathbf{A}\mathbf{N}^{-1}\mathbf{A}^{\mathsf{T}}\right)^{\mathrm{g}}\mathbf{A}\mathbf{N}^{-1}\mathbf{A}^{\mathsf{T}}\right)\mathbf{w}_2, \tag{A.29}$$

where $\mathbf{w}_2$ is an arbitrary column-vector.

Using Eqs. (A.29) and (A.26) in (A.21) with $\mathbf{A}^{\mathsf{T}}\left(\mathbf{I} - \left(\mathbf{A}\mathbf{N}^{-1}\mathbf{A}^{\mathsf{T}}\right)^{\mathrm{g}}\mathbf{A}\mathbf{N}^{-1}\mathbf{A}^{\mathsf{T}}\right) = \mathbf{0}$ similar to Eq. (4.29), we get:

$$\mathbf{u} = \mathbf{u}_0 - \mathbf{A}^{\mathsf{T}}\left(\mathbf{A}\mathbf{N}^{-1}\mathbf{A}^{\mathsf{T}}\right)^{\mathrm{g}}\left(\mathbf{A}\mathbf{N}^{-1}\mathbf{u}_0\right), \tag{A.30}$$

which is the set of control forces consistent with the modeling constraints presented in Eq. (4.30).

Performing the summation of Eq. (A.27) and (A.30), we obtain:

$$\mathbf{a} + \mathbf{N}^{-1}\mathbf{u} = \mathbf{a}_0 + \mathbf{N}^{-1}\mathbf{u}_0 + \mathbf{N}^{-1}\mathbf{A}^{\mathsf{T}}\left(\mathbf{A}\mathbf{N}^{-1}\mathbf{A}^{\mathsf{T}}\right)^{\mathrm{g}}\left(\mathbf{b} - \mathbf{A}\mathbf{a}_0 - \mathbf{A}\mathbf{N}^{-1}\mathbf{u}_0\right), \tag{A.31}$$

which is the closed-loop dynamic presented in Eq. (4.9).

APPENDIX B

B.1 Publications

The list of publications carried out during the Ph.D. course follows below:

- DE OLIVEIRA, É. L. et al. Station-keeping of a ROV under wave disturbance: Modeling and control design. Proceedings of the Institution of Mechanical Engineers, Part M: Journal of Engineering for the Maritime Environment, p. 1–23, 2 set. 2022. <http://journals.sagepub.com/doi/10.1177/14750902221116673>
- DE OLIVEIRA, É. L.; DONHA, D. C. Control of a hydraulic excavator manipulator / Controle de uma escavadora hidráulica manipuladora. Brazilian Journal of Development, v. 8, n. 6, p. 46263–46282, 2022. <https://doi.org/10.34117/bjdv8n6-240>
- DE OLIVEIRA, É. L.; ORSINO, R. M. M.; DONHA, D. C. Modular modeling and coordination control scheme for an underwater cooperative transportation performed by two I-AUVs. Control Engineering Practice, v. 125, n. May, p. 1–21, ago. 2022. <https://doi.org/10.1016/j.conengprac.2022.105198>
- DE OLIVEIRA, É. L. et al. MODELING AND MODEL PREDICTIVE CONTROL (MPC) OF AN UNDERWATER DOUBLE INVERTED PENDULUM (UDIP). Journal of Engineering Research, v. 2, n. 6, p. 2–12, 2022. <https://educapes.capes.gov.br/handle/capes/701820>
- DE OLIVEIRA, É. L. et al. Evaluation of Dynamic Coupling Intensity and Passive Attitude Control of Underwater Vehicle-Manipulator Systems. IFAC-PapersOnLine, v. 54, n. 16, p. 356–363, 2021. <https://doi.org/10.1016/j.ifacol.2021.10.116>
- DE OLIVEIRA, É. L.; ORSINO, R. M. M.; DONHA, D. C. Disturbance-Observer-Based Model Predictive Control of Underwater Vehicle-Manipulator Systems. IFAC-PapersOnLine, v. 54, n. 16, p. 348–355, 2021. <https://doi.org/10.1016/j.ifacol.2021.10.115>
- DE OLIVEIRA, É. L.; DONHA, D. C.; CARDOSO, R. Modeling and Station-Keeping Control of an Underwater Vehicle-Manipulator System Through Reactions Wheels. Vol-

ume 7B: Dynamics, Vibration, and Control. Proceedings...American Society of Mechanical Engineers, 1 nov. 2021. <https://doi.org/10.1115/IMECE2021-69031>

- PESCE, C. P. et al. A Model to Assess the Susceptibility of a Multicolumn FOWT Platform to Vortex-Induced Motions in Early Design Stages. Volume 9: Ocean Renewable Energy. Proceedings...American Society of Mechanical Engineers, 21 jun. 2021. <https://doi.org/10.1115/OMAE2021-65761>

- DE OLIVEIRA, É. L. et al. A Reduced-Order Mathematical Model for the Current-Induced Motion of a Floating Offshore Wind Turbine. ASME 2021 – 3rd International Offshore Wind Technical Conference. Proceedings...American Society of Mechanical Engineers, 16 fev. 2021. <https://doi.org/10.1115/IOWTC2021-3503>

- CARDOSO, R. et al. Integrative backstepping for one link manipulator quadrotor trajectory tracking, CILAMCE 2021 – Proceedings of the XLII Ibero-Latin-American Congress on Computational Methods in Engineering | PANACM 2021 – 3rd Pan American Congress on Computational Mechanics, 9 nov. 2021. <https://cilamce.com.br/anais/arearestrita/apresentacoes/221/9719.pdf>

- DE OLIVEIRA, É. L. et al. Modeling and Model Predictive Control of an Underwater Double Inverted Pendulum. Proceedings of the XLI Ibero-Latin-American Congress on Computational Methods in Engineering, ABMEC, 2020. <https://proceedingscilamce.duckdns.org/>

- PESCE, B.; DE OLIVEIRA, É. L.; PESCE, C. P. Vortex Induced Motions of a Moored Monocolumn Platform. DINAME 2019 – Proceedings of the XV International Symposium on Dynamic Problems of Mechanics. Proceedings... Associação Brasileira de Engenharia e Ciências Mecânicas, 15 mar. 2019. <https://doi.org/10.26678/ABCM.DINAME2019.DIN2019-0213>

- DE OLIVEIRA, É. L.; DONHA, D. C. Control of a hydraulic excavator manipulator. DINAME 2019 – Proceedings of the XV International Symposium on Dynamic Problems of Mechanics. Proceedings... Associação Brasileira de Engenharia e Ciências Mecânicas, 15 mar. 2019. <https://doi.org/10.26678/ABCM.DINAME2019.DIN2019-0118>

- CARDOSO, R.; DE OLIVEIRA, É. L.; DONHA, D. C. Comparison of two sliding mode control techniques applied to a ROV vertical motion. COBEM 2019 – Proceedings of the 25th International Congress of Mechanical Engineering, 20 oct. 2019. <https://doi.org/10.26678/ABCM.COBEM2019.COB2019-1641>

- DE OLIVEIRA, É. L.; ORSINO, R. M. M.; DONHA, D. C. Formation control of AUVs based on the Udwadia-Kalaba equation. MSNDC-2023 (Submitted).
- ORSINO, R. M. M.; DE OLIVEIRA, É. L. Recursive Least-Squares Based Constraint Enforcement Algorithm for Multibody Systems. MSNDC-2023 (Submitted).
- DE OLIVEIRA, É. L.; ORSINO, R. M. M.; DONHA, D. C. Modeling, Simulation and Control of an Underwater Robotic Manipulator. COBEM-2023 (Submitted).
- DE OLIVEIRA, É. L.; DONHA, D. C.; DE BARROS, E. A. Modeling and station-keeping control design of the Mandi-II-ROV under wave disturbance (To be submitted).
- HESS-COELHO, T. A. et al. Modular Modeling Methodology (MMM) applied to kinematically redundant parallel mechanisms (To be submitted).